ISSN 0021-9673

VOL. 638 NO. 2 MAY 28, 1993

THIS ISSUE COMPLETES VOL. 638

**8th Int. Symp. on Capillary Electrophoresis and Isotachophoresis, Rome, October 6–9, 1992**

# JOURNAL OF CHROMATOGRAPHY

## INCLUDING ELECTROPHORESIS AND OTHER SEPARATION METHODS

SYMPOSIUM VOLUMES



ELSEVIER

# JOURNAL OF CHROMATOGRAPHY

INCLUDING ELECTROPHORESIS AND OTHER SEPARATION METHODS

**Scope.** The *Journal of Chromatography* publishes papers on all aspects of **chromatography, electrophoresis** and related methods. Contributions consist mainly of research papers dealing with chromatographic theory, instrumental developments and their applications. The section *Biomedical Applications*, which is under separate editorship, deals with the following aspects: developments in and applications of chromatographic and electrophoretic techniques related to clinical diagnosis or alterations during medical treatment; screening and profiling of body fluids or tissues related to the analysis of active substances and to metabolic disorders; drug level monitoring and pharmacokinetic studies; clinical toxicology; forensic medicine; veterinary medicine; occupational medicine; results from basic medical research with direct consequences in clinical practice. In *Symposium volumes*, which are under separate editorship, proceedings of symposia on chromatography, electrophoresis and related methods are published.

**Submission of Papers.** The preferred medium of submission is on disk with accompanying manuscript (see *Electronic manuscripts* in the Instructions to Authors, which can be obtained from the publisher, Elsevier Science Publishers B.V., P.O. Box 330, 1000 AH Amsterdam, Netherlands). Manuscripts (in English; *four* copies are required) should be submitted to: Editorial Office of *Journal of Chromatography*, P.O. Box 681, 1000 AR Amsterdam, Netherlands, Telefax (+31-20) 5862 304, or to: The Editor of *Journal of Chromatography, Biomedical Applications*, P.O. Box 681, 1000 AR Amsterdam, Netherlands. Review articles are invited or proposed in writing to the Editors who welcome suggestions for subjects. An outline of the proposed review should first be forwarded to the Editors for preliminary discussion prior to preparation. Submission of an article is understood to imply that the article is original and unpublished and is not being considered for publication elsewhere. For copyright regulations, see below.

**Publication.** The *Journal of Chromatography* (incl. *Biomedical Applications*) has 40 volumes in 1993. The subscription prices for 1993 are:

*J. Chromatogr.* (incl. *Cum. Indexes, Vols. 601–650*) + *Biomed. Appl.* (Vols. 612–651):
Dfl. 8520.00 plus Dfl. 1320.00 (p.p.h.) (total *ca.* US$ 5466.75)

*J. Chromatogr.* (incl. *Cum Indexes, Vols. 601–650*) only (Vols. 623–651):
Dfl. 7047.00 plus Dfl. 957.00 (p.p.h.) (total *ca.* US$ 4446.75)

*Biomed. Appl.* only (Vols. 612–622):
Dfl. 2783.00 plus Dfl. 363.00 (p.p.h.) (total *ca.* US$ 1747.75).

**Subscription Orders.** The Dutch guilder price is definitive. The US$ price is subject to exchange-rate fluctuations and is given as a guide. Subscriptions are accepted on a prepaid basis only, unless different terms have been previously agreed upon. Subscriptions orders can be entered only by calender year (Jan.–Dec.) and should be sent to Elsevier Science Publishers, Journal Department, P.O. Box 211, 1000 AE Amsterdam, Netherlands, Tel. (+31-20) 5803 642, Telefax (+31-20) 5803 598, or to your usual subscription agent. Postage and handling charges include surface delivery except to the following countries where air delivery via SAL (Surface Air Lift) mail is ensured: Argentina, Australia, Brazil, Canada, China, Hong Kong, India, Israel, Japan*, Malaysia, Mexico, New Zealand, Pakistan, Singapore, South Africa, South Korea, Taiwan, Thailand, USA. *For Japan air delivery (SAL) requires 25% additional charge of the normal postage and handling charge. For all other countries airmail rates are available upon request. Claims for missing issues must be made within six months of our publication (mailing) date, otherwise such claims cannot be honoured free of charge. Back volumes of the *Journal of Chromatography* (Vols. 1–611) are available at Dfl. 230.00 (plus postage). Customers in the USA and Canada wishing information on this and other Elsevier journals, please contact Journal Information Center, Elsevier Science Publishing Co. Inc., 655 Avenue of the Americas, New York, NY 10010, USA, Tel. (+1-212) 633 3750, Telefax (+1-212) 633 3764.

**Abstracts/Contents Lists** published in Analytical Abstracts, Biochemical Abstracts, Biological Abstracts, Chemical Abstracts, Chemical Titles, Chromatography Abstracts, Current Awareness in Biological Sciences (CABS), Current Contents/Life Sciences, Current Contents/Physical, Chemical & Earth Sciences, Deep-Sea Research/Part B: Oceanographic Literature Review, Excerpta Medica, Index Medicus, Mass Spectrometry Bulletin, PASCAL-CNRS, Referativnyi Zhurnal, Research Alert and Science Citation Index.

**US Mailing Notice.** *Journal of Chromatography* (ISSN 0021-9673) is published weekly (total 52 issues) by Elsevier Science Publishers (Sara Burgerhartstraat 25, P.O. Box 211, 1000 AE Amsterdam, Netherlands). Annual subscription price in the USA US$ 4446.75 (subject to change), including air speed delivery. Second class postage paid at Jamaica, NY 11431. **USA POSTMASTERS:** Send address changes to *Journal of Chromatography*, Publications Expediting, Inc., 200 Meacham Avenue, Elmont, NY 11003. Airfreight and mailing in the USA by Publications Expediting.

**See inside back cover** for Publication Schedule, Information for Authors and information on Advertisements.

---



0021-9673/93/$06.00



Printed in the Netherlands

---

**For Contents see p. 115.**

SYMPOSIUM ISSUE

# EIGHTH INTERNATIONAL SYMPOSIUM ON CAPILLARY ELECTROPHORESIS AND ISOTACHOPHORESIS

*Rome (Italy), October 6–9, 1992*

*Guest Editors*

PETR BOČEK
(Brno)

SALVATORE FANALI
(Rome)

VOL. 638, NO. 2 JOURNAL OF CHROMATOGRAPHY MAY 28, 1993

# CONTENTS

*Journal of Chromatography*, 638 (1993) 117
Elsevier Science Publishers B.V., Amsterdam

CHROM. 24 954

# Preface

The *8th International Symposium on Capillary Electrophoresis and Isotachophoresis* was held in Rome, Italy, from October 6th to 9th, 1992. The Symposium Chairman was Dr. Salvatore Fanali and the Symposium Secretary was Dr. Michele Cristalli. The organizers were the Consiglio Nazionale delle Ricerche, Istituto di Cromatografia e Area della Ricerca di Roma, Università degli Studi di Roma "La Sapienza", Dipartimento di Studi Farmaceutici, and Società Chimica Italiana, Divisione di Chimica Analitica, Gruppo di Cromatografia. The location of the symposium was at the Conference Centre Università "La Sapienza" in Rome.

The symposium included a *Short Course on Capillary Electrophoresis* held at the same location on October 6th, with lectures on fundamental and practical aspects of capillary zone electrophoresis, gel electrophoresis, isoelectric focusing and micellar electrokinetic chromatography and with demonstrations of practical applications carried out with commercial equipment provided by different companies.

The scientific programme included 35 oral presentations arranged in sections on General Aspects and Instrumentation, Capillary Isotachophoresis, Separation of Biopolymers and Micellar Electrokinetic Chromatography and Isoelectric Focusing. Further, two poster sessions including over 70 posters provided space and time for vivid direct discussions in small groups on all aspects of capillary electrophoresis.

There were over 160 participants from fourteen European countries, Japan, Canada and the USA, who contributed with lectures, posters, discussions to the symposium, and, finally, by submitting manuscripts to create this special issue.

The Rome symposium ITP-92 continued the series of European symposia, brought together experts in capillary electrophoresis and showed clearly how broad the field of analytical applications of capillary electrophoresis is, ranging from simple inorganic ions up to biopolymers such as DNA fragments, proteins and polysaccharides.

The exhibition of commercial instrumentation was well organized and clearly confirmed that fully automated unattended overnight analyses by capillary electrophoresis are a practical proposition.

The social programme was organized in an excellent manner and brought together the participants in the evenings. The banquet in the old Palazzo del Drago in Rome was a great experience for everybody.

It is my pleasure to congratulate Drs. Salvatore Fanali and Michele Cristalli who organized this great event from the very beginning until the very end. Further, I thank everyone concerned who contributed to this successful symposium. Finally, I express my appreciation to Dr. Karel Macek for his effort and care in producing this special issue.

*Brno (Czech Republic)* Petr Boček

*Journal of Chromatography*, 638 (1993) 119–135
Elsevier Science Publishers B.V., Amsterdam

CHROM. 24 944

# Options in electrolyte systems for on-line combined capillary isotachophoresis and capillary zone electrophoresis

Ludmila Křivánková* and Petr Gebauer

*Institute of Analytical Chemistry, Czech Academy of Sciences, Veveří 97, 611 42 Brno (Czech Republic)*

Wolfgang Thormann

*Institute of Clinical Pharmacology, University of Berne, Murtenstrasse 35, CH-3010 Berne (Switzerland)*

Richard A. Mosher

*Center for Separation Science, University of Arizona, Tucson, AZ 85721 (USA)*

Petr Boček

*Institute of Analytical Chemistry, Czech Academy of Sciences, Veveří 97, 611 42 Brno (Czech Republic)*

ABSTRACT

A theoretical description of the electrolyte systems that can be used in the on-line combination of isotachophoresis and zone electrophoresis is given. A classification of these systems is presented, based on the type of electrolyte used for the zone electrophoretic separation step. It is shown that transient sample stacking effects always persist from the isotachophoretic step to the beginning of the zone electrophoretic step and that they may negatively influence the zone electrophoretic separation and detection of the sample components. A mathematical description of these effects is given that allows the calculation of their magnitude and consequently the selection of operating conditions such that the stacking is decreased to an acceptable extent. In order to verify the reliability of the theoretical model, a modified PC simulation pack was prepared and used for investigating the behaviour of some model systems.

## INTRODUCTION

The rapidly developing method of capillary zone electrophoresis (CZE) suffers from some serious drawbacks. Some of them can be solved by improvements in the instrumentation used, but others are based on electrophoretic principles. High speed and high efficiency of the separations are achieved by performing the analyses in capillaries with very small inner diameters (0.02–0.01 mm) and injecting very small sample volumes of nanolitres and less. Although a concentration effect can occur at the beginning of the analysis when the sample passes the boundary with the background electrolyte (BGE) [1–5], the sample is diluted by various dispersive effects during the separation process. Therefore, it is advisable to inject a small but reproducible pulse with a high sample concentration. To avoid the dispersion caused by electromigration, the concentration of the sample is, however, recommended to be at least 100 times

* Corresponding author.

0021-9673/93/$06.00 

lower than the concentration of the BGE [1]. In practice this means that nanolitre volumes of the sample are injected hydrodynamically or electrokinetically [6,7]. Technical (exact volume) and principle-related (sample composition changes) drawbacks of these procedures often result in the reproducibility being insufficient for both qualitative and quantitative evaluation [8]. Typical sample concentrations are $10^{-4}$–$10^{-6}$ $M$, which means that the amount present in the zone is $10^{-13}$ mol and less. To increase the sensitivity, very sensitive detectors need to be used; to increase detectability, preconcentration techniques have to be applied.

The preconcentration techniques that can be used during the electrophoretic separation include stacking of the sample at the boundary between the sample zone and the BGE [9–12] and migration in the isotachophoretic (ITP) mode for a certain time due either to the composition of the sample creating ITP conditions for the migration [13,14] or to an ITP system being a constituent part of the BGE both in one capillary [15,16] or in two coupled capillaries [17–20]. The reported increase in sample concentration is about one order of magnitude. The most effective method is the on-line coupling of ITP with CZE where a $10^4$-fold concentration increase can be achieved, and this even for a component present in a $10^5$-fold excess [21,22]. It follows from the principle of the ITP method [23] that the sample zones migrating behind the leading zone are adjusted to its concentration. Usually, tens of microlitres of a sample either more or less concentrated than the leading electrolyte (LE) are injected. After the ITP separation, nanolitre or smaller volumes of about $10^{-2}$ $M$ sample zones can be expected for microcomponents the concentration of which in the sample was about $10^{-6}$ $M$ or less. These zones migrate as a stack between the leading electrolyte (LE) and the terminating electrolyte (TE) with permanently sharp boundaries between them. Such a stack of zones presents an ideal sampling situation for zone electrophoresis. Components of high concentration, the presence of which can cause problems in ZE separations, can be driven out of the separation system during the isotachophoretic stage where their qualitative and quantitative evaluation is reliably performed. In contrast, the detection of components in small amounts can be a problem whenever the zone length is shorter than the width of the detector cell [21,22]. Although such a problem can be solved by adding spacers of suitable mobilities [24], this solution is not simple.

The advantage of the combination of ITP and CZE has been verified practically on different occasions, including the determination of thiamine in blood [17], nitrophenols and amino acids labelled with 2,4-dinitrophenol [21], cyanogen bromide digest of cytochrome *c* [16], the coccidiocide halofuginone in feedstuff [22], *o*-phthaldialdehyde and fluorescein isothiocyanate derivatives of amino acids [19], fluorescein isothiocyanate derivative of angiotensin [20] and protein mixtures [15,18].

A theoretical description of the transition of isotachophoresis to zone electrophoresis can be found in papers by Beckers and Everaerts [25,26] and Gebauer *et al.* [4]. However, no description of processes proceeding during the transition and the way in which they affect the proper zone electrophoretic migration could be found, although some attempts to characterize the ITP–CZE combination with respect to the electrolyte systems applied were reported [15,17,22]. It has been shown that in both ITP and CZE the selection of electrolyte systems in which the separation proceeds is of basic significance [27,28]. It is the composition of the LE [29] (and sometimes also of the TE [30]) in ITP and the BGE in CZE that directly influences the selectivity and separation efficiency [8,31]. In the ITP–ZE combination the proper selection of both electrolyte systems is obviously more difficult if they have to be chosen so that the advantages of both methods are complemented.

This study was aimed at providing a general classification of electrolyte systems applicable for the ITP–ZE combination, a theoretical description of the transition of the zones from the ITP mode to the ZE mode and definition of the conditions for the proper application of the method. A computer simulation program is used to illustrate the behaviour of sample zones in various electrolyte systems.

## EXPERIMENTAL

For computer simulations, the Arizona model [32,33] in its PC-adapted version [34] was executed on an Excel 486 computer (Walz Computer, Berne, Switzerland) running at 50 MHz. The initial conditions for a simulation which must be specified include the distribution of all components, the p$K$ and mobility values of the buffer and sample constituents, the current density and the duration of the current flow, and also the column length and the segmentation. The program outputs concentration, pH and conductivity profiles as functions of time. A conversion program was written that allows the use of a specified slice of a computer-simulated ITP pattern and also the specification of the buffers on either side of the selected region, as the starting distribution for the CZE step.

For the example given in this work, a 10-cm column containing 400 segments was employed. For ITP, a leader composed of 0.01 $M$ HCl and 0.02 $M$ histidine and a terminator containing 0.01 $M$ of a strong acid T (mobility of $25 \cdot 10^{-9}$ $m^2$ $V^{-1}$ $s^{-1}$) and 0.02 $M$ histidine were employed. The input data are given in Table I. For this configuration, the composition of the adjusted terminator was calculated to be 0.00693 $M$ T and 0.01695 $M$ histidine. Two strong acids were chosen as sample components. For the simulation of the BGE–S–BGE system (S = sample), a background electrolyte consisting of 0.02 $M$ histidine and 0.008 $M$ of a strong acid (mobility $35 \cdot 10^{-9}$ $m^2$ $V^{-1}$ $s^{-1}$) was used. The current density and total running time were 20 A $m^{-2}$ and 25 min, respectively. For the simulations of the second (CZE) step, the slice between mesh points 206 and 236 of the 25-min ITP time point having a length of 6.75 mm was chosen. Of this length, *ca.* 3.8 mm ($l_L^*$, see below) were occupied by the leading zone and *ca.* 2.15 mm ($l_T$, see below) by the adjusted terminating zone. The position of the left boundary of this ITP column slice introduced as the sample for the consecutive CZE run was shifted to a 0.5 cm column length prior to application of current (100 A $m^{-2}$).

TABLE I

ELECTROCHEMICAL PARAMETERS USED FOR SIMULATION [33]

| Compound | p$K_1$ | p$K_2$ | Mobility ($10^9$ $m^2$ $V^{-1}$ $s^{-1}$) |
|---|---|---|---|
| Histidine | 6.04 | 9.17 | 20.2 |
| $Cl^-$ | | | 79.1 |
| T | | | 25.0 |
| Sample A | | | 40.0 |
| Sample B | | | 30.0 |
| $H^+$ | | | 362.7 |
| $OH^-$ | | | 198.7 |

## RESULTS AND DISCUSSION

### *Classification of electrolyte systems used in combined ITP–CZE*

In principle there are three ways of performing an ITP–CZE combination technique as far as the electrolyte system is concerned, as follows.

*T–S–T system (Fig. 1a):* the simplest way is to use the terminating electrolyte as the background electrolyte (BGE) for CZE. Here, the preseparation capillary is filled with the leading and terminating electrolytes and the analytical capillary is filled with the terminating electrolyte. In the first stage, the sample is injected in

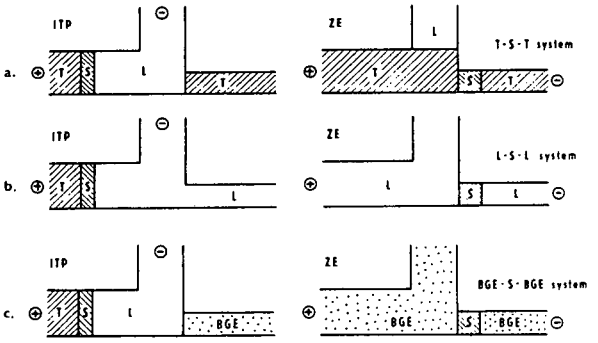


Fig. 1. Classification of electrolyte systems used in the on-line combination of ITP and ZE. The left panel shows the situation in the preseparation capillary at the end of the isotachophoretic separation. The right panel shows the situation in the analytical capillary at the beginning of the zone electrophoretic separation for (a) the terminating electrolyte (T), (b) the leading electrolyte (L) and (c) another background electrolyte (BGE) being used as the electrolyte for the separation by zone electrophoresis. S = Sample zone. The depicted schemes relate to cationic analyses: by changing polarity they apply to anionic systems.

between the leading and terminating electrolytes, current is switched on and passes between the terminating and auxiliary electrodes only through the preseparation capillary. The components of the sample form consecutive isotachophoretic zones with sharp boundaries, arrange themselves in order of decreasing mobilities and change their concentrations depending on the concentration of the leading zone. Before the stack of analytes reaches the bifurcation point between the preseparation and analytical capillaries, the current is switched to the analytical capillary (right panel of Fig. 1a). The ITP stack now becomes the sample for the CZE analysis.

*L–S–L system (Fig. 1b):* in the second approach, the leading electrolyte is employed as the BGE. In this instance, when the stack of isotachophoretically arranged zones of analytes reaches the bifurcation point, the current is switched and the migration of analytes proceeds continuously into the analytical capillary. After the last analyte of the stack has entered the analytical capillary, the current is switched off and the terminating electrolyte within the preseparation capillary is flushed out and replaced with the leading electrolyte. Then the current is again applied (right panel of Fig. 1b).

*BGE–S–BGE system (Fig. 1c):* The third possibility is to use a BGE different from LE or TE. The procedure is similar to the L–S–L system: after the current has been switched off, the terminating electrolyte is replaced by the BGE.

*T–S–T system*

We shall now describe in more detail the first of the systems under consideration (see Fig. 1a). Here the T–S–L stack migrates into the bifurcation block and, after the entire leading zone has migrated to the helping electrode, the electric current is switched off to the analytical electrode and the sample zones are separated zone electrophoretically in the terminating electrolyte. The second panel of Fig. 1a shows this ideal case where the switch-over was performed at the right moment when the leading zone had just migrated out of the preseparation capillary so that only the stack of the sample zones but no leading ion were introduced into the analytical capillary. In practice, however, it is necessary to perform this switching over earlier in order not to lose part of the sample owing to outflow to the auxiliary electrode. Hence some amount of the leading ion is always introduced into the analytical capillary together with the sample. The distance of the tell-tale detector from the end of the preseparation capillary determines the maximum volume of the leading zone which may pass to the analytical capillary because the switching over is usually not performed earlier than the first sample zone reaches the tell-tale detector.

Let us start the description with the just-mentioned time point when the stack of the sample zones is caught by the tell-tale detector. Fig. 2 shows the notation used. In the preseparation capillary (denoted capillary 3), the stack from the ITP step is present. The leading electrolyte zone contains the leading ion L at a concentration $c_{L,3}$ and the common counter ion R; the conductivity of this zone is $\kappa_3$. The analytical capillary (capillary 1) is filled with the terminating electrolyte; it contains the terminating ion T at a concentration $c_{T,1}$ and its conductivity is $\kappa_1$. All ions are assumed to be strong electrolytes,

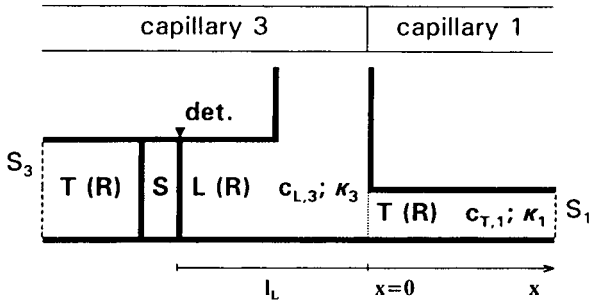


Fig. 2. Scheme of the interface between the preseparation (3) and analytical (1) capillaries serving for the separation in isotachophoretic and zone electrophoretic modes, respectively, in the T–S–T electrolyte system. The situation is depicted at the moment when the sample zone migrating in the ITP mode reaches the tell-tale detector in the preseparation capillary. This capillary of inner cross-section $S_3$ contains terminating (T) and sample (S) zones adjusted to the leading ion (L) of the concentration $c_{L,3}$ and the common counter ion R. The conductivity in the leading zone is $\kappa_3$. The analytical capillary of inner cross-section $S_1$ is filled with the terminating electrolyte, the concentration and conductivity of which are $c_{T,1}$ and $\kappa_1$, respectively. The zero point on the longitudinal axis is positioned at the interface between the capillaries; the length of the leading zone in the preseparation capillary, which will be introduced into the analytical capillary, is $l_L$.

except the counter ion, which is a weak electrolyte. The cross-sections of the analytical and preseparation capillary are $S_1$ and $S_3$, respectively. The one-dimensional coordinate system is positioned so that the origin ($x = 0$) lies at the interface of the preseparation and analytical capillaries. The time count starts ($t = 0$) at the time of switching over to the analytical electrode; it is assumed that the length of the leading zone still present in the preseparation capillary is $l_L$ at this time point. The separation system is assumed to have closed capillaries, *i.e.*, without electroosmotic flow.

The description of the processes that take place in the analytical capillary must be divided into several steps. In the first, which proceeds from the starting situation (Fig. 3a), the leading zone migrates into the analytical capillary, its concentration being readjusted to the Kohlrausch value [31] corresponding to the parameters of the terminating zone. The migration velocity of its rear boundary (equal to the isotachophoretic velocity in capillary 3) is $i_3 u_L/\kappa_3$ ($i_3$ is the electric current density in capillary 3 and $u_L$ is the mobility of ion L) and the time when the entire zone of L had migrated into the analytical capillary is thus given by

$$t_0 = l_L \cdot \frac{\kappa_3}{i_3 u_L} = l_L^* \cdot \frac{\kappa_3}{i_1 u_L} \quad (1)$$

where $l_L^* = l_L S_3/S_1$ is the length of the leading zone in capillary 3 reduced to the cross-section of capillary 1. This is also the time when the sample zones start to enter the analytical capillary (see Fig. 3b).

As was shown previously [35], the front boundary of the leading zone penetrating into the terminating zone is a diffuse one. This diffuse part becomes longer with time, which results in the disappearance of the (isotachophoretic) concentration plateau of the leading zone (Fig. 3c) at the time [4]

$$t_d = l_L^* \cdot \frac{\kappa_3}{i_1(u_L - u_T)} \quad (2)$$

and at the position $x_d$.

At this time, all the sample components that migrated isotachophoretically in capillary 3 are still migrating in stack at the (self-sharpening) rear boundary of the L zone. Since this moment

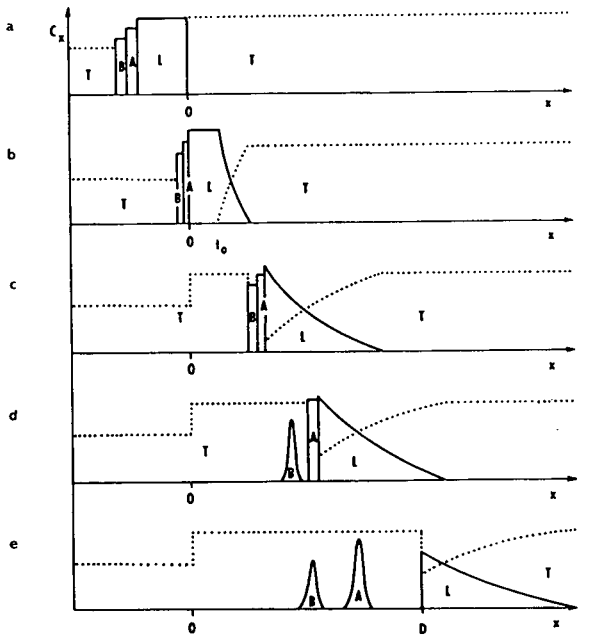


Fig. 3. Scheme of transition of the stack of zones from isotachophoretic migration to zone electrophoretic movement in the T–S–T electrolyte system. The situations are shown at the following time moments: (a) $t = 0$, when the current is switched to the analytical capillary; (b) $t_0$, when the entire zone of the leader electrolyte has just migrated into the analytical capillary; (c) $t_d$, when the ITP concentration plateau of the leading zone has just disappeared; (d) when the zone B has destacked while A is still migrating in the stack; (e) $t_{z,r}$, when all the sample zones migrate in zone electrophoretic mode and the rear boundary of the leading zone just passes the detector, thus opening the time window for detection. L = Leading electrolyte; T = terminating electrolyte; A, B = sample zones; $x$ = longitudinal coordinate; $c_x$ = concentration of a component in the separation system; 0 = interface between the analytical and preseparation capillaries; D = position of the detector.

they are gradually destacked in order of their increasing mobilities (Fig. 3d); the destacking time of a component X is given by [4]

$$t_{X,e} = t_d \left(\frac{u_L - u_T}{u_L - u_X}\right)^2 \quad (3)$$

The longitudinal coordinate where this destacking proceeds is given by [4]

$$x_{X,e} = t_d \cdot \frac{i_1}{\kappa_1} \left(\frac{u_L - u_T}{u_L - u_X}\right)^2 \frac{u_X^2}{u_L} \quad (4)$$

By substituting $t_d$ from eqn. 2, expressing the specific conductivities by $\kappa_3/\kappa_1 = c_{L,3}(u_L + u_R)/$

$c_{T,1}(u_T + u_R)$ and by using the Kohlrausch equation [31] in the form $c_{L,1} = c_{T,1}u_L(u_T + u_R)/u_T(u_L + u_R)$, we obtain

$$x_{X,e} = l_L^* \cdot \frac{c_{L,3}}{c_{L,1}} \cdot \frac{p_{L,T}}{p_{L,X}^2} \quad (5)$$

where $p_{ij} = u_i/u_j - 1$ [36] is the selectivity between components $i$ and $j$. From eqn. 5, it follows that the destacking coordinate of component X depends on the amount of the leading electrolyte introduced into the analytical capillary, on the ratio of concentration readjustment at the interface between both capillaries and on the selectivity between the leading component and component X.

Only after the sample components have been destacked can their zone electrophoretic migration and separation start (Fig. 3e). A general condition can therefore be formulated that the destacking of all components must proceed before they pass the detector, *i.e.*, $x_{X,e} < x_r$, where $x_r$ is the position of the detector in the analytical capillary. The time window for the detection of the sample components starts by the time $t_{z,r}$ when the rear boundary of the L zone passes through a fixed-point detector (Fig. 4). For this time it follows that [4]

$$t_{z,r} = \frac{\kappa_1}{i_1 u_L}\left(\sqrt{x_r} + \sqrt{x_d} \cdot \frac{u_L - u_T}{u_T}\right)^2 \quad (6)$$

In order to obtain complete destacking, for the detection time of the first (fastest) sample component A it must hold that $t_{A,r} \geq t_{z,r} + 4^t\sigma_A$,

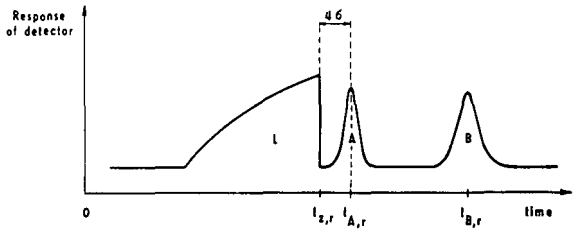


Fig. 4. Record of completely destacked sample components A and B during the separation in the T–S–T electrolyte system. In contrast to Fig. 3, where the concentration profile of the leader shows a concave shape, the respective profile as a function of time is convex here [37]. $t_{z,r}$, $t_{A,r}$ and $t_{B,r}$ are the detection times of the rear boundary of the leading zone and of the sample zones A and B, respectively.

where $^t\sigma_A$ is the time-based variance of the concentration profile of zone A. The detection time of any component X is given by [4]

$$t_{X,r} = x_r \cdot \frac{\kappa_1}{i_1 u_x} + t_d \cdot \frac{(u_L - u_T)^2}{(u_L - u_X)u_L} \quad (7)$$

Evidently, with increasing mobility of a component X, both its detection time $t_{X,r}$ and its destacking time $t_{X,e}$ become close to $t_{z,r}$. The mobility value of the component that would be destacked just when passing through the detector can thus be obtained by setting $t_{z,r} = t_{X,e}$ from eqns. 3 and 6:

$$u_{X,max} = \frac{u_L}{1 + \sqrt{\frac{l_L^*}{x_r} \cdot \frac{\kappa_3}{\kappa_1} \cdot \frac{u_L - u_T}{u_L}}} \quad (8)$$

Fig. 5 shows the calculated dependence of $t_{X,r}$ *vs.* $u_X$ for a model system and for three detection distances $x_r$. Each curve consists of two parts. The linear part (for high $u_X$ values) represents the $t_{z,r}$ value which is independent of $u_X$; it indicates that the substances have not left the

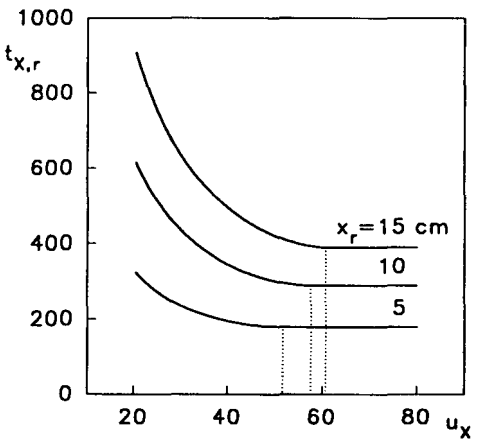


Fig. 5. Calculated dependence of the detection time of a substance X ($t_{X,r}$) on the mobility of this substance ($u_X$) (in $10^{-9}$ m$^2$ V$^{-1}$ s$^{-1}$) for three different positions of the detector, $x_r$, in the T–S–T electrolyte system. Dotted lines designate the mobility of the component that has destacked just when passing the detector, $u_{X,max}$. For $u_X > u_{X,max}$ the sample zones are still migrating in stack when passing the detector whereas for $u_X < u_{X,max}$ they migrate already in the electrophoretic mode. The values used for calculation were $u_L = 80 \cdot 10^{-9}$ m$^2$ V$^{-1}$ s$^{-1}$, $u_T = 20 \cdot 10^{-9}$ m$^2$ V$^{-1}$ s$^{-1}$, $u_R = 40 \cdot 10^{-9}$ m$^2$ V$^{-1}$ s$^{-1}$, $l_L^* = 0.01$ m, $c_{L,3} = c_{T,1} = 0.01$ *M*, $i = 500$ A m$^{-2}$.

stack yet when passing the detector. For $u_X < u_{X,max}$, the curve rises as $u_X$ decreases, which corresponds to sample zones passing the detector already destacked and later than the (stack at the) sharp rear boundary of the L zone.

From the above, it follows that it is desirable to keep the destacking times of all components as short as possible. The possibilities follow directly from the comment after eqn. 5. The major and most straightforward possibility for suppressing the sample stacking in the analytical capillary is to keep the length of the L zone introduced into the analytical capillary as short as possible. This can be achieved either by decreasing the length of the leading zone in the preseparation capillary at the moment of current switching or by increasing the readjustment ratio at the interface of both capillaries, *viz.*, by increasing the electrolyte concentration in the analytical capillary, $c_{T,1}$. The effect of both these parameters on the destacking distance $X_{X,r}$ can be clearly seen from Fig. 6 calculated for a model system.

The possibilities of decreasing the amount of the leader introduced are limited, however, and depend on the instrumentation used. Therefore, the other possibility must be taken into account, consisting in increasing the selectivity between the leading component and the sample components under investigation. As follows from eqn. 5, $x_{X,e}$ is indirectly proportional to the square of $p_{L,X}$ so that it can be decreased very effectively by selecting a leader of sufficiently high mobility. Fig. 7 shows how the value of $x_{X,e}$ decreases with increasing the value of $u_L - u_X$ and reveals the group of sample components that will be still migrating in stack when passing a fixed-point detector (see the parts of the curves above the dashed line when $x_r < x_{x,e}$).

Fig. 8 illustrates the theory by an example of a computer-simulated system. Fig. 8a shows the simulation of the first step resulting in rectangular concentration profiles as is usual in ITP. In Fig. 8b, the evolution of the concentration profiles in the analytical capillary is shown. At the beginning we can see very sharp peaks still migrating in the transient ITP stack, whereas dispersion of the zones appears whenever they leave the stack and migrate in the ZE mode. The

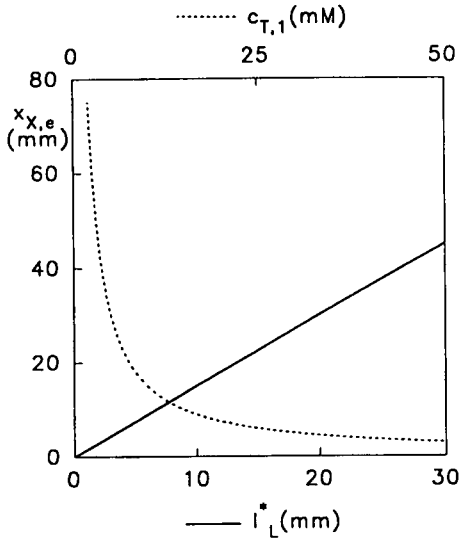


Fig. 6. Calculated dependence of the destacking distance of a sample zone ($x_{X,e}$) on the length of the leading zone cut into the analytical capillary ($l^*_L$, full line) and on the concentration of the terminator used as the BGE in the analytical capillary ($c_{T,1}$, dashed curve) in the T–S–T electrolyte system. The values used for calculation were $u_L = 80 \cdot 10^{-9}$ $m^2$ $V^{-1}$ $s^{-1}$, $u_T = 20 \cdot 10^{-9}$ $m^2$ $V^{-1}$ $s^{-1}$, $u_R = 40 \cdot 10^{-9}$ $m^2$ $V^{-1}$ $s^{-1}$, $u_X = 40 \cdot 10^{-9}$ $m^2$ $V^{-1}$ $s^{-1}$. The first dependence was calculated using $l^*_L = 0.01$ m; for the second, the concentration $c_T = 0.01$ *M* was chosen.

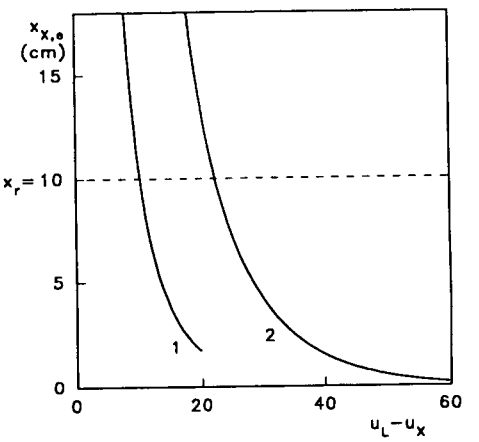


Fig. 7. Calculated effect of the difference between leading and sample mobilities ($u_L - u_X$) (in $10^{-9}$ $m^2$ $V^{-1}$ $s^{-1}$) on the distance where destacking proceeds ($x_{X,e}$) for two model examples. The intersection of the dependence with the position of the detector designates the group of substances that are not destacked prior to their passage through the detector (parts of the curves above the dashed line). For the values used for calculation, see Table I.

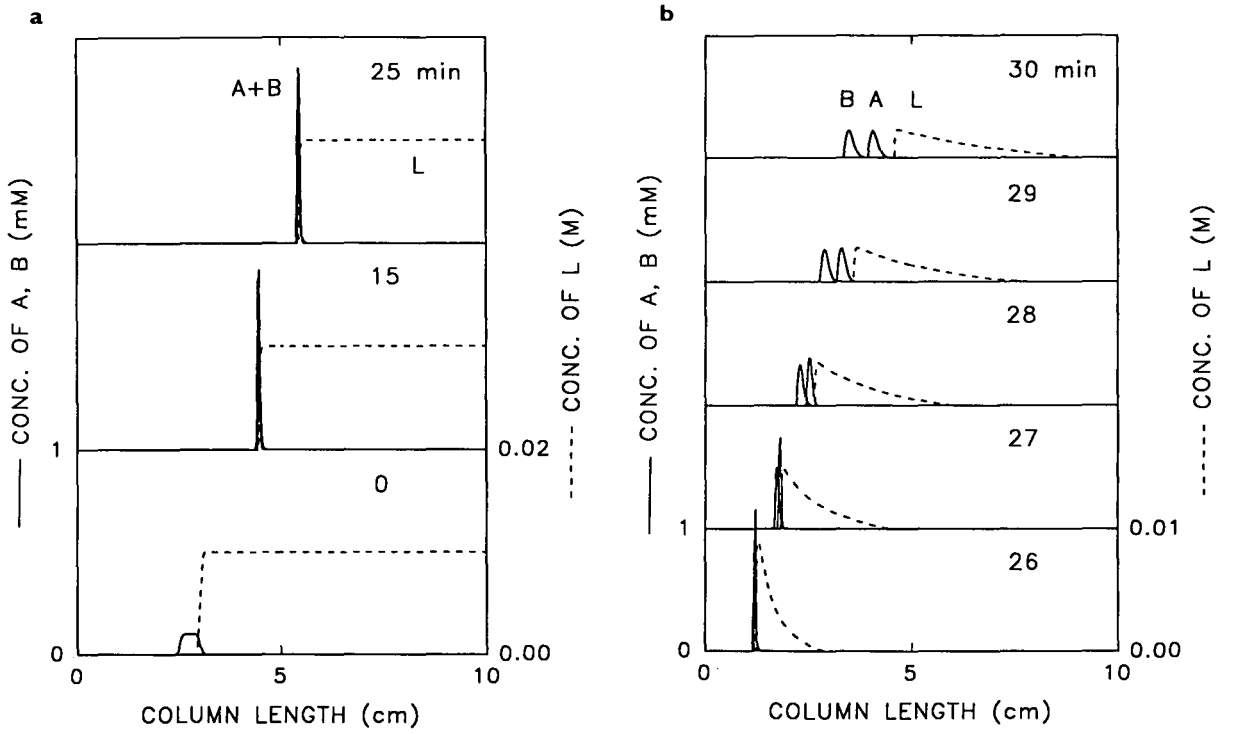


Fig. 8. Computer simulation of the separation of a pair of analytes A and B by the ITP–ZE combination in the T–S–T system. (a) Isotachophoretic step; (b) zone electrophoretic step. The concentration profiles shown correspond to the denoted time intervals. The values used for calculations were $u_L = 80 \cdot 10^{-9}$ m$^2$ V$^{-1}$ s$^{-1}$, $u_T = 25 \cdot 10^{-9}$ m$^2$ V$^{-1}$ s$^{-1}$, $u_R = 30 \cdot 10^{-9}$ m$^2$ V$^{-1}$ s$^{-1}$, $u_A = 40 \cdot 10^{-9}$ m$^2$ V$^{-1}$ s$^{-1}$, $u_B = 30 \cdot 10^{-9}$ m$^2$ V$^{-1}$ s$^{-1}$, $l_L^* = 6.75 \cdot 10^{-3}$ m, $c_T = 0.0069$ *M*, $c_R = 0.0169$ *M*, $i$ = (a) 20 and (b) 100 A m$^{-2}$.

destacking times calculated from eqn. 3 (27.2 min for component A and 26.4 min for component B) agree well with the simulation result.

*L–S–L system*

In the second type of electrolyte combination, the first stage of the separation proceeds just in the same way as in the T–S–T system (Fig. 1b); the difference is that the analytical capillary is filled with the leading electrolyte. After the current has been switched over and the sample zones have migrated into the analytical capillary (for the ideal case, see the second panel in Fig. 1b), the analysis is stopped and the contents of the preseparation capillary are filled with leading electrolyte as well. Then the analysis is continued.

Fig. 9 shows the starting situation of this second step as it corresponds to current practice where, together with the sample zones, some

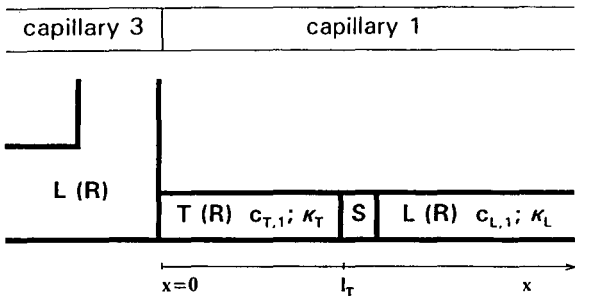


Fig. 9. Scheme of the interface between the preseparation and analytical capillaries serving for the separation in isotachophoretic and zone electrophoretic modes, respectively, in the L–S–L electrolyte system. The situation is depicted at the moment when the current is switched on across both capillaries after the terminator (T) in the preseparation column has been replaced by the leading (L) electrolyte. The concentration of T, $c_{T,1}$, is Kohlrausch-adjusted according to $c_{L,1}$; the conductivities in zones T and L are $\kappa_T$ and $\kappa_L$, respectively. The zero point on the longitudinal axis is positioned at the interface between the capillaries; the length of the terminating zone cut into the analytical capillary is $l_T$.

amount of the terminator has been introduced into the analytical capillary (see also Fig. 10a). This terminating zone of length $l_T$, with its concentration $c_{T,1} = c_{T,3}$ adjusted to the concentration of the leader ($c_{L,1} = c_{L,3}$), is necessary to ensure the quantitative transfer of all sample zones into the analytical capillary. This again leads to the unwanted stacking effects that have to be minimized.

A detailed mathematical description of this type of stacking has not been described previously; a simple way to derive the necessary equations is shown below. The resulting relationships are similar to those for stacking by the leading substance.

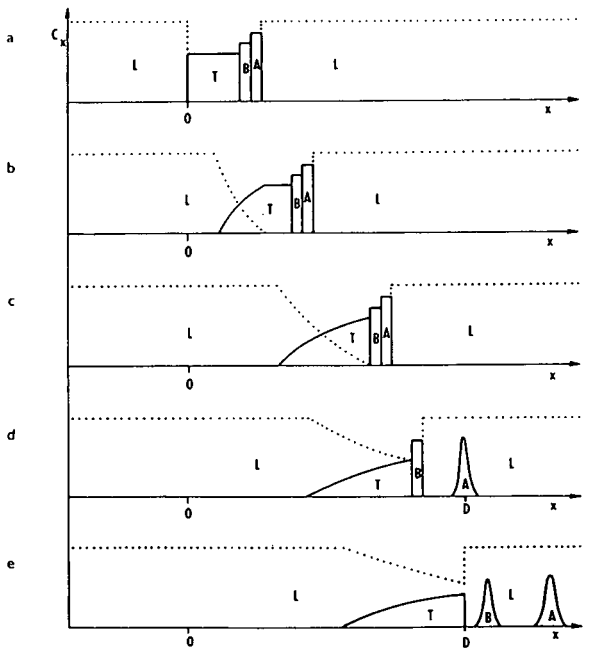


Fig. 10. Scheme of transition of the stack of zones from isotachophoretic migration to zone electrophoretic movement in the L–S–L electrolyte system. The situations are shown at the following time moments: (a) $t = 0$, when the current is again switched on over the system of both capillaries after the terminator (T) in the preseparation capillary was replaced with the leading electrolyte (L) and the separation in the ZE mode starts; (b) $t > 0$, when an ITP plateau of zone T still exists; (c) $t_d$, when the pure zone of T has just disappeared and only the transition mixed zone of T and L is present; (d) $t_{A,r}$, when the zone A is already destacked and passes the detector while B is still migrating in the stack; (e) $t_{z,r}$, when both sample zones migrate in the zone electrophoretic mode and the front boundary of the T zone is just passing the detector. L = Leading electrolyte; T = terminating electrolyte; A, B = sample zones; $x$ = longitudinal coordinate; $c_x$ = concentration of a component in the separation system; 0 = interface between the analytical and preseparation capillaries; D = position of the detector.

At the beginning of the second stage of the separation after replacement of the electrolyte in capillary 3 (start of migration in capillary 1, $t = 0$), the front boundary of the terminator zone and also the T–S–L zone stack migrate still isotachophoretically and the velocities of all the sharp boundaries are equal and given by

$$v_{T\text{-}L} = i_1 \cdot \frac{u_T}{\kappa_T} = i_1 \cdot \frac{u_L}{\kappa_L} \tag{9}$$

The rear boundary of the zone of the terminator (L–T boundary) develops into a diffuse one which forms a growing region of concentration transitions of both substances T and L (see Fig. 10b). The velocities of the rear and front edges of this transition are equal to the velocities of a single ion T and L in the isotachophoretic zone L and T, respectively:

$$v_1 = i_1 \cdot \frac{u_T}{\kappa_L} \qquad v_2 = i_1 \cdot \frac{u_L}{\kappa_T} \tag{10}$$

The balance written for the velocity difference $v_2 - v_{T\text{-}L}$ and for $l_T$ provides the time when the isotachophoretic concentration plateau of zone T disappears (see Fig. 10c):

$$t_d = l_T \cdot \frac{\kappa_L}{i_1} \cdot \frac{u_T}{u_L(u_L - u_T)} \tag{11}$$

For times longer than $t_d$, the L–T boundary remains sharp although the isotachophoretic zone of component T no longer exists (Fig. 10d). Its velocity decreases with time and so does the concentration of component T at this boundary. From ref. 35 we obtain for the ascending concentration profile of T

$$c_{T,L\text{-}T} = \frac{c_{L,1}u_T}{u_L - u_T} \cdot \frac{u_L + u_R}{u_T + u_R}\left(1 - \sqrt{v_1 \cdot \frac{t}{x}}\right) \tag{12}$$

and for the descending concentration profile of L

$$c_{L,L\text{-}T} = \frac{c_{L,1}u_T}{u_L - u_T}\left(\sqrt{v_2 \cdot \frac{t}{x}} - 1\right) \tag{13}$$

and the conductivity of any point $x$ of this profile at time $t$ is thus given by

$$\kappa_{L-T} = \kappa_{L,1}\sqrt{v_1 \cdot \frac{t}{x}} \tag{14}$$

For the velocity of the front boundary of zone T at times $t > t_d$ we can then write

$$\frac{dx_z}{dt} = \frac{i_1 u_T}{\kappa_z} = \sqrt{v_1 \cdot \frac{x_z}{t}} \tag{15}$$

where the subscript $z$ relates to the parameters of the transition zone at this boundary. Rearrangement and integration of this equation from $x_d$ to $x$ and from $t_d$ to $t$ provides

$$\sqrt{x_z} = \sqrt{v_1 t} + \sqrt{x_d} \cdot \frac{u_L - u_T}{u_L} \tag{16}$$

The destacking process starts at time $t_d$; the destacking of a component X proceeds at the time $t_{X,e} > t_d$ when the velocity of the stacking front boundary of zone T has decreased so that it became equal to the velocity of free component X in the leading electrolyte, *i.e.*, $v_z = v_{X,L} = i_1 u_X / \kappa_L$:

$$\sqrt{v_1 \cdot \frac{x_z}{t_{X,e}}} = i_1 \cdot \frac{u_X}{\kappa_L} \tag{17}$$

Substitution from eqn. 16 and rearrangement provide the destacking time of component X:

$$t_{X,e} = t_d \left(\frac{u_L - u_T}{u_X - u_T}\right)^2 \tag{18}$$

Obviously the sample zone is stacked the longer the lower is its mobility. The destacking coordinate is obtained by introducing $t_{X,e}$ into eqn. 16:

$$x_{X,e} = t_d \cdot \frac{i_1}{\kappa_L}\left(\frac{u_L - u_T}{u_X - u_T}\right)^2 \frac{u_X^2}{u_T}$$

$$= l_T \cdot \frac{(u_L - u_T)u_X^2}{(u_X - u_T)^2 u_L} \tag{19}$$

From this equation it is seen that the destacking coordinate again depends on the length of the zone of the stacking component (here T) and on the mobilities of L, X and T. As we assume the same leader concentrations in both capillaries 1 and 3, there is no effect of the readjustment ratio, which is unity. In the opposite case, however, $l_T$ would of course involve this ratio also.

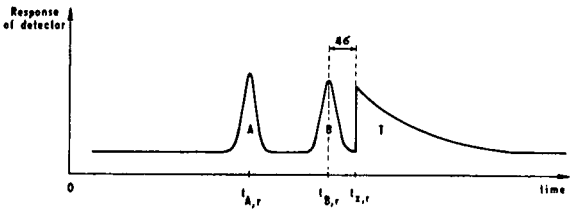


Fig. 11. Record of completely destacked sample components A and B during the separation in the L–S–L electrolyte system. In contrast to Fig. 10, where the concentration profile of the terminator shows a convex shape, the respective profile as a function of time is concave here [37]. $t_{z,r}$, $t_{A,r}$ and $t_{B,r}$ are the detection times of the front boundary of the terminating zone and of the sample zones A and B, respectively.

As already mentioned, the stacking is an effect which should be eliminated as only destacked zones can be separated in the zone electrophor-

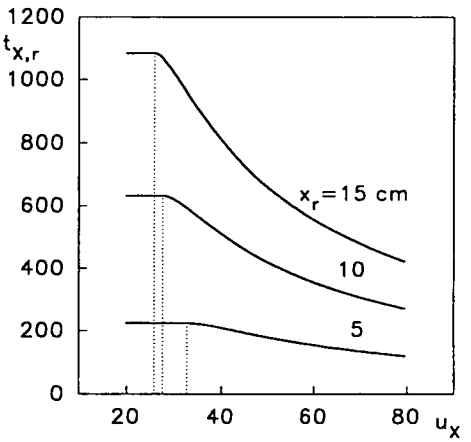


Fig. 12. Calculated dependence of the detection time of a substance X ($t_{X,r}$) on the mobility of this substance ($u_X$) (in $10^{-9}$ m$^2$ V$^{-1}$ s$^{-1}$) for three different positions of the detector, $x_r$, in the L–S–L electrolyte system. Dotted lines designate the mobility of the component that has destacked just when passing the detector, $u_{X,max}$. For $u_x < u_{X,max}$ the sample zones are still migrating in stack when passing the detector whereas for $u_X > u_{X,max}$ they migrate already in the electrophoretic mode. The values used for calculation were $u_L = 80 \cdot 10^{-9}$ m$^2$ V$^{-1}$ s$^{-1}$, $u_T = 20 \cdot 10^{-9}$ m$^2$ V$^{-1}$ s$^{-1}$, $u_R = 40 \cdot 10^{-9}$ m$^2$ V$^{-1}$ s$^{-1}$, $l_T = 0.01$ m, $c_L = 0.01$ $M$, $i = 500$ A m$^{-2}$.

etic mode and detected. For the detection time of component X it holds that

$$t_{X,r} = t_{X,e} + \frac{x_r - x_{X,e}}{v_{X,L}}$$

$$= x_r \cdot \frac{\kappa_L}{i_1 u_X} - t_d \cdot \frac{(u_L - u_T)^2}{(u_X - u_T)u_T} \qquad (20)$$

which is a similar expression to eqn. 7.

Fig. 11 shows that a condition can be formulated for the slowest substance B which still is destacked before detection, *viz.*, $t_{B,r} \leq t_{z,r} + 4'\sigma_B$. From the preceding section it follows that in the limiting case of the substance just being destacked when passing the detector not only $t_{X,r}$ and $t_{z,r}$ but also $t_{X,e}$ become equal. The respective mobility, $u_{X,min}$, thus can be obtained by combining eqns. 18 and 20:

$$u_{X,min} = \frac{u_T}{1 - \sqrt{\frac{l_T}{x_r} \cdot \frac{u_L - u_T}{u_L}}} \qquad (21)$$

Fig. 12 shows, in analogy to Fig. 5, the calculated dependence of $t_{X,r}$ *vs.* $u_X$ for three detection distances $x_r$. Here the linear parts of the lines now correspond to low $u_X$ values of substances that have not left the stack yet when passing the detector. The respective values of $u_{X,min}$ are indicated by the dotted lines; for $u_X > u_{X,min}$, the curves fall as $u_X$ increases which corresponds to sample zones passing the detector already destacked and earlier than the (stack at the) sharp front boundary of the T zone.

As follows from eqns. 18 and 20, by increasing the length of the stacking zone (here expressed in the term of $t_d$; see eqn. 11), the destacking time of the sample zones is increased and their detection time is decreased as the substances are accelerated during their migration in stack. This is the opposite situation to that in the previous case where the stack retards the zones so that a longer zone of the stacking component (*i.e.*, longer destacking times) cause longer detection times. A comparison of both cases is shown in Fig. 13, where the dependences of the detection

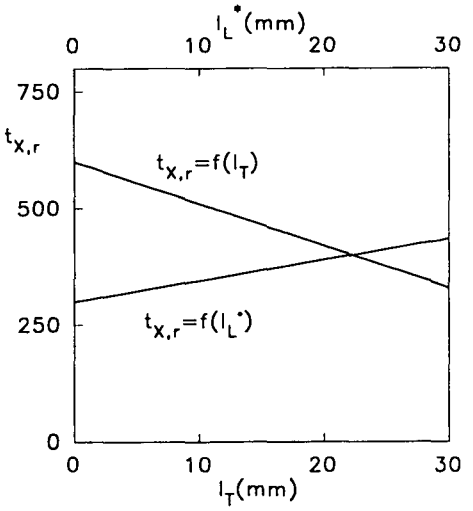


Fig. 13. Calculated dependence of the detection time on the length of the segment of zone L or T cut into the analytical capillary in the T–S–T or L–S–L electrolyte combination, respectively. The values used for calculation were $u_L = 80 \cdot 10^{-9}$ m$^2$ V$^{-1}$ s$^{-1}$, $u_T = 20 \cdot 10^{-9}$ m$^2$ V$^{-1}$ s$^{-1}$, $u_R = 40 \cdot 10^{-9}$ m$^2$ V$^{-1}$ s$^{-1}$, $u_X = 40 \cdot 10^{-9}$ m$^2$ V$^{-1}$ s$^{-1}$, $i = 500$ A m$^{-2}$, $x_r = 0.1$ m. For $t_{X,r} = f(l_L^*)$, $c_T = 0.01$ *M*; for $t_{X,r} = f(l_T)$, $c_L = 0.01$ *M*.

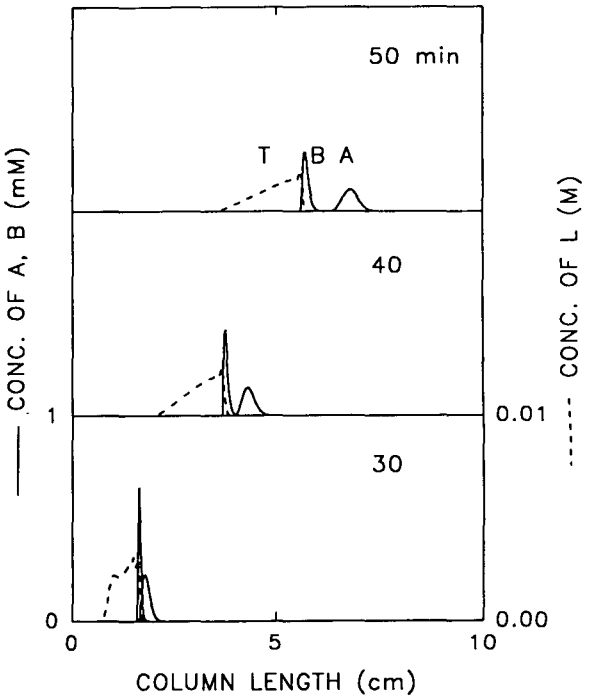


Fig. 14. Computer simulation of the separation of a pair of analytes A and B by the ITP–ZE combination in the L–S–L system. The isotachophoretic step was the same as shown in Fig. 8a. The concentration profiles shown correspond to the denoted time intervals. For the values used for calculations, see Table I.

time on the starting length of the stacking zone are calculated for the same model system.

Fig. 14 again illustrates the theory by a computer-simulated example with two sample components (A and B) and the stacking zone T. Here the mobility difference between B and T is three times lower than that between A and T, which causes much earlier destacking of component A (calculation using eqn. 18 provided the values 27.7 and 49.3 min for components A and B, respectively).

*BGE–S–BGE system*

The third system is the most general. Here, in the second step, the zone electrophoretic separation is performed in a background electrolyte that is different from both leader and terminator from the first step. First, after the sample zones have been detected by the tell-tale detector, the switch-over of the current to the analytical capillary is performed in the same way as was described for the T–S–T system. The remaining zone of the leader migrates into the analytical capillary, followed by the stack of the sample zones and the terminator. After some amount of the terminating zone has also migrated into the analytical capillary, the current is (in analogy to the L–S–L system) switched off, the preseparation capillary filled with the background electrolyte and the analysis continued (Fig. 1c). The behaviour of such a system and the way to

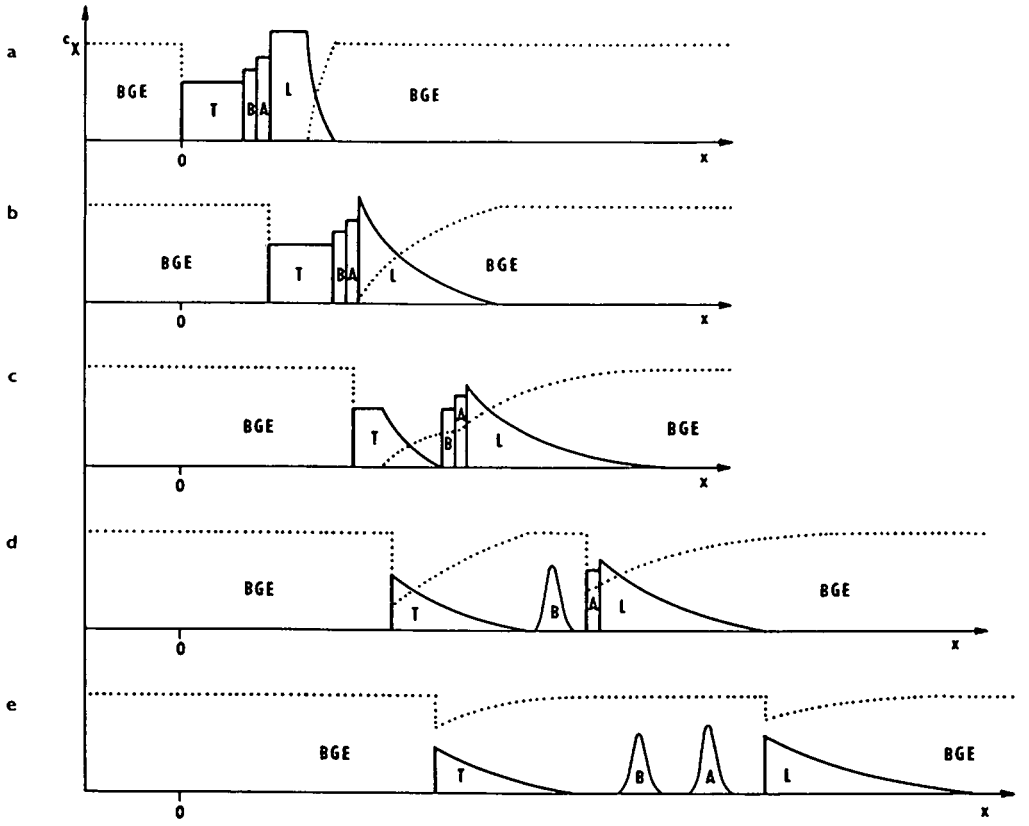


Fig. 15. Scheme of transition of the stack of zones from isotachophoretic migration to zone electrophoretic movement in the BGE–S–BGE electrolyte system for the case when the background electrolyte co-ion (BGC) possesses the lowest mobility of the system, $u_{BGC} < u_T < u_L$. The situations are shown at the time moments when: (a) the current is again switched on over the system of both capillaries after the terminator (T) in the preseparation capillary has been replaced with the BGE; the front boundary of zone L has already developed into a diffuse one; (b) the ITP concentration plateau of the L zone just disappeared; (c) the destacking of the T zone proceeds; (d) zones T and B have destacked while zone A is still migrating in stack behind L; (e) all the zones present in the BGE are destacked and migrating in the ZE mode. L = Leading electrolyte; T = terminating electrolyte; BGE = background electrolyte; A, B = sample zones; $x$ = longitudinal coordinate; $c_X$ = concentration of a component in the separation system; 0 = interface between the analytical and preseparation capillaries.

describe it depend on the mobility of the background electrolyte co-ion, $u_{BGC}$.

$u_{BGC} < u_T < u_L$. In this instance the system behaves similarly to the T–S–T system (Fig. 15). The background co-ion (BGC) is the slowest ion present and therefore the diffuse transition zone is started to be formed at the front boundary of the L zone which controls the migration of the zone stack (Fig. 15a). All other boundaries remain sharp, including the rear boundary of zone T. After the isotachophoretic plateau of zone L has disappeared and the BGE penetrates through the following zones, their destacking proceeds in the same way as described for the T–S–T system. First the zone of the terminator is destacked (Fig. 15c) and then the sample zones follow in order of increasing mobilities (Fig. 15d and e). For the calculation of the destacking time, destacking coordinate and detection time of a sample component X, eqns. 3, 5 and 7, respectively, can be used directly with the only change that the subscript T is replaced by BGC everywhere.

$u_T < u_L < u_{BGC}$. This arrangement resembles the L–S–L system (Fig. 16). The background electrolyte co-ion is the fastest ion and thus the diffuse transition is formed at the rear boundary of the terminating zone which plays the controlling role here (Fig. 16b). The destacking process starts with the zone of the highest mobility,

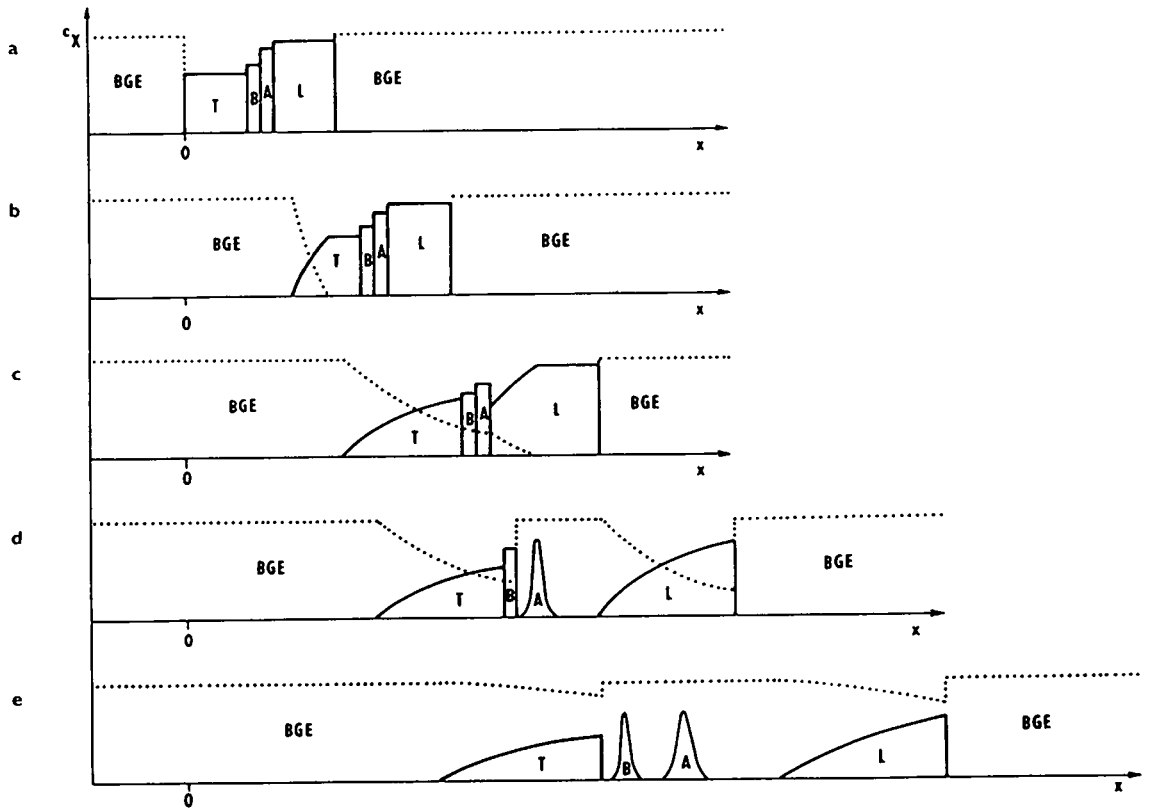


Fig. 16. Scheme of transition of the stack of zones from isotachophoretic migration to zone electrophoretic movement in the BGE–S–BGE electrolyte system for the case when the BGE co-ion (BGC) possesses the highest mobility of the system, $u_T < u_L < u_{BGC}$. The situations are shown at the time moments when: (a) the current is again switched on over the system of both capillaries after the terminator (T) in the preseparation capillary has been replaced with the BGE and zone electrophoretic separation starts; (b) an ITP plateau of zone T still exists; (c) the plateau of pure zone T has disappeared; (d) zones L and A have left the stack while zone B is still migrating in stack in front of T; (e) all the zones present in the BGE are destacked and migrating in the ZE mode. L = Leading electrolyte; T = terminating electrolyte; BGE = background electrolyte; A, B = sample zones; $x$ = longitudinal coordinate; $c_X$ = concentration of a component in the separation system; 0 = interface between the analytical and preseparation capillaries.

which is the L zone (Fig. 16c–e). For the calculation of the destacking time, destacking coordinate and detection time of a sample component X, eqns. 18, 19 and 20, respectively, can be used with the change that the subscript L is replaced by BGC everywhere. Note that these equations hold for the already readjusted zone of the terminator in capillary 1; its concentration and length must be calculated in a suitable way using the amount of terminator introduced into the analytical capillary and the Kohlrausch relationship.

$u_T < u_{BGC} < u_L$. This case represents a combination of the two previous ones (Fig. 17). The background electrolyte co-ion has an intermediate mobility. Both the front boundary of the L zone and the rear boundary of the T zone thus develop into diffuse transition zones (Fig. 17b and c). After the background co-ion has penetrated through the whole system, the zone stack splits into two separate parts, one being the L zone with a zone stack at its rear boundary and the other the T zone with a zone stack at its front boundary (Fig. 17d). The value of $u_{BGC}$ controls which of the two stacks a sample zone approaches: samples with $u_X > u_{BGC}$ stay at the

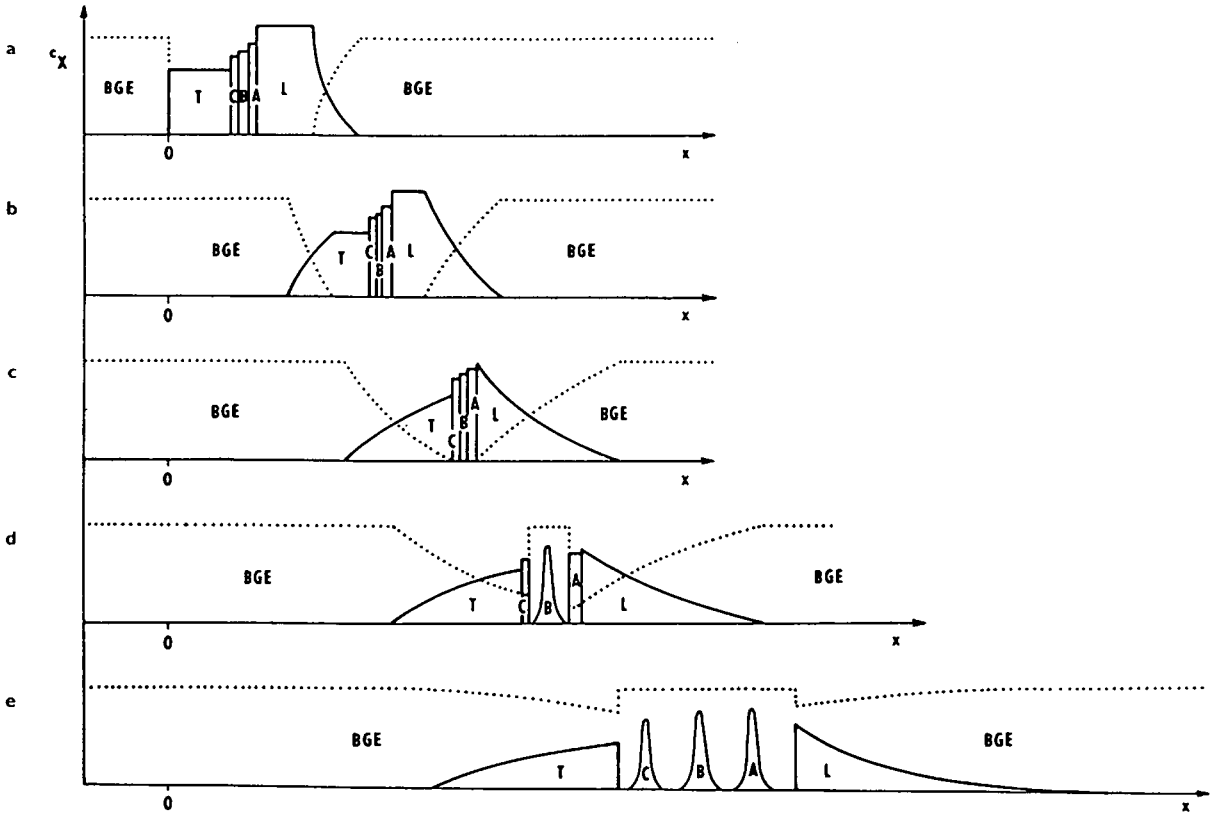


Fig. 17. Scheme of transition of the stack of zones from isotachophoretic migration to zone electrophoretic movement in the BGE–S–BGE electrolyte system for the case when the mobility of the BGE co-ion (BGC) is within the mobility of leader and terminator, $u_T < u_{BGC} < u_L$. The situations are shown at the time moments when: (a) the current is again switched on over the system of both capillaries after the terminator (T) in the preseparation capillary has been replaced with the BGE; the front boundary of zone L has already changed its sharp boundary into a diffuse one; (b) ITP plateaux of both zones L and T still exist; (c) the plateaux of pure zones T and L have disappeared; (d) zone B has left the stack and migrates zone electrophoretically while zones A and C are still migrating in stack behind L and in front of T, respectively; (e) all the zones present in the BGE are destacked and migrating in the ZE mode. L = Leading electrolyte; T = terminating electrolyte; BGE = background electrolyte; A, B, C = sample zones; $x$ = longitudinal coordinate; $c_X$ = concentration of a component in the separation system; 0 = interface between the analytical and preseparation capillaries.

L-zone stack and samples with $u_X < u_{BGC}$ stay at the T-zone stack. The destacking proceeds at each stack independently; at the L zone as it was described under $u_{BGC} < u_T < u_L$ and at the T zone as was described under $u_T < u_L < u_{BGC}$. Of course, in both instances the sample zones the mobilities of which are closest to the value of $u_{BGC}$ are destacked first.

Fig. 18 shows the dependence of the destacking coordinate on the mobility difference between the background co-ion and the sample ion for three different $u_{BGC}$ values. Note that the stacking effect becomes very pronounced when the difference is more than *ca.* $10 \cdot 10^{-9}$ m$^2$ V$^{-1}$ s$^{-1}$. Fig. 19 shows an illustration of such a combined system by computer simulation. Here the two sample substances were selected so that $u_A > u_{BGC}$ and $u_B < u_{BGC}$; this means that the destacking process of component A is controlled by component L and the destacking process of component B is controlled by component T. As $u_B$ is much closer to $u_T$ than $u_A$ is to $u_L$, B does not leave the stack as easily as does A. This is confirmed by the calculated destacking times,

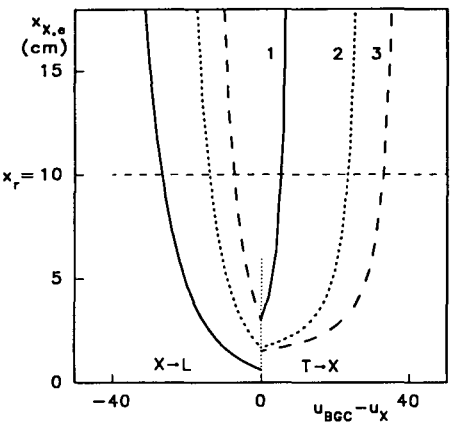


Fig. 18. Calculated dependence of the destacking distance of a sample zone ($x_{X,e}$) on the difference between its mobility and the mobility of background co-ion (in $10^{-9}$ m$^2$ V$^{-1}$ s$^{-1}$) in the BGE–S–BGE system from Fig. 17. For $u_X > u_{BGC}$, the system resembles the T–S–T system and L possesses the controlling role in destacking; for $u_X < u_{BGC}$, the system resembles the L–S–L system and T possesses the controlling role. The values used for calculation were $u_L = 80 \cdot 10^{-9}$ m$^2$ V$^{-1}$ s$^{-1}$, $u_T = 20 \cdot 10^{-9}$ m$^2$ V$^{-1}$ s$^{-1}$, $u_R = 40 \cdot 10^{-9}$ m$^2$ V$^{-1}$ s$^{-1}$, $l_T = l_L = 0.01$ m, $c_L = 0.01$ *M*, $u_{BGC}$ = (1) $30 \cdot 10^{-9}$, (2) $50 \cdot 10^{9}$ and (3) $60 \cdot 10^{-9}$ m$^2$ V$^{-1}$ s$^{-1}$.

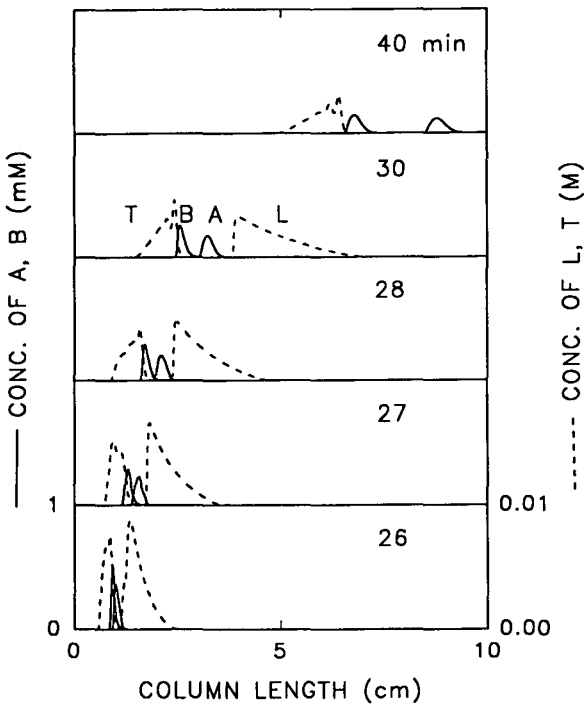


Fig. 19. Computer simulation of the separation of a pair of analytes A and B by the ITP–ZE combination of the BGE–S–BGE electrolyte system from Fig. 17. The isotachophoretic step was the same as shown in Fig. 8a. The concentration profiles shown correspond to the denoted time intervals. For the values used for calculations, see Table I. The rear part of the profile of the T zone is distorted owing to minor oscillations generated during the simulation.

which are 26.8 min for component A and 35.2 min for component B.

## CONCLUSIONS

The on-line combination of capillary ITP and CZE is a very important technique especially for the separation of complex biological fluids. The concentrating capabilities of ITP, which is used as the first separation step, are combined with the resolving power and detection sensitivity of CZE, thus allowing efficient determinations of trace components in complicated sample matrixes. Although the final step of such an analysis is performed in the zone electrophoretic mode, simple rules that hold for single zone electrophoretic analysis cannot be applied here directly. The reason is that the stack of zones introduced

into the zone electrophoretic step always involves some amounts of both leading and terminating zones. Thus, for a certain transient time, the ITP process survives and significantly affects the zone electrophoretic migration. The sample components leave the transient ITP stack gradually, depending on their mobilities, and hence each sample component starts its zone electrophoretic migration at a different time point and at a different column position. This brings about variations of migration times which are used for the qualitative evaluation of zone electrophoretic analyses and the magnitude of this effect depends on the electrolyte used for the zone electrophoretic step and on the amount of either the leader or terminator introduced into this second step. Moreover, if the mentioned amount is too large, some sample components may reach the detector being still stacked and thus not resolved.

The mathematical description presented in this paper provides a detailed insight into the processes that occur during the zone electrophoretic step for all possible types of electrolyte used, especially when the leader or the terminator is used directly as the background electrolyte. The theory allows one to predict the parameters necessary for a given analysis, especially the time when a sample component passes the detector (eqn. 7 or 20) or the position in the capillary where a component starts to migrate zone electrophoretically (eqn. 4 or 19). Based on this, the operating conditions and the amount of the leader and/or terminator introduced into the zone electrophoretic step can be selected so that the stacking effects are substantially reduced and controlled. The destacking process is illustrated by computer simulations that confirm also the values of individual parameters calculated by using the equations following from the theory presented here.

## SYMBOLS

$c_{i,j}$ concentration of substance $i$ in capillary $j$ or zone $j$
$i_j$ electric current density in capillary $j$
$l_L$ length of the leading zone in the preseparation capillary to be cut into the analytical one (T–S–T system)
$l_L^*$ value of $l_L$ reduced to the cross-section of the analytical capillary
$l_T$ length of the terminating zone in the analytical capillary (L–S–L system)
$p_{i,j}$ selectivity between substances $i$ and $j$
$S_1$ cross-section of the analytical capillary
$S_3$ cross-section of the preseparation capillary
$t$ time
$t_d$ time when the isotachophoretic plateau of the stacking zone in the analytical capillary disappears
$t_{X,e}$ time when substance X leaves the stack
$t_{X,r}$ time when zone X passes through the detector
$t_{z,r}$ time when the sharp boundary of the stacking zone passes through the detector
$t_0$ time when the entire zone of L has migrated into the analytical capillary (T–S–T system)
$u_X$ electrophoretic mobility of ion X
$u_{X,max}$ mobility of the ion X which is destacked just when passing through the detector (T–S–T system)
$u_{X,min}$ mobility of the ion X which is destacked just when passing through the detector (L–S–L system)
$v_{T-L}$ isotachophoretic velocity in the analytical capillary
$v_z$ velocity of the sharp boundary of the L–T transition zone
$v_1$ velocity of a single ion T in zone L
$v_2$ velocity of a single ion L in zone T
$x$ longitudinal coordinate
$x_d$ coordinate at which the isotachophoretic plateau of the stacking zone in the analytical capillary disappears
$x_r$ position of the detector
$x_{X,e}$ coordinate at which substance X leaves the stack
$x_z$ position of the sharp boundary of the L–T transition zone
$\kappa_L$ specific conductivity of the leading electrolyte in the analytical capillary (L–S–L system)
$\kappa_{L-T}$ specific conductivity of the L–T transition zone
$\kappa_T$ specific conductivity of the terminating electrolyte in the analytical capillary (L–S–L system)

$\kappa_z$ specific conductivity of the L–T transition zone at its sharp boundary

$\kappa_1$ specific conductivity of the terminating electrolyte in the analytical capillary (T–S–T system)

$\kappa_3$ specific conductivity of the leading electrolyte in the preseparation capillary (T–S–T system)

${}^t\sigma_X$ time-based variance of zone X

ACKNOWLEDGEMENT

This work was partly sponsored by the Swiss National Science Foundation.

REFERENCES

1 F.E.P. Mikkers, F.M. Everaerts and Th.P.E.M. Verheggen, *J. Chromatogr.*, 169 (1979) 1.
2 F.E.P. Mikkers, F.M. Everaerts and Th.P.E.M. Verheggen, *J. Chromatogr.*, 169 (1979) 11.
3 R.L. Chien and D.S. Burgi, *Anal. Chem.*, 64 (1992) 489A.
4 P. Gebauer, W. Thormann and P. Boček, *J. Chromatogr.*, 608 (1992) 47.
5 B. Gaš, J. Vacík and I. Zelenský, *J. Chromatogr.*, 545 (1991) 225.
6 S. Terabe, K. Otsuka, K. Ichikawa, A. Tsuchiya and T. Ando, *Anal. Chem.*, 56 (1984) 113–116.
7 J.W. Jorgenson and K.D. Lukacs, *Anal. Chem.*, 53 (1981) 1298.
8 F. Foret, L. Křivánková and P. Boček, *Capillary Zone Electrophoresis*, VCH, Weinheim, in press.
9 R. Aebersold and H.D. Morrison, *J. Chromatogr.*, 516 (1990) 79.
10 E. Kenndler and K. Schmidt-Beiwl, *J. Chromatogr.*, 545 (1991) 397.
11 G. Bondoux, P. Jandik and W.R. Jones, *J. Chromatogr.*, 602 (1992) 79.
12 S.E. Moring, J.C. Colburn, P.D. Grossman and H.H. Lauer, *LC·GC*, 8 (1989) 34.
13 A.C. Schoots, T.P.E.M. Verheggen, P.M.J.M. De Vries and F.M. Everaerts, *Clin. Chem.*, 36 (1990) 435.
14 Th.P.E.M. Verheggen, A.C. Schoots and F.M. Everaerts, *J. Chromatogr.*, 503 (1990) 245.
15 Ch. Schwer and F. Lottspeich, *J. Chromatogr.*, 623 (1992) 345.
16 V. Dolník, K.A. Cobb and M. Novotny, *J. Microcol. Sep.*, 2 (1990) 127.
17 F. Foret, V. Šustáček and P. Boček, *J. Microcol. Sep.*, 2 (1990) 229.
18 F. Foret, E. Szoko and B.L. Karger, *J. Chromatogr.*, 608 (1992) 3.
19 D.S. Stegehuis, H. Irth, U.R. Tjaden and J. Van Der Greef, *J. Chromatogr.*, 538 (1991) 393.
20 D.S. Stegehuis, U.R. Tjaden and J. Van Der Greef, *J. Chromatogr.*, 591 (1992) 341.
21 D. Kaniansky and J. Marák, *J. Chromatogr.*, 498 (1990) 191.
22 L. Křivánková, F. Foret and P. Boček, *J. Chromatogr.*, 545 (1991) 307.
23 F.M. Everaerts, J.L. Beckers and Th.P.E.M. Verheggen, *Isotachophoresis—Theory, Instrumentation and Applications*, Elsevier, Amsterdam, 1976.
24 G. Erikson, *Anal. Biochem.*, 109 (1980) 239.
25 J.L. Beckers and F.M. Everaerts, *J. Chromatogr.*, 508 (1990) 3.
26 J.L. Beckers and F.M. Everaerts, *J. Chromatogr.*, 508 (1990) 19.
27 L. Křivánková, F. Foret, P. Gebauer and P. Boček, *J. Chromatogr.*, 390 (1987) 3.
28 S. Hjertén, in G. Milazzo (Editor), *Topics in Biochemistry and Bioenergetics*, Vol. 2, Wiley, New York, 1978, pp. 89–128.
29 P. Gebauer and P. Boček, *J. Chromatogr.*, 267 (1983) 49.
30 P. Gebauer, L. Křivánková and P. Boček, *J. Chromatogr.*, 470 (1989) 3.
31 P. Boček, M. Deml, P. Gebauer and V. Dolník, *Analytical Isotachophoresis*, VCH, Weinheim, 1988.
32 M. Bier, O.A. Palusinski, R.A. Mosher and D. Saville, *Science*, 219 (1983) 1281.
33 R.A. Mosher, D.A. Saville and W. Thormann, *The Dynamics of Electrophoresis*, VCH, Weinheim, 1992.
34 R.A. Mosher, P. Gebauer, J. Caslavska and W. Thormann, *Anal. Chem.*, 64 (1992) 2991.
35 H. Weber, *Die Partiellen Differential-Gleichungen der Mathematik und Physik*, Vol. I, Friedrich Vieweg, Braunschweig, 1910, p. 503.
36 P. Gebauer and P. Boček, *J. Chromatogr.*, 320 (1985) 49.
37 V. Šustáček, F. Foret and P. Boček, *J. Chromatogr.*, 545 (1991) 239.

*Journal of Chromatography*, 638 (1993) 137–146
Elsevier Science Publishers B.V., Amsterdam

CHROM. 24 931

# Capillary zone electrophoresis of complex ionic mixtures with on-line isotachophoretic sample pretreatment

D. Kaniansky*, J. Marák, V. Madajová and E. Šimuničová

*Department of Analytical Chemistry, Faculty of Natural Sciences, Komenský University, Mlynská Dolina CH-2, 842 15 Bratislava (Slovak Republic)*

ABSTRACT

Separation modes provided by the column-coupling configuration of the separation unit in an on-line combination of capillary isotachophoresis (ITP) with capillary zone electrophoresis (CZE) were studied from the point of view of their potential in the (trace) determination of ions present in complex ionic matrices. Urine was arbitrarily chosen as such a matrix while sulphanilate and 3,5-dinitrosalicylate (currently not present in urine) served as model analytes. In one of these modes, ITP was employed to remove only the most abundant sample constituent (chloride) and concentrate the rest of those migrating between the leading and terminating zones for injection into the ZE stage. In the other mode, ITP was employed for maximum sample clean-up. Here, only the analyte(s) with a minimum of the matrix constituents was transferred for a final separation in the ZE stage. The fraction to be transferred was defined via a pair of discrete spacers added to the sample. Although a highly efficient sample clean-up was typical in this instance, the use of identical migration regimes in both stages (the separations according to ionic mobilities) did not prove the resolution of one of the analytes (sulphanilate) from the matrix constituent(s) in the ZE stage. A considerable improvement in this respect was achieved easily when the ITP clean-up was based on the separation according to p$K$ values while the constituents present in the transferred fraction were finally separated via differences in their ionic mobilities. This two-dimensional approach provided a way to achieve a 150 ppb ($10^{-6}$ mol $l^{-1}$) concentration detection limit for sulphanilate in a 1-$\mu$l volume of urine taken for the electrophoretic run.

## INTRODUCTION

High separation efficiencies as typically achieved in capillary zone electrophoresis (CZE) favour the use of this technique for the determination of ionogenic compounds present in multi-component mixtures. This is a feature favouring its applicability in trace analysis, especially, when the samples are characterized by complex, multi-component ionic matrices (*e.g.*, determination of trace constituents present in samples of biological and environmental origins). However, the low load capacities of currently used columns and/or high concentration detection limits attainable by current detectors limit the wider use of CZE for such purposes. In this context, it should be noted that improvements in the detection systems (see *e.g.*, refs. 1–5) can provide only a partial solution to these problems as from a general point of view [6] a high frequency of peak overlaps (mixed zones) may be a key task to be solved.

Recently, considerable attention has been paid to various approaches enabling the concentration detection limits in CZE to be improved via higher sample loads. Many of them employ the inherent concentrating capability of zone electrophoretic (ZE) separation [7–10]. The sample preconcentration based on this capability is useful, *e.g.*, in the determination of ions present in water for steam generation in power plants [11]

* Corresponding author.

0021-9673/93/$06.00 

or in the analysis of liquid chromatographic fractions when in-column neutralization of matrix ions is possible [12]. However, it cannot improve the concentration detection limits when the analytes are present in complex ionic matrices (see, *e.g.*, ref. 13).

Disc electrophoresis [14,15], *i.e.*, the sequential use of ITP concentration with ZE separation, was shown to be a convenient approach to the separations of dilute peptide solutions [16] and proteins [17]. A similar sequence of ITP and ZE is applied in the CZE analysis of samples containing a large excess of very mobile ions when the composition of the carrier electrolyte meets certain requirements [18–21]. The practical utility of these alternatives is limited when the number of matrix constituents is very high (peak overlaps) and/or the matrix is highly variable (*e.g.*, variabilities of the migration times of the separands from sample to sample). In this respect, a tandem arrangement of a pair of columns with the possibility of washing the ITP column after the analytes and the constituents migrating in front of them are transferred into the CZE column [22] will probably also be less effective in such situations.

It was shown by Mikkers [23] that the column-coupling configuration of the separation unit for ITP is convenient for electrophoretic separations in discontinuous buffer systems, *i.e.*, for a tandem arrangement of ITP with CZE. However, it is apparent that this concept of capillary electrophoresis instrumentation [23–25] provides wider possibilities, especially from the point of view of on-line ITP sample pretreatment before the CZE separation. We have already demonstrated some of them in previous work [26]. The determination of halofuginone in feedstuffs [27] showed the practical utility of combined ITP–CZE when performed with the column-coupling instrument. The analytical potential of this approach can be further improved from the point of view of concentration detection limits by using very sensitive detectors in the CZE stage [28,29].

As already mentioned, peak overlaps (mixed zones) occur with a high frequency in the separation of complex mixtures also when very high separation efficiencies are achieved [6]. Coupled-column separation systems provide a way to solve these problems in high-efficiency chromatographic techniques [6,30]. Undoubtedly, it is reasonable to expect that such an approach will also be effective in capillary electrophoresis and the column-coupling configuration of the separation unit offers analytical benefits analogous to those of its chromatographic counterparts. In addition, when used with an ITP–CZE combination, some specific features of the ITP step (preconcentration of the analytes; a high sample load; transfer of a well defined fraction to CZE; ideal sample injection for CZE) can further increase these benefits. Previously, however, no attention has been paid to the use of this tandem arrangement to the determination of ions present at low concentrations in complex ionic matrices. The aim of this work was to carry out a feasibility study along these lines and various alternatives of tandem ITP–CZE in the column-coupling configuration of the separation unit were investigated from the point of view of their applicability to such analytical problems. Urine, containing hundreds of acids at very differing concentrations [31], represented such a matrix in this study. Sulphanilate and 3,5-dinitrosalicylate (not reported to be currently present in urine) added at appropriate concentrations to urine samples served as trace analytes.

## EXPERIMENTAL

### *Instrumentation*

A prototype of a micro-trace capillary electrophoresis system (Unitec, Vienna, Austria), assembled in the column-coupling mode, was employed. The samples were injected with the aid of a valve (25-$\mu$l sample loop). The columns provided with 0.30 mm I.D. capillary tubes (O.D. *ca.* 0.65 mm) made of fluorinated ethylene–propylene (FEP) copolymer were employed in both the preseparation (ITP) and analytical (ZE) stages. The analytical column was provided with an on-column UV detector. A rectangular slit (0.25 mm in height) defined the detection cell. The same type of detector was used in some experiments in the ITP stage to record a UV profile of the sample after the ITP separation. Detection was performed at 254 nm.

ZE experiments were carried out in the

column employed in the analytical stage of the separation unit. In this instance the column was directly connected to a CZE valve. The valve, suitable for various capillary electrophoresis techniques, was provided with a 200-nl internal sample loop in this work.

*Chemicals*

Chemicals used for the preparation of the electrolyte solutions were bought from Serva (Heidelberg, Germany), Sigma (St. Louis, MO, USA) and Lachema (Brno, Czech Republic). Methylhydroxyethylcellulose 30 000 (MHEC), obtained from Serva, was used as an anticonvective additive in the electrolyte solutions. A 1% (w/v) aqueous solution of the cellulose derivative was demineralized on a mixed-bed ion exchanger (Amberlite MB-1; BDH, Poole, UK).

Water from a Rodem-1 demineralization unit (OOP, Tišnov, Czech Republic) was further purified by circulation through laboratory-made polytetrafluoroethylene cartridges packed with Amberlite MB-1 mixed-bed exchanger. The solutions used throughout were prepared from freshly recirculated water.

*Samples*

Urine samples were obtained from healthy individuals (mid-stream fractions). After receipt they were diluted fivefold with demineralized water to avoid gradual precipitation of the anionic constituents. When required, the samples or their aliquots were spiked at appropriate concentrations with sulphanilic and/or 3,5-dinitrosalicylic acids. No preservatives were added to the samples.

## RESULTS AND DISCUSSION

*Analysis of constituents present in complex ionic matrices by CZE and ITP*

When CZE is applied to the determination of constituents present in biological and environmental matrices without an appropriate sample pretreatment, usually very small amounts of sample are injected on to the column to avoid its overloading. Consequently, higher concentration detection limits are typical for the analytes present in such matrices in comparison with samples in which they are accompanied by ionic constituents at lower concentrations. In some instances, however, it is advisable to overload the column with the sample as also under such circumstances reliable data can be obtained for some analytes (see, *e.g.*, refs. 20 and 21). This approach, inherently combining ITP and ZE separation principles, has certain analytically relevant implications [18,19]. The electropherograms in Fig. 1 illustrate some of them. For example, it can be seen that sulphanilate (migrating at a considerably longer migration time in comparison with the runs in which only aqueous solutions of this constituent were injected) was unresolved from matrix constituents and, in addition, its (very sharp) peak was fronting. This fronting, resembling the situation in the starting phase of the separation in ZE (see Fig. 3 in ref. 19), can be probably ascribed to the existence of a mixed zone of sulphanilate with more mobile macroconstituents (undetected at 254 nm). In

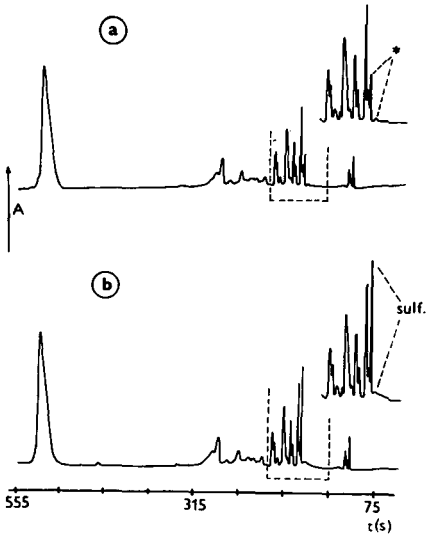


Fig. 1. Electropherograms from the separations of (a) urine and (b) urine spiked with sulphanilate at $2 \cdot 10^{-4}$ mol/l. Volumes of 200 nl of the samples diluted with water (1:5, v/v) were injected by a valve. The separations were carried out in the carrier electrolyte ZE-1 (Table I). The driving current was 150 $\mu$A. The parts of the electropherograms marked with dashed lines indicate the positions of the magnified details shown above the corresponding electropherograms. The asterisk marks the migration positions of sulphanilate in the unspiked urine. $A$ = increasing light absorption; sulf. = sulphanilate.

experiments carried out with the same sample in the column-coupling configuration of the separation unit (see, *e.g.*, Fig. 5), such a fronting was not observed while sulphanilate remained unresolved from matrix constituents. As in these experiments removal of chloride from the separation compartment after the ITP stage was, in fact, the only difference in comparison with the CZE runs shown in Fig. 1, the above explanation of the fronting (a transient mixed zone) seems reasonable. Analytical consequences of the described behaviour of the separands in CZE are obvious (uncertainty in the identification; systematic error in the quantification). We can expect that in the analysis of complex ionic mixtures such situations will arise and there may not be simple means for their detection, especially for trace analytes.

When ITP is considered for use in the above analytical application, it is apparent that the load capacities [23,32] of current single-column separation compartments are not sufficient when the analytical evaluation is to be derived from the response of a high-resolution universal detector (a.c. or d.c. conductivity). ITP used in the spike mode (see, *e.g.*, refs. 33 and 34) is in this respect more convenient. The isotachopherograms given in Fig. 2 (obtained for the same samples as in CZE in Fig. 1) illustrate the advantages and drawbacks of the spike mode for this type of application, especially, when less selective spectrophotometric detection (254 nm) is employed for evaluation. The high concentrating power of ITP is clearly visible from these isotachopherograms. At the same time, however, it can be seen that the sample constituents focused in the migration position of sulphanilate (defined by the zones of spacing constituents, $S_1$, and, $S_2$) may introduce a serious systematic error into its determination and/or make its identification problematic. The use of more appropriate spacing constituents could decrease this bias, but a search for ideal spacers may be a tedious task for the matrix of interest [35].

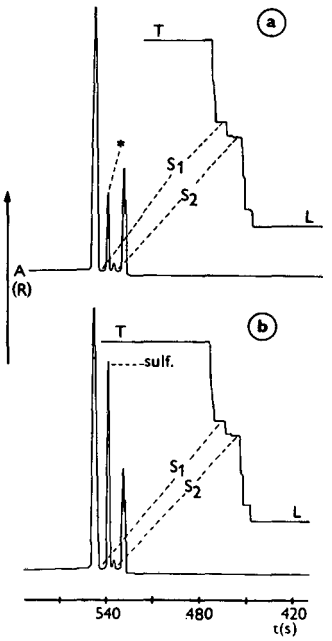


Fig. 2. Isotachopherograms from the separations of (a) urine and (b) urine spiked with sulphanilate at $2 \cdot 10^{-4}$ mol/l. Volumes of 25 $\mu$l of the samples diluted with water (1:250, v/v) were taken for the analyses. The electrolyte system ITP-1 (Table I) was used. The driving current was 150 $\mu$A. The injected samples contained iminodiacetate ($S_1$) and $\beta$-bromopropionate ($S_2$), each at a $3 \cdot 10^{-4}$ mol/l concentration, as discrete spacers. L, T = leading and terminating zones, respectively; $A$ = increasing light absorption; $R$ = increasing resistance.

*ITP in the sample injection mode for ZE*

Experiments carried out with model mixtures in our previous work [26] and the results presented by other workers [16,17,22,27–29] clearly show that ITP can be used as a very convenient sample injection technique for CZE. When the column-coupling configuration of the separation unit is used in this mode of operation (see Fig. 3), it is apparent that the sample need not be injected completely into the ZE stage. Its injection can be combined with removal of constituents having effective mobilities higher than or equal to that of the leading ions. Such a possibility may be of interest, *e.g.*, in the analysis of various biological fluids (containing $Cl^-$ and $Na^+$ at high concentrations) to avoid some of the problems discussed above. From the scheme in Fig. 3 we can deduce that this mode represents a tandem arrangement of the columns in the separation system with limitations inherent to this arrangement from the point of view of multidimensional separations [30].

In the ITP phase not only are the sample

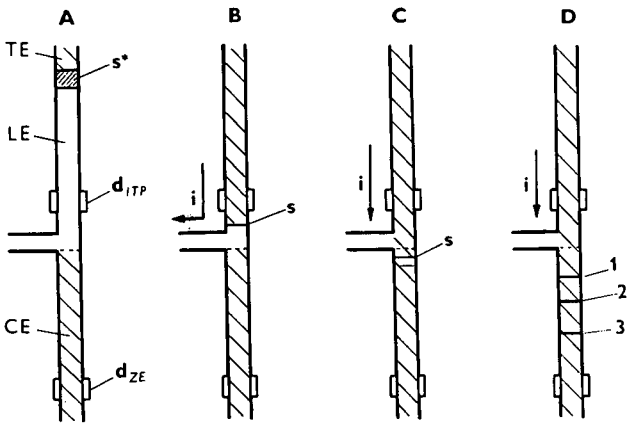


Fig. 3. Schematic illustration of the use of ITP for sample injection into ZE in the column-coupling configuration of the separation unit. (A) Starting phase; (B) end of the ITP separation; (C) transfer of the sample into the ZE stage; (D) ZE separation. s* = Injected sample; s = sample after the ITP stage; 1–3 = constituents separated by ZE; $i$ = direction of the driving current; LE, TE, CE = leading, terminating and carrier electrolytes, respectively; $d_{ITP}$, $d_{ZE}$ = detectors in the ITP and ZE columns, respectively.

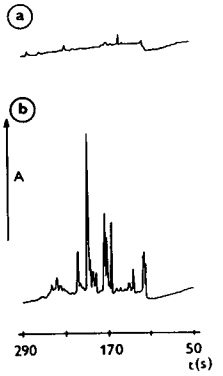


Fig. 4. Influence of impurities preconcentrated from the electrolyte solutions in the ITP stage on the ZE profile of urine. (a) ZE profile of ionogenic constituents accumulated between the leading and terminating zones in a blank ITP run preceding the ZE separation (the solution of the terminating electrolyte served as a sample); (b) ZE profile of urine (diluted 1:250 with water) with ITP injection, 25-$\mu$l volumes of the samples being taken for the analyses. ITP-1 and ZE-1 electrolyte systems (Table I) were used in the ITP and ZE stages, respectively. The driving current in both stages was 150 $\mu$A. $A$ = increasing light absorption.

constituents separated and concentrated (diluted) in a well known way [23,32,36], but also the corresponding impurities present in the electrolyte solutions are focused between the leading and terminating zones in accordance with principles of moving boundary electrophoresis [36–38]. Hence the ITP stage can introduce some disturbances into the CZE analysis. The electropherograms in Fig. 4 show the effect of impurities accumulated between the leading and terminating anions in the ITP stage on the CZE profile of a urine sample. Here, a blank ITP run which gave a maximum background in the ZE stage in terms of the number of peaks and their total area was chosen amount those obtained with the electrolyte solutions employed in this work.

The electropherograms in Fig. 5 were obtained from the separations of urine and urine spiked with 3,5-dinitrosalicylate and sulphanilate. For the reasons mentioned above, chloride present in the sample was removed from the separation compartment after the ITP stage and the sample amount (in terms of total ionics) loaded on to the CZE column was thus considerably reduced. The electropherograms show that whereas 3,5-dinitrosalicylate was resolved from the matrix constituents, sulphanilate migrated unresolved from them. Optimization of the separation conditions could probably solve this particular resolution problem but a detailed study along these lines was beyond the scope of this work.

*ITP sample clean-up with the injection of the analyte-containing fraction into the ZE stage*

The above results suggest that the injection mode combined with removal of very mobile sample macroconstituents can be convenient, *e.g.*, in a CZE profiling of various samples or in a multi-component analysis of ions when the qualitative complexity of the sample is not high. In the analysis of constituents present in complex mixtures of ionogenic compounds, however, a sample clean-up step may become essential. The separation unit as used in this work enables such a clean-up to be carried out on-line when used in the mode shown in Fig. 6. Here, a pair of appropriately chosen spacing constituents added to the sample defines in a straightforward way the fraction to be transferred from the ITP stage for a final ZE separation in the second column. Iminodiacetate ($S_1$ in Fig. 7) and $\beta$-bromo-

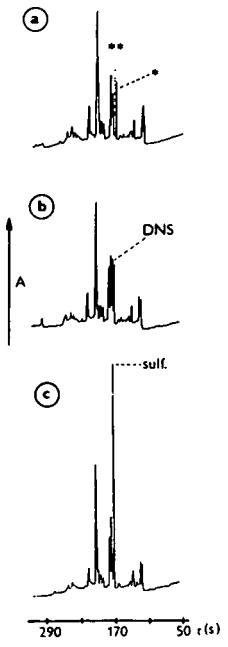


Fig. 5. ZE profiles of urine and urine spiked with the studied analytes in the column-coupling instrument with ITP used for the sample injection. (a) Urine diluted with water (1:250, v/v; *, * * = migration positions of sulphanilate and 3,5-dinitrosalicylate, respectively); (b) the same sample as in (a) except that it was spiked with 3,5-dinitrosalicylate (DNS) at a $10^{-4}$ mol/l concentration before dilution; (c) the same as in (b) except sulphanilate (sulf.) was the analyte. Other conditions as in Fig. 4.

propionate ($S_2$) were found to be convenient spacing constituents for sulphanilate and 3,5-dinitrosalicylate in the ITP phase when the separation was carried out in the electrolyte system ITP-1 (Table I).

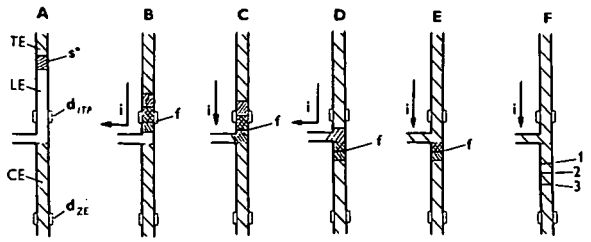


Fig. 6. Schematic illustration of the use of ITP as a sample clean-up technique for ZE. (A) Starting phase of the separation; (B) end of the ITP separation; (C) transfer of the fraction containing the analyte (f) into the ZE stage; (D) removal of the sample constituents migrating behind the transferred fraction; (E) starting phase in the ZE stage; (F) ZE separation. Other conditions as in Fig. 3.

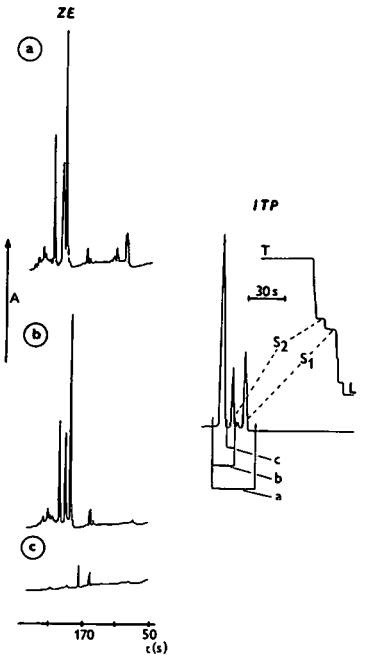


Fig. 7. Alternatives of the ITP clean-up of a urine sample with the use of a pair of discrete spacers. (a) Fraction a [marked on the isotachopherogram (ITP) from the UV detector] was transferred for a final ZE separation; (b) ZE profile of fraction b; (c) ZE profile of fraction c. Volumes of 25 $\mu$l of diluted urine (1:250, v/v) containing iminodiacetate ($S_1$) and $\beta$-bromopropionate ($S_2$) as discrete spacers (each at a $3 \cdot 10^{-4}$ mol/l concentration) were taken for the separations. L, T = leading and terminating zones, respectively. Other conditions as in Figs. 2 and 4.

The electropherograms in Fig. 7 illustrate alternatives of the clean-up attainable under these conditions for a urine sample. In the run shown in Fig. 7a, only the main part of the chloride and the sample constituents migrating zone electrophoretically in the terminating zone were removed from the separation compartment after the ITP stage. As in this instance the sample constituents migrating between the leading and terminating zones (including the spacers) were injected into the ZE stage it may serve as a reference to which the runs in Fig. 7b and c are related. In the run shown in Fig. 7b, the sample fraction transferred into the ZE stage was defined by the spacing constituent $S_1$ and by the terminating zone. The overall sample clean-up was not high in this instance as the main part of the UV-absorbing separands migrated in the ITP stage behind the rear spacer. On the other hand,

TABLE I

ELECTROLYTE SYSTEMS

| Parameter | Electrolyte[a] | | | | Carrier | |
|---|---|---|---|---|---|---|
| | ITP-1 | | ITP-2 | | ZE-1 | ZE-2 |
| | Leading | Terminating | Leading | Terminating | | |
| Solvent | $H_2O$ | $H_2O$ | $H_2O$ | $H_2O$ | $H_2O$ | $H_2O$ |
| Anion | $Cl^-$ | $MES^-$ | $Cl^-$ | $Prop^-$ | $MES^-$ | Prop |
| Concentration (m$M$) | 40 | 10 | 25 | 10 | 100 | 50 |
| Counter ion | HIS | HIS | BALA | BALA | HIS | HIS |
| pH | 6.0 | 6.0 | 3.3 | 4.0 | 5.2 | 4.8 |
| Additive | MHEC | – | MHEC | – | MHEC | MHEC |
| Concentration (%, w/v) | 0.2 | – | 0.2 | – | 0.2 | 0.2 |

[a] MHEC = Methylhydroxyethylcellulose; MES = morpholinoethanesulphonic acid; HIS = histidine; BALA = $\beta$-alanine; Prop = propionic acid.

95% removal of the matrix constituents (when compared via the peak areas with the run in Fig. 7a) was achieved when only the separands migrating between the spacers were transferred into the CZE stage (Fig. 7c). It should be noted that such results could be expected from a general model describing the clean-up efficiency in two-dimensional ITP analysis of ions present in complex matrices [35].

The electropherograms in Fig. 8 illustrate the impact of the ITP clean-up on the resolutions of the studied analytes from the urine matrix. It is apparent that 3,5-dinitrosalicylate was baseline resolved from the matrix constituents transferred with it into the ZE stage (compare Fig. 8a and b). A comparison with the run in which ITP was used for the same sample in the injection mode (Fig. 5b) clearly shows an overall improvement of the analytical conditions for this analyte owing to the clean-up step. On the other hand, sulphanilate was not resolved from the matrix constituent(s) under identical clean-up conditions (Fig. 8c). Although optimizations of the separation conditions could improve the resolution of this model analyte, no investigations along these lines were performed in this work.

### *Multi-dimensional approach in CZE coupled with ITP sample pretreatment*

In the experiments described above, no special attention was paid to the choice of electrolyte systems. Considering the acid–base properties of sulphanilic acid ($pK_a = 3.23$), it is apparent that in both columns its effective mobility was determined mostly by its ionic mobility. An evaluation of the electrolyte systems for ITP from the point of view of

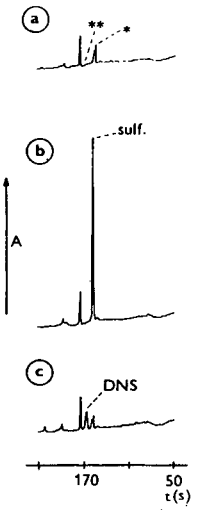


Fig. 8. Electropherograms from the separations of urine fractions obtained by the ITP clean-up. (a) Urine (diluted 1:250, v/v; *, * * = migration positions of sulphanilate and 3,5-dinitrosalicylate, respectively); (b) urine spiked with sulphanilate (sulf.) at a $1 \cdot 10^{-4}$ mol/l concentration [dilution as in (a)]; (c) urine spiked with 3,5-dinitrosalicylate (DNS) at a $10^{-4}$ mol/l concentration [dilution as in (a)]. Volumes of 25 $\mu$l of the samples were injected. The electrolyte systems and driving currents were the same as in Fig. 4. For further details, see the text.

information theory [39] suggests that in the coupled column systems our chance of achieving a desired resolution of the sample constituents will be significantly higher when using electrolyte solutions characterized by low similarities (*e.g.*, by combining the separations according to ionic mobilities and p$K$ values). It was shown recently [35] that the choice of electrolyte systems following this general rule provides, for example, maximum benefit in two-dimensional separations by ITP. Undoubtedly, the ITP–CZE tandem arrangement in the separation unit used in this work can also follow this rule. Therefore, to resolve sulphanilate from a urine matrix the electrolyte system ITP-2 (Table I) was used in the ITP stage. Its role was to minimize the number of isotachophoretically migrating constituents and provide their separations according to p$K$ values. The ZE separations were performed in the carrier electrolyte ZE-2 (Table I). Here, the resolution of separands was governed mostly by the differences in their ionic mobilities.

The separations were carried out in both the sample injection (Fig. 3) and clean-up (Fig. 6) modes to demonstrate their various capabilities under otherwise identical working conditions. To avoid disturbances which can occur in a "pure" sample injection mode (see Fig. 1 and the accompanying discussion), chloride present in the sample was removed from the separation compartment after the ITP stage.

From the electropherograms in Fig. 9 it can be seen that in comparison with the corresponding runs in Fig. 5 an improved resolution of sulphanilate from the matrix was obtained, probably because the electrolyte system used in the ITP stage was more restrictive for the ITP migrations of the anionic sample constituents (lower pH) than its counterpart used in the runs shown in Fig. 5.

A pair of spacing constituents (tartrate and citrate) were added to the sample when it was analysed by ITP in the sample clean-up mode (Fig. 10). These constituents were chosen in the way described elsewhere [35] and their capability to space sulphanilate from the other separands is clear from the isotachopherogram obtained with the UV detector (ITP, in Fig. 10). Electropherograms for the analyses of the transferred ITP fractions (ZE, in Fig. 10) of relevant samples show that the analyte was resolved from the comigrants accompanying it in the migration position in the ITP stage. When we consider differences in pH values of the electrolyte systems, the pH sequence of these systems in the coupled columns and the removal of the main part of the sample constituents from the separation compartment after the first separation stage, it seems reasonable to assume that a two-dimensional separation approach was also responsible for the resolution achieved.

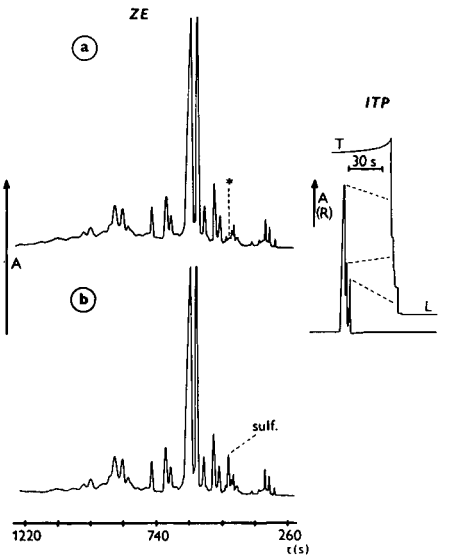


Fig. 9. Electropherograms from the separations of urine and urine spiked with sulphanilate ($1 \cdot 10^{-4}$ mol/l) at pH 4.8 with the ITP preseparation carried out at pH 3.3. Isotachopherograms (ITP) as obtained from the conductivity and UV detectors show ITP profiles of the sample constituents transferred into the ZE stage. (a) Urine (diluted 1:250, v/v); (b) the same as (a) except the injected sample contained sulphanilate (sulf.). ITP-2 and ZE-2 electrolyte systems were used for the separation in the ITP and ZE stages, respectively. The driving currents in both stages were 150 $\mu$A.

Considerable overloading of the CZE column was unavoidable when a 25-$\mu$l volume of urine diluted 1:25 (v/v) was taken for the analysis and in the ITP stage only chloride was removed from the separation compartment (Fig. 11). Obviously, in this instance hardly any useful information can be obtained from the response of the detector in the ZE stage. On the other hand, the ITP sample clean-up improved the situation in the

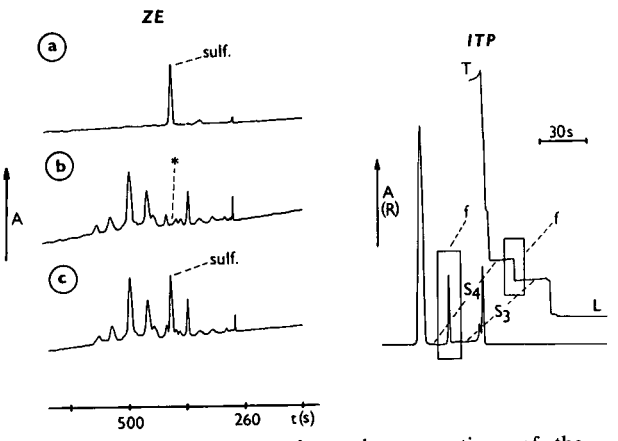


Fig. 10. Electropherograms from the separations of the constituents present in a urine fraction obtained by the ITP clean-up. (a) Control run with sulphanilate ($4 \cdot 10^{-7}$ mol/l concentration in an aqueous solution containing also $Na_2SO_4$ as an adsorption-eliminating additive at a $1 \cdot 10^{-3}$ mol/l concentration); (b) urine (diluted 1:250, v/v); (c) urine spiked with sulphanilate at $1 \cdot 10^{-4}$ mol/l (diluted 1:250, v/v). The samples contained tartrate ($S_3$) and citrate ($S_4$) as spacing constituents (each at a $3 \cdot 10^{-4}$ mol/l concentration). The fractions f [marked by boxes on the isotachopherograms (ITP)] from the conductivity and UV detectors were transferred into the ZE stage. Volumes of 25 $\mu$l of the samples were taken for these runs. Other conditions as in Fig. 9.

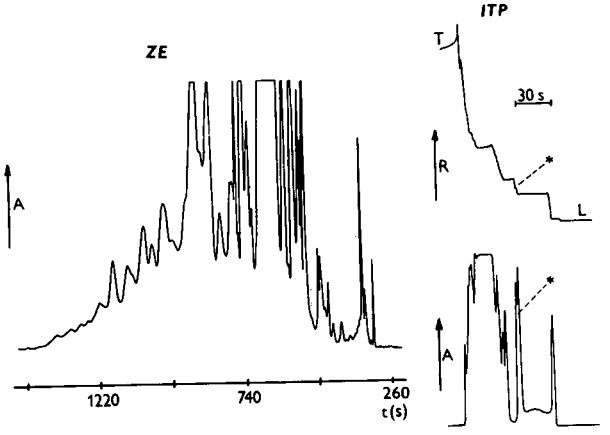


Fig. 11. Electropherograms from the separations of urine with a high sample load. A 25-$\mu$l volume of urine (diluted 1:25, v/v) was taken for the separation. All sample constituents after the ITP stage (see isotachopherograms on the right) were transferred for a final ZE separation. The asterisk marks the migration position of sulphanilate. Other conditions as in Fig. 9.

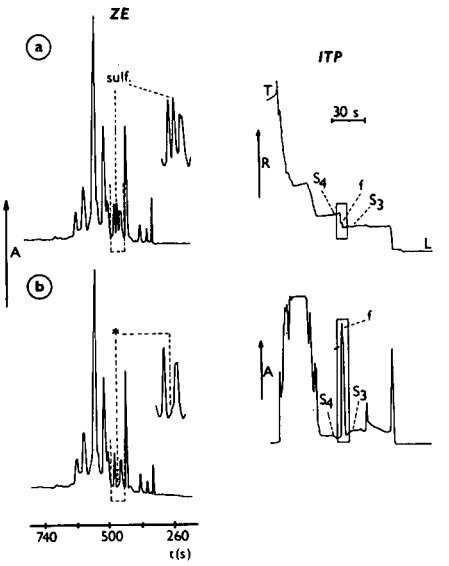


Fig. 12. Electropherograms from the separations of urine fractions obtained by the ITP clean-up for a high sample load. (a) Urine spiked with sulphanilate at $1 \cdot 10^{-5}$ mol/l (diluted 1:25, v/v); (b) urine (diluted 1:25, v/v). The parts of the electropherograms marked with dashed lines indicate the positions of the magnified details shown above the corresponding electropherograms. The injected samples (25 $\mu$l) contained the same spacers as in Fig. 10 to define the fractions to be transferred for the ZE separations. The fractions (f) are marked with boxes on the isotachopherograms (ITP) as obtained from the conductivity and UV detectors. The asterisk indicates the migration position of sulphanilate. Other conditions as in Figs. 9 and 10.

ZE stage dramatically (Fig. 12). In this way almost baseline resolution of sulphanilate from the matrix constituents was achieved. In addition, a high sample load provided the possibility of decreasing the concentration detection limit for this analyte. We found that its value under our working conditions was *ca.* 150 ppb ($10^{-6}$ mol $l^{-1}$), *i.e.*, a tenfold improvement in comparison with the run (Fig. 10) in which the same sample was diluted 1:250 (v/v).

## CONCLUSIONS

This work has shown that various modes of the on-line combination of ITP with CZE in the column-coupling configuration of the separation unit provide very promising possibilities for the CZE analysis of complex ionic mixtures. The use of ITP for sample clean-up seems very conveni-

ent for trace analysis problems in which matrix constituents with physico-chemical properties close to those of the analyte(s) are key interferents. The two-dimensional features of this mode can considerably increase the means available for the optimization of the working conditions.

The 150 ppb concentration detection limit achieved for one of the model analytes (sulphanilate) in urine is obviously not an ultimate minimum. For example, in the analysis of model mixtures containing various ionic constituents we were able to detect it with confidence at the 5 ppb level for a 25-$\mu$l injection volume. A further improvement in the concentration detection limit of the ITP–CZE tandem system by increasing the injection volume is closely related to the load capacity of the ITP stage. However, a very high ratio of the load capacity of the ITP column to that of the CZE column may require sample splitting [29] and thus an inefficient use of the ITP pretreatment. A detailed investigation along these lines can define limits of the combination of ITP and CZE in trace analysis applications. Obviously, the potential associated with the use of more sensitive and/or more selective detectors should also be taken into consideration in such an investigation.

## REFERENCES


1 W.G. Kuhr and C.A. Monnig, *Anal. Chem.*, 64 (1992) 389R.
2 K.C. Waldron and N.J. Dovichi, *Anal. Chem.*, 64 (1992) 1396.
3 T.T. Lee and E.S. Yeung, *J. Chromatogr.*, 595 (1992) 319.
4 T. Wang, J.H. Aiken, C.W. Huie and R.A. Hartwick, *Anal. Chem.*, 63 (1991) 1372.
5 J.P. Chervet, R.E.J. van Soest and M. Ursen, *J. Chromatogr.*, 543 (1991) 439.
6 J.C. Giddings, *Unified Separation Science*, Wiley, New York, 1991.
7 F.E.P. Mikkers, F.M. Everaerts and Th.P.E.M. Verheggen, *J. Chromatogr.*, 169 (1979) 1.
8 F.E.P. Mikkers, F.M. Everaerts and Th.P.E.M. Verheggen, *J. Chromatogr.*, 169 (1979) 11.
9 J.L. Beckers, Th.P.E.M. Verheggen and F.M. Everaerts, *J. Chromatogr.*, 452 (1988) 591.
10 R.-L. Chien and D.S. Burgi, *Anal. Chem.*, 64 (1992) 489 A.
11 G. Bondoux, P. Jandik and W.R. Jones, *J. Chromatogr.*, 602 (1992) 79.
12 R. Aebersold and H.D. Morrison, *J. Chromatogr.*, 516 (1990) 79.
13 B.J. Wildman, P.E. Jackson, W.R. Jones and P.G. Alden, *J. Chromatogr.*, 546 (1991) 459.
14 L. Ornstein, *Ann. N.Y. Acad. Sci.*, 121 (1964) 321.
15 B.J. Davis, *Ann. N.Y. Acad. Sci.*, 121 (1964) 404.
16 V. Dolník, K.A. Cobb and M. Novotný, *J. Microcol. Sep.*, 2 (1990) 127.
17 S. Hjertén, K. Elenbring, F. Kilár, J.-L. Liao, A.J.C. Chen, C.J. Siebert and M.-D. Zhu, *J. Chromatogr.*, 403 (1987) 47.
18 J.L. Beckers and F.M. Everaerts, *J. Chromatogr.*, 508 (1990) 3.
19 J.L. Beckers and F.M. Everaerts, *J. Chromatogr.*, 508 (1990) 19.
20 Th.P.E.M. Verheggen, A.C. Schoots and F.M. Everaerts, *J. Chromatogr.*, 503 (1990) 245.
21 A.C. Schoots, Th.P.E.M. Verheggen, P.M.J.M. De Vries and F.M. Everaerts, *Clin. Chem.*, 36 (1990) 435.
22 F. Foret, V. Šustáček and P. Boček, *J. Microcol. Sep.*, 2 (1990) 229.
23 F.E.P. Mikkers, *Thesis*, University of Technology, Eindhoven, 1980.
24 F.M. Everaerts, Th.P.M. Verheggen and F.E.P. Mikkers, *J. Chromatogr.*, 169 (1979) 21.
25 D. Kaniansky, *Thesis*, Komenský University, Bratislava, 1981.
26 D. Kaniansky and J. Marák, *J. Chromatogr.*, 498 (1990) 191.
27 L. Křivánková, F. Foret and P. Boček, *J. Chromatogr.*, 545 (1991) 307.
28 D.S. Stegehuis, H. Irth, U.R. Tjaden and J. van der Greef, *J. Chromatogr.*, 538 (1991) 393.
29 D.S. Stegehuis, U.R. Tjaden and J. van der Greef, *J. Chromatogr.*, 591 (1992) 341.
30 C.J. Giddings, *J. High Resolut. Chromatogr. Chromatogr. Commun.*, 10 (1987) 319.
31 H.M. Liebich and C. Foerst, *J. Chromatogr.*, 525 (1990) 1; and references cited therein.
32 F.E.P. Mikkers, F.M. Everaerts and J.A.F. Peek, *J. Chromatogr.*, 168 (1979) 293.
33 M. Svoboda and J. Vacík, *J. Chromatogr.*, 119 (1976) 539.
34 D. Kaniansky, V. Madajová, J. Marák, E. Šimuničová, I. Zelenský and V. Zelenská, *J. Chromatogr.*, 390 (1987) 51.
35 J. Marák, J. Laštinec, D. Kaniansky and V. Madajová, *J. Chromatogr.*, 509 (1990) 287.
36 F.M. Everaerts, J.L. Beckers and Th.P.E.M. Verheggen, *Isotachophoresis: Theory, Instrumentation and Applications*, Elsevier, Amsterdam, 1976.
37 J. Vacík, *D. Sc. Thesis*, Charles University, Prague, 1980.
38 V. Dolník, *Thesis*, Institute of Analytical Chemistry, Czechoslovak Academy of Sciences, Brno, 1987.
39 E. Kenndler, *Anal. Chim. Acta*, 173 (1985) 139.

*Journal of Chromatography*, 638 (1993) 147–153
Elsevier Science Publishers B.V., Amsterdam

CHROM. 24 917

# Equipment for multifunctional use in high-performance capillary electrophoresis

Theo P.E.M. Verheggen* and Frans M. Everaerts

*Laboratory of Instrumental Analysis, Eindhoven University of Technology, P.O. Box 513, 5600 MB Eindhoven (Netherlands)*

ABSTRACT

Instrumental aspects of capillary electrophoresis are reported. The instrument discussed can operate in the "open" and "closed" modes. All kinds of capillaries and capillary diameters can be applied. With this apparatus it is possible to perform analysis in free solutions, such as zone electrophoresis, isotachophoresis and isoelectric focusing. Gel-filled columns can also be used and systems making use of micellar electrokinetic chromatography. Several examples of separations of mixtures of organic acids in the open and closed modes are given. A separation of DNA restriction digest in a gel-filled column in the open and closed modes is described. A rapid analysis in an open system of guanine from mites in house dust is reported.

## INTRODUCTION

Because of its high efficiency, high-performance capillary electrophoresis (HPCE), which includes various modes of capillary electrophoresis, is widely used in various fields. Sometimes electroosmotic plug flow (EOF) is suppressed [1,2] and in some experiments EOF is used as a pumping mechanism [3]. A reduction of EOF can lead to an improvement in the resolution of the sample components.

For analytical separation techniques, the results obtained must be reproducible and repeatable. The influence of operating parameters on the reproducibility in capillary electrophoresis has been discussed by Foret and Boček [4].

When liquid levels in the buffer reservoirs at the capillary ends are unequal, hydrostatic flow (HF) results. The HF is parabolic in nature and therefore HF can contribute to zone broadening, making the experimental efficiency less than the theoretical value. This was extensively described by Grushka [5]. In isotachophoretic (ITP) analyses, the EOF is not constant in all zones, but commonly increases in the direction of the terminating zone [2]. This effect increases the turbulence of the liquid in each zone, while still an overall EOF is obtained.

In a study by Ackermans *et al.* [6], problems in quantitative analysis in open systems using ITP were discussed. In 1990, Verheggen *et al.* [7] investigated the reproducibility of migration times of serum components in a completely closed instrument by HPCE. A relative standard deviation of 0.7% was obtained. The instrument was limited to 0.2 mm PTFE capillaries and operated in the "closed" mode.

In this paper, it is shown that the HF can be blocked by membrane and simultaneously the EOF can be suppressed by additives. It is also possible to bypass the membrane, so that the EOF plays a role in the separation. Also, all kinds of capillaries and capillary diameters can easily be inserted. The construction of the electrode block [8], especially constructed for these analyses, and the first test results are given.

* Corresponding author.

0021-9673/93/$06.00 

## EXPERIMENTAL

### *Zone electrophoresis*

The equipment used is described in detail under Results and Discussion. Separation capillaries (100 and 50 $\mu$m I.D.) made of fused silica (Siemens, Mühlheim, Germany) and PTFE capillaries (200 $\mu$m I.D., 350 $\mu$m O.D.) (Habia, Breda, Netherlands) were used. Flat cellulose polyacetate membranes were used in the electrode compartment. A Spectra 100 variable-wavelength UV absorbance detector was used (Spectra-Physics, San Jose, CA, USA). The power supply (type HCN 35-500) was obtained from FUG Electronik (Rosenheim, Germany).

### *Data acquisition*

The software used was the Caesar program (B*Wise, Geleen, Netherlands) running on an Olivetti M250 computer. As the interface a multilab (TUE-TS, Eindhoven Technical University) was applied.

### *Chemicals*

The components of the test mixture, the buffer constituents and cetyltrimethylammonium bromide (CTAB), all of analytical-reagent grade, were purchased from Merck (Darmstadt, Germany). Mowiol poly(vinyl alcohol) (PVA) was supplied by Hoechst (Frankfurt, Germany). Ultra-pure water was used to prepare the buffers and all buffer and sample solutions were filtered through a 0.45-$\mu$m filter.

## RESULTS AND DISCUSSION

The basic unit is shown schematically in Fig. 1. The separation capillary C is mounted between the electrode compartment A and the vessel B. The capillary is surrounded by PTFE tubing used for cooling by forced air. The electrode compartment A is composed of two blocks: the electrode vessel (1) with the earth electrode (2) and block (3), which has a channel through which the system can be rinsed and filled with electrolyte, using valves 4a and 4b. The capillary is introduced at one end through a septum (5) in the channel of block 3. A steel needle is mounted in the septum holder (7). By manual pressure on

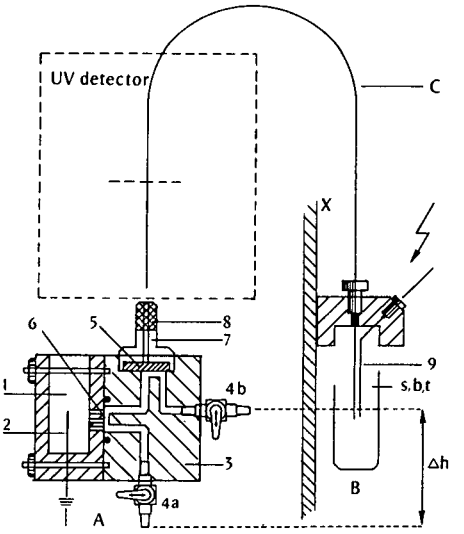


Fig. 1. Schematic diagram of electrophoretic equipment used for capillary electrophoresis (open/closed modes). A = Electrode compartment; B = vessel [buffer (b), samples (s), terminator (t)]; C = separation capillary; X = support; 1 = electrode vessel; 2 = earth electrode; 3 = block with channel; 4a and b = valves; 5 = septum; 6 = membrane; 7 = septum holder; 8 = knob with steel needle; 9 = high-voltage electrode.

knob 8, the needle will penetrate the channel through the septum. In this way it is easy to insert all kinds of capillaries and capillary diameters. After the introduction of the capillary into the channel, the needle is retracted and remains on top of the septum (5).

The channel in block 3 connects the electrode vessel (1) with the capillary C. Between the electrode vessel (1) and the block (3), a flat semi-permeable membrane (6) is clamped with two screws and an O-ring [2]. This means that the capillary is closed at one end by this membrane. Any gas produced at the electrode (2) will not affect the analysis. Liquid applied through valves 4a and 4b will pass and rinse the membrane. The volume of the channel in block 3 is large compared with that of the separation compartment. The potential drop in this channel, over and near the membrane, is small for the same reason. Therefore, it takes a long time before pH jumps, entering the capillary through the membrane, will reach the detector and thus influence the analyses [9].

Tiny movements of the membrane will affect

the reproducibility of the injection and migration times, hence the membrane surface area is limited by three narrow channels of 0.5 mm diameter connecting the electrode vessel (1) with the capillary C. The electrode vessel is filled with ultra-pure water, to prevent the formation of any compounds by electrode reactions. On the other side of the capillary, vessel B and a high-voltage electrode (9) are situated. The vessel can easily be replaced in a vertical direction at any position along the support X, which is used for variable gravity injection [10].

Via valve 4a the channel in the block and the capillary C can be filled with buffer. For the introduction of the sample, the entrance of the capillary is dipped into the sample vessel(s). By opening valve 4a for a fixed time, the sample is introduced by gravity flow, where $\Delta h$ is the driving force. After changing the sample vessel with either buffer (b) or terminating vessel (t), the system can be operated in any HPCE mode. When both valves 4a and 4b are closed, a closed system is obtained. By opening valve 4b, an open system utilizing the electroosmotic flow is created. In the latter instance, it is of great importance, of course, that the liquid level in the buffer vessel is at the same height as the outlet of valve 4b.

To test the equipment, non-coated fused-silica and PTFE capillaries were used. The reproducibility of migration times was tested in a system of $\beta$-alanine (0.05 $M$)–acetate (pH 3.8) using an anionic test mixture. The sample consisted of potassium dichromate, pyrazine-2,3-dicarboxylate, pyrazole-3,5-dicarboxylate, orotate, sulphanilate, dihydroxy-2,4-benzoate, 4-nitrobenzoate, hippurate, 2,4,6-trimethoxybenzoate and benzoate. The separation compartment was a 100-$\mu$m fused-silica capillary with an effective length of 44 cm.

Injection was made by gravity flow, with $\Delta h$ = 5 cm and an injection time of 15 s. The voltage used was 20 kV. The analysis was carried out in the closed mode.

Fig. 2 shows the separation of the anion test mixture. Note that no additives are used in the electrolyte. At low pH the EOF is small and does not influence the separation. In Table I the test mixture composition, the migration times,

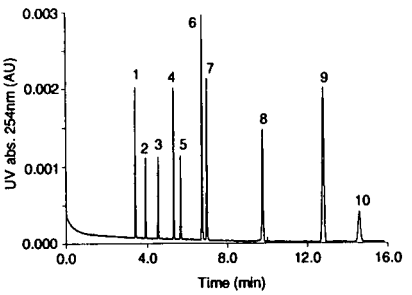


Fig. 2. Zone electropherogram of a test mixture of anions at pH 3.8 (closed mode). For peak numbers, see Table I. Further details are given in the text.

R.S.D. ($n$ = 6) of the migration times and plate numbers are given. High plate numbers are obtained, which means that the EOF is small. In the closed system the hydrodynamic flow is blocked by the membrane, but the EOF still takes place at the capillary wall surface and is compensated for by the EOF counterflow along the capillary axis. This leads to disturbances of the zones [2,4,11].

The $\zeta$-potential of the untreated capillary wall increases with increase in pH. An experiment at higher pH will illustrate this. The system used was Tris (0.02 $M$)–phosphoric acid (pH 7). The same capillary diameter, length and voltage were

TABLE I

AVERAGE VALUES ($n$ = 6) AND RELATIVE STANDARD DEVIATIONS (R.S.D.) OF THE MIGRATION TIMES, $t$, AND PLATE NUMBERS ($N$) IN CZE (CLOSED MODE)

Effective length of the capillary (100 $\mu$m I.D.), 44 cm; system pH, 3.8; voltage, 20 kV.

| No. | Component | $t_{av}$ (min) | R.S.D. (%) | $N$ |
|---|---|---|---|---|
| 1 | Potassium dichromate | 3.42 | 0.80 | 82 000 |
| 2 | Pyrazine-2,3-dicarboxylate | 3.95 | 0.80 | 118 000 |
| 3 | Pyrazole-3,5-dicarboxylate | 4.59 | 0.84 | 141 000 |
| 4 | Orotate | 5.36 | 0.90 | 192 000 |
| 5 | Sulphanilate | 5.71 | 1.11 | 193 000 |
| 6 | Dihydroxy-2,4-benzoate | 6.78 | 1.03 | 165 000 |
| 7 | 4-Nitrobenzoate | 7.02 | 0.99 | 159 000 |
| 8 | Hippurate | 9.80 | 1.05 | 118 000 |
| 9 | 2,4,6-Trimethoxybenzoate | 12.82 | 1.02 | 91 000 |
| 10 | Benzoate | 14.36 | 1.10 | 71 000 |

used. The capillary was rinsed with 0.1 *M* HCl, 0.1 *M* KOH and water. The sample consisted of chromate, pyrazine 2,3-dicarboxylate, sulphanilate, orotate, urate, hippurate and *o*-iodohippurate. In Fig. 3a the separation is shown of the seven components in the closed mode. The separation is unsatisfactory owing to EOF disturbance. Cetyltrimethylammonium bromide (CTAB) is known to decrease and even change the sign of the $\zeta$-potential of the capillary wall [12]. By adding a small concentration ($1 \cdot 10^{-4}$ *M*) of CTAB, the $\zeta$-potential of the capillary wall was decreased, but the results did not improve (see Fig. 3b).

For the next separation, the capillary was extensively rinsed with water. PVA (0.05%) was added to the standard electrolyte. This will also decrease the $\zeta$-potential of the capillary wall and, in addition, it may increase the liquid viscosity at the capillary wall. There was also no improvement (see Fig. 3c). The combination of both $0.5 \cdot 10^{-4}$ *M* CTAB and 0.025% PVA gives excellent results in the closed mode, as shown in Fig. 3d. In the open mode (Fig. 3e) excellent results were also obtained. This effect of the combination of these two constituents is not clear, and is still under investigation. The migration times between the two analyses are different. In this instance the migration times of the components in the open system are faster, because the EOF is in the same direction as the electrophoretic velocity of the separands. This means that $\zeta$-potential of the capillary wall has changed polarity and is now slightly positive owing to the addition of CTAB. The EOF direction follows from the comparison between the two analyses in the open and closed modes. In Table II the test mixture composition and the average plate numbers in the open and closed modes are given for the analyses in Fig. 3d and e.

By observing the outlet of valve 4b (see Fig. 1) in the electrode block during analyses in the open mode, it can be seen directly if the EOF is near zero or the direction in which the liquid flows. For a closed system, slightly suppressing EOF gives a sufficient separation. In Fig. 4 an

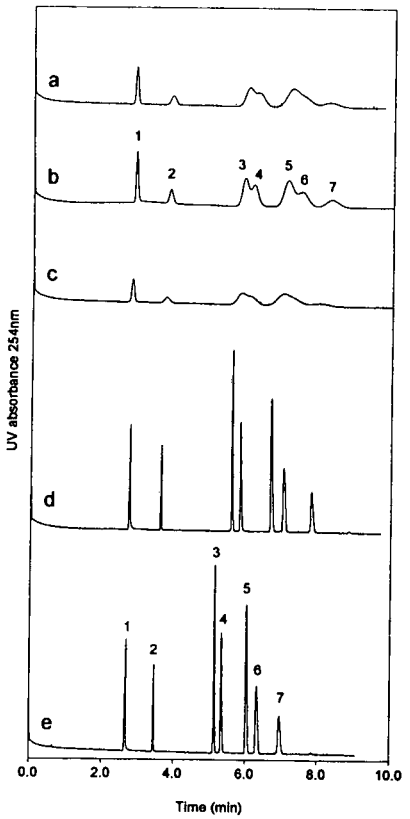


Fig. 3. Zone electropherograms of a test mixture of anions at pH 7. For peak numbers, see Table II. (a) No additives in the electrolyte (closed mode); (b) electrolyte with $1 \cdot 10^{-4}$ *M* CTAB (closed mode); (c) electrolyte with 0.05% PVA (closed mode); (d) electrolyte with $0.5 \cdot 10^{-4}$ *M* CTAB + 0.025% PVA (closed mode); (e) electrolyte as in (d) (open mode). The height of peak 3 is 0.004 absorbance units. The same gain was used for all analyses.

TABLE II

AVERAGE PLATE NUMBERS ($n = 6$) OBTAINED WITH THE OPEN AND CLOSED SYSTEM

Effective length of the capillary (100 $\mu$m I.D.), 44 cm; system, pH 7; voltage, 20 kV.

| No. | Component | Closed | Open |
|---|---|---|---|
| 1 | Chromate | 71 000 | 66 000 |
| 2 | Pyrazine-2,3-dicarboxylate | 262 000 | 241 000 |
| 3 | Sulphanilate | 227 000 | 216 000 |
| 4 | Orotate | 165 000 | 158 000 |
| 5 | Urate | 108 000 | 106 000 |
| 6 | Hippurate | 68 000 | 62 000 |
| 7 | *o*-Iodohippurate | 86 000 | 67 000 |

analysis is shown of the same standard mixture (Table II), where the EOF was higher but not in the "reversed" mode. The system used was Tris (0.02 *M*)–phosphoric acid (pH 7). In Fig. 4a, the separation of the anions is shown in the closed mode. The full analysis of the seven components is completed in 10 min. The peaks are not so sharp owing to the EOF disturbance. In Fig. 4b, the results of the analysis in the open mode are given. In the same analysis time (10 min) only three components are detected owing to the EOF counterflow. The migration order in both analyses remains similar.

In the next experiment, the separation was effected in an open system, where the EOF is not suppressed, but optimized. A similar length and diameter of the capillary were used. Again the test mixture of anions mentioned above was separated at pH 7. The high positive voltage was at the injection side.

In Fig. 5a, after the EOF marker (mesityl oxide) slowly migrating anions are detected first. Ions that are too fast, with respect to the EOF, will not reach the detector. In the analysis in Fig. 5b, the migration order is reversed by changing the polarity at the electrodes. The analysis was

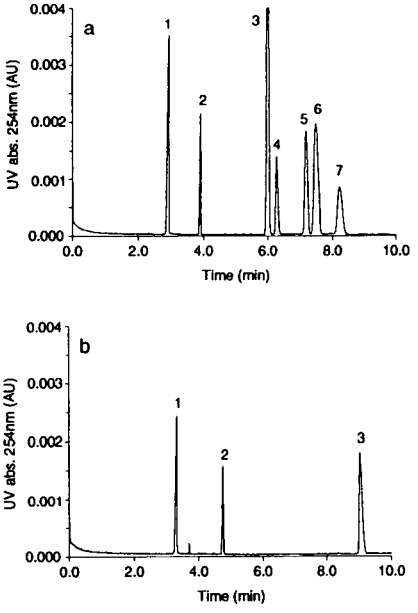


Fig. 4. Zone electropherogram of a test mixture of anions at pH 7. For peak numbers, see Table II. (a) Closed mode; (b) open mode.

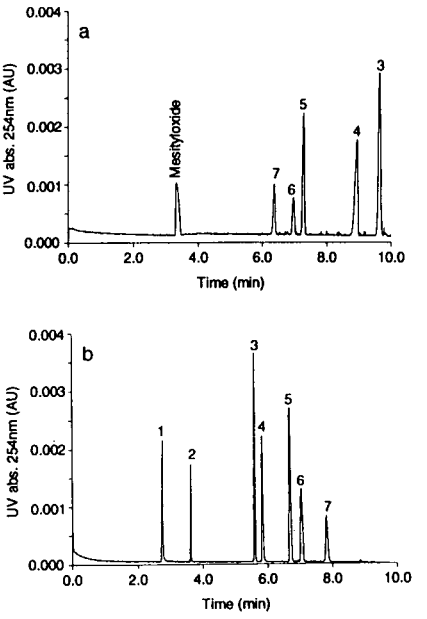


Fig. 5. Zone electropherogram of a text mixture of anions at pH 7. For peak numbers, see Table II. (a) Open mode; (b) closed mode and reversed polarity. For further details, see text.

made in the closed mode. The buffer contained CTAB and PVA as additives. All seven components are detected. From these analyses (Fig. 5a and b) we can conclude that in the closed mode, suppressing the EOF and hydrodynamic flow, the analysis is faster, the resolution is better and the plate numbers are higher.

In the next experiment a PTFE capillary was used (200 $\mu$m I.D. and 350 $\mu$m O.D.). The electrolyte system was $\beta$-alanine (0.01 *M*)–acetate (pH 3.8). The separands were potassium dichromate, pyrazole-3,5-dicarboxylate, orotate, sulphanilate, dihydroxy-2,4-benzoate, 4-nitrobenzoate and hippurate. The buffer contained no additive. The separation, performed in the closed mode, is shown in Fig. 6. Even in PTFE capillaries wavelengths down to 200 nm can be used successfully [13]. Here variable-wavelength detection shows in addition the sensitivity–selectivity trade-off.

One of the HPCE modes, ITP, is not discussed in this paper. It will be evident from the preceding description that ITP can also be performed with the instrument used. ITP in the closed mode using capillaries down to 50 $\mu$m I.D. is

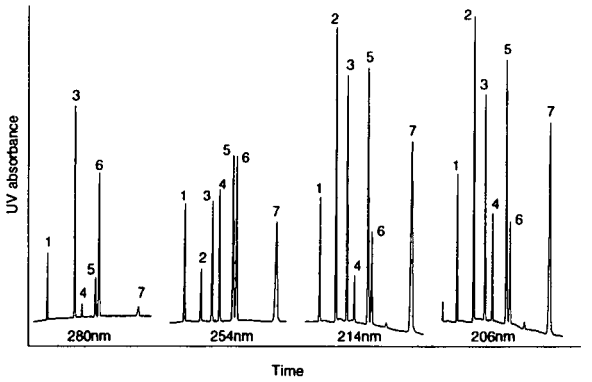


Fig. 6. Zone electropherograms of a text mixture at pH 3.8 in a PTFE capillary at different wavelengths. 1 = Potassium dichromate; 2 = pyrazole-3,5-dicarboxylate; 3 = orotate; 4 = sulphanilate; 5 = dihydroxy-2,4-benzoate; 6 = 4-nitrobenzoate; 7 = hippurate. The detector attenuation was the same for all analyses.

now within reach, with the restriction that as yet there is no universal conductivity detector available for the present prototype. This would decrease the minimum zone volume that can be determined by a considerable factor.

*Application*

A gel-filled column was mounted in the same modular equipment. DNA restriction fragments [14] were analysed in the open and closed modes. A fused-silica capillary of 100 $\mu$m with an effective length of 30 cm and total length of 40 cm was used. The buffer contained 0.1 *M* Tris–acetate and 2 m*M* EDTA (pH 8.3). Electromigration was used for sample introduction (10 s, 2 kV). The separation voltage used was 5 kV. A sample of $\phi$X-174 RF DNA Hae III was

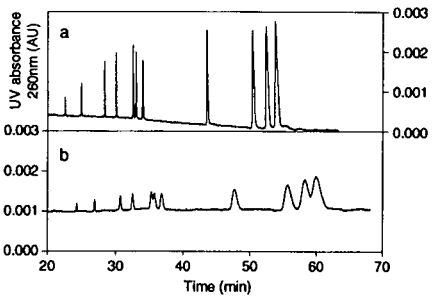


Fig. 7. Zone electropherogram of DNA restriction fragments in a gel-filled capillary. (a) Open mode; (b) closed mode (UV detection at 260 nm). For further details, see text.

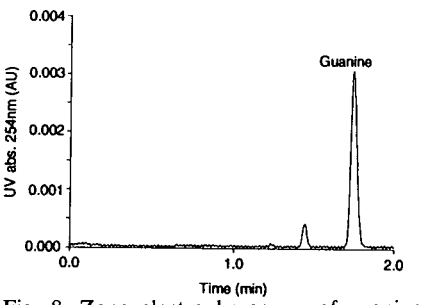


Fig. 8. Zone electropherogram of guanine in a sample of house dust mite (open mode). For further details, see text.

analysed. Comparison of the open and closed modes shows that there is a difference in the efficiency (see Fig. 7a and b). This subject is under investigation.

A Danish study [15] revealed that 60% of asthma cases are due to excretion of allergenic compounds by house dust mites in homes. The guanine (2-amino-6-hydroxypurine) content proved to be a reliable indicator [16]. The HPCE method introduced is superior to the HPLC method [17] (time, variable costs) and more accurate than the commercial Acarex test. The HPLC sample pretreatment procedure [17] was slightly modified and used for HPCE. In the HPCE determination, guanine was measured as a cation in the system glycine (0.01 *M*)–tartrate (pH 3). Determination as an anion at higher pH was unsatisfactory owing to the lower selectivity. The separation compartment was a 50-$\mu$m fused-silica capillary with an effective length of 26.5 cm. The voltage used was 30 kV. Analysis for 2 min gave a more than sufficient resolution of guanine, so that a shorter capillary would have been sufficient (see Fig. 8).

## CONCLUSIONS

The equipment presented facilitates the evaluation of experimental conditions in any HPCE mode in a flexible manner. By comparing analyses in the open and closed modes, the effect of EOF on migration can be determined more readily, also in systems where EOF is suppressed by additives, coating the capillary or in gel columns. A number of phenomena observed can thus be investigated further. In addition, when

sample matrix effects on migration are suspected, dual analyses in both modes will yield decisive information.

The equipment is in principle suitable for automation and can be extended with a commercial autoinjector. As in almost all analytical separation techniques, especially in HPCE, a wide choice of capillary diameters and lengths makes it easy to optimize applications in terms of efficiency and detection selectivity. For all basic HPCE techniques, configurations can easily be selected to achieve such an optimum without changing the equipment used.

ACKNOWLEDGEMENT

J.C. Reijenga is thanked for helpful discussions.

REFERENCES

1 A.J.P. Martin and F.M. Everaerts, *Proc. R. Soc. London, Ser. A*, 316 (1970) 493.
2 F.M. Everaerts, J.L. Beckers and Th.P.E.M. Verheggen, *Isotachophoresis: Theory, Instrumentation and Applications*, Elsevier, Amsterdam, 1976.
3 J.W. Jorgenson and K.D. Lukacs, *J. Chromatogr.*, 218 (1981) 209.
4 F. Foret and P. Boček, in A. Chrambach, M.J. Dunn and B.J. Radola (Editors), *Capillary Electrophoresis (Advances in Electrophoresis*, Vol. 3), VCH, Weinheim, 1989, pp. 273–342.
5 E. Grushka, *J. Chromatogr.*, 559 (1991) 81.
6 M.T. Ackermans, F.M. Everaerts and J.L. Beckers, *J. Chromatogr.*, 545 (1991) 283.
7 Th.P.E.M. Verheggen, A.C. Schoots and F.M. Everaerts, *J. Chromatogr.*, 503 (1990) 245.
8 Th.P.E.M. Verheggen, *Final Report: Capillary Electrophoretic Diagnostic Unit, BIOLAB Workstation; Phase A2, July 1991*, Comprimo Consulting Services, Amsterdam, 1991.
9 F.M. Everaerts, J. Vacik, Th.P.E.M. Verheggen and J. Zuska, *J. Chromatogr.*, 49 (1970) 262.
10 T. Tsuda, K. Nomura and G. Nakagawa, *J. Chromatogr.*, 264 (1983) 385.
11 R. Virtanen, *Acta Polytech. Scand.*, 123 (1974) 1.
12 J.C. Reijenga, G. Aben, Th.P.E.M. Verheggen and F.M. Everaerts, *J. Chromatogr.*, 260 (1983) 241.
13 Th.P.E.M. Verheggen, F.M. Everaerts and J.C. Reijenga, *J. Chromatogr.*, 320 (1985) 99.
14 M.J. van der Schans, *Graduation Report*, University of Technology, Eindhoven, 1992.
15 J. Korsgaard, *Am. Rev. Respir. Dis.*, 128 (1983) 231.
16 J.E.M.H. van Bronswijk, E. Bischoff, W. Schirmacher and F.M. Kniest, *J. Med. Entomol.*, 26 (1989) 55.
17 E.R.C. Bischoff, F.M. Kniest and W. Schirmacher, *Environ. Technol.*, 13 (1992) 377.

*Journal of Chromatography*, 638 (1993) 155–164
Elsevier Science Publishers B.V., Amsterdam

CHROM. 24 941

# Computer simulation and experimental validation of the electrophoretic behavior of proteins

# III. Use of titration data predicted by the protein's amino acid composition

Richard A. Mosher

*Center for Separation Science, University of Arizona, Tucson, AZ 85721 (USA)*

Petr Gebauer[☆] and Wolfgang Thormann*

*Department of Clinical Pharmacology, University of Berne, Murtenstrasse 35, CH-3010 Berne (Switzerland)*

ABSTRACT

To simulate the electrophoretic behavior of a protein, a diffusion coefficient and a tabular representation of net charge *vs.* pH (titration curve) are required. So far data taken from the literature have been employed, the tables being extracted from experimentally determined titration curves. The construction of data tables from the amino acid composition of proteins is reported and compared with those from the literature. The predicted data serve as a rough approximation only, because p$K$ values are dependent on the local environment. Shifting the curve along the pH axis to match the experimentally determined p$I$ is shown to yield simulation data which is in better agreement with experimental data. However, the predicted protein charge numbers are typically too large. Reduction by a pH-independent factor is shown to provide meaningful data for computer simulation. The utility of the titration data employed is documented with good agreement between simulation and experimental data obtained by capillary isotachophoresis.

## INTRODUCTION

Computer simulation of electrophoresis has become an important research tool. Qualitative and quantitative agreement of simulation data with experimental results have confirmed the utility of simulations for the prediction of separability, separation dynamics, zone characteristics and boundary structure, and for the reproduction and explanation of some experimentally observed phenomena [1]. Most of the simulation work performed so far has been limited to low-molecular-mass compounds. Few computer models are available that treat proteins. The complexity inherent in dealing with these macromolecules arises primarily from the lack of a straightforward mathematical procedure for dealing with their ionization [2–4]. The simulation model used in this work has been described in detail previously [2,4]. It is one-dimensional, based on the principles of electroneutrality and conservation of mass and charge and assumes isothermal conditions. Relationships between the concentrations of the

* Corresponding author.
☆ Permanent address: Institute of Analytical Chemistry, Czech Academy of Sciences, CS-611 42 Brno, Czech Republic.

0021-9673/93/$06.00 

various species of a low-molecular-mass component are described by equilibrium constants. The large number of dissociating groups on a protein generates a population of molecules that possess an average net charge at any given pH. The mean square charge of this population is used to describe the contribution of the protein to the current density. In order to make the protein mobility a function of ionic strength, the Linderstrøm–Lang approach is employed [4].

To simulate the behavior of a protein and to calculate its net mobility, two inputs are required, a diffusion coefficient (serving for calculation of the protein radius and diffusive mass transport) and a tabular representation of net charge *vs.* pH (titration curve). So far data taken from the literature have been employed, the table being extracted from experimentally determined titration curves [1,2,4,5]. It is important to note that such titration data are dependent on the ionic strength and are measured at one or more fixed ionic strengths. Titration data that have been extrapolated to zero ionic strength were used when available. Data taken at low ionic strength have generally been found to yield simulation data that are in good agreement with experimental data obtained in media of low ionic strength, such as those employed in isotachophoresis (ITP) [4].

Protein titration curves [6], and also electrophoretic mobilities [7] and p*I* values [8], can be predicted from the protein's amino acid content by applying a model based on the Henderson–Hasselbalch equation. This approach assumes that any specific ionizing group has the same p*K* everywhere on the molecule. For two proteins with known, experimentally determined p*K* values of the residues, calculated input tables have been shown to be in good agreement with experimental titration data [1]. However, the availability of either experimental titration data or accurate p*K* values for the residues within a protein is limited to a small number of proteins. Therefore, titration data generated using the amino acid composition of a protein and p*K* values of free amino acids have been evaluated for use in the simulation of protein electrophoretic behavior.

## THEORETICAL CONSIDERATIONS

For simplicity, it is assumed that each specific ionizing group of a protein has the same p*K* everywhere on the molecule. Hence the net charge of a protein molecule is given by

$$\text{net charge} = \sum_i \frac{n_i}{\frac{K_i}{[H^+]} + 1} - \sum_j \frac{n_j}{\frac{[H^+]}{K_j} + 1} + z_L \quad (1)$$

where $n_i$ and $K_i$ denote the number and ionization constant, respectively, of a weakly basic group $i$, $n_j$ and $K_j$ the corresponding values of a weakly acidic group $j$ and $z_L$ represents the total charge of ligands bound to the protein. Typically there are four different basic groups ($i = 4$), which includes the $\alpha$-amino group, the imidazole group of histidine, the $\varepsilon$-amino group of lysine and the guanidinium group of arginine. The common weakly acidic groups comprise the $\alpha$-carboxyl group, the $\beta$- and $\gamma$-carboxyl groups of aspartic and glutamic acid, respectively, the phenolic group of tyrosine and the thiol of cysteine, yielding a value of 5 for $j$. There are $n$ of each group present and it is assumed that the

TABLE I

RESIDUE-SPECIFIC p*K* VALUES USED IN THIS WORK

| Residue | Tanford and Hauenstein [10] | Compton [7] | GCG [11] |
|---|---|---|---|
| *Basic* | | | |
| Arg | 12.00 | 12.00 | 12.50 |
| Lys | 10.10 | 10.40 | 10.79 |
| His | 6.50 | 6.40 | 6.50 |
| t-$NH_2$ | 7.80 | 8.20 | 8.56 |
| *Acidic* | | | |
| Glu | 4.60 | 4.50 | 4.25 |
| Asp | 4.60 | 4.00 | 3.91 |
| Cys | – | 9.00 | 8.30 |
| Tyr | 9.60 | 10.00 | 10.95 |
| t-COOH | 3.75 | 3.20 | 3.56 |

TABLE II

AMINO ACID COMPOSITION OF PROTEINS USED IN THIS WORK

Amino acid composition according to GCG [11].

| Amino acid | RNase | BLB | OVA | CYTC |
|---|---|---|---|---|
| Arg | 4 | 3 | 15 | 2 |
| Lys | 10 | 15 | 20 | 19 |
| His | 4 | 2 | 7 | 3 |
| t-$NH_2$ | 1 | 1 | 1 | 1 |
| Glu | 5 | 16 | 33 | 9 |
| Asp | 5 | 10 | 14 | 3 |
| Cys | 8 | 5 | 6 | 2 |
| Tyr | 6 | 4 | 10 | 4 |
| t-COOH | 1 | 1 | 1 | 1 |

dissociation constants ($K$) are equal for all members of a group. Charged ligands bound to the protein are typically metal ions, such as $Fe^{2+}$ in hemoglobin for which $z_L$ equals 8 or $Fe^{3+}$ in cytochrome $c$ (CYTC) with $z_L = 3$. A variety of values for the p$K$s of free amino acids, and the N (t-$NH_2$) and C (t-COOH) termini of proteins, can be found in the literature [9]. Three sets of these values have been compared in this work (Table I). One of these is based on experimental values for a specific protein [10], one from the recent literature [7] and one from the Genetics Computer Group (GCG) database of protein amino acid composition [11] (Table II).

## EXPERIMENTAL

### *Chemicals*

The chemicals used were of analytical-reagent or research grade. Ribonuclease A (RNase) from bovine pancreas and CYTC from horse heart were obtained from Sigma (St. Louis, MO, USA), ovalbumin (OVA) from chicken egg from Serva (Heidelberg, Germany) and $\beta$-lactoglobulin B (BLB) from bovine milk from Koch-Light (Haverhill, UK).

### *Computer simulations*

The extended and PC-adapted model of Mosher *et al.* [4] was used. A Mandax AT 286 12 MHz computer (Panatronic, Zürich, Switzerland) running at 12 MHz and featuring a mathematical coprocessor or an Excel AT 486 computer (Walz Computer, Berne, Switzerland) running at 50 MHz were employed throughout this work. Initial conditions that must be specified for a simulation include the distribution of all components, the diffusion coefficients and net charge–pH relationships of the proteins, the p$K$ and mobility values of the buffer constituents, the current density and the duration of the current flow. The program outputs concentration, pH and conductivity profiles as functions of time. The input data for low-molecular-mass components are summarized in Table III. The net charge–pH relationships for the proteins were calculated using eqn. 1 together with the p$K$ values and amino acid compositions listed in Tables I and II, respectively. The experimental net charge–pH relationships and diffusion coefficients for the proteins were taken from literature data [12–19].

### *Experimental validation by capillary ITP*

The experiments were performed on a Tachophor 2127 isotachophoretic capillary analyzer (LKB, Bromma, Sweden) equipped with a

TABLE III

ELECTROCHEMICAL PARAMETERS OF SMALL MOLECULES USED IN SIMULATION

| Compound[a] | p$K_1$ | p$K_2$ | Mobility ($m^2/V \cdot s \times 10^9$) |
|---|---|---|---|
| Acetic acid | 4.76 | | 42.4 |
| $K^+$ | | | 79.1 |
| TPA | | | 18.1 |
| GABA | 4.23 | 10.43 | 32.0 |
| $H^+$ | | | 362.7 |
| $OH^-$ | | | 198.7 |

[a] TPA = Tetrapentylammonium; GABA = $\gamma$-aminobutyric acid.

28 cm × 0.5 mm I.D. PTFE capillary and a conductivity and UV detector (iodine lamp and 277-nm filter) at the column end. Zone patterns were recorded on a two-pen strip-chart recorder as they migrated across the points of detection. The cationic electrolyte systems used consisted of 0.01 *M* potassium acetate and acetic acid ($pH_L$ 4.75) as the leader and 0.01 *M* acetic acid as the terminator. Unless stated otherwise, all measurements were performed at a constant current of 150 μA (the initial and final voltages were about 2.5 and 8.5 kV, respectively) provided by the Tachophor 2127 power supply (500 μA maximum; 30 kV maximum). Samples (1–4 μl containing mg/ml and m*M* concentrations of proteins and spacers, respectively) were injected with a 10-μl syringe (Hamilton, Bonaduz, Switzerland).

## RESULTS AND DISCUSSION

The titration curves for four proteins, bovine pancreas RNase, horse heart CYTC, bovine milk BLB and hen egg OVA, whose amino acid compositions are given in Table II, were determined using eqn. 1. Plots for one protein, RNase, calculated using the three different sets of p*K* values listed in Table I, are presented in Fig. 1A. The data of Compton [7] and Tanford and Hauenstein [10] are in close agreement when cysteine (Cys) with a p*K* of 9 is incorporated for both curves. Larger differences are seen with the p*K*s of GCG. All three calculated graphs deviate from the experimental titration curve [10] (broken line), with the deviation being most pronounced in the pH range above 8, *i.e.*, around the isoelectric point. Calculated p*I* values of the four proteins of interest, using each of the three sets of p*K* values, are given in Table IV. Table IV also includes experimental data, together with p*I* values calculated without including Cys, as was originally suggested for RNase by Tanford and Hauenstein [10]. For BLB and OVA, omitting Cys has no impact on the p*I*, whereas for RNase and CYTC lower p*I* values are predicted with inclusion of Cys. Eqn. 1 also permits the consideration of charges contributed by tightly bound molecules or ions which are not part of the protein's primary

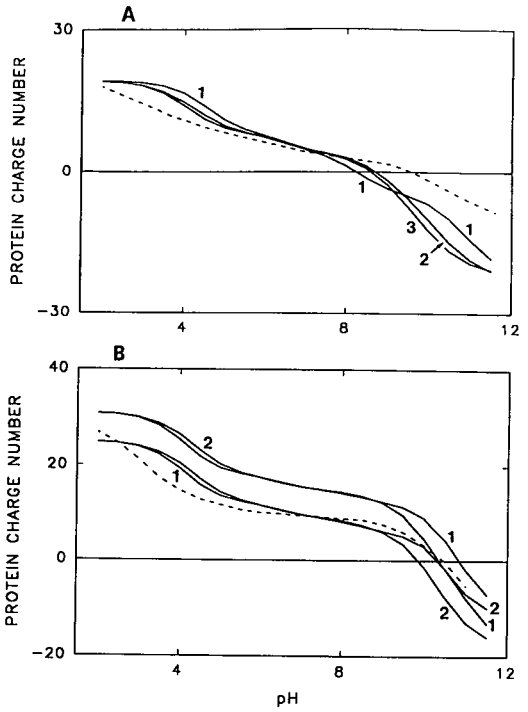


Fig. 1. Calculated (solid lines) and experimental (broken lines) titration data for (A) RNase and (B) CYTC. The curves obtained with the amino acid p*K*s of GCG [11], Compton [7] and Tanford and Hauenstein [10] are denoted 1, 2 and 3, respectively. Upper and lower graphs in (B) refer to a ligand charge of 3 and 0, respectively.

TABLE IV

CALCULATED AND EXPERIMENTAL p*I* VALUES

Amino acid composition according to GCG [11] and p*I* determination extracted from the titration curve calculated by eqn. 1 and using the p*K* values of Tanford and Hauenstein [10], Compton [7] and GCG [11], respectively (Table I).

| Parameter | Protein | | | | |
|---|---|---|---|---|---|
| | RNase (0)[a] | BLB (0)[a] | OVA (0)[a] | CYTC | |
| | | | | 0[a] | 3[a] |
| p*I* [10][b] | 9.20 | 5.15 | 5.48 | 9.71 | 10.23 |
| p*I* [10][c] | 8.59 | 5.15 | 5.48 | 9.58 | 10.07 |
| p*I* [7] | 8.69 | 4.89 | 5.31 | 9.87 | 10.37 |
| p*I* [11] | 8.23 | 4.70 | 5.10 | 10.34 | 10.85 |
| p*I* (exp.) | 9.60 [10] | 5.18 [13] | 4.90 [16] | 10.49 [18] | |

[a] Ligand charge.
[b] No Cys considered.
[c] With inclusion of Cys using a p*K* of 9.

structure. As an example, titration data for CYTC with and without inclusion of the three positive charges of the $Fe^{3+}$ ion were calculated. As is shown in Table IV and Fig. 1B, incorporation of the three charges produces a p*I* shift of about +0.5 pH unit (Table IV) and increased protein charge numbers (Fig. 1B). Unexpectedly, disregarding the contribution of $Fe^{3+}$ produced a better agreement between calculated and experimental (broken line in Fig. 1B) titration curves.

Table V gives the titration data obtained with the GCG input data which were employed for the simulations performed. Table VI presents the different input conditions and predicted ITP zone characteristics of cationically migrating BLB, RNase, CYTC and OVA using 10 m*M* potassium acetate adjusted with acetic acid to pH 4.75 as leader and acetic acid as terminator. The model predicted the formation of an ITP zone with a characteristic plateau concentration and distinct protein mobility for each case. The protein zone properties, however, are clearly dependent on the titration curve employed. For each protein, the first line of data was obtained with the calculated titration curve listed in Table V, whereas the characteristics predicted with the use of experimental titration data are listed in the last line. Additionally, Table VI presents cationic protein ITP data obtained with calculated titration data which were modified by a specified pH shift and/or a factor which reduced the calculated charge number. The data are discussed in turn. The goal is a calculated titration curve that closely reproduces the simulation behavior obtained with an experimental titration curve.

TABLE V

PROTEIN INPUT DATA

Data calculated using the GCG data in Tables I and II.

| pH | RNase | CYTC | BLB | OVA |
|---|---|---|---|---|
| 2.0 | 18.88 | 24.89 | 20.76 | 42.62 |
| 2.5 | 18.64 | 24.65 | 20.27 | 41.82 |
| 3.0 | 17.97 | 23.98 | 18.84 | 39.49 |
| 3.5 | 16.38 | 22.33 | 15.32 | 33.62 |
| 4.0 | 13.70 | 19.36 | 8.98 | 22.64 |
| 4.5 | 10.88 | 15.93 | 1.89 | 9.77 |
| 5.0 | 9.04 | 13.53 | −2.86 | 0.85 |
| 5.5 | 8.03 | 12.29 | −5.08 | −3.53 |
| 6.0 | 7.13 | 11.45 | −6.14 | −6.02 |
| 6.5 | 5.91 | 10.52 | −6.97 | −8.38 |
| 7.0 | 4.56 | 9.61 | −7.75 | −10.57 |
| 7.5 | 3.19 | 8.91 | −8.58 | −12.26 |
| 8.0 | 1.21 | 8.17 | −9.85 | −14.04 |
| 8.5 | −1.40 | 7.23 | −11.60 | −16.21 |
| 9.0 | −3.62 | 6.26 | −13.18 | −18.15 |
| 9.5 | −5.12 | 5.16 | −14.47 | −19.87 |
| 10.0 | −6.82 | 3.01 | −16.37 | −22.69 |
| 10.5 | −9.94 | −1.48 | −20.12 | −28.50 |
| 11.0 | −14.46 | −7.92 | −25.47 | −37.10 |

Fig. 2 presents the simulated ITP steady-state distributions of a two-protein system (RNase and CYTC) using (A) the experimental input data and (B) the calculated titration data. Protein concentrations (upper graphs) and conductivity and pH profiles (lower graphs) are shown for 150 min of current flow. In both instances RNase and CYTC are predicted to behave as typical ITP samples, forming a stack of continuous plateau-shaped zones between the leader (L) and terminator (T) with CYTC appearing immediately behind the leader. This predicted order and the characteristic, step-like conductivity changes have been confirmed experimentally (Fig. 2C). The experimental data represent the UV absorption (277 nm) and conductivity (expressed as increasing resistance *R*) capillary ITP data measured with the Tachophor. Owing to the serial mounting of the two detectors at the capillary end, there is a small shift of detection time, the UV absorbance response being recorded before the conductivity. Although the current densities employed differ by more than two orders of magnitude (experiment, *ca.* 765 $A/m^2$; simulation, 10 $A/m^2$) there is similarity between predicted and experimental protein zone shapes and conductivity distributions. These data demonstrate that calculated, unmodified titration curves can sometimes be used to predict relative net mobilities of two proteins in a given ITP buffer system.

Fig. 3A indicates that calculated titration curves are not always effective predictors of experimental behavior. The computer-predicted dynamics of the separation of RNase, BLB and OVA using the calculated titration data (Table

TABLE VI

INPUT AND SIMULATION RESULTS FOR CATIONIC ITP OF DIFFERENT PROTEINS

Titration data were calculated with eqn. 1 using amino acid composition and $pK$ values according to GCG (Tables I and II). All simulations were performed with the model incorporating the Linderstrøm–Lang approximation (for details see ref. 4). Diffusion coefficients for proteins employed were BLB 7.48 [14], RNase 13.6 [15], CYCT 13.3 [19] and OVA $7.76 \cdot 10^{-11}$ $m^2/s$ [17].

| Line No. | Protein | Titration curve modification | | p$I$ | Protein concentration (m$M$) | Acetate concentration (m$M$) | Conductivity ($S/m \times 10^2$) | pH | Net mobility ($m^2/V \cdot s \times 10^9$) | |
|---|---|---|---|---|---|---|---|---|---|---|
| | | Shift | Factor | | | | | | Protein | Acetate |
| 1 | RNase | – | – | 8.23 | 0.639 | 17.04 | 5.12 | 4.58 | 34.3 | 16.8 |
| 2 | RNase | 0.7 | – | 8.93 | 0.553 | 17.96 | 6.65 | 4.64 | 44.6 | 18.4 |
| 3 | RNase | 1.4 | – | 9.63 | 0.495 | 18.62 | 8.00 | 4.69 | 53.7 | 19.4 |
| 4 | RNase | 1.4 | 0.603 | 9.63 | 0.641 | 17.02 | 5.14 | 4.58 | 34.4 | 16.9 |
| 5 | RNase | 0.7 | 0.603 | 8.93 | 0.691 | 16.51 | 4.38 | 4.53 | 29.4 | 15.8 |
| 6 | RNase | – | 0.603 | 8.23 | 0.768 | 15.80 | 3.42 | 4.45 | 23.0 | 13.9 |
| 7 | RNase | Tanford and Hauenstein [10] | | 9.60 | 0.686 | 16.56 | 4.47 | 4.54 | 30.0 | 16.0 |
| 8 | CYTC[a] | – | – | 10.34 | 0.526 | 18.08 | 6.88 | 4.65 | 46.2 | 18.6 |
| 9 | CYTC[a] | – | 0.603 | 10.34 | 0.660 | 16.61 | 4.52 | 4.54 | 30.3 | 16.0 |
| 10 | CYTC | Theorell and Akesson [18] | | 10.49 | 0.583 | 17.43 | 5.77 | 4.61 | 38.7 | 17.7 |
| 11 | BLB | – | – | 4.70 | 0.387 | 15.33 | 1.80 | 4.12 | 12.1 | 7.9 |
| 12 | BLB | 0.5 | – | 5.20 | 0.368 | 15.19 | 2.60 | 4.34 | 17.4 | 11.7 |
| 13 | BLB | 0.5 | 0.603 | 5.20 | 0.394 | 14.99 | 1.94 | 4.19 | 13.0 | 9.0 |
| 14 | BLB | – | 0.603 | 4.70 | 0.366 | 16.15 | 1.52 | 3.96 | 10.2 | 5.8 |
| 15 | BLB | Cannan *et al.* [13] | | 5.18 | 0.368 | 15.19 | 2.58 | 4.34 | 17.4 | 11.6 |
| 16 | OVA | – | – | 5.10 | 0.364 | 15.63 | 3.00 | 4.38 | 20.1 | 12.6 |
| 17 | OVA | −0.5 | – | 4.60 | 0.407 | 15.32 | 1.83 | 4.13 | 12.3 | 8.04 |
| 18 | OVA | −0.2 | – | 4.90 | 0.390 | 15.27 | 2.44 | 4.30 | 16.3 | 10.9 |
| 19 | OVA | −0.5 | 0.603 | 4.60 | 0.391 | 15.94 | 1.60 | 4.00 | 10.7 | 6.33 |
| 20 | OVA | −0.2 | 0.603 | 4.90 | 0.406 | 15.22 | 1.97 | 4.18 | 13.2 | 8.85 |
| 21 | OVA | – | 0.603 | 5.10 | 0.396 | 15.19 | 2.32 | 4.27 | 15.6 | 10.4 |
| 22 | OVA | −0.2 | 0.244 | 4.90 | 0.352 | 16.96 | 1.45 | 3.87 | 9.72 | 4.81 |
| 23 | OVA | Cannan *et al.* [16], $I \rightarrow 0$ | | 4.90 | 0.406 | 15.52 | 1.65 | 4.06 | 11.0 | 7.01 |

[a] No ligand charge considered.

V) for each protein are presented. Again, all proteins are predicted to behave as typical ITP samples, forming a stack of contiguous plateau-shaped zones between the leader and terminator with RNase (zone 1) appearing immediately behind the leader, followed by OVA (zone 5) and BLB (zone 3). This predicted order is not consistent with that obtained using the experimental titration curves (Fig. 3D), which predict BLB located between RNase and OVA.

The measured isotachopherogram (Fig. 4A) agrees with the simulation data obtained with the experimental input data. This is also reflected in the net mobilities predicted using the calculated titration curves (lines 11 and 16 in Table VI) which are inverted with respect to those predicted employing the experimental titration data (lines 15 and 23). These results reveal the limited utility of calculated titration curves for the simulation of ITP behavior. The discrepancy in the p$I$ values with respect to experimental data is one obvious shortcoming of this approach. The effect of simply shifting the calculated titration curves along the pH axis to the experimental p$I$ values

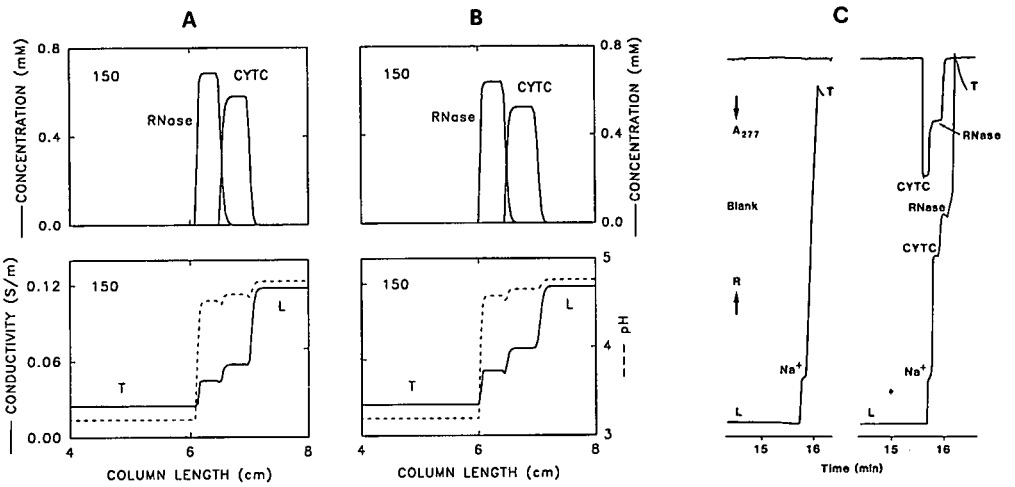


Fig. 2. Cationic ITP of RNase and CYTC. (A) and (B) show the predicted steady-state concentration distributions (upper half) and pH and conductivity profiles (broken and solid lines, respectively, in lower half) after 150 min of current flow (10 A/m$^2$) using experimental and calculated (corresponding to lines 1 and 8 in Table VI) protein input data, respectively. (C) Experimental Tachophor records of blank (left isotachopherogram) and the detected ITP stack with CYTC and RNase as sample (right isotachopherogram). Both the steady-state absorbance at 277 nm (upper graphs) and conductivity profile expressed as increasing resistance *R* (lower graphs) are presented. For the simulation the initial sample pulses (between 0.6 and 1 cm) contained CYTC and RNase (0.7 m*M* each). In the experiment, $Na^+$ represents an impurity and L and T refer to leader and terminator, respectively.

was therefore evaluated. pH shifts of 1.4, 0.5 and −0.2 units for RNase, BLB and OVA, respectively, were implemented (lines 3, 12 and 18 in Table VI). Simulation of the separation of the three proteins using these modified input data predicted the proper migration sequence in this buffer system (compare Fig. 3B and D). There were, however, significant differences in the zone properties, as is reflected in the corresponding data in Table VI.

The shift of 1.4 pH units for RNase produced predicted zone properties (*e.g.*, protein concentration and net mobility) that corresponded to those with experimental titration data less well than did those with the unshifted curve. This is due to the increased charge number of the molecule at the system pH and is reflected in the increased net mobility. The predicted zone properties of OVA with pH shift improved with respect to those obtained with the experimental titration curve. The shift decreased the charge number on the protein. For BLB, the pH shift brought the predicted zone properties into excellent agreement with those produced by the experimental titration data. These data are consistent with two conclusions. The first is that the titration curve used for simulation must reflect the experimental p*I*. This is of obvious importance for the simulation of the isoelectric focusing behavior of proteins and clearly also for simulating ITP and zone electrophoretic behavior. The second conclusion is that calculated titration curves with accurate p*I*s generally, although not always, overestimate the charge on a molecule. The calculated, unshifted titration curve of RNase produced zone properties that were serendipitously close to those produced by the experimental curve. When shifted to the experimental p*I*, the molecule displayed a substantially increased charge at the system pH. The net mobility in this buffer system is much higher with the calculated, shifted curve than with the experimental curve (lines 3 and 7 in Table VI). This is true for OVA (lines 18 and 23) and for CYTC (lines 8 and 10). The titration curve was not shifted for this last example, but the conclusion is valid. The shift would move the p*I* away from the system pH, thus increasing the net charge on the molecule and its net mobility in the buffer system (compare lines 1–3 and 11 with

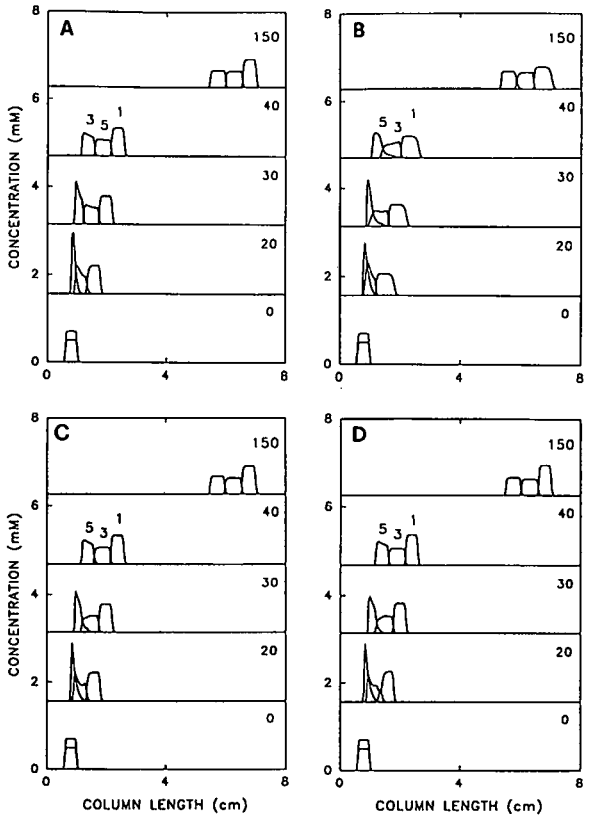


Fig. 3. Computer-simulated separation dynamics of OVA (5), BLB (3) and RNase (1) using (A) calculated titration data, (B) calculated titration data shifted −0.2, 0.5 and 1.4 pH units for the three proteins, respectively, (C) titration data as in (B) with the charge numbers of OVA and RNase being multiplied by 0.603 and (D) experimental titration data. For the simulation, the initial conditions included pulses of OVA, BLB and RNase at 0.5, 0.5 and 0.7 m*M*, respectively, located between 0.6 and 1 cm of the column length. The current density was 10 A/m$^2$. All panels show the concentration profiles of the three proteins at the indicated time intervals between 0 and 150 min.

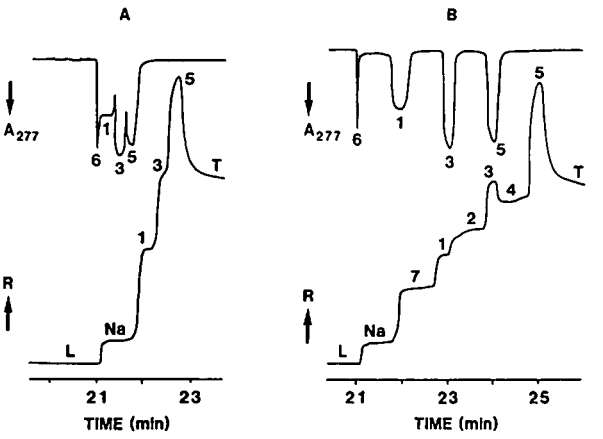


Fig. 4. Experimental ITP data (adapted from ref. 4) showing the steady-state distribution of (A) RNase (1), BLB (3) and OVA (5) and (B) the same protein mixture spaced with TPA (2) and GABA (4). Absorbance at 277 nm (upper graphs) and conductivity profiles expressed as increasing resistance *R* (lower graphs) are presented. While recording the experimental data, the current was reduced to 50 μA. Zone 6 and Na represent impurities and zone 7 represents tris-(hydroxymethyl)aminomethane, which was used to isolate the impurities from the proteins. L and T refer to leader and terminator, respectively.

12). Correspondingly, a shift that would move the p*I* towards the system pH would result in a decrease in net charge and mobility (compare lines 16–18).

There is a clear requirement to reduce the charge numbers calculated for proteins. This need arises from the role of electrostatic charge suppression in decreasing the apparent valence of proteins [20]. As it has been shown that the electrophoretic mobility of a protein is directly proportional to charge number over the entire pH range [7], a pH-independent factor can be employed. Longsworth [12] used 0.603 to approach a similar problem with OVA and his value was arbitrarily chosen as a starting point. The data in Table VI show that reducing the protein valence by this factor yields predicted zone characteristics for RNase (line 4) which are in better agreement with those produced using the experimental titration curve than are the zone characteristics produced with the shifted curve. A clear improvement is also obtained with OVA. As the predicted data for BLB were already in good agreement after the pH shift, reducing the valence resulted in zone characteristics that agreed less well with the data produced using the experimental curve. Corresponding simulated protein zone distributions of the separation of RNase, BLB and OVA (Fig. 3C) are shown to agree well with those obtained with the experimental input data (Fig. 3D). It is important to note that valence reduction without pH shift (lines 6, 9, 14 and 21 in Table VI) did not provide accurate data for the four proteins.

An important aspect of protein separation by

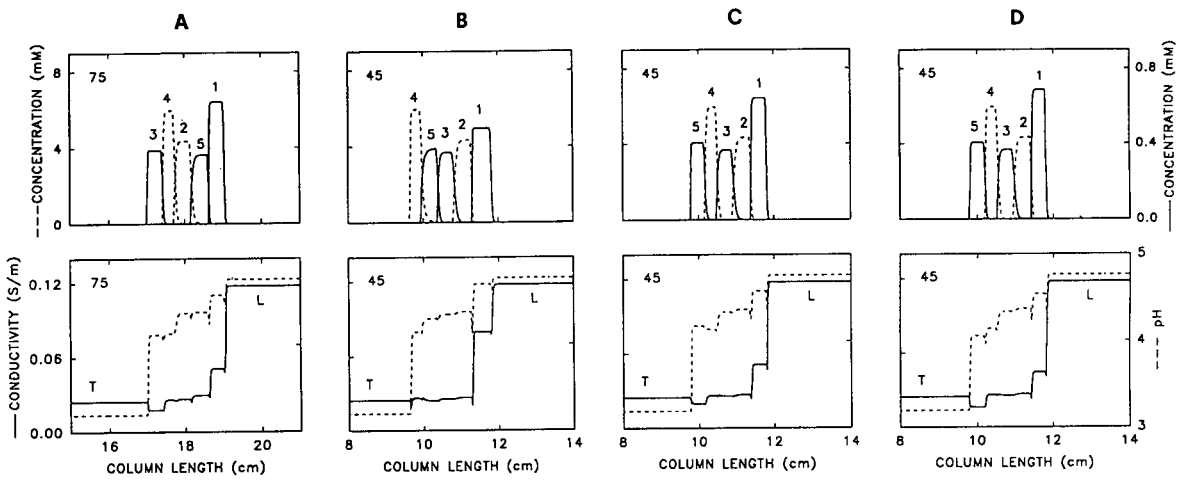


Fig. 5. Computer prediction of the ITP separation of RNase (zone 1), TPA (2), BLB (3), GABA (4) and OVA (5) using (A) calculated titration data, (B) calculated protein titration data shifted 1.4, 0.5 and −0.2 pH units for the three proteins, respectively, (C) titration data as in (B) with the charge numbers of OVA and RNase being multiplied by 0.603 and (D) experimental titration data. The initial sample pulse (between 0.64 and 0.96 cm) consisted of 0.5 m*M* OVA, 0.5 m*M* BLB, 0.8 m*M* RNase, 6 m*M* TPA and 6 m*M* GABA. The current density was 60 A/m$^2$. All panels show the concentration profiles (upper graphs) and the conductivity and pH distributions (solid and broken lines, respectively, lower graphs) at the indicated time intervals.

ITP involves the use of low-molecular-mass molecules as spacers to achieve the fractionation of complex mixtures into several sub-mixtures or to separate completely two proteins that would otherwise migrate contiguously. The simulated behavior of a system composed of the same three proteins (RNase, BLB and OVA) and two low-molecular-mass spacers [tetrapentylammonium (TPA) and γ-aminobutyric acid (GABA)] is presented in Fig. 5. The predicted zone properties of the low-molecular-mass compounds are given in Table VII. The predicted migration order with the use of the experimental protein input data is RNase, TPA, BLB, GABA and OVA (Fig. 5D). Hence the spacers are predicted to separate the three proteins. This migration order has been confirmed experimentally (Fig. 4B). Performing the same simulation with calculated protein titration data produced a different behavior (Fig. 5A), with the prediction of a completely different steady-state zone sequence. Shifting of the protein input data along the pH

TABLE VII

SIMULATED ITP ZONE PROPERTIES OF LOW-MOLECULAR-MASS COMPOUNDS

| Parameter | Zone | | | |
|---|---|---|---|---|
| | Leader ($K^+$) | Samples | | Terminator ($H^+$) |
| | | TPA | GABA | |
| Concentration (m*M*) | 10 | 4.34 | 5.93 | 0.0634 |
| Acetate concentration (m*M*) | 20 | 15.11 | 17.34 | 23.75 |
| pH | 4.76 | 4.37 | 4.14 | 3.20 |
| Conductivity (S/m × $10^2$) | 11.79 | 2.70 | 2.63 | 2.48 |
| Mobility ($m^2/V \cdot s \times 10^9$) | 79.10 | 18.10 | 17.67 | 16.62 |
| Acetate mobility ($m^2/V \cdot s \times 10^9$) | 21.24 | 12.29 | 8.18 | 1.13 |

axis to the correct isoelectric point resulted in the steady-state pattern shown in Fig. 5B, in which zones 4 and 5 are in reverse order compared with the experimentally confirmed pattern in Fig. 5D. Reduction of the charge numbers of RNase and OVA with the pH-independent factor of 0.603 (see above) provided the correct zone pattern (Fig. 5C), which is in good agreement with that obtained with the experimental protein titration data (Fig. 5D).

The good agreement between the data in Fig. 5C and D indicated that protein titration curves useful for the simulation of electrophoretic behavior can be generated employing the GCG database of amino acid composition and p$K$ values and eqn. 1 to generate a titration curve. This curve must then be shifted along the pH axis to match the experimental p$I$, and the calculated charge numbers reduced throughout the pH range by 0.603. The limitation of this approach is shown by BLB, which required no reduction in charge number to reflect the experimental data. The selection of a charge reduction factor is at present an arbitrary process. Compton and O'Grady [6] attempted to predict such factors. Their suggested value of 0.244 for OVA was found to be too small to allow accurate simulation of ITP behavior (lines 22 and 23 in Table VI). Much more work is needed on this subject.

## ACKNOWLEDGEMENTS

The authors are grateful to Dr. M. Solioz for providing access to the GCG database. This work was supported by the Swiss National Science Foundation.

## REFERENCES

1 R.A. Mosher, D.A. Saville and W. Thormann, *The Dynamics of Electrophoresis*, VCH, Weinheim, 1992.
2 R.A. Mosher, D. Dewey, W. Thormann, D.A. Saville and M. Bier, *Anal. Chem.*, 61 (1989) 362.
3 G.O. Roberts, P.H. Rhodes and R.S. Snyder, *J. Chromatogr.*, 480 (1989) 35.
4 R.A. Mosher, P. Gebauer, J. Caslavska and W. Thormann, *Anal. Chem.*, 64 (1992) 2991.
5 W. Thormann and R.A. Mosher, *Electrophoresis*, 11 (1990) 292.
6 B.J. Compton and E.A. O'Grady, *Anal. Chem.*, 63 (1991) 2597.
7 B.J. Compton, *J. Chromatogr.*, 539 (1991) 357.
8 A. Sillero and J.M. Ribeiro, *Anal. Biochem.*, 179 (1989) 319.
9 V. Kašička and Z. Prusík, *J. Chromatogr.*, 569 (1991) 123.
10 C. Tanford and J.D. Hauenstein, *J. Am. Chem. Soc.*, 78 (1956) 5287.
11 J. Devereux, P. Haeberly and O. Smithies, *Nucleic Acids Res.*, 12 (1984) 387.
12 L.G. Longsworth, *Ann. N.Y. Acad. Sci.*, 41 (1941) 267.
13 R.K. Cannan, A.H. Palmer and A.C. Kibrick, *J. Biol. Chem.*, 142 (1942) 803.
14 A.L. Lehninger, *Biochemistry*, Worth, New York, 2nd ed., 1975, p. 176.
15 D.M. Greenberg, *Amino Acids and Proteins*, Charles C. Thomas, Springfield, IL, 1951, p. 394.
16 R.K. Cannan, A.C. Kibrick and A.H. Palmer, *Ann. N.Y. Acad. Sci.*, 41 (1941) 243.
17 A. Tiselius and H. Svensson, *Trans. Faraday Soc.*, 36 (1940) 16.
18 H. Theorell and A. Akesson, *J. Am. Chem. Soc.*, 63 (1941) 1818.
19 J.T. Adsall, in H. Nerath and K. Baile (Editors), *The Proteins, Chemistry, Biological Activity and Methods*, Vol. 1, Part B, Academic Press, New York, 1953, p. 634.
20 C. Tanford and J.G. Kirkwood, *J. Am. Chem. Soc.*, 79 (1957) 5333.

*Journal of Chromatography*, 638 (1993) 165–178
Elsevier Science Publishers B.V., Amsterdam

CHROM. 24 918

# Towards new formulations for polyacrylamide matrices, as investigated by capillary zone electrophoresis

Pier Giorgio Righetti*

*Chair of Biochemistry, Faculty of Pharmacy and Department of Biomedical Sciences and Technologies, University of Milan, Via Celoria 2, 20133 Milan (Italy)*

Marcella Chiari

*Department of Biomedical Sciences and Technologies, University of Milan, Via Celoria 2, 20133 Milan (Italy) and Istituto di Chimica degli Ormoni, CNR, Via Mario Bianco 9, 20131 Milan (Italy)*

Marina Nesi and Silvia Caglio

*Chair of Biochemistry and Department of Biomedical Sciences and Technologies, University of Milan, Via Celoria 2, 20133 Milan (Italy)*

ABSTRACT

Several new aspects of polyacrylamide gel polymerization were investigated. First, a series of mono- and disubstituted acrylamide monomers were evaluated as potential candidates of a novel class of polyacrylamide matrices, exhibiting high hydrophilicity, high resistance to hydrolysis and larger pore size than conventional polyacrylamide gels. A series of cross-linkers were also assessed and their contributions to the gel stability and hydrophilicity evaluated. A novel method of photopolymerization is described, consisting of photoinitiating the reaction with methylene blue in the presence of a redox couple (sodium toluenesulphinate and diphenyliodonium chloride). The photobleaching curve gives direct information on the conversion efficiency of monomers into the growing polymer. In addition, photopolymerized gels have a better elastic modulus than peroxodisulphate-initiated gels. A unique correlation is described between the Phantom modulus and protein mobilities as a function of the percentage of cross-linker: a maximum of Phantom modulus corresponds to a minimum of mobility and both of these values occur at 5% of cross-linker. A novel method is described for producing extremely large-pore gels: polymerization in presence of a preformed, hydrophilic polymer (typically PEG 20 000 or PEG 10 000). In the presence of the latter polymers (up to 2–2.5%), "lateral-chain aggregation" occurs, with an extremely large expansion of pore size. For example, while a 5%T, 4%C gel typically has an average pore diameter of 5–6 nm, the same gel, in the presence of a "laterally aggregating agent" exhibits an average pore size of 500 nm.

## INTRODUCTION

Polyacrylamide matrices, for separation in zone electrophoresis, were introduced in 1959 by Raymond and Weintraub [1] and further promoted for use in disc electrophoresis by Davis [2], Ornstein [3] and Hjertén [4]. Their popularity as electrophoretic supports stems from some fundamental properties, such as optical transparency, including the ultraviolet region, electrical neutrality, due to the absence of charged groups, and the possibility of synthesizing gels with a wide interval of porosities. The monomer that has attained the greatest popularity is acrylamide, coupled to a cross-linker, N,N'-methylene bisacrylamide [5]. However, several defects of such a matrix have been observed on

* Corresponding author.

0021-9673/93/$06.00 

prolonged use. The greatest drawback is its instability at alkaline pH: after an electrophoretic run (most electrokinetic separations occur at alkaline pH for both proteins and nucleic acids), the dangling amido bonds are partly hydrolysed, leading to carboxylic groups, which remain covalently bound to the polymer, which is thus transformed into a polyacrylate. This phenomenon generates strong electroendosmosis, with matrix swelling and considerable distortions. In practice, after only a single electrophoretic run, the polyacrylamide matrix cannot be re-used. This strongly limits its use in large-scale projects, such as the sequencing of the human genome, where the availability of re-usable matrices would greatly shorten the analysis time and allow for rapid progress of such a project around the world. Stable matrices would also be useful in capillary zone electrophoresis (CZE), as the capillary has to be discarded when the gel filling is partially hydrolysed or malfunctioning [6].

Another common problem is the limited range of molecular sizes that can be efficiently sieved by polyacrylamides. Such a porosity range encompasses pore sizes from 2–3 to *ca.* 20–30 nm in highly diluted matrices [7]. This limits the use of polyacrylamides to protein separations, whereas agarose gels are today almost exclusively used for separations of nucleic acid fragments. Highly porous polyacrylamide matrices would thus allow the fractionation also of nucleic acids into some intervals of length.

A third problem is linked to the use of the standard redox couple of catalysts: peroxodisulphate and N,N,N′,N′-tetramethylethylenediamine (TEMED). As this is a redox couple, it is able to oxidize many substances containing amino groups (from primary to tertiary), thus producing N-oxides. Such N-oxides, which remain in the gel even after discharging excess of peroxodisulphate to the anode, are able to oxidize proteins, especially the –SH residues to disulphide bonds (–S–S–) [8].

Some earlier patent applications have addressed a few of the problems described above and have proposed different types of monomers. In one instance [9], Trisacryl [N-acryloyltris-(hydroxymethyl)aminomethane, NAT] has been advocated for producing hydrophilic, large-pore gels for electrophoresis. The Trisacryl monomer had in fact been proposed for chromatographic support media by Girot and Boschetti [10]. As will be shown in this paper, this monomer, although strongly hydrophilic, suffers from inherent instability, as it degrades with zero-order kinetics. Its use for, *e.g.*, re-usable or long-term storage matrices cannot be clearly advocated. In another patent application [11], acrylamido sugars have been proposed, such as N-acryloyl(or methacryloyl)-1-amino-1-deoxy-D-glucitol or the corresponding D-xylitol derivative. This class of acrylamido monomers, which certainly possess good hydrophilicity and a higher molecular mass than unsubstituted acrylamide, is also extremely unstable, as it degrades with zero-order kinetics and thus does not seem to be a valid alternative, similarly to poly(NAT) mentioned above [12].

In another application [13], a broad class of N-mono- and -disubstituted acrylamido monomers have been proposed as electrophoretic support media, including some of the monomers mentioned above. However, of this large class of potential monomers, Shorr and Jain [13] have enucleated (and commercialized) only two preferred mixtures, as follows (verbatim quotation): "in one preferred embodiment, the polymers are formed by cross-linking polymerization of N,N-dimethylacrylamide with ethylene glycol methacrylate. In another preferred embodiment, the polymers are formed by cross-linking polymerization of N,N-dimethylacrylamide and hydroxyethyl methacrylate with N,N-dimethylacrylamide". These formulations also do not appear to be optimum. As will be shown in this paper, N,N-dimethylacrylamide, and similar alkyl-substituted acrylamides, are too hydrophobic, and the various methacrylate cross-linkers are too prone to hydrolysis and also are hydrophobic [14]. As a result, the commercialized product containing these formulations (Hydrolink) has to contain detergents to help in solubilizing the monomers. The corresponding emulsion often flocculates. Needless to say, when the Hydrolink matrix is applied to protein separations, strong hydrophobic interactions, precipitation at the application site and smears are regularly experienced. These examples show

that the problems formulated above, namely the design of new matrices possessing simultaneously a high hydrophilicity, a high resistance to hydrolysis and a larger pore size, have not been addressed properly and are far from being solved.

In the past, we have addressed various problems connected with the polymerization of hydrophilic gels; in particular, the extent of conversion of monomers into the polymer phase was investigated as a function of temperature [15], amount and type of cross-linker [16] and type of catalyst [17]. We also described the problems connected with preparation of highly porous gels by using high levels of cross-linker (typically, above 20%C) [18], especially when the latter was an allyl compound, *i.e.*, an effective inhibitor of gel polymerization [19]. We even ventured to describe two new monomers, acryloylmorpholine and bisacrylylpiperazine [20], believed to open up new horizons, as they permitted electrophoresis in aqueous–organic solvents. However, as it turned out, we (and we suspect many other scientists in the field) were avoiding a key issue, namely how to obtain matrices exhibiting simultaneously high hydrophilicity and extreme resistance to alkaline hydrolysis, an impossible marriage indeed.

In this paper, we address all three aspects mentioned above: the search for new monomers and cross-linkers, novel photopolymerization methods and gel polymerization conditions leading to extremely large pore sizes. In all these aspects, capillary zone electrophoresis (CZE) was instrumental in assessing the fate of the different monomers and their conversion efficiencies.

## EXPERIMENTAL

### *Materials*

Six monomers were analysed: acrylamide (Acr), N-methylacrylamide (MMA), N,N-dimethylacrylamide (DMA), N-acryloyltris-(hydroxymethyl)aminomethane (Trisacryl, Tris-A or NAT), N-acryloyldimethylhydroxymethylaminomethane (dideoxy-Trisacryl, DD-NAT) and N-acryloylmorpholine (ACM). Their synthesis has been described [3,12]. In addition, the following four cross-linkers were analysed: N,N′-methylenebisacrylamide (Bis), N,N′-(1,2-dihydroxyethylene)bisacrylamide (DHEBA), N,N′-diallyltartardiamide (DATD) and N,N′-bisacrylylcystamine (BAC). Gels were prepared by using acrylamide as a monofunctional monomer and any of the four cross-linkers. Acrylamide, TEMED, the four cross-linkers and ammonium peroxodisulphate were obtained from Bio-Rad Labs. (Richmond, CA, USA). Fused-silica capillaries (50 and 100 $\mu$m I.D., 370 $\mu$m O.D.) were purchased from Polymicro Technologies (Phoenix, AZ, USA). Methylene blue (puriss. DAB), toluene-4-sulphinic acid (sodium salt, anhydrous, purum, 98%), diphenyliodonium chloride (purum, 99%) and p$K$ 4.6 acrylamido buffer, used as internal standard in CZE runs, were obtained from Fluka (Buchs, Switzerland). Polyethylene glycol (PEG) 2000, 6000 and 10 000 were purchased from Merck (Darmstadt, Germany) and PEG 20 000 from Baker (Deventer, Netherlands).

### *Capillary zone electrophoresis*

CZE was performed on a Waters Quanta 4000 system (Millipore, Milford, MA, USA) in a 50 cm × 100 $\mu$m I.D. capillary from Polymicro Technologies. All runs were carried out at 25°C in 100 m$M$ borate buffer (pH 9.0), either as such or with 50 m$M$ sodium dodecyl sulphate (SDS) added (micellar electrokinetic chromatography) [21]. All runs were made in the cathodic direction at 5 kV and 35 $\mu$A. Samples were loaded for 10 s by the "hydrostatic injection" method. Sample zones were revealed at 214 nm.

### *Partition coefficient*

In order to establish a hydrophobicity scale, the various acrylamido monomers were subjected to partitioning in water–1-octanol as described by Purcell *et al.* [22]. The partition coefficient $P$ is defined as the ratio between the molarity of a given compound in the organic *vs.* the aqueous phase. Partitioning was performed as follows: each monomer was dissolved (50 m$M$) in water saturated with 1-octanol; 3.5 ml of this solution and 3.5 ml of 1-octanol were transferred into a separating funnel and shaken for 2 min. After decanting for 1 h, the aqueous phase

was collected and centrifuged for 75 min at 4000 *g*. All operations were performed at 25°C. The clarified solution was diluted to *ca.* 1 m*M*, internal standard (0.5 m*M* p*K* 9.3 Immobiline) added and the mixture analysed in CZE as described above. The decrease in the peak area in the aqueous phase allows the assessment of the amount of monomer remaining in that phase and thus, by difference, the amount dissolved in the organic phase.

*Titration of acrylate groups in polyacrylamides by frontal analysis*

In order to assess the amount of protolytic groups (acrylic acid) produced on extensive hydrolysis of the different types of polyacrylamides, the gels were cast not as continuous layers but as beads (with a concentration of 10%T and 8%C[a]) by emulsion polymerization [23]. The beads were extensively washed, dehydrated in methanol and dried *in vacuo*. A known amount of dry beads (from 0.25 to 1 g) was then reswollen in water and then subjected to different hydrolytic conditions: in 0.1 *M* NaOH at 70°C for up to 60 h and in 0.1 *M* HCl at 70°C for up to 12 h. After extensive washing in water (to negligible conductivity) the beads were loaded on a 1.6 cm diameter column to a bed height of *ca.* 10 cm. Titration was performed with 0.1 *M* HCl and the eluate pumped at a constant rate (1.5 ml/min, LKB peristaltic pump) through a micro-conductimetric cell (4-$\mu$l volume, Orion conductimeter, 10 mS full-scale). The signal was traced on a Kipp & Zonen recorder (20 mV full-scale, 10 mm/min chart speed). When the conductivity curve had reached a plateau (corresponding to the conductivity of the titrant, diluted by the dead volume of the resin), the titration was stopped and a solution, with half the titrant molarity, was injected directly into the conductimeter cell: this was necessary in order to measure the inflection point of the curve.

For calculating the total amount of protolytic groups (acrylic acid) generated on the resin by alkaline or acidic hydrolysis ($C_{tot}$), the following equation applies:

$$C_{tot} = [V/L(L_1 - L_0) - G_v]M_{tit}$$

where $V$ is the volume of titrant utilized (in ml, as measured with a burette), $L$ is the total length of the recorder tracing (in cm) for this $V$ value, $L_0$ is the length of the recorder tracing corresponding to the dead volume of all connecting tubings, $L_1$ is the length of the recorder tracing (in cm) up to the inflection point (as measured when pumping in the titrant at half molarity), $G_v$ is the total gel volume (in ml) and $M_{tit}$ is the molarity of the titrant. In our case, the value of $C_{tot}$ obtained is divided by the resin dry mass, so that our data are expressed in $\mu$equiv. per gram of dry beads. These data are finally converted into percentage hydrolysis with time (see Fig. 3A and B).

*Alkaline hydrolysis of free monomers*

All monomers were dissolved (20 m*M* each) in 0.1 *M* NaOH and incubated at 70°C for up to 6 h. At given time intervals (see the relevant figures) aliquots were collected and diluted (to *ca.* 1 m*M*) in 0.1 *M* sodium borate buffer (pH 9.0) containing 50 m*M* SDS. After adding 2 m*M* Immobiline p*K* 4.6 as internal standard, the samples were analysed by CZE as described above. The decrease in the peak area, as compared with a reference, non-hydrolysed sample, was used for calculating the rate of hydrolysis.

*Photopolymerization*

All experiments were performed in 100 m*M* Tris–phosphate buffer (pH 8.2), in general using a monomer mixture of 6%T, 4%C. As a routine, the solutions were first degassed with a water pump for 10 min and then bubbled with argon for an additional 10 min. Stock solutions of catalysts were prepared in distilled water as follows: 2 m*M* methylene blue, 20 m*M* sodium toluenesulphinate (reducer) and 1 m*M* diphenyliodonium chloride (oxidizer). They were kept refrigerated in the dark and used for only one working week (except for the dye, which we have used for up to seven months with no decrease in efficiency). Under standard conditions, the gels were made to contain 100 $\mu M$ dye, 1 m*M* reducer and 50 $\mu M$ oxidizer. Photopolymerization was activated by placing the

[a] C = g Bis/% T; T = (g acrylamide + g Bis)/100 ml solution.

cassette between two light boxes (neon tubes, 12 W each) at a 10-cm distance from each source. Completion of reaction was evident by photobleaching.

*Assessment of photobleaching*

Photobleaching was measured by performing polymerization in plastic cuvettes of a spectrophotometer (1-cm light path) and covering the liquid surface with a layer of light paraffin oil (so as to avoid oxygen adsorption). At regular time intervals, the cuvette was quickly placed inside the spectrophotometer and the absorbance decreases read at 600 nm. In photofading experiments utilizing gel layer thicknesses from 0.5 to 2 mm, the gel cassette was assembled with two microscope glasses, kept apart by appropriate spacers, as described previously [18]. These cassettes were used as both polymerization containers and cuvettes for spectrophotometric readings.

*Other types of polymerization*

Gels were also polymerized with peroxodisulphate and TEMED (1 $\mu$l of 40% peroxodisulphate and 1 $\mu$l of pure TEMED per millilitre of gelling solution) or with riboflavin 5′-phosphate ($1.16 \cdot 10^{-5}$ mmol/ml). In some experiments, peroxodisulphate–TEMED-initiated gels were polymerized in the presence of a "laterally aggregating agent" (2.5% PEG 10 000) to produce macroporous structures.

*Spectrophotometric reading*

The turbidity of "laterally aggregated" gels was studied with a Varian (Palo Alto, CA, USA) DMS-90 UV–Vis spectrophotometer at 600 nm against a water blank. All gels were prepared at 5%T, 4%C matrices in the presence of variable amounts of preformed linear polymers, as follows: for the PEG series the concentrations added ranged from 0.1 up to 25% (w/v), for polyvinylpyrrolidone (PVP) from 0.2 up to 15% (w/v) for hydroxymethyl cellulose (HMC) of $M_r$ $10^6$ from 0.01 up to 0.1% (w/v). To all solutions were added 1 $\mu$l/ml of TEMED and 1 $\mu$l/ml of 40% ammonium peroxodisulphate. Each sample was run in triplicate in plastic cuvettes and was allowed to polymerize for 1 h at room temperature.

*Electron microscopy*

The following procedure proved to be optimum for sample preparation for the scanning electron microscope. The polymerized gels (as prepared in a spectrophotometric cuvette, in the presence of increasing amounts of PEG 10 000 from 0 up to 2.5%) are first fractured into several segments (not by cutting, but by breaking them), which are then equilibrated for 2 days in 2.5% PEG 10 000 (*i.e.*, the plateau concentration giving maximum turbidity and thus maximum chain aggregation). The fragments are quickly frozen in liquid nitrogen and immediately lyophilized without allowing melting during the entire process. It was found that, in the absence of the PEG 10 000 equilibration step, all samples containing either no PEG or smaller amounts showed variable degrees of disintegration of the gel structure during the various sample manipulations prior to microscopic observations. The samples were then spread with a gold–palladium thin layer in an Edwards 306 metallizer (Edwards High Vacuum, Crawley, UK) and then observed with a Stereoscan 250 scanning electron microscope (SEM) from Cambridge Scientific Instruments (Cambridge, UK) at 20 kV. Photographs were taken with a Kodak TRI-X PAN 120 film.

*Elastic measurements*

For elastic measurements the gel matrices were polymerized at room temperature in vertically placed rectangular glass cassettes of 10 mm thickness and 125 × 125 mm size. Photoinitiation was carried out by illuminating the chamber through one of the wide sidewalls by a four-tube lamp situated 10 cm from the chamber. At fixed time points the illumination was stopped, several (usually nine) cylindrical samples of 25 mm diameter were cut from the gel slabs and subjected to measurements with a dynamometer from Instron Engineering (Canton, MA, USA). A pulling force of 10 N full-scale was selected, and the traction was stopped at 3 N, at which point the compressed gel was left to expand. The experimental points plotted in Fig. 5 are statisti-

cal data for the series. Note that, as the gels dry quickly, the matrices were prepared immediately before the measurements and kept in a closed box during the experiment, and each sample was cut just before being subjected to measurements.

## RESULTS

### *Properties of novel monomers and cross-linkers*

For investigating several parameters of the various monomers, such as hydrolytic stability, partition coefficient and incorporation efficiency, we have standardized a separation and quantification method based on micellar electrokinetic chromatography. Fig. 1 gives a typical example of such separations: when investigating the incorporation efficiency of monomers and cross-linkers, the gel extracts were analysed by CZE in 50 m*M* SDS and revealed at 214 nm. This method allowed a clear separation of acrylamide from bisacrylamide, based on the different partition coefficients in the SDS micelle. The p*K* 4.6 Immobiline, admixed to the sample prior to injection, was used as an internal standard for quantification purposes.

Based on the results obtained by CZE, we established a degradation scale of the different monomers, as shown in Fig. 2A: it is seen that whereas almost all acrylamido derivatives exhibit first-order degradation kinetics, one of them

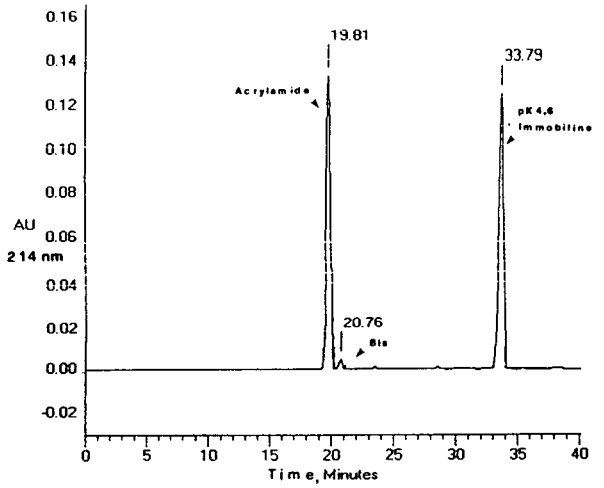


Fig. 1. Representative CZE analysis of ungrafted monomers. After eluting from the gel and adding the internal standard (2 m*M* p*K* 4.6 Immobiline), the monomer mixture was analysed by CZE in a 50 cm × 75 μm I.D. fused-silica capillary at 4000 V, 31 μA and room temperature. The buffer was 100 m*M* Tris–borate–50 m*M* SDS (pH 9.0). The sample was injected by gravity for 10 s. Detection was at 214 nm. The numbers on each peak represent the transit time.

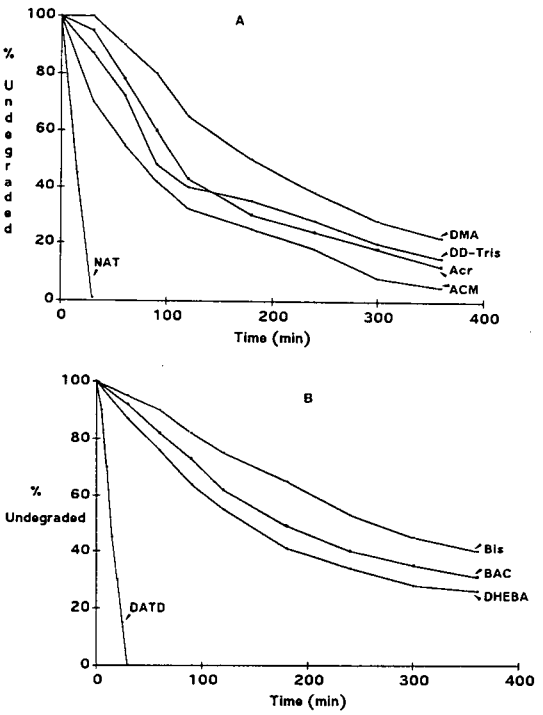


Fig. 2. Kinetics of hydrolysis of different acrylamide monomers (A) and cross-linkers (B). Hydrolysis has been performed in 0.1 *M* NaOH at 70°C for the times indicated. The amounts were assessed by harvesting triplicates at each point, neutralizing and injecting into the CZE instrument (Waters Quanta 4000). Conditions: 100 m*M* borate–NaOH buffer (pH 9.0), 15 kV, 86 μA at 25°C. Uncoated fused-silica capillary (50 cm × 75 μm I.D.). (A) Hydrolysis rate of different monomers, as follows: NAT = Trisacryl; Acr = acrylamide; MMA = monomethylacrylamide; DMA = N,N-dimethylacrylamide; ACM = acryloylmorpholine; DD-NAT = dideoxy-Trisacryl. Note that whereas all other monomers exhibit first-order kinetics, NAT follows zero-order degradation kinetics. (B) kinetics of hydrolysis of different cross-linkers. Abbreviations: Bis = N,N′-methylenebisacrylamide; DHEBA = N,N′-(1,2-dihydroxyethylene)bisacrylamide; DATD = N,N′-diallyltartardiamide; BAC = N,N′-bisacrylylcystamine. Note that whereas all other cross-linkers exhibit first-order kinetics, DATD follows zero-order degradation kinetics.

(Trisacryl) shows zero-order kinetics, suggesting that such a monomer is intrinsically unstable. Similar results were obtained with the four different cross-linkers (Fig. 2B): whereas most of them exhibit first-order degradation kinetics, as expected, one of them, DATD, displays a zero-order degradation process, suggesting that such a monomer, just like Trisacryl, is intrinsically unstable.

A unique picture emerges when the stability of the same monomers is analysed not as free species, but incorporated into the polymer network. For this purpose, all monomers were cross-linked with Bis and polymerized into beads, subjected to hydrolysis and then titrated by frontal analysis (this titration, being a chromatographic process, can only be performed with pearls, not with continuous beds). Fig. 3A shows the degradation kinetics of the monomers into the polymer phase, on alkaline degradation. It is now seen that poly(DMA) is extremely resistant to hydrolysis, as compared with both a polyacrylamide and a poly(Trisacryl). Whereas polyacrylamide, after 2 h of hydrolysis, is already degraded 30%, poly(DMA) exhibits only 0.07% hydrolysis. Hence there is a 500-fold difference between the susceptibility to degradation of the two classes of matrices. Even when prolonging the incubation to 60 h, poly(DMA) shows only 1.22% amido groups hydrolysed. Such a unique behaviour prompted an investigation of the hydrolysis rate also under acidic conditions. As shown in Fig. 3B, the hydrolysis rates in an acidic environment are accelerated by a factor of three compared with analogous conditions in NaOH. In any event, the excellent resistance to hydrolysis of poly(DMA) is confirmed even under acidic conditions.

We next established a hydrophobicity scale, based on partitioning in water–1-octanol phases and determining the remaining concentration in the aqueous phase by CZE. Table I summarizes the results for all the monomers and cross-linkers investigated. It is seen that the $P$ values span all ranges, from extreme hydrophilicity (for Trisacryl $P = 0.01$) to extreme hydrophobicity (for BAC $P = 10$). Fortunately, most values lie in the range $P = 0.2$–$0.4$, *i.e.*, acceptable values for still producing hydrophilic matrices.

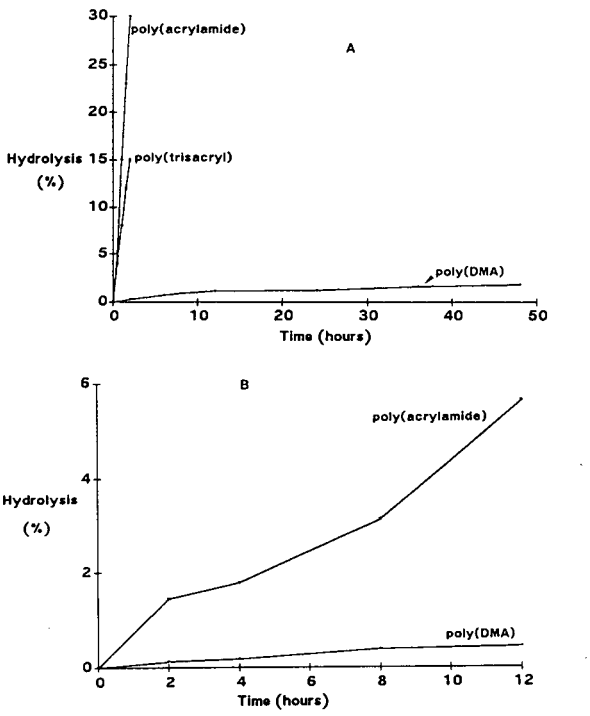


Fig. 3. Hydrolysis kinetics of different monomers after incorporation in a gel matrix. The extent of hydrolysis was assessed by measuring the equivalents of acrylic acid liberated in the polymer beads by frontal analysis. These equivalents were converted into the percentage of total amide groups hydrolysed in the polymer. (A) hydrolysis in 0.1 *M* NaOH at 70°C for up to 60 h. Poly(DMA) = polydimethylacrylamide. Note that there is a 500-fold difference in reactivity between polyacrylamide and poly(DMA). (B) Hydrolysis kinetics of poly(DMA) and polyacrylamide under acidic conditions (70°C, 0.1 *M* HCl) for up to 12 h.

*Photopolymerization*

Another important aspect of polyacrylamide chemistry is the correct choice of the catalyst system. We have recently found that chemical polymerization with the redox couple peroxodisulphate–TEMED is oxidizing, as it produces N-oxide species on all amino groups present in solution. Such N-oxides, during the electrophoretic analysis, can easily oxidize free –SH groups in proteins migrating through the gel phase [24]. We therefore reinvestigated photopolymerization, especially with riboflavin, and found that photoinitiation indeed occurs without concomitant oxidation [8,25].

TABLE I

PARTITION COEFFICIENTS OF MONOMERS AND CROSS-LINKERS

| Compound | Partition coefficient ($P$) |
|---|---|
| *Monomers* | |
| Trisacryl | 0.01 |
| Acrylamide | 0.2 |
| Monomethylacrylamide | 0.38 |
| Dimethylacrylamide | 0.5 |
| Acryloylmorpholine | 0.78 |
| Dideoxy-Trisacryl | 0.896 |
| *Cross-linkers* | |
| DATD | 0.18 |
| DHEBA | 0.27 |
| Bis | 0.82 |
| BAC | 10 |

Another catalyst system that we are currently evaluating is photoinitiation with methylene blue, coupled to the redox system toluenesulphinate–diphenyliodonium chloride. This system has some unique properties, as shown below. First, we found that the monitoring of the rate of photobleaching (*i.e.*, dye destruction during polymerization under light irradiation) gives a precise indication of the extent of conversion of monomers into the polymer phase. This is shown in Fig. 4: photobleaching was assessed by transferring the polymerization cassette (made of two microscope slides with a 0.5 mm gasket as spacer) into the spectrophotometer at the times indicated, and conversion efficiency was measured by extracting the gel and determining the ungrafted monomers by CZE. It is seen that, with this catalyst system, 70% conversion is obtained after 5 min of irradiation and >95% conversion is achieved after 50 min, when the dye is almost completely bleached. Hence the measurement of photobleaching appears to be a simple and reliable method for assessing the rate of polymer formation.

Gels obtained by photopolymerization also exhibit unique viscoelastic properties: as shown in Fig. 5, the elastic modulus of methylene blue-polymerized gels is better than that of peroxodisulphate gels, which in turn is considerably higher than that of peroxodisulphate gels in the

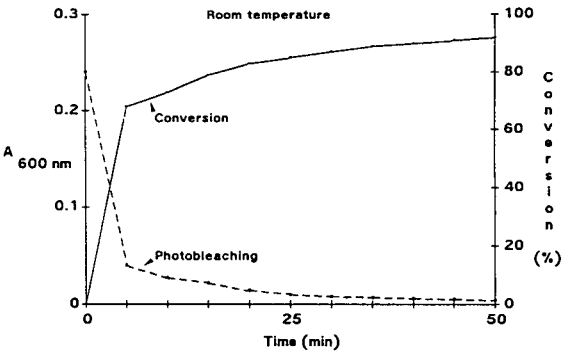


Fig. 4. Correlation between dye photobleaching and conversion efficiency. Photobleaching was assessed spectrophotometrically. For the incorporation efficiency, aliquots were harvested at 5-min intervals along the illumination curve, the monomers extracted, separated by CZE and determined as in Fig. 1. Note the extremely high incorporation efficiency in the first few minutes of illumination (70% in only 5 min), followed by a very slow rate of monomer uptake. Conversions >95% are ensured on illumination for 1 h in gel thicknesses up to 1 mm.

case of lateral aggregation. It should be noted that there is no contradiction between Figs. 4 and 5. In the former, we stated that 70% conversion was obtained in only 5 min. In Fig. 5, it is seen that the elastic modulus (which also is an indicator of the extent of conversion) reaches a plateau in 4–5 h for methylene blue, and in only 1 h for peroxodisulphate. It should be remembered that the conversion rate, in all

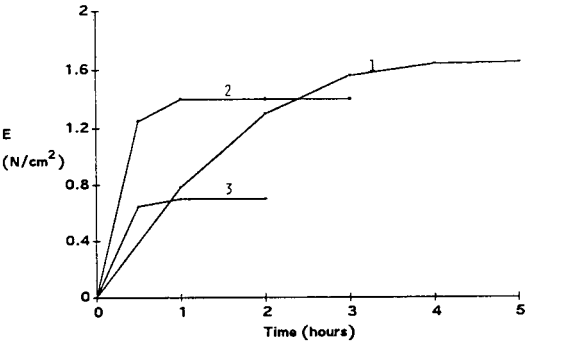


Fig. 5. Dependence of the elastic modulus ($E$, in N/cm$^2$) on the polymerization time in the case of methylene blue polymerization (1), peroxodisulphate (2) and peroxodisulphate in the presence of laterally aggregating agents (3). In the last instance the gel was chemically polymerized in the presence of 2% PEG 10 000. Note that although a plateau is reached at a slower rate, the best elastic properties are exhibited in the case of photopolymerization.

photopolymerization processes, is thickness dependent (which, of course, is not the case in peroxodisulphate-driven polymerization), as the outer liquid strata in the gel cassette absorb much of the incident light. In order to use the dynamometer, we were forced to adopt a 1-cm layer thickness, as opposed to 0.5 mm in Fig. 4.

We next investigated the Phantom modulus of methylene blue gels as a function of the percentage of cross-linker and correlated it with protein migration rates in the gel phase. As shown in Fig. 6, the Phantom modulus (expressed in $N/mm^2$) reaches a maximum at 5% cross-linker; conversely the migration velocity of proteins (expressed in mm/min) reaches a minimum at the same 5% cross-linking value. This is a unique observation and fully confirms the data first proposed by Fawcett and Morris in 1966 [26] that, for any family of %T gels, a minimum of porosity is always found at 5% cross-linker. These data also suggest another important correlation: a good "elastic body" (at least with polyacrylamides) is also a matrix exhibiting a minimum of porosity.

Another unique aspect of photoinitiation is illustrated in Fig. 7. It is well known that, in peroxodisulphate initiation, the polymerization efficiency decreases at acidic pH values (although the conversion had not been assessed before). In

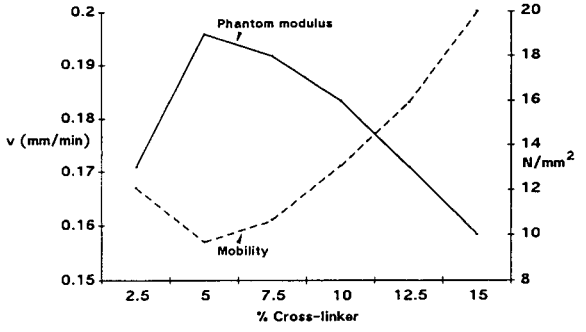


Fig. 6. Comparison between the gel elastic properties (Phantom modulus) and porosity as a function of percentage of cross-linker at constant %T. The gel porosity was assessed by measurement of the velocity of a protein marker (human serum albumin). The Phantom modulus data were measured with a dynamometer. The values on the scale of elastic measurements (in $N/mm^2$) should be multiplied by $10^3$. Note that the minimum of mobility and the maximum of elasticity coincide at 5%C.

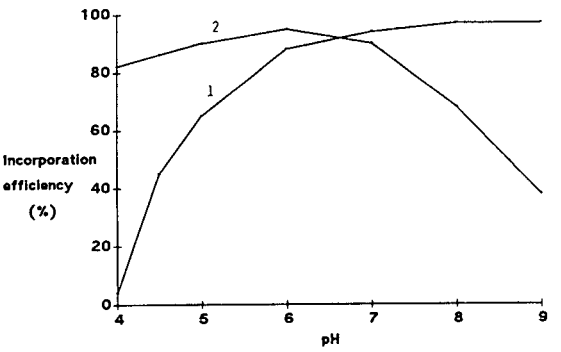


Fig. 7. Conversion efficiencies *vs.* pH of the gel solution in the cases of peroxodisulphate (1) polymerization and riboflavin (2) catalysis. The incorporation efficiencies were assessed in 5%T, 4%C gels after a standard polymerization time of 1 h at room temperature by extracting the ungrafted monomers and determining them in a CZE run (see Fig. 1). All solutions were prepared as follows: in 100 m*M* acetate buffer (pH 4 and 5); in 100 m*M* phosphate buffer (pH 6 and 7); in 100 m*M* Tris–chloride buffer (pH 8 and 9). All the various pH values were readjusted to the corrected pH after addition of TEMED (which usually increased the solution pH by *ca.* 0.5).

Fig. 7, it is shown that a plateau is reached in the pH range 7–9 (with maximum incorporation efficiency of *ca.* 95%), but that incorporation decreases steadily with decreasing pH until, at pH 4.0, no gelation occurs. An opposite behaviour is shown in riboflavin catalysis: the efficiency decreases substantially at alkaline pH values, with maximum incorporation efficiency around pH 6.0–6.4. However, in the entire pH 4–7 interval, gelation still occurs and the incorporation efficiency is still around 85–90% even at adverse pH values, such as pH 4 and 5. This offers a new insight into polyacrylamide catalysis: by selecting the proper catalyst (riboflavin in the pH range 4–6.5 and peroxodisulphate in the pH range 6.5–9), one can ensure satisfactory conversion efficiency throughout the entire operational pH interval. This is a novel finding not reported previously.

*Laterally aggregated gels*

This is a novel aspect of polyacrylamide chemistry, which we have recently discovered [7]. We shall highlight here some of the results obtained. It should be emphasized that, in the classic Ornstein–Davis system [2,3], the only

way to obtain highly porous polyacrylamide matrices was to increase dramatically the amount of cross-linker (%C) at a fixed and low total amount of monomers (%T). As demonstrated by Righetti *et al.* [18], 3%T gels, with up to 60%C cross-linking can reach average pore diameters as high as 500–600 nm. However, such gels are of no practical interest as they are highly hydrophobic and exude water, so that they represent a hazard (electric short-circuits) in open-face gel slab electrophoresis. We have recently found that, if polymerization is conducted in presence of a preformed, hydrophilic polymer in solution, a unique phenomenon occurs, which we have termed "lateral chain aggregation", resulting in a very large increase in pore size at normal values of %T and %C, *e.g.*, 5–6%T and 4–5%C. The process can be monitored by an increased gel turbidity as "lateral chain aggregation" progresses, as shown in Fig. 8. A typical polymer inducing such aggregation is polyethylene glycol (PEG), with an efficiency correlated with the mean molecular mass: a PEG 20 000 polymer drives the full transition (plateau level) already at 1.5% in solution, whereas *ca.* 10% PEG 2000 is needed for a similar transition (Fig. 8).

In Fig. 9, we have depicted what we think could happen during such a unique polymerization process: in the absence of PEG, the gel is truly a "random meshwork of fibres", as previous literature data suggest. This would give a

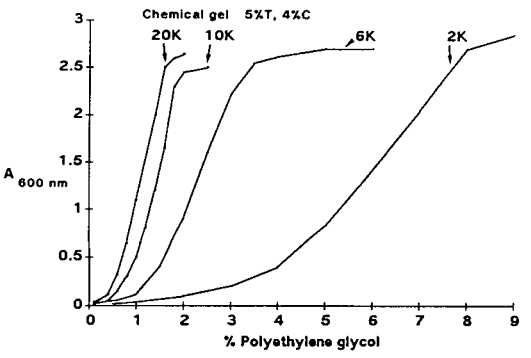


Fig. 8. Gel turbidity *vs.* type and percentage of laterally aggregating agents. 5%T, 4%C gels were polymerized in the presence of increasing amounts of PEG 2000 (2K), 6000 (6K), 10 000 (10K) and 20 000 (20K). The gel opacity was read on a Varian spectrophotometer at 600 nm.

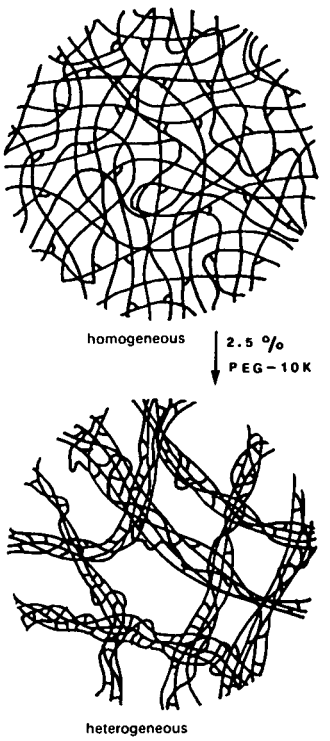


Fig. 9. Hypothetical model for "laterally aggregated" gels. The top drawing could represent the structure of a control gel (a random meshwork of fibres). This gel is homogeneous in the sense that all fibres have random orientations in the three-dimensional space. The bottom drawing could represent a gel polymerized in the presence of hydrophilic polymers. Owing to bundling of individual fibres (chain clustering), the average porosity is greatly increased.

three-dimensional structure resembling the "homogeneous" gel at the top of Fig. 9, consistent with a minimum of porosity. Conversely, in the presence of PEG, bundling or "lateral chain aggregation" occurs, resulting in a matrix with a much increased pore size (Fig. 9, bottom). Note that, in some ways, such a structure could resemble that of agaroses, known to form helices and super-helices (aggregates or pillars of 7–11 helices) on gelation. How can PEG [and other hydrophilic polymers, such as polyvinylpyrrolidone, poly(vinyl alcohol) and hydroxymethylcellulose] induce such a transition? We believe it to be mostly due to inter-chain hydrogen bonding, as such a process is greatly inhibited by the presence of 8 *M* urea in solution and by high temperatures. As PEG is a highly

hydrophilic molecule (coordinating up to 1.5 molecules of water per oxygen residue), as the nascent polyacrylamide strings grow in solution they tend to become hydrogen bonded among themselves, owing to the water-sequestering action of PEG. Once the cross-linking event has occurred, the "bundles" of chains are then irreversibly structured in the gel three-dimensional structure.

That our model in Fig. 9 might not be too far from reality is demonstrated by Fig. 10: by freeze-fracture, scanning electron microscopy, we can observe a smooth, apparently non-porous structure in a regular, control polyacrylamide (6%T, 4%C; Fig. 10A). In the presence of 0.8% PEG 10 000 in solution, a pitted and irregular surface appears (Fig. 10B). When the level is increased to 2% and 2.5% PEG (Fig. 10C and D, respectively), two phenomena are evidenced: fibres of 200–300 nm diameter appear, delimiting "holes" of *ca.* 500 nm diameter. The presence of such large bundles explains the light-scattering properties of such gels. However, in contrast to highly cross-linked gels, which reach similar porosities but are totally useless (at least for electrokinetic processes), the present gels appear to be excellent for electrophoretic fractionation. We have run, in such matrices, double-stranded DNAs up to 22 000 base pairs (bp), a size that cannot even penetrate a regular 6%T, 4%C gel (unpublished work). Moreover, in such highly porous matrices, focusing (including immobilized pH gradients) occurs in a fraction of the time needed in conventional matrices. Thus we believe that such a novel matrix will open up unique possibilities in electrophoretic separations exploiting polyacrylamide matrices.

## DISCUSSION

### *Monomer chemistry*

For at least 15 years our laboratory has been connected with the study of polyacrylamide gels and the development of new matrices. The first impulse came from an invitation by NASA (Dr. R. Snyder, Huntsville, AL, USA) in 1979, at that time strongly interested in developing space electrophoresis. We set out to measure the maximum pore size that could be produced in agarose and polyacrylamides under earth gravity. We derived an empirical equation, linking the pore

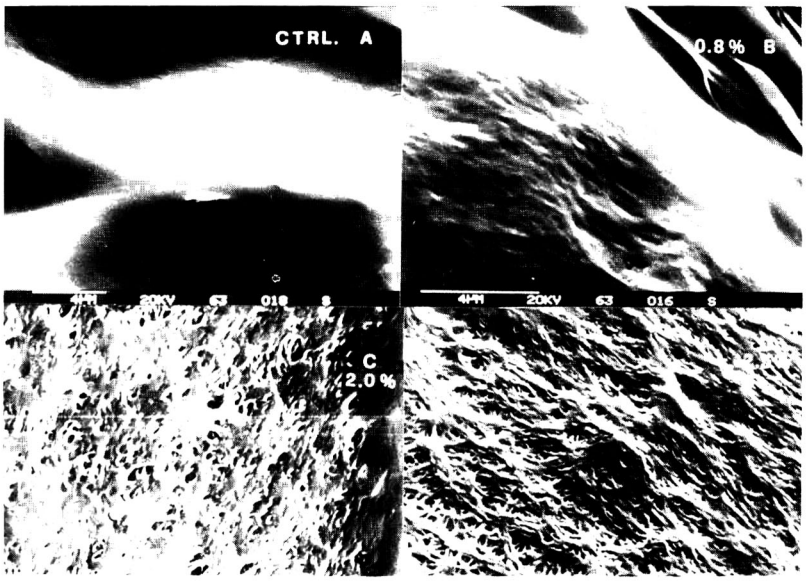


Fig. 10. Scanning electron micrographs of (A) control and (B–D) "laterally aggregated" gels. (B) 5%T, 4%C gel in the presence of 0.5% PEG 10 000; (C) same, but polymerized after adding 2% PEG 10 000; (D) same, but with 2.5% PEG 10 000 added. Note the smooth surface of the control gel, with no visible pores, and the progressive opening of the pore sizes in (C) and (D). In the last gel (D) the surface is seen to be made by regular bundles of 2–300 nm thickness, delimiting "holes" of *ca.* 0.5 $\mu$m diameter.

diameter $p$ of agarose gels to their concentration $C$, in the form [18]

$$p = 140.7C^{-0.7}$$

At that time, there was a great confusion regarding this dependence, and all sorts of relationships were proposed, with factors $C^{-0.3}$, $C^{-0.5}$ and even $C^{-1}$. As it turned out, we were fairly close to the true dependence, established to be $C^{-0.75}$ [27], as also proposed by Slater *et al.* [28]. We then set out to study the properties of highly cross-linked gels and established the fact that one cross-linker, diallyltartardiamide, was in all practical effects an inhibitor of gel polymerization, thus ending a curious myth in biochemical analysis [19].

In 1981, we set out to reinvestigate gel polymerization kinetics as a function of temperature [15], amount and type of cross-linker [16] and type of catalyst [17]. Some basic rules were defined in those studies, such as the fact that the polymerization temperature strongly affects the quality of the final gel: polymerization at low temperatures (as recommended by several workers) resulted in poor conversion of the monomers into the polymer and in a modest incorporation of the cross-linker (Bis), which seems to form poorly reacting clusters at 5–10°C. Polymerization at 50°C was advocated and in fact adopted for achieving proper conversion of the Immobiline chemicals in the IPG technique [29]. However, it was only in 1984 that we first proposed a new reacting couple: acryloylmorpholine as a monomer and bisacrylylpiperazine as a cross-linker [20]; the idea for adopting these new monomers was based on the observation that they are amphiphilic, so that, once incorporated in a gel, they could favour reswelling also in aqueous–organic solvents. Later, we also adopted Trisacryl as a highly hydrophilic monomer [30], as simultaneously advocated by Kozulic *et al.* [31] for DNA analysis. For the reasons given in the Introduction, it is now clear that we were far from having reached a satisfactory solution. Gels based on the acryloylmorpholine monomer turned out to be too hydrophobic and to be opaque. Conversely, gels formed with Trisacryl were extremely hydrophilic but extremely susceptible to hydrolytic degradation even in mildly alkaline solutions (see Figs. 2 and 3). A novel, unique monomer seemed to be dimethylacrylamide: as shown in Fig. 2, it is fairly resistant to hydrolysis as a free species and extremely resistant in the polymer phase (Fig. 3A and B). We had in fact already adopted such a matrix, in a commercial preparation called Hydrolink, which however could only be used to some extent for DNA separations [32]. All our attempts at using it for protein separations were unsuccessful, as the monomer is already too hydrophobic ($P = 0.5$, see Table I). Hence the search for novel monomers has to continue; we have fund the rules that govern strong hydrolytic stability, but we still have to couple it to strong hydrophilicity, an essential feature for proper electrophoresis of proteins. Concerning the chemistry of cross-linkers, clearly DATD should be discarded, as discussed above. Also BAC should be used with great caution; given its extreme hydrophobicity, its use in protein separations should be discouraged. In fact, when first advocated, BAC was adopted only for nucleic acid analysis, as such polymers are not prone to hydrophobic interactions with the matrix.

*Photopolymerization*

Photopolymerization chemistry has now been well elucidated, and it appears to offer some unique features that could render it more preferable in biochemical applications than chemical polymerization: this process proceeds with a very high polymerization rate; by optimizing the reaction parameters very high conversions of monomer into the polymer phase can be obtained; photopolymerization does not need high-temperature conditions and proceeds successfully at room temperature; (d) photosensitizers, which can be used in very low concentrations compared with chemical initiators, do not oxidize proteins in gel matrices; and by varying the incident light intensity it is possible to produce gels of graded porosities. A unique finding appears to be the inverse proportionality between the elastic modulus and the gel pore size, as illustrated by the two curves in Fig. 6. As is known [26], the pore size of the polyacrylamide gels depends in a

non-monotonic fashion on the cross-linker concentration. The lower curve in Fig. 6 is the pore size evaluation performed by electrophoresis of protein markers for gel matrices polymerized at different cross-linker concentrations. The upper curve displays the dependence of the elastic modulus of polyacrylamide gels on the cross-linker concentration. As one can appreciate, in the latter instance a non-monotonic dependence has been obtained, with a maximum at 5%C, corresponding to the mobility (*i.e.*, porosity) minimum at the same concentration of cross-linker. Hence an increase in cross-linker concentration leads to an increase in elastic modulus and to a decrease in pore size at low concentrations of the cross-linker and to opposite dependences at concentrations higher than 5%, which illustrates the inverse proportionality of elastic modulus and pore size. Note that the change in the dependence of the elastic modulus on the cross-linker concentration is found to be connected with the transition from transparent to opaque gels. Thus, curiously, a "good elastic body" appears to be also a "body" exhibiting minimum permeability, both properties being coincident at 5%C (see also Fig. 5). A possible explanation could be that, at 5%C, the distribution of cross-links along the chains is fairly uniform, resulting in chain segments (or springs) possessing a good elastic memory. At high %C values, chain clustering or bundling could result in a loss of elastic memory and an inability to respond to a compression stress.

*Laterally aggregated gels*

How can the pore size of polyacrylamide matrices be manipulated? According to the Ogston model [33],

$$R = 1/\sqrt{4\pi nL}$$

where $R$ is the radius of a sphere which can be accommodated within the "open" spaces of a gel, $L$ is half the length of the gel fibre and $n$ is the number of fibres per $cm^3$ of gel volume. Note, however, that the above equation can only be applied for networks consisting of very long fibres having a negligible thickness, *i.e.*, $r = 0$, here $r$ is the fibre radius). In our case, given the substantial thickness of the gel fibres, their radius has to be subtracted from the computed value of the most frequent pore size population [34]. Thus,

$$R = (1/\sqrt{4\pi nL}) - r$$

There appear to be two ways of accommodating larger objects in a gel network (thus increasing the pore size): either by reducing the fibre length or by decreasing the number of fibres per unit volume (or both!). The manipulation of pore sizes in polyacrylamides by maintaining %T constant and progressively increasing %C seems to rely on the simultaneous shortening of $L$ and thickening of the fibre diameter. Thus Fawcett and Morris [26] suggest that, while a 5%T gel has an average fibre diameter of 0.5 nm, a high %C gel has an upper value of fibre diameter of 6 nm. The procedure adopted by us is based on a different strategy: we drastically diminish the number of fibres per unit gel volume, while possibly not reducing the average $L$ value (as %C is low and constant). This is accomplished by gelling the monomers in the presence of a hydrophilic polymer; we believe that such a polymer (notably PEG 10 000 or 20 000) acts by sequestering the water to the growing chains and forcing them to form large bundles, held together by preferentially (but perhaps not solely) interchain hydrogen bonds. It is in fact known that PEG coordinates large amounts of water around its coil (on the average, 1.5 water molecules per oxygen atom in the chain); this perturbation of the solvent phase could force the growing polyacrylamide strings to seek hydrogen bonding among themselves, rather than with the surrounding solvent. Once such large chain aggregates are formed, they are then stabilized in an irreversible structure by the crosslinks.

Fig. 9 gives a hypothetical representation of this "bundling" phenomenon. How large could such bundles be? We believe that the thickness of such fibres is much more than the 6 nm estimated by Fawcett and Morris [26]; a rough estimate of the diameters of these fibres, as clearly visible in the electron micrographs in Fig. 10D, suggests values of several hundred nanometres, in agreement also with the strong

light-scattering properties of such "laterally aggregated" gels. The process of drastically reducing $n$ (the number of individual fibres per unit volume) has to have as a consequence enlargement of the average pore diameters; again, by measurements of pore sizes in Fig. 10D, we obtain an average value of 0.5 $\mu$m. We believe these values to be real, not artefacts of the sample manipulation prior to microscopic observations. The important step here was to equilibrate all samples in 2.5% PEG 10 000 prior to freezing and lyophilizing; in the absence of cryoprotectant, the gel membranes "exploded" and cavities as large as 100 $\mu$m could be seen. As a final remark, we emphasize that Gersten *et al.* [35] have also reported polymerization of polyacrylamide gels in presence of various hydrophilic polymers. Curiously, however, they did not report the huge increase in pore size that we experienced; on the contrary, they seemed to observe a general retardation of migration of SDS–protein complexes. Therefore, in the absence of additional data, it is impossible to compare our data with those of Gersten *et al.* [35].

ACKNOWLEDGEMENTS

This work was supported in part by grants from the Agenzia Spaziale Italiana (ASI), the European Space Agency (ESA) and the Consiglio Nazionale delle Ricerche (CNR, Rome), Progetti Finalizzati Chimica Fine II and Biotecnologie e Biostrumentazione. We thank Drs. A. Alloni and P. De Besi for help with the experiments reported in Fig. 2A and B and Dr. T. Lyubimova for performing the viscosity measurements.

REFERENCES

1 S. Raymond and L. Weintraub, *Science (Washington, D.C.)*, 130 (1959) 711–712.
2 B.J. Davis, *Ann. N.Y. Acad. Sci.*, 121 (1964) 404–427.
3 L. Ornstein, *Ann. N.Y. Acad. Sci.*, 121 (1964) 321–349.
4 S. Hjertén, *J. Chromatogr.*, 11 (1963) 66–70.
5 P.G. Righetti, *J. Biochem. Biophys. Methods*, 19 (1989) 1–20.
6 M. Chiari, M. Nesi, M. Fazio and P.G. Righetti, *Electrophoresis*, 13 (1992) 690–697.
7 P.G. Righetti, S. Caglio, M. Saracchi and S. Quaroni, *Electrophoresis*, 13 (1992) 587–595.
8 M. Chiari, C. Micheletti, P.G. Righetti and G. Poli, *J. Chromatogr.*, 598 (1992) 287–297.
9 B. Kozulic, K. Mosbach and M. Pietrzak, *Anal. Biochem.*, 170 (1988) 478–484.
10 P. Girot and E. Boschetti, *J. Chromatogr.*, 213 (1981) 389–396.
11 B. Kozulic, *Eur. Pat.*, 88810717.4 (1988).
12 C. Gelfi, P. De Besi, A. Alloni and P.G. Righetti, *J. Chromatogr.*, 608 (1992) 333–341.
13 R. Shorr and T. Jain, *Eur. Pat.*, 89107791.9 (1989).
14 C. Gelfi, P. De Besi, A. Alloni and P.G. Righetti, *J. Chromatogr.*, 608 (1992) 343–348.
15 C. Gelfi and P.G. Righetti, *Electrophoresis*, 2 (1981) 220–228.
16 C. Gelfi and P.G. Righetti, *Electrophoresis*, 2 (1981) 213–219.
17 P.G. Righetti, C. Gelfi and A. Bianchi-Bosisio, *Electrophoresis*, 2 (1981) 291–295.
18 P.G. Righetti, B.C.W. Brost and R.S. Snyder, *J. Biochem. Biophys. Methods*, 4 (1981) 347–463.
19 A. Bianchi-Bosisio, D. Loherlein, R. Snyder and P.G. Righetti, *J. Chromatogr.*, 189 (1980) 317–330.
20 G. Artoni, E. Gianazza, M. Zanoni, C. Gelfi, M.C. Tanzi, C. Barozzi, P. Ferruti and P.G. Righetti, *Anal. Biochem.*, 137 (1984) 420–428.
21 S. Terabe, *Trends Anal. Chem.*, 8 (1989) 129–134.
22 W.P. Purcell, in W.P. Purcell, G.E. Bass and J.M. Clayton (Editors), *Strategy of Drug Design: a Guide to Biological Activity*, Wiley-Interscience, New York, 1973, pp. 126–143.
23 M. Chiari, L. Pagani and P.G. Righetti, *J. Biochem. Biophys. Methods*, 23 (1991) 115–130.
24 P.G. Righetti, M. Chiari, E. Casale and C. Chiesa, *Theor. Appl. Electrophoresis*, 1 (1989) 115–121.
25 M. Chiari, C. Ettori, P.G. Righetti, S. Colonna, N. Gaggero and A. Negri, *Electrophoresis*, 12 (1991) 376–377.
26 J.C. Fawcett and C.J.O.R. Morris, *Sep. Sci.*, 1 (1966) 9–23.
27 P.D. Grossman and D.S. Soane, *J. Chromatogr.*, 559 (1991) 257–266.
28 G.W. Slater, J. Rousseau, J. Noolandi, C. Turmel and M. Lalande, *Biopolymers*, 27 (1988) 509–514.
29 P.G. Righetti, K. Ek and B. Bjellqvist, *J. Chromatogr.*, 291 (1984) 31–42.
30 P.G. Righetti, C. Gelfi, M.L. Bossi and E. Boschetti, *Electrophoresis*, 8 (1987) 62–70.
31 M. Kozulic, B. Kozulic and K. Mosbach, *Anal. Biochem.*, 163 (1987) 506–512.
32 P.G. Righetti, M. Chiari, E. Casale, C. Chiesa, T. Jain and R. Shorr, *J. Biochem. Biophys. Methods*, 19 (1989) 37–49.
33 A.G. Ogston, *Trans. Faraday Soc.*, 54 (1958) 1754–1757.
34 D. Tietz, *Adv. Electrophoresis*, 2 (1988) 109–170.
35 D.M. Gersten, H. Kimball and E. Bijwaard, *Anal. Biochem.*, 197 (1991) 59–64.

*Journal of Chromatography*, 638 (1993) 179–186
Elsevier Science Publishers B.V., Amsterdam

CHROM. 24 925

# Electrically controlled electrofocusing of ampholytes between two zones of modified electrolyte with two different values of pH

J. Pospíchal*, M. Deml and P. Boček

*Institute of Analytical Chemistry, Czech Academy of Sciences, Veveří 97, 611 42 Brno (Czech Republic)*

ABSTRACT

A method is described for the separation and concentration of ampholytes from their mixtures with other ionic species. In a quadrupole electromigration column, two zones of different pHs are created by using controlled flows of the solvolytic ions ($H^+$ and $OH^-$) from appropriate electrode chambers at opposite sides of the column. Thus, a time-variable interface is created between two zones with a sharp change of pH. The position of the interface in the column, the direction and velocity of its movement and the difference in pH across the interface–pH gap can be adjusted by electric currents. This arrested interface is reasonably stable with time and has the following separation properties: ampholytes with p*I* values between the pHs of both zones are focused into a zone at interface; and other types of ampholytes and other weak or strong ions are not trapped at the interface. The basic properties of the above system are described and experiments showing the effects of the type of sample (ampholyte, weak ion), time, the concentration of primary electrolyte and the additives changing the viscosity, solubility or p*I* of ampholyte are given. The method proposed offers the following advantages: the ampholytes in the sample may be concentrated several hundred-fold; the focused zones have sharp boundaries (zones 0.1 mm in length were prepared) and high concentrations of the trapped species; the zone of a trapped ampholyte contains the ampholyte proper and simple ions of primary electrolyte (KCl) only; and the zones can be shifted to any selected position in the column (potentially to the location of a detector cell or a collection device).

## INTRODUCTION

Separation and concentration of amphoteric substances play an important role in biochemistry. Both steps can be carried out gently in one run using an electromigration separation method such as isotachophoresis (ITP) or isoelectric focusing (IEF). A free solution variant of these techniques is especially valuable for the isolation of enzymes and peptides without losing their biological activity.

In ITP, when the steady state is reached, the substances separated according to their effective mobilities migrate through the column in the form of consecutive adjacent zones. To prevent remixing of the zones with the separated impurities during collection, spacers are used, spatially separating the zones from each other [1]. The selection of suitable spacers, with known mobilities and p*K* values, and the effective mobility of the substance of interest, complicates this method.

IEF, in contrast to ITP, has been accepted as a standard procedure for characterizing and separating ampholytes from their mixtures [2]. Substances, separated according to their p*I*s in the pH gradient created by a mixture of synthetic carrier ampholytes (SCAMs) are always contaminated by SCAMs, which must be removed by other separation techniques, if necessary.

The cost of SCAMs and their ability to create complexes with analytes led to attempts to create stable pH gradients without SCAMs. Such gradients were created by self-diffusion or mixing of

* Corresponding author.

0021-9673/93/$06.00 

buffers having different pHs [3–8]; electrolysis or electromigration separation of a mixture of buffers [9–17]; or by changing the p$K$ value of the buffering component by controlling the temperature, dielectric constant and/or complexation [18–21].

The preparation of a pH gradient by diffusion or mixing of two buffers of different pH belongs to the oldest techniques. MacDonald and Williamson [3] created these gradients by using HCl or citric acid on one side and NaOH or sodium citrate on the other side of the separation chamber. A sample, dissolved in distilled water, was applied between them. Kolin [4] used acetate or barbital buffer with the pH adjusted with HCl, Hoch and Barr [5] used phosphate buffer. The advantages of this arrangement are the very short time of analysis (Kolin reported a few minutes) and simple preparation; the disadvantage is movement of the gradient under the influence of electric current. An improvement in the system stability was achieved by Martin and Hampson [6] and Rilbe [7], by maintaining constant flows of the buffer components from electrode chambers. This was achieved in Rilbe's steady-state rheoelectrolysis by mixing the contents of electrode vessels. Stable systems were suggested and verified by computer simulation and experimentally by Mosher *et al.* [8], who pointed out that the stability of the system decreases with increasing pH differences on both sides of the column.

pH gradients created by electrolysis are used on the evolution of solvolytic ions by the decomposition of electrolyte on the electrodes. Solvolytic ions penetrate into the column and thus create a pH gradient. This is the principle of classical IEF, as was suggested by Svensson [9]. Williams and Waterman [10] used a fourteen-chamber apparatus, Tiselius [11] used his classical apparatus and Sova [12] developed a large-scale apparatus (tens of litres in volume) for industry. The theory describing such a system was published by Hagedorn and Kuhr [13].

pH gradients created by moving boundary electrophoresis of mixtures of strong and weak acids, bases or simple ampholytes were used by Petterson [14], Stenmann and Grasbeck [15] and Chrambach and Nguyen [16]. This method, called buffer electrofucusing, gives sufficiently stable and linear pH gradients. Buffer premixtures are available commercially. The theory, developed by Hjelmeland and Chrambach [17], enables one to find the optimum composition of the buffer mixture; a further advantage is the possibility of gradient engineering.

Luner and Kolin [18], Lundahl and Hjertén [19] and Lochmüller *et al.* [20] created pH gradients based on the dependence of the p$K$ value of the buffer on temperature. A temperature gradient superposed along the column with electrolyte of a constant composition gives a rise to a pH gradient. The preparation of the gradient is very rapid and, as mentioned by Kolin, the p$I$ of the separated substance can be determined from the temperature of the solution.

Troitski *et al.* [21] used the dependence of the p$K$ value of the buffering component on the dielectric constant or on complexation with polyols. Complexes of polyols and boric acid were also used for continuous IEF fractionation.

All the methods of IEF described so far can be characterized by a situation where, in the steady state, a balance exists between the diffusion flow of an ampholyte out of a zone and electromigration flow into it. The result is a Gaussian distribution profile of concentration of the focused substance. For the separation and subsequent isolation it is convenient to create a sharp zone of the substance with constant concentration, similarly to ITP. This requirement is fulfilled in the method of Righetti *et al.* [22], where the sample components are separated by isoelectric membranes in a multi-compartment electrolyser. Only amphoteric species with p$I$ values that lie between the pH values of the neighbouring membranes can be found in the respective compartment. The precision of the determined p$I$ values was 0.001 pH unit.

In this paper, an isoelectric separation method in free solution is suggested, where the zone of a purified ampholyte is sharp, *i.e.*, its concentration profile is pulse-like, it has a constant composition and contains in addition to focused substances only easily separable low-molecular-mass ions.

## THEORETICAL

It is of key importance for the study of the separation and isolation of substances in pH gradients to investigate first the fundamental aspect, *i.e.*, the neutralization reaction boundary, where sharp pH changes occur. Such a boundary, for the accomplishment of successful separations of ampholytes, must have the following separation properties: weak and strong acids and bases pass through the boundary; ampholytes with p*I* values within the range of pH values on both sides (pH gap) are trapped at the boundary; and ampholytes with p*I* values outside the pH gap pass through the boundary. Further, the boundary should also fulfil the following demands: it must have fixed position in the column; the span of the pH gap must be regulated; and the boundary must be sufficiently stable with time.

Let us discuss the properties of the boundary first. Without the presence of ampholytes in the electrolyte system, only one neutralization boundary can be created in the column. Its velocity is given by the magnitudes of the flows of solvolytic ions. With respect to the stoichiometry of the neutralization reaction, the boundary is stationary if the flows are equal, *i.e.*,

$$J_H = J_{OH} \quad (1)$$

where $J_H$ and $J_{OH}$ are flows of $H^+$ and $OH^-$ ions, respectively. To ensure some background conductivity along the column and to give the system the possibility of controlling the pH gap at the boundary, the presence of a primary (background) electrolyte (*e.g.*, KCl) in the column is necessary.

As shown in earlier work [23], the magnitude of the ion flows can be regulated in a column equipped with pairs of electrode chambers on each side. This enables one to control the magnitude of flow of $H^+$, $J_H$, by setting the ratio of the flows of $H^+$ and its co-ion on one side and the magnitude of the flow of $OH^-$, $J_{OH}$, by setting ratio of the flows of $OH^-$ and its co-ion on the other side. In such a way, the span of the pH gap is easily controlled and it changes symmetrically around *ca.* pH 7 for a strong electrolyte (KCl).

For the determination of the time stability of the boundary (system), it is convenient to start from a description of the system using flows of ions as shown in Fig. 1. In our considerations, we chose a case that is as simple as possible: the strong primary electrolyte, KCl, is modified from the left, anodic, side by a flow of cations $H^+$ and from the right, cathodic, side by a flow of anions $OH^-$. Hence from the anodic side, the flows of $H^+$ and $K^+$, $J_H$ and $J_K$, enter the boundary and the flow of $Cl^-$, $J_{Cl}$, leaves the boundary. From the right side, by analogy, there is input $J_{OH}$ and $J_{Cl}$ and output $J_K$. Owing to the presence of a chemical reaction at the boundary,

$$H^+ + OH^- \rightleftharpoons H_2O \quad (2)$$

the flows of $K^+$ and $Cl^-$ on the two sides of the stationary boundary are not equal:

$$J_K^A \neq J_K^C \quad (3)$$

The flows of potassium and chloride in modified zones can be derived from the knowledge of solvolytic flows. The anodic flow of potassium, $J_K^A$, is equal to the flow of potassium in the non-modified electrolyte, $J_K^P$, decreased by the flow of potassium replaced by $H^+$. The cathodic flow of potassium, $J_K^C$, is equal to the flow of

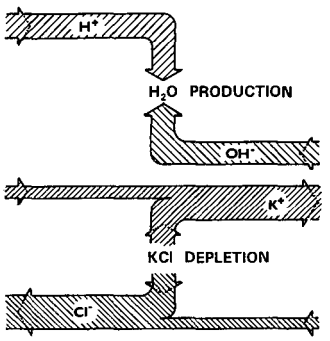


Fig. 1. Scheme of the flows of ions in the separation column. Anode is on the left, cathode is on the right. For further explanation, see text.

potassium in the non-modified primary electrolyte, $J_K^P$, which is decreased by the flow of potassium relevant to the flow of chlorides, replaced by $OH^-$, and increased by the flow of potassium, relevant to replacement by $OH^-$ Because the flows are substituted into the ratios of transference numbers, we can write

$$J_K^A = J_K^P - J_H^A \cdot \frac{T_K^{KCl}}{T_H^{HCl}} \quad (4)$$

$$J_K^C = J_K^P - J_{OH}^C \cdot \frac{T_K^{KCl} - T_K^{KOH}}{T_{OH}^{KOH}} \quad (5)$$

where $T_x^y$ is the transference number of ion $x$ in the electrolyte $y$. Similarly, we can derive for the flows of chloride in the cathodic and anodic part of the column:

$$J_C^C = J_C^P - J_{OH}^C \cdot \frac{T_C^{KCl}}{T_{OH}^{KOH}} \quad (6)$$

$$J_C^A = J_C^P - J_H^A \cdot \frac{T_C^{KCl} - T_C^{HCl}}{T_H^{HCl}} \quad (7)$$

For the depletion flows of the potassium and chloride from the boundary site, we can write

$$\Delta J_C = J_C^C - J_C^A; \quad \Delta J_K = J_K^C - J_K^A \quad (8)$$

By combining previous equations, we obtain the expressions

$$\Delta J_C = J_S \cdot \frac{T_{OH}^{KOH}(T_C^{KCl} - T_C^{HCl}) - T_H^{HCl} T_C^{KCl}}{T_H^{HCl} T_{OH}^{KOH}} \quad (9)$$

$$\Delta J_K = J_S \cdot \frac{T_H^{HCl}(T_K^{KCl} - T_K^{KOH}) - T_{OH}^{KOH} T_K^{KCl}}{T_{OH}^{KOH} T_H^{HCL}} \quad (10)$$

and thus

$$\Delta J_C = \Delta J_K = -J_S \cdot \frac{U_K U_C (U_H + U_{OH})}{U_H U_{OH}(U_K + U_C)}$$

$$= J_S \cdot \text{constant} \quad (11)$$

where $U_K$, $U_C$, $U_H$ and $U_{OH}$ are ionic mobilities of potassium, chloride, hydrogen and hydroxyl ions, respectively, and $J_S$ is flow of solvolytic ions $H^+$ or $OH^-$. From eqn. 11, it follows that depletion flows of potassium and chloride from the non-moving neutralization boundary are equal, and only neutral KCl is depleted from the boundary site. The depletion rate of KCl is dependent on the magnitudes of flows of solvolytic ions. The numerical value of the constant in eqn. 11 is 0.29, which means that 0.29 mol of KCl is depleted from the boundary per mole of neutralization water formed. Comparing the concentration of water (55.5 $M$) with the concentration of primary electrolyte (*e.g.*, 0.01 $M$), it is seen that the effect of neutralization water created on the boundary is negligible. The neutralization boundary behaves as an ideal sink of solvolytic ions and a source of ions of primary electrolyte, *e.g.*, $K^+$ and $Cl^-$, which maintains the background conductivity of the system. Because electric current passes through the boundary, depleted KCl must be replenished to a certain extent. This is possible only by diffusion from the surroundings of the boundary. With constant current, a diffusional flow of KCl, $J_{dif}$, must be equal to electromigration depletion:

$$J_{dif} = \Delta J_K = \Delta J_C \quad (12)$$

A break of the electric circuit at the boundary occurs with time, when the concentration of the background electrolyte (KCl) decreases to zero. This time and the variation of the concentration profile of KCl with time can be easily calculated if a model of linear diffusion is adopted, *i.e.*, with a constant gradient of concentration. For the evaluation of the time dependence of the concentration profile of the electrolyte along the $x$-axis, eqn. 13 can be used [24]:

$$C_{KCl} = C_0 - \frac{2\Delta J T^{1/2}}{(D\pi)^{1/2}} \cdot \exp\left\{-\frac{x^2}{4Dt} + \frac{\Delta J}{D} \cdot \text{erfc}\left[\frac{x}{2(DT)^{1/2}}\right]\right\} \quad (13)$$

where $C_0$ is the initial concentration of KCl, $D$ is the diffusion coefficient, $T$ is time and $\Delta J$ is the mass flow from the boundary. After rearrangement for $x = 0$ and $C_{KCl} = 0$, we obtain

$$t = \pi D \left(\frac{C_0}{2\Delta J}\right)^2 \quad (14)$$

It can be seen from eqn. 14 that the time stability of the boundary $t$ is proportional to the square of the concentration of primary elec-

trolyte and inversely proportional to the square of the depletion flow. There are possibilities for controlling the time stability, namely by decreasing the driving current, which decreases the absolute value of the depletion flow and yielding diffusion, or by increasing the concentration of the primary electrolyte.

## EXPERIMENTAL

### *Apparatus*

A three-pole column, described previously [23], was rebuilt and now permits the regulation of any solvolytic flow from both sides of the capillary and ensures its constancy. The apparatus consists of a high-voltage (HV) power supply, equipped with two regulators of the ratio of driving currents and of the separation column. The power supply electric circuit provide the column by four adjustable and measured electric currents. These currents pass through two pairs of electrode chambers, each on the proper side of the separation capillary according to the polarity. In each pair, one chamber is filled with primary electrolyte and the other is filled with a modification electrolyte. The anodic or cathodic modification electrolyte is a solution of strong acid or base. The flows of ions from the electrolyte chambers pass through the washed membranes into the separation channel, which is a glass capillary of 100 mm × 0.3 mm I.D. A scale glued on the side of the capillary serves for measuring the position and length of the zones. Sample can be introduced via a septum on each side of the column.

### *Chemicals*

All chemicals were purchased from Lachema (Brno, Czech Republic) with the exception of the model substances, synthetic low-molecular-mass p*I* markers, which were a kind gift from Tessek (Prague, Czech Republic). The electrolyte systems used were 0.01 and 0.05 *M* solutions of KCl modified with $H^+$ and $OH^-$.

### *Focusing procedure*

After filling the electrode chambers with the modification and primary electrolytes and switching on the membrane washing (to prevent any electrolysis products from entering capillary), a separation channel was filled with the sample dissolved in the primary electrolyte. The separation was started by setting up the ratio of the driving currents on both regulators and switching on the main driving current. Solvolytic ions penetrated into the channel and brought about the dissociation of the sample ampholyte, which migrated to the centre of the column and created the zone. The zone was photographed and its length and position were evaluated from the photograph.

## RESULTS AND DISCUSSION

The first part of the experimental work was aimed at verification of the possibility of creating the stationary neutralization boundary in the column with the outlined separation properties.

The working pH range is depicted in Fig. 2a, where the dependence of the pH for both modified electrolytes on the ratio of the driving current in cathodic part of the column, as calculated for equal flows of solvolytic ions, is shown. This case corresponds to a stationary boundary. A concentration of the primary electrolyte (KCl) is parametrically selected. It can be seen that a pH gap ranging from *ca.* 1 to 13 pH units can be prepared in the given electrolyte system. It is symmetrical around the value pH 7.12.

The practical range of pH is limited by the stability with time. As follows from Table I, the time stability of the boundary was calculated for 0.01 and 0.05 *M* KCl as the primary electrolyte. In each instance the times needed to reach total depletion of the ions of KCl from the boundary (100%) and the times needed to reach 10% depletion of the ions (the pH is decreased by *ca.* 0.1) are given. It is clear from Table I that the practically useful ranges of pH are 10–4 in 0.01 *M* electrolyte and 11–3 in 0.05 *M* electrolyte. In Fig. 2b the dynamics of the KCl depletion from the boundary are illustrated. Under reasonable conditions, *i.e.*, pH range 4.26–10, the boundary is fairly stable.

Experimental verification of the stability of the boundary was carried out by adding a small amount of pH indicator (bromothymol blue or

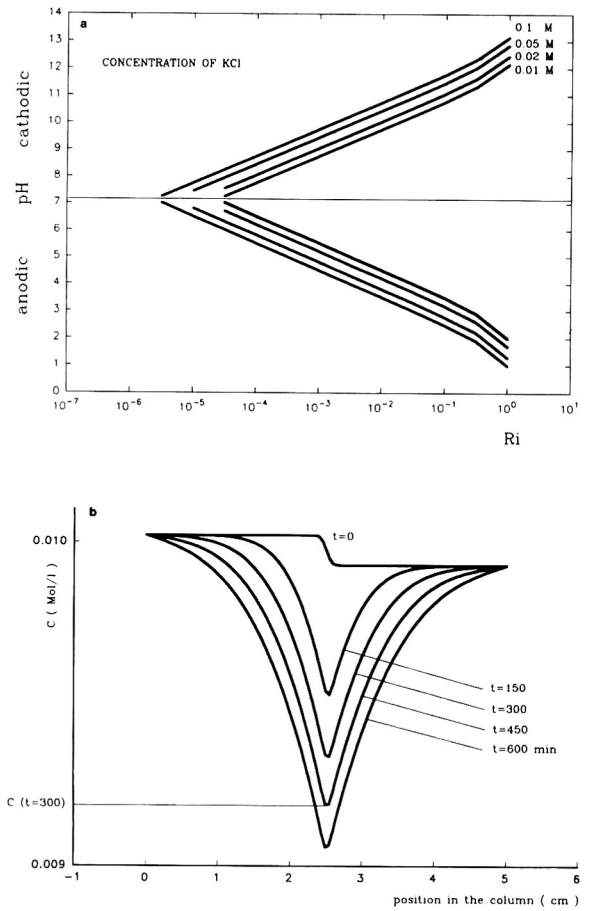


Fig. 2. (a) Dependence of the $pH_a$ and $pH_c$ on the ratio of the driving current on the cathodic side of the column for a different concentration of the primary electrolyte (KCl). (b) Calculated dependence of the concentration of KCl on time and position in the column. $I = 10$ A/m$^2$. Program kindly provided by Dr. W. Thormann (see ref. 8).

phenol red) at a concentration of 0.0001 *M* to the primary electrolyte so that the position of the boundary was made visible (Fig. 3). A boundary with a pH gap of 4.26–10 was stable for *ca.* 90 min in the column. By changing the ratio of the driving currents the boundary is mobilized or shifted.

It is not easy to find a suitable model coloured ampholyte with known p*I*; finally, we selected methyl red, which is a commonly used p*I* indicator in classical isoelectric focusing. Fig. 4 shows a photograph of the focused zone of methyl red. The indicator was loaded as a solution in the primary electrolyte. During the

TABLE I

TIME STABILITY OF THE BOUNDARY FOR 0.01 AND 0.05 *M* KCl AS A PRIMARY ELECTROLYTE AS A FUNCTION OF pH ON CATHODIC SIDE, $pH_c$

| $pH_c$ | Time (s) | | | |
|---|---|---|---|---|
| | 0.01 *M* KCl | | 0.05 *M* KCl | |
| | 100% | 10% | 100% | 10% |
| 8 | $4.72 \cdot 10^7$ | $4.72 \cdot 10^5$ | $2.96 \cdot 10^1$ | $2.96 \cdot 10^8$ |
| 9 | $4.72 \cdot 10^5$ | $4.72 \cdot 10^3$ | $2.94 \cdot 10^8$ | $2.94 \cdot 10^6$ |
| 10 | $4.75 \cdot 10^3$ | $4.76 \cdot 10^1$ | $2.96 \cdot 10^6$ | $2.95 \cdot 10^4$ |
| 11 | $5.07 \cdot 10^1$ | $5.0 \cdot 10^{-1}$ | $2.99 \cdot 10^4$ | $3.00 \cdot 10^2$ |
| 12 | $2.0 \cdot 10^{-1}$ | $2.0 \cdot 10^{-3}$ | $3.3 \cdot 10^2$ | $3.30 \cdot 10^0$ |

focusing in the column the concentration of the methyl red exceeded its solubility and a precipitate was formed. To prevent this precipitation, the addition of 75% ethylene glycol to the primary electrolyte was used. It is obvious that the methyl red created a sharp focus in the column. By changing the ratio of the driving current, the focused zone may be shifted along

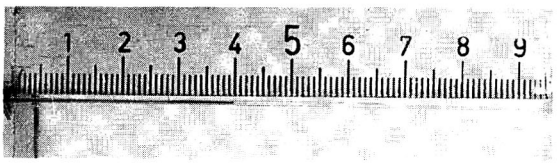


Fig. 3. Neutralization boundary created in the column revealed by addition of 0.0001 *M* phenol red to the primary electrolyte. Conditions: primary electrolyte, 0.01 *M* KCl; modifying electrolytes, 0.01 *M* KCl + 0.001 *M* HCl, 0.01 *M* KCl + 0.02 *M* ammonia solution; total current through column, 400 $\mu$A; $I_H = 50$ $\mu$A; $I_{OH} = 100$ $\mu$A. Photograph taken in 5 min.

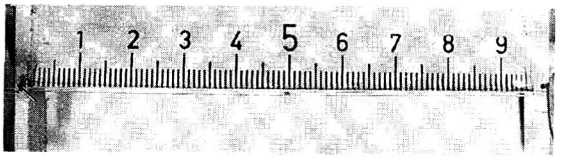


Fig. 4. Focused zone of methyl red (p*I* standard). Conditions: primary electrolyte, 0.05 *M* KCl; modifying electrolytes, 0.05 *M* KCl + 0.0025 *M* HCl, 0.05 *M* KCl + 0.1 *M* ammonia solution, all in 75% ethylene glycol; total current through column, 400 $\mu$A; $I_H = 160$ $\mu$A; $I_{OH} = 400$ $\mu$A. Photograph taken in 60 min.

the column, with a velocity that can be controlled and is proportional to the bias of the magnitude of the solvolytic flows from their balance. Up to a certain extent methyl red moves within the neutralization boundary; however, if the velocity of the boundary is higher than the maximum electromigration velocity attainable by methyl red, the dye lags behind the boundary and migrates in a zone electrophoretic mode.

In the next experiments, model coloured ampholytic substances readily soluble in water were chosen. Substances now produced commercially as p*I* markers are available with a broad range of p*I* values and have high absorption in the visible part of the spectrum. This enables us to avoid an expensive detection device. Fig. 5 shows the focused zone of a model substance (Tessek p*I* Marker 6) of p*I* 6. The substance focuses very well in the column.

Fig. 6 shows the separation of an ampholyte and strong ion. First, a zone of ampholyte was focused in the column and then the sample was injected (ferroin cationic indicator) via septum on the anodic part of the column. It is clear that ferroin passed through the focused zone of ampholyte without disturbing it. A slight movement of the focused zone was caused by side-effects, due to mechanical movement during the injection and also to the effect of the pH of the sample, which was not identical with that in the column.

The possibility of influencing the span of the pH gap and to utilize it for the separation a reaction slurry of Tessek p*I* Markers with a span of p*I* 6–9 is demonstrated in Fig. 7. The sample was first focused into one zone at the boundary having a sufficiently large span of the pH gap

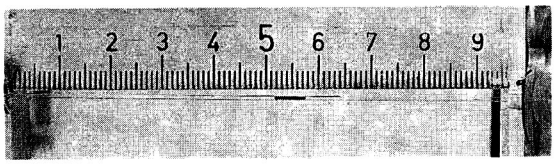


Fig. 5. Focused zone of Tessek p*I* Marker 6. Conditions, primary electrolyte, 0.01 *M* KCl; modifying electrolytes, 0.01 *M* KCl + 0.001 *M* HCl, 0.01 *M* KCl + 0.02 *M* ammonia solution; total current through column, 400 $\mu$A; $I_H$ = 20 $\mu$A; $I_{OH}$ = 50 $\mu$A. Photograph taken in 20 min.

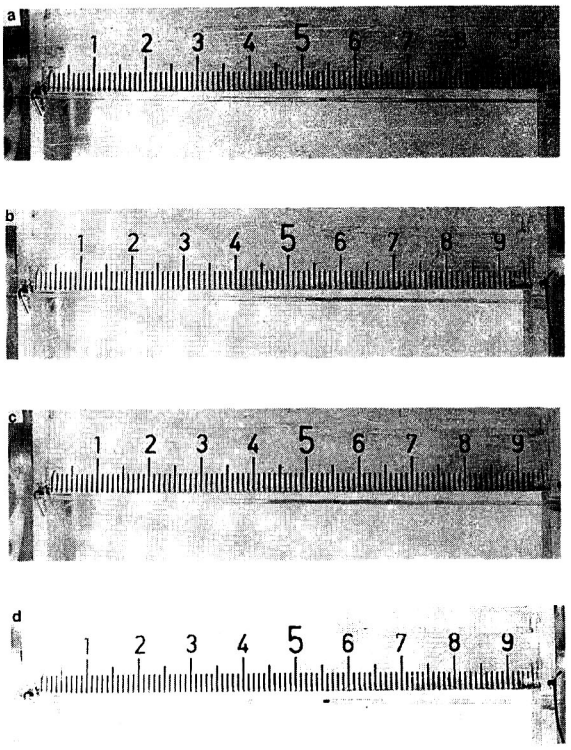


Fig. 6. Separation of the ampholyte and strong ion. Strong ion ferroin injected from the cathodic side of the column passes through focused zone of ampholyte (Tessek p*I* Marker 6). Conditions: primary electrolyte, 0.05 *M* KCl; modifying electrolytes, 0.05 *M* KCl + 0.0025 *M* HCl, 0.05 *M* KCl + 0.1 *M* ammonia solution; total current through column, 400 $\mu$A; $I_H$ = 35 $\mu$A; $I_{OH}$ = 100 $\mu$A. Photographs (a), (b), (c) and (d) taken in 30, 32, 33 and 35 min, respectively.

(4.25–10). Then, by changing the solvolytic flows, the span of the pH gap was reduced (*ca.* 5.75–8.5), which matches the focusing of the ampholyte of p*I* 6 only. As can be seen, more basic ampholytes migrate out of column, and the ampholyte of p*I* 6 remains focused. This depicts the way in which ampholytes can be separated step by step.

The described method, in contrast to classical isoelectric focusing, exhibits some characteristic features of isotachophoresis. With a steady state of the solvolytic flows, the length of the zone of an ampholyte is proportional to the amount of a sample injected and to the concentration of the primary electrolyte at a constant ratio of the driving currents. This feature is depicted in Fig. 8. The dependence of the length of zone on the

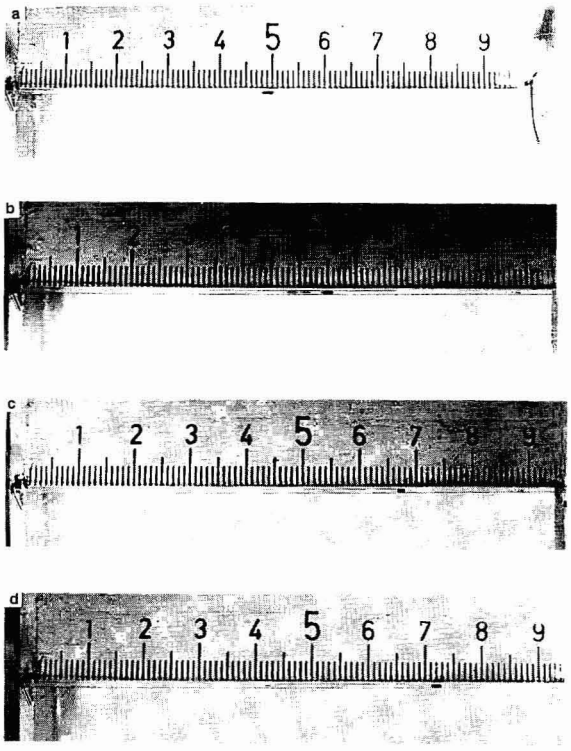


Fig. 7. Separation of a reaction slurry of ampholytes by a change in the span of the pH gap. Focused zone at larger span (a) is separated after its decrease (b–d). Conditions: primary electrolyte, 0.05 *M* KCl; modifying electrolytes, 0.05 *M* KCl + 0.005 *M* HCl, 0.05 *M* KCl + 0.1 *M* ammonia solution; total current through column, 400 $\mu$A; $I_H$ = 60 $\mu$A and $I_{OH}$ = 200 $\mu$A up to 27 min, then decreased to $I_H$ = 6 $\mu$A and $I_{OH}$ = 10 $\mu$A. Photographs (a), (b), (c) and (d) taken in 27, 30, 32 and 34 min, respectively.

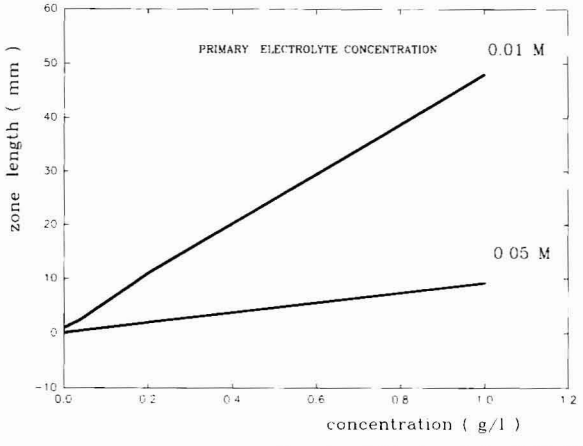


Fig. 8. Calibration lines of Tessek p*I* Marker 6 for 0.01 *M* KCl and 0.05 *M* KCl as a primary electrolyte. For conditions see Figs. 5 and 6, respectively.

injected amount for 0.01 *M* KCl is fairly linear; the small intercept is of experimental origin, as the focused zones of low load were only 50 $\mu$m in length, and this length was difficult to read from photographs. For the similar calibration line for 0.05 *M* KCl serving as primary electrolyte the dependence is fairly linear with a five times smaller slope.

## REFERENCES

1 J. Caslavska, P. Gebauer, A. Odermatt and W. Thormann, *J. Chromatogr.*, 545 (1991) 315.
2 P.G. Righetti, M. Faupel and E. Wenish, in A. Chrambach, M.J. Dunn and B.J. Radola (Editors), *Advances in Electrophoresis*, Vol. 5, VCH, Weinheim, 1992, pp. 159–200.
3 H.J. MacDonald and M.B. Williamson, *Naturwissenschaften*, 42 (1955) 461.
4 A. Kolin, *J. Chem. Phys.*, 22 (1954) 1628.
5 H. Hoch and G.H. Barr, *Science*, 122 (1955) 101.
6 A.J.P. Martin and F. Hampson, *J. Chromatogr.*, 159 (1978) 101.
7 H. Rilbe, *J. Chromatogr.*, 159 (1978) 193.
8 R.A. Mosher, W. Thormann, A. Graham and M. Bier, *Electrophoresis*, 6 (1985) 545.
9 H. Svensson, *Acta Chem. Scand.*, 15 (1961) 325.
10 A.R. Williams and R.E. Waterman, *Proc. Soc. Exp. Biol. Med.*, 27 (1959) 56.
11 A. Tiselius, *Sven. Kem. Tidskr.*, 53 (1941) 305.
12 O. Sova, *J. Chromatogr.*, 320 (1985) 15.
13 R. Hagedorn and G. Kuhr, *Electrophoresis*, 11 (1990) 281.
14 E. Petterson, *Acta Chem. Scand.*, 23 (1969) 2631.
15 U.K. Stenmann and R. Grasbeck, *Biochim. Biophys. Acta*, 286 (1972) 243.
16 A. Chrambach and N.Y. Nguyen, in B.J. Radola and D. Graesslin (Editors), *Electrofocusing and Isotachophoresis*, Walter de Gruyter, Berlin, 1977, pp. 51–58.
17 L.M. Hjelmeland and A. Chrambach, *Electrophoresis*, 4 (1983) 20.
18 S.J. Luner and A. Kolin, *Proc. Natl. Acad. Sci. U.S.A.*, 66 (1970) 898.
19 P. Lundahl and S. Hjertén, *Ann. N.Y. Acad. Sci.*, 209 (1973) 94.
20 C.H. Lochmüller, S.J. Breiner and C.S. Ronsick, *J. Chromatogr.*, 480 (1989) 293.
21 G.V. Troitski, V.P. Savialov, I.F. Kirjukhin, V.M. Abramov and G.J. Agitski, *Biochim. Biophys. Acta*, 400 (1975) 24.
22 P.G. Righetti, E. Wenisch, A. Jungbauer, H. Katinger and M. Faupel, *J. Chromatogr.*, 500 (1990) 681.
23 J. Pospíchal, M. Deml, P. Gebauer and P. Boček, *J. Chromatogr.*, 470 (1989) 43.
24 J. Dvořák and J. Koryta, *Elektrochemie*, Academia, Prague, 1983.

*Journal of Chromatography*, 638 (1993) 187–193
Elsevier Science Publishers B.V., Amsterdam

CHROM. 24 863

# Experimental aspects of capillary isoelectric focusing with electroosmotic zone displacement

Sarah Molteni and Wolfgang Thormann*

*Department of Clinical Pharmacology, University of Berne, Murtenstrasse 35, CH-3010 Berne (Switzerland)*

ABSTRACT

The investigation of different parameters affecting separation and resolution in capillary isoelectric focusing (CIEF) with electroosmotic zone displacement is reported. Focusing is performed in an uncoated, open-tubular fused-silica capillary of length 50–100 cm and 75 $\mu$m I.D. An experiment proceeds by first filling the entire capillary with the catholyte containing the neutral polymer(s). Sample composed of carrier ampholytes and proteins is introduced at the anodic capillary end, the initial zone length being 10–50% of the effective capillary length. After application of power, two electrokinetic effects occur concurrently, the formation of a longitudinal pH gradient with the separation of proteins (isoelectric focusing) and, owing to the negative surface charge of untreated fused silica, the displacement of the entire zone pattern towards the cathode (electroosmosis). Basic proteins reach the detector prior to neutral and acidic compounds. The concentrations of the polymers, different protein solubilizing additives, carrier ampholytes, anolyte and catholyte, and also the initial sample zone length, the applied voltage, the capillary length and the rinsing procedures are shown to affect focusing in CIEF. A knowledge of the effects of these parameters leads to optimization of protein separation and resolution and provides an insight into the pros and cons of this method.

## INTRODUCTION

In the past few years increasing attention has been paid to protein isoelectric focusing (IEF) in capillaries with the ultimate aim of developing a fully instrumental approach to this high resolution method. First, free fluid focusing was studied in capillaries of rectangular cross-sections [1–5], in glass [6–8] or PTFE capillaries [9,10] of 200–500 $\mu$m I.D., and also in coated, open-tubular fused-silica capillaries of very small I.D. [11–16]. These approaches operated with minimized electroosmosis in which stationary steady-state zone patterns were established. Zones were detected either by the use of array detection or by visual inspection [1–5], and also by UV absorption measurement [6–15] or concentration gradient monitoring [16] towards one column end which required that after focusing the proteins had to be mobilized and swept past a stationary detector. Essentially two approaches for mobilization were studied. The first method consisted of the use of hydrodynamic flow which was applied after focusing was attained and without interruption of the current flow [6]. Second, electrophoretic mobilization was achieved through power interruption after focusing and replacement of one of the two electrode buffers prior to reapplication of current [6–15].

Recently, Mazzeo and Krull [17,18] and Thormann *et al.* [19] independently described two similar isoelectric focusing methods with electroosmotic zone displacement. In these studies it was discovered that small amounts of a neutral polymer (hydroxypropylmethylcellulose or methylcellulose) added to the buffer allowed IEF of proteins to be performed in untreated, open-tubular fused-silica capillaries, *i.e.*, in the presence of an electroosmotic flow along the separation axis. The added polymer provides a dynamic coating of the capillary surface which reduced

* Corresponding author.

0021-9673/93/$06.00 

both the protein–wall interactions and the electroosmotic flow. This, and also the plug flow characteristics of electroosmosis, were important prerequisites for low sample dispersion and therefore for efficient focusing. Electroosmotic zone displacement was shown to make mobilization after focusing obsolete. Mazzeo and Krull [17,18] described a configuration in which the column was initially completely filled with the sample, this requiring the further addition of a strong base to the sample in order to be able to detect basic proteins [9,14]. In our experiments a relatively short initial sample zone was employed, the remainder of the capillary being filled with catholyte. After power application the electroosmotic flow gradually displaced the developing zone pattern towards and eventually across the point of detection, making the addition of the strong base unnecessary. Further, fast-scanning multi-wavelength detection was shown to permit the simultaneous monitoring of proteins and carrier ampholytes, and the temporal behaviour of the current was found to provide information on the degree of focusing prior to sample detection at a specified location towards the capillary end [19].

In this paper, experimental data allowing the elucidation of factors affecting separation of proteins in our fully dynamic method of capillary isoelectric focusing (CIEF) are reported. Separation and resolution of model protein mixtures are shown to be dependent on instrumental variables, including applied power, capillary length, initial zone length and the capillary cleaning procedure, and on the chemical variables, such as the concentration of sample, polymer, carrier ampholytes, anolyte and catholyte.

## EXPERIMENTAL

### *Chemicals and sample preparation*

All chemicals were of analytical-reagent grade. Cytochrome *c* (CYTC) from horse heart ($M_r$ 12 384, p*I* 9.3), carbonic anhydrase (CA) from bovine erythrocytes ($M_r$ 31 000, p*I* 6.2), bovine serum transferrin (b-TF), iron free ($M_r$ 77 000, p*I* 5.2–5.8), human serum transferrin (h-TF), iron saturated ($M_r$ 79 570, p*I* 5–6), hydroxypropylmethylcellulose (HPMC) and methylcellulose (MC) with a viscosity of 4000 cP each (2% aqueous solution at 25°C) were obtained from Sigma (St. Louis, MO, USA), equine myoglobin (MYO) from skeletal muscle ($M_r$ 17 800, p*I* 6.8–7.3) from Serva (Heidelberg, Germany) and ampholines (pH 3.5–10, 4–6, 5–7 and 7–9) from Pharmacia–LKB (Bromma, Sweden). Proteins were dissolved in Ampholine solution at specified concentrations. Unless stated otherwise, HPMC and/or MC were added to the catholyte only.

### *Instrumentation*

Two different instruments were employed. Most of the experiments were performed on an ABI 270A capillary electrophoresis system (Applied Biosystems, Foster City, CA, USA). Typically, this instrument was equipped with a fused-silica capillary of 75 $\mu$m I.D. and effective and total separation lengths of 50 and 70 cm, respectively (Polymicro Technologies, Phoenix, AZ, USA). Electropherograms were recorded using a Model D-2000 chromato-integrator (Merck–Hitachi, Darmstadt, Germany). An automated ABI 270A-HT capillary electrophoresis system (Applied Biosystems), a similar instrument to that described above but featuring a larger autosampler, was also used. The capillary employed had effective and total lengths of 52 and 73.5 cm, respectively, and I.D. 75 $\mu$m (Polymicro Technologies). Data collection and evaluation were performed with a data acquisition system consisting of a PC Integration Pack (version 2.50) (Kontron, Zurich, Switzerland) together with a Mandax AT 286 computer system. This integration pack features automatic range switching and a dynamic sampling rate, allowing a data sampling rate of up to 100 Hz for quickly changing signals.

### *Standard running conditions*

Unless stated otherwise, 20 m*M* NaOH containing 0.06% (w/v) HPMC and 10 m*M* $H_3PO_4$ were used as catholyte and anolyte, respectively. Using the ABI 270A instrument, the applied voltage was 10 kV (initial currents 25–30 $\mu$A; minimum currents 1–2 $\mu$A; for explanations, see ref. 19) and the sample loading time (with

vacuum) was 20 s, providing an initial sample zone length covering about 20% of the effective column length. Ampholine was used at a concentration of 2.5% and the concentration of the proteins was about 0.16 mg/ml. Electropherograms were recorded at 200 nm (carrier ampholytes) and 280 nm (proteins) using the Model D-2000 chromato-integrator. Between runs, capillaries were rinsed with catholyte for 10 min.

## RESULTS AND DISCUSSION

A CIEF experiment is commenced with a sample zone at the anodic end covering typically <50% of the effective capillary length, the remainder being filled with catholyte. On application of power, isoelectric focusing is performed in an electroosmotic stream flowing towards the cathode. For the investigation of a range of parameters, model protein mixtures composed of CYTC, MYO and b-TF or CYTC, MYO and CA were used. Unless stated otherwise, experiments were performed in a 50-cm column (effective length) using the ABI 270A instrument, which features vacuum injection [20 and 5 in.Hg (1 in.Hg = 3386.4 Pa) for rinsing and sample loading, respectively]. Parameters examined on each electropherogram included protein separation, resolution, elution time and absorbance at 280 nm.

As reported previously [19], CIEF in a configuration without the addition of a polymer to the catholyte was found to be irreproducible. Consequently, HPMC concentrations of 0.15, 0.1, 0.06, 0.03 and 0.015% (w/v) were investigated in order to find the optimum conditions. The separation of CYTC, MYO and b-TF was fairly good in all instances. However, the HPMC concentration was found to affect the resolution of specific proteins (Fig. 1). The best results were obtained with 0.06 and 0.1% of HPMC. Further, conditioning of the capillary prior to sample application with catholyte was established to be essential for the performance of dynamic CIEF. Addition of the polymer to the sample was found to improve the separation of proteins or isoforms with close p*I* values (see below), whereas no changes in resolution were observed with HPMC in the anolyte (data not shown). It appears that the loaded sample is indirectly influenced by the polymer concentration. With vacuum injection at a specified time interval it was observed that the lower the polymer concentration was, the more sample became introduced. The electropherograms shown in Fig. 1 clearly show this effect, particularly when the CYTC peaks are compared. With a longer initial sample zone less NaOH is present in the capillary at the beginning of the experiment, causing a smaller net electroosmotic flow and thereby increased retention times (see below).

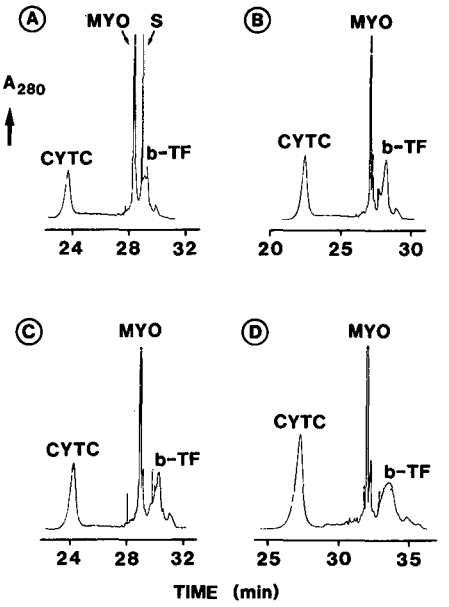


Fig. 1. Effect of HPMC concentration in the catholyte. CIEF of CYTC, MYO and b-TF with (A) 0.15, (B) 0.10, (C) 0.06 and (D) 0.03% of HPMC is shown under otherwise standard conditions using the ABI 270A instrument. The trace denoted by S is believed to be a spike originating from a particle (protein precipitate) that is transported through the detection cell.

MC at concentrations of 0.15, 0.1, 0.06 and 0.03% (w/v) were also investigated (data not shown). Compared with HPMC and in agreement with the method of Mazzeo and Krull [17,18], no significant differences were observed with regard to electroosmotic flow and protein interaction with the capillary walls. However, lower MC concentrations provided better resolution of the isoforms, particularly for b-TF. This effect could be attributed to a specific

protein–polymer interaction which differs from protein to protein. Good results were also obtained when a mixture of HPMC and MC at low concentrations (typically HPMC 0.03% and MC 0.015%) was used. Finally, an insignificant improvement of separation was noted with the addition of urea (1 *M*), glycine or glycylglycine [1% (w/v) each] to the sample (data not shown).

The effects of anolyte and catholyte concentrations were first analysed by keeping one solution at a constant concentration and varying the concentration of the other. CYTC, MYO and CA were used as sample proteins and MC (0.03%) was employed as the polymer in the catholyte. Variation of NaOH concentration was found to have a considerable effect on retention times, *i.e.*, on the electroosmotic flow. Retention became longer with increased catholyte concentration, permitting an improvement of the separation of certain isoforms. It was interesting that modification of the anolyte ($H_3PO_4$) concentration had an opposite effect, *i.e.*, a higher concentration led to shorter retention times. On increasing both the anolyte and catholyte concentrations while maintaining their ratio at $NaOH:H_3PO_4 = 2$, the retention times became larger. Typical electropherograms are presented in Fig. 2. It can be concluded that the catholyte (NaOH) essentially dominates the generation of the electroosmotic flow, thereby acting as the pump for mobilization and permitting the control of elution by selection of its concentration.

The concentration of the carrier ampholytes represents another parameter to be considered. In our investigation, Ampholine (pH 3.5–10) concentrations of 1, 2.5 and 5% (w/v) were employed. Under the chosen conditions with CYTC, MYO and b-TF as sample proteins and vacuum injection, 5% Ampholine was observed to provide faster elution than 2.5% carrier ampholyte. Under otherwise standard conditions, the elution time intervals of the three proteins were 18.4, 21.4 and 21.9 min (5%) and 24.1, 28.9 and 30.2 min (2.5%), respectively. Moreover, with 1% Ampholine, mobilization was even slower. In that case and with an applied voltage of 25 kV, CYTC eluted after 24.5 min and b-TF did not reach the detector within 45 min (data not shown). Again, it is assumed that with higher ampholyte concentrations a shorter initial sample zone length is obtained, thereby allowing for a longer NaOH zone, which induces increased electroosmotic pumping. The data depicted in Fig. 3 illustrate that, in addition to all the parameters mentioned above, pH gradient adjustment has to be employed to obtain the highest resolution of isoforms. For CIEF of b-TF and h-TF, a pH gradient ranging from pH 4 to 9 was found to resolve isoforms almost completely, a state which was not achieved with the broad

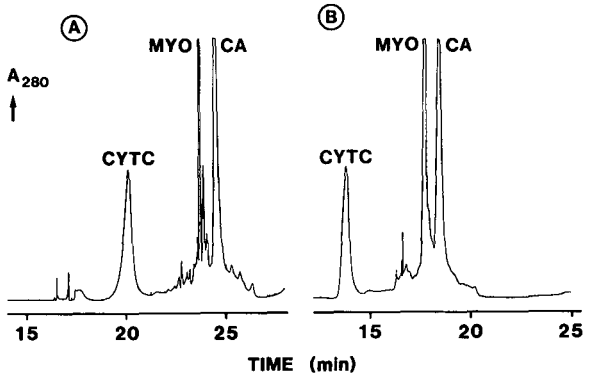


Fig. 2. Effect of catholyte and anolyte concentrations. CIEF of CYTC, MYO and CA having a catholyte (NaOH with 0.03% MC) and anolyte ($H_3PO_4$) of (A) 20 and 20 m*M* and (B) 10 and 5 m*M*, respectively, and using the ABI 270A instrument. All other parameters as given under standard conditions.

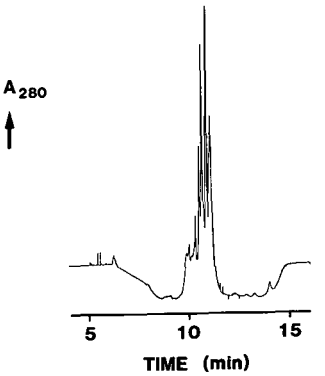


Fig. 3. CIEF of iron-saturated h-TF (0.4 mg/ml) employing the ABI 270A-HT instrument with 2.5% carrier ampholytes composed of Ampholine of pH 4–6, 5–7 and 7–9 (3:6:1, respectively), 0.03% MC in catholyte and sample, sample injection time 60 s (the initial sample zone length was about 50% of effective capillary length) and applied voltage 20 kV. All other parameters as given under standard conditions.

range (pH 3.5–10) preparation. The resolution shown in Fig. 3 is almost as good as that reported by Kilàr and Hjertén [11]. It is important to understand that the data in Fig. 3 were obtained with the addition of the polymer to both sample and catholyte.

With an ABI 270A instrument, most experiments were performed in capillaries of 70 cm total length (50 cm to the detector). In order to evaluate the effect of the electric power, experiments were executed with a constant voltage of 10, 15 or 20 kV. Not surprisingly, an increased voltage resulted in shorter retention times. While separation of the three test proteins was observed in all three instances, there was no resolution of isoforms at 20 kV (Fig. 4). Thus, with a given capillary length, achievement of the required resolution or speed of analysis depends on the proper selection of the ampholyte concentration and voltage. Further, for a given chemical configuration and at the expense of larger run times, longer capillaries were found to provide increased resolution. Investigations of the influence of the initial sample zone length on CIEF were executed via variation of the time interval of vacuum injection (10–30 s on the ABI 270A and up to 1 min on the ABI 270A-HT instrument with effective capillary lengths of 50 cm). Two major phenomena were observed (data not shown). First, with increased sample zone length a higher protein resolution is obtained. Second, the ampholyte front reaches the detector within a shorter time interval and the time required for detection of the entire gradient increases with longer sample zones. These effects are attributed to the increased sample zone length and a decreasing electroosmotic flow caused by the shorter part of the capillary filled with catholyte. Longer sample zones generate a flatter pH gradient so that the resolution of proteins with close p*I* values (isoforms) is increased.

Reproducibility was evaluated using CYTC, MYO and CA as test proteins. Typically for quadruplicates a relative standard deviation (R.S.D.) of 1.5–3% for retention times and 4–9% for peak areas was obtained (Fig. 5, Table

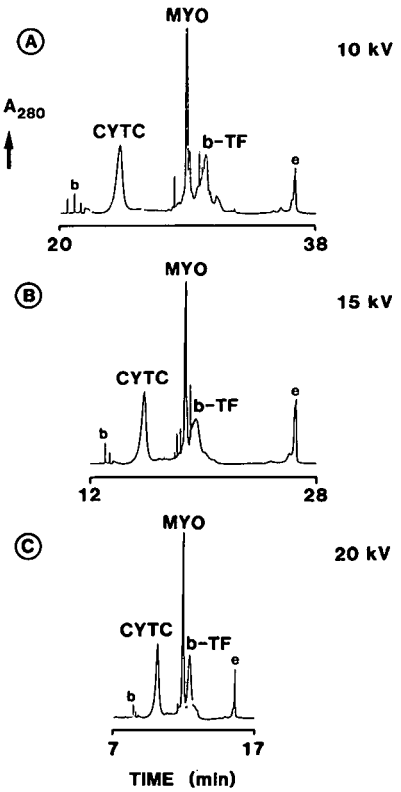


Fig. 4. Effect of applied voltage. CIEF of CYTC, MYO and b-TF using the ABI 270A at (A) 10, (B) 15 and (C) 20 kV and otherwise the specified standard conditions. The beginning and end of the detection of the carrier ampholytes are denoted by b and e, respectively.

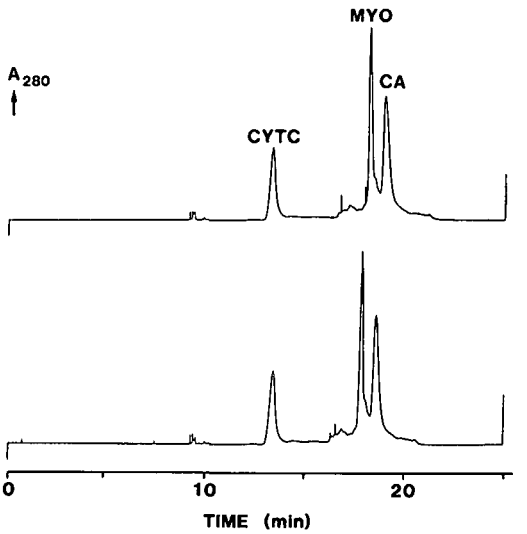


Fig. 5. Reproducibility. CIEF of CYTC, MYO and CA using the ABI 270A instrument and having 10 m*M* NaOH (with 0.03% MC) and 5 m*M* $H_3PO_4$ as catholyte and anolyte, respectively. All other parameters as given under standard conditions.

TABLE I

REPRODUCIBILITY DATA ($n = 4$) FOR TYPICAL CIEF RUNS

Data corresponding to the electropherograms shown in Fig. 5.

| Protein | Retention time | | Peak area | |
|---|---|---|---|---|
| | Mean (min) | R.S.D. (%) | Mean ($\mu$V s) | R.S.D. (%) |
| CYTC | 13.53 | 1.44 | 174 727 | 8.82 |
| MYO | 18.17 | 2.98 | 318 400 | 3.93 |
| CA | 18.89 | 2.97 | 350 545 | 5.44 |

I). In this approach, capillaries were first conditioned with catholyte (10 min). On working for longer periods with the same capillary it was observed that the conditioning of the capillary was not constant. In a series of ten experiments on the ABI 270A-HT instrument and using a similar protein mixture, a constant increase in retention time was observed, leading to poor reproducibility of both retention times and peak areas. Therefore, different conditioning procedures were investigated. Instead of rinsing the capillary for a long time with catholyte, the rinsing procedure was changed to a cleaning period with 0.1 or 1 *M* NaOH (destruction of conditioning) followed by a short dynamic conditioning with catholyte. The effect of an in-between rinse with distilled water was also evaluated. Typical data (CYTC peak only) for four different procedures are shown in Fig. 6. First, the capillary was rinsed with 0.1 *M* NaOH and catholyte for 3 and 10 min, respectively (Fig. 6A). Data obtained with sequential flushing using 0.1 *M* NaOH, water and catholyte (5 min each) are shown in Fig. 6B and those measured with a reversed sequence of water and 0.1 *M* NaOH in Fig. 6C. The fourth procedure (Fig. 6D) involved the use of 1 *M* NaOH for 1 min, followed by water and catholyte (5 min each). This approach clearly provided the best results with R.S.D. values of 2.7 and 4.0% for retention times and areas of CYTC, respectively. Corresponding values for procedures A, B and C were 4.6/17, 2.7/6.6 and 9.8/11.3%, respectively. Because of possible damage to the capillary with frequent use of 1 *M* NaOH, the conditions employed for Fig. 6B are recommended.

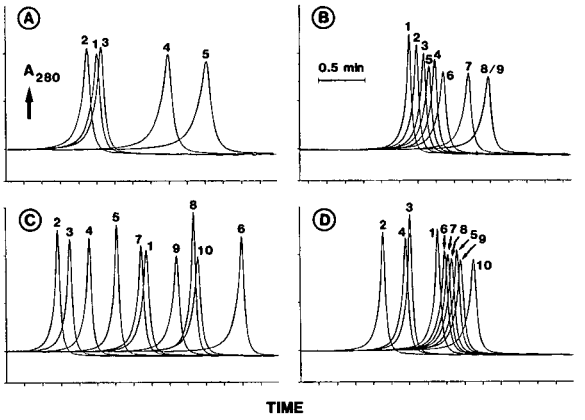


Fig. 6. Effect of capillary conditioning. CIEF of CYTC, MYO and CA (0.08 mg/ml each) employing the ABI 270-HT instrument with computerized data acquisition using the following rinsing procedures: (A) 0.1 *M* NaOH (3 min) and catholyte (10 min); (B) 0.1 *M* NaOH (5 min), water (5 min) and catholyte (5 min); (C) water (5 min), 0.1 *M* NaOH (5 min) and catholyte (5 min); and (D) 1 *M* NaOH (1 min), water (5 min) and catholyte (5 min). Sample injection time, 60 s (about 50% of the effective column length); applied voltage, 20 kV. Data for a 3-min time interval (CYTC peak only) are shown. The numbers in the four panels refer to the injections.

## CONCLUSIONS

In CIEF, a relatively short section of the capillary is occupied with the sample and isoelectric focusing is performed in one step, focusing and mobilization occurring simultaneously. Electroosmosis provides the flow for mobilization; hence in this technique this property plays a very central role. Generally, the electroosmotic flow is dependent on surface charge (pH), the electric field determined by current density and conductivity (composition of the solutions present in the capillary) and viscosity. In the described configuration, these three parameters are not constant during focusing. At any given time the sample is moving with a velocity defined as the mean of the electroosmotic velocities of the different longitudinally arranged fluid elements present. Its value changes with time, as (i) the catholyte is gradually leaving and the anolyte entering the column and (ii) the pH gradient is formed. As

the electroosmotic flow has a direct influence on retention, its control and reproducibility are of great importance, or else drastic changes can be observed from run to run. Optimized conditions for CIEF are shown to depend on a number of parameters, most notably the use of a neutral polymer in the catholyte, the concentrations of catholyte and carrier ampholytes, the applied voltage and capillary length, as well as the initial sample zone length.

The results show that different polymers (HPMC and MC) and combinations can be employed as additives to the catholyte. Further, higher resolution is obtained with the inclusion of the polymer in the sample solution whereas no improvement is achieved through introduction of the capillary conditioner to the anolyte. The catholyte (NaOH) is shown to be the major contributor to the electroosmotic flow. Variations of its concentration and that of the carrier ampholytes affect the resolution and migration time. Higher NaOH and/or lower carrier ampholyte concentrations increase the residence time and resolution. With the sample loading time (initial sample zone length) the steepness of the pH gradient can be manipulated, this having an effect on the resolution, efficiency of separations and the speed of analysis. From the instrumental side, the applied voltage and capillary length are the two parameters with which resolution and retention times are influenced. Increased voltage/capillary length are shown to result in shorter/longer retention times, configurations which are obtained at the expense/benefit of resolution, respectively. Finally, the rinsing procedure between runs is shown to have a strong effect on reproducibility. Etching of the capillary surface (with 1 *M* NaOH) followed by a short renewal of the dynamic coating is shown to provide data of the highest reproducibility.

The proteins used in this study are characterized by large differences in p*I*. Under the investigated conditions, they are generally well separated. The resolution of isoforms of proteins, however, is shown to require favourable conditions, which appear to be protein specific. Further work is needed to define the limit of resolution of components with very close p*I* values. Other topics of interest include improved control of electroosmosis (*e.g.*, with external electric fields [20,21]), the description of the complete separation and transport dynamics of CIEF and a careful comparison between the method described here and that of Mazzeo and Krull [17,18].

ACKNOWLEDGEMENTS

The authors acknowledge stimulating discussions with J. Chmelík. This work was partly sponsored by the Research Foundation of the University of Berne and the Swiss National Science Foundation.

REFERENCES

1 W. Thormann, R.A. Mosher and M. Bier, *J. Chromatogr.*, 351 (1986) 17.
2 W. Thormann, N.B. Egen, R.A. Mosher and M. Bier, *J. Biochem. Biophys. Methods*, 11 (1985) 287.
3 W. Thormann, A. Tsai, J.P. Michaud, R.A. Mosher and M. Bier, *J. Chromatogr.*, 389 (1987) 75.
4 R.A. Mosher, W. Thormann, R. Kuhn and H. Wagner, *J. Chromatogr.*, 478 (1989) 39.
5 J. Wu and J. Pawliszyn, *Anal. Chem.*, 64 (1992) 224.
6 S. Hjertén and M. Zhu, *J. Chromatogr.*, 346 (1985) 265.
7 S. Hjertén, J.L. Liao and K. Yao, *J. Chromatogr.*, 387 (1987) 127.
8 S. Hjertén, K. Elenbring, F. Kilàr, J. Liao, J.C. Chen, C.J. Siebert and M. Zhu, *J. Chromatogr.*, 403 (1987) 47.
9 M.A. Firestone and W. Thormann, *J. Chromatogr.*, 436 (1988) 309.
10 W. Thormann and M.A. Firestone, in J.C. Janson and L. Riden (Editors), *Protein Purification*, VCH, Weinheim, 1989, p. 469.
11 F. Kilàr and S. Hjertén, *Electrophoresis*, 10 (1989) 23.
12 F. Kilàr and S. Hjertén, *J. Chromatogr.*, 480 (1989) 351.
13 F. Kilàr, *J. Chromatogr.*, 545 (1991) 403.
14 M. Zhu, D.L. Hansen, S. Burd and F. Gannon, *J. Chromatogr.*, 480 (1989) 311.
15 M. Zhu, R. Rodriguez and T. Wehr, *J. Chromatogr.*, 559 (1991) 479.
16 J. Wu and J. Pawliszyn, *Anal. Chem.*, 64 (1992) 219.
17 J.R. Mazzeo and I.S. Krull, *Anal. Chem.*, 63 (1991) 2852.
18 J.R. Mazzeo and I.S. Krull, *J. Microcol. Sep.*, 4 (1992) 29.
19 W. Thormann, J. Caslavska, S. Molteni and J. Chmelík, *J. Chromatogr.*, 589 (1992) 321.
20 C.S. Lee, W.C. Blanchard and C.T. Wu, *Anal. Chem.*, 62 (1990) 1550.
21 K. Ghowsi and R.J. Gale, *J. Chromatogr.*, 559 (1991) 95.

*Journal of Chromatography*, 638 (1993) 195–203
Elsevier Science Publishers B.V., Amsterdam

CHROM. 24 919

# Project ILSAP: an inter-laboratory study on accuracy and precision in isotachophoresis

J.C. Reijenga* and R.G. Trieling

*Department of Chemical Engineering, Eindhoven University of Technology, P.O. Box 513, 5600 MB Eindhoven (Netherlands)*

D. Kaniansky

*Institute of Chemistry, Faculty of Science, Komensky University, 84215 Bratislava (Slovak Republic)*

ABSTRACT

In a collaborative study by seventeen laboratories, six aqueous sample solutions also containing 0.9% (w/v) NaCl were analysed for lactate and creatinine using isotachophoresis. A split-level study was carried out with three levels of the order of 3, 10 and 30 mmol/l, two sublevels and without blind duplicates. A calibration graph was constructed at five concentrations, using citrate and Tris as internal standards, added on a mass basis. The concentrations in the sample were determined in singular. After elimination of a few outliers using the Grubbs test at a 1% confidence level, data were treated according to ISO 5725. For low, medium and high concentration levels, the repeatability values $r$ were 0.41, 0.40 and 1.67 mmol/l, respectively, for lactate and 0.63, 0.53 and 1.43 mmol/l, respectively, for creatinine. The reproducibility values $R$ were 0.59, 1.12 and 2.05 mmol/l, respectively, for lactate and 1.33, 0.88 and 2.66 mmol/l, respectively, for creatinine.

## INTRODUCTION

This paper describes the results of a collaborative study on capillary isotachophoresis, decided upon by a number of participants during the *7th International Symposium on Capillary Electrophoresis and Isotachophoresis* in the High Tatras, Czechoslovakia, in 1990. The preparation of the collaborative study and analyses were carried out in 1991.

The aim of the study was to evaluate the accuracy and precision of capillary isotachophoresis. It was decided to use universal detection (zone length measurement) because of the simple and sound theoretical basis of this detection principle. The sample components determined should be of interest from a practical point of view and include both cations and anions. Their number should be limited in order to avoid too much work on calibration. Lactate and creatinine were considered suitable candidates. As for the sample matrix, 0.9% NaCl in an aqueous solution was considered a good compromise between a purely synthetic matrix and a physiological matrix.

After consulting the relevant literature [1], it was decided to organize a split-level study with three levels and two sublevels and without blind duplicates. The levels were chosen such that they were within the dynamic range of the instrument with the same injection volume, depending of course on the sample load of the instrument.

A number of laboratories were invited to take part in the study. Invitations were sent to those laboratories having practical experience with capillary isotachophoresis on an analytical scale for a number of years, resulting in publications and contributions to symposia on isotachophoresis. Eighteen of those agreed to par-

* Corresponding author.

0021-9673/93/$06.00 

ticipate. A draft proposal was then sent to the participants, requesting suggestions for improvement. These were incorporated in the final procedure, distributed together with all chemicals and sample solutions.

Results were received from seventeen laboratories. Some of these submitted additional results, obtained under different operating conditions. These results were not averaged. For statistical treatment, a single result was taken from each laboratory. Outlier tests were applied to both calibration data and individual results. For those laboratories having submitted more than one result, these are listed separately. For correlations between individual results and operating conditions, all results, including the sub-laboratory results and the outliers, were taken. The idea behind this was that outliers may have been caused by the operating conditions.

## EXPERIMENTAL

### *Equipment*

The equipment used was either laboratory made or commercially available, provided that it was designed for analytical and not preparative purposes. The method of injection was either by syringe (in twenty cases, 1–5 $\mu$l) or a fixed volume sample valve (in seven cases, 0.2–30 $\mu$l). The method of detection was universal: a.c. (21), high-frequency (h.f.) (1) or d.c. (5) conductivity detection. The driving current (15–150 $\mu$A) was kept constant during detection and adjusted to the inside diameter (0.2–0.55 mm) and length (133–400 mm) of the separation capillary in order to reach an end voltage acceptable for the proper performance of the instrument. In nine instances column coupling was used.

A strip-chart recorder or a microcomputer was used for registration of the detector signals in such a way that the time resolution (paper speed or A/D sampling rate) was sufficiently high in order to determine zone lengths accurately. The method of zone-length measurement was based on the fact that the zone lengths are marked by an inflection point in the detector signal (a distinct maximum in the time differential of the signal).

### *Samples*

The sample matrix consisted of 10-ml amounts of 0.9% (w/v) NaCl solution. The sample solutions were prepared in 1-l volumes using an analytical balance with a 0.1-mg digital readout and calibrated volumetric glassware. The sample components to be determined were lactic acid and creatinine, both at 3, 10 and 30 mmol/l concentration levels.

The split-level study included two solutions of high, two of medium and two of low concentration levels of a sample constituent. Sample solutions were labelled A, B, C, D, E and F. An additional practice sample (labelled P) of approximately 6 mmol/l concentration for both constituents in 0.9% (w/v) NaCl was also provided.

All sample solutions were stored in a refrigerator on receipt and analysed as soon as possible.

### *Chemicals*

Chemicals for leading and terminating operational systems and for calibration were provided by the organizers in sufficient amount and of the highest purity normally available. Care was taken that the chemicals were from a single production batch. These chemicals were a generous gift from Merck (Darmstadt, Germany).

All solid chemicals were stored in a dry location at room temperature. In addition, lithium lactate was first dried in an oven for 3 h at 110°C and subsequently stored in a desiccator (a 1% mass loss was observed).

### *Operational systems*

All operational systems were made up in at least 1-l amounts, dissolved in deionized water and stored in a refrigerator for not longer than 2 weeks.

The operational system for anionic analysis was as follows:

| | |
|---|---|
| leading electrolyte: | 0.01 mmol/l histidine |
| | 0.01 mol/l histidine hydrochloride |
| terminating electrolyte: | 0.005 mol/l glutamic acid |
| | 0.01 mol/l histidine |

and that for cationic analysis was as follows:

| | |
|---|---|
| leading electrolyte: | 0.01 mol/l sodium glutamate<br>0.002 mol/l glutamic acid |
| terminating electrolyte: | 0.005 mol/l glutamic acid. |

Prior to the analysis of standards or samples, a blank run was performed using the same current and recording paper speed as in the subsequent analyses. No detectable step height should have occurred at the step height of either sample component or internal standard.

*Calibration and analysis*

Determinations of standards and samples were carried out using an internal standard (I.S.). For cationic analyses trishydroxymethylaminomethane (Tris) was used and for anionic analyses citric acid. Each time, 1–5 ml of I.S. solution were added to an equal volume of sample/standard solution using a calibrated pipette. These dilutions were carried out on a mass basis using an analytical balance with a 0.1-mg readout.

The concentration of the I.S. solution was 10.00 mmol/l for both analytes. The anionic and cationic internal standards were combined in one solution, in deionized water.

Five standard solutions were prepared, having sample component concentrations of 0, 2.00, 5.00, 15.0 and 30.0 mmol/l. Again, standard solutions for anionic and cationic analyses were combined in one solution, also containing 0.9% (w/v) NaCl. The combinations were such that 0 mmol/l creatinine was combined with 30.0 mmol/l lithium lactate, 2.00 mmol/l creatinine with 15.0 mmol/l lithium lactate, etc. Participants were advised to prepare 1-l volumes of each.

*Injection and injection sequence*

For each analysis, equal amounts of I.S. and sample/standard were mixed as described previously and injected. The amount injected was adjusted to the separation capacity of the instrument. With equipment using syringe injection, a fixed-volume adapter was used. When using sample valve injection, a dilution could be necessary. Deionized water was used in that event.

For each of the two sample components to be determined (creatinine and lactic acid), all injections took place in 1 day. This meant a minimum of twelve injections per day. If any of the injections or the blank run was "unsuccessful", it could be repeated, but the sequence of injection remained unchanged. If, as a result, a series of injections could not be completed in 1 day, the sequence was started from the beginning. The sequence of injection was such that standard and sample solutions were alternately injected in approximately increasing concentration.

*Submission of results*

Results were submitted on a computer diskette, containing a program to gather raw data and calculate results according to the procedure described above. Laboratory data were stored in a binary file with a file name extension LAC or CRE. Isotachopherograms of a blank, a standard and a sample run were also submitted.

When submitting sub-laboratory results in addition (different equipment and/or operator), an additional digit was added to the laboratory code.

## TREATMENT OF EXPERIMENTAL DATA

*Calculations carried out by all participants*

For each of the analyses, step heights of standard/sample components were measured relative to that of the I.S. and used for within-laboratory identification purposes. They were not reported. For each of the analyses, zone lengths of standard/sample components were measured relative to that of the I.S.:

$$RZL = \text{zone length}_{\text{standard/sample}} / \text{zone length}_{\text{I.S.}} \quad (1)$$

The 1:1 dilution of standard/sample and internal standard solution was carried out on a mass basis. The relative corrected zone length ($RCZL$) was then calculated as

$$RCZL = 1.0058RZL \cdot \text{mass}_{\text{I.S.}} / \text{mass}_{\text{standard/sample}} \quad (2)$$

In this equation, the factor 1.0058 is the ratio of the average density of the sample and the average density of the internal standard solution. A calibration graph of the five standard solutions was then constructed using linear regression [2]. The slope and intercept of the calibration graph of relative corrected zone length (*RCZL*) *vs.* concentration (*c*) were finally reported:

$$RCZL_{\text{standard}} = \text{slope} \cdot c_{\text{standard}} + \text{intercept} \quad (3)$$

The relative corrected zone lengths, *RCZL*, as calculated with eqn. 2, were now considered *y*-data and the concentrations in the calibration solutions *x*-data. The slope, intercept and correlation coefficient were then calculated in the usual manner [2].

The sample concentrations were then calculated from

$$c_{\text{sample}} = (y_c - \text{intercept})/\text{slope} \quad (4)$$

where $y_c$ is the relative corrected zone length (*RCZL*) of the sample.

The calculation of the following parameters might require some explanation. First the following quantities, also needed for the correlation coefficient, were determined:

$$S_{xx} = \sum_{i=1}^{N} (x_i - x_{\text{mean}})^2 \quad (5)$$

$$S_{yy} = \sum_{i=1}^{N} (y_i - y_{\text{mean}})^2 \quad (6)$$

where $x_{\text{mean}}$ and $y_{\text{mean}}$ are mean values of standard concentrations and corresponding *RCZL*, respectively, and $N$ is the number of calibration points ($N = 5$). The standard deviation about regression, $s_{\text{reg}}$, and the standard deviation of the slope, $s_{\text{slope}}$, for the particular laboratory were then calculated:

$$s_{\text{reg}} = [(S_{yy} - \text{slope}^2 \cdot S_{xx})/(N - 2)]^{1/2} \quad (7)$$

$$s_{\text{slope}} = (s_{\text{reg}}^2/S_{xx})^{1/2} \quad (8)$$

Finally, the standard deviation, $s_c$, of the results obtained from the calibration graph was calculated:

$$s_c = \frac{s_{\text{reg}}}{\text{slope}} [1/M + 1/N + (y_c - y_{\text{mean}})^2 / S_{xx} \cdot \text{slope}^2]^{1/2} \quad (9)$$

Here $M = 1$ because results were obtained from a measurement performed in singular. This value $s_c$ was used as the within-laboratory standard deviation.

*Elimination of outliers [3]*

After receiving all results from all participants, data were combined into one database in which first outliers were determined. The outliers distinguished were laboratory outliers and individual results outliers.

First, laboratory outliers were detected by observing the calibration data, for instance if the calibration graph parameters slope, intercept or correlation coefficient deviated substantially from the laboratory-to-laboratory average. We applied the Grubbs outlier test [3] for a 1% confidence level for any of the three parameters, using the laboratory-to-laboratory standard deviation of these values, with the restriction that for the correlation coefficient, which may not be normally distributed, only outliers on the lower side were considered.

After elimination of the laboratory outliers, individual results outliers were detected by comparing the individual value with the mean. Here we also applied the Grubbs outlier test for a 1% confidence level using the laboratory-to-laboratory standard deviation. The Grubbs test was applied to check if the highest or lowest value was an outlier. If this was the case, the outlier was removed and the mean and standard deviation were calculated again. This was repeated until there were no more outliers. Outliers are indicted by asterisks in the tables.

*Repeatability and reproducibility [4]*

In the split-level study, each of the sub-levels was analysed once. For each of the three concentration levels, the following quantities were then calculated according to the required procedure [4]: the repeatability standard deviation $s_r$ and variance $s_r^2$, the between-laboratory standard deviation $s_L$ and variance $s_L^2$, the reproducibility

standard deviation $s_R$ and variance $s_R^2$ and the grand mean $m$. The repeatability values $r$ and the reproducibility values $R$ are 2.8 times $s_r$ and $s_R$, respectively.

## RESULTS AND DISCUSSION

### *Calibration graph data*

First, the statistics of the calibration graphs were determined, using the mass-corrected internal standard method described. Here, one laboratory outlier (laboratory I) had to be eliminated first because of a correlation coefficient for lactate that was obviously too low (0.9955 compared with a minimum value of 0.9990 for the others).

The lactate calibration graphs had an average slope of 0.04807 with a standard deviation of 0.00325, an average intercept of 0.00676 with a standard deviation of 0.0123 and an average correlation coefficient of 0.99980.

The creatinine calibration graphs had an average slope of 0.10166 with a standard deviation of 0.00813, an average intercept of −0.00769 with a standard deviation of 0.0154 and an average correlation coefficient of 0.99977.

The relative standard deviations of the calibration graph slopes (6.8 and 8.0% for lactate and creatinine, respectively) indicate that the method can be transferred and used without recalibration in different laboratories if the required precision is 10%, a value not uncommon in routine analysis.

### *Individual results*

The results of the study are reported in two different ways. For the collaborative study, results of different laboratories were compared. Therefore, from each laboratory one result was taken and sub-laboratory results were disregarded. Then, the results were checked for outliers, according to the criteria mentioned, first for laboratory outliers, then for individual outliers. The data remaining were used to calculate averages, standard deviations and other parameters according to ISO 5725 [4].

Results of lactate and creatinine determinations are summarized in Tables I and II, in which also the standard deviation of the concentration of an average sample ($C$) is given. This parameter $s_c$ is a more sensitive parameter for the quality of the regression than the correlation coefficient. Considerable differences between laboratories are shown. The outlier status of laboratory I for lactate is obvious. After elimination of the corresponding value, the average within-laboratory standard deviations for lactate and creatinine are approximately the same (0.2 mmol/l for lactate and 0.3 mmol/l for creatinine). The $s_c$ value is directly related to the detection limit of the procedure used. Note that significant differences between the laboratories exist: 0.02–0.7 mmol/l for lactate and 0.03–0.6 mmol/l for creatinine. This is related to some extent to the relative sharpness of the zone transitions, as can be seen in Fig. 1, an example of typical lactate isotachopherograms.

Owing to different non-linearities of the detector electronics, significant laboratory-to-laboratory differences in relative step height (*RSH*) values for lactate remain. The within-laboratory standard deviation of the *RSH* values, however, is generally much better (1% or less). Finally, the citrate step is not perfect in several instances, an effect we have observed before when analysing multivalent ions with a.c. conductivity detection.

Mixed zones were reported by some laboratories determining creatinine with a non-corrected version of the procedure, where the pH was too low owing to a glutamate counter-ion concentration that was too high. An erratum was sent to correct this. Laboratory J also reported a mixed zone between leading zone and citrate in the lactate determination. The sample was diluted prior to injection to avoid this effect. The *RSH* value of this mixed zone is low, so that the step from leading zone to mixed zone is easily overlooked and mistaken for the leading zone. For instance, laboratory A, using equipment identical with that of laboratory J, did not report such a mixed zone.

### *Repeatability and reproducibility*

Calculations according to ISO 5725 [4] were carried out with each of the three levels of both lactate and creatinine. The results are given in Table III.

TABLE I

LACTATE RESULTS IN mmol/l

| Laboratory | Sample[a] | | | | | | $s_c$[b] |
|---|---|---|---|---|---|---|---|
| | A | B | C | D | E | F | |
| A | 3.18 | 4.48 | 11.21 | 10.33 | 28.02 | 31.19* | 0.28 |
| B | 3.04 | 4.16 | 10.17 | 9.16 | 26.87 | 28.55 | 0.15 |
| C | 2.96 | 4.15 | 9.92 | 8.67 | 28.43 | 27.24 | 0.48 |
| D | 3.11 | 4.15 | 10.30 | 9.07 | 27.61 | 28.19 | 0.02 |
| E | 3.30 | 4.32 | 10.66 | 9.49 | 27.52 | 28.14 | 0.38 |
| F | 3.07 | 4.09 | 10.16 | 9.33 | 27.02 | 28.52 | 0.06 |
| G | 2.98 | 4.48 | 11.23 | 9.75 | 28.13 | 29.07 | 0.24 |
| H | nd[c] | 4.05 | 10.16 | 9.24 | 26.96 | 27.82 | 0.04 |
| I | 6.21* | 3.90* | 7.91* | 6.60* | 18.99* | 18.67* | 1.50* |
| J | 3.23 | 4.26 | 10.20 | 9.32 | 26.73 | 27.59 | 0.18 |
| K | 2.51 | 3.89 | 10.01 | 9.16 | 27.04 | 28.75 | 0.29 |
| L | 3.14 | 4.15 | 10.22 | 9.14 | 26.72 | 27.89 | 0.06 |
| M | 3.13 | 4.19 | 10.40 | 9.26 | 27.58 | 28.79 | 0.13 |
| N | 2.66 | 4.29 | 10.56 | 9.85 | 26.17 | 28.83 | 0.67 |
| O | 3.16 | 4.11 | 10.32 | 9.20 | 26.58 | 27.81 | 0.07 |
| P | 3.11 | 4.25 | 10.22 | 9.15 | 26.43 | 27.78 | 0.14 |
| Q | 3.13 | 4.06 | 9.93 | 9.14 | 26.62 | nd | 0.28 |
| *n* | 15 | 16 | 16 | 16 | 16 | 14 | 16 |
| True | 3.04 | 4.07 | 10.10 | 9.04 | 26.98 | 28.15 | |
| Mean | 3.05 | 4.19 | 10.35 | 9.33 | 27.15 | 28.21 | 0.22 |
| S.D. | 0.21 | 0.15 | 0.39 | 0.38 | 0.66 | 0.55 | 0.18 |

[a] Outliers are marked with asterisks.
[b] $s_c$ is the within-laboratory standard deviation of the concentration of sample, *C*.
[c] nd = Not determined.

In terms of repeatability standard deviation, both low and medium concentration levels are around 0.2 mmol/l whereas the 27 mmol/l concentration level scores significantly higher: 0.6 mmol/l for lactate and 0.5 mmol/l for creatinine. A relative value of 1–2% over the whole concentration range, however, is acceptable.

Concerning the between-laboratory standard deviation, a high value for the 27 mmol/l creatinine level is observed. Here the true and mean values also differ significantly. A possible reason might be that for this level, decomposition in some laboratories cannot be excluded, in spite of the precautions taken. Some delivery problems reported might also be at the origin.

*Sub-laboratory results*

A considerable number of participants also reported results from sub-laboratories with different equipment, operating conditions, operator or data evaluation method. It was considered incorrect to average these results together with data from other laboratories. The experimental data supplied describe the experimental conditions in considerable detail. An additional aim of this study was to correlate results with experimental data. For these correlations, all results submitted were used, including the outliers. The reason is that outliers are possibly outliers because of experimental conditions. In this way outliers and other results may be explained.

When comparing lactate sub-levels for all (sub-)laboratories, it was observed that in only one instance were the lower and higher sub-levels distinguished incorrectly. When doing the same with the creatinine sub-levels, it was observed that in only two instances were the lower and higher sub-levels distinguished incorrectly. In only a few instances did the difference be-

TABLE II

CREATININE RESULTS IN mmol/l

| Laboratory | Sample[a] | | | | | | $s_c$[b] |
|---|---|---|---|---|---|---|---|
| | A | B | C | D | E | F | |
| A | 28.46 | 26.81 | 8.37 | 9.68 | 3.18 | 4.21 | 0.61 |
| B | 27.13 | 26.17 | 8.27 | 9.51 | 2.44 | 3.10 | 0.24 |
| C | 27.63 | 27.86 | 8.12 | 9.75 | 2.39 | 2.68 | 0.48 |
| D | 27.79 | 27.09 | 8.72 | 9.80 | 3.27 | 4.33 | 0.46 |
| E | 28.28 | 26.28 | 8.94 | 10.12 | 2.85 | 3.66 | 0.19 |
| F | 27.23 | 25.96 | 8.69 | 9.93 | 2.84 | 3.69 | 0.03 |
| G | 26.71 | 24.70 | 8.34 | 9.39 | 2.69 | 3.33 | 0.41 |
| H | nd[c] | 25.77 | 7.95 | 9.82 | 2.73 | 2.98 | 0.31 |
| K | 27.54 | 24.91 | 7.59 | 9.45 | 2.37 | 2.32 | 0.35 |
| L | 27.55 | 26.90 | 8.50 | 9.79 | 2.98 | 3.76 | 0.19 |
| M | 28.07 | 26.47 | 8.36 | 9.69 | 2.94 | 3.74 | 0.12 |
| N | 25.54 | 24.37 | 6.92 | 8.50* | 1.47* | 1.98 | 0.09 |
| O | 27.37 | 26.05 | 8.55 | 9.79 | 2.79 | 3.39 | 0.14 |
| P | 27.25 | 25.79 | 8.39 | 9.60 | 2.66 | 3.52 | 0.20 |
| *n* | 13 | 14 | 14 | 13 | 13 | 14 | 14 |
| True | 28.24 | 27.05 | 8.94 | 10.30 | 3.03 | 3.86 | |
| Mean | 27.43 | 26.08 | 8.26 | 9.72 | 2.78 | 3.34 | 0.27 |
| S.D. | 0.74 | 0.96 | 0.51 | 0.20 | 0.28 | 0.67 | 0.17 |

[a–c] See Table I.

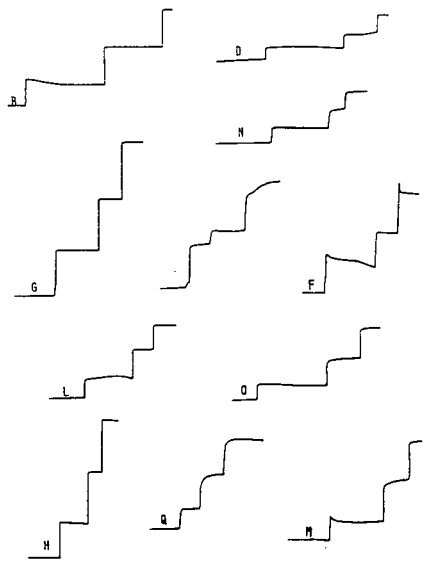


Fig. 1. Isotachopherograms for a typical lactate analysis. Time is from left to right; the vertical axis shows increasing resistance. Zones are chloride (leading), citrate (internal standard), lactate (sample) and glutamate (terminator). The time base is not the same; the figure intends to illustrate qualitative differences.

tween two sub-laboratory results significantly exceed the repeatability standard deviation, $s_r$, of this laboratory.

*Three calibration methods*

For two injection techniques, syringe and loop, three different calibration methods were compared: (i) I.S. + M: internal standard on a mass basis, using the dimensionless relative corrected zone length *RCZL*, as *y*-data in the calibration graph; (ii) I.S.: internal standard, using the dimensionless relative zone length, *RZL*, as *y*-data in the calibration graph; and (iii) E.S.: external standard, using the absolute zone length, *ZL*, in arbitrary units as *y*-data for the calibration graph.

In order to compare the three methods, the relative standard deviations of the slope of the calibration line ($s_{slope}$/slope · 100%) were calculated. As with the $s_c$ values, significant differences between laboratories were observed. Comparing average values therefore does not lead to general conclusions. In some instances, using an internal standard significantly improved the qual-

TABLE III

REPEATABILITY AND REPRODUCIBILITY IN mmol/l (ISO 5725 [4])

| Parameter | Lactate | | | Creatinine | | |
|---|---|---|---|---|---|---|
| | Low | Medium | High | Low | Medium | High |
| Number | 15 | 16 | 14 | 13 | 13 | 13 |
| True mean value | 3.56 | 9.57 | 27.57 | 3.45 | 9.60 | 27.65 |
| Grand mean $m$ | 3.62 | 9.84 | 27.67 | 3.11 | 9.04 | 26.77 |
| Repeatability S.D. $s_r$ | 0.15 | 0.14 | 0.60 | 0.23 | 0.19 | 0.51 |
| Between-laboratory S.D. $s_L$ | 0.15 | 0.37 | 0.43 | 0.42 | 0.25 | 0.80 |
| Reproducibility S.D. $s_R$ | 0.21 | 0.40 | 0.73 | 0.47 | 0.31 | 0.95 |
| Repeatability value $r$ | 0.41 | 0.40 | 1.67 | 0.63 | 0.53 | 1.43 |
| Reproducibility value $R$ | 0.59 | 1.12 | 2.05 | 1.33 | 0.88 | 2.66 |

ity of calibration. In others, where I.S. calibration significantly decreased the performance, it must be concluded that the I.S. method was not properly carried out.

In cases where mass correction did not improve I.S. calibration, it must be concluded that the 1:1 dilution on a volume basis was carried out with sufficient precision, in other words, mass correction did not improve the precision.

*Injection and reproducibility*

The possible difference between syringe and loop injection can be investigated by averaging the standard deviation of the regression, $s_{reg}$, or the within-laboratory standard deviation, $s_c$, of a sample of medium concentration $C$ (see Table IV).

From the results for both lactate and creatinine it can be concluded that loop injection gives a slightly better repeatability than syringe injection. The difference is not very distinct statistically. In addition, it was seen that in spite of using syringe injection, some laboratories performed excellently, explaining the large standard deviation $s_c$ for syringe injection.

TABLE IV

INJECTION AND REGRESSION

| Injection | Lactate | | Creatinine | |
|---|---|---|---|---|
| | $s_{reg}$ [a] | $s_c$ [a] | $s_{reg}$ [a] | $s_c$ [a] |
| Syringe | $n = 18$ | $n = 18$ | $n = 15$ | $n = 15$ |
| Mean | 0.017 | 0.347 | 0.036 | 0.355 |
| S.D. | 0.024 | 0.408 | 0.054 | 0.462 |
| Loop | $n = 7$ | $n = 7$ | $n = 6$ | $n = 6$ |
| Mean | 0.005 | 0.124 | 0.016 | 0.174 |
| S.D. | 0.003 | 0.080 | 0.005 | 0.047 |

*Reproducibility of I.S. zone length*

As the concentration of I.S. is in principle the same in all samples and calibration solutions, the relative standard deviation of the I.S. zone length within a laboratory can be attributed mainly to differences in injection volume. Significant differences between individual laboratories were observed (1–35%). Overall, it cannot be concluded that loop injection performs better in this respect.

*Accuracy*

From the bottom lines of Tables I and II, conclusions can be drawn regarding the accuracy of the procedure for lactate and creatinine, respectively. It appears that in most instances the true and mean values differ less than the between-laboratory standard deviation. This is not so, however, with some of the creatinine samples, where the mean is always less. In spite of the provisions taken in the procedure, decomposition of the sample cannot be excluded.

Accuracy problems may be encountered in individual laboratories due to overloading. This cannot be analysed from the data provided because an unknown number of laboratories used column coupling without explicitly stating

so. In these instances, the effective volume of the capillary between injection and detection cannot be calculated from the inside diameter and length. In addition, those laboratories using loop injection reported the injected volume and not the dilution factor, so that sample load calculations are impossible.

Laboratory J reported problems with the occurrence of mixed zones. The sample was diluted with water to prevent mixed zone formation. How would mixed zones affect the results? Consider lactate, where the citrate internal standard migrates directly behind the leading ion. A mixed zone between leading zone and citrate, if not noticed, may lead to a systematically lower citrate zone length and a different calibration graph slope. As the citrate concentration in all injections is the same, a very reproducible injection may lead to a mixed zone length that is almost constant. Otherwise, a larger standard deviation is expected, in addition to a different slope.

## CONCLUSIONS

Overall, the procedure using an internal standard yielded good results. A weighing correction of the 1:1 dilution step probably did not add to the precision of the method. The linearity over the concentration range used was excellent. The standard deviation of a single determination, using the calibration graph, however, showed large differences between the individual laboratories. In general, only few outliers were reported. It can be concluded that isotachophoresis is a technique suitable for accurate and precise determinations using a straightforward procedure that is easily transferred from one laboratory to another.

## ACKNOWLEDGEMENTS

The chemicals used in this study were a generous gift from Merck (Darmstadt, Germany). Cooperation by the following participants (in random order with respect to laboratory codes) is gratefully acknowledged: J. Caslavska and W. Thormann, University of Berne, CH-3010 Berne, Switzerland; J. Ellis, Staatliches Untersuchungsamt, 6200 Wiesbaden, Germany; B. Gaš and I. Zusková, Charles University, 12840 Prague, Czech Republic; T. Hirokawa, Hiroshima University, Higashi-Hiroshima 724, Japan; P. Janssen and M. Langenhuizen, Organon International, 5340 BH Oss, Netherlands; V. Kašicka and Z. Prusík, Academy of Science, 16610 Prague, Czech Republic; E. Kenndler and W. Friedl, University of Vienna, A-1090 Vienna, Austria; M. Koval, LABECO, Spisska Nova Vess, Czech Republic; L. Krivánková, Institute of Analytical Chemistry, 61142 Brno, Czech Republic; J. Marák, Comenius University, 84215 Bratislava, Slovak Republic; J. Polonsky, Slovak Technical University, 81237 Bratislava, Slovak Republic; J. Sollenberg, National Institute of Occupational Health, S-17184 Solna, Sweden; K. Strikwerda and P. van Dijk, Keuringsdienst, 9700 AL Groningen, Netherlands; J. Tkácová, Comenius University, 84215 Bratislava, Slovak Republic; Th.P.E.M. Verheggen, University of Technology, 5600 MB Eindhoven, Netherlands; and D. Vinjamoori, Monsanto, St. Louis, MO 63167, USA.

## REFERENCES

1 W.D. Pocklington, *Guidelines for the Development of Standard Methods by Collaborative Study*, Laboratory of the Government Chemist, London, 1978.
2 D.A. Skoog, D.M. West and F.J. Holler, *Fundamentals of Analytical Chemistry*, Saunders, New York, 5th ed., 1988.
3 F.E. Grubbs, *Technometrics*, 11 (1969) 1–22.
4 *Precision of Test Methods, Determination of Repeatability and Reproducibility for a Standard Test Method by Inter-Laboratory Tests*, ISO 5725, International Organization for Standardization, Geneva, 1986.

*Journal of Chromatography*, 638 (1993) 205–214
Elsevier Science Publishers B.V., Amsterdam

CHROM. 24 862

# Efficient computerized data acquisition and evaluation for capillary isotachophoresis in quiescent and flowing solution with single detectors placed towards the capillary end

J. Caslavska, T. Kaufmann, P. Gebauer[☆] and W. Thormann[*]

*Department of Clinical Pharmacology, University of Berne, Murtenstrasse 35, CH-3010 Berne (Switzerland)*

ABSTRACT

The use of a commercial, inexpensive, computerized data acquisition system and different data evaluation schemes for isotachophoresis in capillaries is reported. Data acquisition features two channels, automatic range switching and a unique dynamic sampling rate between 0.0125 and 100 Hz which provides compressed data files and smoother signals compared with sampling at a constant rate. Software termed UNIclip was written for data evaluation based on zone length measurements of conductivity and/or UV absorption signals and the chromatographic integration software was employed for data evaluation based on peak areas of baseline-resolved UV absorption peaks. In a configuration with minimized electroosmosis, high-quality data with linear calibration graphs were obtained. In the presence of electroosmosis, and also electroosmosis combined with a vacuum generated co-flow, in principle UV absorbance data with excellent linear calibration and high reproducibility could be obtained. However, the occurrence of outliers and the detection of uneven zone plateaux made accurate quantification difficult using an automated instrument with a single detector placed towards the capillary end.

## INTRODUCTION

In capillary isotachophoresis (CITP), computerized data acquisition and evaluation are prerequisites for automation [1–3], in addition to a more convenient and accurate approach for quantification compared with the customary use of strip-chart recorders and manual data handling [4,5]. During the past decade, computer-based data acquisition systems for laboratory-made [6,7] and commercial [2,3] instruments featuring narrow-bore (200–500 $\mu$m I.D.) PTFE capillary tubes with suppressed electroosmosis have been reported. In other approaches, instrumentation with array [8,9] or scanning [10] detectors along the capillary together with appropriate hardware and software for data collection and evaluation has been developed. Depending on the sophistication and availability of detectors, the programs for data evaluation permit the determination of isotachophoretic zone lengths (zone areas) for calibration and quantification, of step heights for automated zone assignment, of differential detector responses and reconstructed analogue data displays with labelled and quantified zones.

Recently, instrumentation for electrokinetic separations in fused-silica capillaries of very small I.D. (25–75 $\mu$m) became available and the first papers reporting its use for CITP appeared [11,12]. In these configurations using untreated, open-tubular capillaries, the longitudinal electroosmotic flow was found not to disturb isotachophoretic (ITP) zone formation of low-molecular-mass substances, but to make quantifica-

* Corresponding author.
☆ Permanent address: Institute of Analytical Chemistry, Czech Academy of Sciences, 611 42 Brno, Czech Republic.

0021-9673/93/$06.00 

tion more difficult than in classical CITP [13]. Further, it was discovered that small amounts of hydroxypropylmethylcellulose added to the buffer allowed high-resolution isotachophoretic determinations of proteins in the presence of electroosmosis [14]. Similarly, the use of coated capillaries exhibiting minimized electroosmosis for the determination of low-molecular-mass compounds [11] and proteins [15,16] was discussed. Thus, the recent advances in laboratory-made and commercial instruments for capillary electrophoresis offer broad access to CITP with very interesting features for solute monitoring, such as the use of on-column fast scanning polychrome detection [17] or on-line coupling with mass spectrometry [18].

In this study, the detector outputs of two commercial instruments, one of the old generation with a PTFE capillary (Tachophor, in an electroosmosis-free configuration) and a new, automated instrument with a fused-silica capillary (ABI 270A-HT, configuration with strong electroosmosis), were interfaced to a commercial two-channel data acquisition system featuring automatic range switching and a unique, dynamic sampling rate which provides compressed data files compared with data gathering at a constant sampling rate. Software termed UNIclip was written for CITP data evaluation based on zone length measurements of conductivity and/or UV absorption signals and the chromatographic integration software was employed for data evaluation based on peak areas of baseline-resolved UV absorption peaks. With these approaches, quantification in the presence of suppressed or active electroosmosis, and also electroosmosis combined with a vacuum generated co-flow, is compared and a discussion of the pros and cons of CITP in fused-silica capillaries is presented.

## EXPERIMENTAL

### *Chemicals*

All chemicals were of analytical-reagent or research grade. Histidine, histidine hydrochloride, sodium glutamate, glutamic acid, citric acid, lithium lactate, creatinine (CREAT), sodium chloride, tris(hydroxymethyl)aminomethane (Tris) and procaine hydrochloride were purchased from Merck (Darmstadt, Germany), γ-amino-*n*-butyric acid (GABA) and hydroxypropylmethylcellulose (HPMC) from Sigma (St. Louis, MO, USA) and ovalbumin (OVA) from chicken egg, lysozyme (LYSO) from chicken egg white and conalbumin (CAL) from Serva (Heidelberg, Germany).

### *Instrumentation and running conditions*

Experiments with minimized electroosmosis were performed on a Tachophor 2127 analyser (LKB, Bromma, Sweden). This instrument was equipped with a 28 cm × 0.5 mm I.D. PTFE capillary and a conductivity and a UV detector (filter 277 nm) at the column end. The measurements were performed at a constant current of 150 μA. Samples were injected with a 10-μl syringe (Hamilton, Bonaduz, Switzerland). If not stated otherwise, the sample volume applied was 4 μl. The data were registered with a PM8252A two-channel strip-chart recorder (Philips, Eindhoven, Netherlands) and/or using the PC integration pack (PCIP, version 3.0) (Kontron, Zurich, Switzerland). Data storage and computations were executed on a Mandax AT 286 computer (Panatronic, Zurich, Switzerland).

Experiments in flowing solution were performed on an automated Model 270A-HT electrophoresis system (Applied Biosystems, Foster City, CA, USA) featuring fused-silica capillaries of either 50 μm I.D. (total and effective lengths 72 and 52 cm) (Applied Biosystems) or 75 μm I.D. (total and effective lengths 73.5 and 52 cm) (Polymicro Technologies, Phoenix, AZ, USA). A constant voltage of 20 kV was applied, the temperature was set to 35°C and detection was effected at 280 nm. The data were registered with the PCIP (version 3.0) (Kontron). For cationic analyses, the leader and terminator were placed in the cathodic and anodic electrolyte vials, respectively [11]. Prior to each experiment, the capillary was rinsed by vacuum aspiration (20 in.Hg; 1 in.Hg = 3386.4 Pa) with 0.1 *M* sodium hydroxide and leading buffer for 2 and 5 min, respectively. Sample injection was effected with application of a 5.0 in.Hg vacuum for 5, 10 or 20

s. This vacuum was also applied to generate a buffer co-flow during power application.

*Computerized data acquisition and evaluation*

The commercial PCIP together with a Mandax AT 286 computer system was used for data acquisition and raw data storage for the experiments performed on the Tachophor and the ABI 270A-HT. The PCIP features (i) automatic range switching, (ii) a dynamic sampling rate (between 0.0125 and 100 Hz) allowing sampling every 10 ms for quickly changing signals and, depending on the slope of the detector response, with a time interval between 0.01 and 80 s (this providing greatly compressed data files compared with data gathering at a constant sampling rate) and (iii) two channels for the simultaneous recording of the signals of two detectors on an equal time base (see Fig. 1).

The peak areas of UV absorbance data were determined through integration provided by the chromatographic software of the PCIP. Quantification was based on external calibration but could also have been performed using an internal standard. In ITP, quantitative results are typically obtained through zone length measurements,

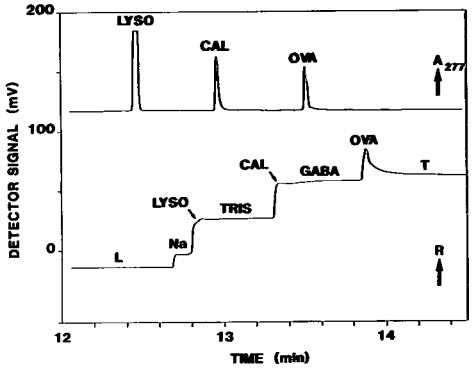


Fig. 1. Cationic CITP data for a model mixture consisting of three proteins and two low-molecular-mass spacers obtained in the Tachophor interfaced to the PCIP system. The UV absorption data (277 nm, top) and the conductivity data (expressed as resistance $R$, bottom) are presented. A 1-$\mu$l volume of a protein mixture containing OVA (2.6 mg/ml), LYSO (2.9 mg/ml) and CAL (2.2 mg/ml) and 1 $\mu$l of a spacer solution consisting of Tris and GABA (several m$M$ each) were injected. L and T refer to leader and terminator, respectively (buffer system C2 in Table I).

particularly when evaluating conductivity or potential gradient data [4,5]. Thus, a software package termed UNIclip was developed that permits the determination of zone lengths from PCIP raw data files, the establishment of linear calibration graphs based on external or internal calibration from a specified set of up to five calibration data files and quantification of a target compound in up to twenty sample runs employing the computer-stored calibration.

The basic program, which includes a shell with guidance through a menu in addition to the data, was written in Clipper (version summer 1987) (Nantucket, Los Angeles, CA, USA), whereas the programs for zone length and height determination and the graphical display were written in Turbo-C$^{++}$ (version 1.0 in ANSI-C standard) (Borland International, Scotts Valley, CA, USA). The algorithm used for zone length determination is based on the slope between two data points, *i.e.*, the difference in signal magnitude divided by the difference in sampling time of these points. A slope higher than that of a preselected value indicates the beginning of a plateau whereas the zone end is characterized by a lower slope than the specified threshold value. Zone assignment is based on comparison of plateau values. Initially a control sample (placed as the first sample to be evaluated) is analysed for plateau values and lengths, their values being written on the screen. The target zone and, if applicable, internal standard zone are then marked, followed by carrying out the complete calibration and evaluation of data. During this procedure, zone heights of each isotachopherogram are corrected based on the relative change between the measured property of its leading zone compared with that of the control sample. Corrected plateau zone values differing by less than a specified value (typically 1–2 mV) from the marked value of the calibration zone are assigned to the zone to be evaluated. Zone lengths and heights are given in units of 0.01 s and mV, respectively. With this procedure, noisy signals might be broken up into several short plateaus of very similar zone height instead of one long zone. For reassessment of such cases, a zone height range (typically 5–20 mV) can be input and used as a second criterion for the

proper determination of the correct plateau length.

## RESULTS AND DISCUSSION

Typical detector signals produced in CITP are depicted in Fig. 1. They represent (top) UV and (bottom) conductivity data of a cationic analysis of LYSO, TRIS, CAL, GABA and OVA using the Tachophor instrument together with the PCIP data acquisition system. The leader and terminator were 10 m*M* potassium acetate–acetic acid (pH 4.75) and 10 m*M* acetic acid, respectively. Depending on sample amount, UV signals represent either rectangular pulses (if sufficient sample for plateau formation is present, as is shown for LYSO) or spikes (CAL and OVA). On the other hand, conductivity data are characterized by a step-like change from the level of the leader (L) to that of the terminator (T). The CITP data format is significantly different to that observed in capillary zone electrophoresis and many forms of chromatographic analyses. Thus, CITP requires different data evaluation strategies, the chromatographic approaches being of little value for most ITP applications. The UNIclip software was developed for quantification by zone length measurements, primarily by the plateau lengths obtained with universal (*e.g.*, conductivity) detectors. It was also found to be applicable for zone lengths of UV signals. Prior to evaluating data obtained in a flowing stream, the performance of UNIclip was investigated

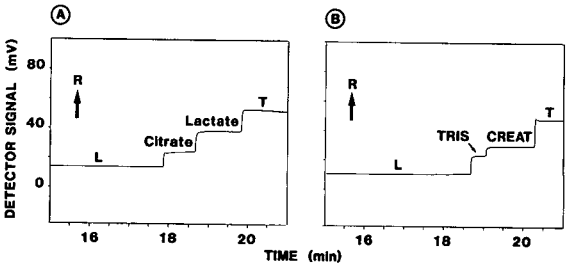


Fig. 2. CITP conductivity PCIP data expressed as resistance *R* for (A) lactate and citrate in buffer system A1 (Table I) and (B) CREAT and Tris in buffer system C1 (Table I). A 4-$\mu$l volume of a sample composed of lactate (30 m*M*), CREAT (30 m*M*), citrate (5 m*M*), Tris (5 m*M*) and 0.9% NaCl was injected. L and T refer to leader and terminator, respectively.

TABLE I

ISOTACHOPHORETIC ELECTROLYTE SYSTEMS

| System | Leader | Terminator |
|---|---|---|
| A1 | 0.01 *M* histidine–0.01 *M* histidine hydrochloride–0.2% HPMC | 0.005 *M* glutamic acid–0.01 *M* histidine |
| C1 | 0.01 *M* sodium glutamate–0.002 *M* glutamic acid (pH 4.95) | 0.005 *M* glutamic acid |
| C2 | 0.01 *M* potassium acetate–acetic acid (pH 4.75) | 0.01 *M* acetic acid |

TABLE II

INSTRUMENTAL CONDITIONS

| System No. | Instrument | Detector | Electroosmosis | Sample compound | Buffer system | Calibration range (m*M*) |
|---|---|---|---|---|---|---|
| 1 | Tachophor | Conductivity | Minimized | Creatinine | C1 | 0–30 |
| 2 | Tachophor | Conductivity | Minimized | Lactate | A1 | 0–30 |
| 3 | Tachophor | UV absorbance | Minimized | Procaine | C1 | 0–30 |
| 4 | ABI 270A-HT | UV absorbance | Yes | Procaine | C1 | 0–30 |

with data obtained on the Tachophor. The electrolyte configurations employed and instrumental conditions are summarized in Tables I and II, respectively.

In a first approach, the use of UNIclip for the evaluation of Tachophor conductivity data of samples provided by an inter-laboratory study on accuracy and precision in CITP [19] was investigated. The cationic determination of creatinine and the anionic determination of lactate in aqueous samples containing 0.9% NaCl was undertaken. Tris and citric acid (5 m*M* each) served as internal standards, respectively. Typical isotachopherograms are presented in Fig. 2. Calibration was performed with five standard solutions having sample concentrations of 0, 2, 5, 15 and 30 m*M*. Excellent linear correlations were obtained with both internal (*i.e.*, inclusion of internal standard) and external calibration (see Systems 1 and 2 in Table III). As example, the output protocol showing the calibration and analysis data for creatinine is presented in Fig. 3. The sequence of the samples consists of the five calibrators in reversed order (data files JC1.381–301), followed by five samples (JC1.311–391). For calibration, the zero value was included. Not surprisingly for this case with little sample preparation, there is good agreement between data evaluated with (A) internal and (B) external calibration. The creatinine levels obtained were found to compare favourably (within a few per cent) with those produced in other laboratories [19]. Similar data were obtained for lactate. Thus UNIclip is shown to handle the evaluation of these data properly.

UNIclip was also employed for the evaluation of Tachophor UV absorption data, such as the cationic CITP of procaine in the electrolyte system C1 (Fig. 4A). Calibration of zone length *versus* sampled amount provided linear relationships with small intercepts when using four or five calibration points (System 3 in Table III). An alternative approach for data evaluation represents the determination of peak areas. For the very simple case of procaine, excellent correlations between peak areas determined by the PCIP integration software and sampled amount were obtained (System 3 in Table III). Thus UNIclip and PCIP software can both be employed for the evaluation of UV absorption data monitored with the Tachophor. UNIclip is capable of recognizing and assigning plateaux whose zone heights differ more than a specified value (typically 1–2 mV). The use of the chromato-

TABLE III

TYPICAL LINEAR REGRESSION ANALYSIS DATA FOR TACHOPHOR CALIBRATIONS

| System No. | I.S.[a] | Evaluated zone property[b] | $n$[c] | Slope | $y$-Intercept[d] | Correlation coefficient |
|---|---|---|---|---|---|---|
| 1 | Yes | Length | 5 | 0.115 | −0.041 | 0.99975 |
| | No | Length | 5 | 240.1 | −37.86 | 0.99993 |
| 2 | Yes | Length | 5 | 0.050 | −0.018 | 0.99983 |
| | No | Length | 5 | 230.2 | −89.37 | 0.99980 |
| 3 | No | Length | 5 | 277.6 | −15.02 | 0.99997 |
| | No | Length | 4 | 278.0 | −24.06 | 0.99997 |
| 3 | No | Area | 5 | 1.561 | 0.29 | 0.99992 |
| | No | Area | 4 | 1.553 | 0.47 | 0.99996 |

[a] Internal standard.
[b] Area determined with PCIP (mV min) and length obtained with UNIclip (0.01 s).
[c] Number of calibrators; with $n = 5$ the zero value was included.
[d] The $y$-intercept units for area, length with I.S. and length without I.S. determinations are mV min, ratio (dimensionless) and 0.01 s, respectively.

(A) UNIclip data: creatinine

Calibration data

| File name | length | length IS | ratio | concentration |
|---|---|---|---|---|
| JC1.301 | 0 | 2410 | 0.0000000 | 0.0000000 |
| JC1.321 | 449 | 2364 | 0.1899323 | 2.0000000 |
| JC1.341 | 1105 | 2279 | 0.4848618 | 5.0000000 |
| JC1.361 | 3574 | 2123 | 1.6834668 | 15.0000000 |
| JC1.381 | 7170 | 2100 | 3.4142857 | 30.0000000 |

Results

| File name | length | length IS | ratio | concentration |
|---|---|---|---|---|
| JC1.381 | 7170 | 2100 | 3.4142857 | 30.0591261 |
| JC1.361 | 3574 | 2123 | 1.6834668 | 15.0017127 |
| JC1.341 | 1105 | 2279 | 0.4848618 | 4.5743416 |
| JC1.321 | 449 | 2364 | 0.1899323 | 2.0085764 |
| JC1.301 | 0 | 2410 | 0.0000000 | 0.3562433 |
| JC1.311 | 544 | 2326 | 0.2338779 | 2.3908849 |
| JC1.331 | 2291 | 2207 | 1.0380607 | 9.3869450 |
| JC1.351 | 1886 | 2268 | 0.8315697 | 7.5905577 |
| JC1.371 | 6224 | 2201 | 2.8278055 | 24.9569896 |
| JC1.391 | 6425 | 2058 | 3.1219631 | 27.5160392 |

(B) UNIclip data: creatinine

Calibration data

| File name | zone length | concentration |
|---|---|---|
| JC1.301 | 0 | 0.0000000 |
| JC1.321 | 449 | 2.0000000 |
| JC1.341 | 1105 | 5.0000000 |
| JC1.361 | 3574 | 15.0000000 |
| JC1.381 | 7170 | 30.0000000 |

Results

| File name | zone length | concentration |
|---|---|---|
| JC1.381 | 7170 | 30.0151598 |
| JC1.361 | 3574 | 15.0406110 |
| JC1.341 | 1105 | 4.7591424 |
| JC1.321 | 449 | 2.0274116 |
| JC1.301 | 0 | 0.1576751 |
| JC1.311 | 544 | 2.4230129 |
| JC1.331 | 2291 | 9.6979119 |
| JC1.351 | 1886 | 8.0114012 |
| JC1.371 | 6224 | 26.0758041 |
| JC1.391 | 6425 | 26.9128131 |

Fig. 3. UNIclip output protocol for the calibration and determination of creatinine using (A) internal and (B) external calibration.

graphic integration software, however, is restricted to situations with zones being bracketed by non-absorbing spacers, *i.e.*, with baseline-resolved signals resembling either spikes or rectangular peaks [Fig. 1 (top) and Fig. 4A] and not step-like functions [Fig. 1 (bottom) and Fig. 2].

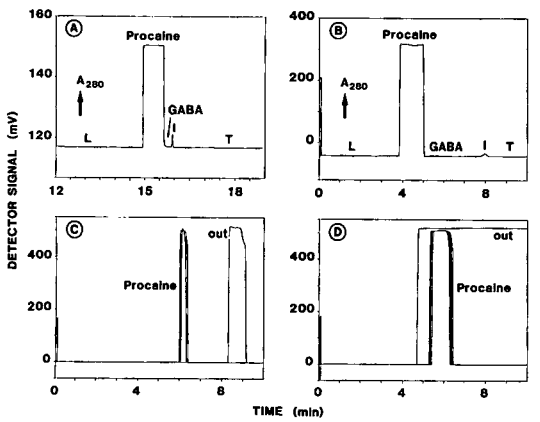


Fig. 4. UV absorption (280 nm) PCIP data for procaine in buffer system C1 using (A) the Tachophor with 2 $\mu$l of a 15 m*M* procaine sample, (B) the ABI 270A-HT with a 50 $\mu$m I.D. capillary and 20-s injection of a 15 m*M* procaine sample, (C) the ABI with a 75 $\mu$m I.D. capillary and 5-s injection of a 5 m*M* procaine sample and (D) the ABI with a 75 $\mu$m I.D. capillary and 5-s injection of a 15 m*M* procaine sample. The experiments in (A) and (B) were executed with addition of GABA for removal of the impurity (I) from the procaine peak. (C) and (D) display data with typical outliers (out) obtained with three and eight consecutive injections, respectively. For the data in (B)–(D), 100 mV corresponds to 0.1 absorbance.

Configurations exhibiting electroosmotic zone displacement are of particular interest because they can easily be implemented on both commercial and laboratory-made instrumentation. Experiments with procaine performed on the automated ABI 270A-HT employing untreated fused-silica capillaries of 50 and 75 $\mu$m I.D. (Fig. 4B) provided calibration data of equal linearity but with larger *y*-intercepts compared with those obtained with the Tachophor (Table IV). The combined application of vacuum-driven buffer flow towards the detector and power, a feature which is provided by the ABI 270A-HT, was also investigated. For one capillary (75 $\mu$m I.D.) procaine calibration data with a hydrodynamic co-flow produced through application of a 5 in.Hg vacuum during detection are presented in Table IV. Again, almost perfect linear behaviour was obtained. The combination of electroosmotic and pressure-driven flows is an attractive feature for cases with low electroosmotic flows, for dual ITP (*i.e.*, the simultaneous monitoring of cationic and anionic zone structures [11]) and to maintain the net zone displacement constant, an approach which would require a special flow control mechanism. Excellent reproducibility was achieved in the presence of electroosmosis

TABLE IV

TYPICAL LINEAR REGRESSION ANALYSIS DATA FOR PROCAINE CALIBRATIONS ON THE ABI270A-HT

System No. 4 without the use of an internal standard.

| Capillary I.D. ($\mu$m) | Injection time (s) | Vacuum during detection | Evaluated zone property[a] | $n$[b] | Slope | $y$-Intercept[c] | Correlation coefficient |
|---|---|---|---|---|---|---|---|
| 50 | 10 | Off | Length | 3 | 234.0 | −863.4 | 0.99986 |
| 50 | 10 | Off | Area | 4 | 15.16 | 5.33 | 0.99998 |
| 50 | 20 | Off | Length | 4 | 375.4 | −305.3 | 0.99212 |
| 50 | 20 | Off | Area | 4 | 23.14 | 16.0 | 0.99399 |
| 75 | 5 | Off | Length | 3 | 349.2 | −1954.8 | 0.98991 |
| 75 | 5 | Off | Area | 4 | 32.03 | −12.29 | 0.99897 |
| 75 | 5 | On | Area | 4 | 5.847 | −0.108 | 0.99976 |
| 75 | 15 | On | Area | 3 | 15.43 | 6.29 | 0.99994 |

[a] Area determined with PCIP (mV min) and length obtained with UNIclip (0.01 s).
[b] Number of calibrators (zero value was not included).
[c] The $y$-intercept units for area and length (without I.S.) determinations are mV min and 0.01 s, respectively.

as shown by the R.S.D. values for nine injections (Table V), the R.S.D.s of area determinations with PCIP integration software (1.3–1.4%) being lower than those based on zone lengths using UNIclip (1.6–2.2%). The same applies for the R.S.D.s of the concentration levels (Table V). Thus, based on these data, CITP in the presence of electroosmosis alone or in combination with vacuum-driven flow should constitute attractive analytical methods. This view, however, is hampered by a number of observations which are discussed in turn.

Despite automatic sampling, every set of runs was characterized with outliers, such as those seen in Fig. 4C and D, which are attributed to changes in electroosmosis. Careful conditioning did not overcome the occurrence of zones with much increased length, making quantification impossible without considering running the samples in duplicate or even triplicate, a time-consuming task. Further, with a single detector placed towards the capillary end (as in all commercial instruments), proper quantification by zone length measurements can only be performed when, during detection, the net displacement of the ITP zones remains constant. This

TABLE V

REPRODUCIBILITY DATA FOR PROCAINE IN PRESENCE OF ELECTROOSMOSIS

| Capillary I.D. ($\mu$m) | Injection time (s) | Evaluated zone property[a] | $n$[b] | Zone property | | Zone concentration | |
|---|---|---|---|---|---|---|---|
| | | | | Mean[a] | R.S.D. (%) | Mean (m$M$) | R.S.D. (%) |
| 50 | 10 | Length | 9 | 3160.3 | 2.18 | 15.52 | 1.80 |
| 50 | 10 | Area | 9 | 247.43 | 1.41 | 15.43 | 1.43 |
| 75 | 5 | Length | 9 | 5058.3 | 1.61 | 15.91 | 1.36 |
| 75 | 5 | Area | 9 | 499.23 | 1.30 | 15.96 | 1.27 |

[a] Area determined with PCIP (mV min) and length obtained with UNIclip (0.01 s).
[b] Number of measurements with a sample containing about 15 m$M$ procaine.

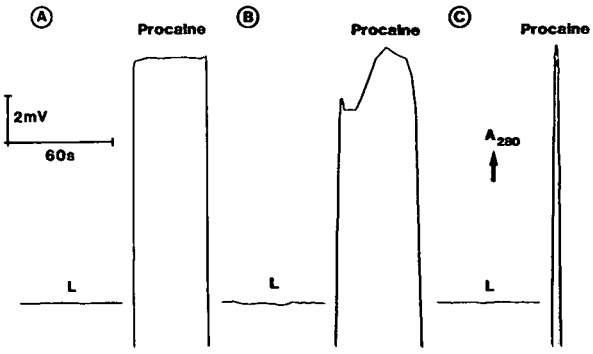


Fig. 5. UV absorption (280 nm) PCIP data with greatly expanded signal scale for leader (L) and procaine zone plateau in buffer systems C1 using (A) the Tachophor with 2 $\mu$l of a 15 m*M* procaine sample, (B) the ABI 270A-HT with a 75 $\mu$m I.D. capillary and 5-s injection of a 15 m*M* procaine sample and (C) the ABI with a 75 $\mu$m I.D. capillary, 5-s injection of a 15 m*M* procaine sample and application of 5 in.Hg vacuum during detection (beginning of co-flow after 3 min of current application).

condition, however, is difficult to meet because the electroosmotic flow is typically changing owing to the gradual change of buffer composition within the column [13]. This problem, however, is not expected in configurations of minimized electroosmosis. Second, data obtained with different capillaries showed considerable variations in noise and shape of the zone plateaux (Fig. 5). Thus, for some cases proper plateau recognition became more demanding and could not be achieved with the algorithm based on the slope between two data points, *i.e.*, the difference in signal magnitude divided by the difference in sampling time of these points. In this approach, in which a slope higher than that of a preselected value indicates the beginning of a plateau whereas the zone end is characterized by a lower slope than the specified threshold value, noisy signals were broken up into several short plateaux of very similar zone height instead of one long zone. With the use of a specified zone height range (typically 5–20 mV above and below the average plateau height) as a second condition, correct plateau lengths could be determined.

The impact of the selection of slope and height range parameters on zone length determination is shown by the data presented in Table VI. Increasing the slope parameter from 50 to 100 or 150 (lines 1, 3 and 6 of Table VI) provides longer mean zone lengths and lower R.S.D. values. A similar effect is seen with increasing height range values (compare lines 3–5). With a range value ±20 mV, equal calculated properties were obtained for all three slope values. Small deviations in zone concentrations were observed with all settings except a slope of 50 and no range value. Thus, a slope of 100 was typically chosen, the

TABLE VI

IMPACT OF SLOPE AND HEIGHT RANGE PARAMETERS ON UNICLIP ZONE LENGTH AND CONCENTRATION DETERMINATION FOR PROCAINE IN PRESENCE OF ELECTROOSMOSIS

Based on nine consecutive experiments with a 15 m*M* procaine sample, 10-s injection and a 50 $\mu$m I.D. capillary.

| Slope[a] (V/s) | Height range (mV)[b] | Mean zone length (0.01 s) | R.S.D. (%) | Mean concentration (m*M*) | R.S.D. (%) |
|---|---|---|---|---|---|
| 50 | – | 2806.0 | 5.21 | 16.61 | 3.90 |
| 50 | 20 | 3160.3 | 2.18 | 15.52 | 1.80 |
| 100 | – | 2920.4 | 3.72 | 15.45 | 2.83 |
| 100 | 10 | 3112.1 | 2.48 | 15.48 | 2.03 |
| 100 | 20 | 3160.3 | 2.18 | 15.52 | 1.80 |
| 150 | – | 3022.0 | 3.13 | 15.55 | 2.48 |
| 150 | 20 | 3160.3 | 2.18 | 15.52 | 1.80 |

[a] The value of the slope is 15 000 times higher than the actual number employed.
[b] The height range value represents the signal magnitude (mV) above and below a specified zone height, defining the range used for zone length determination.

range value being dependent on the quality of the signal. No height range value was necessary for zone length determinations of the Tachophor data whereas most sets of data obtained on the ABI 270A-HT were treated with a range value of 5–20 mV.

The difference in signal noise and shape between the two instruments is illustrated by the data presented in Fig. 5. First, it is apparent that PCIP data gathering with a dynamic sampling rate provides much smoother reponses than sampling at a fixed rate, such as 100 Hz (data not shown), making data smoothing prior to evaluation [20] obsolete. With the Tachophor, an almost perfect rectangular pulse was monitored (Fig. 5A). This, however, was rarely the case in the presence of electroosmosis and with a combination of electroosmosis and co-flow (Fig. 5B and C, respectively). It is interesting that with a slope parameter of 100 and without the use of the height range constraint, the odd-shaped procaine zone in Fig. 5B could be determined as one zone. This was not the case, however, for frequently observed signals with sharply changing noise (data not shown).

In conclusion, PCIP data gathering and automated UNIclip data evaluation provide simple, efficient and relatively inexpensive (<$3500) means for CITP in instruments featuring PTFE or fused-silica capillaries and single, on-column detectors placed towards the capillary end. The PCIP integration software can also be employed for the evaluation of baseline-resolved absorption data. This, however, is restricted to manual operation because CITP detection times are strongly dependent on the sample matrix. CITP in fused-silica capillaries with electroosmotic zone displacement along the capillary is an attractive approach for qualitative characterization of samples, such as the fractions obtained in purification [21] or body fluids received for drug screening [22]. Quantification is difficult for systems in which a significant change in electroosmosis is observed, changes which are dependent not only on the discontinuous buffer system used but also on the sample matrix [13]. Quantification is also hampered by the occurrence of outliers with a drastically different net transport across the point of detection (Fig. 4C and D), by the formation of uneven plateaux (Fig. 5B) and by the loss of certain proteins during the course of an experiment [14]. Concomitant application of a feedback-controlled, pressure- or vacuum-driven flow, however, would not only allow proper performance of dual ITP analyses [11] but would also make the net zone transport constant and therefore accurate quantification possible. The external control of the electroosmotic flow [23,24] would be an alternative to this approach.

ACKNOWLEDGEMENT

This work was supported in part by the Swiss National Science Foundation.

REFERENCES

1 W. Thormann, *J. Chromatogr.*, 334 (1985) 83.
2 F.S. Stover, K.L. Deppermann, W.A. Grote and D.V. Vinjamoori, *J. Chromatogr.*, 390 (1987) 61.
3 H. Carchon and E. Eggermont, *Anal. Chim. Acta*, 219 (1989) 247.
4 F.M. Everaerts, J.L. Beckers and Th.P.E.M. Verheggen, *Isotachophoresis —Theory, Instrumentation and Applications* (*Journal of Chromatography Library*, Vol. 6), Elsevier, Amsterdam, 1976.
5 P. Boček, M. Deml, P. Gebauer and V. Dolník, *Analytical Isotachophoresis*, VCH, Weinheim, 1988.
6 J.C. Reijenga, W. van Iersel, G.V.A. Aben, Th.P.E.M. Verheggen and F.M. Everaerts, *J. Chromatogr.*, 292 (1984) 217.
7 B.J. Wanders, A.A.G. Lemmens, F.M. Everaerts and M.M. Gladdines, *J. Chromatogr.*, 470 (1989) 79.
8 E. Schumacher, D. Arn and W. Thormann, *Electrophoresis*, 4 (1983) 390.
9 T. Hirokawa, K. Nakahara and Y. Kiso, *J. Chromatogr.*, 463 (1989) 39.
10 T. Hirokawa, Y. Yokota and Y. Kiso, *J. Chromatogr.*, 538 (1991) 403.
11 W. Thormann, *J. Chromatogr.*, 516 (1990) 211.
12 J.L. Beckers, F.M. Everaerts and M.T. Ackermans, *J. Chromatogr.*, 537 (1991) 429.
13 M.T. Ackermans, F.M. Everaerts and J.L. Beckers, *J. Chromatogr.*, 545 (1991) 283.
14 P. Gebauer and W. Thormann, *J. Chromatogr.*, 558 (1991) 423.
15 W. Thormann, M.A. Firestone, J.E. Sloan, T.D. Long and R.A. Mosher, *Electrophoresis*, 11 (1990) 298.
16 S. Hjertén and M. Kiessling-Johansson, *J. Chromatogr.*, 550 (1991) 811.
17 P. Gebauer and W. Thormann, *J. Chromatogr.*, 545 (1991) 299.

18 H.R. Udseth, J.A. Loo and R.D. Smith, R.D., *Anal. Chem.*, 61 (1989) 228.
19 J.C. Reijenga, R.G. Trieling and D. Kaniansky, *J. Chromatogr.*, 638 (1993) 195.
20 J.C. Reijenga, *J. Chromatogr.*, 545 (1991) 337.
21 J. Caslavska, P. Gebauer and W. Thormann, *J. Chromatogr.*, 585 (1991) 145.
22 J. Caslavska, S. Lienhard and W. Thormann, *J. Chromatogr.*, 638 (1993) 335.
23 C.S. Lee, W.C. Blanchard and C.T. Wu, *Anal. Chem.*, 62 (1990) 1550.
24 K. Ghowsi and R.J. Gale, *J. Chromatogr.*, 559 (1991) 95.

*Journal of Chromatography*, 638 (1993) 215–223
Elsevier Science Publishers B.V., Amsterdam

CHROM. 24 922

# Study of isotachophoretic separation behaviour of metal cations by means of particle-induced X-ray emission

# V. Fractionation of platinum group elements from a model solution of nuclear fuel waste by means of continuous free-flow isotachophoresis

Takeshi Hirokawa*, Takao Ohta, Isamu Tanaka, Ken-ichiro Nakamura, Wen Xia, Fumitaka Nishiyama and Yoshiyuki Kiso☆

*Applied Physics and Chemistry, Faculty of Engineering, Hiroshima University, Kagamiyama 1, Higashi-hiroshima 724 (Japan)*

ABSTRACT

The fractionation of platinum group elements from a model solution of a high-level liquid waste was investigated using a continuous free-flow isotachophoretic analyser. The leading electrolytes used contained α-hydroxyisobutyric acid (HIB) and tartaric acid as the complex-forming agent, where 20 m*M* $NH_4^+$ was the leading ion and acetic acid was the pH buffer (pH 4.8). The fractions were analysed off-line by means of particle-induced X-ray emission (PIXE). It was found that Fe and platinum group elements split into two zones of cations and non-ions when HIB was used, but all of them was recovered as non-ions when tartaric acid was used. In both electrolyte systems, 100% recovery as cations was obtained for $Cs^+$, $Rb^+$, $Ba^{2+}$, $Sr^{2+}$, $Na^+$, $Cr^{2+}$, $Mn^{2+}$, $Ni^{2+}$, $La^{3+}$, $Ce^{3+}$, $Pr^{3+}$, $Nd^{3+}$, $Sm^{3+}$, $Eu^{3+}$, $Gd^{3+}$ and $Y^{3+}$. It was concluded that free-flow isotachophoresis would be very useful for fractionating platinum group elements from other metal ions.

## INTRODUCTION

In the preceding paper [1] we reported the isotachophoretic (ITP) separation behaviour of a model mixture of a high-level liquid waste (HLLW) by the use of a capillary-type isotachophoretic analyser [1]. An HLLW is generated in the reprocessing stage of a nuclear fuel cycle to recover Pu and U and it contains 30 or more elements: the constituents are the fission products of U (light lanthanides, Cs, Sr and platinum group elements), the fuel cladding materials (Zr) and solidifying agent ($NaNO_3$). An actual HLLW contains considerable amounts of platinum group metals, such as palladium, which have very low radioactivity and may be useful as a catalyst material. For this purpose, they must be separated from the co-existing long-lived and highly radioactive nuclides such as Cs and Sr.

In order to clarify the possibility of using ITP as a fractionating method for HLLW, in this work the separation behaviour of platinum group elements in a model HLLW was investigated by the use of a continuous free-flow ITP apparatus. The fractions were analysed off-line by particle-induced X-ray emission (PIXE). Two kinds of

* Corresponding author.
☆ Present address: Hijiyama Women's College, Ushita-shin-machi, Hiroshima, 732, Japan.

0021-9673/93/$06.00 

complex-forming agents, α-hydroxyisobutyric acid and tartaric acid, were used. The recovery of the components, migration order and separation efficiency of the HLLW components are reported.

## THEORETICAL

### *Processing ability of a free-flow isotachophoretic instrument*

In capillary ITP, the boundary velocity at the steady state remains constant with time provided that a constant current is supplied. However, in free-flow ITP, the boundary velocity decreases during the transit time, even if the migration current is kept constant, because the distribution of migration current in the separation chamber is not homogeneous, that is, the current density decreases from the sample inlet to the outlet with the development of the ITP terminating zone.

Apart from the above point, there is no fundamental difference between capillary ITP and continuous free-flow ITP. The amount of sample separable depends on the amount of electricity during the migration process [2,3]. In the actual instrument, the suppliable amount of electricity depends linearly on the load of the leading electrolyte [2,3]; to increase the load to a capillary ITP analyser, it is necessary to use a long separation tube and/or a concentrated leading electrolyte. Similarly, the separability of a free-flow ITP instrument depends on the volume of the separation chamber occupied by the leading electrolyte and the concentration of the electrolyte.

The separable sample amount ($SA$) of a free-flow ITP analyser during the transit time [$t$ (s)] may consist of three factors:

$$SA = SIt \quad (1)$$

where $S$ denotes the separability of the sample (mol/C) under the electrolyte system and $I$ is the migration current (A). The current $I$ may be set so as not to generate an excess migration voltage, *i.e.*, to keep the target zones within the fractions. Therefore, the current $I$ is closely related to the flow-rate of the electrolyte in the sample chamber. If a high flow-rate is necessary to reduce the transit time, a high migration current can be applied within the practical limit of the cooling unit used. If a long transit time is allowed, the migration current must be set low to prevent overmigration. Consequently, the amount of electricity ($Q$) is automatically determined by the volume of the separation chamber occupied by the leading electrolyte.

In principle, the separability $S$ is the same as in capillary ITP, provided that the same electrolyte system is used at the same temperature.

The processing ability ($P$) of the apparatus per unit time (mol/h) can be defined as

$$P = SI \cdot 3600 \quad (2)$$

The actual sampling rate must be smaller than $P$. It should be noted that the sum of the zone lengths of the sample components cannot exceed the effective width of the sample chamber.

Hence the processing ability of a free-flow ITP instrument for a sample can be estimated from the separability of a capillary ITP analyser.

## EXPERIMENTAL

### *Samples*

A non-radioactive model solution of HLLW (MW-2), which contained 27 kinds of metal ions, was used as the sample [1]. The composition of MW-2 was simulated by Power Reactor and Nuclear Fuel Development (Tokyo, Japan). As the original solution was strongly acidic (2.5 mol/l nitric acid solution), it was not suitable as the sample for ITP. Therefore, the solution was dried to remove nitric acid using an evaporator, and the residue was dissolved by adding deionized water. This process was repeated three times. The solution obtained (pH ≈ 1.5) was diluted with deionized water to 1/350 of the concentration of the original solution. The solution obtained (pH 3.2) was used as the sample. The component concentrations are given in Table I. Small amounts of cationic dyes, toluidine blue (TB) and astrazon pink (AP), were added to the above sample in order to monitor the positions of the zones.

TABLE I

CONCENTRATIONS OF COMPONENTS OF THE MODEL WASTE MW-2

| Z | Element | Form[a] | Concentration ($\mu M$) | Z | Element | Form | Concentration ($\mu M$) |
|---|---|---|---|---|---|---|---|
| 11 | Na | $NaNO_3$ | 2802.9 | 46 | Pd | $Pd(NO_3)_2$ | 24.74 |
| 13 | Al | Al | 0.13 | 47 | Ag | $AgNO_3$ | 1.00 |
| 15 | P | P | 36.3 | 48 | Cd | $Cd(NO_3)_2$ | 1.40 |
| 24 | Cr | $Cr(NO_3)_3$ | 11.29 | 50 | Sn | Sn | 0.94 |
| 25 | Mn | $Mn(NO_3)_2$ | 37.46 | 52 | Te | $TeO_2$ | 10.20 |
| 26 | Fe | $Fe(NO_3)_3$ | 222.0 | 55 | Cs | $CsNO_3$ | 46.00 |
| 28 | Ni | $Ni(NO_3)_2$ | 26.77 | 56 | Ba | $Ba(NO_3)_2$ | 27.77 |
| 34 | Se | $Na_2SeO_3$ | 1.54 | 57 | La | $La_2(CO_3)_3$ | 23.46 |
| 37 | Rb | $RbNO_3$ | 10.40 | 58 | Ce | $Ce(CO_3)_2$ | 168.3 |
| 38 | Sr | $Sr(NO_3)_2$ | 25.09 | 59 | Pr | $Pr_6O_{11}$ | 21.31 |
| 39 | Y | $Y_2O_3$ | 13.91 | 60 | Nd | $Nd_2O_3$ | 71.43 |
| 40 | Zr | $ZrO(NO_3)_2$ | 103.1 | 62 | Sm | $Sm_2O_3$ | 14.57 |
| 42 | Mo | $Na_2MoO_4$ | 87.43 | 63 | Eu | $Eu_2O_3$ | 2.29 |
| 44 | Ru | $Ru(NO_3)_3$ | 48.29 | 64 | Gd | $Gd_2O_3$ | 1.11 |
| 45 | Rh | $Rh(NO_3)_3$ | 9.69 | 72 | U | $UO_2(NO_3)_2$ | 12.13 |

[a] Chemical forms of the reagents used.

*Electrolyte system*

Two leading electrolytes were used, as shown in Table II. One was 20 m$M$ ammonia solution containing 10 m$M$ $\alpha$-hydroxyisobutyric acid (HIB) as the complex-forming agent. The pH of the leading electrolyte ($pH_L$) was adjusted to 4.8 by adding acetic acid. This system is referred to as $WNH_4Ac$–HIB. The other was 20 m$M$ ammonia solution containing 1 or 2 m$M$ tartaric acid as the complex-forming agent. The pH of the leading electrolyte ($pH_L$) was adjusted to 4.8 also by adding acetic acid. This system is referred to as $WNH_4Ac$–Tar. Hydroxypropylcellulose (HPC) was added to both leading electrolytes (0.1%, w/w) to suppress electroosmotic flow. The terminating electrolyte used was 10 m$M$ carnitine hydrochloride for both leading electrolytes.

The operational electrolyte systems used permits two-dimensional isotachophoresis [4,5], *i.e.*, both cations and anions can migrate isotachophoretically toward the respective electrodes. The leading anion was 10 m$M$ $Cl^-$ and the terminating ion was 10 m$M$ HIB or 1 m$M$ Tar.

All the reagents used were purchased from

TABLE II

ELECTROLYTE SYSTEMS USED IN ISOTACHOPHORETIC SEPARATIONS

HIB = $\alpha$-hydroxyisobutyric acid; Tar = tartaric acid; HPC = hydroxypropylcellulose.

| Parameter | $WNH_4Ac$–HIB | $WNH_4Ac$–Tar |
|---|---|---|
| Leading electrolyte | 20 m$M$ $NH_3$ solution | 20 m$M$ $NH_3$ solution |
| Complexing agent | 10 m$M$ HIB | 1 m$M$ Tar |
| pH buffer | Acetic acid | Acetic acid |
| pH | 4.80 | 5.00 |
| Additive | 0.1% HPC | 0.1% HPC |
| Terminating electrolyte | 10 m$M$ carnitine hydrochloride | |
| pH | 2.5 | |

Tokyo Kasei (Tokyo, Japan). pH measurements were carried out using a Horiba (Tokyo, Japan) Model F7ss expanded pH meter.

*Free-flow isotachophoretic instrument*

The preparative instrument used was a Bender and Hobein Elphor Vap 22. Fig. 1 illustrates the electrolyte circuits of the apparatus when it was operated in the ITP mode. The effective size of the separation chamber (SC) was 10 cm wide, 50 cm high and 0.5 mm thick. The sample solution (S) was supplied by a sixfold peristaltic pump (P1) together with the leading electrolyte (L2) and the terminating electrolyte (T2). Ninety fractions were obtained using a 90-fold peristaltic pump (P2). The leading and terminating electrolytes (L1 and T1) used for the electrode compartments (L and T) were 2 l in volume and they were circulated by pumps (PL and PT) during migration. The separation chamber was thermostated at 15°C.

*PIXE analysis*

For the measurement of PIXE spectra, a Model AN-2500 Van de Graaff accelerator (Nisshin High Voltage, Tokyo, Japan) at the Faculty of Engineering, Hiroshima University, was used. The energy of the $H^+$ beam was 2.0 MeV and the beam current was 20–50 nA. A typical single run for ITP fractions took 190–260 s. The detector used was a high-purity Ge detector (ORTEC Model GLP-10180) and the multi-channel analyser used was a Laboratory Equipment (Tokyo, Japan) Model AMS-1000.

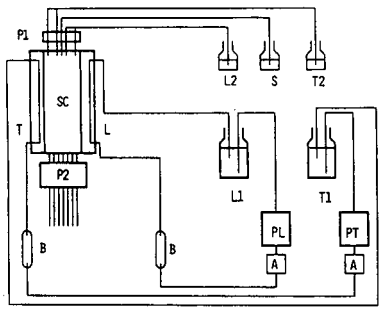


Fig. 1. Electrolyte circuits of free-flow isotachophoresis instrument. SC = separation chamber; L = leading electrolyte and electrode compartment; T = terminating electrolyte and electrode compartment; P1 = peristaltic pump to feed sample and electrolyte; P2 = 90-fold peristaltic pump for fractionation; S = sample solution reservoir; L1 and L2 = leading electrolyte reservoir; T1 and T2 = terminating electrolyte reservoir; PL and PT = electrolyte circulation pumps; A = flow-rate adjuster; B = bubble trap.

The Nuclepore filter used as the target backing material was of thickness 5 $\mu$m and pore size 0.1 $\mu$m, and was mounted on an aluminium flame. Each fraction was sampled using a 5-$\mu$l pipette (Eppendorf Model 4700) on to the filter. The diameter of the fraction spot was *ca.* 3 mm. A PIXE spectrum was measured for each fraction after drying in a desiccator. In order to calibrate the PIXE sensitivities, standard samples (5 $\mu$l, 1000 ppm solution for atomic absorption spectrometry; Tokyo Kasei) were used.

A few or more components were contained in a fraction when the abundances were low. The computer code PIXS developed previously [6] was used to analyse the PIXE spectra. Least-squares fitting for spectrum deconvolution was carried out utilizing the X-ray relative intensity database, which was optimized to our measurement system. Calculations were carried on an NEC (Tokyo, Japan) PC-9801RA microcomputer (CPU = 80 386, co-processor = 80 387, clock = 20 MHz). It took 1 min to analyse the spectrum of one fraction.

## RESULTS AND DISCUSSION

*Determination of sample rate*

As the present sample was inorganic, a longer transit time caused no problems. We selected the minimum value appropriately as *ca.* 500 s. In the actual experiments, the transit time was calculated from the flow-rate and the volume of the sample chamber ($10 \times 50 \times 0.25$ cm) and the sample flow-rate was adjusted to give a residence time of 500 s. The total flow-rates of the leading electrolyte, terminating electrolyte and the sample solution were 191.4, 125 and 96 ml/h, respectively. The electrolytes were supplied to the separation chamber by a sixfold peristaltic pump, where one port was for the sample solution, three ports were for the leading electrolyte and two ports were for the terminating electrolyte. The same transit times were calculated as 471, 720 and 937 s, respectively, and the migration current $I$ was fixed at 30 mA.

Capillary ITP experiments have shown that the separability of MW-2 using the $WNH_4Ac$–HIB system was 1.14 $\mu$mol/C at 25°C [1]. From this value and the migration current, the processing ability ($P$ in eqn. 2) can be calculated as 123 $\mu$mol/h. To achieve this value at a flow-rate of 31.9 ml/h, the original model solution was diluted 1:350. Therefore, the molar sampling rates at the other flow-rates were 80 and 60 $\mu$mol/h.

*Separation behaviour of MW-2 with the $WNH_4Ac$–HIB system*

The migration order of MW-2 components using the $WNH_4Ac$–HIB system was ascertained from capillary ITP experiments to be $Cs^+$, $Rb^+$, $Ba^{2+}$, $Sr^{2+}$, $Na^+$, $Mn^{2+}$, $Fe^{2+}$, ($Cr^{2+}$, $Rh^{2+}$, $Cd^{2+}$), $Ni^{2+}$, $La^{3+}$, $Ce^{3+}$, $Pr^{3+}$, $Nd^{3+}$, $Sm^{3+}$, $Eu^{3+}$, $Gd^{3+}$, $Y^{3+}$, ($Fe^{3+}$, $Ru^{3+}$, $Rh^{3+}$, $ZrO^{2+}$). It should be noted that mobilities of $Cs^+$ and $Rb^+$ are larger than that of the leading ion $NH_4^+$ and therefore these ions migrate zone electrophoretically in the leading zone. A concentrated colloidal zone containing Fe, Ru, Rh and ZrO was observed just before the terminating zone. Although the cation recovery was 100% for $Ba^{2+}$, $Sr^{2+}$, $Na^+$, ($Cd^{2+}$, $Cr^{2+}$), $Ni^{2+}$, $La^{3+}$, $Ce^{3+}$, $Pr^{3+}$, $Nd^{3+}$, $Sm^{3+}$, $Eu^{3+}$, $Gd^{3+}$ and $Y^{3+}$, almost all of $Fe^{3+}$, $Ru^{3+}$ and $Rh^{3+}$ and half of $ZrO^{2+}$ and $Rh^{2+}$ could not be recovered as cations. The components migrating as anions were a part of $MoO_4$, Zr and Se. The low cation recovery of $Fe^{3+}$, $Ru^{3+}$, $Pd^{3+}$ and $Rh^{3+}$ suggested that the remainder might form immobile non-ions [1,7].

Fig. 2 shows the results of PIXE analysis for each of the fractions that were obtained with the continuous free-flow instrument varying the sampling rate of MW-2 at (A) 123, (B) 80 and (C) 60 $\mu$mol/h. Not all of the fractions were analysed. The sample injection port used was positioned approximately above the 55th fractionating port. Although the electrolyte system used permits two-dimensional ITP, the anionic components were not fractionated because of the small width (10 cm) of the separation chamber used and the low abundances [1]. The sample components shown in Fig. 2 were restricted to the representative components Fe, Ce, Ba, Cs and platinum metals. The distribution of Na was not determined (PIXE inactive) but it has already been found in experiments using capillary ITP that an Na zone existed between the Ba and Ce zones [1].

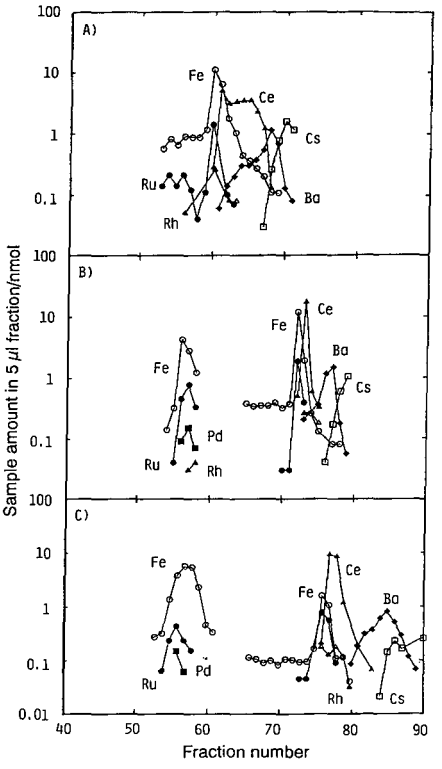


Fig. 2. Analytical results for the cationic and non-ionic fractions of MW-2 obtained by means of PIXE with the $WNH_4Ac$–HIB system. The molar sampling rate was (A) 123, (B) 80 and (C) 60 $\mu$mol/h. For the electrolyte system, see Table II; migration current = 30 mA; temperature of separation chamber = 15°C.

Apparently from Fig. 2, the separability depended on the sampling rate. In fact, we could observe the separation process of the MW-2 components by changing the sampling rate. At 123 $\mu$mol/h the separation was in the initial stage, and at 60 $\mu$mol/h the separation was still incomplete. Better results will be obtained at the lower sampling rate, although the present experiments gave enough information on the separation behaviour of MW-2. The actual processing ability was thus smaller than that calculated from capillary ITP experiments, which might be main-

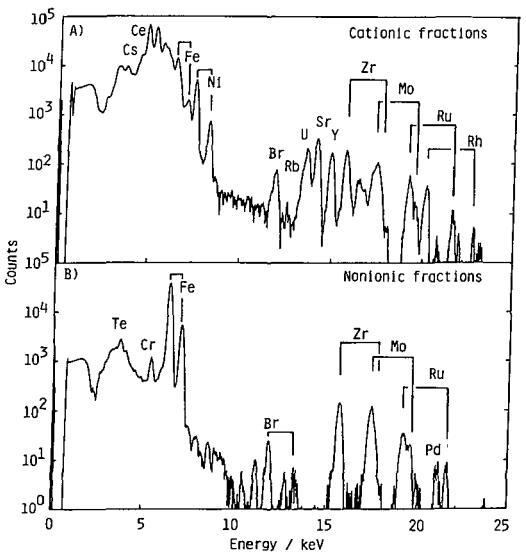


Fig. 3. Merged PIXE spectra of (A) the cationic fractions and (B) the non-ionic fractions. Electrolyte system, $WNH_4Ac$–HIB; $E_p = 2$ MeV.

ly due to the fact that the temperature of the separation chamber was thermostated at 15°C.

Fig. 3 shows the merged PIXE spectra of the cationic fractions and non-ionic fractions. Obviously from Fig. 3, Fe, Zr, Mo and platinum group elements (Ru, Rh and Pd) split into two zones of non-ions and cations. This is the significant feature of the separation behaviour when this electrolyte system is used.

Table III summarizes the component amounts determined by PIXE together with the cation and anion recoveries. Most of the component amounts agreed with each other within experimental errors. The significant decrease in the Cs and Rb levels was due to the fact that not all of the zones were analysed and at the lowest sampling rate (Fig. 2C) the Cs and Rb zones migrated into the leading electrode compartment.

In Fig. 2B, the Fe zone shows a long tail. This suggested that the colloidal Fe zone migrating just before the terminating zone was not stable and the amount of Fe in the Fe zone decreased gradually during migration. Table IV gives the relative abundances of MW-2 components in the original sample and the fractions where Ce was normalized as 100. The abundance of Fe non-ions and Fe cations were 86% and 14% at 123 μmol/h and 17% and 83% at 60 μmol/h, respectively. A similar change was observed for platinum group elements, although not as large. Moreover, the total amount of Fe decreased slightly.

This observation was not an experimental error, as we observed the formation of a red-brown precipitate of Fe compounds in the separation chamber as a narrow stream with 60 μmol/h operation, and the precipitate was found at the bottom of the fractions tubes which corresponded to the non-ions.

The relative abundances of the components agreed well with each other among three experiments, as shown in Table IV. However, in comparison with the relative abundance of the sample, significant differences were found for Zr, Mo, Ru, Rh and Pd, suggesting that these were not contained in the sample solution. In fact, the original sample was the filtered solution of the original mixture. Insoluble substances consisted mainly of Zr. Small amounts of Mo, Ru, Rh, Pd and other elements were also found in the precipitate.

*Separation behaviour of MW-2 with the $WNH_4Ac$–Tar system*

Fig. 4 shows the analytical results for the fractions. Although the separation behaviour was very similar to that for the $WNH_4Ac$–HIB system for many components, very different separation behaviour was observed for Fe, Zr, Mo and platinum group elements, *i.e.*, the Fe, Zr and Mo zones migrating just before the terminating electrolyte observed with the $WNH_4Ac$–HIB system disappeared completely. Most of Fe was found as non-ions and only a small amount was fractionated at $Fe^{2+}$.

Fig. 5 shows the merged PIXE spectra of the cationic and non-ionic fractions. The above discussion about the migration behaviour of Fe, Zr and Mo is obvious from Figs. 3 and 5. That is, the X-ray bands of Fe, Zr and Mo were significant in Fig. 3A but not in Fig. 5A. One more important observation was that the $UO_2^{2+}$ ion was not observed in the cationic fractions with the $WNH_4Ac$–Tar system, because the effective mobility of $UO_2^{2+}$ with the $WNH_4Ac$–Tar system

TABLE III

SAMPLE AMOUNTS IN FRACTIONS ANALYSED BY PIXE

Electrolyte system: $WNH_4Ac$–HIB. $T$ = total amount (nmol) of sample components found in 5-μl fractions; $C$ = recovery as cations (%); $N$ = recovery as non-ions (%).

| Z | Element | Sampling rate (μmol/h) | | | | | | | | |
|---|---|---|---|---|---|---|---|---|---|---|
| | | 123 | | | 80 | | | 60 | | |
| | | T (nmol) | C (%) | N (%) | T (nmol) | C (%) | N (%) | T (nmol) | C (%) | N (%) |
| 24 | Cr | 1.36 | 100 | 0 | 1.30 | 92 | 8 | 0.76 | 100 | 0 |
| 25 | Mn | 5.30 | 100 | 0 | 4.70 | 100 | 0 | 4.56 | 100 | 0 |
| 26 | Fe | 28.64 | 86 | 14 | 27.22 | 67 | 33 | 23.02 | 17 | 83 |
| 28 | Ni | 3.61 | 100 | 0 | 3.30 | 100 | 0 | 3.02 | 100 | 0 |
| 34 | Se | nd[a] | | | | | | | | |
| 37 | Rb | 0.96 | 100 | 0 | 0.44 | 100 | 0 | 0.07 | 100 | 0 |
| 38 | Sr | 2.94 | 100 | 0 | 2.92 | 100 | 0 | 2.76 | 100 | 0 |
| 39 | Y | 1.21 | 100 | 0 | 1.67 | 100 | 0 | 1.59 | 100 | 0 |
| 40 | Zr | 2.90 | 58 | 42 | 3.96 | 51 | 49 | 2.98 | 43 | 57 |
| 42 | Mo | 4.44 | 63 | 37 | 5.08 | 52 | 48 | 3.96 | 40 | 60 |
| 44 | Ru | 2.53 | 66 | 34 | 3.88 | 59 | 41 | 2.43 | 56 | 44 |
| 45 | Rh | 0.32 | 100 | 0 | 0.40 | 100 | 0 | 0.44 | 100 | 0 |
| 46 | Pd | nd | | | 0.34 | 0 | 100 | 0.14 | 0 | 100 |
| 47 | Ag | nd | | | | | | | | |
| 48 | Cd | nd | | | | | | | | |
| 50 | Sn | nd | | | | | | | | |
| 52 | Te | nd | | | | | | | | |
| 55 | Cs | 4.00 | 100 | 0 | 1.87 | 100 | 0 | 0.64 | 100 | 0 |
| 56 | Ba | 3.93 | 100 | 0 | 3.94 | 100 | 0 | 3.49 | 100 | 0 |
| 57 | La | 3.56 | 100 | 0 | 3.26 | 100 | 0 | 2.89 | 100 | 0 |
| 58 | Ce | 23.85 | 100 | 0 | 21.94 | 100 | 0 | 21.23 | 100 | 0 |
| 59 | Pr | 3.00 | 100 | 0 | 2.69 | 100 | 0 | 2.79 | 100 | 0 |
| 60 | Nd | 10.25 | 100 | 0 | 9.11 | 100 | 0 | 9.15 | 100 | 0 |
| 62 | Sm | 2.08 | 100 | 0 | 1.74 | 100 | 0 | 1.97 | 100 | 0 |
| 63 | Eu | 0.64 | 100 | 0 | 0.78 | 100 | 0 | 0.51 | 100 | 0 |
| 64 | Gd | 0.20 | 100 | 0 | 0.17 | 100 | 0 | 0.20 | 100 | 0 |
| 92 | U | – | – | – | 0.94 | 100 | 0 | 0.81 | 100 | 0 |

[a] nd = Not determined (the elements were in the non-ionic precipitates).

was not so large that it migrated in the terminating zone in a zone electrophoretic mode (Fig. 4).

From Fig. 5, it was expected that most of the Fe, Zr, Mo and platinum group elements were precipitated in the non-ionic fractions. Fig. 6 shows the PIXE spectrum of the red-brown precipitate. The solution of non-ionic fractions was decanted and the residue was used as the PIXE target after drying in a desiccator. Obviously from Fig. 6, the major components in the precipitate were Fr, Zr, Mo and Ru. Rh and Pd were also found in the precipitate.

Table V shows the component amounts determined by PIXE and their relative abundances; Ce was normalized as 100. In comparison with Table IV, the non-ionic abundance was much smaller than that with the $WNH_4Ac$–HIB system. As shown in Fig. 6, several elements (Te, Se, Ag, etc.) were found in the precipitate. These elements were not determined because the precipitate sample was not a so-called "thin target" but a "thick target", where correction of the X-ray absorption and energy down of the proton beam must be taken into account. The program PIXS did not fully support thick target analysis. However, it is obvious that the

TABLE IV

RELATIVE ABUNDANCES OF MW-2 COMPONENTS IN THE FRACTIONS (Ce = 100)

| Z | Element | Relative abundance (%) | | | |
|---|---|---|---|---|---|
| | | Sample | Sampling rate (μmol/h) | | |
| | | | 123 | 80 | 60 |
| 24 | Cr | 6.7 | 5.7 | 5.9 | 3.6 |
| 25 | Mn | 22.3 | 22.2 | 21.4 | 21.5 |
| 26 | Fe | 131.9 | 120.1 | 124.0 | 108.4 |
| 28 | Ni | 15.9 | 15.1 | 15.0 | 14.2 |
| 34 | Se | 0.9 | 0.0 | 0.0 | 0.0 |
| 37 | Rb | 6.2 | 4.0 | 2.0 | 0.3 |
| 38 | Sr | 14.9 | 12.3 | 13.3 | 13.0 |
| 39 | Y | 10.7 | 5.1 | 7.6 | 7.5 |
| 40 | Zr | 61.3 | 12.2 | 18.1 | 14.0 |
| 42 | Mo | 52.0 | 18.6 | 23.2 | 18.7 |
| 44 | Ru | 28.7 | 10.6 | 17.7 | 11.5 |
| 45 | Rh | 5.8 | 1.3 | 1.8 | 2.1 |
| 46 | Pd | 14.7 | nd[a] | 1.6 | 0.7 |
| 47 | Ag | 0.6 | nd | | |
| 48 | Cd | 0.8 | nd | | |
| 50 | Sn | 0.6 | nd | | |
| 52 | Te | 6.1 | nd | | |
| 55 | Cs | 27.3 | 16.8 | 8.5 | 3.0 |
| 56 | Ba | 16.5 | 16.5 | 18.0 | 16.4 |
| 57 | La | 13.9 | 14.9 | 14.9 | 13.6 |
| 58 | Ce | 100.0 | 100.0 | 100.0 | 100.0 |
| 59 | Pr | 12.7 | 12.6 | 12.3 | 13.1 |
| 60 | Nd | 42.4 | 43.0 | 41.5 | 43.1 |
| 62 | Sm | 8.7 | 8.7 | 7.9 | 9.3 |
| 63 | Eu | 1.4 | 2.7 | 3.6 | 2.4 |
| 64 | Gd | 0.7 | 0.8 | 0.8 | 0.9 |
| 92 | U | | 0.0 | 4.3 | 3.8 |

[a] nd = Not determined (the elements were in the non-ionic precipitates).

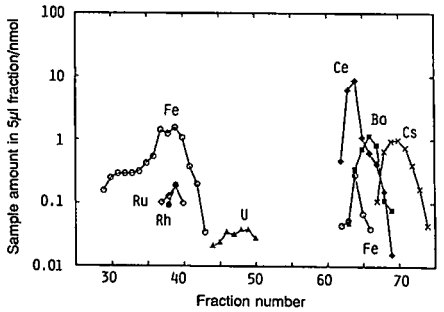


Fig. 4. Analytical results for the cationic and non-ionic fractions of MW-2 obtained by means of PIXE with the $WNH_4Ac$–Tar system. Molar sampling rate, 80 μmol/h; migration current = 30 mA; temperature of separation chamber = 15°C.

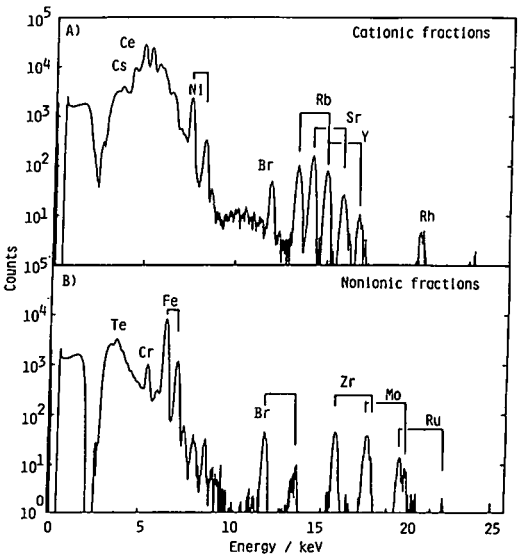


Fig. 5. Merged PIXE spectra of (A) the cationic fractions and (B) the non-ionic fractions. Electrolyte system, $WNH_4Ac$–Tar; $E_p = 2$ MeV.

$WNH_4Ac$–Tar system is suitable for fractionating platinum group elements by means of free-flow ITP.

As the electrolyte system used is two-directional, simultaneous fractionation of anions, non-ions and cations was tried using the Elphor Vap 22 instrument. However, it was unsuccessful. The width of the separation chamber (10 cm) of the present instrument seems to be too small for two-dimensional fractionation of the present model waste. Better fractionation might be

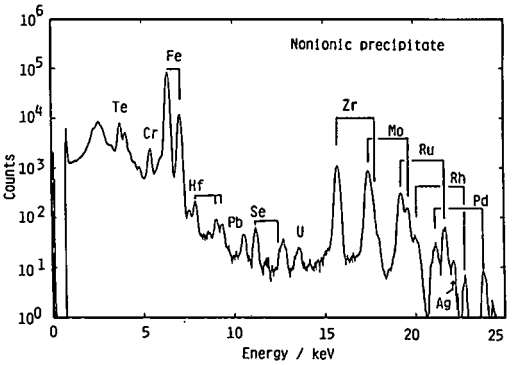


Fig. 6. PIXE spectra of the non-ionic precipitate in non-ionic fractions. Electrolyte system, $WNH_4Ac$–Tar; $E_p = 2$ MeV.

TABLE V

COMPONENT AMOUNTS DETERMINED BY PIXE

Electrolyte system: $WNH_4Ac$–Tar. $T$ = total amount (nmol) of sample components found in 5-$\mu$l fractions; $C$ = recovery as cations (%); $N$ = recovery as non-ions (%).

| Z | Element | T (nmol) | Relative abundance (%) | C (%) | N (%) |
|---|---|---|---|---|---|
| 24 | Cr | 0.54 | 3.1 | 100 | 0 |
| 25 | Mn | 4.15 | 23.6 | 100 | 0 |
| 26 | Fe | 8.84 | 50.3 | 6 | 94 |
| 28 | Ni | 2.76 | 15.7 | 100 | 0 |
| 34 | Se | nd[a] | | | |
| 37 | Rb | nd | | | |
| 38 | Sr | 2.41 | 13.7 | 100 | 0 |
| 39 | Y | 1.15 | 6.6 | 100 | 0 |
| 40 | Zr | 0.56 | 3.2 | 0 | 100 |
| 42 | Mo | 0.73 | 4.2 | 0 | 100 |
| 44 | Ru | 0.20 | 1.1 | 0 | 100 |
| 45 | Rh | 0.14 | 0.8 | 100 | 0 |
| 46 | Pd | nd | | | |
| 47 | Ag | nd | | | |
| 48 | Cd | nd | | | |
| 50 | Sn | nd | | | |
| 52 | Te | nd | | | |
| 55 | Cs | 4.15 | 23.6 | 100 | 0 |
| 56 | Ba | 3.25 | 18.5 | 100 | 0 |
| 57 | La | 2.42 | 13.8 | 100 | 0 |
| 58 | Ce | 17.56 | 100.0 | 100 | 0 |
| 59 | Pr | 2.08 | 11.9 | 100 | 0 |
| 60 | Nd | 7.74 | 44.1 | 100 | 0 |
| 62 | Sm | 1.56 | 8.9 | 100 | 0 |
| 63 | Eu | 0.63 | 3.6 | 100 | 0 |
| 64 | Gd | 0.18 | 1.0 | 100 | 0 |
| 92 | U | 0.21 | 1.2 | 100 | 0 |

[a] nd = Not determined (the elements were found only in the non-ionic precipitates).

achieved by using a separation chamber of width 50 cm or more.

ACKNOWLEDGEMENT

The authors express their thanks to Power Reactor and Nuclear Fuel Development (Tokyo, Japan) for financial support of part of this work. T.H. also wishes to thank the Ministry of Education, Science and Culture of Japan for support of part of this work under a Grant-in-Aid for Scientific Research (No. 04650683).

REFERENCES

1 T. Hirokawa, M. Ueda, A. Ijyuin, S. Yoshida, F. Nishiyama and Y. Kiso, *J. Chromatogr.*, 633 (1993) 261.
2 F.E.P. Mikkers, F.M. Everaerts and J.A.F. Peek, *J. Chromatogr.*, 168 (1979) 293.
3 F.E.P. Mikkers, F.M. Everaerts and J.A.F. Peek, *J. Chromatogr.*, 168 (1979) 317.
4 W. Thormann, D. Arn and E. Schumacher, *Electrophoresis*, 6 (1985) 10.
5 T. Hirokawa, K. Watanabe, Y. Yokota and Y. Kiso, *J. Chromatogr.*, 633 (1993) 251.
6 T. Hirokawa, F. Nishiyama and Y. Kiso, *Nucl. Instr. Methods*, B31 (1988) 525.
7 P. Boček and F. Foret, *J. Chromatogr.*, 313 (184) 189.

*Journal of Chromatography*, 638 (1993) 225–229
Elsevier Science Publishers B.V., Amsterdam

CHROM. 24 870

# Photometric detection of amino-containing compounds in capillary isotachophoresis based on reaction with copper(II) ions

Dušan Kaniansky* and Imrich Zelenský

*Department of Analytical Chemistry, Faculty of Natural Sciences, Komenský University, Mlynská Dolina CH-2, 842 15 Bratislava (Slovak Republic)*

ABSTRACT

Some basic aspects of the photometric detection of amines, amino acids and peptides via their complexes (chelates) formed with $Cu^{2+}$ ions in capillary isotachophoresis (ITP) were studied. Experiments performed in this feasibility study were focused on the complexes of separands formed on the addition of $Cu^{2+}$ ions to the sample solution and the cationic mode of migration. The results suggest that only the compounds that form chelates with more than one ring are detectable photometrically as probably only this type of chelate did not bleed during the separation (migration). Detection limits for these ITP separands were in the range $10^{-7}$–$10^{-6}$ mol/l (30-$\mu$l sample volumes) when detection was carried out at 580 nm. ITP runs with various sample matrices indicate a high analytical selectivity of this mode of detection.

## INTRODUCTION

Capillary isotachophoresis (ITP) is a convenient technique for the separation and analysis of amines, amino acids and peptides present in various matrices (see, *e.g.*, refs. 1–6). As many of these constituents do not respond to ITP-selective detectors, their detection by universal conductivity detectors is often the only alternative [1–6]. However, this is a disadvantage when they need to be determined at trace concentrations and/or in complex ionic matrices. In such instances, the use of selective detectors, preferably in the spike mode [7,8], is advantageous. In conjunction with these detectors, pre-column reactions labelling the analyte(s) with appropriate chromophore(s) [9] or fluorophore(s) [10] may also be very useful.

It is well known that many amino-containing compounds form intensely blue complexes (chelates) with $Cu^{2+}$ ions. From the point of view of ITP analysis, it is apparent that these reactions may form a basis for their selective photometric detection. Although complexes of amino acids with $Cu^{2+}$ have been employed to optimize their ITP separation conditions [6,11], no attention was paid to the use of these reactions for detection in ITP or in any of the related capillary electrophoretic techniques. This work was intended to study some basic aspects of the photometric detection of amines, amino acids and peptides via their complexes (chelates) with $Cu^{2+}$ ions in ITP.

## EXPERIMENTAL

### *Instrumentation*

A CS isotachophoretic analyser (Labeco, Spišská Nová Ves, Slovak Republic) was used in the column-coupling configuration of the separation unit. The analytical column of the analyser was provided with a laboratory-made photometric detector with an LQ 1411 light-emitting diode

* Corresponding author.

0021-9673/93/$06.00 

(Tesla, Rožnov, Czech Republic) as a monochromatic source of light at 580 nm. A KPX 81 phototransistor (Tesla) served as a photosensing element of this detector, described in detail elsewhere [12].

*Chemicals*

Chemicals were obtained from Serva (Heidelberg, Germany), Sigma (St. Louis, MO, USA), Lachema (Brno, Czech Republic), Reanal (Budapest, Hungary), K & K (Plainview, NY, USA) and Fluka (Buchs, Switzerland). The chemicals used for the preparation of the leading and terminating electrolytes were purified by conventional methods.

Hydroxyethylcellulose 4000 (HEC) (Serva) or methylhydroxyethylcellulose 30 000 (MHEC) (Serva), after purification on a mixed-bed ion exchanger (Amberlite MB-1; BDH, Poole, UK), was added to the leading electrolytes at a 0.1% (w/v) concentration.

Water delivered by a Rodem 1 two-stage demineralization unit (OPP, Tišnov, Czech Republic) was further purified by circulation through laboratory-made PTFE cartridges packed with a mixed-bed ion exchanger (Amberlite MB-1; BDH). Freshly recirculated water was used for the preparation of solutions.

## RESULTS AND DISCUSSION

*Migration behaviour of the complexes*

There are several ways in which complex equilibria can be employed for the separation [13–16] and detection [17] of ions in ITP. Experiments carried out in this feasibility study were focused on the detection of various amino-containing constituents via their complexes (chelates) formed on addition of $Cu^{2+}$ ions. We preferred this alternative as it provides the possibility of a complete conversion of the constituents of interest into light-absorbing species. On the other hand, it is clear that it cannot be of general use as many complexes will decompose during the migration in an analogous way to that described for the chelates of metals with EDTA [13]. In this respect, considering the behaviour of the studied constituents as ligands in the reactions with $Cu^{2+}$ [18–22], we can classify them as follows:

(a) constituents that can form chelates with more than one ring {diethylenetriamine (DETA); triethylenetetramine (TETA); histidine (HIS); 1,3-bis[tris(hydroxymethyl)methylamino]propane (bis-tris-propane or BTP); spermine; anserine; carnosine};

(b) constituents that can form single-ring chelates (ethylenediamine; 1,2-diaminopropane; 1,3-diaminopropane; histamine);

(c) constituents that probably cannot form chelates [spermidine; 1,4-diaminobutane; 1,5-diaminopentane; 1,6-diaminohexane; 1,8-diaminooctane; 1,10-diaminodecane; tris(hydroxymethyl)aminomethane (Tris); bis(2-hydroxyethyl) iminotris(hydroxymethyl)methane (bis-tris); ethanolamine; imidazole; guanidine; pyridine; 2-aminopyridine; dimethylaniline; *p*-toluidine; quinoline; dimorpholinoethane; creatinine].

We found that under the ITP working conditions employed (Table I), only the constituents which are expected to form with $Cu^{2+}$ ions chelates with more than one ring [group (a)] did not bleed from these chelates during the separation. Consequently, they could be detected by the photometric detector at 580 nm. The stabilities of the complexes (chelates) of the remainder of the constituents were not sufficient

TABLE I

OPERATIONAL SYSTEM

The driving currents were 200 and 35 μA in the preseparation and analytical columns, respectively.

| Parameter | Electrolyte[a] | |
|---|---|---|
| | Leading | Terminating |
| Solvent | $H_2O$ | $H_2O$ |
| Cation | $NH_4^+$ | $EACA^+$ |
| Concentration (m*M*) | 10 | 10 |
| Counter ion | $MES^-$ | $AC^-$ |
| pH | 6.1 | *ca.* 5.0 |
| Additive | HEC (MHEC) | – |
| Concentration (%, w/v) | 0.1 | – |

[a] EACA = ε-Aminocaproic acid; MES = morpholinoethanesulphonic acid; HEC = hydroxyethylcellulose; MHEC = methylhydroxyethylcellulose; AC = acetic acid.

for them to be detected, at least partially. Although separations (migrations) at a higher pH should be favourable from the point of view of complex formation, the values of the stability constants [18–22] and the hydrolytic behaviour of $Cu^{2+}$ [23] suggest that a considerable improvement in this respect can hardly be expected.

*Detection limits and competition of the separands for $Cu^{2+}$*

The values of the detection limits (DETA $10^{-6}$ mol/l, BTP $10^{-7}$ mol/l and HIS $2 \cdot 10^{-7}$ mol/l for a 30-$\mu$l injection volume) were determined using the spike mode of detection [8]. The isotachopherograms in Fig. 1 were obtained from the photometric detector and they show responses of the detector for the constituents forming cationically migrating chelates with $Cu^{2+}$ at concentrations close to their detection limits. From the isotachopherogram in Fig. 1b it can be seen that the complex (chelate) of DETA present in the sample at a concentration of $5 \cdot 10^{-7}$ mol/l was decomposed during the migration. This seems to be the most appropriate explanation for the fact that this amine was not detected via the complex particles. From this we can also deduce that the above value of the detection limit could be lower for separations performed in shorter capillary tubes or in the separation compartment with a lower load capacity [24].

The isotachopherograms in Fig. 2 are intended to illustrate competitions of the separands (ligands) for the central ion. The isotachopherogram in Fig. 2b shows that an excess of BTP added to the sample (relative to the concentration of $Cu^{2+}$ in the sample) is accompanied by the formation of a zone of this constituent (BTP in Fig. 2b) in front of the zone of the chelate (Cu–BTP in Fig. 2b). When we also consider the behaviour of the Cu–DETA complex (see above), it is surprising that the presence of free BTP in the sample did not lead to the decomposition of Cu–DETA. The complete disappearance of the Cu–BTP complex on the addition of histidine (Fig. 2c) is also unexpected.

*Detection of complex-forming constituents in various matrices*

Ampholytic buffers for isoelectric focusing contain mixtures of polyaminopolycarboxylic, polyaminopolyphosphonic and polyaminopolysulphonic acids or their salts [25,26]. The isotachopherogram in Fig. 3 shows that many of these constituents form strongly visible light-absorbing and cationically migrating complexes

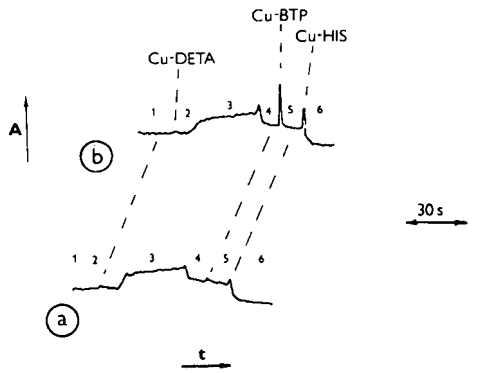


Fig. 1. Migration behaviour of the complexes of DETA, BTP and HIS at concentrations close to their detection limits. (a) Blank run with the sample containing $1 \cdot 10^{-4}$ mol/l $Na^+$ (2), $5 \cdot 10^{-5}$ mol/l tetraethylammonium (4) and $5 \cdot 10^{-5}$ mol/l bis-tris (5) as discrete spacers and $10^{-4}$ mol/l $Cu^{2+}$ (3). (b) Run as in (a) except that the sample contained DETA, BTP and HIS at $5 \cdot 10^{-7}$ mol/l (symbols of the corresponding complexes mark the peaks and/or indicate the migration positions). 1,6 = Zones of the leading and terminating constituents, respectively (see Table I). $A$ = Light absorption (580 nm); $t$ = time.

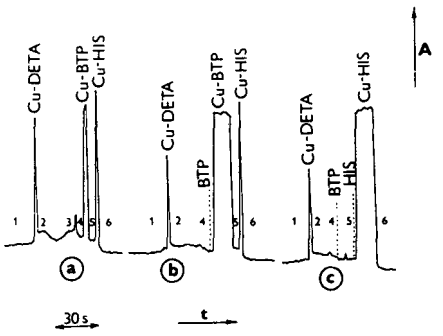


Fig. 2. Competition of the amino-containing separands for $Cu^{2+}$ ions. (a) Same mixture of discrete spacers as in Fig. 1 containing $Cu^{2+}$ (3) at $1 \cdot 10^{-4}$ mol/l and each of the analytes (DETA, BTP and HIS) at $1 \cdot 10^{-5}$ mol/l. (b) Same sample as in (a) except that BTP was present at $4 \cdot 10^{-5}$ mol/l. (c) Same sample as in (a) except that HIS was present at $4 \cdot 10^{-5}$ mol/l. Other symbols as in Fig. 1. For separation conditions, see Table I.

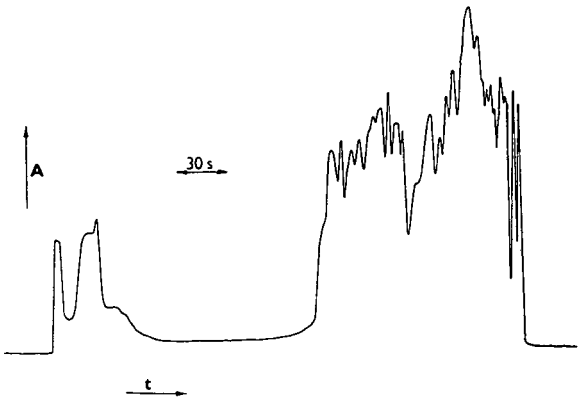


Fig. 3. Isotachophoretic profiling of cationically migrating complexes formed by ampholytic constituents with $Cu^{2+}$ cations. The sample solution was prepared by diluting a Servalyt buffer for isoelectric focusing (pH 2–11; Serva) with water in the ratio 1:1000 (v/v). The concentration of $Cu^{2+}$ ions in the diluted buffer was $5 \cdot 10^{-4}$ mol/l. A 30-$\mu$l volume of the sample solution was taken for the separation performed under the conditions described in Table I.

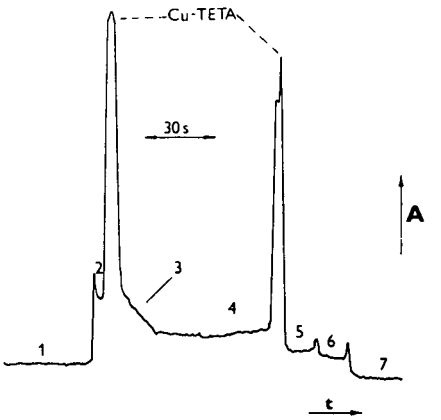


Fig. 4. Isotachophoretic separation and photometric detection of cationically migrating $Cu^{2+}$ complexes of triethylenetetraamine (Cu–TETA) of technical-grade purity. TETA was present in the sample at $5 \cdot 10^{-5}$ mol/l while the final $Cu^{2+}$ concentration was $2 \cdot 10^{-4}$ mol/l. Bis-tris (6), tetraethylammonium (5), $Na^{+}$ (3) and $Ca^{2+}$ (2) served as spacing constituents. 1,7 = Zones of the leading and terminating constituents, respectively.

(chelates) with $Cu^{2+}$ ions. Differences in the absorptivities of the complexes make the resolutions of these contiguous zones possible in spite of the fact that their resolution can hardly be achieved by a high-resolution conductivity detector.

Triethylenetetramine, available in technical-grade purity, under our separation conditions (Table I) forms several zones detectable with a conductivity detector. The isotachopherogram from the photometric detector shown in Fig. 4 indicates that at least two of these constituents form isotachophoretically migrating chelates with $Cu^{2+}$. In this respect it should also be noted that the sample concentration was close to that corresponding to the detection limit from the response of the conductivity detector. The detection limit with the photometric detector was found to be *ca.* 100 times lower ($10^{-7}$ mol/l), *i.e.*, in the range favourable for some environmental applications (see ref. 1 and references cited therein).

A dilute urine sample mixed with discrete spacers and with $Cu^{2+}$ ions was profiled for constituents that form cationally migrating complexes (chelates) with this metal. The isotachopherograms in Fig. 5 clearly show that with the aid of the spacers used we were able to resolve at least two constituents that form complexes with $Cu^{2+}$ and detectable at 580 nm. In spite of the fact that we did not identify these constituents, it seems reasonable to suggest that one of them could be 3-methylhistidine (a degradation product of actin and myosin proteins) which is excreted in urine and which is a good index of skeletal muscle protein degradation [27,28].

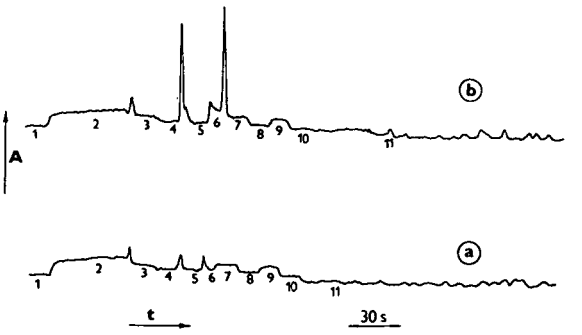


Fig. 5. Profiling of complex forming constituents present in human urine. (a) Blank run with spacing constituents [2-aminopyridine (3), tetraethylammonium (4), bis-tris (5), pyridine (6), dimethylaniline (7), *p*-toluidine (8), quinoline (9), creatinine (10)]. $Cu^{2+}$ was present in the samples at $1 \cdot 10^{-4}$ mol/l. (b) Urine (diluted 1:100 immediately after collection) containing the same constituents as the blank sample (a). 1,11 = Zones of the leading and terminating cations, respectively.

REFERENCES


1 J. Sollenberg and L. Hansén, *J. Chromatogr.*, 390 (1987) 133.
2 A. Kopwillem, U. Moberg, G. Westin-Sjoedahl, R. Lundin and H. Sievertsson, *Anal. Biochem.*, 67 (1975) 166.
3 V. Kašička and Z. Prusík, *J. Chromatogr.*, 569 (1991) 123.
4 T. Hirokawa, T. Gojo and Y. Kiso, *J. Chromatogr.*, 369 (1986) 59.
5 T. Hirokawa, T. Gojo and Y. Kiso, *J. Chromatogr.*, 390 (1987) 201.
6 F.M. Everaerts, J.L. Beckers and Th.P.E.M. Verheggen, *Isotachophoresis. Theory, Instrumentation and Applications*, Elsevier, Amsterdam, 1976.
7 M. Svoboda and J. Vacík, *J. Chromatogr.*, 119 (1976) 539.
8 D. Kaniansky, V. Madajová, J. Marák, E. Šimuničová, I. Zelenský and V. Zelenská, *J. Chromatogr.*, 390 (1987) 51.
9 A. Šišková, *Graduation Report*, Komensky University, Bratislava, 1987.
10 R. Jarofke, *J. Chromatogr.*, 390 (1987) 161.
11 F.S. Stover, *J. Chromatogr.*, 470 (1989) 131.
12 P. Havaši and D. Kaniansky, *J. Chromatogr.*, 325 (1985) 137.
13 P. Gebauer, P. Boček, M. Deml and J. Janák, *J. Chromatogr.*, 199 (1980) 81.
14 D. Kaniansky and F.M. Everaerts, *J. Chromatogr.*, 148 (1978) 441.
15 P. Gebauer and P. Boček, *Folia Fac. Sci. Nat. Univ. Purkynianae Brun., Chem.*, 20 (1985) 37.
16 H. Yoshida, S. Tanaka, T. Kaneta and Y. Hirama, *Anal. Sci.*, 7 (1991) 673.
17 I. Zelenský, D. Kaniansky, P. Havaši, Th.P.E.M. Verheggen and F.M. Everaerts, *J. Chromatogr.*, 470 (1989) 155.
18 R.J. Angelici, in G.L. Eichhorn (Editor), *Inorganic Biochemistry*, Vol. 1, Elsevier, Amsterdam, 1973, p. 63.
19 H.C. Freeman, in G.L. Eichhorn (Editor), *Inorganic Biochemistry*, Vol. 1, Elsevier, Amsterdam, 1973, p. 121.
20 S. Kotrlý and L. Šucha, *Handbook of Chemical Equilibria in Analytical Chemistry*, Wiley, Chichester, 1985.
21 A.E. Martell and R.M. Smith, *Critical Stability Constants, Vol. 1: Amino Acids*, Plenum Press, New York, 1974.
22 R.M. Smith and A.E. Martell, *Critical Stability Constants, Vol. 2: Amines*, Plenum Press, New York, 1975.
23 R.M. Smith and A.E. Martell, *Critical Stability Constants, Vol. 4: Inorganic Complexes*, Plenum Press, New York, 1976.
24 F.E.P. Mikkers, F.M. Everaerts and J.A.F. Peek, *J. Chromatogr.*, 168 (1979) 293.
25 P.G. Righetti and J.W. Drysdale, *Isoelectric Focusing*, North-Holland, Amsterdam, 1976.
26 B.J. Radola and G. Graesslin (Editors), *Electrofocusing and Isotachophoresis*, Walter de Gruyter, Berlin, 1977.
27 T. Nagasawa, T. Sakai and R. Onodera, *J. Chromatogr.*, 566 (1991) 223.
28 L. Dalla Libera, *J. Chromatogr.*, 536 (1991) 283.

*Journal of Chromatography*, 638 (1993) 231–234
Elsevier Science Publishers B.V., Amsterdam

CHROM. 24 859

# Short Communication

# Isotachophoretic analysis of some antidepressants

T. Buzinkaiová, J. Sádecká, J. Polonský* and E. Vlašičová

*Faculty of Chemical Technology, Slovak Technical University, Radlinského 9, 812 37 Bratislava (Slovak Republic)*

V. Kořínková

*Medical Faculty of Comenius, Department of Psychiatry, Bratislava (Slovak Republic)*

ABSTRACT

Optimal electrolyte systems for the analysis of the substances with tricyclic structure, clomipramine and imipramine, and tetracyclic, maprotiline, were determined. The analysis conditions were applied to the determination of these compounds in antidepressant drugs.

## INTRODUCTION

Depressive illnesses are very often treated with antidepressant drugs. These drugs can be divided into three groups. The first-generation drugs were thymoleptics with a tricyclic structure. The second generation of tetracyclic antidepressants share a number of the basic therapeutic properties of tricyclics in various kinds of depression (endogenous, somatogenic, etc.). The third and newest generation of drugs enhance serotoninergic neurotransmission.

To control the amount of antidepressants in drugs and human blood, plasma or serum chromatographic analytical techniques are used. Reviews of GC, HPLC and HPTLC for tricyclic antidepressants are presented in refs. 1 and 2. Other methods of preconcentration and derivatization of antidepressants were published later [3–6].

Electrophoretic methods have not often been used. Seven tricyclic antidepressants were analysed by capillary electrophoresis [7], and some of them were determined by capillary isotachophoresis [8,9].

Isotachophoresis (ITP) with coupled columns can provide both qualitative and quantitative analysis on ionic solutes without sample pretreatment in a relatively short analysis time. Most antidepressants are in ionic form. If they are not, changing the pH of their water solutions makes it possible to analyse them in electrolyte systems for cations. ITP analysis of compounds of our

* Corresponding author.

0021-9673/93/$06.00 

interest—imipramine and clomipramine tricyclic antidepressants and maprotiline, a second-generation antidepressant—has not yet been published. These compounds are the basic substances in the drugs very often prescribed by psychiatrists. The optimal conditions for ITP analysis of these compounds were applied for the ITP analysis of antidepressant drugs.

## EXPERIMENTAL

### *Instrumentation*

For the isotachophoretic separations a coupled column system in a ZKI 02 instrument (Spišská Nová Ves, Slovak Republic) and a conductivity detector were used. The preseparation column was 160 mm × 0.8 mm I.D. The zone of antidepressants was trapped in the analytical column which was 160 mm × 0.3 mm I.D. The columns were made from a copolymer of fluorinated ethylene and propylene. The voltages varied between 1 and 15 kV.

A PC AT with twelve-bit A/D–D/A converter with 100-Hz sample frequency and connected on-line to the ITP instrument was used, and the results were processed with the ITP-PC version 2 program by KasComp (Bratislava, Slovak Republic).

### *Chemicals*

All chemicals were of analytical grade or additionally purified by the usual methods. Imipramine, clomipramine and maprotiline (all as hydrochlorides) were obtained from Ciba-Geigy (Basle, Switzerland). Analysed drugs Anafranil and Ludiomil were produced by Ciba-Geigy and Melipramine by Egis Pharmaceutical (Hungary).

## RESULTS AND DISCUSSION

Two tertiary amines (imipramine and clomipramine) were chosen because there is only small difference in their chemical structure (R = H or Cl). Their $pK_a$ in water reaches 9.8. Maprotiline is a tetracyclic compound which differs chemically from the others by virtue of a bridge in the central ring. Its $pK_a$ in water is 10.5. The structures of imipramine, clomipramine and maprotiline are shown in Fig. 1.

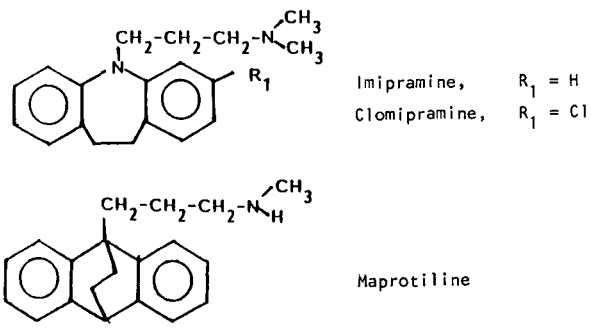


Fig. 1. Structures of analysed antidepressants.

Tested electrolyte systems which are the same in preseparation and separation columns are listed in Table I.

The best leading systems contained sodium acetate and sodium glutamate. The driving current in the preseparation column was 250 $\mu$A and in the analytical column 40 $\mu$A. The terminating components $\beta$-alanine, $\varepsilon$-caproic acid, acetic acid and glutamic acid were tested. Acetic acid as a terminator was too quick for the very large antidepressant molecules. The values of the principal qualitative parameter, $r_{s,h}$, for analysed standards are given in Table II.

In systems with sodium glutamate as the leading electrolyte and glutamic acid or $\beta$-alanine as the terminating electrolyte, clomipramine, imipramine and maprotiline can be distinguished in a mixture. In other systems the separation of these three antidepressants was not explicit. However, their separation is not important because these three compounds are not found together in drugs, nor are they used together in multiple therapy.

TABLE I

LEADING ELECTROLYTE SYSTEMS FOR ITP ANALYSIS OF ANTIDEPRESSANT CATIONS

| Leading electrolyte | Concentration (*M*) | Counter-constituent | pH |
|---|---|---|---|
| Sodium acetate | 0.01 | Acetic acid | 4.6 |
| Potassium acetate | 0.02 | Acetic acid | 4.6 |
| Calcium hydroxide | 0.01 | Acetic acid | 4.5 |
| Sodium glutamate | 0.01 | Glutamic acid | 5.3 |

TABLE II

PARAMETER $r_{s,h}$ OF ANALYSED COMPOUNDS

| Leading electrolyte | Terminating *electrolyte* | $r_{s,h}$[a] | | |
|---|---|---|---|---|
| | | Clomipramine | Imipramine | Maprotiline |
| Sodium acetate | β-Alanine | 0.482 | 0.431 | 0.444 |
| Calcium acetate | ε-Caproic acid | 0.737 | 0.753 | 0.769 |
| Sodium glutamate | Glutamic acid | 0.959 | 0.803 | 0.839 |
| Sodium glutamate | β-Alanine | 0.734 | 0.647 | 0.870 |

[a] $r_{s,h}$ = Relative step height = $(h_x - h_L)/(h_T - h_L)$.

The determination of clomipramine, maprotiline and imipramine as basic substances in the drugs Anafranil, Ludiomil and Melipramine was achieved by the calibration and standard addition methods and statistically evaluated by linear regression. Seven calibration points repeated five times were measured with standard solutions. Samples of drugs as tablets and injections containing various amounts of the basic compounds were tested. Ten tablets and five injections for each type of drug were analysed, and every analysis was repeated five times (Fig. 2). Changes in analysed solutions from day to day were not observed. The relative standard deviation for a drug concentration 0.1 mg/ml was less than 0.5%, for the concentration range 0.01–0.1 mg/ml less than 3% and for concentrations less than 0.01 mg/ml reached 8%. The limits of detection of clomipramine, imipramine and maprotiline were around 200 ng/ml, and correlation coefficients ranged from 0.9996 to 0.9999. Table III shows the overall determinations of the basic substances in several drugs.

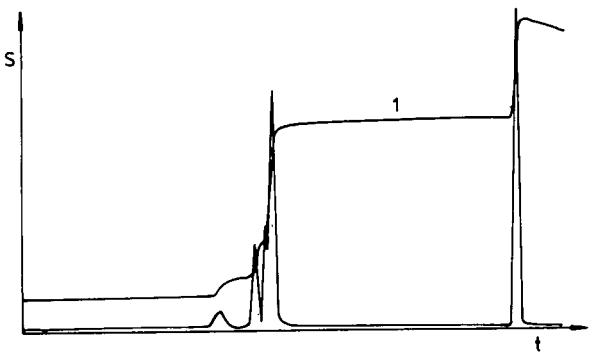


Fig. 2. Isotachopherogram of a Melipramin tablet in the following electrolyte system: leading electrolyte, sodium acetate + acetic acid pH 4.6; terminating electrolyte, β-alanine. 1 = Imipramine.

TABLE III

AMOUNTS OF THE BASIC COMPOUNDS FOUND IN TABLETS AND INJECTIONS

The amounts declared by the manufacturers are: 25 or 10 mg in tablets and 25 mg per 2-ml injection of solution; $n = 2$

| Drug | Amount of basic compound (mg per tablet or injection) |
|---|---|
| Anafranil tablet | 24.72 ± 0.111 |
| Anafranil tablet | 9.41 ± 0.050 |
| Anafranil injection | 24.55 ± 0.160 |
| Melipramin tablet | 24.92 ± 0.115 |
| Melipramin tablet | 9.94 ± 0.045 |
| Melipramin injection | 25.11 ± 0.133 |
| Ludiomil tablet | 26.73 ± 0.150 |
| Ludiomil tablet | 9.98 ± 0.050 |
| Ludiomil injection | 26.81 ± 0.174 |

## CONCLUSIONS

It is shown that the ITP technique is well suited to the analysis of Anafranil, Tofranil and Ludiomil, out of this important group of drugs. The limit of detection of these drugs (around 200 ng/ml) was obtained with the injection of 50 μl of drug solution and zone width of 0.1 mm. The multiple injections of these volumes (50 μl) of plasma could be a problem in ITP detection systems.

ACKNOWLEDGEMENT

The authors are indebted to A. Suter of Ciba-Geigy Ltd. for extending drug standards with full chemical specifications.

REFERENCES

1 T.R. Norman and K.P. Maguire, *J. Chromatogr.*, 340 (1985) 173.
2 R.N. Gupta, *J. Chromatogr.*, 576 (1992) 183.
3 J.R. Hughes and M. Osselton, *J. Anal. Toxicol.*, 13 (1989) 77.
4 H. Hattori, E. Takashima and T. Yamada, *J. Chromatogr.*, 529 (1990) 189.
5 M.P. Segatti, G. Nisis and F. Grossi, *J. Chromatogr.*, 536 (1991) 319.
6 G.L. Lensmeyer, D.A. Weibe and B.A. Darcey, *J. Chromatogr. Sci.*, 29 (1991) 444.
7 K. Salomon, S. Dean Burgi and J.C. Helmer, *J. Chromatogr.*, 549 (1991) 375.
8 V. Jokl, J. Mokrá-Pospíchalová and B. Vítkovič, *Česk. Farm.*, 38 (1989) 294.
9 Z. Chmela and Z. Stránský, *Česk. Farm.*, 39 (1990) 172.

*Journal of Chromatography*, 638 (1993) 235–240
Elsevier Science Publishers B.V., Amsterdam

CHROM. 24 932

# Determination of ascorbic acid by isotachophoresis with regard to its potential in neuroblastoma therapy

Sabine Gebhardt, Katharina Kraft, Holger N. Lode and Dietrich Niethammer
*Children's Hospital, University of Tübingen, Rümelinstrasse 23, W-7400 Tübingen (Germany)*

Karl-Heinz Schmidt
*Department of Surgery, University of Tübingen, Tübingen (Germany)*

Gernot Bruchelt*
*Children's Hospital, University of Tübingen, Rümelinstrasse 23, W-7400 Tübingen (Germany)*

ABSTRACT

Analytical capillary isotachophoresis was used to determine ascorbic acid (AA) in different matrices (cell-free system, neuroblastoma cell extracts and urine). The system for purging bone marrow of neuroblastoma cells, including 6-hydroxydopamine (6-OHDA) and AA, was analysed with regard to the interaction of AA with 6-OHDA and its autoxidation product, hydrogen peroxide. Furthermore, analyses concerning the uptake of AA into neuroblastoma cells as well as its excretion in urine after uptake of large amounts were carried out.

## INTRODUCTION

Neuroblastoma is a tumour of the sympathetic nervous system, which in its disseminated form has a poor prognosis [1]. One new therapeutic approach in the treatment of this tumour is autologous bone marrow transplantation. Since neuroblastoma cells metastasize into bone marrow, bone marrow cells have to be cleared of neuroblastoma cells prior to reinfusion. Among other substances, the neurotoxin 6-hydroxydopamine (6-OHDA) has been used as a purging agent [2]. It is supposed that since 6-OHDA is a catecholaminergic compound it is incorporated specifically into neuroblastoma but not into bone marrow stem cells. Inside the cells it can autoxidize, leading to cytotoxic oxygen compounds such as superoxidanion, hydrogen peroxide and hydroxyl radicals (Fig. 1). Ascorbic acid (AA), added in a ten-fold excess, has been shown to enhance the cytotoxic effects of 6-OHDA [3]. It acts a redox cycler and reduced 6-OHDA-chinon (which is formed during the oxidation of 6-OHDA [4]), allowing the next round of cycling to generate reactive oxygen compounds. However, as will be shown in this paper, some of the suppositions mentioned above have proved to be incorrect. This was demonstrated by investigating the interaction of AA with 6-OHDA and hydrogen peroxide using isotachophoresis (AA), HPLC (6-OHDA) and the Clark electrode (oxygen consumption).

## EXPERIMENTAL

### *Chemicals*

6-OHDA, EDTA, 1,10-phenanthroline and

* Corresponding author.

0021-9673/93/$06.00 

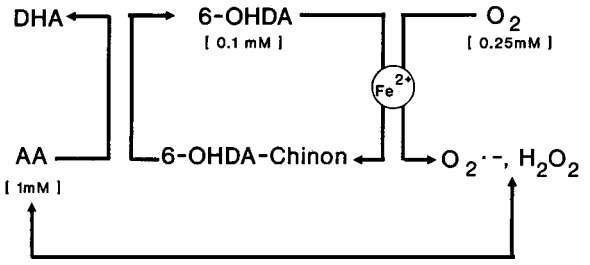


Fig. 1. Redox cycling of 6-OHDA in the presence of excess AA. In the presence of oxygen and traces of iron, 6-OHDA oxidizes to 6-OHDA-chinon, leading to the formation of reactive oxygen compounds such as the superoxide anion ($O_2^{\bullet -}$) and hydrogen peroxide ($H_2O_2$). The molarities indicate the concentrations present in the bone marrow-purging system. DHA = Dehydroascorbic acid.

ascorbic acid were from Sigma (Munich, Germany); desferrioxamine (Desferal, DFO) was obtained from Ciba (Basle, Switzerland).

*Isotachophoresis*

Experiments were performed on a LKB Tachophor 2127 equipped with UV (254 nm) and conductivity detectors. 0.01 *M* HCl adjusted with β-alanine to pH 3.65 plus 0.3% (w/v) methylcellulose 4000 (Fluka, Buchs, Switzerland) was used as the leading electrolyte and 0.01 *M* caproic acid (Merck, Darmstadt, Germany) as the terminating electrolyte. Analysis was carried out at 15°C in a 230 × 0.5 mm I.D. capillary. Usually, the current during signal detection was 7.5 μA. Chart speed during detection was 10 cm/min.

*Other methods*

Oxygen consumption during autoxidation of 6-OHDA experiments was measured with a Clark-type electrode (Hansa-Tech, UK, [5]).

HPLC (electrochemical detection) was used for the determination of 6-OHDA.

*Cell culture*

The human neuroblastoma cell line SK-N-SH was cultivated in RPMI (Rosewell Park Memorial Institute) 1640 cell culture medium supplemented with 2 m*M* L-glutamine, penicillin/streptomycin and 10% foetal calf serum. AA was added in a final concentration of 1 m*M*. After different incubation times, cell culture medium was removed and cell pellets were extensively washed and lysed in 50 μl of 0.1 *M* hydrochloric acid. A 5-μl volume was injected into the Tachophor.

## RESULTS AND DISCUSSION

*Identification of asorbic acid in different matrices*

Fig. 2 shows isotachopherograms of AA in different matrices [phosphate-buffered saline (Fig. 2a) cell lysates of the neuroblastoma cell

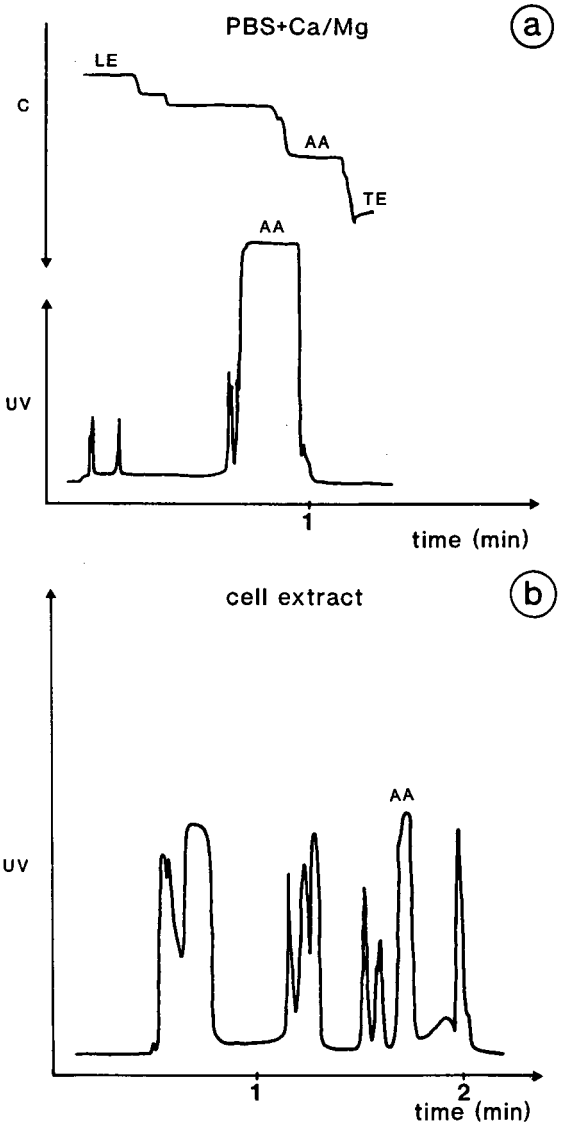


Fig. 2.

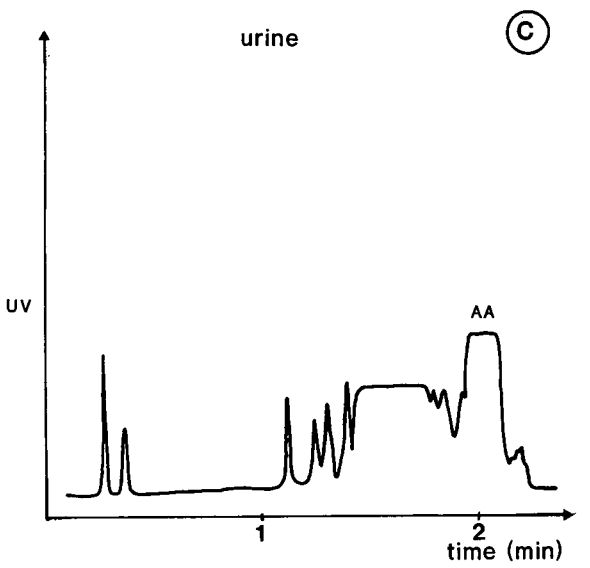


Fig. 2. Isotachopherograms of AA in different biological matrices (UV, UV signal, 254 nm; C, conductivity). (a) AA 5 m*M* in phosphate-buffered saline. (b) AA in extracts of $3.6 \cdot 10^6$ SK-N-SH cells after 4 h incubation with 1 m*M* ascorbate. (c) AA in 1:1 diluted morning urine after uptake of 1 g of ascorbic acid the night before. LE = Leading electrolyte; TE = terminating electrolyte.

line SK-N-SH (Fig. 2b) and 1:1 diluted urine (Fig. 2c)]. AA was identified by its characteristic UV pattern at 254 nm, its conductivity signal, and by addition of AA to neuroblastoma cell extracts and urine. Calibration curves were linear in all three matrices (data not shown).

*Interaction of 0.1 mM 6-OHDA with 1 mM ascorbic acid*

The combination of 0.1 m*M* 6-OHDA and 1 m*M* AA has been used clinically to purge bone marrow of neuroblastoma cells. The kinetics of 6-OHDA autoxidation and its interaction with AA was investigated and is shown in Fig. 3a–c. Within 15 mins, about 70% of 6-OHDA was metabolized in the presence of AA (Fig. 3a). Although present in a tenfold molar excess compared with 6-OHDA, only 18% of AA was consumed during this period of time (Fig. 3b) and 37% after 60 mins. It was expected that in the presence of a tenfold excess of ascorbic acid several redox cycles would be possible. However, the limiting factor for redox cycling proved to be not ascorbic acid but the oxygen concentration in the reaction mixture (about 250 $\mu$mol/l [4], Fig. 3c, compared to 100 $\mu M$ 6-OHDA and 1000 $\mu M$ AA). Therefore, even with a tenfold excess of ascorbate compared with

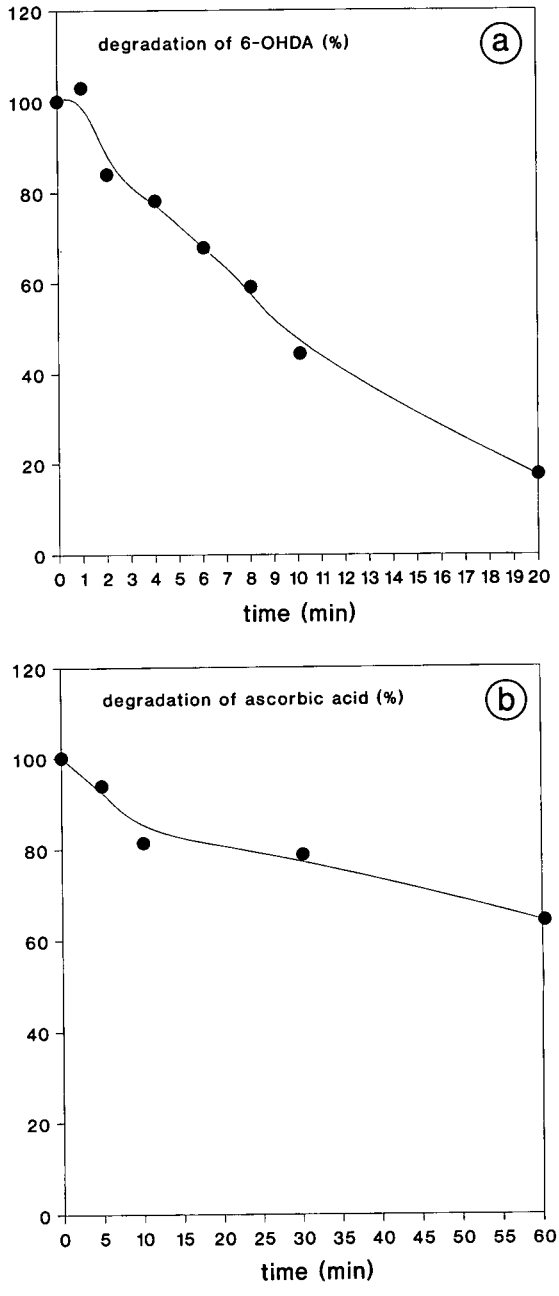


Fig. 3.

(Continued on p. 238)

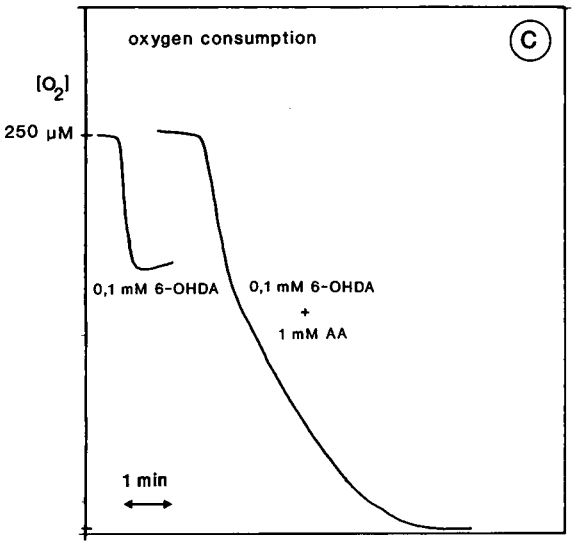


Fig. 3. Kinetics of the interaction between 0.1 m*M* 6-OHDA and 1 m*M* AA. (a) Time course of degradation of 6-OHDA (HPLC analysis). (b) Decrease of ascorbic acid (isotachophoresis). (c) Oxygen consumption (total sample volume: 1 ml).

6-OHDA, only about 1.5-fold redox cycling is possible until oxygen is completely consumed.

Nevertheless, after complete consumption of oxygen the tenfold excess of AA did not reduce, but even further enhanced, the toxic effects of the reaction mixture on neuroblastoma cells [3]. The major explanation is its interaction with hydrogen peroxide, which is formed during 6-OHDA oxidation (Table I). The cytotoxic effects of AA are probably due to the formation of highly cytotoxic hydroxyl radicals in the Fenton reaction [6]:

$$H_2O_2 + Fe^{2+} \rightarrow Fe^{3+} + OH^{\bullet} + OH^{-}$$

AA is able to reduce $Fe^{3+}$ to $Fe^{2+}$, thus allowing this reaction to proceed. The important role of iron in the interaction of AA with hydrogen peroxide is documented in Fig. 4. The degradation rate of AA in the presence of hydrogen peroxide under different conditions was enhanced in the presence of additional iron, but reduced in the presence of the iron chelators Desferal and 1,10-phenanthroline. These experiments indicate that traces of iron, which are

TABLE I

DECREASE IN ASCORBIC ACID AFTER 30 min INCUBATION WITH HYDROGEN PEROXIDE[a]

| AA (m*M*) | Hydrogen peroxide (m*M*) | Zone length of AA signal (mm) | Percentage of control |
|---|---|---|---|
| 1 | – | 22.0 | 100 |
| 1 | 0.1 | 19.9 | 90.4 |
| 1 | 0.25 | 18.3 | 83.3 |
| 1 | 1 | 9.5 | 43.0 |

[a] AA, 1 m*M*, was incubated with different concentrations of hydrogen peroxide (0.1–1 m*M*) in 1 ml of phosphate-buffered saline, pH 7.4 at 37°C for 30 min. Subsequently 5 µl of the reaction mixture were injected into the Tachophor.

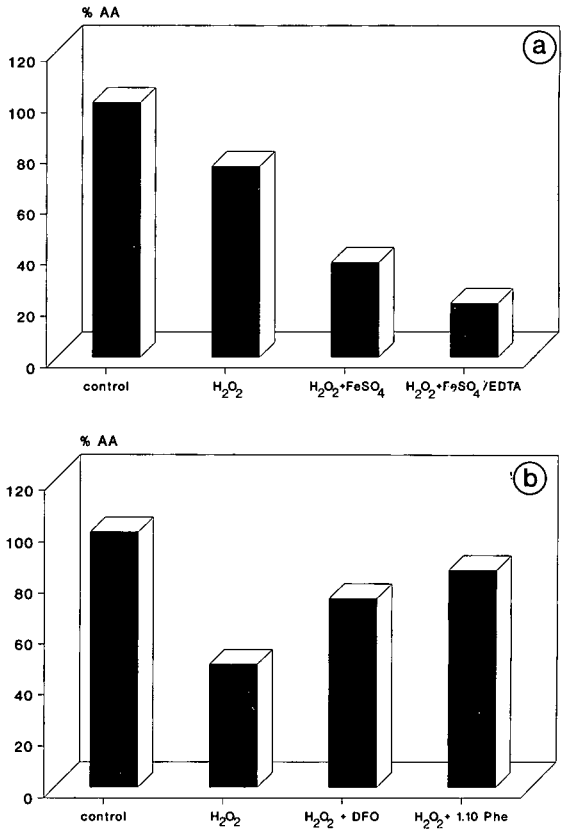


Fig. 4. Role of iron in the degradation of AA in the presence of hydrogen peroxide. (a) In the presence of elevated iron concentrations (AA, 10 m*M*; hydrogen peroxide 10 m*M*). (b) In the presence of the iron chelators Desferal (DFO) and 1,10-phenanthroline (1.10 Phe) (each 5 mmol/l): AA, 2.5 m*M*; hydrogen peroxide, 1 m*M*.

normally present in the reaction mixture, enable the Fenton reaction to occur.

The biological significance of this reaction is given by the observation that neuroblastoma cells endogenously generate hydrogen peroxide in elevated amounts [7], and that they contain elevated levels of ferritin from which iron can be released by AA [8,9]. Since AA is enriched in neuroblastoma cells in a time-dependent manner, the cytotoxic hydroxyl radicals could be formed (0.71 nmol of AA were found in $10^6$ SK-N-SH cells after incubation with 1 m*M* ascorbic acid for 1 h, 2.5 nmol after 4 hs; Fig. 2b).

## CONCLUSION

The present study shows that some of the ideas concerning the specific cytotoxicity of 6-OHDA on neuroblastoma cells in the presence of a tenfold excess of AA are not correct. The main limitation in using 6-OHDA/AA as a bone marrow-purging system is the fast capacity of 6-OHDA to autoxidize at neutral pH. Most of its autoxidation product, hydrogen peroxide, is already formed outside the neuroblastoma cells before significant amounts of 6-OHDA can enter the cells. Furthermore, oxygen, not AA, is the limiting factor for the generation of reactive oxygen substrates during redox cycling. Nevertheless, the mixture of 6-OHDA and ascorbate proved to be more toxic the more ascorbate was present, probably because of the interaction of hydrogen peroxide and ascorbate, which, in the presence of traces of iron, leads to the formation of hydroxyl radicals.

Therefore, 6-OHDA/AA cannot be recommended as a bone marrow-purging agent. In addition, another conclusion concerning the therapeutic use of AA may be drawn from these experiments. Since neuroblastoma cells produce elevated amounts of hydrogen peroxide, and since they contain elevated amounts of ferritin from which iron can be released by ascorbic acid, daily application of large amounts of this vitamin to patients suffering from neuroblastoma may be a useful therapeutic approach for destruction of the tumour cells. Although ascorbate is excreted in large amounts in urine after its uptake in the gram range (Figs. 2c and 5), an increasing amount of it will accumulate in the body if it is given for an unlimited period of time. Continuous application of ascorbate may therefore be a mild therapy that could help destroy neuroblastoma cells.

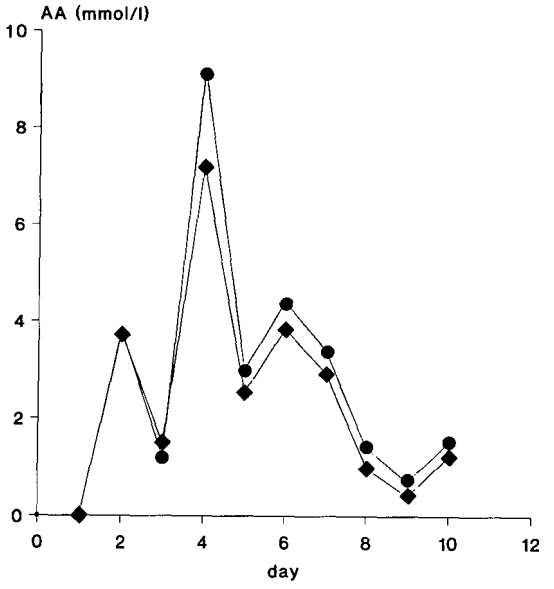


Fig. 5. Ascorbate concentration in morning urine after daily uptake of 1 g for 7 days (day 1: before uptake). AA in urine was determined in 1:1 diluted urine by isotachophoresis (●) and by a commercially available test [◆, 3-(4,5-dimethylthiazol-2-yl)-2,5-diphenyltetrazolium bromide (MTT) test, Böhringer Mannheim]. Correlation between both methods: $r^2 = 0.99$.

## ACKNOWLEDGEMENT

This study was supported by the Deutsche Krebshilfe, Grant 54/89/Ni4.

## REFERENCES

1 C.R. Pinkerton, *Br. J. Cancer*, 61 (1990) 351–353.
2 G. Cohen and R.E. Heikkila, *J. Biol. Chem.*, 249 (1974) 2447–2452.
3 C.P. Reynolds, D.A. Reynolds, E.P. Frenkel and R.G. Smith, *Cancer Res.*, 42 (1982) 1331–1336.
4 E. Heikkila and G. Cohen, *Mol. Pharmacol.*, 8 (1972) 241–248.
5 T. Delieu and D.A. Walker, *New Phytol.*, 71 (1972) 201–225.
6 H.J.H. Fenton, *J. Chem. Soc.*, 65 (1894) 899–910.

7 T.P. Szatrowski and C.F. Nathan, *Cancer Res.*, 51 (1991) 794–798.
8 T.C. Iancu, H. Shilo and A. Kedar, *Cancer*, 61 (1988) 2497–2502.
9 R.F. Boyer, T.W. Grabill and R.M. Petrovich, *Anal. Biochem.*, 174 (1988) 17–22.

*Journal of Chromatography*, 638 (1993) 241–246
Elsevier Science Publishers B.V., Amsterdam

CHROM. 24 861

# Capillary isotachophoresis of organic acids produced by selected microorganisms during lactic acid fermentation

J. Karovičová, J. Polonský*, M. Drdák, P. Šimko and V. Vollek

*Faculty of Chemical Technology, Slovak Technical University, Radlinského 9, 812 37 Bratislava (Slovak Republic)*

ABSTRACT

Organic acids present in samples of vegetables [green peas, carrots, celery, paprika (capsicum) and onions] after lactic acid fermentation by selected microorganisms were determined by capillary isotachophoresis. Lactic, acetic, phosphoric, citric, propionic and butyric acid and potassium sorbate were determined.

## INTRODUCTION

Preservation by lactic fermentation uses the ability of microorganisms to produce substances that prolong the natural storage time of foods [1]. The objectives for using lactic acid bacteria are to make the food durable, to improve its taste and to maintain the nutritive, physiological and hygienic value of the fermentation products. Lactic fermentation is a complex microbiological process that is influenced by using factors, such as the concentration of salt, temperature, microorganisms and air exclusion [2].

The by-products of lactic fermentation consist mainly of acetic acid with small amounts of formic, propionic, valeric, succinic and caproic acid. They contribute to finishing and rounding of the taste. Butyric acid, produced by bacteria of lactic fermentation, has an adverse effect owing to its particular smell and is therefore undesirable [3,4].

There is commercial interest in the production of vegetable juices fermented by lactic fermentation. Spontaneous fermentation or inoculation of selected and tested cultures of microorganisms is used for the production of the juices. Cultures of microorganisms are required that deepen the aroma and make possible a rapid decrease in the pH of the juices. Lactic fermentation is suitable especially for processing vegetables, mainly cabbage and cucumbers, but also sugar beet, carrots, cauliflower, kohlrabi, paprika (capsicum), onions, asparagus and vegetable mixtures.

Many workers are engaged in research on new products fermented by lactic fermentation, either conserved vegetables or vegetables or fruit juices fermented by lactic fermentation [5–7]. Yu [8] effected the lactic fermentation of soya milk by the strains *Lactobacillus casei* and *Kluyveromyces fragilis*. Manan [9] accomplished laction fermentation of potato slices in salty brine. Ogbadu and Okagbue [10] were engaged in lactic fermentation of soy beans with a starting culture of *Lactobacillus plantarum*. Valdez *et al.* [11] achieved the lactic fermentation of green peas, sweet black pepper and cabbage. Oyewole and Odunfa [12] divided and characterized the cultures of lactic fermentation.

Methods for the identification and determination of organic acids in foods and their advantages, including capillary isotachophoresis, were published by Karovičová and co-workers [13,14]. The aim of this study was to follow the production of organic acids, especially lactic acid and also acetic acid, during lactic fermentation of

* Corresponding author.

0021-9673/93/$06.00 

vegetables by different microorganisms. On the basis of results obtained for the production of lactic acid, suitable microorganisms can be selected for use in the production of fermented vegetables that can be employed for the production of vegetables for preparing vegetable drinks or salads.

Capillary isotachophoresis, owing to its advantages (simple sample preparation, short time of analysis), is comparable to other chromatographic methods and is suitable for the determination of organic acids.

## EXPERIMENTAL

### *Fermentation*

Fermentation experiments were carried out with different kinds of vegetables: green peas, carrots, celery, paprika (capsicum) and onions. The experiments were performed in fermentation flasks in such a way that after the inoculation of a microorganism anaerobic conditions were maintained. The fermentation lasted 7–10 days at 23–26°C.

For the inoculation of fermented vegetables in the fermentation flasks, the following lyophilized microorganisms were used: *Lactobacillus* sp. "S", $3.04 \cdot 10^8$ microorganisms (MO)/ml; *Pediococcus acidilactici*, $3.52 \cdot 10^7$ MO/ml; *Pediococcus* sp. "CSL", $2.05 \cdot 10^7$ MO/ml; *Lactobacillus fermentum*, $7.08 \cdot 10^7$ MO/ml; *Lactobacillus* sp. "U", $2.60 \cdot 10^7$ MO/ml; *Lactobacillus* spp., $5.40 \cdot 10^8$ MO/ml; *Lactobacillus bucheri*, $1.32 \cdot 10^8$ MO/ml; and *Lactobacillus brevi*, $2.40 \cdot 10^8$ MO/ml.

For the experiments the cultivation base according to Rogos was used [19]. The cultivation lasted 3 days at 37°C.

*Fermentation of green peas.* Frozen green peas were used. Brine of the required concentrations of salt and reducing sugars was prepared after thawing and after the basic analyses (determination of reducing sugars, titriatable acids, pH). The concentration of reducing sugars for samples A1–3 was 2.40% and the adjusted concentration of reducing sugars for samples A4–7 was 3.57%. The brine in samples A1–7 was 1.5% NaCl and the ratio of mixing the brine and green peas was 5:4. The fermentation lasted 7 days at 23°–26°C.

*Fermentation of carrots.* Stored, cleaned and grated carrots with brine of 1.5% NaCl were used. For samples B1–8, 0.1% $CaCl_2$ and 0.1% potassium sorbate were added; sample B9 was without potassium sorbate. Better anaerobic conditions were created by nitrogen bubbling. The ratio of carrots to brine was 5:9. The fermentation lasted 10 days.

*Fermentation of celery.* Stored celery was cut into cubes and immersed in brine (celery to brine ratio = 3:4) before fermentation. For samples C1–5 0.1% potassium sorbate was added and for samples C3–5 nitrogen bubbling was also applied. A higher concentration of phytoncide substance (0.01%) was applied to the C6–8 and a lower concentration (0.005%) to samples C9 and 10. The brine used for all samples C1–10 was 1.5% NaCl.

*Fermentation of paprika (capsicum).* Frozen paprika was cut into strips and immersed in brine (paprika to brine ratio = 4:5) before fermentation. The brine contained 1.5% NaCl and 0.1% $CaCl_2$ for samples D1–8, and was also 0.1% potassium sorbate for samples D3 and 4. A higher concentration of phytoncide substance (0.01%) was applied to samples D5 and 6 and a lower concentration (0.005%) to samples D7 and 8. The fermentation lasted 10 days.

*Fermentation of onions.* Onions (E) were cleaned and cut into round pieces and immersed in brine (onion to brine ratio = 2:3) before fermentation. The brine was 1.5% NaCl. The fermentation lasted 7 days.

### *Isotachophoresis*

Fermented samples were homogenized and filtered before isotachophoretic analyses. Measurements were made on a CS ZKI 01 isotachophoretic analyser (Spišská Nová Ves, Slovak Republic) equipped with a conductivity detector and a TZ 4200 double line recorder.

The samples were analysed at a driving current of 200 $\mu$A in the preseparation column and 50 $\mu$A in the analytical column. For identification and determination the electrolytic system applied had the following composition: concentration of leading electrolyte, 0.01 *M* HCl; counter ion, $\varepsilon$-aminocaproic acid; pH, 4.5; additive, methylhydroxyethylcellulose (0.1%); terminat-

TABLE I

CHARACTERISTIC CONSTANTS OF THE STANDARDS OF ORGANIC ACIDS AND THE PARAMETERS OF THE CALIBRATION LINES ($y = a + bx$)

R.s.h. = Relative step height = $(h_i - h_L)/(h_T - h_L)$, where $h_i$ is the line of the $i$th ion, $h_L$ is the line of the leading electrolyte and $h_T$ is the line of the terminating electrolyte; r = correlation coefficient; $a$ = intercept on ordinate (mm); $b$ = slope (mm/mmol).

| Organic acid | R.s.h. | $a$ | $b$ | $r$ |
|---|---|---|---|---|
| Phosphoric acid | 0.299 | 2.4163 | 9.5581 | 0.9971 |
| Lactic acid | 0.310 | −1.6584 | 17.5145 | 0.9968 |
| Acetic acid | 0.327 | 1.7064 | 11.5406 | 0.9916 |
| Citric acid | 0.227 | −0.0988 | 19.8256 | 0.9973 |
| Propionic acid | 0.600 | 0.7776 | 17.1076 | 0.9989 |
| Butyric acid | 0.777 | 0.9442 | 16.7729 | 0.9994 |

ing electrolyte, $5 \cdot 10^{-3}$ $M$ caproic acid–$5 \cdot 10^{-3}$ $M$ histidine (pH 4–5).

Samples diluted 1:25 with water were injected into the column using the four-way valve of the instrument. The duration of the analysis was 20–30 min. Quantitative analysis was performed by calibration. Based on the presumed presence of organic acids, standard solutions of lactic, acetic, citric, phosphoric, propionic and butyric acid and potassium sorbate of concentration 0.01 $M$ were prepared. Values of the characteristic constants (relative step heights) of the standards of organic acids and the parameters of the calibration lines are given in the Table I.

## RESULTS AND DISCUSSION

The study was aimed at the investigation of the suitability of the various microorganisms as starting cultures during the lactic fermentation of vegetables. The selection of the microorganisms was based mainly on the production of lactic acid and also on the sensory evaluation of the fermented vegetables. We wanted to retain the hardness of the vegetables and to gain a typical sour taste and adequate aroma. The designations of the analysed samples, the microorganisms used, and the average contents of the determined organic acids calculated from three measurements are given in Tables II–VI. The samples were always taken after the fermentation had finished.

The results of isotachophoretic analysis of the samples of green peas are presented in Table II. Only lactic and acetic acid were present in the samples of green peas. The measured amount of lactic acid ranged from 6.75 to 14.56 g $l^{-1}$. The best producer of lactic acid was the microorganism *Pediococcus* sp. "CSL". Its production was the highest at the different concentrations of reducing sugars. This microorganism also showed a very suitable production of acetic acid, which gave a good taste and aroma to the product.

Recently there has been a demand to lower the amounts of chemical preservatives added to food products. With regard to this problem, our task was to establish and use the preservation effects of phytoncides at two different concentrations. Phytoncides inhibit the growth of many microorganisms. They may have different chemical compositions, taste and aroma and many are characteristic, strong and pervasive. They are components of some spices and herbs. Phytoncides are the subject of research as additional preservation agents. We obtained products with a pleasant sour taste, excellent appearance and the same hardness after fermentation for 1 week with application of phytoncides.

Table III gives the organic acids in the samples of fermented carrots after 10 days of fermentation. We tested a large number of microorganisms during the fermentation of carrots. We identified lactic, acetic, phosphoric, citric, propi-

TABLE II

ORGANIC ACIDS IN GREEN PEA SAMPLES

| Sample | Microorganism | Contents of organic acids (g $l^{-1}$) | |
|---|---|---|---|
| | | Lactic | Acetic |
| A1 | *Pediococcus* sp. "CSL" | 9.67 | 2.83 |
| A2 | *Lactobacillus* sp. "S" | 7.24 | 1.69 |
| A3 | *Pediococcus acidilactici* | 6.75 | 2.36 |
| A4 | *Lactobacillus* sp. "S" | 11.64 | 5.40 |
| A5 | *Pediococcus acidilactici* | 7.77 | 6.85 |
| A6 | *Pediococcus* sp. "CSL" | 14.56 | 4.90 |
| A7 | *Lactobacillus* sp. "U" | 14.52 | 5.64 |

TABLE III

ORGANIC ACIDS IN CARROT SAMPLES

| Sample | Microorganism | Contents of organic acids (g $l^{-1}$) | | | | | |
|---|---|---|---|---|---|---|---|
| | | Lactic | Acetic | Phosphoric | Citric | Propionic | Butyric |
| B1 | *Lactobacillus buchneri* | 8.80 | 4.59 | 0.19 | 1.47 | – | – |
| B2 | *Pediococcus* sp. "CSL" | 13.21 | 4.85 | 0.15 | – | – | 1.31 |
| B3 | *Lactobacillus* sp. "U" | 8.04 | 3.28 | – | – | 0.43 | – |
| B4 | *Lactobacillus fermentum* | 9.69 | 4.28 | – | – | – | – |
| B5 | *Lactobacillus* spp. | 7.53 | 2.56 | – | – | 0.24 | 0.27 |
| B6 | *Pediococcus acidilactici* | 7.01 | 3.32 | – | – | 0.36 | 0.45 |
| B7 | *Lactobacillus* brevi | 4.89 | 4.60 | – | 0.18 | 0.79 | – |
| B8 | *Lactobacillus* sp. "S" | 9.36 | 4.19 | 1.47 | 0.42 | 0.62 | – |
| B9 | *Lactobacillus* sp. "S" | 8.39 | 2.40 | – | – | 0.22 | – |

onic and butyric acid in the individual fermentation samples. Under the same conditions, *Lactobacillus fermentum*, *Lactobacillus* sp. "S" and *Pediococcus* sp. "CSL" produced the most lactic acid, but butyric acid was also produced, which is not desirable for the sensory aspect of the product. The measured amounts of lactic acid ranged from 4.89 to 13.21 g $l^{-1}$. Fig. 1 shows the analysis of a carrot sample.

Table IV lists the organic acids present in the samples of fermented celery. The samples were taken after 10 days of fermentation. Lactic, acetic, phosphoric, citric and propionic acid and potassium sorbate were identified. A concentration of 0.98 g $l^{-1}$ of potassium sorbate was determined in sample C2. Most lactic acid was determined in sample C2 with the microorganism *Lactobacillus* sp. "S", and similar results were obtained with samples C3–5. Nitrogen bubbling was also used in the fermentation of celery. We found that the product without nitrogen bubbling had a typical sour taste and aroma. We also tried omitting the use of preservatives with this product. We tested two different concentrations of phytonicide substance. With regard to the sensory aspect, both tested concentrations of phytoncide substance were convenient for this product.

Lactic, acetic and propionic acid were determined by isotachophoretic analysis of the samples of paprika (Capsicum) (Table V). A 0.98 g $l^{-1}$ concentration of potassium sorbate was determined in samples D3 and 4. The highest content of lactic acid in samples D1–4 was in sample D2 when *Lactobacillus* sp. "S" was used, but at the same time there was also a fairly high content of acetic acid (up to 5.08 g $l^{-1}$).

In the literature there are numerous contradictory discussions about the effect of acetic acid

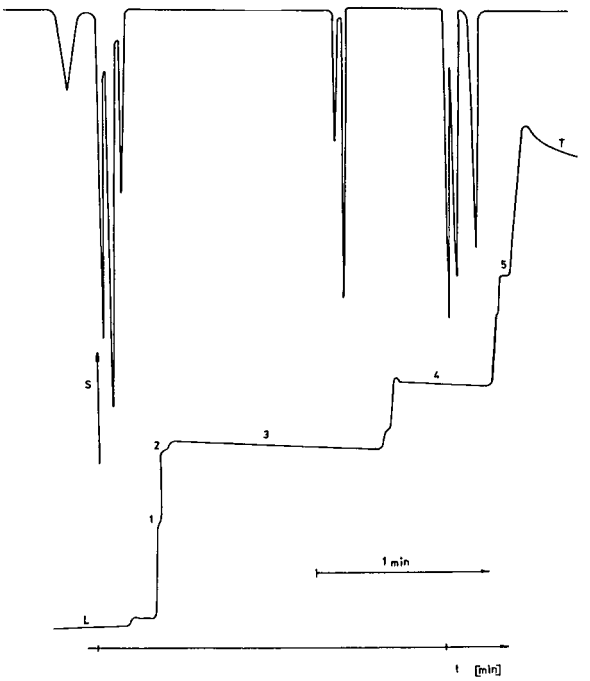


Fig. 1. Isotachopherogram of organic acids in the carrot B8 sample. *S* = Response of conductivity detector; L = leading electrolyte; T = terminating electrolyte. 1 = Citric acid; 2 = phosphoric acid; 3 = lactic acid; 4 = acetic acid; 5 = propionic acid.

TABLE IV

ORGANIC ACIDS IN CELERY SAMPLES

| Sample | Microorganism | Contents or organic acids (g $l^{-1}$) | | | | |
|---|---|---|---|---|---|---|
| | | Lactic | Acetic | Phosphoric | Citric | Propionic |
| C1 | *Lactobacillus* sp. "U" | 9.23 | 4.84 | 0.65 | 0.99 | 0.34 |
| C2 | *Lactobacillus* sp. "S" | 11.42 | 2.65 | 0.63 | 1.38 | 0.51 |
| C3 | *Lactobacillus* sp. "U" | 6.48 | 3.28 | 0.40 | 0.68 | 0.69 |
| C4 | *Lactobacillus* sp. "S" | 8.47 | 3.34 | 0.67 | 0.69 | 0.51 |
| C5 | *Lactobacillus fermentum* | 7.03 | 3.13 | 0.19 | 0.70 | 0.61 |
| C6 | *Lactobacillus* sp. "S" | 13.39 | 7.77 | 0.41 | 0.95 | – |
| C7 | *Lactobacillus fermentum* | 11.29 | 6.48 | 1.08 | 0.69 | – |
| C8 | *Lactobacillus* sp. "U" | 9.38 | 6.47 | – | 0.69 | – |
| C9 | *Lactobacillus fermentum* | 10.76 | 8.00 | 0.19 | 0.68 | – |
| C10 | *Lactobacillus* sp. "U" | 8.80 | 7.46 | 1.10 | 0.69 | – |

TABLE V

ORGANIC ACIDS IN PAPRIKA (CAPSICUM)

| Sample | Microorganism | Contents of organic acids (g $l^{-1}$) | | | |
|---|---|---|---|---|---|
| | | Lactic | Acetic | Citric | Propionic |
| D1 | *Lactobacillus fermentum* | 7.49 | 5.08 | 0.82 | 0.27 |
| D2 | *Lactobacillus* sp. "S" | 7.61 | 4.86 | 0.69 | 0.27 |
| D3 | *Lactobacillus fermentum* | 6.44 | 4.65 | 0.95 | 0.27 |
| D4 | *Lactobacillus* sp. "S" | 6.60 | 4.55 | 0.69 | 0.27 |
| D5 | *Lactobacillus* sp. "S" | 7.18 | 2.15 | 0.82 | 0.21 |
| D6 | *Lactobacillus fermentum* | 7.34 | 3.24 | 0.69 | 0.22 |
| D7 | *Lactobacillus* sp. "S" | 6.89 | 2.03 | 0.69 | 0.31 |
| D8 | *Lactobacillus fermentum* | 4.09 | 1.34 | 0.69 | 0.31 |

concentration on the quality of fermented products. It is known that the absence of acetic acid leads to products which have a unilaterally sour taste and an atypical and flat aroma [15]. Similarly to the samples of celery, paprika was also fermented with addition of phytoncide substance. *Lactobacillus fermentum* (D6) was the best producer of lactic acid in samples D5–8. During the experiments, 0.1% $CaCl_2$ was always added to the brine to maintain the hardness of the product.

Lactic, acetic, phosphoric, citric and propionic acid were determined by isotachophoretic analysis of samples of onions. The average values are given in Table VI. The highest content of lactic acid was present in sample E1 (7.71 g $l^{-1}$) with the use of *Lactobacillus* sp. "S". After fermentation for 1 week onions had pleasant taste, became slightly softer and were suitable for salads or for the production of vegetable drinks. Butyric acid at 0.45 g $l^{-1}$ was also determined in sample E2 with the use of *Lactobacillus fermentum*, which adversely influenced the sensory characteristics of the product.

The production of lactic acid during the cultivation time period indicated that the production of lactic acid depends on the type of microorganism used and not directly on time.

From the evaluation of the effect of NaCl we can say that an increased NaCl concentration does not affect the activity of microorganisms unfavourably. As some fermented products were already softened after 2 days of storage, we added 0.1% $CaCl_2$ to subsequent samples. Mi-

TABLE VI

ORGANIC ACIDS IN ONION SAMPLES

| Sample | Microorganism | Contents of organic acids (g $l^{-1}$) | | | | | |
|---|---|---|---|---|---|---|---|
| | | Lactic | Acetic | Phosphoric | Citric | Propionic | Butyric |
| E1 | *Lactobacillus* sp. "S" | 7.71 | 2.40 | – | – | – | – |
| E2 | *Lactobacillus fermentum* | 2.61 | 1.53 | 0.65 | 2.23 | 0.31 | 0.45 |
| E3 | *Lactobacillus* sp. "U" | 6.32 | 1.34 | – | 2.23 | 0.31 | – |
| E4 | *Lactobacillus* spp. | 6.81 | 1.34 | 0.30 | 1.20 | 0.27 | – |

croorganisms produce only a small amount of acids at a low concentration of sugar. If the total concentration of reducing sugars is so low that the pH drops to 4.1 after the fermentation, butyric acid may be produced, which worsens the sensory characteristics of the product. Hence it is necessary to ensure that the content of reducing sugars is about 4% in the whole product before fermentation.

For the determination of organic acids in individual fermented samples, the standard deviations $s_x$ [16] were as follows: lactic acid, 0.06–0.09; acetic acid, 0.09–0.19; phosphoric acid, 0.01–0.15; citric acid, 0.01–0.07; and propionic acid, 0.01–0.02 g $l^{-1}$. The relative standard deviations $s_r$ were 0.62–2.55%.

In conclusion, capillary isotachophoresis is a suitable method for the determination of organic acids in foods [17,18] and fermented samples, because it gives information about the production of all organic acids and on the use of selected microorganisms in a relatively short time.

Other methods for the determination of organic acids have various disadvantages when compared with isotachophoretic methods. They often require special processing of the samples (derivatization, matrix elimination), which increases the time of analysis and also decreases the accuracy of determination.

Controlled fermentation should satisfy the sensory demands of users and it should also enrich the products with substances that are essential for humans. In this case the fermentation process starts earlier and nutritively important substances are preserved to a greater extent. This is why it is necessary to monitor especially the content of lactic, acetic and other organic acids which are produced by fermentation and essential and total amino acids and vitamins of group B in products fermented by lactic fermentation.

REFERENCES

1 V. Kyzlink, *Základy Konzervace Potravin*, SNTL, Prague, 1980, p. 513.
2 M. Drdák, *Technológia Rastlinných Neudržných Potravín*, Alfa, Bratislava, 1989, p. 300.
3 R. Binnig, *Flüssiges Obst., Sonderheft*, 3a (1982) 204.
4 H.P. Fleming and R.F. McFeeters, *Food Technol.*, 1 (1981) 84.
5 K. Gierschner, *Flüssiges Obst.*, 58 (1991) 236.
6 H. Buckenhüskes, B. Schwartz and K. Gierschner, *Dtsch. Lebensm.-Rundsch.*, 83 (1987) 319.
7 L.M. Beltrán-Edeza and H. Hernandéz-Sánchez, *Lebensm.-Wiss. Technol.*, 22 (1989) 65.
8 J.H. Yu, *Korean J. Food Sci. Technol.*, 20 (1988) 518.
9 J.K. Manan, *J. Food Sci. Technol.*, 24 (1987) 139.
10 L. Ogbadu and R.N. Okagbue, *J. Appl. Bacteriol.*, 65 (1988) 353.
11 G.F. Valdez, G.S. Giori, M. Garro, F. Mozzi and G. Oliver, *Microbiol. Aliment. Natur.*, 8 (1990) 175.
12 O.B. Oyewole and S.A. Odunfa, *J. Appl. Bacteriol.*, 68 (1990) 145.
13 J. Karovičová, M. Drdák and J. Polonský, *J. Chromatogr.*, 509 (1990) 283.
14 J. Karovičová, J. Polonský and A. Príbela, *Nährung*, 34 (1990) 665.
15 H. Buckenhüskes, A. Gessler and K. Gierschner, *Ind. Obst- Gemüseverwert.*, 73 (1988) 454.
16 K. Eckschlager, I. Horsák and Z. Kodejš, *Vyhodnocování Analytických Výsledků a Metod*, SNTL, Prague, 1980, p. 224.
17 L. An and Z. Yan, *Shipin Kexue*, 112 (1989) 1.
18 Z. Stránský, P. Peč, M. Kudlová, M. Mergl and J. Žabková, *Živočíšna Výroba*, 33 (1988) 211.
19 *Potravinářské rýrobky, Stanovení počtu baktérií rodu Lactobacillus*, ČSN 56 0094, 1988.

*Journal of Chromatography*, 638 (1993) 247–253
Elsevier Science Publishers B.V., Amsterdam

CHROM. 24 951

# Use of charged and neutral cyclodextrins in capillary zone electrophoresis: enantiomeric resolution of some 2-hydroxy acids

Annalisa Nardi and Alexey Eliseev[☆]

*Istituto di Cromatografia del CNR, Area della Ricerca di Roma, via Salaria Km 29 300, C.P. 10, 00016 Monterotondo Scalo (Rome) (Italy)*

Petr Boček

*Institute of Analytical Chemistry, Czechoslovak Academy of Scienees, Veveří 97, 611 42 Brno (Czech Republic)*

Salvatore Fanali*

*Istituto di Cromatografia del CNR, Area della Ricerca di Roma, via Salaria Km 29 300, C.P. 10, 00016 Monterotondo Scalo (Rome) (Italy)*

ABSTRACT

Enantiomers of racemic 2-hydroxy acids, namely 2-phenyllactic, 3-phenyllactic, mandelic, *m*-hydroxymandelic, *p*-hydroxymandelic and 3,4-dihydroxymandelic acid, were resolved by capillary zone electrophoresis. The separation was achieved by using the background electrolyte with addition of cyclodextrins. The effects of the type of cyclodextrin, the pH of the electrolyte and the shape of analyte compounds on the migration time and resolution were studied. Good resolution was obtained with background electrolytes in the pH range 5–7, supplemented with 2-hydroxypropyl, $6^{A}$-methylamino- and $6^{A},6^{D}$-dimethylamino-$\beta$-cyclodextrin.

## INTRODUCTION

The resolution of enantiomers in racemic mixtures of hydroxy acids is an interesting field of application in analytical chemistry, especially in pharmaceutical analysis and metabolism studies [1].

Gas chromatography (GC) and liquid chromatography (LC) have so far been used for the resolution of 2-hydroxy acid enantiomers [2–5].

In LC the resolution is obtained by using chiral compounds either in the stationary phase or in the mobile phase, *e.g.*, metal complexes with chiral amino acids, cyclodextrins or triacetylcellulose.

Capillary zone electrophoresis (CZE) is a recent method that allows rapid separations to be obtained with high efficiency and high resolution of compounds with different effective electrophoretic mobilities [6]. When the electrophoretic analysis of a racemic mixture is carried out in an achiral background electrolyte (BGE), the two enantiomers are usually not resolved because they have the same mobilities. Hence the use of a suitable chiral additive in the background electrolyte is required in order to

* Corresponding author.
☆ Permanent address: Department of Chemistry, Moscow State University, Moscow, Russian Federation.

0021-9673/93/$06.00 

interact selectively with enantiomers to give a difference in their mobilities and hence allow their separation. This can be done, *e.g.*, by using some equilibria with chiral additives by forming diastereoisomeric complexes with the analytes. Among several mechanisms used in CZE, inclusion complexation seems to be interesting for the resolution of several classes of enantiomers.

Cyclodextrins (CDs) have already been successfully used for these purposes, added either to the BGE or to the gel or bonded to the capillary walls [7–11]. Recent developments in the electrophoretic separation of optical isomers can be found elsewhere [12–14]. CDs are chiral, natural oligosaccharides with a shape similar to a truncated cone with a relatively hydrophobic cavity able to form inclusion complexes with analytes (aromatic groups are preferred). The outside of the CD is more hydrophilic [15]. The enantioselectivity arises from the chiral carbon of the glucose units in the CDs. The formation of inclusion complexes between enantiomers and CDs is strongly influenced not only by the hydrophobic interaction in the cavity but also by bonding between the hydroxyl groups (or other substituents) on the rim of CDs and substituent groups of the asymmetric centre of the analytes.

This paper describes a continuation of our studies on chiral separations in CZE by using CDs as chiral additives to the BGE [16–19]. This work was aimed at an experimental study of the effects of the type and concentration of the CD and the pH of the BGE on the migration time and the resolution of DL-2-phenyllactic, DL-3-phenyllactic, DL-mandelic, DL-*m*-hydroxymandelic, DL-*p*-hydroxymandelic and DL-3,4-dihydroxymandelic acid. We selected β-CD and some modified β-CDs, namely, heptakis(2,6-di-O-methyl)-, 2-hydroxypropyl, $6^A$-methylamino- and $6^A$,$6^D$-dimethylamino-β-cyclodextrin for electrophoretic experiments. The modified CDs can provide greater effectiveness in enantiomeric resolution because they possess different properties with respect to the parent compounds, *e.g.*, the solubility can be higher, the cavity can be deeper (dimethyl-β-CD) or the presence of charged groups can stabilize the inclusion complex etc.

## EXPERIMENTAL

Sodium dihydrogenphosphate, phosphoric acid, sodium acetate, acetic acid and L- and D-mandelic acid (MA) were purchased from Carlo Erba (Milan, Italy), DL-3-phenyllactic acid (3-PhL), L-3-phenyllactic acid, DL-*m*-hydroxymandelic acid (*m*-MA), DL-*p*-hydroxymandelic acid (*p*-MA), DL-3,4-dihydroxymandelic acid (3,4-di-MA) and β-cyclodextrin from Sigma (St. Louis, MO, USA), DL-atrolactic acid hemihydrate (2-PhL) from Fluka (Buchs, Switzerland) and heptakis(2,6-di-O-methyl)-β-cyclodextrin (di-Me-β-CD) and 2-hydroxypropyl-β-cyclodextrin (2-PRO-β-CD) from Chinoin (Budapest, Hungary). $6^A$-Methylamino-β-cyclodextrin (6-NH-β-CD) was synthesized through tosylated intermediates [20] with subsequent substitution of the tosyl groups by methylamine [21]. $6^A$,$6^D$-Dimethylamino-β-cyclodextrin (6-di-MeNH-β-CD) was prepared by the reaction of methylamine [21] with $6^A$,$6^D$-(biphenyl-4,4′-disulphonyl)-β-cyclodextrin, obtained by a regioselective capping procedure in accordance with ref. 22. Analytical data for the aminated cyclodextrins are presented elsewhere [23]. The formulae of the racemic acids, their abbreviations and the symbols used in the figures are shown in Fig. 1.

### *Apparatus*

A Bio-Rad HPE 100 apparatus (Bio-Rad Labs., Richmond, CA, USA) equipped with an

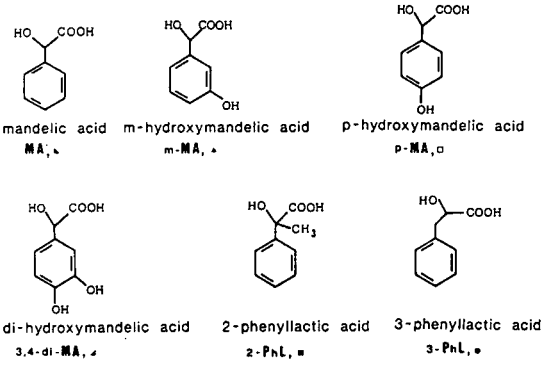


Fig. 1. Structures of mandelic acid and derivatives.

on-column UV detector operated at 206 nm was used for electrophoretic experiments. The high-voltage power supply was operated in either a constant-voltage or constant-current mode. The electrophoretic analyses were performed in a capillary (20 cm × 0.025 mm I.D.) with a coated inner wall mounted in a cartridge (Bio-Rad Labs.). This capillary showed negligible electroosmosis. Samples were injected by the electromigration method at constant voltage. The electropherograms were recorded by using a Model 2210 line recorder (LKB, Bromma, Sweden).

*Background electrolyte (BGE)*

Stock solutions 0.1 *M* sodium dihydrogenphosphate titrated with either phosphoric acid or sodium hydroxide at pH 6 and 7 were used for electrophoretic experiments. For the separations at pH 5, 0.1 *M* sodium acetate titrated with acetic acid was used. The appropriate amount of a selected CD was added to the stock solutions before the experiments.

The resolution ($R$) of the enantiomers was calculated by using the following equation:

$$R = \frac{2(t_L - t_D)}{w_L + w_D} \quad (1)$$

where $t$ is the migration time, $w$ the width of the peak at the baseline and L and D represent the two enantiomers.

## RESULTS AND DISCUSSION

Considering the requirement that the acids in question (see Fig. 1) should be sufficiently dissociated and considering the data from ref. 24, we selected a BGE in the pH range 5–7 for electrophoretic experiments. Under these conditions all the analyte compounds migrated anodically. In the absence of CDs the migration times of the analytes were short (less than 5 min) and, as expected, the racemic mixtures were not resolved. When enantiomers of the same compound have to be separated it is necessary to modify selectively their mobility and this can be done, *e.g.*, by using some equilibria with chiral additives by forming diastereoisomeric complexes with analytes. Among several mechanisms used in CZE, inclusion complexation seems to be interesting for the resolution of several classes of enantiomers.

Fig. 2 shows the effect of the concentration of β-CD added to the BGE at pH 5 on the migration time of the analyte compounds. By increasing the amount of CD in the BGE the migration time of all the analytes increased. The effect was most evident for 3-phenyllactic and 2-phenyllactic acid. The resolution of enantiomers was obtained only for 3-PhL ($R = 0.5$) and 2-PhL ($R = 0.8$). By performing similar electrophoretic experiments with the BGE at pH 6 and 7 an increase in the migration times with increasing amount of CD was observed in all instances, but no resolution of enantiomers was obtained.

The increase in the migration times of the acids investigated when CD was added to the BGE shows that inclusion complexation takes place. The stronger the complexation, the larger is the increase in migration time.

By using di-Me-β-CD as the additive to BGE (up to 80 m*M*), the migration time of all the racemic compounds was increased in proportion to the amount of CD added, but no resolution was observed in any instance. The effect was greater for the two phenyllactic acids than the other compounds, probably owing to the forma-

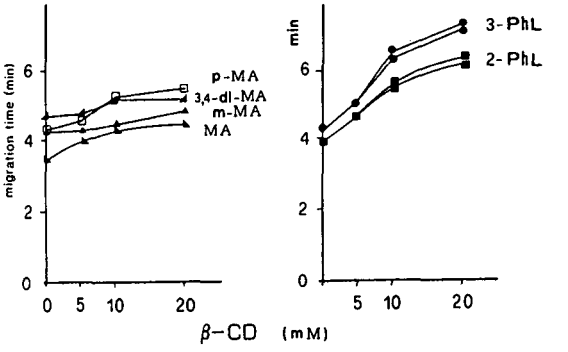


Fig. 2. Effect of the amount of β-cyclodextrin (β-CD) added to the BGE at pH 5 on the migration times of 2-hydroxy acids. Electrophoresis, 12 μA (constant), 7 kV; sampling, electromigration at 8 kV, 8 s.

tion of inclusion complexes with higher stability constants; the effect was more evident when the BGE at pH 7 was used.

When we used 2-PRO-β-CD as an additive to the BGE, the migration time of all the compounds increased when the amount of CD increased in all experiments. Fig. 3 shows the effect of the amount of modified CD on the migration times of the compounds when the BGE at pH 6 was used. It is clear that the differences in the migration times of the separated enantiomers are relatively high.

Concerning the enantiomeric resolution, none was observed for *m*-MA or 3,4-di-MA at any pH. MA and *p*-MA were resolved poorly and only when the BGE at pH 6 was used ($R = 0.5$ at 80 m*M* 2-PRO-β-CD). For 2-PhL good enantiomeric resolution was obtained at all pH values. For 3-PhL some enantiomeric resolution was also obtained at all pH values, but the resolution was not satisfactory (the best result obtained was $R = 0.5$ at pH 5 and 20 m*M* 2-PRO-β-CD). In spite of the greater inclusion complexation of 3-PhL than 2-PhL, the former showed a higher degree of resolution, which was strongly related to the concentration of chiral additive (at pH 6, $R = 0.9$ and 1.1 with 20 and 80 m*M* 2-PRO-β-CD, respectively). The higher enantiomeric resolution of 2-PhL than that obtained for 3-PhL can be explained by considering their structures. The chiral carbon is in a different position, α- and β- for 2- and 3-PhL, respectively, and also 2-PhL possesses a methyl group that can interact with the hydroxypropyl substituent of the CD.

Further experiments were carried out with a charged type of CD, namely $6^A$-methylamino-β-CD. Fig. 4 shows the effect of the amount of this CD on the migration times of the 2-hydroxy acids at pH 5.

Generally, all the compounds moved anodically with a reduced velocity when the CD content was increased. 3-PhL showed higher complexation than 2-PhL. The complexation order for mandelic acid and its derivatives was *p*-MA > MA > 3,4-di-MA > *m*-MA. 3,4-Di-MA and *m*-MA are less complexed than the other compounds owing to the hindering effect of OH groups on the aromatic ring. The enantiomeric resolution of all compounds under investigation was obtained in a broad range of added concentrations of this CD, and, it was pH dependent.

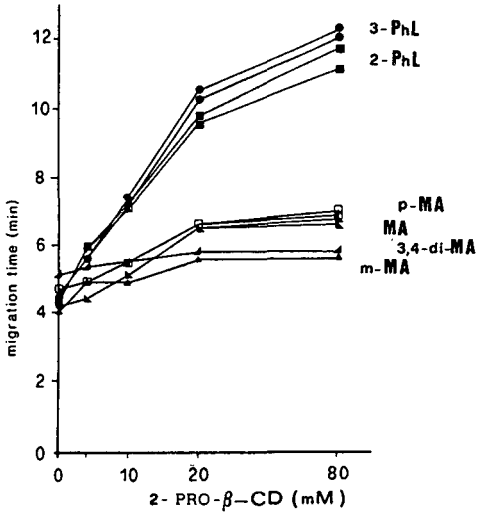


Fig. 3. Effect of 2-hydroxypropyl-β-cyclodextrin (2-PRO-β-CD) concentration on the migration times of 2-hydroxy acids. BGE, pH 6; electrophoresis, 20 μA (constant), 6.5 kV; sampling, electromigration at 8 kV, 8 s.

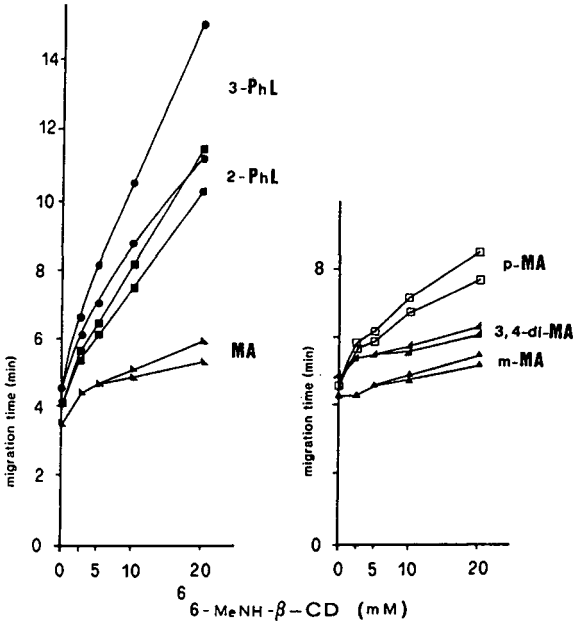


Fig. 4. Effect of $6^A$-methylamino-β-cyclodextrin (6-MeNH-β-CD) on the migration times of 2-hydroxy acids at pH 5.

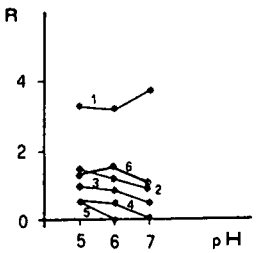


Fig. 5. Effect of the pH on the resolution ($R$) of 2-hydroxy acids: 1 = 3-PhL; 2 = MA; 3 = *p*-MA; 4 = *m*-MA; 5 = 3,4-di-MA; 6 = 2-PhL. BGE containing 10 m*M* $6^A$-methylamino-$\beta$-cyclodextrin.

Fig. 5 depicts this effect and shows plots of $R$ *versus* pH for racemic compounds analysed in presence of 10 m*M* $6^A$-methylamino-$\beta$-CD. By increasing the pH of the BGE the resolution improved for 3-PhL, for 2-PhL it increased at pH 6 and decreased at pH 7 and for MA and its derivatives the resolution decreased.

The results indicate that the presence of the methylamino substituent on the $\beta$-CD ring is very important for improving the complexation and the resolution of racemic mixtures. Inclusion complexation seems to be the main mechanism involved during the electrophoretic process and the complex stability and chiral discrimination are improved by the electrostatic interactions between amino ($\beta$-CD) and carboxylic (analyte) groups.

In order to verify the effect of the methylamino substituent, which brings one positive charge to the CD, on the resolution of hydroxy acids, experiments were also performed (at pH 5) with a disubstituted methylamino-$\beta$-CD ($6^A$,$6^D$-dimethylamino-$\beta$-CD), which has two positive charge. Table I gives the results. Obviously, the migration time and the resolution increased on increasing the amount of CD added. The effect was stronger for 2- and 3-PhL than for the other compounds. When 5 m*M* $6^A$,$6^D$-dimethylamino-$\beta$-CD was used, 2-PhL and 3-PhL gave very broad peaks, probably owing to the slow kinetics of the complexation.

TABLE I

EFFECT OF THE CONCENTRATION OF $6^A$,$6^D$-DIMETHYLAMINO-$\beta$-CYCLODEXTRIN ON THE MIGRATION TIMES AND RESOLUTION OF 2-HYDROXY ACIDS

$t_m$ = Migration time (min); $R$ = resolution.

| 2-Hydroxy acid | $6^A$,$6^D$-Dimethylamino-$\beta$-CD (m*M*) | | | | | | | | | |
|---|---|---|---|---|---|---|---|---|---|---|
| | 0.0 | | 0.5 | | 1.0 | | 2.5 | | 5.0 | |
| | $t_m$ | $R$ | $t_m$ | $R$ | $t_m$ | $R$ | $t_m$ | $R$ | $t_m$ | $R$ |
| MA | 3.5 | – | 3.7<br>3.8 | 0.5 | 4.1<br>4.4 | 1.0 | 4.7<br>5.3 | 2.0 | 6.3<br>7.6 | 3.2 |
| *m*-MA | 4.3 | – | 4.1 | – | 4.2<br>4.3 | 0.5 | 4.4<br>4.7 | 1.1 | 5.3<br>6.0 | 3.4 |
| *p*-MA | 4.4 | – | 4.4<br>4.6 | 0.8 | 4.8<br>5.3 | 1.4 | 5.7<br>6.9 | 2.8 | 9.5<br>13.5 | 4.0 |
| 3,4-Di-MA | 4.7 | – | 4.3 | – | 4.6<br>4.7 | 0.5 | 4.7<br>4.9 | 1.0 | 5.6<br>6.1 | 2.0 |
| 2-PhL | 4.0 | – | 4.5<br>4.8 | 1.0 | 5.3<br>6.0 | 1.3 | 8.2<br>10.5 | 2.3 | n.m.[a] | n.m. |
| 3-PhL | 4.3 | – | 4.6<br>5.5 | 1.6 | 5.8<br>6.3 | 3.5 | 8.8<br>15.3 | 3.2 | n.m. | n.m. |

[a] n.m. = Not measured.

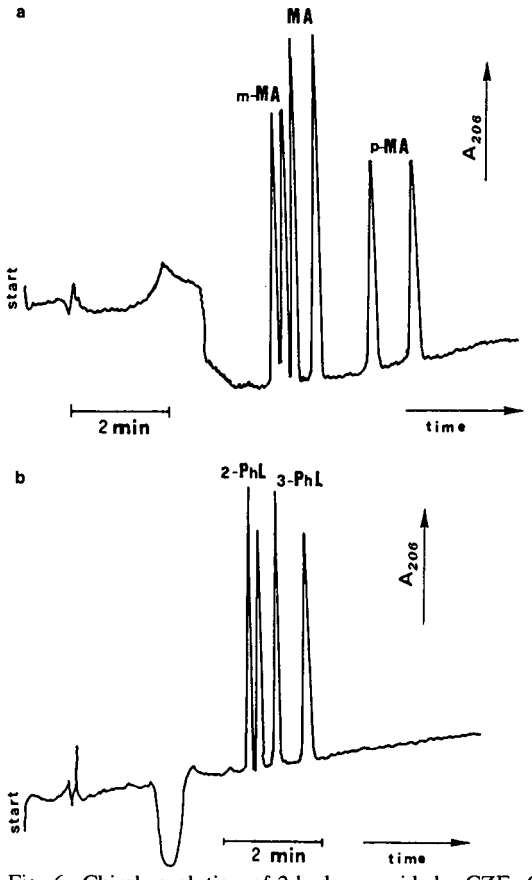


Fig. 6. Chiral resolution of 2-hydroxy acids by CZE. Capillary column, 20 cm × 0.025 mm I.D., coated; BGE, 0.1 *M* acetate buffer (pH 5) containing $6^A$-methylamino-β-cyclodextrin at (a) 20 and (b) 5 m*M*; electrophoresis, 7 kV (constant), 15 μA; sampling, electromigration at 8 kV, 8 s; $10^{-5}$ *M* of each racemic compound.

As an example, Fig. 6a and b show the resolution of a mixture of the racemic 2-hydroxy acids into their enantiomers when the BGE at pH 5 was supplemented with 5 and 20 m*M* $6^A$-methylamino-β-CD, respectively. The migration order was verified by spiking the racemic mixture with pure standards (L- and D-mandelic acid, L-phenyllactic acid). In all instances when β-CD and modified CDs were used, the L-isomer moved more slowly than the D-isomer.

## CONCLUSIONS

It has been demonstrated that CZE can be successfully used for the enantiomeric resolution of racemic mixtures of 2-hydroxy acids when modified CDs serve as the chiral additive to the BGE and thus selective retardation is involved owing to an inclusion complexation mechanism. Among the various cyclodextrins tested, modified β-CD (di-Me-β-CD, 2-PRO-β-CD, $6^A$-MeNH-β-CD and $6^A$,$6^D$-di-MeNH-β-CD) seem to be the most useful for the enantiomeric resolution of this type of compound. The chiral discrimination is influenced by the type of CD, its concentration and the pH of the BGE.

## ACKNOWLEDGEMENTS

Thanks are due to Mr. M. Cristalli and Mr. G. Caponecchi for technical assistance.

## REFERENCES

1 W. Klemisch, A. von Hodenberg and K.O. Vollmer, *J. High Resolut. Chromatogr. Chromatogr. Commun.*, 4 (1981) 535.
2 W.A. Konig, I. Benecke and S. Sieves, *J. Chromatogr.*, 217 (1981) 71.
3 G. Blaschke, *Angew. Chem.*, 92 (1980) 14.
4 G. Gubitz and S. Mihellyes, *Chromatographia*, 19 (1984) 257.
5 J. Debowski, J. Jurczak and D. Sybilska, *J. Chromatogr.*, 282 (1983) 83.
6 F. Foret and P. Bocek, in A. Chrambach, M.J. Dunn and B.J. Radola (Editors), *Advances in Electrophoresis*, VCH, Weinheim, 1989, p. 273.
7 A. Guttman, A. Paulus, A.S. Cohen, N. Grinberg and B.L. Karger, *J. Chromatogr.*, 448 (1988) 41.
8 S. Mayer and V. Schurig, *J. High Resolut. Chromatogr.*, 15 (1992) 129.
9 S. Terabe, *Trends Anal. Chem.*, 8 (1989) 129.
10 J. Snopek, H. Soini, M. Novotny, E. Smolkova-Keulemansova and I. Jelinek, *J. Chromatogr.*, 559 (1991) 215.
11 S. Fanali, *J. Chromatogr.*, 474 (1989) 111.
12 J. Snopek, I. Jelinek and E. Smolkova-Keulemansova, *J. Chromatogr.*, 609 (1992) 1.
13 J. Snopek and E. Smolkova-Keulemansova, *Cyclodextrins in Electromigration Methods (New Trends in Cyclodextrins and Derivatives)*, Edition de Santé, Paris, 1991, Ch. 14, p. 483.
14 R. Kuhn and S. Hoffstetter-Kuhn, *Chromatographia*, 34 (1992) 505.
15 W.L. Hinze, *Sep. Purif. Methods*, 10 (1981) 159.
16 S. Fanali and P. Bocek, *Electrophoresis*, 11 (1990) 757.
17 S. Fanali, *J. Chromatogr.*, 545 (1991) 437.
18 S. Fanali, M. Flieger, N. Steirenova and A. Nardi, *Electrophoresis*, 13 (1992) 39.

19 A. Nardi, L. Ossicini and S. Fanali, *Chirality*, 4 (1992) 56.
20 Y. Matsui and A. Okimoto, *Bull. Chem. Soc. Jpn.*, 51 (1978) 3030.
21 R. Breslow, M.F. Czarniecki, J. Emert and H. Hamaguchi, *J. Am. Chem. Soc.*, 102 (1980) 762.
22 I. Tabushi, K. Yamamura and T. Nabeshima, *J. Am. Chem. Soc.*, 106 (1984) 5267.
23 A.V. Eliseev and A.K. Yatsimirsky, in preparation.
24 V. Sustacek, F. Foret and P. Bocek, *J. Chromatogr.*, 545 (1991) 237.

*Journal of Chromatography*, 638 (1993) 255–261
Elsevier Science Publishers B.V., Amsterdam

CHROM. 24 924

# Prospects of dissolved albumin as a chiral selector in capillary zone electrophoresis

Radim Vespalec*, Vladimír Šustáček and Petr Boček

*Institute of Analytical Chemistry, Czech Academy of Sciences, Veveří 97, 611 42 Brno (Czech Republic)*

ABSTRACT

It has been shown using as examples amino acids, mono- and dicarboxylic acids that the enantioselectivity of dissolved albumin may be employed with advantage in capillary zone electrophoresis (CZE) separations. Slow changes in the enantioselectivity of albumin dissolved in weakly alkaline aqueous solutions can be avoided by a short mild heating of the solution. The efficiency of a separation system for a given solute in CZE is at least one order of magnitude higher than that in LC based on bonded albumin. The good chiral separations obtained here and the high efficiency of CZE separation systems confirm that CZE separations based on dissolved albumin as a chiral selector can compete with analogous LC separations. Perfect qualitative agreement of both enantioselective properties of albumin and factors affecting its enantioselectivity in CZE and LC proves that the knowledge obtained in LC with bonded albumin may be transferred to CZE separation systems.

## INTRODUCTION

The analysis of chiral compounds is of great importance in pharmacy, medicine and biological sciences as a rule. For liquid chromatography (LC) the is shown by the large increase in the number of communications devoted to the problem of enantioselective separations in recent years.

Because of a number of interactions contributing to the enantioselective discrimination, the specificity of particular interactions and further factors affecting the resulting separation selectivity in practice [1], a variety of chiral selectors should be available for routine analyses. Therefore, many chiral selectors of different kinds have been studied in LC [1,2]. Among them, macromolecules of biological origin, *e.g.* proteins, are of importance. Albumin chemically bonded to a proper wide-pore solid matrix is especially suitable for the separation of anionic and amphoteric solutes [3–5]. In LC theory, the enantioselectivity and other properties of the bonded albumin relevant to its functioning as a chiral selector are approximated by those of dissolved albumin [4,6]. The test on the ability of the dissolved albumin to act as a chiral selector in free solution capillary zone electrophoresis (CZE), done in this study is simply the consequence of such theory. In planning the CZE experiments, both experimental findings and ideas originated in LC were employed. Comparison of experimental results with those from LC served for evaluation of experiments as well as for considering the potential of CZE to compete with established LC analyses based on bonded albumin.

## EXPERIMENTAL

Fused-silica capillaries of 80 and 100 $\mu$m I.D. (SGE, Austin, TX, USA and Polymicro Technologies, Phoenix, AZ, USA, respectively) with both laboratory-coated and non-coated inner walls, hanging in free air at room temperature, were used in the laboratory-made set-up with simple siphoning sampling. Non-coated capil-

* Corresponding author.

0021-9673/93/$06.00 

laries, pretreated with 10 m*M* sodium hydroxide and 100 m*M* nitric acid, were rinsed with 10 m*M* sodium hydroxide every day after experiments. Capillaries coated with linear polyacrylamide were prepared using the procedure described by Hjertén [7], but ethanol was used instead of water as a solvent for the silanizing agent.

A laboratory-made power supply unit delivering a constant voltage of ±9.5 kV was employed in experiments using 80 μm I.D. capillaries. In these instances, the current passing through the capillary never exceeded 10 μA. A Spellman CZE 1000 R power supply unit was employed in the experiment using 100 μm I.D. capillaries.

Background electrolytes (BGEs) were obtained by dissolving lyophilized human albumin (HA) or bovine serum albumin (BSA) for laboratory use (Imuna, Šarišské Michalany, Czech Republic) in a proper buffering electrolyte. Buffering electrolytes of pH 8–10 were prepared by dissolving chemicals of analytical grade in boiled deionized water. Details of buffer composition and pH as well as albumin treatment are given in the descriptions of individual experiments. Chemically pure 1:1 racemates D,L-kynurenine, D,L-trypthophan, D,L-3-indole lactic acid N-2,4-dinitrophenyl-D,L-glutamic acid (DNPG), dansyl-D,L-glutamic acid (DSG) as well as 2,3-dibenzoyl-D-tartaric acid and 2,3-dibenzoyl-L-tartaric acid without electrophoretically active admixtures served as samples.

A Jasco 875-UV spectrophotometer equipped with a laboratory-made capillary holder was used for on-line light-absorption detection. The detection window in the outer polyimide capillary coating was made by cutting off the coating with a razor blade. After introductory experiments, the capillary in the holder was sandwiched between quartz lenses having the focal distance of 5 mm at a wavelength of 254 nm. The lenses increased the radial luminous flux through the capillary 10–20 times, depending on the capillary diameter and adjustment of the capillary in the holder. As a result, the intensity of the light beam passing through the capillary of 80–100 μm I.D., where lighted capillary length was 0.6 mm, ranges from 20 to 50% of the intensity of the reference light beam.

Migration times, $t_m$, read from the strip chart record, were converted to apparent mobilities, $\bar{u}$, using the equation $\bar{u} = LlE^{-1}t_m^{-1}$, where $L$ is the total capillary length, $l$ is the distance to the detector and $E$ is the voltage used. Electroosmotic mobility $u_{osm}$ was calculated from the migration time of mesityl oxide or from the vacant peak caused by injection of a large sample volume of albumin-containing electrolytes at detection wavelength less than 330 nm. Separation selectivity is expressed as $|\Delta\bar{u}|$ for each pair of enantiomers. Units $10^{-9}$ m$^2$ V$^{-1}$ s$^{-1}$ were used for all the mobility data.

## RESULTS AND DISCUSSION

Preliminary experiments with bovine serum albumin (BSA) revealed insufficient purity of the available BSA preparation —a ghost peak appeared on the record at wavelengths below 300 nm with detection time independent of the injected solute. No ghost peaks were observed with the human albumin (HA), therefore, only HA was used in the following experiments. Regarding minor differences between BSA and HA [8] and resemblance of BSA and HA enantioselectivities found in LC [9], the qualitative observations and conclusions made in this study with HA are valid for BSA as well.

A 10 mg/ml solution of HA (1% by weight) in 10 m*M* acetic acid–Tris buffer, pH 8, was used to test the applicability of the on-line light absorption detection. The light absorption curve of human albumin in the range 200–600 nm, corrected for the electrolyte background (Fig. 1), demonstrates that the albumin solution is optically transparent at wavelengths ($\lambda$) above 330 nm. At $\lambda < 330$ nm the on-line detection needs the compensation of the background absorption, which is no problem for modern spectrophotometers, such as Jasco 875-UV.

Albumin preferentially retains solutes with negatively charged groups [10]. Enantioselectivity of the bonded albumin to mono- and dicarboxylic acids as well as to amino acids is highest near pH 9 [11,12]. The test on enantioselectivity of the dissolved albumin at pH 9.6 showed a sufficient potential of the freshly dissolved albumin to separate enantiomers of amino acids

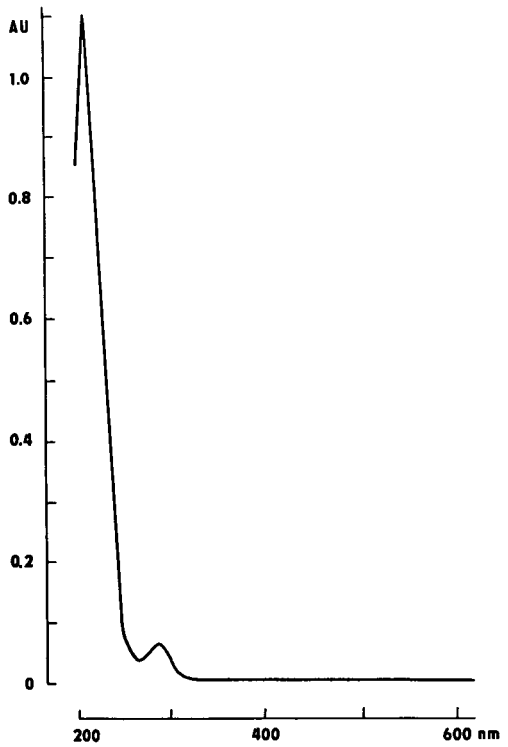


Fig. 1. Light absorption curve of 10 mg/ml human albumin solution, measured in a 100 $\mu$m I.D. fused-silica capillary and corrected for the background absorption of the 10 m*M* acetic acid–Tris buffer, pH 8.

and monocarboxylic acids (Fig. 2); separation of dicarboxylic acids was not satisfactory at an albumin concentration of 1 mg/ml. During a 3-h period, the ability of the albumin, dissolved in electrolyte of pH 9.6, to separate compounds with two carboxylic groups increased, and its enantioselectivity to monocarboxylic compounds decreased. This behaviour is qualitatively the same as that of bonded albumin in LC [12], but the rate of the enantioselectivity changes of the dissolved albumin is at least one order of magnitude higher than that of the albumin bonded in pores of a solid matrix. A decrease in albumin selectivity for amino acids with time in weakly alkaline solutions and its absence in weakly acidic solutions [12] suggests that dissolved albumin is not a proper chiral selector for CZE separations of amino acids.

The stabilization of the enantioselectivity of albumin dissolved in alkaline medium may be accelerated by a short mild heating of the solu-

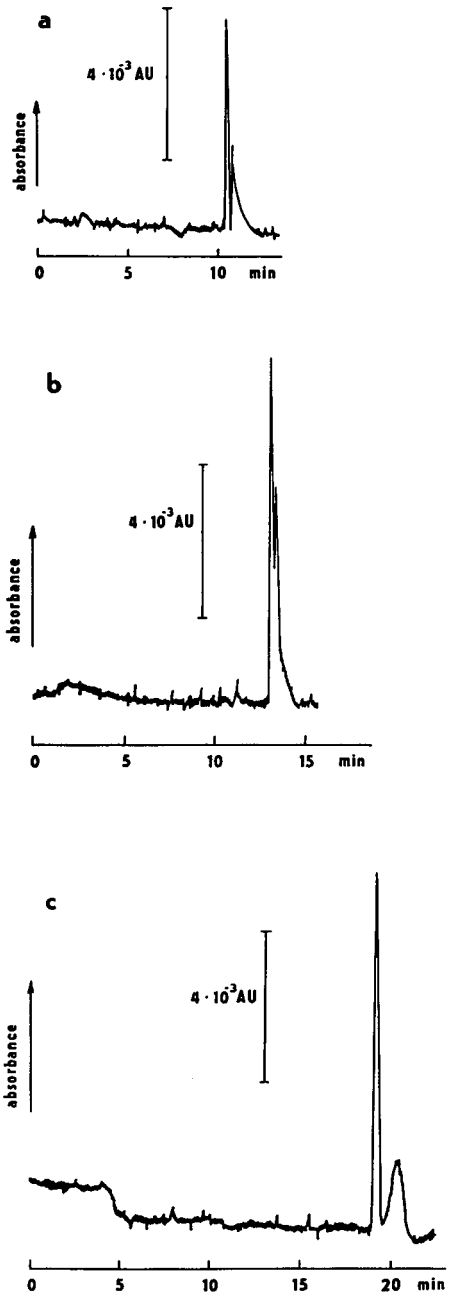


Fig. 2. Separation of (a) 11 pmol of D,L-kynurenine ($\Delta\bar{u}$ = 0.75), (b) 12 pmol of D,L-tryptophan ($\Delta\bar{u}$ = 0.18) and (c) 8 pmol of D,L-3-indole lactic acid ($\Delta\bar{u}$ = 1.3) in freshly prepared solution of 1 mg/ml HA in 10 m*M* boric acid having pH 9.6 adjusted by sodium hydroxide. Experimental details: Non-coated fused-silica capillary [70 cm (54 cm to detector) × 80 $\mu$m I.D.], voltage +9.5 kV, $u_{osm}$ = 45, ambient temperature 24 ± 1°C. Detection: D,L-kynurenine 254 nm, D,L-tryptophan and D,L-3-indole lactic acid 280 nm, using capillary holder without lenses.

tion. For example, heating for 30 min to 60°C at pH 9 is satisfactory. An example of the analysis using the preheated albumin is shown in Fig. 3. After heating the albumin in acetate–Tris solution of pH 9, the final pH 8 at 10 m*M* acetate concentration was adjusted by adding suitable amounts of acetic acid and Tris. The acetic acid–Tris buffer pH 8 was chosen to protect the capillary coating from the damaging action of the high-pH borate buffer. A separation selectivity of $\Delta\bar{u} = 2.3$, observed after injection of 12 pmol of 2,3-dibenzoyl-D,L-tartaric acid to the freshly prepared electrolyte at 29°C, was independent of time. Time-independent enantioselectivities were observed in this system with other tested dicarboxylic acids (DNPG and DSG) as well. Enantioselectivity for amino acids and monocarboxylic acids disappeared with heating, as for bonded albumin in LC [13]. With prolonged heating, *e.g.* for 24 h to 60°C, albumin completely lost its enantioselectivity.

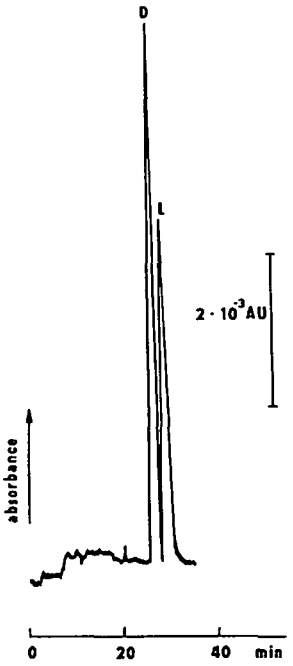


Fig. 3. Separation of 12 pmol of 2,3-dibenzoyl-D,L-tartaric acid in 10 m*M* acetate–Tris buffer, pH 8, containing 3 mg/ml human albumin, heated for 30 min at pH 9 and 60°C. Experimental details: Polyacrylamide-coated fused-silica capillary [76 cm (60 cm to detector) × 80 μm I.D.], voltage −9.5 kV, $u_{osm} < 5$, ambient temperature 29–30°C, detection at 238 nm using capillary holder with quartz lenses.

TABLE I

INFLUENCE OF HUMAN ALBUMIN CONCENTRATION ON SEPARATION SELECTIVITY OF N-2,4-DINITROPHENYL-D,L-GLUTAMIC ACID

Experimental details: Non-coated fused-silica capillary, 70 cm (54 cm to detector) × 80 μm I.D. BGE: 28 m*M* borate buffer, pH 9.0, human albumin heated for 30 min at 60°C. Injection: 0.6 pmol of N-2,4-dinitrophenyl-D,L-glutamic acid. Ambient temperature 20–30°C. Voltage +9.5 kV (0 and 0.5 mg/ml HA) or −9.5 kV (3 mg/ml HA) according to the magnitude of electroosmotic velocity

| HA concentration (mg/ml) | $\lvert\Delta u\rvert$ ($10^{-9}$ m$^2$ V$^{-1}$ s$^{-1}$) |
|---|---|
| 0.0 | 0.0 |
| 0.5 | 0.8 |
| 3.0 | 4.0 |

The effect of the concentration of the preheated albumin on separation selectivity at pH 9.0 was studied in 28 m*M* borate buffer in non-coated capillary (Table I). Owing to the strong dependence of the electro-osmotic flow on the albumin concentration in non-coated capillaries, a polyacrylamide-coated capillary was used in

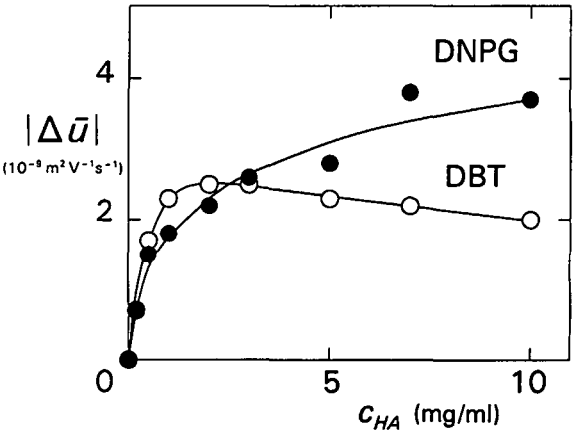


Fig. 4. Selectivity of enantiomeric separations $|\Delta\bar{u}|$ as a function of albumin concentration in 10 m*M* acetate–Tris buffer, pH 8 (DNPG = N-2,4-dinitrophenyl-D,L-glutamate; DBT = 2,3-dibenzoyl-D,L-tartrate). Experimental details: Polyacrylamide-coated fused-silica capillary [70 cm (55 cm to detector) × 100 μm I.D.], sample load 1 pmol, voltage −12 kV, current 10–25 μA, $u_{osm} < 2$, ambient temperature 21–22°C, detection at 380 nm (DNPG) or 254 nm (DBT) using capillary holder with quartz lenses.

the following experiment, shown in Fig. 4. Here the effect was measured in the concentration range 0.2–10 mg/ml albumin in 10 m*M* acetate–Tris buffer, pH 8.0. These two experiments prove the activity of albumin in chiral discrimination. Generally, the chiral selectivity of the system increases with increasing albumin concentration, regardless of pH, temperature, background electrolyte and type of solute. In Fig. 4, the dependence of separation selectivity passes through a maximum for DBT. An increase in the temperature inside the capillary as a result of greater Joule heat produced by the current increasing with albumin concentrations is one probable explanation. However, in addition to increasing enantioselectivity, a higher albumin concentration improves the peak shape and, consequently, the resolution as well. The resolution of peaks increases even if the apparent decrease in selectivity with increasing albumin concentration is observed (Fig. 5). The baseline drift at a concentration of 10 mg/ml HA is due to effects connected with the absorption of the UV light having $\lambda < 330$ nm in relatively concentrated albumin solution.

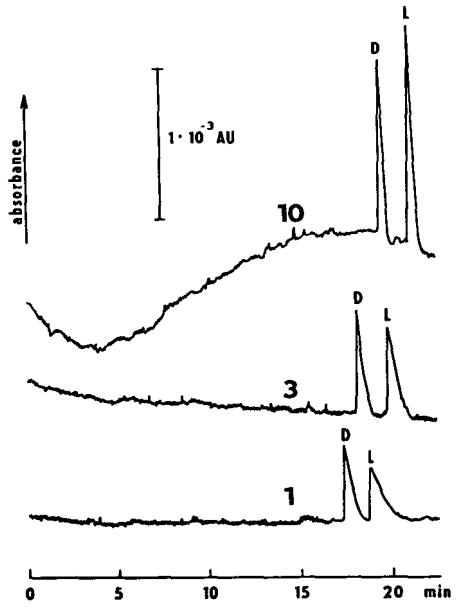


Fig. 5. Influence of albumin concentration (10, 3 and 1 mg/ml HA) on the separation of 1 pmol of 2,3-dibenzoyl-D,L-tartaric acid in 10 m*M* acetate–Tris buffer, pH 8. Experimental details: see Fig. 4.

Efficiency of the proper CZE separation systems based on albumin ranged in this study from 6000 (Fig. 6a) to 80 000 theoretical plates for a capillary of effective length of 60 cm and 20–40 min of analysis time, depending on solute, albumin concentration and its pretreatment as well as on the sample amount.

The efficiency of common LC columns, 15–25 cm in length, packed with sorbents prepared by bonding albumin to silica gel matrix ranges from 500 to 5000 theoretical plates at 10–40 min analysis time for various solutes [1,3–5]. The efficiency may be even lower for columns in which albumin is bonded to an organic polymeric matrix, *e.g.*, HEMA (Fig. 6b).

It is impossible to estimate from the experiments done so far how much the peak broadening in CZE is influenced by the albumin trapped on the capillary wall (albumin mobility is reported to be $-5.9 \cdot 10^{-9}$ m$^2$ V$^{-1}$ s$^{-1}$ at pH 8.6 [8]). In non-coated capillaries, albumin adsorption is manifested by a strong decrease in electroosmosis with increasing albumin concentration. Even in polyacrylamide-coated capillaries, a slight albumin adsorption was observed at high albumin levels as a residual light absorption after replacing the albumin-containing BGE with the same electrolyte solution without albumin.

A typical feature of LC analysis based on bonded albumin is the increase in both solute retention and separation selectivity with decreasing solute amount, being the steeper the lower the solute amount [5,12]. In LC, the combination of a low sorption capacity of albumin for a particular solute [8,14] and an unfavourably low albumin/solute molar concentration ratio is supposed to be the reason. The albumin/solute ratio estimated from albumin content declared by manufacturers and reported sample amounts is usually of the order of $10^{-1}$ to $10^{0}$.

For albumin concentrations of 0.5–1 mg/ml and injections exceeding 5 pmol, the albumin/solute molar concentration ratio was of the order of $10^{-3}$ to $10^{-2}$. The dependence of detection times on sample amount was typical for such experiments at temperatures up to 30°C. The albumin/solute molar concentration ratio of the order of $10^{-1}$ was attainable at 3 mg/ml or higher albumin concentrations and injections of

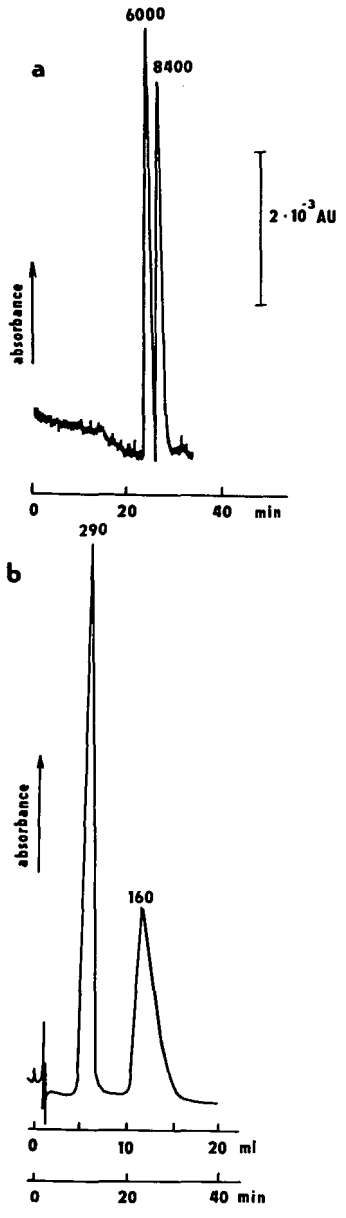


Fig. 6. Comparison of separation efficiencies, given as plate numbers at peak maxima, attained at separations of N-2,4-dinitrophenyl-D,L-glutamic acid in albumin-based systems in (a) CZE and (b) HPLC. Experimental details: (a) Polyacrylamide-coated fused-silica capillary [76 cm (60 cm to detector) × 80 μm I.D.]. BGE: albumin heated in acetate–Tris solution for 30 min at pH 9 and 60°C; final pH 8 at 10 m*M* acetate adjusted with acetic acid and Tris. Injection: 6 pmol of racemate. Voltage −9.5 kV. (b) Commercial 150 mm × 3.3 mm I.D. column packed with Separon HEMA-BIO-BSA (Tessek, Prague, Czech Republic), bonded albumin. Mobile phase: 50 m*M* phosphate buffer, pH 7.8 containing 3% (v/v) 1-propanol, flow-rate 0.5 ml/min. Injection: 5.3 nmol of racemate.

TABLE II

CHANGES IN DETECTION TIMES, $t_i$, AND SELECTIVITIES, $|\Delta u|$, OF N-2,4-DINITROPHENYL-D,L-GLUTAMIC ACID WITH ALBUMIN/SOLUTE MOLAR RATIO AT THE CAPILLARY INLET

Experimental details: Human albumin concentration 3 mg/ml; other details as in Table I

| Albumin/solute molar ratio | $t_1$ (s) | $t_2$ (s) | $\lvert\Delta u\rvert$ ($10^{-9}$ m$^2$ V$^{-1}$ s$^{-1}$) |
|---|---|---|---|
| $4.5 \cdot 10^{-2}$ | 4610 | 6160 | 2.62 |
| $1.8 \cdot 10^{-2}$ | 5300 | 7540 | 2.70 |
| $4.5 \cdot 10^{-1}$ | 5300 | 8040 | 3.10 |

2 pmol or lower. The independence of the detection time on injected amount was observed for the less retained enantiomer of N-2,4-dinitrophenyl-D,L-glutamic acid using heated albumin of 3 mg/ml concentration at 29°C (Table II). This suggests that there is chance to restrict or even eliminate in CZE the unwanted dependence of detection times on solute amount by a proper combination of albumin pretreatment, albumin concentration and elevated capillary temperature. Very long detection times in Table II are the result of a small difference between $u_{osm} = 30$ for 3 mg/ml albumin concentration in non-coated capillary at pH 9 and mobilities of DNPG enantiomers in the system.

ACKNOWLEDGEMENT

This research was supported by the Grant Agency of Czechoslovak Academy of Sciences, Grant No. 43106.

REFERENCES

1 S.G. Allenmark, *Chromatographic Enantioseparations, Methods and Applications*, Ellis Horwood, Chichester, 1988.
2 M. Zief and L.J. Crane (Editors), *Chromatographic Chiral Separations*, (*Chromatographic Science Series*, Vol. 40), Marcel Dekker, New York, 1988.
3 S. Allenmark, B. Bomgren and H. Borén, *J. Chromatogr.*, 316 (1984) 617.
4 S. Allenmark and S. Andersson, *J. Chromatogr.*, 351 (1986) 231.
5 J. Vindevogel, J. van Dijck and M. Verzele, *J. Chromatogr.*, 447 (1988) 297.

6 E. Domenici, C. Bertucci, P. Salvador, G. Félix, I. Cahagne, S. Motellier and I.M. Wainer, *Chromatographia*, 29 (1990) 170.
7 S. Hjertén, *J. Chromatogr.*, 347 (1985) 191.
8 T. Peters, Jr., Serum Albumin, in F.W. Putnam (Editors), *The Plasma Proteins*, Vol. I, Academic Press, New York, 2nd ed. 1975, pp. 133–181.
9 C. Pettersson, T. Arvidsson, A.-L. Karlsson and I. Marle, *J. Pharm. Biomed. Anal.*, 4 (1986) 221.
10 R.H. McMenamy, Albumin Binding Sites, in V. Rosenoer, M. Oratz and M. Rotshild (Editors), *Albumin Structure, Function and Uses*, Pergamon Press, Elmsford, NY, 1977, pp. 143–157.
11 K.K. Stewart and R.F. Doherty, *Proc. Natl. Acad. Sci. USA*, 70 (1973) 2850.
12 Z. Šimek and R. Vespalec, *J. Chromatogr.*, 629 (1993) 153.
13 Z. Šimek, R. Vespalec and J. Šubert, *J. Chromatogr.*, 543 (1991) 475.
14 J.F. Foster, in V. Rosenoer, M. Oratz and M. Rotshild (Editors), *Albumin Structure, Function and Uses*, Pergamon Press, Elmsford, NY, 1977, pp. 53–84.

*Journal of Chromatography*, 638 (1993) 263–267
Elsevier Science Publishers B.V., Amsterdam

CHROM. 24 939

# Chiral separation of β-blockers by high-performance capillary electrophoresis based on non-immobilized cellulase as enantioselective protein

Ludmila Valtcheva, Jamil Mohammad, Göran Pettersson and Stellan Hjertén*

*Department of Biochemistry, University of Uppsala, Biomedical Centre, P.O. Box 576, S-751 23 Uppsala (Sweden)*

ABSTRACT

Optical isomers of some basic parmaceutical drugs (β-blockers) were separated by means of high-performance capillary electrophoresis in a carrier-free solution, using the chiral recognition properties of a cellulase (cellobiohydrolase I). High resolution of the isomers and peaks with satisfactory symmetry were obtained only when the enzyme was dissolved at a high concentration (40 mg/ml; total 10 μg) in a buffer of high ionic strength (0.4 *M* sodium phosphate) supplemented with 2-propanol. Surprisingly, the isomer selectivity was lost when the electrophoresis was carried out in the buffers used for chromatographic separation of the isomers on a bed derivatized with cellulase. At pH 5.1 (the experimental pH), the enantiomers are positively charged and the enzyme is negatively charged. With the cathode at the detection end of the capillary the enzyme accordingly migrated away from the detection point and the enantiomers toward it. Disturbances in the UV detection of the enantiomers otherwise caused by the presence of the enzyme were thus avoided. As the runs are performed in the absence of a supporting medium the analyses can be automated easily, which also facilitates the screening of different proteins for their chiral recognition properties and studies to establish the optimum experimental conditions.

A large number of pharmaceutical drugs contain one or more chiral atoms and thus exist in two or more isomeric forms. In most instances only one of the forms is highly active therapeutically. The other one can be either much less active, inactive or sometimes even toxic. Only the highly active isomers are used in the production of medicines. The requirements of the US Food and Drug Administration for the purity of substances used in the pharmaceutical industry are very strict, and the presence of non-highly active forms is not allowed. For efficient purity control, rapid and sensitive analytical methods are therefore needed.

Most chiral separation methods are based on chromatography. The enantioselective ligands can be synthetic, low-molecular-mass compounds, *e.g.*, β-cyclodextrin and Pirkle phases [1], or natural polymers, such as albumin [2,3], $\alpha_1$-acidic glycoprotein [4,5], conalbumin [6] and α-chymotrypsin [7].

Only low-molecular-mass compounds, such as cyclodextrins, have been used as enantioselective agents for the separations of *R*- and *S*-forms by high-performance capillary electrophoresis (HPCE) [8–11]. In this paper we show the usefulness of a high-molecular-mass enantioselector (a protein) for this purpose.

Cellobiohydrolase I (CBH I), a cellulase produced by the fungus *Trichoderma reesei*, was recently used successfully for chiral recognition chromatography following immobilization on silica [12,13] and piperazine diacrylamide–methacrylamide [14] beds. It was therefore of interest to investigate whether this enzyme could be used also for electrophoretic chiral separations. For this purpose we used HPCE, as this

* Corresponding author.

0021-9673/93/$06.00 

method gives high resolution and short run times and requires only small amounts of sample. The last requirement was essential, as we wanted to develop a method based on simple addition of the enantioselective enzyme to the buffer.

The electrophoresis experiments could therefore be performed in free solution without time-consuming immobilization of the enzyme on a solid support. Such a method is attractive as it permits rapid screening of many substances for their enantioselective properties under different experimental conditions. The method is also easy to automate, as the absence of a solid phase makes it easy to suck washing liquid and fresh enzyme and buffer solutions through the electrophoresis tube for each run.

## EXPERIMENTAL

### *Apparatus*

The experiments were performed with a laboratory-designed HPCE system consisting of a Linear 206 PHD variable-wavelength UV detector, (a kind gift from Mr. K. Weinberger, Linear Instruments, Reno, NV, USA, and Mr. L. Lidman, Metric, Malmö, Sweden), a 10-kV power supply (constructed by Mr. Per-Axel Lidström of this Department) and a W + W 1100 recorder (LKB, Bromma, Sweden). The part of the detector that holds the capillary tube was modified slightly in order to accomodate tubes with small diameters.

### *Materials and reagents*

Fused-silica tubing (75 μm I.D., 150 μm O.D.) was bought from Polymicro Technologies (Phoenix, AZ, USA).

The sodium hydrogenphosphate, disodium hydrogenphosphate and 2-propanol used for the preparation of the electrophoresis buffers were of analytical-reagent grade (Merck, Darmstadt, Germany). The agarose gel plug at one end of the capillary was prepared from agarose zero-$m_r$ (Bio-Rad, Richmond, CA, USA).

Culture filtrate from *Trichoderma reesei*, strain QM 9414, was kindly provided by the Biotechnical Laboratory of the Technical Research Centre of Finland (VTT) (Espoo, Finland).

Cellobiohydrolase I (CBH I), a glycoprotein with a molecular mass of 64 000 and a p*I* of 3.9 [15] was purified as described [16]. The enzyme was concentrated by ultrafiltration (cell UH 100/10 with $M_r$ cut-off *ca.* 10 000; Schleicher & Schüll, Dassel, Germany).

The samples, some drugs of the groups of the β-blockers, vasodilatators and antiadrenergics, were a gift from Dr. Bengt-Arne Persson (Astra Hässle, Mölndal, Sweden). A list of the samples and their structures are given in Table I.

### *Electrophoretic procedure*

The capillary tubes were 11.5 cm long (8.5 cm to the detector) × 75 μm I.D. The polyamide coating was removed from a 2–3-mm zone of the silica wall at the detection point by burning it on a hot Kantal wire [17]. The inner surface of the capillary was coated with non-cross-linked polyacrylamide in order to suppress electroendosmotic flow and interaction between the solutes and the silica wall [18].

Agarose (20 mg) was mixed with 1 ml of electrophoresis buffer. The mixture was first boiled to dissolve the agarose and then cooled to allow gelation. One end of the coated buffer-

TABLE 1

STRUCTURE OF THE DRUGS

| No. | Name | p$K_a$ | Structure |
|---|---|---|---|
| 1 | Propranolol | 9.5 | 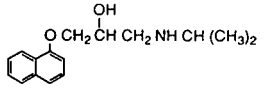 |
| 2 | Alprenolol | 9.5 | 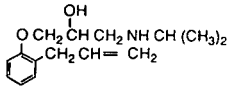 |
| 3 | Metoprolol | 9.7 | 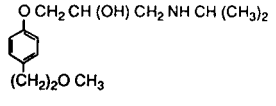 |
| 4 | Pindolol | 9.7 | 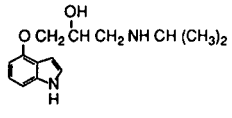 |
| 5 | Labetolol | 7.4 | 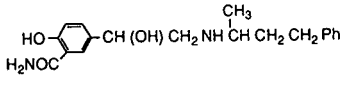 |

filled electrophoresis tube was pressed into the agarose gel. The gel plug thus obtained had a length of a few millimetres.

The enzyme solution was dialysed against the electrophoresis buffer and concentrated by ultrafiltration to a final concentration of 40 mg/ml. An additional dialysis is preferable, as some concentration of buffer ions takes place during the ultrafiltration step.

The electrophoresis buffer used was 0.4 *M* sodium phosphate buffer (pH 5.1) containing different concentrations of 2-propanol (up to 30%). The experiments were carried out as follows. A 7-cm long buffer zone was drawn up into an 11.5-cm coated fused-silica tube from the end where the sample was to be applied. The same end of the tube was then dipped into a vial containing CBH I solution (40 mg/ml in the electrophoresis buffer) to fill, by capillary force, the remainder of the tube with enzyme solution (see Fig. 1). A 2–3-mm long agarose plug was then introduced at the application end as described above to prevent any hydrodynamic flow through the tube.

The sample, 1 mg/ml of a racemate dissolved in electrophoresis buffer diluted tenfold, was applied electrophoretically at 1000 V for 20 s. As the solutes and the enzyme have opposite charges at pH 5.1 they migrate in opposite directions. The basic sample molecules migrate towards the cathode, passing through the CBH I zone, which moves considerably more slowly towards the anode (Fig. 1). This approach ensures that protein molecules do not pass through the detection point and do not disturb the detection of the sample zones. UV detection was performed at 220 nm.

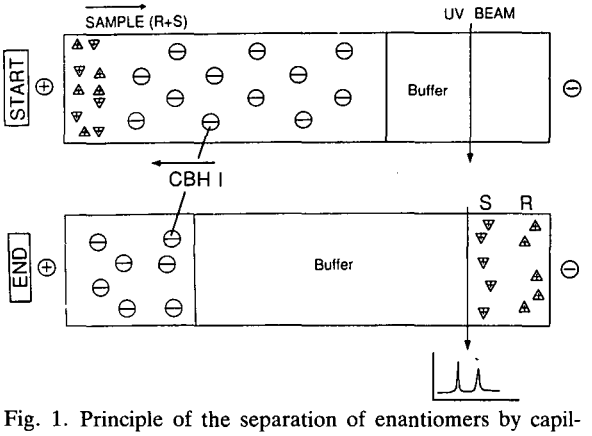


Fig. 1. Principle of the separation of enantiomers by capillary electrophoresis in free solution. The electrophoresis was conducted at a pH such that the enantioselective agent (in this instance cellulase) migrates in a direction opposite to that of the enantiomers. The UV-absorbing cellulase will thus not disturb the UV detection of the enantiomers.

## RESULTS AND DISCUSSION

### *Importance of pH, ionic strength and buffer additive for chiral separation*

The electropherograms in Fig. 2 represent the separation of optical isomers of different drugs. Propranolol (a), pindolol (b) and metoprolol (c) possess one asymmetric atom and therefore appear in two isoforms. The first peak in electropherogram (a) corresponds to the *R*-form of propranolol and the second to the *S*-form. Unfortunately, we could not find standards for the *R*- and *S*-forms of the other drugs. In Fig. 2d and

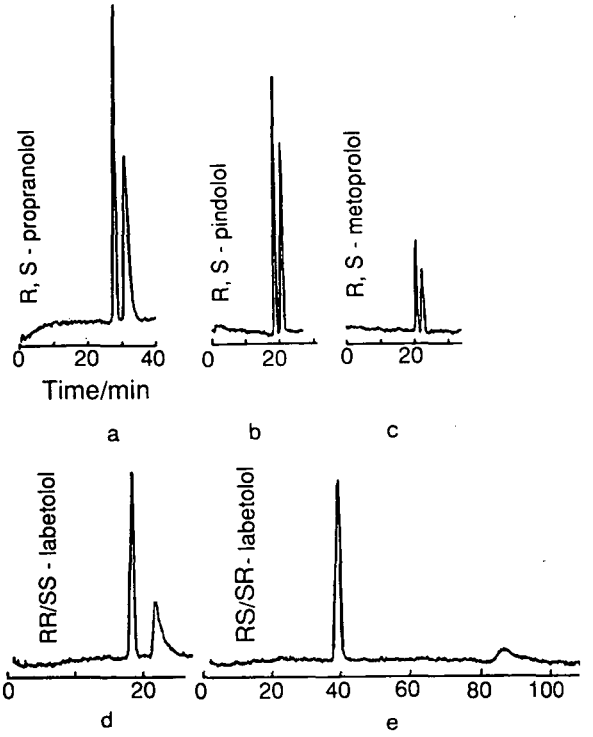


Fig. 2. Separation of (a) (*R*,*S*)-propranolol, (b) (*R*,*S*)-pindolol, (c) (*R*,*S*)-metoprolol, (d) (*RR*/*SS*)-labetolol and (e) (*RS*/*SR*)-labetolol. Buffer, 0.4 *M* sodium phosphate (pH 5.1) supplemented with (a, b, c) 25% and (d, e) 30% 2-propanol.

e a separation of the isomers of labetolol is presented. Labetolol is a diastereomer and thus appears in four isoforms: *RR*, *SS*, *RS* and *SR*. In all runs the isomers were baseline resolved and the peaks showed satisfactory symmetry. The asymmetry factor for the first peaks varied from 1.08 to 1.17 and for the second peaks from 1.6 to 2.7. (For the calculation of the symmetry factor, see ref. 19.)

To resolve the enantiomers we had to perform the experiments under conditions that are unusual for HPCE: a high ionic strength (0.4 *M* sodium phosphate buffer), a high concentration of organic solvent (up to 30% 2-propanol) and a relatively low voltage (the voltage was kept at 1000 V to avoid high temperatures in the electrophoresis tube and thereby the risks of precipitation of CBH I and bubble formation). Without 2-propanol in the buffer the enantiomers separated, but the second peak was extremely broad and asymmetrical, probably owing to a strong hydrophobic interaction with the non-polar patches on the surface of the CBH I molecule. Even at a propanol concentration as high as 10–15%, the tailing was very pronounced. We had to increase the concentration above 20% to obtain a satisfactory peak shape. The asymmetry factor for the second alprenolol peak in the presence of 25% 2-propanol was 2.0. The influence of 2-propanol on the appearance of the peaks is illustrated by the separation of (*R*, *S*)-alprenolol. (Fig. 3). Different samples required different concentrations of 2-propanol to suppress tailing of the second peak (see the legend to Fig. 2), which suggests differences in their hydrophobic interaction with the enzyme. Attempts to suppress the hydrophobic interaction by using ethylene glycol instead of 2-propanol were not successful. Ethylene glycol at high concentrations increases the viscosity of the buffer, thereby extending the run times and increasing the peak broadening.

As we have not studied systematically the influence of each parameter (pH, ionic strength, 2-propanol concentration) there are certainly other experimental conditions that can be used with advantage. The difficulty in finding the optimum conditions for the separation of enantiomers originates from the nature of the chiral

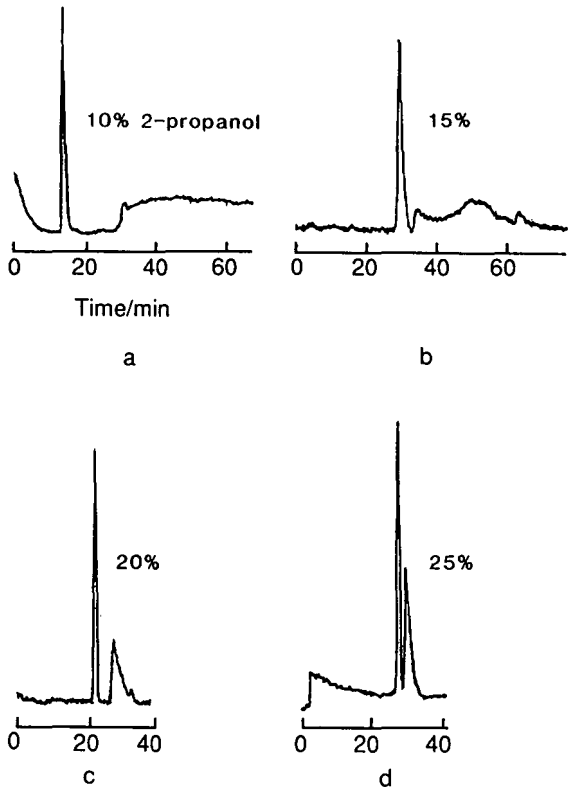


Fig. 3. Influence of the concentration of 2-propanol on the chiral separation of (*R*,*S*)-alprenolol. Buffer, 0.4 *M* sodium phosphate (pH 5.1) supplemented with (a) 10%, (b) 15%, (c) 20% and (d) 25% 2-propanol.

recognition: a complicated multiple (three)-point interaction [20,21], including electrostatic, hydrophobic, $\pi-\pi$, Van der Waals and hydrogen bonds. A strict balance among the interactions is needed to obtain optimum resolution. As the contributions of the different kinds of interactions are a function of, for instance, ionic strength, pH, temperature and the presence of buffer additives, the selectivity is dependent on fine tuning of the separation conditions.

### *Comparison of HPLC and HPCE separations of enantiomers interacting with CBH I*

We also studied the separation of enantiomers of the same drugs by chromatography on a continuous polymer bed (synthesized from piperazine diacrylamide and methacrylamide) to which CBH I had been immobilized [14]. A comparison can therefore be made. The enan-

tioselectivity was lost both for the free enzyme and the enzyme immobilized on the continuous bed when the buffers used for chromatography (0.005–0.1 *M* potassium phosphate, pH 7.5) were employed in the HPCE runs. We have no satisfactory explanation for this unexpected finding. In addition, *RR/SS* and *RS/SR* isomers of labetolol (Fig. 2d and e) could be baseline separated by HPCE but not by chromatography. Obviously, the selectivity of the free (in HPCE) and the immobilized enzyme (in HPLC) is not the same, probably owing to some structural changes in the protein molecules on immobilization. Some non-specific interactions with the supporting material may also explain the differences in selectivity.

*Separation mechanism*

CBH I consists of one cellulose-binding domain, the three-dimensional structure of which has been solved [22], and a catalytically active core. Structural studies on this core, which constitutes the main part of the enzyme, are in progress. As cellobiose, an inhibitor of the enzyme, strongly impairs the enantioselectivity (14,23) it is evident that the active site is involved in the chiral recognition. Interestingly, propranolol inhibits the enzymatic activity [23].

## CONCLUSIONS

We have shown that CBH I, and therefore probably also other proteins enantioselective in HPLC, can be used for the separation of enantiomers by HPCE utilizing the approach described. It is stressed, however, that it is not necessary that the protein and the enantiomers migate in different directions to avoid disturbances in the UV detection; it may be sufficient if they have different migration velocities. The advantage of HPCE over HPLC is that CBH I need not be immobilized. As the enzyme is included in the buffer, it is easy to automate the analyses and to use this method for screening many proteins for stereoselective properties.

## ACKNOWLEDGEMENTS

The work was supported financially by the Swedish Natural Science Research Council and the Knut and Alice Wallenberg and the Carl Trygger Foundations.

## REFERENCES

1 W.H. Pirkle and R. Däppen, *J. Chromatogr.*, 404 (1987) 107.
2 K.K. Stewart and R.F. Doherty, *Proc. Natl. Acad. Sci. U.S.A.*, 70 (1973) 2850.
3 S. Allenmark, B. Bomgren and H. Borén, *J. Liq. Chromatogr.*, 237 (1982) 473.
4 J. Hermansson, *J. Chromatogr.*, 269 (1983) 71.
5 J. Hermansson, K. Ström and R. Sandberg, *Chromatographia*, 24 (1987) 520.
6 N. Mano, Y. Oda, T. Miwa, N. Asakawa, Y. Yoshida and T. Sato, *J. Chromatogr.*, 603 (1992) 105.
7 I. Marle, A. Karlsson and C. Pettersson, *J. Chromatogr.*, 604 (1992) 185.
8 A. Guttman, A. Paulus, A.S. Cohen, N. Grinberg and B.L. Karger, *J. Chromatogr.*, 448 (1988) 41.
9 S. Fanali, *J. Chromatogr.*, 545 (1991) 437.
10 R. Kuhn, F. Stoecklin and F. Erni, *Chromatographia*, 33 (1992) 32.
11 J. Snopek, H. Soini, M. Novotny, E. Smolkova-Keulemansova and I. Teliek, *J. Chromatogr.*, 559 (1991) 215.
12 I. Marle, P. Erlandsson, L. Hansson, R. Isaksson, C. Pettersson and G. Pettersson, *J. Chromatogr.*, 586 (1991) 233.
13 P. Erlandsson, I. Marle, L. Hansson, R. Isaksson, C. Pettersson and G. Pettersson, *J. Am. Chem. Soc.*, 112 (1990) 4573.
14 J. Mohammad, Y.-M. Li, M. El-Ahmad, K. Nakazato, G. Pettersson and S. Hjertén, *Chirality*, in press.
15 J. Ståhlberg, *Doctoral Dissertation*, Almquist and Wiksell International, Stockholm, 1991.
16 R. Bhikhabhai, G. Johansson and G. Pettersson, *J. Appl. Biochem.*, 6 (1984) 336.
17 J.A. Lux, U. Hänsig and G. Schomberg, *J. High Resolut. Chromatogr.*, 13 (1990) 373.
18 S. Hjertén, *J. Chromatogr.*, 347 (1985) 191.
19 L.R. Snyder and J.J. Kirkland, *Introduction to Modern Liquid Chromatography*, Wiley-Interscience, New York, 2nd ed., 1979, Ch. 5.
20 C.E. Dalgliesh, *J. Chem. Soc.*, (1952) 3940.
21 V.A. Davankov, A.A. Kurganov, *Chromatographia*, 17 (1983) 686.
22 P.J. Kraulis, G.M. Clore, M. Nilges, T.A. Jones, G. Pettersson, J. Knowles and A.M. Groneborn, *Biochemistry*, 28 (1989) 7241.
23 G. Pettersson, C. Pettersson, J. Ståhlberg, R. Isaksson and S. Jönsson, Departments of Biochemistry and Pharmaceutical Analytical Chemistry, University of Uppsala, personal communication.

*Journal of Chromatography*, 638 (1993) 269–276
Elsevier Science Publishers B.V., Amsterdam

CHROM. 24 923

# Unfolding of human serum transferrin in urea studied by high-performance capillary electrophoresis

Ferenc Kilár* and Stellan Hjertén

*Institute of Biochemistry, Uppsala University, P.O. Box 576, S-751 23 Uppsala (Sweden)*

ABSTRACT

High-performance capillary electrophoresis (HPCE) was used to monitor the progress of the unfolding of human serum transferrin in urea. Denaturation curves of the transferrin forms were constructed plotting the migration times corrected for the viscosity *vs.* the concentration of urea in the buffer. The practical advantage of capillary zone electrophoresis is the short analysis time, 5–15 min, as compared with slab-gel experiments, which require overnight runs for similar purposes. The resolution increased with the urea concentration, and hence high concentrations are beneficial for quantitative and qualitative analysis of mixtures of transferrin forms. Unfolding intermediates of the isoforms, which interconvert to the unfolded state slowly compared with the time scale of the electrophoretic separation, and also the completely unfolded isoforms were resolved and detected simultaneously when iron-free transferrin was subjected to denaturation by urea at concentrations between 3 and 6 *M*. However, no unfolding intermediates were observed with transferrin isoforms containing two iron atoms (*i.e.* diferric transferrin molecules), which accordingly are strongly resistant to urea denaturation. The unfolding of the transferrin isoforms depends on the iron content of the complexes, but not the carbohydrate content. HPCE in the presence of urea in this mode has the potential to become an analytical tool for diagnosis of diseases in which the transferrin patterns change.

## INTRODUCTION

Monitoring the unfolding of proteins by denaturants by measuring one or more physical parameters as a function of the denaturant concentration gives information about the conformational stability of the molecules. Gel electrophoresis in urea gradients has been shown to be a convenient method for visualization of the conformational transition states of proteins [1,2]. The electrophoretic pattern changes as the unfolding proceeds [3]. However, if the process of unfolding is fast compared with the duration of the electrophoresis run, the possible unfolding intermediates cannot be seen in the electropherogram.

Human serum transferrin, a glycoprotein, has two lobes (N- and C-terminal ones), each having a binding site for iron(III) (see review by Brock [4]). A high degree of homology (42%) is observed between the amino acid compositions of these lobes. The carbohydrate chains are located on the C-terminal lobe. The conformational stabilities of the two lobes are different, as shown by Evans and co-workers [5,6], but measurements of changes in the optical properties of transferrin in urea do not indicate a multistep unfolding [7,8].

The transferrin isoforms (asialo, mono-sialo, 2-sialo, 3-sialo, 4-sialo, 5-sialo, 6-sialo molecules, which contain different carbohydrate chains) and the molecular forms of these isoforms (*i.e.* diferric transferrin, monoferric transferrin with iron bound in the N-terminal or in the C-terminal lobe, and iron-free transferrin, designated $Fe_NTfFe_C$, $Fe_NTf$, $TfFe_C$ and Tf, respectively) have different p*I* values and can be separated by

* Corresponding author. Address for correspondence: Central Research Laboratory, University of Pécs, Medical School, Szigeti út 12, H-7643 Pécs, Hungary.

0021-9673/93/$06.00 

isoelectric focusing [9]. The major component in normal human serum is 4-sialo-transferrin. The amounts of the other components are significantly lower. The transferrin isoforms do not exhibit differences in iron-binding properties [10]. In an earlier report we showed that the iron-free transferrin isoforms (with only one charge unit difference) can be separated by zone electrophoresis in capillaries using a low ionic strength buffer [11].

In this study the unfolding of iron-free and iron-containing isoforms of transferrin in the presence of urea was monitored by high-performance electrophoresis in capillaries. Actually, the original purpose of this study was to develop a rapid method for the analysis of mixtures containing different molecular forms of transferrin.

## EXPERIMENTAL

### *Materials*

Human serum transferrin was purchased from Behring Werke (Marburg, Germany) and was used without further purification. Iron nitrilotriacetate and iron citrate solutions were prepared as described previously [11,12]. The desired degree of iron saturation was achieved by mixing these iron chelate solutions with the calculated volumes of a 150 mg/ml iron-free transferrin solution in a 20 m*M* HEPES buffer (pH 7.5) that contained 20 m*M* sodium hydrogencarbonate. The solutions were left at room temperature for 2 h and then dialysed overnight against 20 m*M* sodium hydrogencarbonate (pH 7.5) in the cold.

The urea was deionized on a mixed-bed ion-exchanger resin column [AG 501-X8(D) Bio-Rad, Richmond, CA, USA] and was stored in a refrigerator for up to 2 weeks in the presence of the resin. The urea-containing buffer was prepared from stock solution of 1.8 *M* Tris–1.8 *M* borate–30 m*M* EDTA (pH 8.4) diluted with an 8.08 *M* urea solution and deionized water to the desired concentration (0–8 *M*). Transferrin samples were prepared in 6 m*M* Tris–6 m*M* borate–0.1 m*M* EDTA (pH 8.4) buffer containing the same amount of urea as the electrophoresis buffer.

### *Capillary zone electrophoresis in the presence of urea*

The electrophoresis experiments performed in glass capillaries (Modulohm, Herlev, Denmark) [13] with 0.1 mm I.D., were conducted in a 18 m*M* Tris–18 m*M* borate–0.03 m*M* EDTA (pH 8.4) buffer containing 0–8 *M* urea. The capillaries were coated as described in ref. 12 to eliminate adsorption and electroendosmosis. The lengths of the capillaries varied between 190 and 200 mm. The samples were applied into the tube by capillary force as previously described [11]. A modified Spectroflow 783 HPLC monitor (Kratos Division, Ramsey, NJ, USA) was used for on-tube detection at 280 nm. The monitoring was performed at a distance of 171–178 mm from one end of the capillary. The electrophoresis was carried out at 8000 V, which gave a current in the tube between 4.5 and 11 $\mu$A (the higher the urea concentration, the lower was the current). The relative viscosity values of the urea-containing buffers were taken from the literature [14]. All experiments were repeated 3–10 times to assess the reproducibility.

## RESULTS

Iron-free and iron-saturated transferrin samples were investigated by zone electrophoresis in capillaries in the absence and in the presence of urea. In the absence of urea the characteristic pattern of iron-free transferrin was observed, showing the 4-sialo transferrin as the major component and the 2-sialo-, 3-sialo-, 5-sialo- and 6-sialo forms as minor ones (Fig. 1a). The separation order of these isoforms is reflected in the differences in their net surface charge densities caused by the differences in the sialic acid contents as discussed earlier [11].

The same number of transferrin isoforms were resolved in the ranges 0–3 *M* and 6–8 *M* urea (Fig. 1b, c, g and h). However, each isoform gave two peaks in the interval 3–6 *M* urea (Fig. 1d–f). The patterns in Fig. 1d–f show that all isoforms of the iron-free transferrin appeared in two different conformations characterized by different migration times. (It is easy to assign the major component, 4-sialo-transferrin, and the surrounding minor ones.) A change in the

5-sialo- and 4-sialo-transferrin peak sizes with time was observed. These changes occur slowly in 4 *M* urea, the ratios changing by only about 10% during 3 h (not shown). Observations made after larger periods in urea solutions were not meaningful since the expressed sulphydryl groups easily become oxidized [15], leading to the formation of "transferrin gels", as has been observed for albumin and ovalbumin [16,17]. However, the ratio of the peak areas in 5 *M* urea changed quickly (see Fig. 1e and f). After 2 h only one conformation of each isoform was detected (not shown).

Fig. 2 shows the electropherograms obtained by analysis of diferric human serum transferrin. The isoforms of the transferrin were clearly resolved. No splitting of the peaks was observed between 0 and 8 *M* urea. The resolution of the transferrin isoforms increased with the urea concentration, as was the case for the experiments presented in Fig. 1 for iron-free transferrin.

In order to follow the unfolding of transferrin, the migration times of the different components were plotted *vs.* the urea concentration. Since the migration rates decrease in the viscous urea solutions, the migration times were corrected by dividing them by the relative viscosity of the buffer. The corrected migration times are thus plotted for the 4-sialo iron-free and diferric transferrin *vs.* the urea concentration in Fig. 3. The curves show that unfolding of the iron-free transferrin is not a simple process. An intermediate conformation of iron-free transferrin exists between 3 and 6 *M* urea. As pointed out above, protein molecules in these intermediate states convert slowly to the unfolded conformation. No unfolding intermediates were observed in the case of diferric transferrin (Fig. 3).

Fig. 4a and b show denaturation curves for all the iron-free and diferric isoforms, respectively.

Since the original purpose of these capillary electrophoresis experiments was to develop a rapid method for the analysis of mixtures containing iron-free and iron-saturated transferrin molecules, artificial transferrin mixtures were analysed in 8 *M* urea. In one sample (Fig. 5a) the mixture was prepared with the intention of having the four molecular forms in a ratio of 1:1:1:1. Fig. 5 shows that the unfolded molecular forms of the different isoforms were well resolved in 8 *M* urea. Upon calculation of the peak

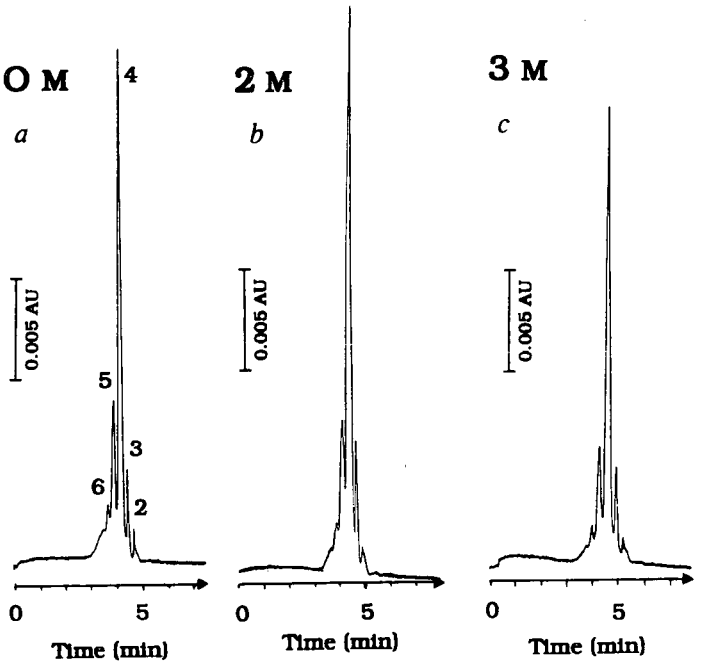


Fig. 1.

(Continued on page 272)

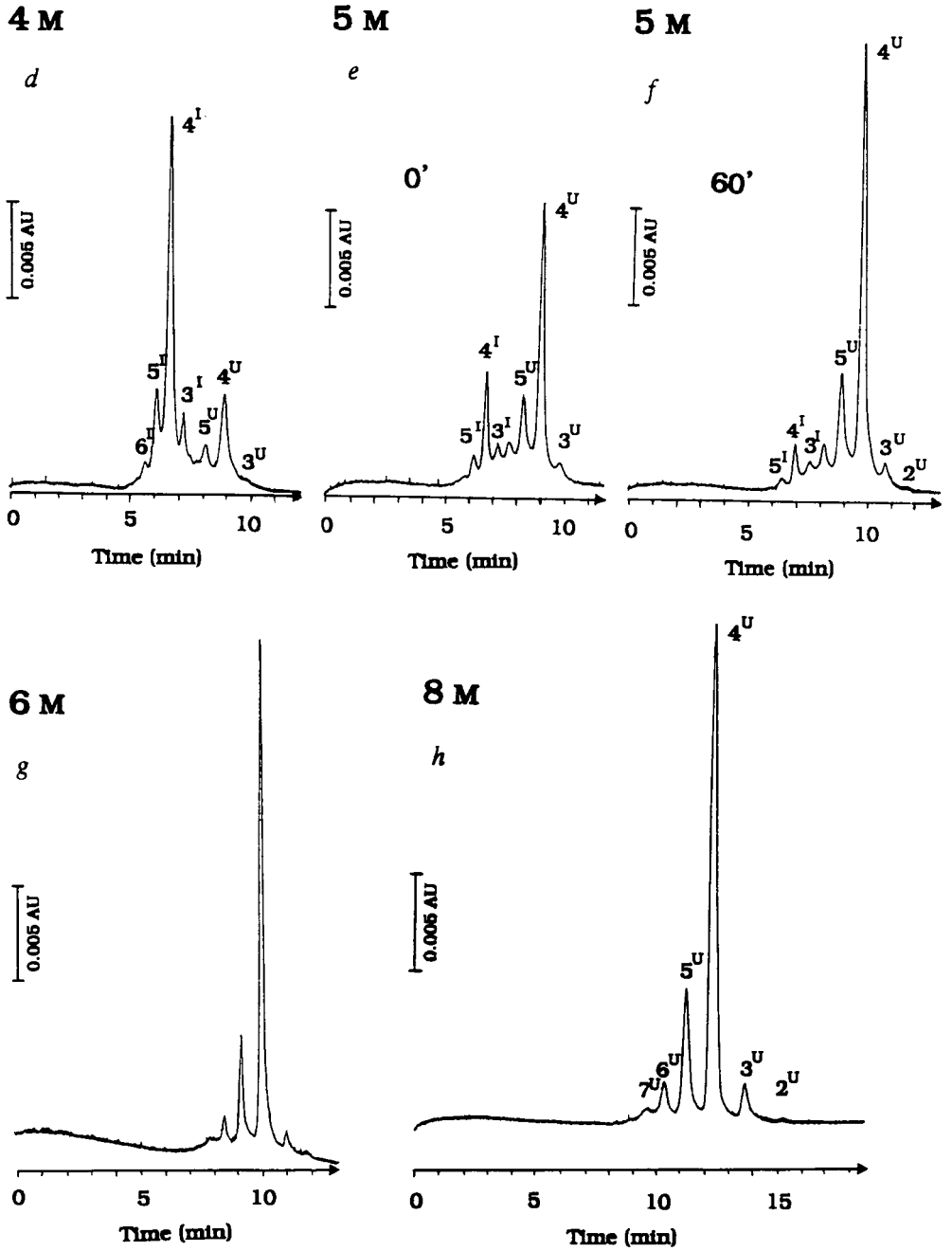


Fig. 1. High-performance electrophoresis of human serum iron-free transferrin in free solution in the absence (a) and presence (b–h) of urea. Experimental conditions: electrophoresis buffer, 18 m*M* Tris–18 m*M* boric acid–0.3 m*M* EDTA, pH 8.4; tube dimensions, 0.1 (I.D.) × 0.3 (O.D.) × 200 mm; voltage, 8000 V; on-tube detection at 280 nm. The current decreased with the increase of the urea concentration from 10 $\mu$A to 4.5 $\mu$A. Transferrin isoforms (2-sialo, 3-sialo, 4-sialo, 5-sialo and 6-sialo marked by 2, 3, 4, 5, 6, respectively) are better resolved at higher urea concentrations. The electrophoresis shows two conformations of the isoforms (I, intermediate; U, unfolded) in 4 *M* (d) and 5 *M* (e and f) urea. The ratio of the amounts of the conformational states changed significantly after 1 h in 5 *M* urea.

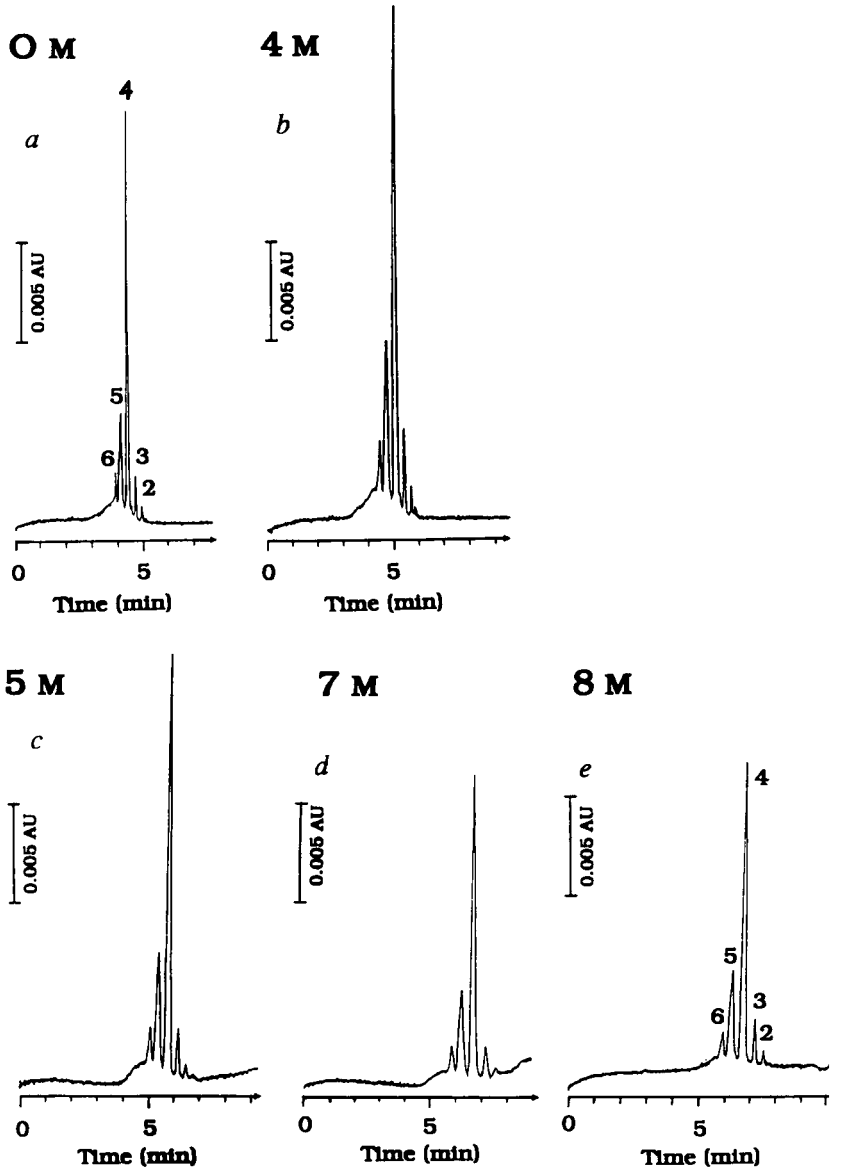


Fig. 2. High-performance electrophoresis of diferric human serum transferrin in free solution in the absence (a) and presence (b–e) of urea. The experimental conditions are the same as in the legend to Fig. 1. Transferrin isoforms (marked by 2, 3, 4, 5 and 6) are better resolved at higher urea concentration. The electrophoretic patterns are the same for all the experiments, although the resolution increases with urea concentration. The migration times of the isoforms increase with an increase in the urea concentration (a–e).

areas of the 4-sialo-transferrin components, we found that the mixture actually contained 30%, 30%, 20% and 20% of $Fe_NTfFe_C$, $Fe_NTf$, $TfFe_C$ and Tf, respectively, with an error of 5%. In another sample (Fig. 5b), the ratios of the different iron-containing isoforms were different, but all of the components were observable (compare with Fig. 5a).

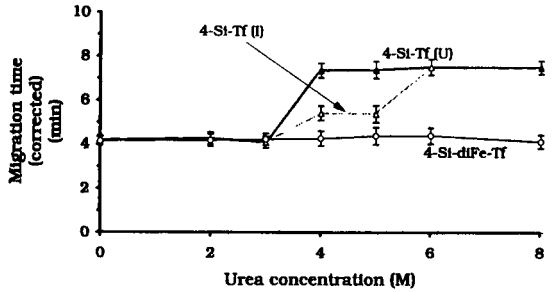


Fig. 3. Denaturation curves of the 4-sialo forms of iron-free (4-Si-Tf) and diferric (4-Si-diFe-Tf) human serum transferrin between 0 and 8 *M* urea (triangles and circles, respectively). The migration times of the 4-sialo isoforms in Figs. 1 and 2 were corrected for the increasing viscosity caused by the presence of urea and plotted *vs.* the concentration of urea in the buffer. An intermediate transition state (I) of the iron-free transferrin exists between 3 and 6 *M* urea together with the unfolded state (U). No unfolding intermediate transition state is observed for the diferric transferrin.

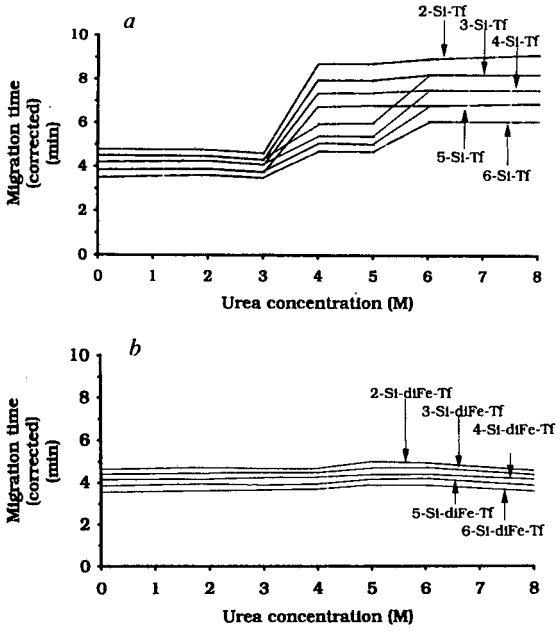


Fig. 4. Denaturation curves of the human serum (a) iron-free and (b) diferric transferrin isoforms between 0 and 8 *M* urea. Corrected migration times for the 2-sialo, 3-sialo-, 4-sialo-, 5-sialo- and 6-sialo-transferrin forms (marked as 2-Si-Tf, 3-Si-Tf, 4-Si-Tf, 5-Si-Tf, 6-Si-Tf or 2-Si-diFe-Tf, 3-Si-diFe-Tf, 4-Si-diFe-Tf, 5-Si-diFe-Tf, 6-Si-diFe-Tf, respectively) *vs.* urea concentration are plotted as in Fig. 3 (*cf.* Fig. 3). Intermediate transition states of the iron-free transferrin (a) isoforms exist between 3 and 6 *M* urea together with the unfolded states. The iron-saturated (diferric) isoforms of transferrin (b) are resistant to urea denaturation.

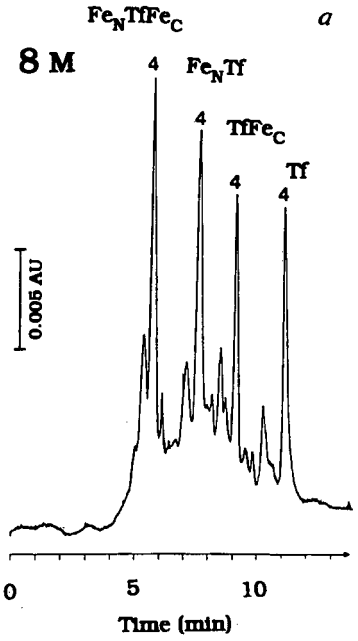


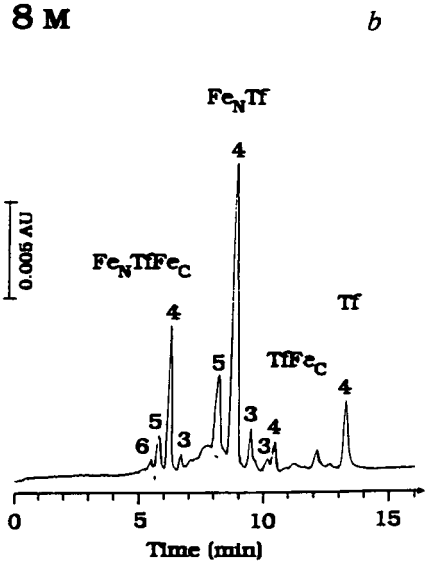


Fig. 5. High-performance capillary electrophoresis of mixtures containing iron-free (Tf), monoferric ($Fe_NTf$ and $TfFe_C$, having iron bound in the N- and C-terminal lobe, respectively), and diferric ($Fe_NTfFe_C$) transferrin components (a) in approximately equal concentrations and (b) with a large amount of monoferric transferrin having iron bound at the N-terminal binding site and with lower amounts of the other forms. The peak sizes of the 4-sialo-transferrin components can be used for determination of the relative amounts of the different iron-containing transferrin forms.

## DISCUSSION

Studies of the unfolding of proteins, for instance using electrophoresis in the presence of urea [3], gives information about the conformational stabilities of the molecules [18,19]. Electrophoresis has an advantage over other methods in that the relative amounts of the components may be determined easily from the electropherograms. However, conventional urea gel electrophoresis is a time-consuming procedure involving gel casting, running, staining and destaining. The use of urea gradient gels makes the procedure even more laborious. Therefore, we have utilized the advantages of capillary zone electrophoresis in free solution to analyse the unfolding of transferrin as well as for the quantitative and qualitative analysis of artificial mixtures of different species of transferrin. With the high-performance capillary electrophoresis technique the speed of the analysis in the presence of urea was increased by a factor of about 100 and the high resolution permitted detection of the unfolding intermediates of the iron-free transferrin isoforms.

The original gel electrophoresis method of Makey and Seal [20] for the analysis of the iron saturation of transferrin was adapted for capillary zone electrophoresis experiments in free solution with a few modifications. For instance, the buffer concentration was decreased to the value given in the Experimental section in order to speed up the analysis.

The unfolding of iron-free transferrin is a two-step procedure [5,6]. The transitions between the folded, unfolding (intermediate) and unfolded states occur between 3 and 6 *M* urea. Fig. 3 shows that the intermediate and the unfolded states of the iron-free transferrin coexist during a certain period of time. It has been proposed [5,6] that in the intermediate conformation the C-terminal lobe of transferrin is unfolded, while the N-terminal lobe remains in the native state. Since gel electrophoresis requires more than 15 h, the intermediate state could not be observed when the run was conducted in 4–6 *M* urea. Only the slowly interconverting conformation could be detected when the urea concentration was 3–4 *M* [5,6]. Measurement of the optical parameters of the transferrin [7,8] did not reveal an intermediate state, probably because the time scale was short compared with the speed of the interconversion.

Iron-saturated transferrin molecules have a more compact conformation than the iron-free forms [21,22] and are therefore more resistant to urea denaturation, as shown earlier [5,6] and also demonstrated in this study (see Figs. 3 and 4b). Accordingly, neither the polypeptide nor the carbohydrate chains are affected by the presence of urea.

Gel electrophoretic techniques are unable to resolve the transferrin isoforms [20,23]. Therefore, we have used capillary electrophoresis in free solution to compare the unfolding properties of the isoforms. Fig. 4a shows that the unfolding follows the same pattern for all of the isoforms in the iron-free transferrin. The differences between the migration velocities of the isoforms, which exist already in buffer without urea, are not caused by differences in the conformation of the carbohydrate moiety, as pointed out above for the iron-saturated isoforms. Hence, and as expected, only the conformation of the polypeptide chain is changed by urea, causing an alteration in net charge density, *i.e.* a change in migration time.

It has been shown previously that one can separate the two monoferric transferrin species in the presence of urea by polyacrylamide gel electrophoresis [20], which means that these species represent different conformational states. This conclusion is in agreement with small-angle X-ray scattering data [21]. However, it is not known how the differences in the conformations of the monoferric species influence the net surface charge density of the proteins and thereby their electrophoretic mobilities. As expected, also capillary electrophoresis in the presence of urea also permitted separation of the two types of the monoferric components. However, the isoforms could be resolved as well, as shown in Fig. 5 (where both monoferric transferrin components of each transferring isoform are separated).

The analytical separation of the isoforms and their species with different iron content shown in Fig. 5a and b is of diagnostic interest in the case

of, for example, alcoholism and analysis of blood from workers exposed to organic solvents [24,25] because these electropherograms can be utilized, for instance, for the quantitation of the 4-sialo- and 2-sialo-transferrin isoforms. Furthermore, it may now be possible to determine the iron content of these isoforms as well.

ACKNOWLEDGEMENTS

This work was supported by the Swedish Natural Science Research Council and by Grants OTKA No. 1981 and OTKA No. T5218 (Hungary).

REFERENCES

1 T.E. Creighton, *J. Mol. Biol.*, 137 (1980) 61.
2 D. Loftus, G.O. Gbenle, P.S. Kim and R.L. Baldwin, *Biochemistry*, 25 (1986) 1428.
3 T.E. Creighton, *Methods Enzymol.*, 131 (1986) 156.
4 J.H. Brock, in P. Harrison (Editor), *Metalloproteins, Part II*, Macmillan, London, 1985, p. 183.
5 R.W. Evans and J. Williams, *Biochem. J.*, 189 (1980) 541.
6 R.W. Evans, J. Williams and K. Moreton, *Biochem. J.*, 201 (1982) 19.
7 B. Teuwissen, K. Schanck, P.L. Masson, P.A. Osinski and J.F. Heremans, *Eur. J. Biochem.*, 42 (1974) 411.
8 J.P. Harrington, J. Stuart and A. Jones, *Int. J. Biochem.*, 19 (1987) 1001.
9 F. Kilár, *J. Chromatogr.*, 545 (1991) 403.
10 G. de Jong and H.G. van Eijk, *Int. J. Biochem.*, 21 (1989) 253.
11 F. Kilár and S. Hjertén, *J. Chromatogr.*, 480 (1989) 351.
12 F. Kilár and S. Hjertén, *Electrophoresis*, 10 (1989) 23.
13 S. Hjertén, *J. Chromatogr.*, 270 (1983) 1.
14 R.C. Weast (Editor) *CRC Handbook of Chemistry and Physics, 1978–1979*, CRC Press, Boca Raton, FL, 59th ed., 1979.
15 Y.L. Xiong and J.E. Kinsella, *Agr. Biol. Chem. Tokyo*, 54 (1990) 2157.
16 C. Huggins, D.F. Tapley and E.V. Jensen, *Nature*, 167 (1951) 592.
17 H.K. Frensdorff, M.T. Watson and W. Kauzmann, *J. Am. Chem. Soc.*, 75 (1953) 5157.
18 T.E. Creighton, *Biochem. J.*, 270 (1990) 16.
19 R. Jaenicke, in G. Jörnvall, H. Höög and R. Gustavsson (Editors), *Methods in Protein Sequence Analysis*, Birkhäuser Verlag, Basle, 1991, p. 387.
20 D.G. Makey and U.S. Seal, *Biochim. Biophys. Acta*, 453 (1976) 250.
21 F. Kilár and I. Simon, *Biophys. J.*, 48 (1985) 799.
22 R. Vígh, L. Cser, F. Kilár and I. Simon, *Arch. Biochem. Biophys.*, 275 (1989) 181.
23 N.D. Chasteen and J. Williams, *Biochem. J.*, 193 (1981) 717.
24 O. Vesterberg, S. Petrén and D. Schmidt, *Clin. Chim. Acta*, 141 (1984) 33.
25 S. Petrén and O. Vesterberg, *Br. J. Ind. Med.*, 44 (1987) 566.

*Journal of Chromatography*, 638 (1993) 277–281
Elsevier Science Publishers B.V., Amsterdam

CHROM. 24 942

# Detection by capillary electrophoresis of restriction fragment length polymorphism

# Analysis of a polymerase chain reaction-amplified product of the DXS 164 locus in the dystrophin gene

Domenico Del Principe*, Maria Paola Iampieri, Daniela Germani and Adriana Menichelli

*Dipartimento di Sanità Pubblica e Biologia Cellulare, Facoltà di Medicina, Università di Roma "Tor Vergata", Via Orazio Raimondo, 000173 Rome (Italy)*

Giuseppe Novelli

*Cattedra di Genetica Umana, Università Cattolica, Rome (Italy)*

Bruno Dallapiccola

*Dipartimento di Sanità Pubblica e Biologia Cellulare, Facoltà di Medicina, Università di Roma "Tor Vergata", Via Orazio Raimondo, 000173 Rome (Italy)*

ABSTRACT

Capillary electrophoresis (CE) was used to characterize restriction fragment length polymorphism (RFLP) in a polymerase chain reaction (PCR)-amplified product of a 740-base pairs DNA fragment from the DXS 164 locus of the dystrophin gene. The polymorphic alleles of 740 and 520/220 base pairs revealed by *Xmn*I digestion were analysed from homozygous and heterozygous individuals by CE. Our studies show that extraction in phenol–chloroform may be useful in PCR-amplified product purification. Excellent separation was obtained in a short time. The data indicate that CE is suitable for genomic analysis such as carrier detection and prenatal diagnosis of X-linked recessive disorders after purification of PCR-amplified products.

## INTRODUCTION

Specific endonucleases digest DNA, producing DNA fragments that differ in size among individuals. By identifying the association between different DNA fragments (known as restriction fragment length polymorphisms or RFLPs) and the appearance of a particular inheritable trait or disorder within a family tree, inheritance patterns in families have been studied and numerous genetic diseases have been detected and mapped to specific chromosomes [1].

Traditionally, DNA polymorphisms have been detected by analysing point mutations in restriction-enzyme sites that give rise to altered length fragments. These are detected using DNA transfer to a solid support and its hybridization with labelled molecular probes [2]. Differences in the banding pattern between individuals whose DNA has been digested with the same enzyme

* Corresponding author.

0021-9673/93/$06.00 

will reveal an RFLP. The polymorphism can be detected quicker and more economically by polymerase chain reaction (PCR) amplification of a stretch of DNA followed by detection of the presence or absence of the restriction-enzyme cutting sites on ethidium-stained agarose gels. PCR coupled to (multiple) restriction digests allows dramatically faster analysis of RFLPs than the Southern-blotting technique [3].

The availability of genetic markers, which reveal DNA polymorphism by restriction-endonuclease analysis, and/or variable number of sequence length repeats on the X chromosome, has improved the prenatal genotype prediction and carrier detection of several X-linked diseases, such as Duchenne muscular dystrophy, ornithine transcarbamyl transferase deficiency, retinitis pigmentosa, adrenal hypoplasia, chronic granulomatous disease and McLeod phenotype [4,5]. Because slab gel electrophoresis is time-consuming, labour-intensive, and difficult to quantify, capillary electrophoresis (CE) may become an attractive alternative to agarose or polyacrylamide gel electrophoresis. In this paper we describe the application of CE in the detection of DXS164/*Xmn*I polymorphism after PCR amplification of genomic DNA.

## EXPERIMENTAL

### *Subjects*

Venous blood samples were obtained from unrelated adult donors at the National Blood Transfusion Center, Italian Red Cross, Rome, Italy. Subjects were of both sexes and from different parts of Italy. The blood samples were collected after informed consent.

### *DNA sample preparation: agarose gel electrophoresis*

Circulating leucocytes were separated from venous blood anticoagulated with 0.5% EDTA. DNA was extracted from the cells by urea lysis, phenol–chloroform extraction, ethanol precipitation and Tris–EDTA resuspension. Human genomic DNA was amplified by PCR under the following conditions: a 100-$\mu$l volume containing 0.5–1 $\mu$g of genomic DNA, with 1 $\mu M$ of each primer (5′-GACTGGAGCAAGGGTCGCC-3′ and 5′-ACAATTTCCCTTTCATTCCAG-3′), 200 $\mu M$ of each deoxynucleotidetriphosphate (dNTP), 0.3 U of Amplitaq (Perkin-Elmer Cetus) and 1 × Perkin-Elmer PCR buffer was subjected to 29 cycles of amplification. PCR was performed on a DNA thermal cycler (PE Cetus Instruments, Norwalk, CT, USA). Cycle temperature conditions were 40 s at 94°C, 1 min at 57°C and 1 min at 72°C.

Amplified DNA was then sequentially digested with *Xmn*I at 37°C overnight. DNA fragments were analysed by agarose gel electrophoresis using 2% agarose gels and TBE buffer (0.089 *M* Tris, 0.089 *M* boric acid, 2 m*M* EDTA, pH 8.5). Run conditions were 60 mA, 70 V, for 5–6 h. DNA was visualized by ethidium bromide staining at a concentration of 10 $\mu$g/ml. For analysis by CE, the digested samples were subjected to phenol–chloroform (3:1, v/v) extraction. DNA size standard low range [72–1350 base pairs (bp)] was used. DNA molecular weight markers (*Hae*III digest of $\phi$X 174 DNA, New England Biolabs, Beverly, MA, USA) were reconstituted in distilled water to a final concentration of 10 $\mu$g/ml.

### *CE instrumentation and buffer system*

CE was performed using the HPE 100 high-performance capillary electrophoresis system from Bio-Rad Labs. (Richmond, CA, USA), with data collection by a Hewlett-Packard 3394A integrator. A 50 cm × 50 $\mu$m I.D. preassembled coated capillary (Bio-Rad) was conditioned with separation buffer and pre-electropheresed before each analysis. Samples and standards were loaded electrophoretically at a negative polarity by applying 180 V/cm for 8 and 15 s, respectively. Separations were performed at negative polarity under constant voltage at 160 V/cm. A typical run lasted 25 min. The separation buffer consisted of a 0.5% hydroxypropyl methylcellulose (HPMC; Sigma, St. Louis, MO, USA) in TBE. The buffer was filtered by a Millipore filter (0.45 $\mu$m) to remove particulates and degassed at 0.01 atm (1 atm = 101 325 Pa) by a standard vacuum pump for 30 min. DNA size standard low range (88–1746 bp) was used (*Eco*RI digest of pBR322 from Bio-Rad). DNA molecular markers were reconstituted in distilled water to a

final concentration of 10 μg/ml. Ultraviolet absorbance was monitored at 260 nm. By serial dilution of the size standard up to 0.0025 μg/ml, a diminution of the peak area was detected. This may be useful when quantification is needed. In any case, no variation in the migration time was observed and the resolution was maintained. The identification of the DNA fragment size was determined by plotting log bp *vs.* the migration time. A good correlation was obtained ($r = 0.977$). In preliminary experiments, the same sample was injected sequentially. The migration time was reduced from run to run by $15 \pm 1$ s (mean ± S.D., $n = 7$), while the electropherograms show the same profile. Since the drift was constant and predictable, we calculated the DNA fragment sizes taking into account this factor.

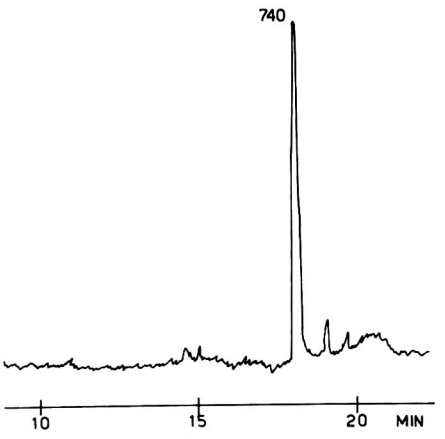


Fig. 2. CE of the PCR-amplified fragment. Detection was by absorbance at 260 nm (0.005 full scale). Migration times (min) are indicated on the *x*-axis.

## RESULTS

Fig. 1 shows the separation of samples from various individuals demonstrating *Xmn*I polymorphism on agarose gel. The amplification product is a fragment of 740 bp, and *Xmn*I digestion distinguished a two-allele polymorphism of 520 and 220 bp. Lane M shows DNA size markers. Lane U shows the amplified fragment, lane d the digested amplified fragment. PCR amplification of the 740-bp DNA fragment from an intron in the DXS 164 locus and subsequent digestion by *Xmn*I yields polymorphic fragments of 520 and 220 bp, corresponding to alleles A1 and A2, respectively. Individuals homozygous for A1 reveal only the 740-bp fragment. Those homozygous for A2 reveal the 520- and 220-bp fragments. Heterozygous individuals (A1–A2) yield three fragments upon electrophoretic separation.

Fig. 2 shows the electropherogram (CE) of the PCR-amplified fragment. The size (740 bp) was determined by comparing the mobility with a calibration run of standard low-range DNA fragments from Bio Rad. On the basis of this calibration, the sizes of the fragments (740, 520, 220 bp) were determined. This result corresponds with that estimated by agarose gel electrophoresis. Digestion of the fragment in an A2

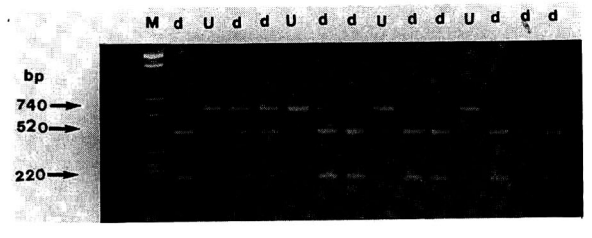


Fig. 1. Separation on agarose gel of samples from various individuals demonstrating *Xmn*I polymorphism. PCR amplification of a 740-bp DNA fragment from an intron in the DXS 164 locus and subsequent digestion by *Xmn*I. For details see text.

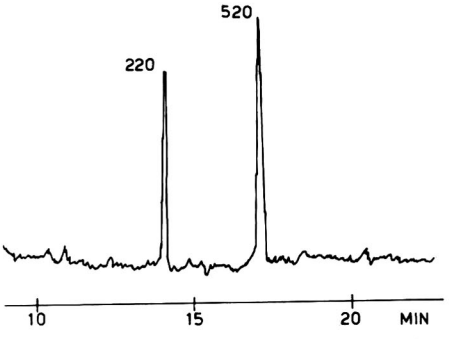


Fig. 3. CE that indicates homozygous alleles (A2–A2). Detection was by absorbance at 260 nm (0.005 full scale). Migration times (min) are indicated on the *x*-axis.

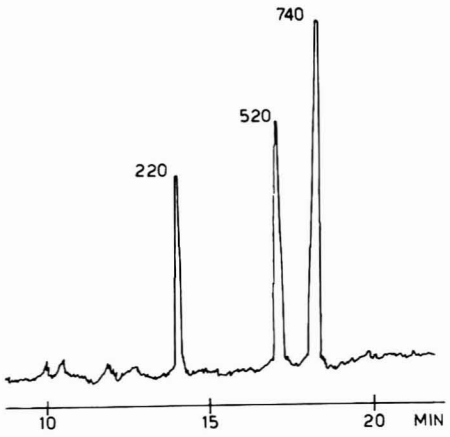


Fig. 4. CE of a sample taken from a woman. The presence of three fragments (744, 520 and 220 bp) demonstrates the heterozygosity of the subject (A1–A2). Detection was by absorbance at 260 nm (0.005 full scale). Migration times (min) are indicated on the *x*-axis.

homozygous sample yields two fragments (520 and 220 bp). The fragments are well separated (Fig. 3). Fig. 4 shows the electropherogram (CE) of a sample taken from a woman. The presence of three fragments (740, 520, 220 bp) demonstrates the heterozygosity of the subject (A1–A2) [6].

## DISCUSSION

Our results demonstrate that CE can be applied to genomic diagnosis using RFLP restriction enzyme-digested PCR samples. Excellent separation is achieved for the DNA restriction fragments. In our study it may be seen that it is possible to determine unambiguously homo- and heterozygous patterns. To improve the detectability in cases in which the samples do not contain enough DNA, it is possible to increase the injection time or the voltage. One solution to the sample detectability problem is to employ more powerful detection schemes, *e.g.*, laser-induced fluorescence or electrochemical detectors [7]. Recently, a method by which more samples can be injected and simultaneously focused into a narrow zone has been introduced, taking advantage of injecting a small water plug [8].

Linear polymers have been used as buffer additives to separate the DNA fragments by acting as molecular sieves [9,10]. In our experiments the use of methylcellulose derivative was essential to adequately separate RLFPs. Good resolution may be obtained only after purification of the PCR products, which we achieved by extraction in phenol–chloroform. Recently, an ultrafiltration method has been introduced [11].

In our experiments, a shift in the migration times was observed. The observed drift is due to the change in temperature of the capillary and its environment. For this reason, the size determination of the DNA fragments based on mobility *vs.* bp number plot of calibration standards can only be a good approximation. However, since the drift was constant and predictable, this method was more than sufficient for our purpose, owing to the large difference in the size of the analysed fragments. It is conceivable that this problem may be overcome by using the instruments, now commercially available, that allow adequate temperature control and heat removal from the capillary.

Determination of DNA restriction fragments with a sieving buffer containing ethidium bromide and a coated capillary has recently been achieved [12]. The ethidium bromide induces significant shifts in mobility of the DNA fragments, depending on their size. Its addition has demonstrated the usefulness of CE in detecting PCR-amplified retroviral DNA sequences, and RFLP of an oncogene [12,13].

CE may be useful for detecting RFLP because it allows a reduction in analysis time compared with the standard method. Samples can be loaded automatically and run overnight unattended, and the same capillary can be used for hundreds of runs. Further optimization of CE conditions would allow a reduction of CE run time (*e.g.*, when larger differences in DNA fragments are analysed) [12]. In future, it will be possible to estimate the size of unknown DNA fragments based on calibration data using special software. Further improvements in quantitation should gain CE wide acceptance in diagnostic and biomedical research applications.

## REFERENCES

1 *Human Gene Mapping 11; Cytogenet. Cell Genet.*, 58 (1991) Nos. 3 and 4.

2 J. Sambrook, E.F. Fritsch and T. Maniatis, in N. Ford, C. Nolan and M. Fergusson (Editors), *Molecular Cloning: A Laboratory Manual*, Vol. 2, Cold Spring Harbor Laboratory Press, Cold Spring Harbor, NY, 2nd ed., 1989, p. 931.
3 R. Reynolds, G. Sensabaugh and E. Blake, *Anal. Chem.*, 63 (1991) 2.
4 E. Bakker, N. Goor, K. Wrogemann, L.M. Kunkel, W.A. Fenton, D. Majoor-Krakauer, M.G.J. Jahoda, G.J.B. Van Ommen, M.H. Hofker, J.L. Mandel, K.E. Davies, H.F. Willard, L. Saundkuyl, A.J. V. Essen, E.S. Sachs and P.L. Pearson, *Lancet*, i (1985) 65.
5 B. Dallapiccola and R. Mingarelli, *Prospettive in Pediatria*, 21 (1991) 267.
6 H.E. Schwartz, K.J. Ulfelder, F.J. Sunzeri, M.P. Busch and R.G. Brownlee, *J. Chromatogr.*, 559 (1991) 267.
7 B.L. Karger, *Anal. Chem.*, 63 (1991) 385A.
8 R.L. Chien and D.S. Burgi, *J. Chromatogr.*, 559 (1991) 141.
9 M. Zhu, D.L. Hansen, S. Burd and F. Gannon, *J. Chromatogr.*, 480 (1989) 311.
10 D.N. Heige, A.S. Cohen and B.L. Karger, *J. Chromatogr.*, 516 (1990) 33.
11 A.M. Krowczynska and M.B. Handerson, *Biotechniques*, 13 (1992) 286.
12 K.J. Ulfelder, H.E. Schwartz, J.M. Hall, F.J. Sunzeri, *Anal. Biochem.*, 200 (1992) 260.
13 P.J. Neufeld and N. Colman, *Sci. Am.*, 262 (1990) 46.

*Journal of Chromatography*, 638 (1993) 283–292
Elsevier Science Publishers B.V., Amsterdam

CHROM. 24 943

# Selectivity of the separation of DNA fragments by capillary zone electrophoresis in low-melting-point agarose sol

Karel Klepárník*

*Institute of Analytical Chemistry, Czech Academy of Sciences, Veveří 97, 611 42 Brno (Czech Republic)*

Salvatore Fanali

*Institute of Chromatography, CNR, Monterotondo Scalo, Rome (Italy)*

Petr Boček

*Institute of Analytical Chemistry, Czech Academy of Sciences, Veveří 97, 611 42 Brno (Czech Republic)*

ABSTRACT

The properties of solutions of low-melting-point agarose for the separation of DNA fragments were investigated as a function of temperature and applied voltage. Giddings *et al.*'s definition of the selectivity of the separation according to molecular size, $S = |(\mathrm{d} \ln u)/(\mathrm{d} \ln p)|$, where $u$ is the electrophoretic mobility and $p$ the number of base pairs, was adopted as a suitable phenomenological description of the capability of the system to separate DNA fragments. It was found that the selectivity of separation in 1% agarose has its maximum at about 600 base pairs, decreases with increasing applied voltage and is a complex function of temperature. No decrease in selectivity was observed even at temperatures above the melting point. The high selectivity of agarose at these temperatures is probably evidence for the positive effect of conformational entropy of DNA molecules. A development of an apparatus for thermostating the capillary within the range 10–70°C that allowed the measurements to be performed is reported.

## INTRODUCTION

Liquefied agarose, in the state of the sol, has been used successfully for separations of oligonucleotides by capillary zone electrophoresis [1–3]. The application of such a low-viscosity sieving medium brings some advantages. The capillary can be filled and refilled with the sol easily and thus a standard separation condition is established before each analysis. The concentration and the type of separation medium can be changed in the same capillary after successive runs. No polymerization or cross-linking of the medium is needed and so the lifetime of the capillary is limited only by that of the capillary wall coating. Even untreated capillaries could be used if the agarose sol was allowed to gel within a capillary below its gelling temperature [4]. The electroosmotic flow inside the untreated capillary filled with a hydroxyethylcellulose solution has been used as a non-selective transport for the separation of DNA fragments [5]. The hydrodynamic injection of the sample can be applied if a low-viscosity medium is used [6].

In addition to the separation efficiency, the selectivity is the other criterion of the quality of a separation, which evaluates the relative dis-

* Corresponding author.

0021-9673/93/$06.00 

placement of the zones of two components [7]. Giddings *et al.* [8] defined the selectivity of the separation of polymers according to their sizes. This definition of selectivity is more informative not only for the quality of separation, but also for the character of migration of a polymer solute through a separation medium.

Despite the fact that the efficiency of the separation of the DNA fragments decreases with increase in temperature, as shown for polyacrylamide gel [9] and for agarose solutions [6], the decrease has no direct connection with the sieving itself and can be avoided. As the efficiency of the separation of polyelectrolytes is intrinsically very high [7,10], the lowered separation efficiency is usually caused by other phenomena such as electromigrational dispersion, interactions with the capillary wall and inhomogeneities of the gel. The impact of all these factors can be decreased independently of the temperature. Hence the selectivity is of paramount importance for optimizing the separation conditions.

In this work, the selectivity of the separation of DNA fragments sized from 9 to 1353 base pairs (bp) in various low-melting-point agaroses was measured at various temperatures and electric field strengths. The relationship to possible migration mechanisms is discussed. Another objective was to prove the feasibility of separation at high temperature and consequently lowered viscosity of the sieving medium.

## THEORY

### *Agarose transient structures*

Gelation is one of the most interesting and complex phase transitions in polymer science and has been subject of considerable theoretical and experimental study. Agarose belongs to a class of polysaccharides that exhibit a marked thermal hysteresis in the sol–gel and gel–sol transitions. Key features of these transitions have been studied by both optical and reheological methods [11–16].

Fig. 1 shows a schematic diagram of the dependence on temperature of the absolute value of a rheological or optical property of an agarose, *e.g.*, viscosity, optical rotation, light scattering or turbidity. The pronounced thermal hysteresis between the gel–sol and sol–gel transition is caused by the existence of the metastable equilibrium. This is observed on cooling the substance (lower curve in Fig. 1), whereas stable equilibrium is attained by heating (upper curve in Fig. 1). The properties of agarose obtained on the cooling curve gradually change to the final equilibrium state on the heating curve. The rates of these relaxation phenomena depend on the temperature and concentration. At 20°C and an

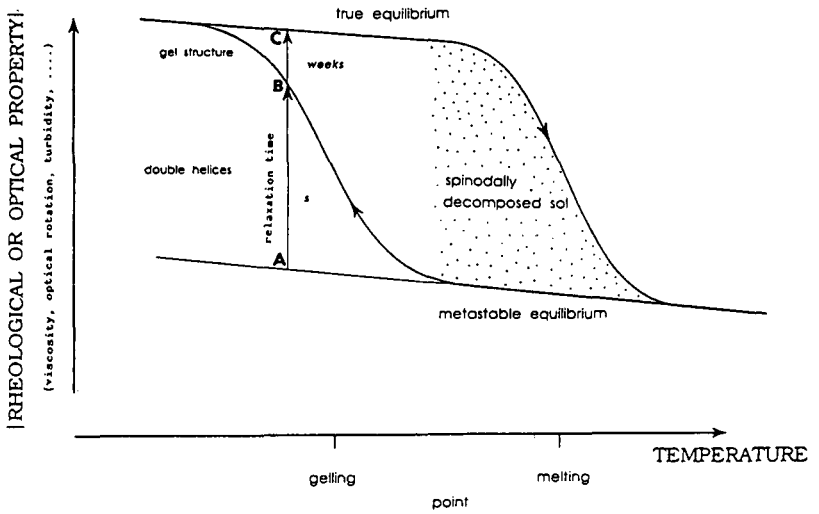


Fig. 1. Schematic dependence of the absolute value of some rheological or optical property (viscosity, optical rotation, turbidity, etc.) of an agarose solution on temperature. The arrows on the hysteresis loop indicate heating and cooling, respectively. The arrows A→B and B→C indicate the transitions to the metastable and true equilibrium, respectively. For explanation, see text.

agarose concentration of 1% the characteristic relaxation time of the sol–gel transition is a few weeks [14]. However, the first increase in viscosity can be observed after several hours. The higher the temperature, the longer is the relaxation time.

At temperatures close to the melting point, the relaxation time is very long and starts after a delay that is interpreted as the spinodal decomposition [17] of the sol, which occurs long before the beginning of gelation [13,15,16]. These sol–sol structural transitions are microscopic transport phenomena that lead to two sets of regions, one with higher and the other lower than average concentrations. The size of the high-concentration regions ranges from a fraction of a micrometre to a few micrometres [16]. In these regions the two random coils→double helix transitions occur, which give rise to the optical activity of the solution as indicated in Fig. 1 by the arrow A→B. The conformational ordering to a coaxial double helix is essentially complete within 100 ms [14].

The final gelation step, indicated by arrow B→C in Fig. 1, is the longest and takes several weeks, as stated above. From the molecular point of view this process is physical cross-linking based on the bundling of double helices. The gelation occurs in the high-concentration regions whereas the low-concentration regions act as early stages of the pores. If the initial concentration of the polymer is high enough, the physical cross-linking between the polymer-rich regions closes the pores, which are essential for the good sieving properties of agarose [16,18].

*Selectivity*

The objective of any separation technique is to obtain an adequate resolution of the bands of separated components. For a quantitative description of the mutual separation of two components the resolution $R_s$ is used. The resolution is defined as the ratio of the distance between the concentration distribution centroids, $\Delta x$, to the mean width of the two peaks near the baseline, taken as $4\sigma$, where $\sigma$ is the mean standard deviation of their concentration distributions [19].

For the separation techniques where the concentration profiles are detected at a fixed point as a dependence of the concentration on time, the resolution should be defined with the help of time quantities as

$$R_s = \Delta t / 4\sigma_t \tag{1}$$

where $\Delta t$ is the absolute value of the difference in the migration times of two separated components and $\sigma_t$ is the standard deviation expressed in units of time. The numerator and denominator on the right-hand side of eqn. 1 describe the selective and the dispersive transport, respectively. The selective transport is the object of this study.

To make the selectivity of electrophoresis independent of applied voltage, the effective mobility difference $\Delta u$ can replace the migration time difference in eqn. 1. This difference can be obtained from the definition of the electrophoretic mobility $u = L/(tE)$ differentiated by $t$, where $L$ is the migration path length and $E$ the electric field strength. Usually the dispersion is expressed by the dimensionless number of the theoretical plates $N$, which is independent on the total migration time and thus on the total length of the migration path. Hence $\sigma_t$ can be replaced with $N$ with the help of the equation $\sigma_t = \bar{t}/(\sqrt{N})$. After these transformations the resolution can be expressed as [7]

$$R_s = \frac{\sqrt{N}}{4} \cdot \frac{|\Delta u|}{u} \tag{2}$$

Now, the selectivity in eqn. 2 is expressed as a relative difference of the effective mobilities of two components. Even more universally, selectivity can be defined if related to a physicochemical parameter of separated components. As the separation of DNA fragments is according to their sizes, the number of base pairs $p$ is accepted here as such a parameter. Consequently, the difference in mobilities can be expressed as $\Delta u = |\mathrm{d}u/\mathrm{d}p| \cdot \Delta p$. However, for the sake of universality it is more convenient to use the derivative according to a relative molecular size. Then

$$\Delta u = \left| \frac{\mathrm{d}u}{\mathrm{d}p/p} \right| \frac{\Delta p}{p} \tag{3}$$

Actually, the molecules are "sized" during the migration through the separation medium on the basis of their absolute lengths and, accordingly, the resolution is a result of relative differences in interactions of molecules with the separation medium. After substituting eqn. 3 into eqn. 2 the final relationship for resolution is [8]

$$R_s = \frac{\sqrt{N}}{4}\left|\frac{du}{dp}\cdot\frac{p}{u}\right|\frac{\Delta p}{p} = \frac{\sqrt{N}}{4}\left|\frac{d\ln u}{d\ln p}\right|\frac{\Delta p}{p} \quad (4)$$

Where the selectivity $S$ is [8]

$$S = \left|\frac{d\ln u}{d\ln p}\right| \quad (5)$$

The ratio $p/\Delta p$ is called the separation power, $f$ [8]:

$$f = p/\Delta p \quad (6)$$

where $\Delta p$ is the difference in base pairs of two polynucleotide molecules of mean size $p$ which are separated with a resolution $R_s = 1$. Then it follows from eqn. 4 for the separation power [8]

$$f = \frac{\sqrt{N}}{4}\cdot S \quad (7)$$

Assuming the difference $\Delta p = 1$, the separation power is the maximum size of the molecules that differ in one base pair and are separated completely.

The selectivity defined by eqn. 5 reflects not only the separating ability of a system but also the character of migration through a separation medium. Now it is interesting to compare the selectivities derived from the two most commonly used models of migration of macromolecules through a gel, the Ogston model [20] in the form extended by Rodbard and Chrambach [21];

$$u \approx \exp(K\, p^{1.2}) \quad (8)$$

where $K$ is a constant and the radius of the equivalent sphere of DNA was taken as proportional to $p^{0.6}$ [22], and the reptation model [23–25]:

$$u \approx 1/p \quad (9)$$

Now after the substitutions of $u$ in eqn. 5 by eqn. 8 for the sieving and by eqn. 9 for the reptation, respectively, the selectivities are proportional as follows:

$$S_{\text{sieving}} \approx p^{1.2} \quad (10)$$

$$S_{\text{reptation}} \approx p^{0} \quad (11)$$

While the selectivity of the sieving is proportional to the size of a molecule, the selectivity of the reptation mechanism is constant. Hence the sieving mode is similar to partition chromatographic techniques and the reptation mode to gel permeation chromatography or field-flow fractionation techniques.

## EXPERIMENTAL

### *Chemicals*

A 123 bp ladder of double-stranded DNA in the size range 123–4182 bp (Gibco BRL No. 5613 SA), a $\phi$X-174 DNA Hae III digest in the range 72–1353 bp and a pBR-322 DNA Msp I digest in the range 9–622 bp (New England Biolabs, Beverly, MA, USA) were used. The solutions were stored overnight at 4°C.

The agaroses used were SeaPrep (Cat. No. 50302; FMC Bioproducts, Rockland, ME, USA) and AcrylAide (Cat. No. 51013, a 2% solution; FMC). Solution of 1% were prepared gravimetrically in 89 m*M* Tris base–89 m*M* boric acid–2.5 m*M* $Na_2EDTA$ (1 × TBE) at boiling temperature and stored at 60°C as described [2].

### *Capillary*

The fused-silica capillary (75 $\mu$m I.D., 367 $\mu$m O.D.) was obtained from Polymicro Technologies (Phoenix, AZ, USA). The capillary was internally coated with linear polyacrylamide [2,26]. The total length of the capillary was 0.41 m and the length from the end to the window was 0.3 m. The window was cut off by a blade under a microscope.

### *Apparatus*

The laboratory-made apparatus [27] was constructed in a similar way to a cartridge of a Varian (Walnut Creek, CA, USA) 2550 variable-wavelength detector and connected to a thermostated water-bath (Multitemp 2209; LKB, Bromma, Sweden) circulating doubly distilled water.

The capillary was coiled inside the cartridge and thermostated by direct contact with the flowing water within the range 10–70°C. The cartridge temperature in that range had no marked effect on the noise and the sensitivity of the detector. A pair of silica lenses, which focused the light beam as a condenser and objective, respectively, were fixed in movable holders that allow for focusing the light prior to any change of the wavelength. Separations were monitored at a single wavelength of 260 nm. After each run of the analysis the capillary was rinsed with fresh agarose solution using an injection syringe. Both the cathodic and anodic chambers, with a volume of 2 ml, were filled with agarose solution. Samples were injected hydrodynamically for 20 s with a level difference of 10 cm. A high-voltage supply (Glassman, Series EH; High Voltage, Whitehouse Station, NJ, USA) was used. The detector signal was monitored with a C-R5A Chromatopac integrator (Shimadzu, Kyoto, Japan).

## RESULTS AND DISCUSSION

Fig. 2 shows an electropherogram of a 123 bp ladder of DNA molecules differing in size by a constant 123 bp. The recorded peaks represent a separation in 1% SeaPrep agarose at 40°C and an electric field strength of 4.9 kV/m. As stated above, the differences in migration times do not indicate much about the real separation properties and are incomparable with other systems. Hence the consecutively decreasing migration time differences of the adjoining fragments do not indicate that the separation ability of the medium is the best for the smallest molecules.

Fig. 3 shows the electrophoretic mobilities of molecules of the 123 bp ladder analysed in 1% SeaPrep agarose at an electric field strength of 4.9 kV/m and within the temperature range 20–60°C. The dependences can be compared with other systems where different lengths of capillaries and different voltages were used. However, it still does not reveal the nature of the selective transport. The higher gradients of the curves at higher temperatures cannot simply be regarded as a symptom of high selectivity but as the non-selective effect of temperature on the mobility.

Fig. 4 shows a third-order least-squares polynomial fit of the selectivity (eqn. 5) on the number of base pairs of DNA molecules at 30, 40 and 50°C. The selectivity values were calculated from the raw experimental results of separations of restriction fragments (pBR-322 DNA

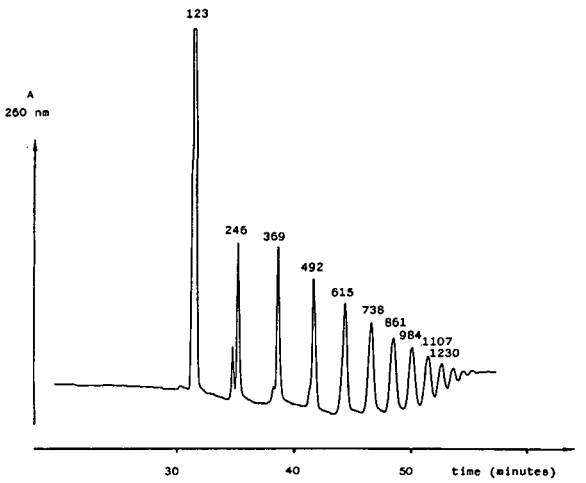


Fig. 2. Electropherogram of the separation of a 123 bp ladder of DNA fragments in 1% SeaPrep agarose. The number of base pairs is given on each peak. Conditions: temperature, 40°C; electric field strength, $E = 4.9$ kV/m.

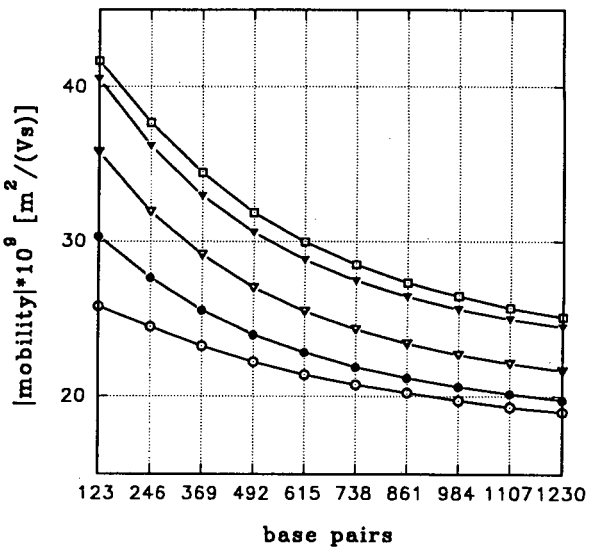


Fig. 3. Dependence of the electrophoretic mobilities of a 123 bp ladder of DNA fragments in 1% SeaPrep agarose at $E = 4.9$ kV/m and temperature of (○) 20, (●) 30, (▽) 40, (▼) 50 and (□) 60°C.

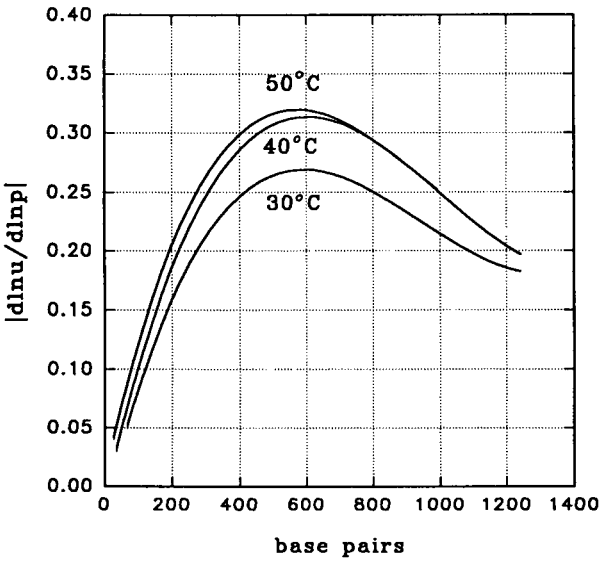


Fig. 4. Dependence of the selectivity on the number of base pairs of restriction fragments (pBR-322 DNA Msp I digest) and a 123 bp ladder of DNA fragments. Conditions: temperature, 30, 40 and 50°C; $E = 4.9$ kV/m; 1% SeaPrep agarose. The plots are polynomial fits of the selectivities calculated from the raw experimental data (eqn. 5).

Msp I digest) and 123 bp ladder of double-stranded DNA at an electric field strength of 4.9 kV/m in 1% SeaPrep agarose.

The increase in selectivity for molecular sizes up to about 400 bp is in accordance with the sieving model (eqn. 10). The existence of maxima at 600 bp indicates the change in the character of molecular migration through the agarose network. Under the optimum selectivity conditions, molecules in the size range *ca.* 400–800 bp are separated. This regime of migration is called entropically regulated transport [28,29]. The transport of molecules larger than 800 bp starts to be driven by another mechanism. It is probably reptation where the selectivity is independent of the molecular size according to eqn. 11. However, there are no other data for the selectivity of the separation of longer molecules to prove the reptation character of migration.

The selectivity of the separation of about 600 bp molecules is the optimum for the whole range of temperatures. This can be interpreted as the absence of a temperature effect on the shape of a polymer coil.

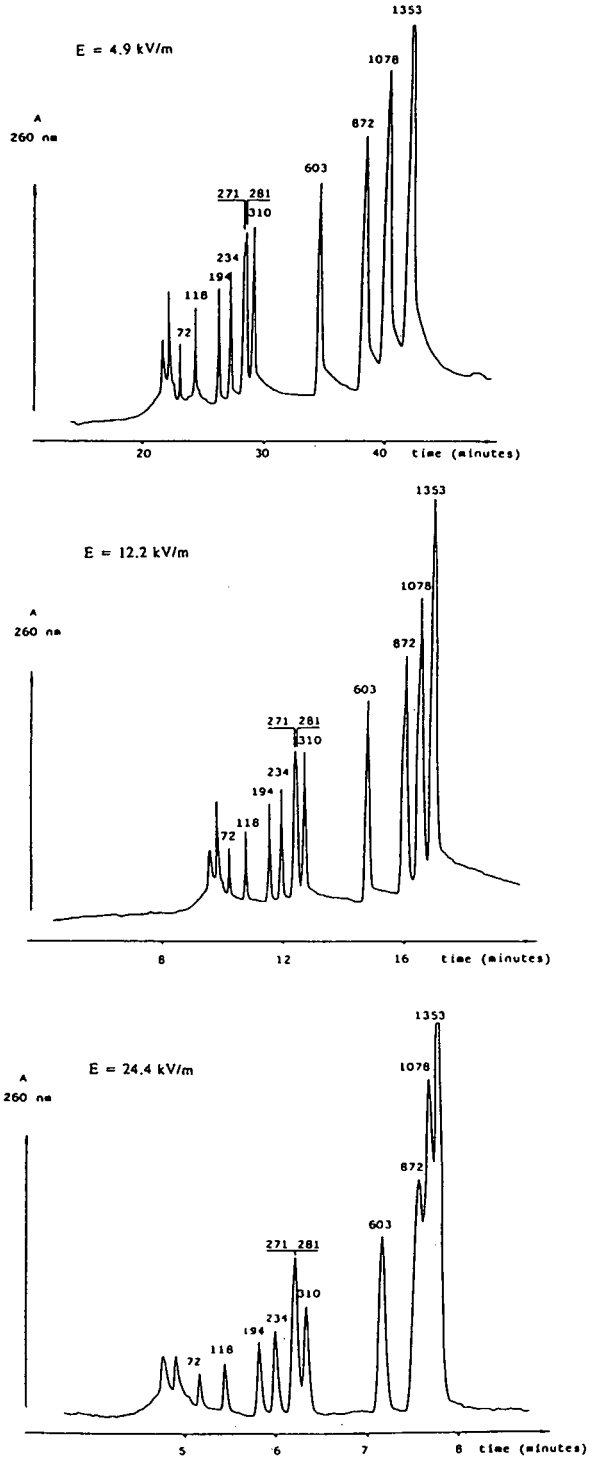


Fig. 5. Three electropherograms of restriction fragments ($\phi$X-174 DNA Hae III digest) at three voltages, 2 kV ($E$ = 4.9 kV/m), 5 kV ($E$ = 12.2 kV/m) and 10 kV ($E$ = 24.4 kV/m), at 50°C in 1% SeaPrep.

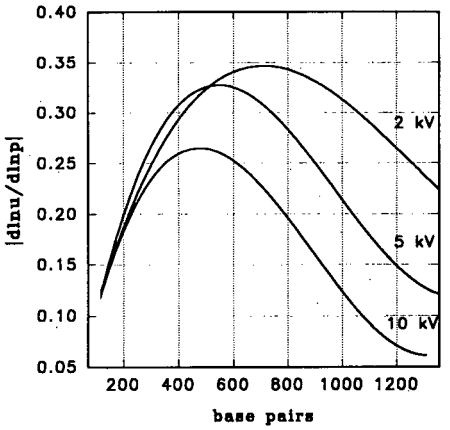


Fig. 6. Dependence of the selectivity on the number of base pairs of restriction fragments ($\phi$X-174 DNA Hae III digest) under the same conditions as in Fig. 5. The data for the plots are treated as in Fig. 4.

The effect of the voltage on the migration of DNA molecules can be elucidated from Figs. 5 and 6. Fig. 5 depicts clearly the negative effect of the electric field strength. There are three separations of restriction fragments ($\phi$X-174 DNA Hae III digest) at electric field strengths 4.9, 12.2 and 24.4 kV/m at 50°C in 1% SeaPrep agarose. It can be concluded that the analysis could be accelerated by higher voltage but at the expense of resolution.

The dependences of the selectivity on the number of base pairs for three values of the electric field strength, 4.9, 12.2 and 24.4 kV/m, are shown in Fig. 6. The three curves were calculated using least-squares three-order polynomial fits of the selectivity to the field strength. The selectivity (eqn. 5) was calculated from the raw experimental data of the separations shown in Fig. 5.

The decrease in the selectivity with applied voltage is followed by a shift of the maxima of the curves to lower numbers of base pairs. This phenomenon can be explained by the biased reptation model [30–32]. The random coil conformation of DNA molecules is stretched by the electric field. The coil becomes more elongated as the strength of the electric field increases and, in the limiting case, the coil becomes a rod [33–36]. Under such a condition the molecules of different lengths migrate at the same velocity and the selectivity of the system approaches zero. The shift of the maxima is an indication that the elongated coils behave as coils of longer molecules.

The effect of temperature on the selectivity of the separation of DNA fragments of 123 bp ladder in 1% AcrylAide and 1% SeaPrep agaroses is shown in Fig. 7. The data were treated in the same way as in Figs. 4 and 6. For the sake of clarity, only the fragments at which the selectivity is increasing with size (*cf.*, Fig. 4) are included here.

The character of the presented curves is determined by the structural changes of the agarose and by conformational changes in the polynucleotide molecule. When working with SeaPrep at 20°C (the gelling point is 17°C), an increase in

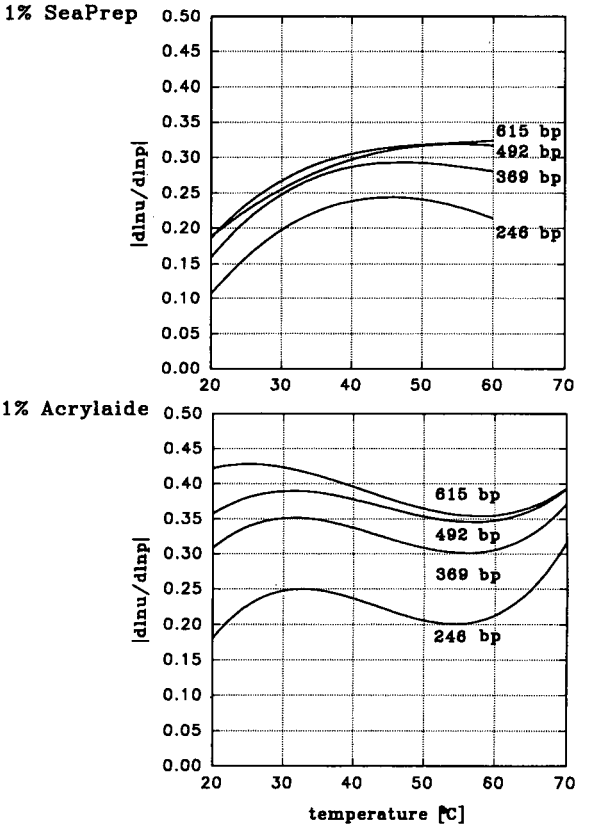


Fig. 7. Comparison of the selectivity dependence on temperature for 1% SeaPrep and 1% AcrylAide agaroses at $E = 4.9$ kV/m. The number of base pairs of selected fragments of 123 bp ladder is indicated on each curve. The data for the plots are treated as in Fig. 4.

the viscosity and therefore the beginning of gelation was obvious. Nevertheless, the selectivity is the lowest at this temperature. In contrast, there is no significant decrease in the selectivity of SeaPrep at temperatures above 50°C, which is its nominal melting point. The AcrylAide agarose exhibits a higher and more varied selectivity versus temperature than that of the SeaPrep. The only available data about AcrylAide agarose is the gelling temperature, given as less than 0°C. With the help of this information, it is possible to explain the different appearances of the two dependences as a shift of the structural transitions of AcrylAide toward the lower temperatures. Thus the graphs belonging to the SeaPrep agarose in the temperature range 20–60°C can be compared with the graphs for AcrylAide shifted downwards by 20°C.

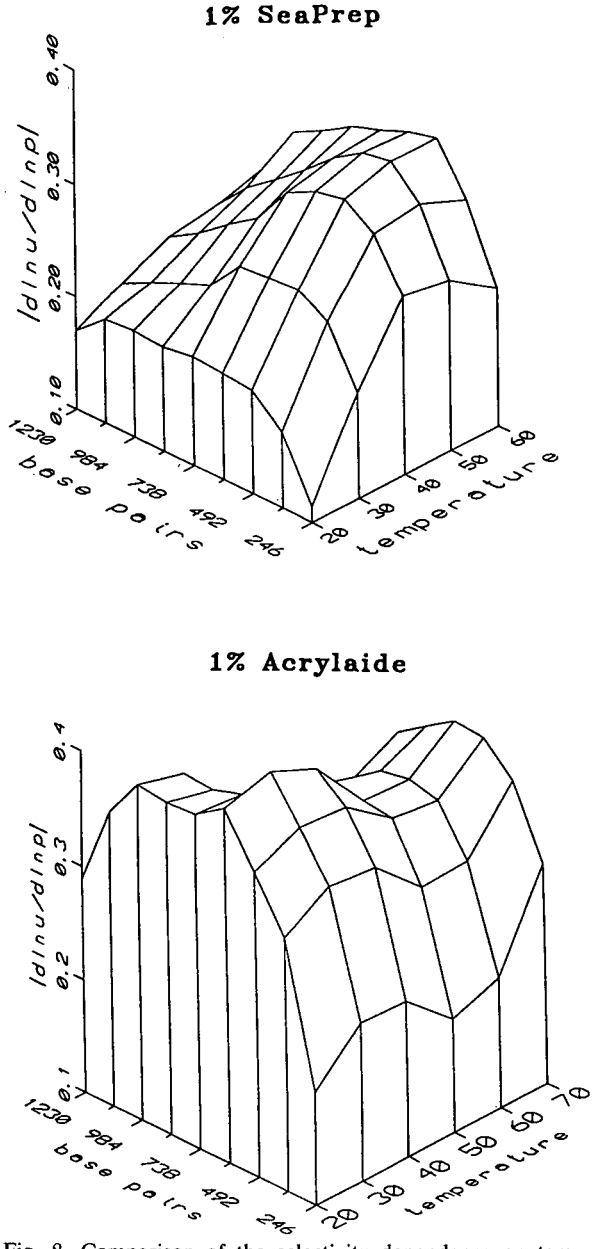


Fig. 8. Comparison of the selectivity dependence on temperature (°C) and number of base pairs for 1% SeaPrep and 1% AcrylAide at $E = 4.9$ kV/m. The selectivities are calculated from the raw experimental data (eqn. 5).

Fig. 8 presents views of the raw experimental data in a three-dimensional plot of the dependence of the selectivity on the molecule size and temperature. These data are the same as those partially used in Fig. 7.

The only explanation for the high selectivity of both agaroses at a temperature near the melting point is the existence of the spinodally decomposed sol and the early structures of the gel. On the other hand, the surprisingly high selectivity even at 60 and 70°C could be due to a closer mutual contact of the polynucleotide and agarose molecules. This is caused either by a large thermal movement or by the beginning of the double helix→single helix transition of the DNA molecule. In this instance even the completely unstructured agarose sol still retains good separation properties. To prove these hypotheses is the object of further study.

## CONCLUSIONS

Giddings *et al.*'s definition of the selectivity (eqn. 5) proved to be a universal and very useful criterion of the quality of the separation of polynucleotides by electrophoresis. The selectivity reflects sensitively the changes in the character of the transport of a polyelectrolyte through a separation medium.

With the help of the selectivity definition (eqn. 5), the proportional relationships for the selectivity of the sieving and reptation models were derived. While the selectivity of the sieving model is nearly linearly proportional to the

number of base pairs (eqn. 10), the selectivity of reptation is independent of the size of a molecule (eqn. 11). Hence, from the point of view of selectivity, the sieving mechanism is similar to partition chromatography and reptation is similar to gel permeation chromatography or field-flow fractionation.

The experimental results show (Figs. 7 and 8) that it is possible to work with low-melting-point agaroses (SeaPrep, AcrylAide) even at temperatures above the melting point without any decrease in selectivity. The speed of an analysis of DNA fragments in a polymer separation medium can be increased at higher temperatures without any significant decrease in resolution, while the application of a higher voltage leads to decreased resolution (Figs. 4, 5 and 8).

The dependence of the selectivity on the molecular size (Fig. 4) indicates that molecules of different sizes migrate through the 1% agarose network under three different regimes. The molecules in the size range up to *ca.* 400 bp migrate in the sieving model. Under the optimum selectivity conditions molecules in the size range ca. 400–800 bp are separated in the regime of entropically regulated transport. The transport of molecules larger than 800 bp starts to be driven by a reptation mechanism.

It seems that the best conditions for the separation of polyelectrolytes are in a medium where the regions of close mutual contact exist together with regions where a molecule is allowed to relax freely. The results show that the spinodally decomposed sol, at a temperature close to the melting point, might be a medium with this feature.

## ACKNOWLEDGEMENTS

We thank Dr. Andreas Chrambach for valuable comments on the manuscript. We gratefully acknowledge Bio-Rad Laboratories (Segrate, Milan, Italy) for material support.

## REFERENCES

1 P. Boček and A. Chrambach, *Electrophoresis*, 12 (1991) 620–623.
2 P. Boček and A. Chrambach, *Electrophoresis*, 12 (1991) 1059–1061.
3 P. Boček and A. Chrambach, *Electrophoresis*, 13 (1992) 31–34.
4 S.R. Motsch, M.H. Kleemiss and G. Schomburg, *J. High Resolut. Chromatogr.*, 14 (1991) 629–632.
5 P.D. Grossman and D.S. Soane, *Biopolymers*, 31 (1991) 1221–1228.
6 K. Klepárník, J. Vala and P. Boček, presented at the *International Symposium "Macromolecules 92", Prague, July 13–17, 1992.*
7 J.C. Giddings, *Sep. Sci.*, 4 (1969) 181–189.
8 J.C. Giddings, Y.H. Youn and M.N. Myers, *Anal. Chem.*, 47 (1975) 126–131.
9 A. Guttmann and N. Cook, *J. Chromatogr.*, 559 (1991) 285–294.
10 E. Kenndler and Ch. Schwer, *Anal. Chem.*, 63 (1991) 2499–2502.
11 S. Arnott, A. Fulmer, W.E. Scott, I.C.M. Dea, R. Moorhouse and D.A. Rees, *J. Mol. Biol.*, 90 (1974) 269–284.
12 P.L. Indovina, E. Tettamanti, M.S. Micciancio-Giammarinaro and M.U. Palma, *J. Chem. Phys.*, 70 (1979) 2841–2847.
13 P.L. San Biagio, F. Madonia, J. Newman and M.U. Palma, *Biopolymers*, 25 (1976) 2255–2269.
14 I.T. Norton, D.M. Goodall, K.R.J. Austen, E.R. Morris and D.A. Rees, *Biopolymers*, 25 (1986) 1009–1029.
15 M. Leone, F. Sciortino, M. Migliore, S.L. Fornili and M.B. Palma-Vittoreli, *Biopolymers*, 26 (1987) 743–761.
16 A. Emanuele, L. Di Stefano, D. Giacomazza, M. Trapanese, M. B. Palma-Vittorelli and M.U. Palma, *Biopolymers*, 31 (1991) 859–868.
17 T. Riste (Editor), *Fluctuations, Instabilities and Phase transitions*, Plenum Press, New York, 1975.
18 P. Serwer, *Electrophoresis*, 4 (1983) 375–382.
19 J.C. Giddings, *Dynamics of Chromatography, Part I*, Marcel Dekker, New York, 1965.
20 A.G. Ogston, *Trans. Faraday Soc.*, 54 (1958) 1754–1757.
21 D. Rodbard and A. Chrambach, *Proc. Natl. Acad. Sci. U.S.A.*, 65 (1970) 970–977.
22 P.J. Flory, *Principles of Polymer Chemistry*, Cornell University Press, Ithaca, NY, 1953.
23 P.G. De Gennes, *J. Chem. Phys.*, 55 (1971) 575–579.
24 M. Doi and S.F. Edwards, *J. Chem. Soc., Faraday Trans. II*, 74 (1978) 1789–1818, 1902–1817, 1818–1829.
25 L.S. Lerman and H.L. Frisch, *Biopolymers*, 21 (1982) 995–997.
26 S. Hjertén, *J. Chromatogr.*, 347 (1985) 191–198.
27 K. Klepárník *et al.*, in preparation.
28 D.L. Smisek and D.A. Hoagland, *Science*, 248 (1990) 1221–1223.
29 E. Arvanitidou, D. Hoagland and D. Smisek, *Biopolymers*, 31 (1991) 435–447.
30 O.J. Lumpkin and B.H. Zimm, *Biopolymers*, 21 (1982) 2315–2316.
31 O.J. Lumpkin, P. Dejardin and B.H. Zimm, *Biopolymers*, 24 (1985) 1573–1593.

32 G.W. Slater, J. Noolandi, C. Turmel and M. Lalande, *Biopolymers*, 27 (1988) 509–524.
33 N.C. Stellwagen, *Biopolymers*, 24 (1985) 2243–2255.
34 H. Hervet and C.P. Bean, *Biopolymers*, 26 (1987) 727–742.
35 D.L. Holmes and N.C. Stellwagen, *Electrophoresis*, 11 (1990) 5–15.
36 B. Nordén. C. Elvingston, M. Jonsson and B. Ackerman. *Q. Rev. Biophys.*, 24 (1991) 103–164.

*Journal of Chromatography*, 638 (1993) 293–301
Elsevier Science Publishers B.V., Amsterdam

CHROM. 24 953

# High-performance liquid chromatography and capillary gel electrophoresis as applied to antisense DNA

Aharon S. Cohen*, Maria Vilenchik, Judith L. Dudley, Mark W. Gemborys and André J. Bourque

*Hybridon Inc., Worcester, MA 01605 (USA)*

ABSTRACT

Reversed-phase and ion-exchange HPLC are compared with both slab gel and capillary gel electrophoresis for the separation of antisense phosphorothioate oligomers. The chromatographic separations were found to be markedly inferior to the electrophoretic separations, especially for oligomers greater than 20 bases in length. The potential of gel high-performance capillary electrophoresis for the analysis of phosphorothioate analogues is shown.

## INTRODUCTION

A new field, "antisense DNA", was born following the discovery that a synthetic 13-mer DNA selectively inhibited gene expression in *Rous Sarcoma* virus [1]. Oligodeoxynucleotides (ODNs) that are complementary or "antisense" to a specific gene or mRNA sequence are potential chemotherapeutic agents [2,3]. Initially, this concept was accepted with skepticism. The half-life of short single-stranded DNA (ssDNA) in a living organism (and *in vitro*) is short; before it penetrates the cell membrane and reaches its target, most of it is digested by exonucleases. Therefore ssDNA is not effective as a targeted therapeutic drug at low dosages. To diminish enzymatic hydrolysis, synthetic analogues of oligonucleotides were synthesized. It is important to the antisense strategy to minimize disruption of the normal formation of hydrogen bonded Watson–Crick base pairs. Thus, antisense DNA modifications should be conservative. The substitution of a sulfur atom for an oxygen atom on the phosphate group is a conservative substitution which increases nuclease resistance without significantly impairing the hybridization of the antisense with the target mRNA [4]. These ssDNA analogues are known as phosphorothioates (SODNs).

SODNs have been successfully used as antiviral agents [5,6] and gene inhibitors [5]. Toxicity and pharmacokinetics of SODN oligomers have been conducted successfully on animals with promising preliminary results [7]. The principle by which such a compound is used is rather simple. Antisense DNA, the complement to a specific segment of mRNA, hybridizes to the target sequence and inhibits the gene's expression. If the product of the inhibited gene (*e.g.*, a protein) is essential to the cell, the cell will perish. Antisense DNA analogues are small synthetic molecules (*i.e.*, $M_r$ *ca.* 10 000). The development and manufacture of antisense pharmaceuticals must address the issues of oligomer length, base composition, base sequence and chemical as well as stereochemical purity.

RP-HPLC is of limited use for the resolution of modified DNA because of the small differences in hydrophobicity with increasing chain length [8]. In addition, the resolution of SODNs may be complicated by stereochemical effects.

* Corresponding author.

0021-9673/93/$06.00 

The substitution of a sulfur for an oxygen atom on the phosphate group results in the formation of a chiral center. Thus, for an oligomer with $n$ SODN linkages, there can be $2^n$ stereoisomers only one of which may represent the most active molecule [4]. The reversed-phase partitioning is complicated by the nature of the DNA backbone, which requires low pH for suppression of SODN ionization. The addition of a cationic ion-pairing reagent increases the efficiency of reversed-phase separations and ODNs with up to 20 bases have been resolved [9]. However, these data were generated with phosphodiester DNA, not the sulfur analogue. Ion-exchange HPLC appears to offer the highest chromatographic resolution of modified oligomers. Polymer based columns yield more predictable behavior and increased longevity over silica based columns [10]. This is probably due to secondary interactions with silanol groups and the chemically labile nature of silica bonded phases. A potential benefit of polymer based columns is the ability to utilize pH extremes to differentiate between oligomers of equal length, but different base sequence [11]. The use of weak or strong anion-exchange columns (WAX/SAX) yielded comparable separations although the selectivity of the WAX column could be modified by pH. The advantage of ion-exchange HPLC over ion-pair HPLC is selectivity; ion-exchange HPLC resolution of SODNs is sequence *and* length dependent while ion-pair HPLC is only length dependent [9].

The length and heterogeneity of natural or modified DNA are best assessed by polyacrylamide gel electrophoresis (PAGE). There is a great deal of interest in the separation and characterization of SODN analogues for use as antisense pharmaceuticals. Synthetic SODNs have become standard reagents in most antisense laboratories using molecular biology techniques. When synthesized, the product is a mixture of truncated oligomers and the desired oligomer. Purification usually involves PAGE and RP-HPLC [12]. The task of purification is a challenging one, because failure sequences differ only in base number and possibly in the sequence of bases. A technique for the rapid separation of SODNs could result in important advances in the molecular biology of antisense pharmaceuticals.

We have demonstrated the high resolution power of PAGE filled capillaries for the separation of low-molecular-mass DNA [13] and enzymatic sequencing reaction mixtures [14]. Capillary gel columns with low monomer concentrations (less than 3% T) generate large numbers of theoretical plates; however, they are not suitable for SODN separations.

In this paper we compare and contrast the separation of SODNs via chromatographic and electrophoretic methods. Several factors which control efficiency and resolution of SODNs by HPCE are explored. The separation conditions for SODNs are significantly different from those recommended for phosphodiesters [14]. The results were used to define conditions where separation of SODNs can be achieved with single-base resolution up to 50 bases in length.

## EXPERIMENTAL

### *Chemicals and reagents*

Water and acetonitrile (ACN) were HPLC grade (J.T. Baker, Phillipsburg, NJ, USA). Tetrabutylammonium phosphate (TBAP) was obtained from Fluka (Ronkonkoma, NY, USA). Sequagel Sequencing System (acrylamide–bisacrylamide, 19:1) purchased from National Diagnostics (Manville, NJ, USA) was used for slab gel preparations. Ultra-pure Tris base, urea, acrylamide, and EDTA were purchased from Schwartz/Mann Biotech (Cleveland, OH, USA). N,N,N′,N′-tetramethylethylenediamine (TEMED) and ammonium persulfate were purchased from Bio-Rad (Richmond, CA, USA). Boric acid was obtained from Sigma (St. Louis, MO, USA). All SODNs were synthesized in-house, desalted, lyophilized and reconstituted in sterile water for injection (Lyphomed, a division of Fujisawa USA, Deerfield, IL, USA). Stains-All (4,5,4′,5′-dibenzo-3,3′-diethyl-9-methylthiacarboncyanine bromide) was purchased from Eastman Kodak (Rochester, NY, USA).

### *HPLC apparatus*

Two HPLC systems were employed in this work: an HP 1090m (Hewlett-Packard, Burlington, MA, USA) and a Waters system consisting of a 600E system controller, a 717 autosampler and a 490E UV detector (Waters, a division of

Millipore, Milford, MA USA). The reversed-phase resolution of SODNs was performed on a NovaPak $C_{18}$, 4 $\mu$m, 150 × 3.9 mm I.D. column (Waters) using the following mobile phases: (I) A: 0.1% formic acid, B: ACN containing 0.1% formic acid; (II) A: 0.1 *M* ammonium acetate ($NH_4Ac$), B: ACN–0.1 *M* $NH_4Ac$ (80:20); (III) A: 50 m*M* $KH_2PO_4$ (pH 4.3), 10 m*M* TEAP, B: ACN–water (80:20) containing 10 m*M* TBAP. Ion-exchange separations were performed on a Partisphere WAX, 5 $\mu$m, 110 × 4.7 mm I.D. GENPAK column (Whatman, Clifton, NJ, USA), a GEN-PAK FAX, 2.5 $\mu$m, 100 × 4.6 mm I.D. column (Waters) and a NucleoPac PA-100, 13 $\mu$m, 250 × 4.0 mm I.D. column (Dionex, Sunnyvale, CA, USA). The mobile phases used for ion-exchange HPLC were (IV) A: 20 m*M* $KH_2PO_4$, 100 m*M* $(NH_4)_2SO_4$ (pH 6.3)–ACN–MeOH (8:2:1, v/v/v), B: 20 m*M* $KH_2PO_4$, 1 *M* $(NH_4)_2SO_4$ (pH 6.3)–ACN–MeOH (8:2:1, v/v/v) and (V) A: 25 m*M*, Tris 1 m*M* EDTA (pH 8.0)–ACN (9:1, v/v), B: 25 m*M* Tris, 1 m*M* EDTA, 2 *M* $NH_4Cl$ (pH 8.0)–ACN (1:9, v/v). All effluents were monitored at 270 nm and gradients were as defined in Table I.

*Slab gel apparatus*

Electrophoresis was carried out in a vertical slab gel apparatus (Model V16, GIBCO BRL, Gaithersburg, MD, USA). The electric field was supplied by a regulated power supply (Model FB 400, Fisher, Pittsburgh, PA, USA). The applied voltage was 250 V, which corresponded to an effective field strength of 19.2 V/cm. Gels were stained with Stains-All and dried on a gel dryer (Buchler Instruments, Lenexa, KA, USA). Electropherograms were obtained on a laser densitometer (Molecular Dynamics, Sunnyvale, CA, USA).

*HPCE apparatus*

The capillary electrophoresis apparatus with

TABLE I

GRADIENT PROGRAMS USED FOR HPLC ANALYSES

| Gradient program | Column | Flow-rate and temperature (ml/min, °C) | Time (min) | Mobile phase composition (%) | |
|---|---|---|---|---|---|
| | | | | A | B |
| I | NovaPak $C_{18}$ | 1.5 at 50°C | 0 | 94 | 6 |
| | | | 3 | 94 | 6 |
| | | | 13 | 26 | 76 |
| II | NovaPak $C_{18}$ | 1.5 at 50°C | 0 | 100 | 0 |
| | | | 2 | 100 | 0 |
| | | | 12 | 0 | 100 |
| III | NovaPak $C_{18}$ | 1.5 at 50°C | 0 | 50 | 50 |
| | | | 2 | 50 | 50 |
| | | | 8 | 50 | 100 |
| IV | Partisphere WAX | 1.5 at room temperature | 0 | 100 | 0 |
| | | | 2 | 100 | 0 |
| | | | 25 | 40 | 60 |
| | | | 30 | 40 | 60 |
| V | GenPak FAX | 0.75 at 65°C | 0 | 40 | 60 |
| | | | 15 | 5 | 95 |
| | | | 15.1 | 0 | 100 |
| | | | 30 | 0 | 100 |
| VI | Nucleopak PA-100 | 2.0 at 70°C | 0 | 90 | 10 |
| | | | 6 | 0 | 100 |
| | | | 10 | 0 | 100 |

UV detection and the preparation of gel-filled capillary for the separation of DNA molecules have been described previously [13,15]. A 30 kV, 500 μA direct current high-voltage power supply (Model ER/DM; Glassman, Whitehouse Station, NJ, USA) was used to generate the potential across the capillary, UV detection of SODNs at 270 nm was accomplished with a Spectra 100 (Spectra-Physics, San Jose, CA, USA). The data were acquired and stored on an AcerPower 486/33 computer (Acer American, San Jose CA, USA) through an analog-to-digital converter (Model 970, Nelson Analytical, Cupertino, CA, USA).

*Gel-filled capillaries*

Fused-silica capillary tubing (Polymicro Technologies, Phoenix, AZ, USA) with 75 μm I.D., 375 μm O.D., effective length of 15–20 cm and the total length of 30–60 cm was treated with (methylacryloxypropyl)trimethoxysilane (Petrarch Systems, Bristol, PA, USA) and then filled with a degassed solution of 13–18% polymerizing linear acrylamide in aqueous or formamide media (0.1–0.3 *M* Tris–borate, 2–6 m*M* EDTA TBE buffer, pH 8.3 containing 7–8.3 *M* urea). Polymerization was achieved by adding ammonium persulfate solution and TEMED. An electric field of 400 V/cm was normally applied unless otherwise is indicated.

## RESULTS AND DISCUSSION

The analysis of SODN antisense compounds is in its infancy. There are few published chromatographic or electrophoretic methods for the baseline resolution of phosphorothioate homologues beyond 20 bases.

*Reversed-phase liquid chromatography*

The separation of large SODN oligomers by RP-HPLC was unsuccessful. The resolution of SODNs of less than 7 bases was possible, but larger oligomers coeluted. Reversed-phase supports are useful for separation of dimethoxytrityl-blocked *vs.* deblocked species. Decreasing the pH of the mobile phase increased the interaction of the phosphorothioates with a hydrophobic stationary phase; however, the peak shape was skewed *vs.* chromatography at pH 6.5 (Fig. 1A and B). In both cases no resolution of individual oligomers was achieved. Aliquots from RP-HPLC (Fig. 1B) were collected and analyzed by PAGE. The aliquots from the front, middle and end of the peak showed the same ratio of oligomers indicating no resolution of bases had occurred. The addition of TBAP to the mobile phase increased the interaction with the hydrophobic support, but the resolution of

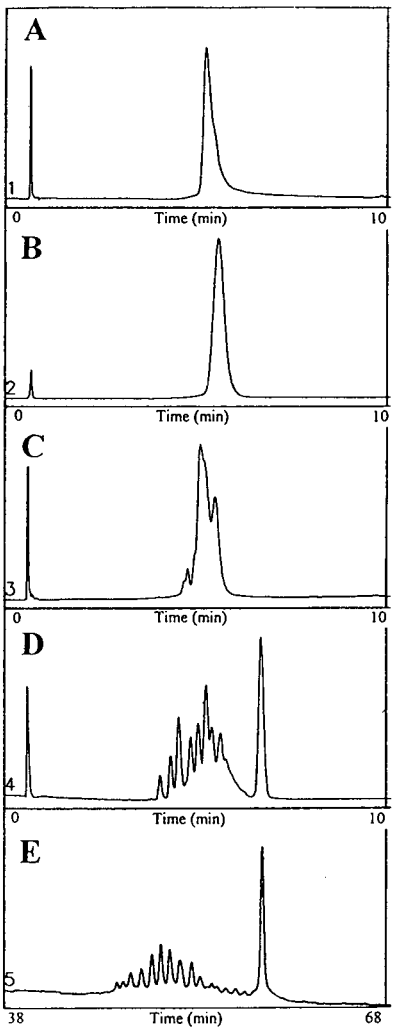


Fig. 1. Resolution of phosphorothioates via HPLC and HPCE. The sample is a crude 25-mer SODN containing failure sequences. (A) RP-HPLC at low pH, Table I, gradient I, (B) RP-HPLC at pH 6.5, gradient II, (C) ion-pair HPLC, gradient III, (D) ion-exchange HPLC, gradient VI, and (E) capillary gel HPCE conditions as in Fig. 4.

the 25-mer from the failure sequences was poor (Fig. 1C). The most effective chromatographic resolutions were obtained on anion-exchange HPLC supports (Fig. 1D). The best separation of this mixture was obtained with capillary gel HPCE (Fig. 1E). The reasons for such high efficiency will be discussed later.

*Anion-exchange chromatography*

Anion-exchange HPLC of the SODNs was possible on weak and strong anion-exchange supports. Reproducibility and efficiency were better with polymer-based supports *vs.* silica-based supports. The chemical stability of the polymer based columns and the absence of secondary effects from residual silanol groups were likely factors in their improved performance. The Partisphere column, a weak anion exchanger based on diethylaminoethyl groups covalently bonded to 10 $\mu$m silica, required several injections of concentrated phosphorothioate before reproducible recoveries were obtained. This presumably covered active sites in the column. The column efficiently resolved over 20 failure sequences from a 25-mer synthesis. However, the gradient program required daily modification because the retention of oligomers decreased by *ca.* 0.5 min per day. The GenPak FAX column and the NucleoPac PA-100 are polymer based pellicular supports. Although the GenPak FAX column contained weak anion-exchange groups and the NucleoPac PA-100 strong anion-exchange groups, the resolutions were virtually identical. Both polymer based columns yielded reproducible separations over several hundred injections. The ability to work at elevated temperature (60–70°C, *i.e.*, denaturing conditions) also reduced the possibility of secondary structure. The interaction of the SODNs increased with increasing temperature due to exposure of more ion-exchange sites on the SODN as the conformation became more relaxed [16]. The resolution of oligomers greater than 23 bases in length proved difficult. This appeared to be exacerbated when the components were present in unequal ratios (Fig. 2A–F). A spiking study was performed to determine the ability to separate oligomers of 23 and 25 bases in length. The retention times of the 23 and 25 mers appeared to be dependent on the relative ratios of the components (Fig. 2A–F). Since the mass load on the column was within the linear range, the reason for this phenomenon is uncertain.

*Slab gel electrophoresis*

Separations of SODN and other DNA analogues have been achieved by flat bed or slab gel electrophoresis [17]. Normal sequencing gel was used to separate SODN analogues with up to 50 bases [17]. We first examined the separation of a mixture of failure sequences ranging from 1 to 50 bases on a sequencing slab gel (Fig. 3). Although

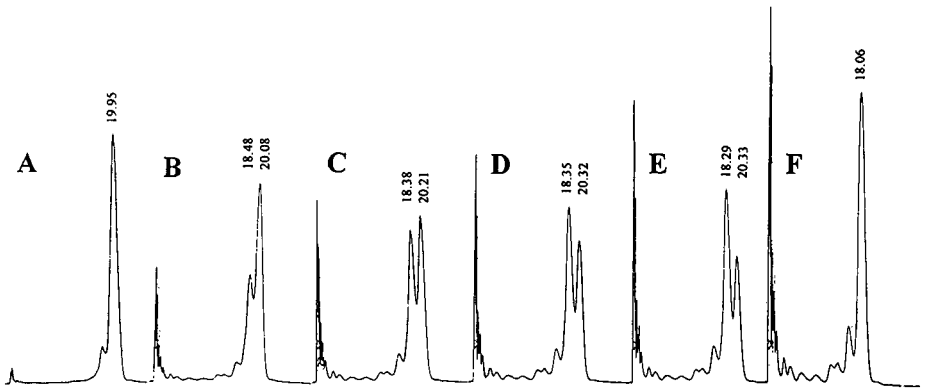


Fig. 2. Ion-exchange HPLC of 23- and 25-mer SODNs. The retention behavior was investigated *vs.* relative concentration of each oligomer. (A) 25-mer, (B) 1:3 (25/23), (C) 2:3, (D) 3:3, (E) 4:3 and (F) 23-mer. The analyses were performed on a GenPak FAX column, gradient V. Injection volume: 20 $\mu$l. Peak numbers indicate retention times in min.

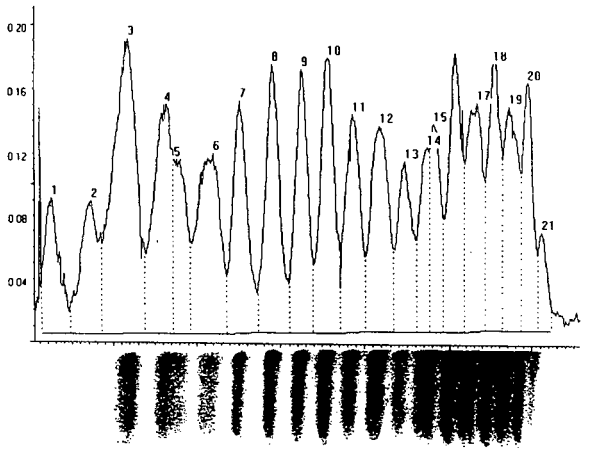

Fig. 3. Separation of failure sequence on a polyacrylamide slab gel. Conditions: 19% T, 1% C containing 8.3 *M* urea, 0.1 *M* TBE (pH 8.3); applied electric field 19.2 V/cm, voltage 250 V. Electropherogram was obtained by laser densitometry, peak numbers indicate delineation of bands by densitometer.

25 distinct bands could be seen on the gel, baseline separation was not obtained by densitometry because of the background from the Stains-All reagent (figure not shown). A laser densitometer gave better results under the exact same conditions (Fig. 3). Although the laser densitometer had better performance than the conventional densitometer, only 21 out of the expected 50 bands were detected. In addition to the problems of background absorbance and reproducibility of the staining, the binding of Stains-All to single-stranded phosphorothioate (ssSODN) was not a linear function of base length. Thus, quantitation or even relative quantitation, was not possible using this approach.

*Gel HPCE separations*

The separations of individual SODNs on gel matrices were investigated. The migration times of the SODNs were longer than the phosphodiester analogues. Electropherograms indicated no linear correlation between migration and SODN length (Fig. 4). Mobility and thus migration time were sensitive to temperature changes (*e.g.*, *ca.* 2%/°C) due to the sensitivity of the gel's viscosity to temperature. Therefore

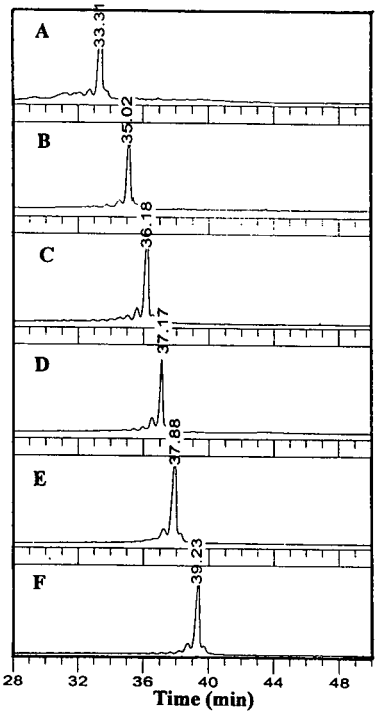


Fig. 4. Gel HPCE migration of SODNs on a capillary gel column. (A) 15-mer; (B) 19-mer; (C) 23-mer; (D) 25-mer; (E) 27-mer and (F) 29-mer. Conditions: 12% T, 0% C, 7 *M* urea, 0.1 *M* TBE (pH 8.3); capillary dimensions: 75 μm I.D., total length 30 cm (effective length 20 cm); applied electric field 300 V/cm, current 10 μA.

care was exercised to keep the Joule heating in the HPCE system below 0.5 W/m.

We approximated the amount of sample injected in Fig. 5 (5 kV for 2 s) by calibrating the capillary detector response in the absence of gel with known concentrations of sample. A linear plot was observed ($r^2 = 0.998$). The analyte concentration in each band passing through the detector was interpolated from this calibration curve. The average concentration of an individual band was determined from the average peak height of the bands in the electropherogram (Fig. 5). The volume of the band was calculated from the baseline peak width and the migration velocity of the species. The estimated peak volume was *ca.* 5 nl and the average mass per peak was 375 pg.

We have used the conventional sequencing gel formulation [14] which was found to have low resolving power (Fig. 4). A higher density gel

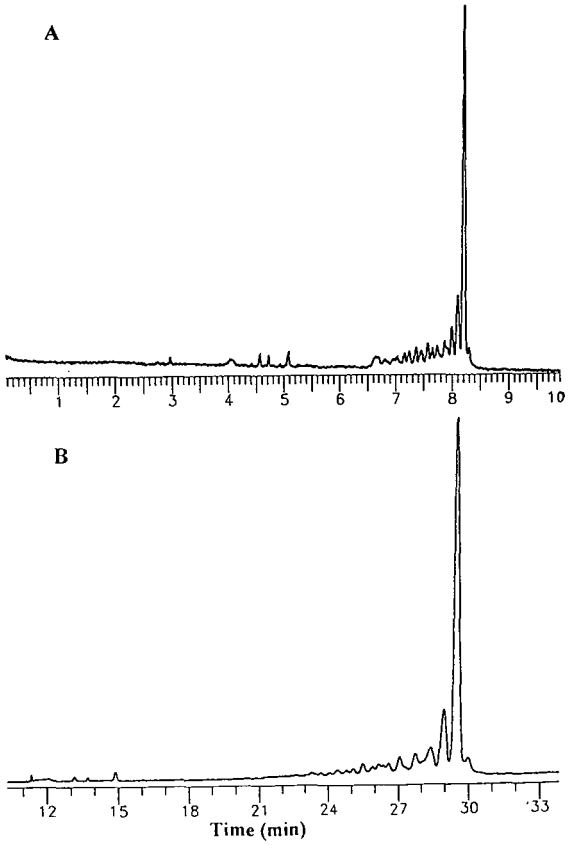


Fig. 5. Gel HPCE separation of a mixture of 23-, 24- and 25-mers of SODNs. (A) effective length 8 cm and (B) effective length 25 cm. Conditions: 13% T, 0% C, 8.3 *M* urea, 0.2 *M* TBE (pH 8.3); applied electric field 400 V/cm.

(*i.e.* higher %T) yielded a better separation (Fig. 5A and B). Artificial mixtures of 23-, 24-, 25-mers of SODNs were separated on a denaturing gel (7 *M* urea, 12% T) in 30 min (Fig. 5B). To reduce analysis time, the column was shortened from 25 to 8 cm (Fig. 5A). The ability of the 8-cm column to maintain high resolution with short run times was remarkable. The calculated efficiency for the 25-mer was $1.9 \cdot 10^6$ plates/m *vs.* $0.34 \cdot 10^6$ plates/m for the longer column. Thus, the shorter columns was three times as efficient in one third the time. Though the efficiency was not as high as expected based on known efficiencies for phosphodiester DNA, the number of possible diastereomers which migrate with the same effective charge was $2^{24}$ for the SODN 25-mer. As expected, the mass sensitivity also increased in the shorter column due to decreased band broadening. Since no efforts were made to thermostat the capillaries, a longer capillary may have experienced more temperature inhomogeneity than a short capillary. This phenomena will be the topic of future investigations.

An artificial mixture of 24- and 25-mers of SODNs was resolved on the 28-cm column, Fig. 6. The time window between the oligomers is large enough to accommodate an additional peak. This peak is presumed to be a failure sequence of the synthesized 25-mer and therefore a 24-mer. Since this peak is migrating right from the main 25-mer under denaturing conditions, we assume that the two 24-mers (possibly two 25-mers) are separated based on the difference in base sequence.

An improved version of the electrophoresis column is currently being developed for the separation of SODN analogues. The gel composition was modified with formamide [18]. Using this modified gel formulation, improved resolution of bases 1 through 50 was obtained (Fig. 7A and B) [18]. When migration time was examined with respect to fragment length, a linear relationship ($r^2 = 0.999$) was observed (Fig. 8). The linear behavior of SODNs ranging from 1 to 50 bases in length (or longer) is an important feature for SODN analyses. It is important to recognize that under these experimental conditions, no peak compression was observed in the

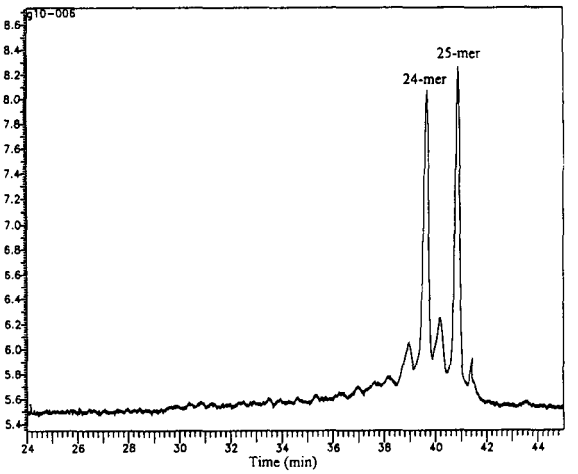


Fig. 6. HPCE separation of an artificial mixture of 24- and 25-mers of SODNs. For experimental conditions see Fig. 5.

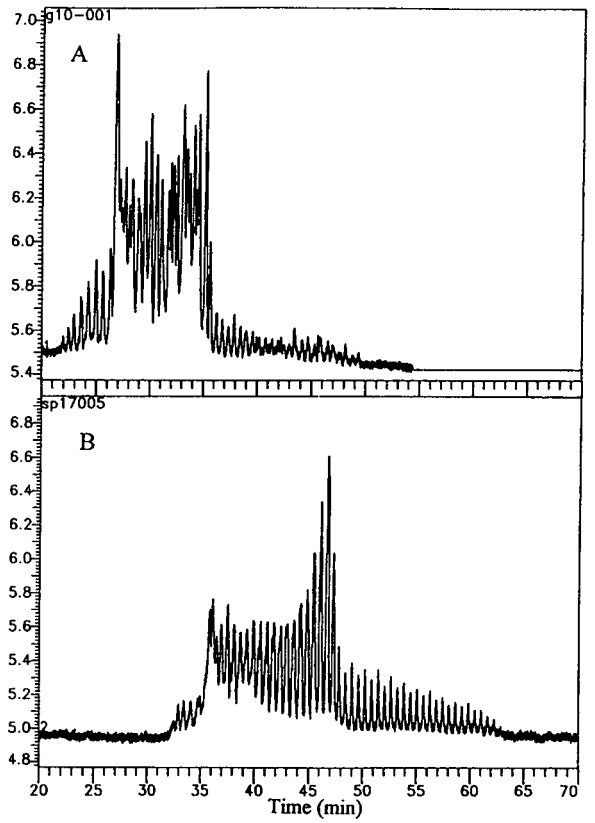


Fig. 7. Electropherograms of failure sequence of SODNs from 1 to 50 bases on (A) regular sequencing gel column and (B) modified sequencing gel column. Conditions: effective length 20 cm, applied electric field 400 V/cm.

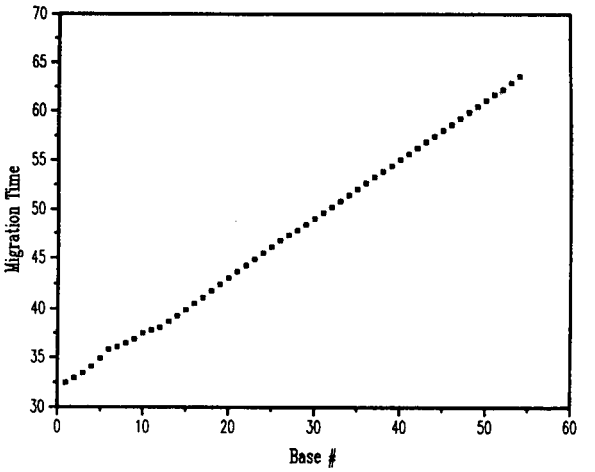


Fig. 8. Calibration plot of migration time *vs.* base length. All conditions identical to those of Fig. 7B.

range of 1 to 50 bases. We are currently investigating resolutions of SODNs beyond the 50 base range.

## CONCLUSIONS

The analysis of SODNs via chromatographic means was possible for short oligomers with less than 30 bases. The highest resolutions were obtained using polymer based pellicular anion-exchange resins. Gel HPCE provides a facile approach to separation, analysis and purity determination of SODNs. High resolving power was possible with these capillary gel columns, permitting rapid separation of SODNs that differ by one base. A significant potential exists for sequencing of SODNs with HPCE gel columns. In addition, rapid assessment of the purity of synthesized oligonucleotides is possible by gel HPCE.

## ACKNOWLEDGEMENTS

The authors deeply acknowledge Dr. Sudhir Agrawal, Dr. Steve Gray and Dr. Tim Noonan for providing us with the SODNs used in this publication.

## REFERENCES

1 P. Zamecnik and M. Stephenson, *Proc. Natl. Acad. Sci. U.S.A.*, 75 (1978) 280.
2 P.S. Miller and P.O.P. Ts'o, *Ann. Rep. Med. Chem.*, 23 (1988) 295.
3 G. Zon, *Pharm. Res.*, 5 (1988) 539.
4 F. Eckstein, *Anal. Biochem.*, 54 (1985) 367.
5 S. Agrawal, T. Ikeuchi, D. Sun, P.S. Sarni, A. Konopka, J. Maizel and P. Zamecnik, *Proc. Natl. Acad. Sci. U.S.A.*, 86 (189) 7790.
6 J.M.E. Leiter, S. Agrawal, P.C. Zamecnik and P. Plese, *Proc. Natl. Acad. Sci. U.S.A.*, 87 (1990) 3430.
7 T.M. Woolf, C.G. Jennings, M. Rebagliatti and D.A. Melton, *Nucleic Acids Res.*, 18 (7) (1990) 1763.
8 S. Agrawal, J.Y. Tang and D.M. Brown, *J. Chromatogr.*, 509 (1990) 396.
9 K. Makino, H. Ozaki, T. Matsumoto, H. Imaiishi and T. Takeuchi, *J. Chromatogr.*, 400 (1987) 271.
10 V. Metelev and S. Agrawal, *Anal. Biochem.*, 200 (1992) 342.
11 Y.-Z. Xu and P.F. Swann, *Anal. Biochem.*, 204 (1992) 185.
12 M.D. Edge, A.R. Greene, G.R. Heathcliffe, P.A. Meacock, W. Schuck, D.B. Scanlon, D.B. Atkinson, T.C.

Newton, C.R. Markham and A.F. Markham, *Nature (London)*, 292 (1981) 756.
13 A.S. Cohen, D.R. Najarian, A. Paulus, A. Guttman, J.A. Smith and B.L. Karger, *Proc. Natl. Acad. Sci. U.S.A.*, 85 (1988) 9660.
14 A.S. Cohen, S. Carson, A.B. Belinkii and B.L. Karger, *Anal. Chem.*, in press.
15 D.N. Heiger, A.S. Cohen and B.L. Karger, *J. Chromatogr.*, 516 (1990) 33.
16 R. Wiem, in E. Heftmann (Editor), *A Laboratory Handbook of Chromatography and Electrophoresis Methods*, Van Nostrand, New York, 3rd ed., 1975, p. 228.
17 D. Rickwood and B.D. James (Editors), *Gel Electrophoresis of Nucleic Acids: A Practical Approach*, IRC Press, Washington, DC, 1983.
18 A.S. Cohen and M. Vilenchik, Patent filed by Hybridon Inc., USA, March 16, 1993.

*Journal of Chromatography*, 638 (1993) 303–309
Elsevier Science Publishers B.V., Amsterdam

CHROM. 24 929

# Capillary electrophoresis for the investigation of illicit drugs in hair: determination of cocaine and morphine

F. Tagliaro*
*Institute of Forensic Medicine, University of Verona, Policlinic, 37134 Verona (Italy)*

C. Poiesi
*Institute of Chemistry, School of Medicine, University of Brescia, Brescia (Italy)*

R. Aiello and R. Dorizzi
*Institute of Forensic Medicine, University of Verona, Policlinic, 37134 Verona (Italy)*

S. Ghielmi
*Institute of Chemistry, School of Medicine, University of Brescia, Brescia (Italy)*

M. Marigo
*Institute of Forensic Medicine, University of Verona, Policlinic, 37134 Verona (Italy)*

ABSTRACT

Toxicological analysis of hair is becoming a popular method for investigating past, chronic use of illicit drugs. Several analytical methods using immunometry, chromatography and mass spectrometry have been reported. In this work, capillary electrophoresis was first used for the determination of illicit drugs, such as cocaine and morphine, in the hair of heroin and cocaine users. After rapid washing, hair samples were incubated overnight in 0.25 *M* HCl at 45°C and the mixtures were extracted with ready-to-use Toxi-tubes A. The organic phase was evaporated and the residue dissolved in a suitable amount of electrophoresis buffer. Free zone capillary electrophoretic determinations of morphine, the main heroin metabolite, and cocaine were accomplished in 0.05 *M* borate buffer (pH 9.2) at a potential of 15 000 V, with UV detection at 214 and 238 nm, respectively. The use of the less selective wavelength of 200 nm allowed the simultaneous detection of both compounds. Efficient separations (up to 350 000 theoretical plates) and accurate and precise determinations (intra-day R.S.D.s in the range 3–5%) of cocaine and morphine in hair extracts were easily achieved. The analytical sensitivity was sufficient to determinate as little as 0.15 ng/mg of cocaine and morphine in hair using 100-mg samples. Interferences from more than 90 therapeutic drugs and drugs of abuse were excluded.

## INTRODUCTION

Capillary electrophoresis (CE), after having been demonstrated to be a powerful tool in biopolymer separations, has rapidly expanded into the field of drug analysis [1,2]. CE possesses some unique characteristics that make it potentially valuable in the analysis of therapeutic and illicit drugs for pharmacological–pharmaceutical, clinical and forensic purposes.

First, CE is based on physical–chemical princi-

* Corresponding author.

0021-9673/93/$06.00 

ples substantially different from those in chromatography and other techniques used in pharmaceutical and toxicological analysis and thus has the potential to become an ideal "complementary" technique in analytical toxicology. An additional facet of CE is the need for minimum amounts of specimens, which makes it important especially when only minute amounts of sample are available, as often happens in forensic cases.

These unique features have prompted some forensic and clinical toxicologists to investigate possible applications of CE in analyses for drugs of abuse. A pioneering paper by Wernly and Thormann [3] demonstrated the effectiveness of micellar electrokinetic capillary chromatography (MECC) in the analysis of urines for common drugs of abuse and their metabolites (*e.g.*, opiates, benzoylecgonine, amphetamines and methaqualone). To the best of our knowledge, however, CE has never found application in the analysis of hair for drugs of abuse, in which this technique could display most of its advantages. This innovative approach to toxicological investigations, first proposed by Baumgartner *et al.* in 1979 [4], is now becoming a powerful means for demonstrating the chronic use of illicit drugs. An excellent overview of this subject has been published by Harkey and Henderson [5].

Several drugs undergoing chronic use become embedded in the hair at the follicle level, during the hair growth, and, lacking any metabolism in this structure, they remain fairly unaltered throughout the entire hair lifetime. The average hair growth being about 1 cm/month, the analysis of few centimetres of hair can provide information on the toxicological behaviour over several months before the collection of the hair sample. This is particularly important if one considers that usually drugs disappear from the blood in a few hours and from urine in a few days.

However, because, for aesthetic problems, only a few milligrams of hair can be collected, and as the concentration of drugs in the hair matrix is in the low ng/mg range, analytical sensitivity is a crucial point. At present, radioimmunoassay (RIA) is generally used for the preliminary screening and gas chromatography, gas chromatography–mass spectrometry, high-performance liquid chromatography (HPLC) or collisional activation mass spectrometry are used for confirmation of the results (for a review, see ref. 5). On this ground, CE, because of its high analytical efficiency and mass sensitivity, could become an important tool of investigation. In addition, its possible coupling with mass spectrometry should be taken into account in view of its possible use for forensic purposes.

The aim of this work was to test the performance of CE in the assay of hair for markers of cocaine and heroin use (*i.e.*, cocaine itself and morphine, the main metabolite of heroin) in comparison with the HPLC methods currently used in our laboratory.

## EXPERIMENTAL

### *CE instrumentation and methods*

A manual capillary electropherograph (Model 3850; Isco, Lincoln, NE, USA) equipped with an on-column UV detector and a split-flow injector was used. Bare silica capillaries (40 cm to the detector) of I.D. 50 $\mu$m were adopted, furnished by Isco. Separations were accomplished using constant potentials of 15 000 V in 0.050 *M* borate buffer (pH 9.2), with resulting currents no higher than 60 $\mu$A. The buffers were filtered through a 0.45-$\mu$m nylon 66 membrane (Alltech, Eke, Belgium) and deareated under reduced pressure (water pump) before use. After each injection the capillary surface was renewed by flushing with 0.1 *M* NaOH and rinsing with the working buffer. Injection was executed manually with a syringe through a splitter with a reported splitting ratio to the column of 1:830.

MECC separations were carried out under conditions mostly resembling those published by Wernly and Thormann [3]. Briefly, 0.010 *M* borate buffer (pH 9.2) containing 0.050 *M* sodium dodecyl sulphate (SDS) was the background buffer and a potential of 20 000 V was applied. The capillary was the same as that described above. Wavelengths of 238 and 214 nm were chosen for the UV detection of cocaine and morphine, respectively, with a detector range of 0.005 AUFS. For calculating the net mobilities,

methanol was used as an electroosmotic flow marker.

*Standards and sample preparation*

Stock standard solutions of cocaine (Sigma, St. Louis, MO, USA) and morphine (Carlo Erba, Milan, Italy) were prepared from the respective hydrochloride salts in methanol to yield concentrations of 1 mg/ml and were stored at −18°C. Working standard solutions of suitable concentrations were prepared on the day of analysis by diluting the stock standard solution with the background buffer diluted 1:2 with water. Tetracaine and nalorphine, used as internal standards (I.S.), were purchased from Sigma.

Standards of therapeutic drugs and drugs of abuse, supplied dried on glass microfibre discs impregnated with silicic acid (Toxi Disc Library) and Toxi-tubes A were purchased from Analytical Systems (Laguna Hills, CA, USA).

The hair sample pretreatment has been fully described elsewhere [6] and it can be summarized as follows. Hair samples (25–100 mg), cut near the scalp, were washed with diethyl ether and 0.01 *M* HCl and then extracted by incubating overnight in 0.25 *M* HCl at 45°C. The incubation mixtures were neutralized with NaOH and extracted twice into the organic phase with ready-to-use Toxi-tubes A. The organic layer was then evaporated to dryness and the residue was reconstituted with 20 $\mu$l of the background buffer, previously diluted 1:2 with water, 5 or 10 $\mu$l of which were injected.

*HPLC instrumentation and methods*

Morphine and cocaine were assayed by HPLC using an isocratic instrument composed of a high-pressure pump (Model 880 PU; Jasco, Tokyo, Japan) and a six-port injection valve (Model 7125; Rheodyne, Cotati, CA, USA) with a 50-$\mu$l loop. For morphine, an amperometric detector (LC 4B/17A; BAS, West Lafayette, IN, USA) with a thin-layer cell and a glassy carbon working electrode (operated at 350 mV *vs.* an Ag/AgCl reference electrode) was used; for cocaine, a UV detector (Model 875 UV; Jasco) set at 235 nm was adopted.

The HPLC separation of morphine was carried out under conditions fully detailed elsewhere [7], using a Bio-Gel PRP 70-5 column (150 mm × 4.6 mm I.D.) (Bio-Rad RSL, Eke, Belgium), packed with 5-$\mu$m spherical particles of polystyrene–divinylbenzene, and a mobile phase of 0.050 *M* sodium phosphate (pH 9.5)–acetonitrile (85:15) at a flow-rate of 0.5 ml/min at 65°C.

Reversed-phase ion-pair liquid chromatographic assay of cocaine was accomplished according to Jatlow and Nadim [8], with minor changes. An ODS silica column (250 mm × 4.6 mm I.D.) packed with 5-$\mu$m Nucleosil 100 (Macherey–Nagel, Düren, Germany) was used with a mobile phase composed of 0.050 *M* phosphate buffer (pH 3.0)–acetonitrile (66:33), containing 0.2% of hexanesulphonic acid, at a flow-rate of 0.5 ml/min at room temperature.

## RESULTS AND DISCUSSION

*CE determination of cocaine*

CE of cocaine under the described conditions results in a sharp and symmetrical peak migrating before the electroosmotic flow. In fact, cocaine ($M_r$ 303.35), having only a tertiary amine as ionizable moiety with a p$K$ of 8.7, is still partially ionized as a cation at the pH of the background buffer (9.2). Its net mobility ($\mu$) was $0.42 \cdot 10^{-4}$ cm$^2$/V s under the adopted conditions; the dependence of $\mu$ on the pH of the buffer is shown in Fig. 1. The efficiency of separation was about 350 000 theoretical plates.

The major metabolite of cocaine, benzoylecgonine, having an additional COOH moiety, was not extracted efficiently with the adopted liquid–

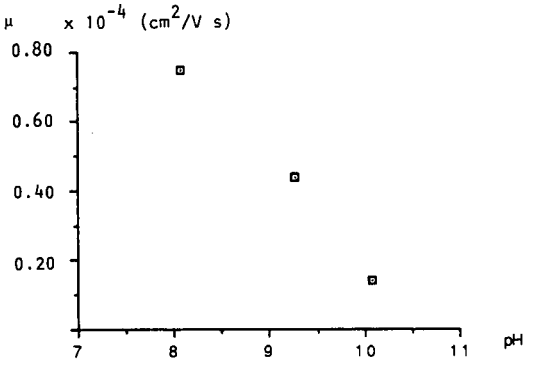


Fig. 1. Dependence of the net mobility ($\mu$) of cocaine on the pH of the background buffer.

liquid extraction method and is a minor compound in the hair of cocaine users. Therefore, it was not investigated further. No interferences were observed from more than 90 therapeutic and illicit drugs at the level of 100 $\mu$g/ml, as shown in Table I, or from the "normal" constituents of hair matrix and common cosmetic treatments. In fact, the electropherograms of blank hair extracts were remarkably clean, allowing the injection of hair extracts reconstituted in very small volumes. This is particularly important because of the modest sensitivity, in terms of concentration, of CE with on-column UV detection. In fact, the limit of detection (LOD) was about 600 ng/ml (with a signal-to-noise ratio of 3), allowing the identification of levels of cocaine as low as 0.15 ng/mg in 100-mg hair samples. Fig. 2 shows the electropherograms of a blank hair sample (in which the addition of the I.S. has intentionally been omitted) and of a sample positive for cocaine at the level of 4.0 ng/mg (from a hair sample of 75 mg). Only a single peak is present in the blank hair electropherogram, which can be ascribed to the bulk of uncharged endogenous compounds co-extracted, which migrate all together at the velocity of the electroosmotic flow.

The determination of cocaine, notwithstanding an "acceptable" reproducibility of the manual split-flow injector in method development, needed the use of an I.S. in order to achieve the required degree of repeatability and accuracy for application to real samples. For this purpose, tetracaine, with $\mu = 0.22$, emerging close to cocaine but baseline resolved, was used at a level of 25 $\mu$g/ml.

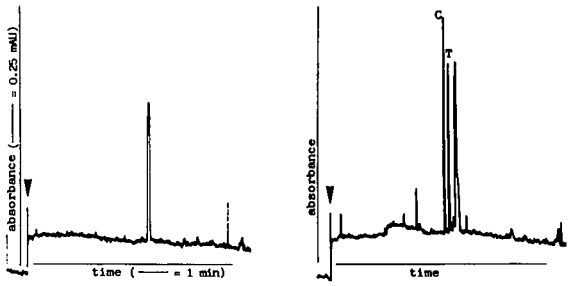


Fig. 2. Typical electropherograms of (left) a blank hair sample (in which the addition of the I.S. was intentionally omitted) and (right) hair (75 mg) from a cocaine user, containing cocaine at the level of 4.0 ng/mg [C = cocaine peak; T = tetracaine (I.S.) peak]. Chart speed, 0.5 cm/min; detection at 238 nm; other conditions are detailed in the text. The arrows indicate injections.

The linearity of the CE determination of cocaine in the range 0.78–100 $\mu$g/ml (corresponding to 0.16–20 ng/mg in 100-mg hair samples) is described by the equation $y = 0.0144 + 0.0747x$ ($r = 0.99990$); Tables II and III summa-

TABLE I

DRUGS INVESTIGATED IN ORDER TO EXCLUDE INTERFERENCES IN THE CE DETERMINATION OF COCAINE AND MORPHINE

No interferences were observed up to levels of 100 $\mu$g/ml.

| | |
|---|---|
| Opiates and antagonists | Codeine, dextromethorphan, dihydrocodeine, diphenoxilate, ethylmorphine, hydrocodone, hydromorphone, meperidine, methadone, naloxone, oxicodone, papaverine, propoxyphene, terpin hydrate |
| Central nervous system active drugs | Amphetamine, amitriptyline, benztropine, carbamazepine, caffeine, chlorprothixene, chlorpromazine, cocaine, diazepam, diphenylhydantoin, doxepin, flurazepam, imipramine, loxapine, meprobamate, methamphetam, methaqualone, methylphenidate, nordiazepam, nortriptyline, phenmetrazine, phentermine, phencyclidine, phetidine, prazepam, protriptyline, strychnine, thioridazine, thiothixene, trifluperazine, triflupromazine |
| Miscellaneous | Acetaminophen, atropine, benzoylecgonine, carisoprodol, chlorpheniramine, cimetidine, diphenhydramine, disopyramide, doxylamine, emetine, erythromycin, glutethimide, hydrocortisone, hydroxyzine, lidocaine, methapyrilene, methocarbamol, nicotine, orphenadrine, pentazocine, phenacetin, pyrilamine, phenolphthalein, phenylpropanola, propranolol, procaine, procainamide, pseudoephedrine, quinine, salicylamide, spironolactone, triamterene, triexyphenidyl, trimeprazine, trimetobenzamide, trimethoprim |

TABLE II

ACCURACY OF COCAINE AND MORPHINE DETERMINATIONS

| Drug | Expected concentration (μg/ml) | Observed concentration (mean ± S.D., $n = 6$) (μg/ml) | Recovery (%) |
|---|---|---|---|
| Cocaine | 50.0 | 49.1 ± 2.07 | 98 |
| | 10.0 | 9.3 ± 0.30 | 93 |
| Morphine | 10.0 | 9.5 ± 0.38 | 95 |
| | 2.5 | 2.1 ± 0.11 | 84 |

TABLE III

PRECISION OF DETERMINATION AND MIGRATION TIMES OF COCAINE AND MORPHINE

| Precision | Drug | Mean concentration ($n = 6$) (μg/ml) ± R.S.D. (%) | Mean migration time ($n = 12$) (min) ± R.S.D. (%) | | | | |
|---|---|---|---|---|---|---|---|
| | | | E.O. flow | Cocaine | Tetracaine | Morphine | Nalorphine |
| Intra-day | Cocaine | 9.3 ± 3.2% | 8.18 ± 0.31% | 7.40 ± 0.91% | 7.69 ± 0.92% | | |
| | | 49.1 ± 4.2% | | | | | |
| | Morphine | 9.5 ± 4.0% | 8.18 ± 0.31% | | | 9.26 ± 0.96% | 9.46 ± 1.12% |
| | | 2.1 ± 5.2% | | | | | |
| Inter-day | Cocaine | 10.2 ± 5.7% | 8.09 ± 0.93% | 7.32 ± 2.26% | 7.55 ± 2.18% | | |
| | | 49.7 ± 7.0% | | | | | |
| | Morphine | 10.1 ± 7.2% | 8.09 ± 0.93% | | | 9.06 ± 2.96% | 9.26 ± 2.90% |
| | | 2.4 ± 8.3% | | | | | |

rize the accuracy and precision data, respectively.

*CE determination of morphine*

Morphine, separated under the described conditions, gave a symmetrical peak migrating after the electroosmotic flow. Morphine ($M_r$ 285.33), having both a tertiary amine and a phenolic group (p$K$ 8.1 and 9.85, respectively) on the whole behaves as an anion at the pH of the background buffer (9.2). The anionic mobility of morphine was $\mu = 0.44 \cdot 10^{-4}$ cm$^2$/V s under the adopted separation conditions; the dependence of $\mu$ on the pH of the buffer, reflecting its amphoteric character, is shown in Fig. 3. The efficiency of separation was about 150 000 theoretical plates.

As for cocaine, no interferences were observed from the compounds listed in Table I. The electropherograms of blank hair extracts did not show interfering peaks at the migration time of morphine. The LOD for morphine was about 600 ng/ml (with a signal-to-noise ratio of 3),

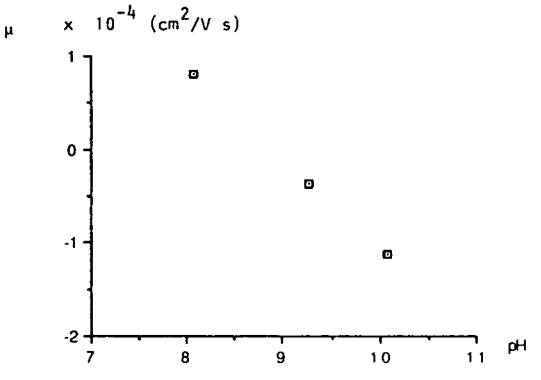


Fig. 3. Dependence of the net mobility ($\mu$) of morphine on the pH of the background buffer.

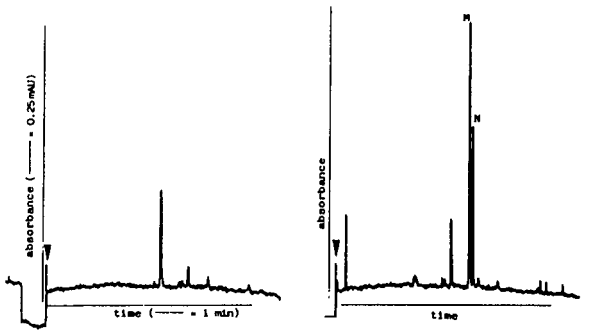


Fig. 4. Typical electropherograms of (left) a blank hair sample (in which the addition of the I.S. was intentionally omitted) and (right) hair (75 mg) from a heroin user, containing morphine at the level of 3.0 ng/mg [M = morphine peak; N = nalorphine (I.S.) peak]. Chart speed, 0.5 cm/min; detection at 214 nm; other conditions are detailed in the text. The arrows indicate injections.

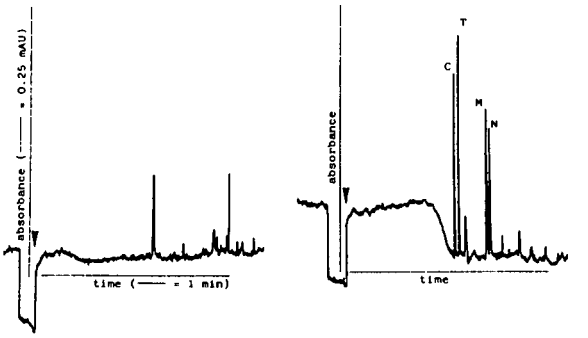


Fig. 5. Electropherograms of (left) a blank hair sample and (right) a hair extract spiked with cocaine (C), tetracaine (T), morphine (M) and nalorphine (N), to simulate a concentration of about 4 ng/mg of each analyte in hair. Chart speed, 0.5 cm/min; detection at 200 nm; other conditions are detailed in the text. The arrows indicate injections.

allowing the identification of levels of morphine as low as 0.15 ng/mg in 100-mg hair samples. Fig. 4 shows the electropherograms of blank hair (without the I.S.) and of a sample positive for morphine at a level of 3.0 ng/mg (from a hair sample of 100 mg).

For the determination, nalorphine, which was baseline resolved from morphine, was used as the I.S. at the level of 15 $\mu$g/ml.

The linearity of the CE determination of morphine in the concentration range 0.62–100 $\mu$g/ml is described by the equation $y = 0.0461 + 0.1295x$ ($r = 0.99980$). Tables II and III give the accuracy and precision data for both concentration and migration times.

*Simultaneous determination of cocaine and morphine*

Because of the different UV absorption maxima of cocaine and morphine, the simultaneous determination of the two analytes was not possible at either of the wavelengths used. UV detection at 200 nm, where both cocaine and morphine absorb, could overcome this problem, as shown in Fig. 5. Unfortunately, determinations at this low and inherently less selective wavelength may suffer from interferences. For this reason, detection at 200 nm is to be used only for screening purposes and positive samples should be reassayed at the more specific wavelengths.

*Comparison with HPLC*

The results of the CE determination of cocaine and morphine in eight real samples were compared with the results given by HPLC on the same extracts. Good correlation coefficients were observed ($r = 0.96$ for morphine and 0.99 for cocaine), but CE showed at least a three times higher productivity than HPLC (Fig. 6). No deterioration of the capillary was observed over several months.

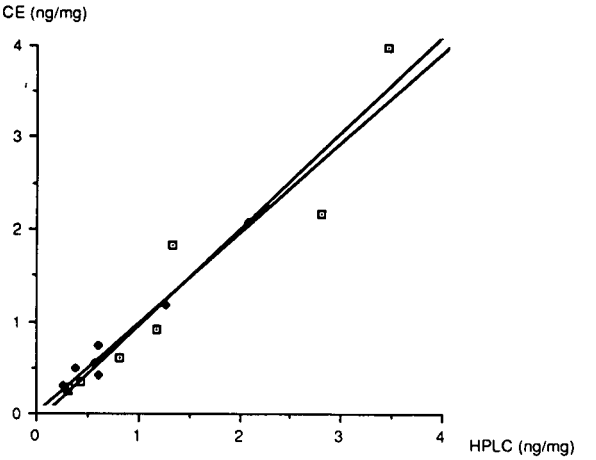


Fig. 6. Correlation between HPLC and CE in the determination of cocaine and morphine observed in the cross-assay of eight hair extracts from opiate and/or cocaine users. □ = Morphine ($y = -0.1018 + 1.0479x$, $r = 0.96$); ◆ = cocaine ($y = 0.0025 + 0.9764x$, $r = 0.99$).

## CONCLUSION

Although the most common approach to the CE analysis of drugs is MECC [3,9], the present study demonstrates that free zone CE is suitable for the determination of charged drugs, such as cocaine and morphine, in rough extracts of human hair. For this purpose, capillary zone electrophoresis proved superior to MECC because the latter technique, although able to provide excellent separations of drugs of abuse, produced, in our hands, complex electropherograms when real hair extracts were injected, with several small peaks potentially interfering with those of the analytes of interest (data not shown). This was probably due to the inherent ability of MECC to "separate" also uncharged molecules, which in this particular instance apparently represent most of the co-extractives from the hair matrix.

On the other hand, free zone CE showed excellent selectivity for the analytes of interest, being suitable also for the determination of cocaine and morphine, meeting the sensitivity, accuracy and precision requirements for a technique suitable for use in forensic work. On-line scanning UV detection, although only preliminarily studied, seems an interesting feature, providing CE analyses with valuable additional information on peak purity and identity [3]. In conclusion, CE can be considered as a powerful technique suitable for wide use in forensic and clinical toxicology. It can be considered not only complementary to liquid and gas chromatography for confirmatory purposes, but could also, because of the possibility of automation, its ruggedness and negligible reagents costs per test [2], be interesting for screening analyses.

## ACKNOWLEDGEMENTS

The cooperation of Dr. G. Sabbatini (Bio-Rad, Milan) is gratefully acknowledged. This study was carried out in the frame of the UNICRI (United Nations Interregional Crime and Justice Research Institute, Rome) research project "Toxicological Hair Analysis".

## REFERENCES

1 G.M. McLaughlin, J.A. Nolan, J.L. Lindahl, R.H. Palmieri, K.W. Anderson, S.C. Morris, J.A. Morrison and T.J. Bronzert, *J. Liq. Chromatogr.*, 15 (1992) 961.
2 M.A. Evenson and J.E. Wiktorowicz, *Clin. Chem.*, 38 (1992) 1847.
3 P. Wernly and W. Thormann, *Anal. Chem.*, 63 (1991) 2878.
4 A.M. Baumgartner, P.F. Jones, W.A. Baumgartner and C.T. Black, *J. Nucl. Med.*, 20 (1979) 748.
5 M.R. Harkey and G.L. Henderson, in R.C. Baselt (Editor), *Advances in Toxicological Analysis*, Vol. II, Year Book Medical, Chicago, 1989, p. 298.
6 M. Marigo, F. Tagliaro, C. Poiesi, S. Lafisca and C. Neri, *J. Anal. Toxicol.*, 10 (1986) 158.
7 F. Tagliaro, G. Carli, F. Cristofori, G. Campagnari and M. Marigo, *Chromatographia*, 26 (1988) 163.
8 P. Jatlow and H. Nadim, *Clin. Chem.*, 36 (1990) 1436.
9 R. Weinberger and I.S. Lurie, *Anal. Chem.*, 63 (1991) 823.

*Journal of Chromatography*, 638 (1993) 311–318
Elsevier Science Publishers B.V., Amsterdam

CHROM. 24 860

# Capillary zone electrophoresis of pharmaceutical peptides

Marleen H.J.M. Langenhuizen and Peter S.L. Janssen*

*Department of Analytical Chemistry, Organon International BV, AKZO Pharma Group, P.O. Box 20, 5340 BH Oss (Netherlands)*

ABSTRACT

In peptide analysis, capillary zone electrophoresis (CZE) gives complementary information to that obtained using high-performance liquid chromatography and capillary isotachophoresis. However, a prerequisite for the implementation of CZE for routine quality control purposes is a simple strategy quickly leading to an adequate separation system. A general approach towards the set-up of such systems is presented. A broad range of peptides were used as representative models, *viz.*, adrenocorticotropic hormone (ACTH), the modified ACTH fragment Org 2766, endorphins, cholecystokinin and fragments thereof. In general, the pH and the concentration of the applied electrophoresis buffers are the most important parameters to be considered in the CZE of pharmaceutical peptides.

## INTRODUCTION

High-performance capillary electrophoresis (HPCE) is a separation technique with a rapidly growing number of applications in the field of protein and peptide analysis. Several groups have reported on the complementary information obtained from reversed-phase high-performance liquid chromatography (RP-HPLC) on the one hand and the HPCE modes [capillary isotachophoresis (CITP) and capillary zone electrophoresis (CZE)] on the other [1–4]. The combination of these techniques proved to be most valuable in the support of the preparation, purification and characterization of natural and synthetic pharmaceutical peptides. However, a prerequisite for the implementation of CZE for routine quality control purposes for pharmaceutical peptides is the availability of rapid and simple optimization procedures. Considering the amphoteric character of peptides, the most important parameter to be manipulated in method optimization is the pH of the buffer system [5,6]. Another important factor that can easily be varied and that may have a beneficial effect on the separation performance is the concentration of the buffer [7]. Moreover, buffer additives such as methanol or acetonitrile or metal salts such as $ZnSO_4$ may also improve the separation [6,7]. Using a broad range of peptides we studied the influence of the above parameters. The intention of this work was to set up a general strategy for the development of CZE procedures to be applied in routine peptide analyses.

## EXPERIMENTAL

### *Instrumentation*

All CZE experiments were performed on a P/ACE System 2100 capillary electrophoresis equipment (Beckman, Palo Alto, CA, USA) equipped with an untreated fused-silica tube (57 cm × 75 $\mu$m I.D.; 50 cm from inlet to detector), an autosampler, a temperature-controlled fluid-cooled capillary cartridge, an automatic injector

* Corresponding author.

0021-9673/93/$06.00 

TABLE I

SEQUENCES OF PARENT PEPTIDES

| | |
|---|---|
| ACTH | H–Ser–Tyr–Ser–Met–Glu–His–Phe–Arg–Trp–Gly–Lys–Pro–Val–Gly–Lys–Lys–Arg–Arg–Pro–Val–Lys–Val–Tyr–Pro–Asn–Gly–Ala–Glu–Asp–Glu–Leu–Ala–Glu–Ala–Phe–Pro–Leu–Glu–Phe–OH |
| Org 2766 | H–Met$O_2$–Glu–His–Phe–D–Lys–Phe–OH |
| β-Endorphin | H–Tyr–Gly–Gly–Phe–Met–Thr–Ser–Glu–Lys–Ser–Gln–Thr–Pro–Leu–Val–Thr–Leu–Phe–Lys–Asn–Ala–Ile–Ile–Lys–Asn–Ala–Tyr–Lys–Lys–Gly–Glu–OH |
| CCK-8(S) | H–Asp(–$SO_3H$)–Tyr–Met–Gly–Trp–Met–Asp–Phe–$NH_2$ |

and a UV source with a set of selectable wavelength filters.

Calculation of the relative mobilities of the peptides was performed using CAS, a peptide mobility software program developed at Eindhoven University of Technology [4].

*Peptide characteristics*

To obtain a good overall insight into the influence of the various buffer parameters on HPCE peptide separations in general, four characteristic peptide groups varying widely in isoelectric point (p*I*), molecular mass and chain

TABLE II

PHYSICO-CHEMICAL CHARACTERISTICS OF THE PEPTIDES

| Peptide group | Sequence[a] | p*I* | Molecular mass | Chain length | Buffer pH | Mobility[b] | Migration order |
|---|---|---|---|---|---|---|---|
| 1 ACTH | 11–24 | 11.69 | 1652 | 14 | 3.8 | 0.0431 | 1 |
| | 1–24 | 10.05 | 2934 | 24 | | 0.0379 | 2 |
| | 1–39 | 9.24 | 4567 | 39 | | 0.0216 | 3 |
| | 1–10 | 7.55 | 1299 | 10 | | 0.0151 | 4 |
| 2 Org 2766 | 3–6 | 9.74 | 578 | 4 | 3.8 | 0.0289 | 1 |
| | 5–6 | 9.70 | 294 | 2 | | 0.0229 | 2 |
| | 2–6 | 7.81 | 707 | 5 | | 0.0222 | 3 |
| | 1–6 | 7.60 | 870 | 6 | | 0.0194 | 4 |
| | 4–6 | 9.82 | 441 | 3 | | 0.0175 | 5 |
| | 2–6 (pyroGlu) | 8.25 | 689 | 5 | | 0.0130 | 6 |
| | 1–3 | 5.15 | 447 | 3 | | 0.0130 | 7 |
| 3 Endorphins | 7–15 | 6.70 | 998 | 9 | 2.2 | 0.0157 | 1 |
| | 6–15 | 6.70 | 1089 | 10 | | 0.0147 | 2 |
| | 6–16 | 6.70 | 1190 | 11 | | 0.0130 | 3 |
| 4 CCK | 2–8 (non-S) | 6.80 | 948 | 7 | 7.5 | −0.0001 | 1 |
| | 1–8 (cyclic S) | – | 1125 | 8 | | – | 2 |
| | 1–8 (non-S) | 3.90 | 1063 | 8 | | −0.0097 | 3 |
| | 2–8 (S) | ~3.90 | 1028 | 7 | | −0.0099 | 4 |
| | 1–8 (S) | ~3.90 | 1143 | 8 | | −0.0184 | 5 |

[a] S = Sulphated.

[b] Mobility = calculated electrophoretic mobility.

length were chosen: (1) adrenocorticotropic hormone (ACTH) and fragments; (2) Org 2766 and fragments; (3) endorphins and fragments; and (4) cholecystokinin (CCK) fragments. For each of the four groups, structurally closely related peptide preparations, giving representative information in critical separations, were selected.

The sequences of the parent peptides are given in Table I and the physico-chemical characteristics of the individual peptides in Table II. The porcine ACTH preparation was obtained from Diosynth (Oss, Netherlands). All other peptide preparations were synthesized by the peptide chemistry group of Organon.

*ACTH and Org 2766.* The principal activity of ACTH is the stimulation of the adrenal cortex to produce and release steroid hormones. The N-terminal part ACTH-(1–24) possesses full biological activity [8]. The (1–10) and (11–24) fragments are the building blocks in the synthesis of ACTH-(1–24). Recently, several studies have shown that ACTH and related peptides also stimulate the recovery of sensorimotor function after nerve damage. The modified ACTH-(4–9) fragment Org 2766 was found to prevent neuropathies induced by cytostatic drugs in both animals and man [9]. In the framework of metabolism studies the separation of Org 2766 and fragments has been investigated [4].

*Endorphins and fragments.* β-Endorphin, the C-terminal 31-peptide of β-lipotropin, was originally isolated from pituitaries of several species. The peptide is a potent opiate-like compound and displays behavioural properties [10]. Metabolic processing of β-endorphin by enzymes generates the N-terminal 16- and 17-peptides called α- and γ-endorphin, respectively. Removal of the N-terminal tyrosine residue of the endorphins, giving the (2–31), (2–17) and (2–16) fragments, results in preparations that have lost their opiate-like activity but have retained their behavioural properties. In order to facilitate metabolism studies of the proposed antipsychotic compound β-endorphin-(6–17) (Org 5878), the separation of the fragments (6–15), (6–16) and (7–15) has been investigated [11].

*Cholecystokinin.* The 58-peptide CCK is important in the control of gastrointestinal function. In addition, high concentrations of a sulphated octapeptide sequence (CCK-8S; the sulphated C-terminal fragment) were demonstrated to be present in several brain regions [12]. CCK-8S and (modified) fragments have been investigated for their separatibility.

*Operational buffer systems*

Five buffer systems, covering the pH range 2.20–8.30, were selected: (1) 25 m*M* phosphoric acid, adjusted to pH 2.20 with 1 *M* NaOH; (2) 20 m*M* formic acid, adjusted to pH 3.80 with β-alanine; (3) 20 m*M* L-histidine, adjusted to pH 6.20 with 2-(N-morpholino)ethanesulphonic acid; (4) 50 m*M* tris(hydroxymethyl)aminomethane (Tris), adjusted to pH 7.50 with acetic acid; and (5) 100 m*M* boric acid, adjusted to pH 8.30 with 1 *M* NaOH.

In addition, the separation performance of the buffers 1, 2 and 4 was studied at higher concentrations, *i.e.*, 50 and 100 m*M* for buffers 1 and 2 and 100 and 200 m*M* for buffer 4. Moreover, the effects of $ZnSO_4$ (50 m*M*), acetonitrile (10%) and methanol (10%), added to the original buffers 1, 2 and 4, was tested.

All chemicals used in the preparation of the buffers were of analytical-reagent grade (J.T. Baker).

*Procedure*

The peptide mixtures 1–4 (see Table II) were prepared in ultrapure water (Milli-Q) at a concentration of *ca.* 0.2 mg/ml of each component.

At the beginning of each day the capillary was rinsed successively with 1 *M* NaOH and ultrapure water for 45 min each. Prior to each analysis the capillary was rinsed for 3 min with the separation buffer. Samples of the peptide mixtures were injected using pressure for 5 s (corresponding to an injection volume of *ca.* 25 nl). Peak assignment was done by single component injection.

The analyses were performed at a voltage of 25 kV, unless stated otherwise. The fused-silica tube was maintained at 25°C. The components were detected by UV absorbance at 214 nm. After each run the capillary was rinsed successively with 0.1 *M* NaOH and ultrapure water for 3 min each.

## RESULTS AND DISCUSSION

### *ACTH peptides (group 1, Table II)*

On applying the operational buffer systems having a neutral or basic pH (3, 4 and 5), the four peptides co-migrated. However, using the acidic buffers (1 and 2), three clearly distinguishable peaks were monitored. The peak shape in the pH 3.8 buffer was slightly better than that in the buffer of pH 2.2. Hence further experiments were performed at pH 3.8. Raising the concentration of this buffer from 20 to 50 mmol/l resulted in a baseline separation of the four peptides in 8 min. Execution of a run at an even higher buffer concentration of 100 mmol/l made it necessary to lower the applied voltage from 25 to 20 kV (prevention of excessive Joule heating: current limit 100 $\mu$A). As a result, the separation time was then 12 min. The electrophoresis patterns obtained with the pH 3.8 buffer at concentrations of 20, 50 and 100 mmol/l are shown in Fig. 1.

An even more pronounced increase in the separation time was found when $ZnSO_4$ was added to the buffer. The high ionic strength of this medium made it necessary to lower the applied voltage to 15 kV. As a result, the separation time was 24 min without an improvement in separation. The organic additives acetonitrile and methanol also proved to be ineffective; in fact, the separation decreased. Whereas in the 10% acetonitrile-containing buffer no significant increase in separation time was found, in the buffer containing 10% methanol the separation lasted 30 min. This observation is in line with the results reported by McLaughlin *et al.* [7].

In summary, a buffer of pH 3.8 with a "medium" concentration of 50 mmol/l performed best in the separation of the four ACTH peptides.

On the basis of the amino acid composition of the peptides, one can calculate the approximate charge of the peptides at a particular pH, using the $pK_a$ values of the amino acid residues [4,13]. Dividing the charge by the two-thirds power of the peptide molecular mass, one obtains an estimate of the relative electrophoretic mobility [4,14–16]. For the four ACTH peptides under investigation these relative mobilities, calculated at pH 3.8, are given in Table II, group 1.

The actual migration order of the peptides is in complete accordance with the order predicted from the estimated mobilities: in order of decreasing mobility, (11–24), (1–24), ACTH itself and finally the (1–10) peptide (Table II, group 1).

### *Org 2766 group (group 2, Table II)*

For the optimum pH of the buffers tested, similar results as for the ACTH group were obtained, *i.e.*, the best separation was achieved in the system of pH 3.8. Four of the seven peptides are clearly separated whereas the separation of the other three peptides is critical (Fig. 2A). Raising the buffer concentration from 20 to

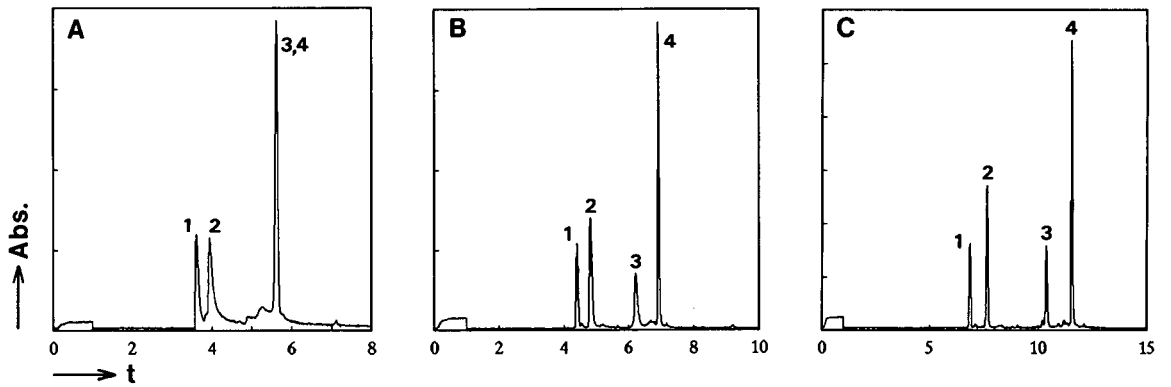


Fig. 1. CZE separation of ACTH peptides in buffer of pH 3.80. Concentration: (A) 20; (B) 50; (C) 100 m*M*. Peaks: 1 = (11–24); 2 = (1–24); 3 = (1–39); 4 = (1–10). *t* = Migration time (min); Abs. = absorbance at 214 nm.

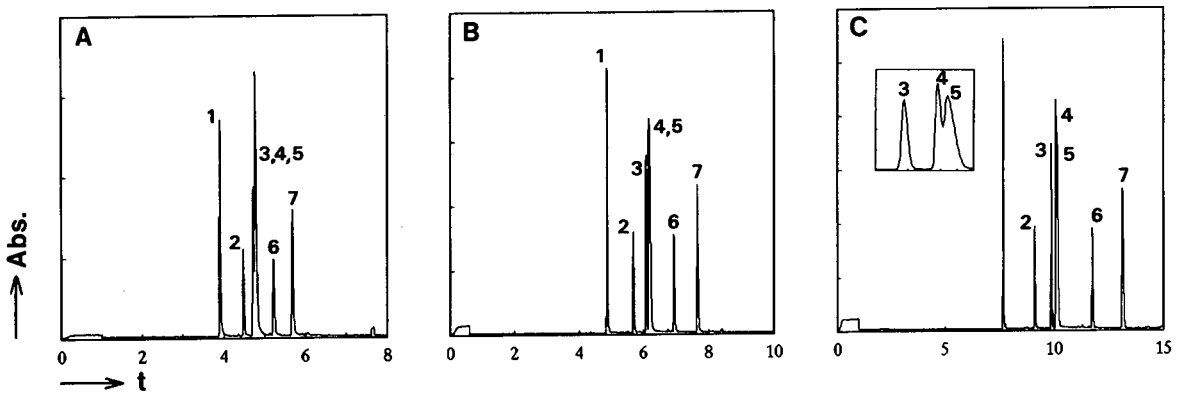


Fig. 2. CZE separation of Org 2766 peptides in buffer of pH 3.80. Concentration: (A) 20; (B) 50; (C) 100 m*M*. Peaks: 1 = (3–6); 2 = (5–6); 3 = (2–6); 4 = (1–6); 5 = (4–6); 6 = (2–6)pyroGlu; 7 = (1–3). The inset in (C) shows the actual separation of peptides 3, 4 and 5. Axes as in Fig. 1.

50 mmol/l improved the resolution: the (2–6) peptide is partly separated from the (1–6) peptide (Org 2766 itself) and the (4–6) peptide. However, the last two peptides still co-migrate (Fig. 2B). Further elevation of the buffer concentration to 100 mmol/l gave the best result, with complete separation of five of the seven peptides and partial separation of the (1–6) and (4–6) peptides (Fig. 2C). Owing to the lower voltage that had to be applied with this buffer, the separation time was 14 min. As with the ACTH peptides, the addition of $ZnSO_4$ gave no improvement in the separation (in this high ionic strength buffer, the voltage had to be lowered to 15 kV, resulting in an analysis time of 24 min). Also, the addition of 10% acetonitrile or 10% methanol was ineffective.

Summarizing these results, the buffer of pH 3.8 at a high concentration of 100 mmol/l gave the best separation.

At the applied pH of 3.8 the actual migration order of the seven peptides was again completely in line with the predicted order derived from the calculated relative electrophoretic mobilities (Table II, group 2).

*Endorphin peptides (group 3, Table II)*

We have previously reported on the separation of $\alpha$-, $\beta$- and $\gamma$-endorphin and their N-terminally shortened des-Tyr fragments [17]. With a system that was not further optimized, *i.e.*, 20 m*M* phosphate buffer (pH 2.80) at 25 kV, a clear separation of the six peptides was obtained (Fig. 3).

As a sequel to that study on closely related endorphin fragments, we investigated the separation of the neutral peptide triad $\beta$-endorphin-(6–16), -(6–15) and -(7–15). This is considered to be a severe test for the current strategy as these peptides have similar molecular masses and an identical p*I* value of 6.70. Again, the acidic buffers performed best. In this instance the most acidic buffer of pH 2.2 gave the best result, with three partially separated peaks, whereas at pH 3.8 two components co-migrated. Raising the concentration of the pH 2.2 buffer from 25 to 50

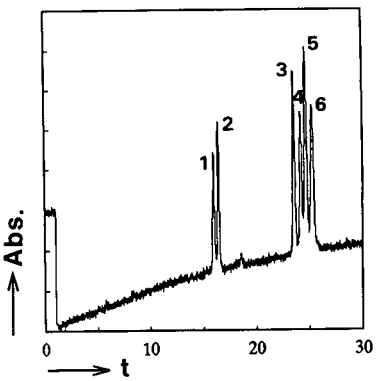


Fig. 3. CZE separation of $\alpha$-, $\beta$- and $\gamma$-endorphin and their N-terminally shortened des-Tyr fragments in buffer of pH 2.80. Peaks: 1 = des-Tyr $\beta$-endorphin, (2–31); 2 = $\beta$-endorphin, (1–31); 3 = des-Tyr $\gamma$-endorphin, (2–17); 4 = des-Tyr $\alpha$-endorphin, (2–16); 5 = $\gamma$-endorphin, (1–17); 6 = $\alpha$-endorphin, (1–16). Axes as in Fig. 1.

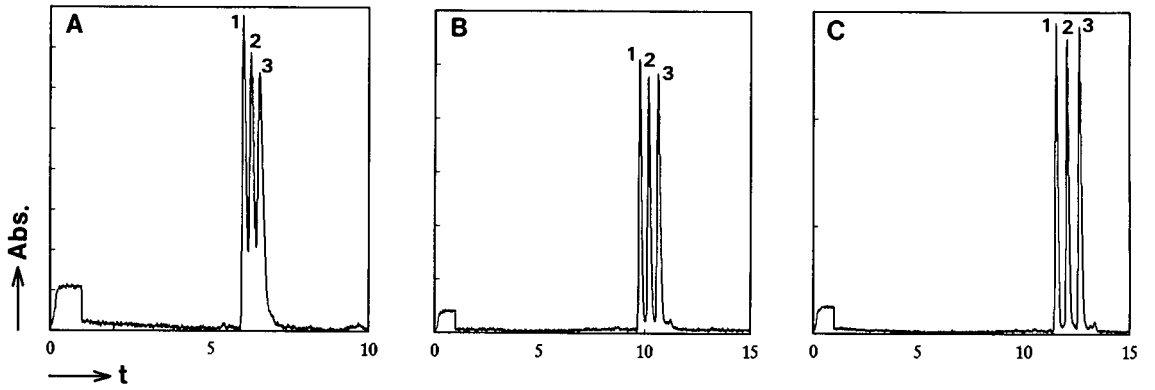


Fig. 4. CZE separation of β-endorphin fragment peptides in buffer of pH 2.20. Concentration: (A) 25; (B) 50; (C) 100 m*M*. Peaks: 1 = (7–15); 2 = (6–15); 3 = (6–16). Axes as in Fig. 1.

mmol/l resulted in a nearly baseline separation of the three peptides. As the applied voltage had to be lowered from 25 to 20 kV with the 50 mmol/l buffer, the separation time was increased by *ca.* 5 min (Fig. 4A and B). A further increase in the buffer concentration to 100 mmol/l (applied voltage again 20 kV) gave a further minor improvement of the separation (Fig. 4C). Addition of $ZnSO_4$ was ineffective, giving long migration time of 25 min (applied voltage 15 kV) and no improvement in separation. Addition of acetonitrile or methanol decreased the resolution.

In summary, for these neutral peptides the buffer of pH 2.2 at a molarity of 100 m*M* gave the best separation.

Also for these peptides the migration order found corresponded with the predicted order (Table II, group 3).

*CCK fragments (group 4, Table II)*

For the acidic CCK peptide fragments a completely different electrophoretic behaviour to that with the basic and neutral peptides was found. The low-pH buffers gave inadequate separation. However, using the neutral or basic buffers the separation improved considerably. The best result was obtained with the pH 7.50 buffer in which a reasonable separation of the five peptides was obtained (Fig. 5A). Raising the buffer concentration to 100 mmol/l further improved the peak shape, although the separation

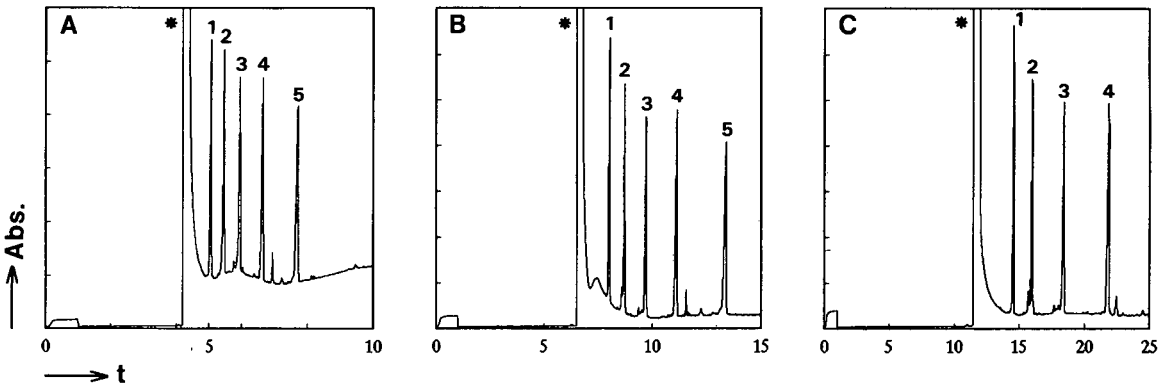


Fig. 5. CZE separation of CCK peptides in buffer of pH 7.50. Concentration: (A) 50; (B) 100; (C) 200 m*M*. Peaks: 1 = (2–8)non-S; 2 = (1–8)cyclic-S; 3 = (1–8)non-S; 4 = (2–8)S; 5 (1–8)S (S = sulphated); * = dimethylformamide (solvent constituent). Axes as in Fig. 1.

time was doubled owing to the lower voltage of 20 kV that had to be applied (Fig. 5B). At a concentration of 200 mmol/l at 15 kV, only four of the five components migrated within 25 min (Fig. 5C). Addition of $ZnSO_4$, acetonitrile or methanol to the buffer gave no improvement in separation.

Hence for these acidic peptides the neutral buffer of pH 7.5 at a "medium" concentration of 100 mmol/l performed best.

Again, the experimentally found order of migration corresponded with the calculated migration order (Table II, group 4).

## CONCLUSIONS

In the set-up of standard CZE procedures to be used in the quality control of closely related peptides, a simple strategy for obtaining adequate information is needed. In this work we investigated the parameters that may have a major impact on the separation. In line with earlier observations [5,6], the buffer pH is the most important parameter to be considered. However, it turned out that the optimum buffer pH depends strongly on the p*I* values of the peptides. Using five "standard" buffers, we found that for peptides with a basic and neutral character, the best separation is achieved in the low-pH region. Additional advantages of the low-pH buffers are the substantial reduction in the electroosmotic flow and the elimination of solute–wall interactions, resulting in a better reproducibility of the separation [18]. For peptides with an acidic character, the neutral pH region is preferred for a good separation.

After careful adjustment of the buffer pH, the second parameter to be considered for an optimum separation is the buffer concentration. In general we found that "medium" and "high" concentration buffers, *i.e.*, 50–100 mmol/l, performed best. For the peptide groups investigated, no beneficial effect on the separation was found with the buffer additives $ZnSO_4$, 10% acetonitrile or 10% methanol.

An additional guide in setting up an optimum separation is the calculation of the expected relative mobilities at a particular pH. For all the peptide groups investigated, the experimentally found migration order corresponded with the order estimated from the calculated relative mobilities. In this respect, plotting the calculated relative mobilities against the pH, as proposed by Van de Goor *et al.* [4], is a further extension of this approach. Taking the three endorphins as a representative example, such a plot is shown in Fig. 6.

In conclusion, we propose the following strategy for the rapid optimization of an adequate routine CZE analysis of closely related peptides: for basic and neutral peptides low-pH standard buffers should be tested first, and for acidic peptides the optimization should be started with buffers of neutral pH. If necessary, further improvement in the separation can be obtained by careful fine tuning of the buffer pH and/or using a higher buffer concentration. Using this strategy, CZE can be applied to the analysis of pharmaceutical peptides on a routine basis. Together with the complementary information from RP-HPLC and CITP, a valuable quality control system for these peptides may be established.

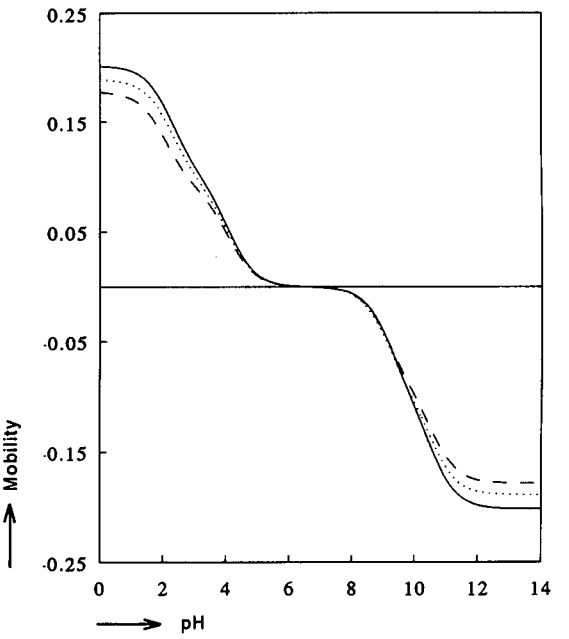


Fig. 6. Calculated relative electrophoretic mobilities over the pH range 0–14 for the three endorphin fragment peptides. Solid line, (7–15); dotted line, (6–15); dashed line, (6–16).

ACKNOWLEDGEMENTS

The authors gratefully acknowledge Professor F.M. Everaerts, Th.P.E.M. Verheggen, T.A.A.M. van de Goor and B.J. Wanders (Eindhoven University of Technology) for stimulating discussions and the use of the CAS mobility software program.

REFERENCES

1 R.G. Nielsen, R.M. Riggin and E.C. Rickard, *J. Chromatogr.*, 480 (1989) 393.
2 D. Corradini, C. Bohler and V. Brizzi, presented at the *4th International Symposium on High Performance Capillary Electrophoresis, Amsterdam, February 9–12, 1992.*
3 P.S.L. Janssen, J.W. van Nispen, M.J.M. van Zeeland and P.A.T.A. Melgers, *J. Chromatogr.*, 470 (1989) 171.
4 T.A.A.M. van de Goor, P.S.L. Janssen, J.W. van Nispen, M.J.M. van Zeeland and F.M. Everaerts, *J. Chromatogr.*, 545 (1991) 379.
5 P.D. Grossman, K.J. Wilson, G. Petrie and H.H. Lauer, *Anal. Biochem.*, 173 (1988) 265.
6 H.J. Issaq, G.J. Janini, I.Z. Atamna, G.M. Muschik and J. Lukszo, *J. Liq. Chromatogr.*, 15 (1992) 1129.
7 G.M. McLaughlin, J.A. Nolan, J.L. Lundahl, R.H. Palmieri, K.W. Anderson, S.C. Morris, J.A. Morrison and T.J. Bronzert, *J. Liq. Chromatogr.*, 15 (1992) 961.
8 H.P.J. Bennett and C. McMartin, *Pharmacol. Rev.*, 30 (1979) 247.
9 R. Gerritsen van der Hoop, C.J. Vecht, M.E.L. van der Burg, A. Elderson, W. Boogerd, J.J. Heimans, E.P. Vries, J.C. van Houwelingen, F.G.I. Jennekens, W.H. Gispen and J.P. Neijt, *N. Engl. J. Med.*, 322 (1990) 89.
10 C.H. Li (Editor), *Hormonal Proteins and Peptides, Vol. X: β-Endorphin*, Academic Press, New York, 1981.
11 P.S.L. Janssen, J.W. van Nispen, P.A.T.A. Melgers and R.L.A.E. Hamelinck, *Chromatographia*, 21 (1986) 461.
12 G.N. Woodruff, D.R. Hill, P. Bodem, R. Pinnock, L. Singh and J. Hughes, *Neuropeptides*, 19 (Suppl.) (1991) 45.
13 R.M.C. Dawson, D.C. Elliot and K.M. Jones, *Data for Biochemical Research*, Orford University Press, Oxford, 1974.
14 R.E. Offord, *Nature (London)*, 211 (1966) 591.
15 Z. Deyl, V. Rohlicek and M. Adam, *J. Chromatogr.*, 480 (1989) 371.
16 E.C. Rickard, M.M. Strohl and R.G. Nielsen, *Anal. Biochem.*, 197 (1991) 197.
17 P.S.L. Janssen, presented at the *2nd International Symposium on High Performance Capillary Electrophoresis, San Francisco, CA, January 29–31, 1990.*
18 R.M. McCormick, *Anal. Chem.*, 60 (1988) 2332.

*Journal of Chromatography*, 638 (1993) 319–326
Elsevier Science Publishers B.V., Amsterdam

CHROM. 24 950

# Analysis of pilocarpine and its *trans* epimer, isopilocarpine, by capillary electrophoresis

W. Baeyens*, G. Weiss, G. Van Der Weken and W. Van Den Bossche

*Department of Pharmaceutical Analysis, Faculty of Pharmaceutical Sciences, University of Ghent, Harelbekestraat 72, B-9000 Ghent (Belgium)*

C. Dewaele

*Bio-Rad RSL, Begoniastraat 5, B-9810 Nazareth (Belgium)*

ABSTRACT

Capillary zone electrophoresis was used for the separation of pilocarpine from its epimer, isopilocarpine, using coated fused-silica capillaries of 20 cm × 25 $\mu$m I.D., 8 kV running voltage, migration buffer of 0.1 *M* sodium dihydrogenphosphate pH 8, detection at 217 nm and injection by electromigration. Injections of aqueous, acid and basic solutions were compared. Linearity of the signal for pilocarpine hydrochloride up to 200 $\mu$g ml$^{-1}$ in 0.05 *M* hydrochloric acid was obtained, using naphazoline nitrate as internal standard. Optimization of migration buffer pH using coated silica capillaries of 50 cm × 50 $\mu$m I.D. showed that at pH 6.9 pilocarpine can be separated from isopilocarpine. Inclusion of $\beta$-cyclodextrin in the buffer allows full baseline separation of both epimers. The method was applied to the analysis of a commercial ophthalmic pilocarpine solution.

## INTRODUCTION

Pilocarpine, the parasympathomimetic principle isolated from *Pilocarpus jaborandi* (*Rutaceae*), is frequently used in ophthalmic solutions as an antiglaucoma, miotic agent. It is an imidazole-derived alkaloid containing a butyrolactone group, at which both substituents appear in the *cis* configuration. Isopilocarpine, occurring in the plant as well, is the *trans* epimer.

Pilocarpine is more stable at low than at high pH values. The two degradative reactions of pharmaceutical interest are the hydrolysis of the ester linkage of the lactone ring, resulting in pilocarpic acid, and the epimerization about the $\alpha$-carbon to isopilocarpine, which is further degraded by hydrolysis to isopilocarpic acid [1,2] (Fig. 1). Recent literature data illustrate an increased interest in the area of pilocarpine prodrugs as a means of improving ocular delivery [3–6].

The literature includes reports of several assays for pilocarpine, isopilocarpine, pilocarpic acid and isopilocarpic acid applying HPLC [7–10], analysing commercial pilocarpine preparations in which no significant contamination with the isomer isopilocarpine or the degradation products, pilocarpic acid or isopilocarpic acid, was found [11,12]. In the present study, similar conclusions can be drawn. Preliminary results on the application of capillary zone electrophoresis to the separation of pilocarpine from isopilocar-

* Corresponding author.

0021-9673/93/$06.00 

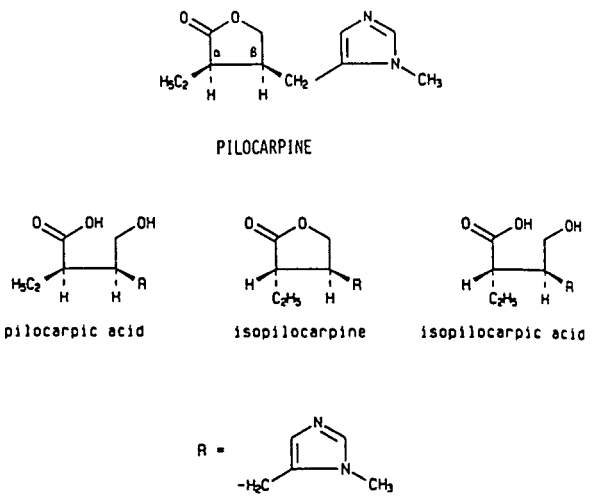


Fig. 1. Structure of pilocarpine, isopilocarpine and their hydrolysis products, pilocarpic acid and isopilocarpic acid.

pine are shown. Inclusion of β-cyclodextrin in the pH 6.9 phosphate eluent buffer using coated columns and UV detection at 217 nm allows full baseline separation of both compounds. The method could be applied to the determination of a commercial ophthalmic solution.

## EXPERIMENTAL

### *Materials and instruments*

Pilocarpine hydrochloride and isopilocarpine nitrate were obtained from Aldrich-Chemie (Beerse, Belgium), pilocarpine nitrate from Merck (Darmstadt, Germany) and naphazoline nitrate and β-cyclodextrin from Janssen Chimica (Beerse, Belgium).

Normo-glaukon, a preparation of 2% pilocarpine in the form of 10-ml sterile eyedrops (Dr. Mann Pharma, Berlin, Germany), has the following composition: pilocarpine hydrochloride 20.0 mg, metipranolol hydrochloride 1.118 mg, benzalkonium chloride, disodium EDTA, sodium chloride, dilute hydrochloric acid, water for injections up to 1 ml.

Capillary electrophoresis was performed on a HPE 100 instrument from Bio-Rad, equipped with a variable-wavelength detector. Commercial cartridges (Bio-Rad) containing fused-silica columns were used, with the following specifications: HPE Microsampler cartridge, 20 cm × 25 μm I.D., coated, and Microsampler 100 cartridge, 50 cm × 50 μm I.D., coated. Samples were injected on the anodic side by electromigration, using different loading times and voltages. A constant-voltage mode was applied for the separation of the analytical solutions. For detection, the absorbance was measured at a wavelength (λ) of 217 nm (though any wavelength between 206 and 220 nm may be used), and peak integration was performed by a Shimadzu Chromatopac C-R3A integrator system. Aqueous sodium phosphate buffer solutions were used throughout.

UV absorption spectra were taken on a Perkin-Elmer Lambda 15 double-beam UV spectrophotometer.

### *Hydrolysis*

Hydrolysis of pilocarpine nitrate and of isopilocarpine nitrate was carried out by refluxing 50 mg of each compound (0.184 mmol) for 1 h in about 30 ml of 0.1 *M* sodium hydroxide solution while stirring, followed by cooling of the reaction mixture to room temperature. Next, the solution was treated with 0.5 *M* hydrochloric acid solution to produce a final pH of 7.0, followed by dilution with water up to 50 ml. This solution, containing the hydrolysis products from an original alkaloid concentration of 1 mg $ml^{-1}$ (3.686 m*M*) is used for the UV absorptiometric and capillary electrophoretic experiments. Apart from the hydrolysed solutions of pilocarpine nitrate and of isopilocarpine nitrate, similar hydrolysis was performed on the pilocarpine hydrochloride salt, providing, as expected, completely similar analytical results.

### *Analysis of a commercial pilocarpine preparation*

The ophthalmic solution containing 20.0 mg $ml^{-1}$ pilocarpine hydrochloride solution was diluted 100-fold using 0.05 *M* hydrochloric acid and then mixed with an equal volume of the naphazoline nitrate internal standard solution (50 μg $ml^{-1}$ in 0.05 *M* hydrochloric acid). This sample solution, containing 100 μg $ml^{-1}$ pilocarpine hydrochloride and 25 μg $ml^{-1}$ naphazoline nitrate, was injected onto the column by electromigration at least three times. A standard

solution containing 100 $\mu$g ml$^{-1}$ pilocarpine hydrochloride and 25 $\mu$g ml$^{-1}$ naphazoline nitrate in 0.05 *M* hydrochloric acid was injected under similar conditions at least three times. By calculating the peak-area ratios of analyte to internal standard in both sample and standard solutions, the pilocarpine content of the eye-drops can be calculated.

## RESULTS AND DISCUSSION

As expected, the UV absorption spectra for pilocarpine and isopilocarpine are similar (pilocarpine hydrochloride, $\lambda_{max.} = 214$ nm; pilocarpine nitrate, 206–220 nm plateau; isopilocarpine nitrate, 206–220 nm plateau; all values in water). The spectra from their base-hydrolysed and neutralized solutions are similar to the parent spectra.

### *Capillary electrophoresis*

Coated fused-silica capillaries (see Experimental section) were used throughout so as to decrease electro-endosmosis.

Preliminary experiments were done using short coated columns (20 cm × 25 $\mu$m I.D.) at a detection wavelength of 206 nm for aqueous solutions of pilocarpine nitrate, isopilocarpine nitrate, naphazoline nitrate (a suitable internal standard for quantitative work) at concentrations of 50 $\mu$g ml$^{-1}$ and equal-volume mixtures of these solutions, applying a loading time of 8 s and a loading voltage of 8 kV (both values experimentally determined to be optimal), and using a 0.1 *M* phosphate buffer pH 8.0. Under these conditions, pilocarpine and isopilocarpine migrate together (about 2.0 min), being separated from the internal standard naphazoline nitrate (about 1.2 min). Reproducibility problems with respect to migration times and peak areas are solved by replacing water with 0.05–0.2 *M* hydrochloric acid as a solvent.

An explanation of the migration and peak-area reproducibility problems depending on the nature of the solution to be injected is as follows. The pilocarpine base has two p$K$ values (p$K_1$ = 7.15; p$K_2$ = 12.57, both at 20°C). On injection of aqueous solutions, pilocarpine will not be sufficiently protonated to be quantitatively loaded onto the capillary by electromigration. When the pH of the medium is reduced below 7.15, the base becomes diprotonated and the resulting ion will be easily loaded. At pH values between p$K_1$ and p$K_2$, pilocarpine is present as the monoprotonated ion, whilst in strong alkaline medium (pH > 12.57) the molecule remains in the non-ionized state. Analyses cannot be carried out starting from basic pilocarpine solutions, which was verified by injecting solutions in sodium hydroxide medium (0.02 *M* and higher), when no peaks could be seen in the electropherograms. Similar problems in quantitatively injecting samples by electromigration may occur when variable amounts of organic solvents (*e.g.* methanol) are present.

The hydrolysed and *ex tempore* acidified solutions of pilocarpine and of isopilocarpine provide an electropherogram showing two non-separated peaks (between 9 and 12 min), without any parent molecule present. When the hydrolysed solutions are acidified down to pH 1.6, in the course of time (days, room temperature) the hydrolysed fraction (non-resolved pilocarpic and isopilocarpic acids) decreases in favour of pilocarpine formation (see *Stability of pilocarpine* section).

### *Calibration curves*

Linear calibration graphs on 20 cm × 25 $\mu$m I.D. coated columns were obtained in the 0–200 $\mu$g ml$^{-1}$ range ($n = 10$) of pilocarpine nitrate in 0.05 *M* hydrochloric acid ($r = 0.9993$), using naphazoline nitrate as internal standard and applying peak-area ratio calculations. A pilocarpine detection limit of about 1 $\mu$g ml$^{-1}$ injected solution ($S/N = 2$) could be reached, though during some analyses this value unexpectedly increased at least five-fold ($\geq$5 $\mu$g ml$^{-1}$), possibly because of a decreased electromigration loading efficiency. Fig. 2 shows a typical electropherogram from pilocarpine in the presence of naphazoline. Under these conditions, isopilocarpine nitrate migrates identically to pilocarpine nitrate, which was confirmed by the addition of isopilocarpine nitrate to a mixture of pilocarpine and naphazoline, the pilocarpine peak remaining qualitatively unaltered. Changing the running buffer pH from 5.0 to 8.0 could

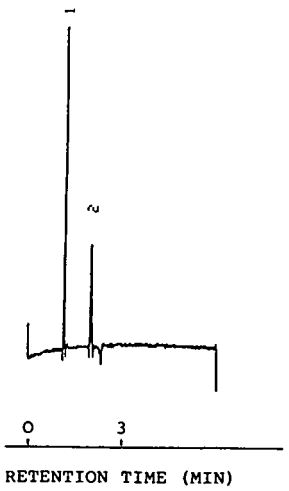


Fig. 2. Electropherogram of a mixture of pilocarpine nitrate and naphazoline nitrate (each at 25 $\mu$g ml$^{-1}$ in 0.05 *M* hydrochloric acid). Conditions: 20 cm × 25 $\mu$m I.D. coated column; loading by electromigration, 8 s at 8 kV (from + to −); running buffer, 0.1 *M* phosphate buffer pH 8.0; running voltage, 8 kV; detection at 217 nm. Peaks: 1 = naphazoline (1.15 min); 2 = pilocarpine (2.01 min).

not separate the epimers, in spite of the excellent shape and reproducible character of the obtained peaks. The present investigations indicate that the use of longer capillaries may solve this problem.

*Separation of pilocarpine and isopilocarpine*

*Influence of running buffer pH.* Mixtures of pilocarpine nitrate and isopilocarpine nitrate were injected onto a 50 cm × 50 $\mu$m I.D. coated column applying 0.1 *M* phosphate running buffer solutions with pH values between 6.7 and 7.5, based on the overall identical migration pattern of both molecules over a wider pH range: it was noticed that from pH 5.0 to pH 6.5, both molecules migrate identically (one peak when mixed). From pH 6.6 up to about pH 7.8, separation is observed, whereas at pH 8.0 and 9.0 both compounds again migrate equally. Fig. 3 illustrates the pH effect of the running buffer from pH 6.8 to 7.0. A pH value of 6.9 provides the best electropherogram, though baseline separation is not achieved. Peaks were assigned by repetitive injections of solutions of both compounds, after the addition of each component.

*Influence of running voltage.* The effect of the running voltage on the separation of pilocarpine nitrate and isopilocarpine nitrate was investigated at the optimum running buffer pH of 6.9. Fig. 4 shows the results on the migration times of both molecules for voltages between 4 and 9 kV. Based on the peak shape, a running voltage of 8 kV was chosen for further experiments. None of the applied voltages could provide a baseline separation.

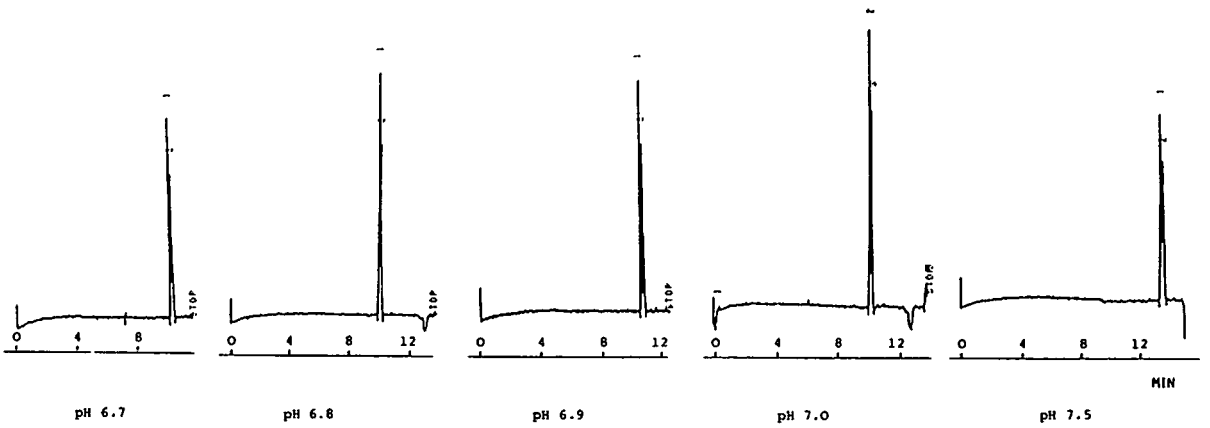


Fig. 3. Electropherogram of a mixture of pilocarpine nitrate and isopilocarpine nitrate (each at 100 $\mu$g ml$^{-1}$ in 0.05 *M* hydrochloric acid) at pH 6.7, 6.8, 6.9, 7.0 and 7.5. Conditions: 50 cm × 50 $\mu$m I.D. coated column; loading by electromigration, 8 s at 8 kV (from + to −); running buffer, 0.1 *M* phosphate buffer; running voltage, 8 kV; detection at 217 nm. Peaks: 1 = pilocarpine (10.69 min at pH 6.9); 2 = isopilocarpine (10.85 min at pH 6.9).

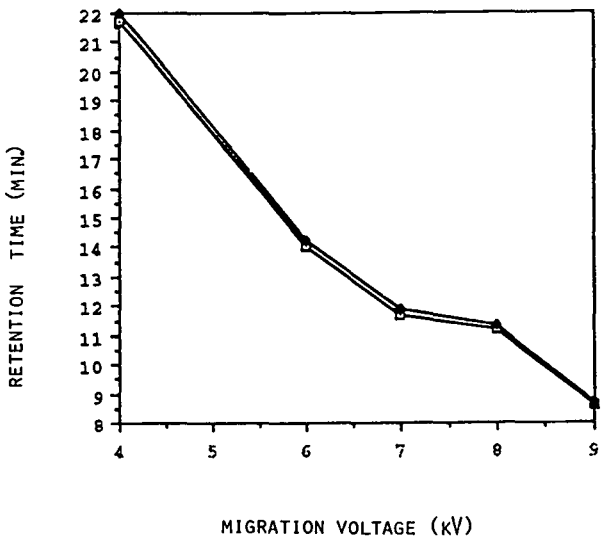


Fig. 4. Influence of migration voltage on the separation of pilocarpine nitrate (□) and isopilocarpine nitrate (◆). Conditions: see Fig. 3 (running buffer pH 6.9).

*Influence of β-cyclodextrin.* The effect of β-cyclodextrin inclusion in the buffer upon the capillary electrophoretic pilocarpine–isopilocarpine separation was investigated, based on the general use of β-cyclodextrin and similar cyclodextrins as inclusion-complexing and performance-increasing agents in chromatography, spectroscopy and capillary electrophoresis [13–15]. Mixing the pH 6.9 phosphate buffer with an equal volume of 0.02 *M* aqueous β-cyclodextrin under the optimized electrophoretic conditions yielded the electropherogram shown in Fig. 5A, providing baseline separation of the two epimers. Fig. 5B clearly shows that the separation effect is definitely caused by the presence of cyclodextrin in the buffer solution. It is assumed that the increased separation of the two alkaloids, possessing only minor stereochemical differences, is the result of a difference in their interaction with the typical conically shaped β-cyclodextrin molecule, featuring a polar outer surface and a rather non-polar internal cavity.

The influence of the concentration of β-cyclodextrin on the migration difference between both epimers is shown in Fig. 6. Apparently, increasing the β-cyclodextrin concentration of the buffer enhances the difference in the retention time of both migrating compounds. However, at a concentration of 0.03 *M* added β-cyclodextrin onwards (0.015 *M* final concentration), practical problems occur, as cyclodextrin crystallizations in the buffer are noticed. Hence, the capillary flow may be seriously hindered, in addition to the light-scattering effects encountered in the detector, resulting in unstable

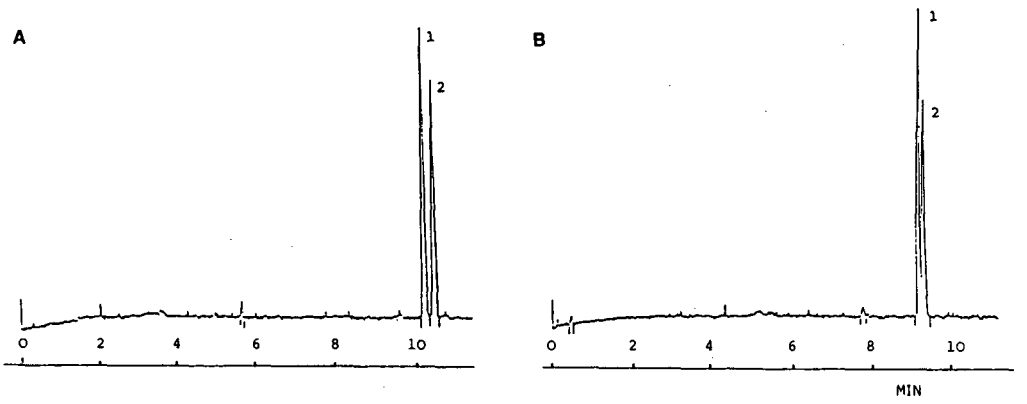


Fig. 5. (A) Electropherogram of a mixture of pilocarpine nitrate and isopilocarpine nitrate (each at 100 μg $ml^{-1}$ in 0.05 *M* hydrochloric acid). Conditions: 50 cm × 50 μm I.D. coated column; loading by electromigration, 8 s at 8 kV (from + to −); running buffer solution, 0.1 *M* phosphate buffer pH 6.9 containing β-cyclodextrin 0.01 *M*; running voltage, 8 kV; detection at 217 nm. Peaks: 1 = pilocarpine; 2 = isopilocarpine. (B) Electropherogram similar to (A), replacing the β-cyclodextrin solutions with pure water.

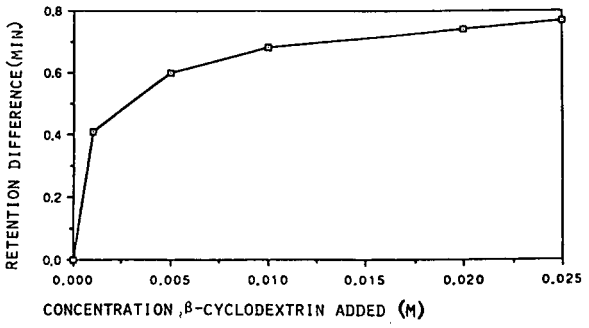


Fig. 6. Influence of β-cyclodextrin concentration on the difference in migration times between pilocarpine nitrate and isopilocarpine nitrate. Conditions as in Fig. 5A with varying β-cyclodextrin concentrations.

baselines. For these reasons, an optimum final β-cyclodextrin concentration of 0.01 *M* was chosen. Peak assignment in the optimized separating system was carried out by injecting mixtures of both alkaloids at different concentrations.

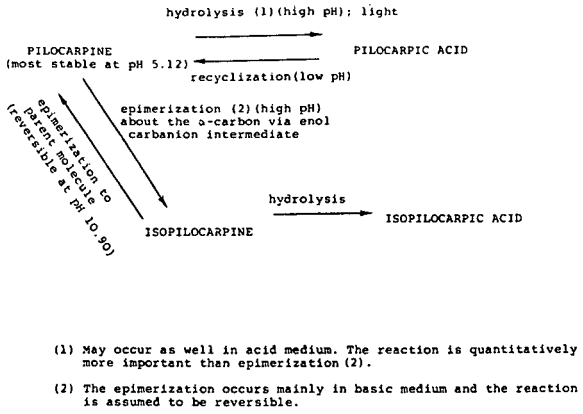


Fig. 7. Chemical stability of pilocarpine and general decomposition reactions [2].

*Stability of pilocarpine*

A previous report on the chemical stability of pilocarpine [2] states that the hydrolysis of the ester linkage of pilocarpine occurs much faster than the epimerization in alkaline medium. The epimerization reaction of pilocarpine is reversible at pH 10.90. Pilocarpine and isopilocarpine are susceptible to hydrolysis to the same extent at pH 10.90; the hydrolysis reaction of isopilocarpine is probably irreversible in either acid or basic medium. A general scheme on pilocarpine stability is given in Fig. 7.

The fact that pilocarpine is more stable at lower than at higher pH values, with maximum stability at pH 5.12, should be taken into account, *e.g.*, when preparing ophthalmic solutions. In the present study, some useful data on pilocarpine decomposition reactions were obtained. Fig. 8 shows the electropherogram of base-hydrolysed pilocarpine nitrate, adjusted to pH 1.6 and analysed after 1 day and 1 week standing at room temperature. Both electropherograms indicate that pilocarpine nitrate is transformed during the alkaline hydrolysis to isopilocarpine nitrate and hydrolysate. Note that pilocarpic and isopilocarpic acids cannot be separated under the given conditions. When considering peak areas of the different peaks, it could be demonstrated that after 1 week at pH 1.6 the

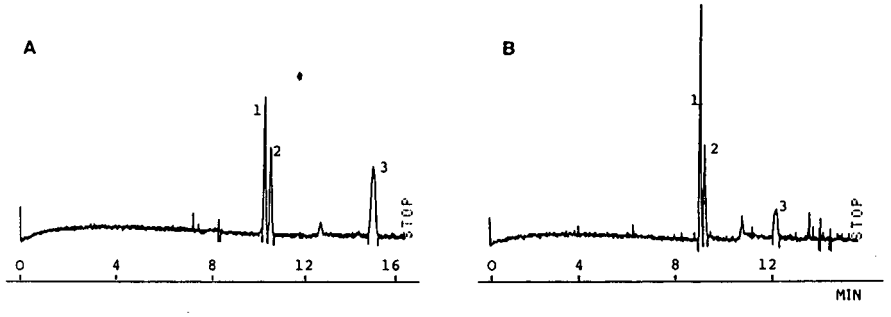


Fig. 8. Electropherogram of base-hydrolysed pilocarpine nitrate (150 μg $ml^{-1}$), adjusted to pH 1.6 and injected after 1 day (A) and 1 week (B) standing at room temperature. Conditions: see Fig. 5A; detection at 217 nm. Peaks: 1 = pilocarpine; 2 = isopilocarpine; 3 = hydrolysate peak.

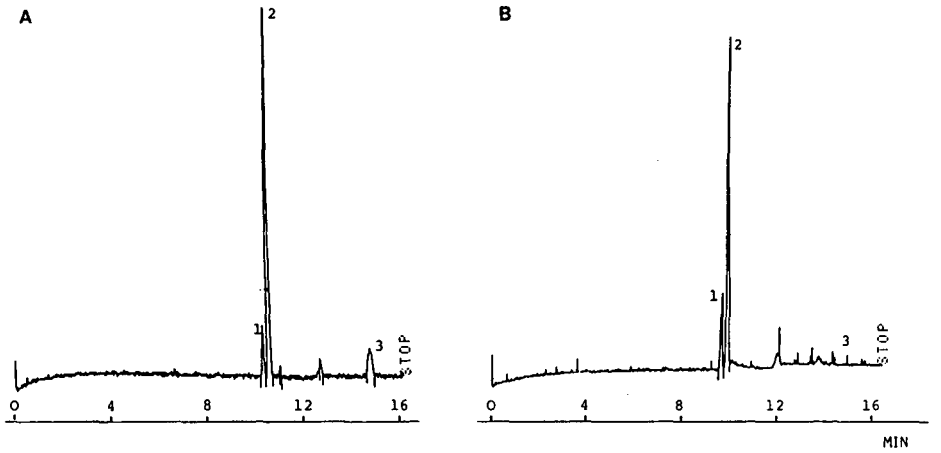


Fig. 9. Electropherogram of base-hydrolysed isopilocarpine nitrate (150 $\mu$g ml$^{-1}$), adjusted to pH 1.6 and injected after 1 day (A) and 1 week (B). Conditions: see Fig. 5A; detection at 217 nm. Peaks: 1 = pilocarpine; 2 = isopilocarpine; 3 = hydrolysate peak (with adjusted integrator attenuation).

(total) acids peak had markedly decreased in favour of a strongly increased pilocarpine nitrate peak. It is assumed that pilocarpic acid is converted into pilocarpine in acid medium. As isopilocarpic acid is not converted to isopilocarpine, the area of the iosopilocarpine nitrate peaks nearly remains unchanged. The same phenomenon could be seen with base-hydrolysed isopilocarpine nitrate, of which the alkaline hydrolysis solution was adjusted to pH 1.6. The obtained electropherograms are illustrated in Fig. 9. Again, three peaks are seen, those of pilocarpine nitrate, isopilocarpine nitrate and the acids. With time, the last peak decreases in favour of pilocarpine nitrate, the isopilocarpine nitrate peak remaining constant. The results of

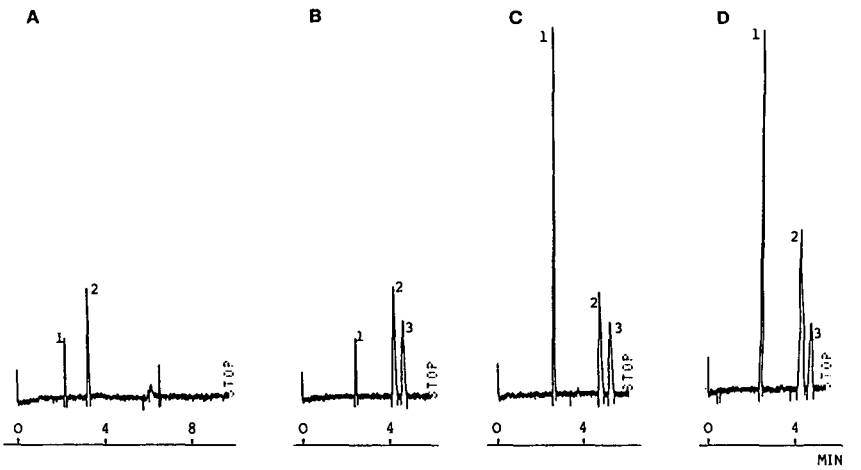


Fig. 10. Electropherograms of solutions of pilocarpine hydrochloride (200 $\mu$g ml$^{-1}$) and naphazoline nitrate (25 $\mu$g ml$^{-1}$) in 0.05 *M* hydrochloric acid (A), to which are subsequently added +4 mg of isopilocarpine nitrate per 20 ml (= 200 $\mu$g ml$^{-1}$ final concentration) (B), +4 mg of naphazoline nitrate (C), and +4 mg of pilocarpine hydrochloride (D). Peaks: 1 = naphazoline; 2 = pilocarpine; 3 = isopilocarpine. Conditions: 20 cm × 25 $\mu$m I.D. coated column; loading by electromigration, 8 s at 8 kV (from + to −); running buffer, 0.1 *M* phosphate buffer pH 6.9 containing 0.01 *M* $\beta$-cyclodextrin; running voltage, 8 kV; detection at 217 nm.

the electrophoretic experiments could be confirmed by TLC experiments, a technique that clearly offers poorer resolving capacity than capillary electrophoresis.

*Analysis of a commercial pilocarpine preparation*

The relative standard deviation of six replicate standard injections was 1.04%. Calibration standard solutions were prepared such that a range of 80–120% of the concentration claimed on the label was covered. A plot of the peak-area ratios of pilocarpine–naphazoline (internal standard) *versus* the amount of pilocarpine in the standard solutions was linear ($r = 0.9995$). The results of the quantitation, calculated for six independently prepared commercial sample solutions, were 101.3% (R.S.D. = 1.43%) with respect to the label claim. It is assumed that the coefficient of variation can be lowered when applying a non-electromigration loading system. Fig. 10 shows the electropherograms, with peak assignment, obtained from standard solutions, indicating the absence of isopilocarpine, which is baseline separated in the electropherogram provided by this system. Fig. 11 shows the electropherogram from the sample solution. As can be seen, the metipranolol peak does not interfere with the peaks of interest. No other pilocarpine decomposition peaks can be identified in the sample solution.

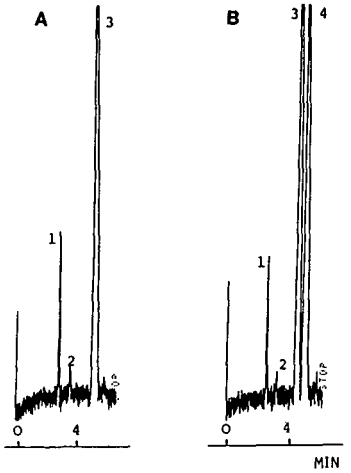


Fig. 11. Electropherogram of a sample solution of the eyedrop preparation (A) and of the same solution after the addition of isopilocarpine nitrate (B). Conditions as for Fig. 8 (with adjusted integrator attenuation). Peaks: 1 = naphazoline; 2 = metipranolol (confirmed by injecting 5 $\mu$g ml$^{-1}$ standard solutions); 3 = pilocarpine; 4 = isopilocarpine.

In conclusion, pilocarpine can be separated from its epimer isopilocarpine by applying capillary electrophoresis on coated columns using a 0.1 *M* phosphate buffer pH 6.9 and UV detection; the inclusion of $\beta$-cyclodextrin in the buffer allows baseline separations. The method allows quantitative analysis of a commercial ophthalmic preparation using naphazoline as an internal standard. The suggested system opens up the possibility of further analytical research on the chemical stability testing of pilocarpine and related alkaloids.

REFERENCES

1 *The Merck Index*, Merck, Rahway, NJ, 11th ed., 1989, p. 7395.
2 K.A. Connors, G.L. Amidon and V.J. Stella (Editors), *Chemical Stability of Pharmaceuticals*, Wiley, New York, 2nd ed., 1986, pp. 675–684.
3 T. Järvinen, S. Auriola, P. Peura, P. Suhonen, A. Urtti and J. Vepsäläinen, *J. Pharm. Biomed. Anal.*, 9 (1991) 457.
4 T. Järvinen, P. Suhonen, H. Naumanen, A. Urtti and P. Peura, *J. Pharm. Biomed. Anal.*, 9 (1991) 737.
5 T. Järvinen, P. Suhonen, S. Auriola, J. Vepsäläinen, A. Urtti and P. Peura, *Int. J. Pharm.*, 75 (1991) 249.
6 T. Järvinen, P. Suhonen, A. Urtti and P. Peura, *Int. J. Pharm.*, 75 (1991) 259.
7 T. Urbanyi, A. Piedmont, E. Willis and G. Manning, *J. Pharm. Sci.*, 65 (1976) 257.
8 J.D. Weber, *J. Assoc. Off. Anal. Chem.*, 59 (1976) 1409.
9 A. Noordam, K. Waliszewski, C. Olieman, L. Maat and H.C. Beyerman, *J. Chromatogr.*, 153 (1978) 271.
10 J.J. O'Donnell, R. Sandman and M.V. Drake, *J. Pharm. Sci.*, 69 (1980) 1096.
11 A. Noordam, L. Maat and H.C. Beyerman, *J. Pharm. Sci.*, 70 (1981) 96.
12 M.V. Drake, J.J. O'Donnell and R.P. Sandman, *J. Pharm. Sci.*, 71 (1982) 358.
13 W.R.G. Baeyens, B. Lin Ling, P. De Moerloose, B. del Castillo and C. De Jonge, *An. Real Acad. Farm. (Madrid)*, 54 (1988) 698.
14 H. Nishi, T. Fukuyama and S. Terabe, *J. Chromatogr.*, 553 (1991) 503.
15 V. Schurig and S. Mayer, in P. Sandra and M.L. Lee (Editors), *Proceedings of the XIVth International Symposium on Capillary Chromatography*, Foundation for the International Symposium on Capillary Chromatography, FL, 1992, p. 587.

*Journal of Chromatography*, 638 (1993) 327–334
Elsevier Science Publishers B.V., Amsterdam

CHROM. 24 952

# Optimization of phenylthiohydantoinamino acid separation by micellar electrokinetic capillary chromatography

Massimo Castagnola*, Diana Valeria Rossetti, Loredana Cassiano, Rita Rabino, Giuseppina Nocca and Bruno Giardina

*Istituto di Chimica e di Chimica Clinica, Facoltà di Medicina e Chirurgia "A. Gemelli", Università Cattolica, e/o Centro di Studio per la Chimica dei Recettori e delle Molecole Biologicamente Attive, CNR, Largo F. Vito 1, 00168 Rome (Italy)*

ABSTRACT

Optimization of phenylthiohydantion (PTH)-amino acid separation by micellar electrokinetic capillary chromatography was achieved by the use of a weighted variable-size simplex algorithm. The optimization procedure concerned the pH of the aqueous buffer, the sodium dodecyl sulphate concentration and the percentage of organic solvent; the organic solvent used was either methanol or acetonitrile. In both instances the optimization procedure led to very similar final experimental conditions and migration order and times of the PTH-amino acids, showing that the organic solvent probably provides a better polydispersity of the micellar phase. The elution pattern observed in the two instances suggests that ionic interactions and polar repartition play a role in the separation mechanism, but other types of interaction cannot be excluded.

## INTRODUCTION

Micellar electrokinetic capillary chromatography (MECC) is a separation technique, deriving from capillary electrophoresis (CE), that allows very sensitive analysis [1,2]. The use of sodium dodecyl sulphate (SDS) in the separation buffer at a concentration higher than its critical micellar concentration (CMC) generates a biphasic system: the aqueous phase migrates towards the cathode because of the electro-osmotic flow and can be considered as the chromatographic mobile phase; the micellar phase, moving towards the anode owing to its negative charge, can be regarded as a pseudo-stationary phase. Solutes are separated as a function of their different thermodynamic interactions with the two pseudo-phases, such as an electro-driven chromatographic separation.

The molecular mechanism is complex, as many forces such as ionic or polar interactions play an important role in the separation [1,2]. Further, the improvement of the separation and the selectivity also depend on the presence of an organic solvent and on the pH of the aqueous phase, all these experimental parameters being connected with each other. In spite of this complex experimental picture, the separation capacity of MECC is interesting, because in a few minutes it allows the detection of analytes at a sensitivity in the femtomole ($10^{-15}$ mol) range.

This study was devoted to the MECC separation of phenylthiohydantoin (PTH)-amino acids. The reliable detection of these derivatives in the low femtomole range could represent a real improvement in manual and automatic sequencing strategies (of almost three orders of magnitude), as LC methods show a sensitivity at the low picomole level. Some workers [3,4] have demonstrated that a sensitive separation of PTH-amino acids is obtainable by MECC.

* Corresponding author.

0021-9673/93/$06.00 

The possibility of varying several experimental parameters permits a useful manipulation of the selectivity of the separation, but this is accompanied by long and tedious attempts to find the optimum separation parameters. As the theory of MECC separation is complex and a prediction on the basis of the thermodynamics of the system is impossible, we adopted for the optimization of the separation of PTH-amino acids a weighted variable-size simplex algorithm, which explores the parameter range without requiring information on the physics of the separation system or the behaviour of any individual solute. The simplex optimization was applied to three experimental parameters: the pH of the aqueous buffer, the percentage of organic solvent in the separation buffer and the concentration of SDS.

## EXPERIMENTAL

### *Materials*

All common reagents were of analytical-reagent grade purchased from Carlo Erba (Milan, Italy) or Merck (Darmstadt, Germany). SDS was obtained from Merck, the PTH-amino acid standards used were the PTH-amino acids standard kit from Pierce (Rockford, IL, USA) or the PTH-amino acids standard, complete, from Sigma (St. Louis, MO, USA). Methanol and acetonitrile were of HPLC grade from Baker (Deventer, Netherlands) and were used as received. All aqueous buffers, prior to the CE separation, were filtered through 0.2-$\mu$m flowpore FN filters obtained from Flow Labs. (McLean, VA, USA).

### *Methods*

The CE experiments were performed using a Beckman (Palo Alto, CA, USA). P/ACE 2000 system. The PTH-amino acids were dissolved in methanol or acetonitrile so as to give a 0.2 mmol/l concentration of each PTH-amino acid; a small increase in the concentration of a single PTH-amino acid in the complete mixture was used for the final identification of PTH-amino acids. Prior to injection, the mixture of PTH-amino acids was diluted 1:1 (v/v) with the separation buffer. The capillary used was the standard capillary provided by Beckman in the cartridge; its dimensions were 56.5 cm total length, 50.0 cm to the detection window and 75 $\mu$m I.D. The sample injection, unless stated otherwise, was always performed by pressure, with a time ranging from 1 to 5 s. The wavelength of detection was 254 nm. The compositions of the solutions are described in the Results section; the aqueous buffer used was sodium phosphate (40 mmol/l)–sodium tetraborate (10 mmol/l) adjusted to the desired pH value in the experiment. The SDS concentration and the percentage of organic solvent used are described in the Results section. Unless stated otherwise the MECC separation was performed at 35°C and at a constant voltage of 18 kV.

### *Weighted variable-size simplex algorithm*

As described in the Introduction, the parameters (or coordinates or factors) studied in the optimization algorithm were the pH of the aqueous buffer, the percentage of organic solvent and the concentration of SDS. The choice of these three factors was made on the basis of preliminary experiments (not reported), which demonstrated that these are the major factors responsible for modulation of the selectivity of the separation of PTH-amino acids. The efficiency of the MECC separation was analysed, as usual, in terms of the mean resolution, $R_{s_m}$; the resolution $R_s$ between two peaks, as is well known, is defined as

$$R_s = 2(t_2 - t_1)/(w_2 + w_1)$$

where $t_2$ and $t_1$ are the elution times measured at the maximum peak height and $w_1$ and $w_2$ are the peak widths measured at the peak base. If the separation allows the detection of $n$ peaks, the mean resolution, $R_{s_m}$ can be calculated as:

$$R_{s_m} = \frac{\sum_{z=2}^{z=n} 2(t_z - t_{z-1})/(w_z + w_{z-1})}{L - 1}$$

where $L$ corresponds to the total number of substances under analysis (in this instance the 20 PTH-amino acids). In general, care must be taken in the use of this parameter as a general representation of the efficiency of separation as (hypothetically in some instances) a better $R_{s_m}$ can be obtained in a chromatogram with a small number of peaks, $n$, less than the number of

substances, $L$, under analysis. As the final optimization procedure should offer a chromatogram in which each substance is resolved from any other, accurate control of the calculated $R_{s_m}$ should be exercized in any step of the simplex algorithm to avoid erroneous interpretations of the response of a factorial point.

The simplex optimization strategy starts from a minimum number of initial experiments established as $k + 1$, where $k$ represents the number of experimental factors that are explored [5]. Here, as the experimental factors under study were the pH of aqueous buffer, the SDS concentration and the percentage of organic solvent (three factors), a minimum of four starting experiments were required, organized, in the space defined by each parameter, as the four vertices (corners) of a tetrahedron. After a measure of the response of the experiments, in the fixed-size simplex algorithm, the worst vertex $W$ was eliminated and a new vertex is generated by a reflection $R$:

$$R = P + (P - W)$$

obtained by extending the line segment $WP$ beyond $P$ by the operation where $P$ is the centroid of the face defined by the three vertices of the tetrahedron remaining when $W$ is eliminated from the starting simplex [5]. The response of the new vertex $R$ of the tetrahedron is established and the elimination of the new worst vertex is the second step of the algorithm, and so on through further new steps until an optimum response or a complete separation is obtained. This strategy presents some disadvantages that can be summarized as follows: (i) it is impossible to reduce the dimensions of the tetrahedron from the starting ones; (ii) a local optimum may be the final result; (iii) little insight into the response surface is obtained; and (iv) the centroid $P$ is obtained by considering the three vertices of the face with the same experimental statistical weight.

Disadvantage (i) obliges one to choose a small starting tetrahedron with a subsequent large number of experiments required for the optimization. An effective solution to this problem was first described by Nelder and Mead [6] and makes use of other operations besides the reflections, such as contractions or expansions. This is called a variable-size simplex algorithm and these movements in the parameter space were adopted in our optimization strategy. It is difficult to eliminate disadvantage (ii); a possibility for finding the global optimum instead of a local optimum is to restart the simplex procedure from different sets of initial factor points and to verify if the same final result is obtained; however, this is in conflict with the large number of experiments required for the total optimization process; in any event, it is impossible, at the end of the optimization procedure by the simplex algorithm, to have the assurance that the global optimum is the final result. Disadvantage (iii) was in part avoided by starting the experiments with an initial scouting factorial design that allowed a partial exploration of the parameter space (see Results). Finally, disadvantage (iv) can increase the number of experiments necessary to reach the optimum; it was partly corrected for by calculating the centroid $P$ not as the simple mean of the values of each factor under study, but by considering in the mean each point with a statistical weight proportional to its response. In fact, the coordinates (factors) of a vertex in the parameter space can be defined as $a_v, b_v, c_v, \ldots, k_v$. The coordinates of the $k + 1$ vertices chosen in the starting set of experiments can be organized in the array

$$(V) = \begin{matrix} a_1 & b_1 & c_1 & \cdots & k_1 \\ a_2 & b_2 & c_2 & \cdots & k_2 \\ a_3 & b_3 & c_3 & \cdots & k_3 \\ \vdots & \vdots & \vdots & & \vdots \\ a_k & b_k & c_k & \cdots & k_k \\ a_{k+1} & b_{k+1} & c_{k+1} & \cdots & k_{k+1} \end{matrix}$$

which can be ordered in the rows from the best to the worst response; in this instance the vertex that must be eliminated during the simplex strategy is that corresponding to the $(k + 1)$th row. Then, in normal simplex algorithm, the coordinate $i_p$ of the centroid $P$ for a general factor (array column) can be obtained by the mean

$$i_p = \frac{\sum_{z=1}^{z=k} i_z}{k}$$

In this mean, any vertex used to calculate the

coordinates of the centroid $P$ has the same statistical weight. We preferred to define a weighted centroid $P_w$ obtained as follows after calculation of $R_{s_m}$, a statistical weight for any row $j$ of the matrix was established as

$$sw(j) = \frac{R_{s_m}(j)}{\sum_{z=1}^{z=k} R_{s_m}(z)}$$

and the weighted coordinates of the centroid $P_w$ were established as

$$i_p = \sum_{z=1}^{z=k} i(z)sw(z)$$

The centroid $P_w$ is then used in substitution of $P$ for the common operations suggested by Nelder and Mead [6] in the variable-size simplex algorithm, which are:

(Reflection) $R = P_w + (P_w - W)$

(Expansion) $E = R + (P_w - W)$

(Contraction towards reflection) $C_r = P_w + [(P_w - W)/2]$

(Contraction towards worst res.) $C_w = P_w - [P_w - W)/2]$

## RESULTS

The initial set of experiments chosen to explore the parameter space is reported in Table I. It was initially established that reasonable ranges for the three parameters under optimization were as follows:

(a) A pH range of the aqueous buffer ranging from 7.00 to pH 9.50. The lowest limit was established to ensure always an acceptable electroosmotic flow and the highest value was fixed so as to avoid instability of PTH-amino acids at high pH values.

(b) The limits of SDS concentration were established as 30 and 60 mmol/l, respectively: the lowest limit to ensure a sufficient total concentration of the micellar phase and the highest to avoid too high an ionic strength and a consequent too high current during the separation, for the purpose of maintaining a constant voltage of 18 kV. A constant voltage is essential when using $R_{s_m}$ as an index of the separation performance; in fact, $R_{s_m}$ is directly linked to the applied voltage. Further, too high an SDS concentration can easily generate capillary obstructions.

(c) The limits of the percentage of organic solvent were established as 10 and 40% (v/v), respectively. Less than 10% of organic solvent strongly reduces the resolution, whereas greater than 40% strongly reduces the electroosmotic flow.

### *Organic solvent methanol*

As shown in Table I, the best response among the four scouting vertices was observed for the point B, where an $R_{s_m}$ about twice than at any other point was obtained. The low resolution of the points A, C, D suggests that their conditions are probably far from a local or a global optimum. For this reason, the simplex strategy was started from the conditions of point B. The initial experimental design was prepared by

TABLE I

SCOUTING EXPERIMENTS FOR THE OPTIMIZATION

Organic solvent: methanol.

| Vertex | pH | SDS (m*M*) | Methanol (%) | *n* (No. of peaks) | $R_{s_m}$ |
|---|---|---|---|---|---|
| A | 9.50 | 30 | 10 | 12 | 2.36 |
| B | 7.00 | 30 | 10 | 14 | 6.10 |
| C | 7.00 | 30 | 40 | 9 | 3.63 |
| D | 7.00 | 60 | 10 | 12 | 3.74 |

considering a variation of 0.5 pH unit in the aqueous buffer, a 5% variation in the concentration of methanol and a 5 mmol/l variation in the SDS concentration.

The starting tetrahedron (or factorial design) was obtained by fractional replication and is shown in Table II. From this starting tetrahedron, a series of simplex movements in the parameter space were performed and they are also reported in Table II. The optimization continued to the eleventh step, which must be considered as the final step as the next movement is very close to the previous conditions.

In Fig. 1 the MECC separation of PTH-amino acids obtained at the eleventh step of the optimization is shown, in Fig. 2 the performance obtained at any step is reported and in Fig. 3 the conditions used in the steps of the optimization are reported. The conditions of the eleventh step are pH 7.27, 9% methanol and 34.8 mmol/l SDS. The number of resolved peaks is 18, as the pairs PTH-gln–PTH-gly and PTH-met–PTH-val migrate as a unique peak.

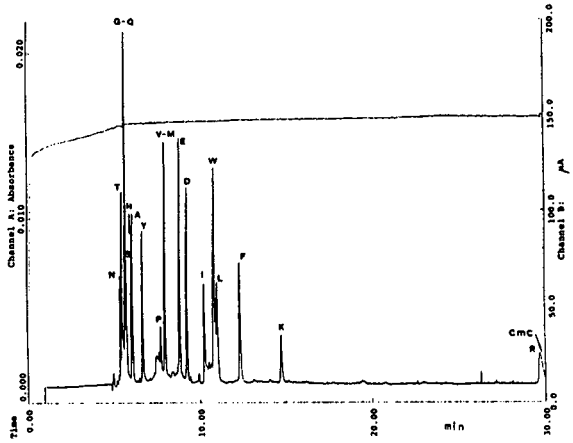


Fig. 1. MECC separation of the PTH-amino acids (the one-letter code is utilized; CmC = carboxymethyl cysteine) obtained at the eleventh step of the optimization using methanol as organic solvent.

*Organic solvent acetonitrile*

The optimization of the separation (of PTH-amino acids using acetonitrile instead of methanol is reported in Table III. In this instance the good resolution observed using the conditions of the starting four scouting vertices suggested performing the optimization starting from these conditions. The separation of the PTH-amino acids obtained at the tenth step of the optimization is shown in Fig. 4.

The performance of the optimization, represented in Fig. 5, showed a serious decrease in the performance at the fifth step, the first after the scouting experiments. The separation was so bad that a definition of $R_{s_m}$ and of the number of the peaks was impossible. The next step restored acceptable separation conditions. The optimiza-

TABLE II

VARIABLE-SIZED WEIGHTED SIMPLEX OPTIMIZATION

Organic solvent: methanol.

| Vertex | pH | Methanol (%) | SDS (m$M$) | $n$ (No. of peaks) | $R_{s_m}$ | Rejected vertex | Simplex operation[a] |
|---|---|---|---|---|---|---|---|
| 1 | 7.00 | 10.0 | 30.0 | 14 | 6.10 | – | Start 1 |
| 2 | 7.50 | 10.0 | 35.0 | 13 | 10.98 | – | Start 2 |
| 3 | 7.00 | 15.0 | 35.0 | 10 | 2.67 | – | Start 3 |
| 4 | 7.50 | 15.0 | 30.0 | 13 | 7.43 | – | Start 4 |
| 5 | 7.76 | 8.0 | 29.4 | 14 | 6.46 | 3 | $R$ |
| 6 | 8.14 | 12.0 | 34.0 | 15 | 6.29 | 1 | $R$ |
| 7 | 7.85 | 11.5 | 33.0 | 14 | 6.05 | 1 | $C_r$ |
| 8 | 7.28 | 10.5 | 31.0 | 14 | 9.98 | 1 | $C_w$ |
| 9 | 7.05 | 14.9 | 35.0 | 13 | 5.93 | 5 | $R$ |
| 10 | 7.22 | 13.2 | 33.6 | 15 | 7.01 | 9 | $C_w$ |
| 11 | 7.27 | 9.0 | 34.8 | 18 | 11.76 | 4 | $C_r$ |

[a] The symbols used for the simplex operations are explained under *Weighted variable-size simplex algorithm.*

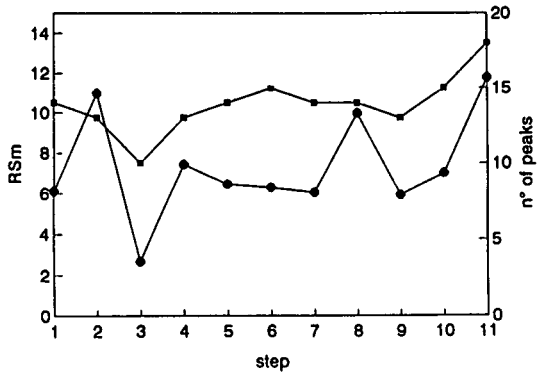


Fig. 2. (●) Mean resolution and (■) number of peaks obtained through the optimization of the separation of PTH-amino acids using methanol as organic solvent.

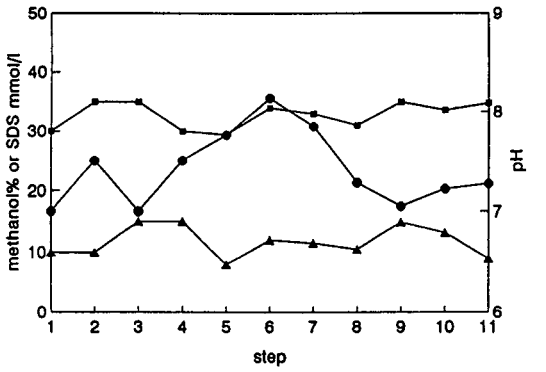


Fig. 3. Experimental conditions utilized through the optimization of the separation of PTH-amino acids using methanol as organic solvent. ▲ = Methanol (%); ■ = SDS (mmol/l); ● = pH.

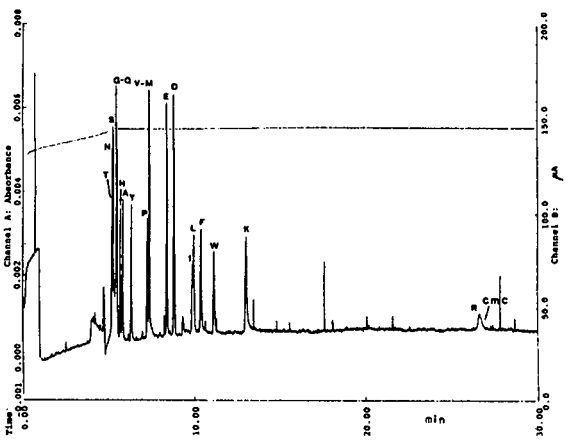


Fig. 4. MECC separation obtained at the tenth step of the optimization using acetonitrile as organic solvent.

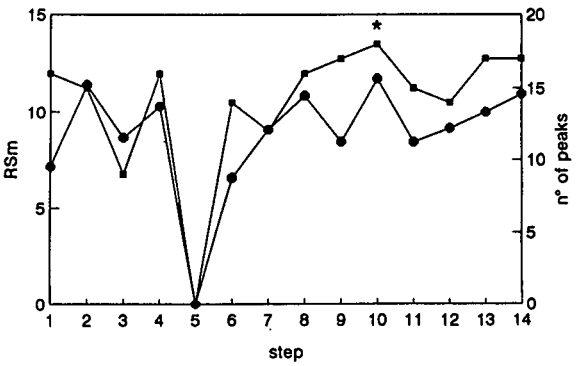


Fig. 5. (●) Mean resolution and (■) number of peaks obtained through the optimization of the separation of PTH-amino acids using acetonitrile as organic solvent. The asterisk indicates the best step.

tion reached its maximum at the tenth step, where a pH of 7.09, an acetonitrile concentration of 10.2% and an SDS concentration of 33.0 mmol/l were utilized; in further steps the optimization lead to a stabilization of the pH and of the acetonitrile percentage, as shown in Fig. 6, and further increases in the SDS concentration resulted in a decrease in performance. Also, with the use of acetontrile a separation of 18 peaks was the best performance and a close agreement of the migration order of the PTH-amino acids with that obtained using methanol as organic solvent was observed.

With the exception of the fifth step, a better mean resolution was obtained with the use of acetonitrile. For this reason, using the conditions of the tenth point, a change in the applied voltage and the temperature of the capillary was attempted, with the aim of verifying whether a further increase in resolution was possible. As shown in Figs. 7 and 8, a change in either the voltage or the temperature resulted in a decrease in $R_{s_m}$ and did not give a complete separation of all 20 PTH-amino acids.

## DISCUSSION

The optimization procedure adopted seems to represent an efficient way to find the optimum conditions for MECC separation. Whereas the usual variable-size simplex algorithm reaches an optimum response after about 20–30 steps, the

TABLE III

VARIABLE-SIZED WEIGHTED SIMPLEX OPTIMIZATION

Organic solvent: acetonitrile.

| Vertex | pH | Acetonitrile (%) | SDS (m*M*) | *n* (No. of peaks) | $R_{s_m}$ | Rejected vertex | Simplex operation[a] |
|---|---|---|---|---|---|---|---|
| 1 | 9.50 | 10.0 | 30.0 | 16 | 7.13 | – | Start 1 |
| 2 | 7.00 | 10.0 | 30.0 | 15 | 11.42 | – | Start 2 |
| 3 | 7.00 | 40.0 | 30.0 | 9 | 8.63 | – | Start 3 |
| 4 | 7.00 | 10.0 | 60.0 | 16 | 10.30 | – | Start 4 |
| 5 | 7.27 | 25.0 | 35.0 | Not acceptable | Not acceptable | 3 | $C_w$ |
| 6 | 7.40 | 17.5 | 37.4 | 14 | 6.57 | 5 | $C_w$ |
| 7 | 7.47 | 13.7 | 38.5 | 12 | 9.05 | 6 | $C_w$ |
| 8 | 7.50 | 11.1 | 39.1 | 16 | 10.86 | 7 | $C_r$ |
| 9 | 6.03 | 10.2 | 48.0 | 17 | 8.41 | 1 | $C_r$ |
| 10 | 7.09 | 10.2 | 33.0 | 18 | 11.75 | 9 | $C_w$ |
| 11 | 7.26 | 10.6 | 20.5 | 15 | 8.40 | 4 | $C_r$ |
| 12 | 7.22 | 10.5 | 27.1 | 14 | 9.13 | 11 | $C_w$ |
| 13 | 7.20 | 10.4 | 30.4 | 17 | 9.98 | 12 | $C_w$ |
| 14 | 7.19 | 10.4 | 32.0 | 17 | 10.95 | 13 | $C_w$ |

[a] The symbols used for the simplex operations are explained under *Weighted variable-size simplex algorithm.*

weighed procedure adopted seems to reach the same result after about 10–15 steps [7]; the determination of the coordinates of the point *P* is the crucial operation in the performance of the simplex algorithm. When a numerical value of the separation response is available, such as $R_{s_m}$ in this study, a choice of the coordinates of the point *P* proportionally near to the best response should offer a fast approach to optimum conditions [7]. Further studies are in progress on a rigorous comparison between the performances of the different simplex optimization procedures.

Comparison of the two optimization paths (with methanol and acetonitrile) led to surprising results: the paths are very different in the step performance, showing that the behaviour of MECC is sensitively dependent on the solvent. With respect to $R_{s_m}$, the two solvents show comparable performance, but surprisingly the two optimization procedures, starting from dif-

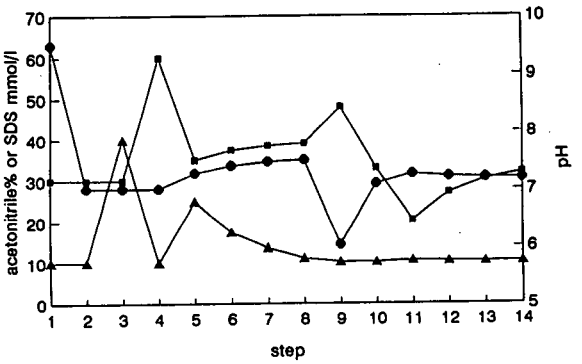


Fig. 6. Experimental conditions utilized through the optimization of the separation of PTH-amino acids using acetonitrile as organic solvent. ▲ = Acetonitrile (%); ■ = SDS (mmol/l); ● = pH.

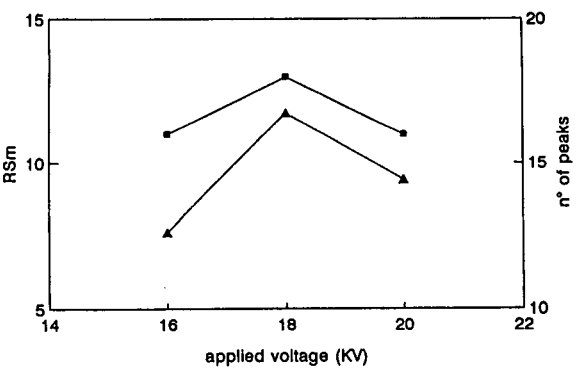


Fig. 7. Mean resolution measured using the experimental conditions of the tenth step of the acetonitrile optimization, changing the applied voltage. ▲ = $R_{s_m}$; ■ = No. of peaks.

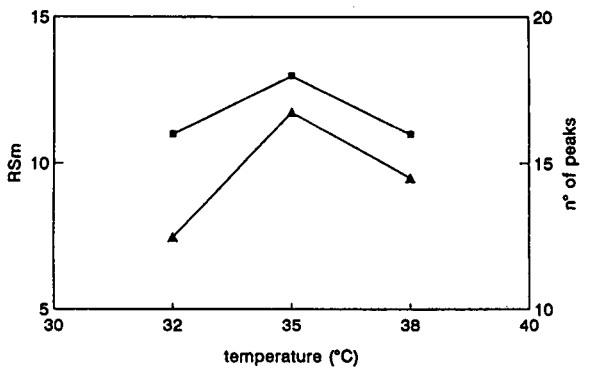


Fig. 8. Mean resolution measured using the experimental conditions of the tenth step of the acetonitrile optimization, changing the temperature of the separation. ▲ = $R_{s_m}$; ■ = No. of peaks.

ferent initial conditions, arrive at very close final pH values, SDS concentration and percentage of organic solvent. Further, the migration orders of the PTH-amino acids are very similar in the two solvents. This result should not be fortuitous; it probably indicates that the role of the organic solvent is mainly connected with a reduction in the polydispersity of the micellar pseudo-stationary phase. The molecular basis of the separation seems to be connected mainly to a strong ionic interaction between the PTH-amino acids and the micellar phase. This interaction could justify the long migration time of PTH-lys and PTH-arg with respect to other PTH-amino acids. In addition to this ionic interaction, a partition mechanism also plays an important role, as in reversed-phase LC separations. The mixed aqueous–organic mobile phase should represent the polar phase, whereas the micellar pseudo-stationary phase should represent the apolar phase. In fact, generally the non-polar PTH-amino acids are retarded in the separation compared with the polar compounds. However, a strong ionic interaction and a partition mechanism cannot explain the behaviour of some PTH-AAs with respect to others, e.g., the migration time of PTH-thr being shorter than that of PTH-ser, that of PTH-glu shorter than that of PTH-asp, that of PTH-leu shorter than that of PTH-leu and that of PTH-lys noticeably shorter than that of PTH-arg. These migration times are all the reverse of those observed in reversed-phase LC separation, suggesting that some other unknown interactions make important contributions to the separation.

By the use of the optimization procedures reported here, the complete separation of all 20 PTH-amino acids was not achieved; obviously this does not exclude that by using other conditions this goal could be obtainable. Further, under the experimental conditions explored by the optimization, we did not have complete assurance that the global optimum was reached.

## REFERENCES

1 S. Terabe, K. Otsuka, K. Ichikawa, A. Tsuchiya and T. Ando, *Anal. Chem.*, 56 (1984) 111.
2 S. Terabe, K. Otsuka and T. Ando, *Anal. Chem.*, 57 (1985) 834.
3 K. Otsuka, S. Terabe and T. Ando, *J. Chromatogr.*, 332 (1985) 219.
4 K.C. Waldron, S. Wu, C.W. Earle, H.R. Harke and N.J. Dovichi, *Electrophoresis*, 11 (1990) 777.
5 D.L. Massart, B.G.M. Vandeginste, S.N. Deming, Y. Michotte and L. Kaufman (Editors), *Chemometrics: a Textbook* (*Data Handling in Science and Technology*, Vol. 2), Elsevier, Amsterdam, 1988, Ch. 18, p. 299.
6 J.A. Nelder and R. Mead, *Comput. J.*, 7 (1965) 308.
7 M.W. Routh, P.A. Swartz and M.B. Denton, *Anal. Chem.*, 49 (1977) 1422.

*Journal of Chromatography*, 638 (1993) 335–342
Elsevier Science Publishers B.V., Amsterdam

CHROM. 24 940

# Comparative use of three electrokinetic capillary methods for the determination of drugs in body fluids

# Prospects for rapid determination of intoxications

J. Caslavska, S. Lienhard and W. Thormann*

*Department of Clinical Pharmacology, University of Berne, Murtenstrasse 35, CH-3010 Berne (Switzerland)*

ABSTRACT

Three electrokinetic capillary methods, micellar electrokinetic capillary chromatography, capillary zone electrophoresis and capillary isotachophoresis, are shown to be well suited for the rapid screening and confirmation of drugs in serum and urine of patients with medical drug overdoses (intoxications), situations where rapid identification without precise quantification is needed. Patients' samples obtained from the emergency care unit were analysed in an instrument featuring on-column, fast forward-scanning multi-wavelength detection and the data were compared with those obtained by conventional methods. The drugs studied included salicylate, acetaminophen (paracetamol) and antiepileptics. In cases with high drug concentrations, body fluids can be injected directly or may have only to be diluted (urine) or ultrafiltered (serum) prior to analysis, providing results within about 30 min. Thus, electrokinetic capillary methods can be employed for rapid drug screening, provided that instrumentation with a database for peak identification is available.

## INTRODUCTION

Emergency qualitative drug screening can provide valuable information to physicians faced with a confusing clinical presentation, atypical symptoms or signs and little or no history. For such cases, anticipated laboratory results may affect short-term management of a patient, this making drug screening an important part of a clinical service station [1]. Currently used analytical methods for drug screening are based on the principles of spectrophotometry, immunoassays and chromatography, with thin-layer chromatography [2] probably being most frequently employed. All of these techniques have advantages and disadvantages. The reagents for many of the immunological assays are available in kit form, together with highly automated instrumentation. This permits such analyses to be performed easily and rapidly. However, immunological techniques are prone to disturbances by molecules of similar structure (cross-reactivity). Many antibodies involved not only recognize the drug of interest, but also some of its metabolites. Moreover, these techniques are by nature unsuited to the simultaneous monitoring of several drugs and metabolites [3]. Chromatographic assays, on the other hand, provide specific results for multiple compounds but typically require extensive sample preparation and/or derivatization. Thus automation of chromatographic drug screening is complex [4].

For many years, analytical capillary isotachophoresis (CITP) performed in narrow-bore PTFE tubes of 200–500 $\mu$m I.D. was applied to drug monitoring [5]. Applications were developed in laboratories specializing in electro-

* Corresponding author.

0021-9673/93/$06.00 

phoretic techniques. However, partly owing to its complexity and the lack of automated instrumentation, CITP was never adopted as a routine drug assay methodology. Recently, instrumentation for electrokinetic separations in fused-silica capillaries of very small I.D. (25–75 $\mu$m) was developed [6–10] and the first papers reporting its use for drug monitoring in body fluids have appeared [11–23]. This type of instrumentation was shown to be suitable for high-resolution separations based on the principles of capillary zone electrophoresis (CZE), CITP and micellar electrokinetic capillary chromatography (MECC) [24,25].

For rapid analysis, minimum sample preparation is desirable. Sample preparation methods include simple liquid handling procedures (*e.g.*, centrifugation, dilution, filtration), release of the analyte from the biological matrix (*e.g.*, hydrolysis, sonication), the removal of endogenous compounds (*e.g.*, precipitation, ultrafiltration and extraction) and the enhancement of selectivity and sensitivity by analyte derivatization. In previous papers from our laboratory, the values of direct sample injection [18,19] and extraction [18–22] for drug screening by MECC was reported. In this work, MECC, CZE and CITP performed in the same instrument and with minimum sample pretreatment, including direct sample injection, dilution and ultrafiltration, were evaluated. Patients' samples obtained from the emergency care unit were analysed in an instrument featuring on-column, fast forward-scanning multi-wavelength detection and the data were compared with those obtained by conventional methods. The drugs studied include salicylate, acetaminophen (paracetamol) and antiepileptics. The data were employed to elucidate the pros and cons of the different electrokinetic capillary approaches for emergency analyses.

## EXPERIMENTAL

### *Chemicals, origin of samples and routine methods of analysis*

All chemicals were of analytical-reagent or research grade. The drugs employed as reference compounds were of European Pharmacopeia quality. Our own serum and urine were employed as blank matrices. Patients' samples were collected in our routine drug assay laboratory where they were received for drug screening. Salicylate, paracetamol, ethosuximide and primidone levels in serum were determined by automatic fluorescence polarization immunoassays (FPIA) on a TDx Analyzer (Abbott Labs., Irving, TX, USA). Phenobarbital was monitored by an automated enzyme immunoassay technique (EMIT) (Syva, Palo Alto, CA, USA) on a Cobas Fara centrifugal analyzer (Hoffmann-La Roche, Diagnostica, Basle, Switzerland). The immunoassays were performed according to the manufacturer's instructions using their reagent kits. Salicylate in urine was determined spectrophotometrically as the Fe(III) complex in acidic solution according to the method of Trinder [26], but without employing the precipitation reagent for proteins. Samples were stored at −20°C until further analysis.

### *Electrophoretic instrumentation and running conditions*

The instrument with multi-wavelength detection employed in this work has been described previously [18–20]. Briefly, it featured a 75 $\mu$m I.D. fused-silica capillary of about 90 cm length (Product TSP/075/375; Polymicro Technologies, Phoenix, AZ, USA) together with a UVIS 206 PHD fast-scanning multi-wavelength detector with a No. 9550-0155 on-column capillary detector cell (both from Linear Instruments, Reno, NV, USA) towards the capillary end. The effective separation distance was 70 cm. Multi-wavelength data were read, evaluated and stored employing a Mandax AT 286 computer system and running the Model 206 detector software package version 2.0 (Linear Instruments) with windows 286 version 2.1 (Microsoft, Redmont, WA, USA). Throughout this work the Model 206 detector was employed in the high-speed polychrome mode by scanning from 195 to 320 nm at 5-nm intervals (26 wavelengths). With these settings the sampling rate was 3.69 data points per second and wavelength.

For all three methods, a constant voltage of 20 kV was applied and the cathode was on the detector side. Sample application was effected manually through dipping the anodic capillary

end into the sample vial and lifting it *ca.* 34 cm for a specified time interval. Conditioning between runs was achieved by rinsing the capillary with 0.1 *M* NaOH for 5 min and with buffer for 10 min. For MECC, a buffer composed of 75 m*M* sodium dodecyl sulphate (SDS), 6 m*M* $Na_2B_4O_7$ and 10 m*M* $Na_2HPO_4$ (pH ≈ 9.1) was employed. CZE analyses were executed with a 33 m*M* phosphate buffer of pH 8.3 (1.23 m*M* $KH_2PO_4$–32.1 m*M* $Na_2HPO_4$). CITP was performed with a leader of 10 m*M* HCl and histidine (pH 6.0) and a terminator composed of 10 m*M* 2-(N-morpholino)ethanesulphonic acid (MES) and histidine (pH 6.0). As described previously, the leader was placed in the anodic electrode vessel and the terminator was in the cathodic compartment and in the capillary [27]. All standard drug solutions were prepared in buffer or methanol at concentrations of 100–300 μg/ml. Spiking of blank and patients' samples was effected by addition of known aliquots of these standard solutions to the plain or pretreated body fluids.

*Sample pretreatment for electrokinetic capillary analyses*

Serum and urine samples were either injected as received or, prior to injection, centrifuged at 1500 *g* for 10 min and/or filtered using 0.2-μm Nalgene (25-mm diameter) disposable syringe filters (Nalge, Rochester, NY, USA). For the removal of the proteins, the samples were ultrafiltered at 1500 *g* for 20 min using the Centrifree Micropartition System (Grace, Amicon Division, Wallisellen, Switzerland).

## RESULTS AND DISCUSSION

For three different cases, a comparative study of drug monitoring by MECC, CZE and CITP is presented. The first sample was serum of a patient with a suspected overdose of analgesics, the second a similar case for which both urine and serum were available and the third serum from a patient under multiple anticonvulsant pharmacotherapy.

Fig. 1 presents MECC data obtained for a patient's serum sample that was received for the

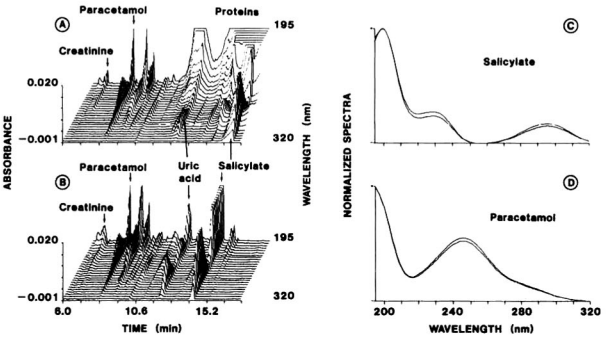


Fig. 1. Three-dimensional MECC data for (A) directly injected and (B) ultrafiltered patient's serum containing salicylate and paracetamol; (C) and (D) depict spectral identity proofs for salicylate and paracetamol, respectively. Sample injection time, 5 s; applied voltage, 20 kV; current, *ca.* 80 μA.

determination of salicylate and paracetamol. Using FPIA assays, the investigated serum was found to contain 3730 μ*M* salicylate and 160 μ*M* paracetamol, drug levels which are above those of the usual therapeutic ranges (salicylate 1100–2200 μ*M*, paracetamol 66–132 μ*M* [28]). With direct serum injection (Fig. 1A), the MECC data reveal a clear zone for paracetamol, and also peaks for the two endogenous marker substances, creatinine and uric acid. Also obtained is an indication of the presence of salicylate, which is shown to elute within unresolved matrix compounds, particularly proteins [19]. However, with ultrafiltration these interferences are removed and salicylate is also well monitored (Fig. 1B). For both drugs, excellent agreement between the extracted normalized absorbance spectra with those of a model run is obtained (Fig. 1C and D), revealing the unambiguous identification and purity of these zones. Thus, MECC of ultrafiltered serum has the potential to analyse rapidly for serum salicylate and paracetamol.

Comparing the electropherograms in Fig. 1A and B reveals interesting matrix effects. Ultrafiltration is shown to remove substantially interferences at elution times above about 12 min, permitting the formation of much improved zones of uric acid and salicylate. Second, the elution time intervals of all zones with serum injection are higher than those with the ultrafil-

trate. For example, paracetamol, uric acid and salicylate in Fig. 1A/B were detected after 8.59/8.33, 13.12/12.14 and 16.91/14.31 min, respectively. These data clearly emphasize the need for multi-wavelength detection for identification purposes. Retention (detection) times are not reliable parameters for zone assignment.

Omitting the solubilization of proteins (as with SDS in MECC) in an electrokinetic capillary system featuring untreated fused-silica capillaries makes direct injection of proteinaceous samples, particularly serum, difficult. Therefore, CZE and CITP analyses of ultrafiltered serum samples only were investigated. Analysing the patient's sample in Fig. 1 by CZE in a phosphate buffer of pH 8.3 gave the results presented in Fig. 2. Fig. 2A and B depict three-dimensional electropherograms of ultrafiltered serum blank and patient's serum, respectively. In this assay, paracetamol and salicylate are shown to produce clear peaks that elute in the same relative order with respect to uric acid as in MECC (Fig. 1) and to be clearly identifiable by normalized absorbance spectra (Fig. 2C and D).

Owing to the discontinuous buffer configuration, the data format in CITP is different to those obtained in MECC and CZE. Fig. 3 presents CITP electropherograms of (A) a blank and (B) an analysis of a model mixture of paracetamol and salicylate. Fig. 3A shows the complete three-dimensional UV data plot recorded with 5-nm increments for the wavelength

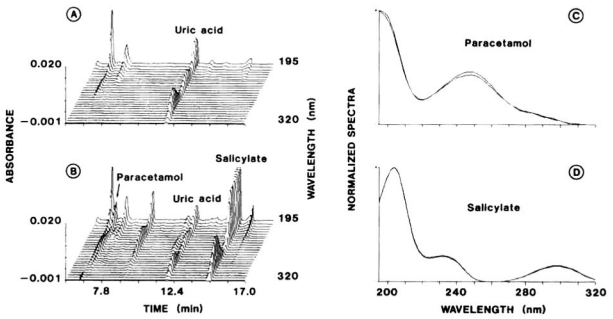


Fig. 2. Three-dimensional CZE data for (A) an ultrafiltered serum blank and (B) an ultrafiltered patient's serum (same as in Fig. 1B) together with the peak and reference spectra of (C) paracetamol and (D) salicylate. Sample injection time, 5 s. The applied voltage was a constant 20 kV and the current was observed to increase from about 70 to 78 $\mu$A during the experiment.

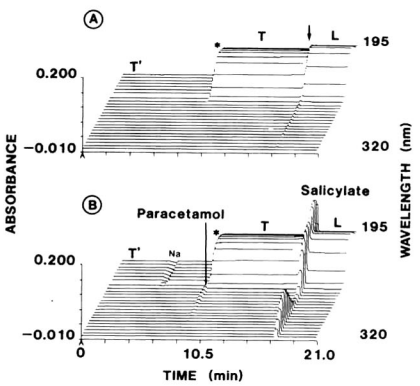


Fig. 3. Three-dimensional CITP data for (A) the blank and (B) a model sample consisting of salicylate (2.5 m$M$) and paracetamol (330 $\mu M$) having a sample injection time of 12 s. Leader (anolyte), adjusted terminator and initial terminator (catholyte) zones are marked L, T and T′, respectively. The arrow and asterisk mark the leader–terminator boundary and the location of the initial leader–terminator interface (sample zone), respectively. The applied voltage was 20 kV. During the experiment a gradual current increase from 2 to about 6 $\mu$A was observed.

range 195–320 nm (absorbance *vs.* detection time *vs.* wavelength). Note that the total zone movement in this anionic CITP configuration proceeds in the direction opposite to that of electromigration [27,29]. The discontinuity at *ca.* 8.4 min (marked with an asterisk) represents the detection of the stationary boundary which is moved by the electroosmotic flow across the point of detection. The absorbance change observed originates from the change in the histidine concentration between the original (T′) and the adjusted (T) terminator solutions. At the beginning of an experiment the UV absorbance was set to zero across the entire wavelength range. Finally, the leader–terminator interface (marked with an arrow) is monitored at *ca.* 16.8 min. The data presented in Fig. 3B reveal that salicylate is migrating isotachophoretically within the leader–terminator frame whereas paracetamol remains as an uncharged compound in the initial sample compartment and is therefore monitored within the T′–T transition. Sodium from the sample migrates zone electrophoretically and is detected through indirect absorption at low wavelengths at about 5 min.

CITP data obtained with (A) ultrafiltered

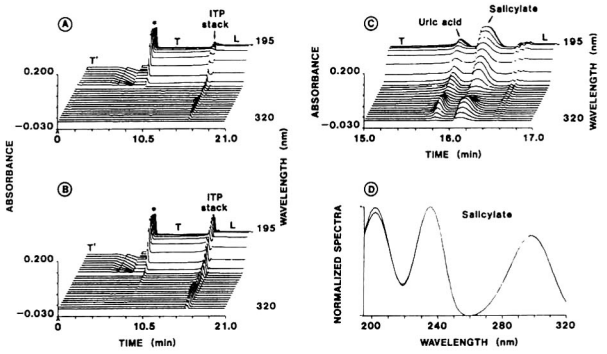


Fig. 4. Three-dimensional CITP data for (A) an ultrafiltered serum blank, (B) an ultrafiltered patient's serum (same as in Fig. 1B), (C) the ITP stack with an expanded time scale of (B) and (D) the peak and reference spectra of salicylate. The injection time was 6 s in all instances. Other conditions as in Fig. 3.

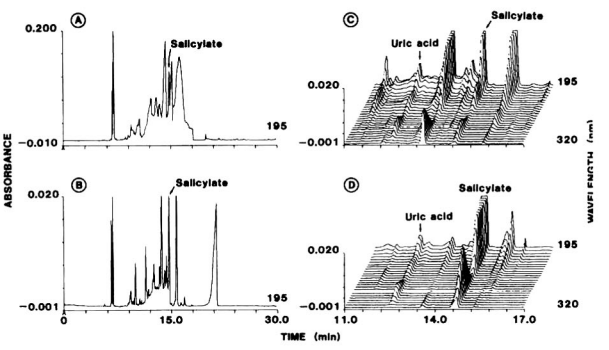


Fig. 5. Single-wavelength (195 nm) MECC data for (A) a directly injected patient's urine and (B) a tenfold diluted patient's urine, and multi-wavelength MECC data for (C) the tenfold diluted patient's urine (only part of the data with an expanded time axis are shown) and (D) an ultrafiltered serum from the same patient. Other conditions as in Fig. 1.

serum blank and (C and D) a patient's sample (same sample as used for Figs. 1B and 2B) are depicted in Fig. 4. Comparison of the electropherograms of the serum blank (Fig. 4A) with the buffer blank (Fig. 3A) shows that some endogenous compounds migrate isotachophoretically, forming a so-called ITP stack, whereas others remain between T′ and T or migrate zone electrophoretically within T′. Within the ITP stack, the substance with the characteristic absorption spectrum in the range 230–320 nm could be identified as uric acid. The ultrafiltered patient's serum provided an electropherogram (Fig. 4B) similar to that of serum blank (Fig. 4A). At first glance, it appears to be difficult to analyse salicylate in such a system. However, looking at the data depicted in Fig. 4C (which represent the ITP stack in Fig. 4B simply drawn on the expanded time scale) reveals the presence of salicylate. Identification of this zone was achieved by comparison of the background-subtracted, normalized absorbance spectrum with that in Fig. 3B. The good agreement between these spectra is depicted in Fig. 4D. Thus, CITP executed in fused-silica capillaries can easily be used to identify salicylate in ultrafiltered serum. Although paracetamol produces a small absorbance change in the 225–260 nm range at the T′–T interface (marked by an asterisk), its confirmation is impossible in that electrolyte system. No efforts were made to find a suitable electrolyte system for the CITP analysis of this drug.

MECC, CZE and CITP data obtained with a urine and a serum sample from a patient with suspected salicylate intoxication are presented in Figs. 5, 6 and 7, respectively. Using FPIA, the serum was found to contain 2998 $\mu M$ of salicylate. The urine specimen tested markedly positive (>1 m$M$) for salicylate employing the modified spectrophotometric method of Trinder [26] (see above). MECC data for directly injected urine are depicted in Fig. 5A, for tenfold diluted urine in Fig. 5B and C and for ultrafiltered serum in Fig. 5D. In contrast to the analysis of the serum, direct injection of untreated urine is shown to

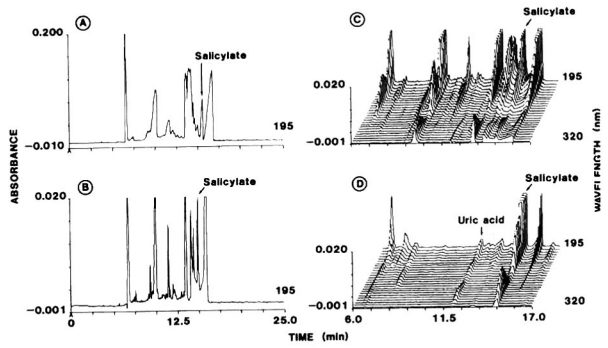


Fig. 6. Single-wavelength (195 nm) CZE data for (A) a directly injected patient's urine and (B) a tenfold diluted patient's urine, and multi-wavelength CZE data for (C) a tenfold diluted patient's urine and (D) an ultrafiltered serum from the same patient. Other conditions as in Fig. 2.

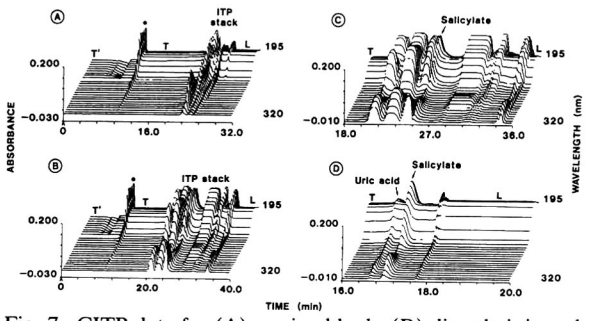


Fig. 7. CITP data for (A) a urine blank, (B) directly injected patient's urine (same as in Fig. 5), (C) ITP stack of the data of (B) with an expanded time scale and (D) ultrafiltered serum from the same patient. Injection time, 6 s. Other conditions as in Fig. 3.

overload the capillary column. Thus, for that example, sample dilution is required for the satisfactory determination of salicylate in urine. Comparison of the urine and serum data (Fig. 5C and D) reveals comparable salicylate concentrations in these two body fluids. However, the electropherogram obtained with urine is much more complex than that of ultrafiltered serum. The CZE analysis provided similar data (Fig. 6), which suggests that serum is the preferred body fluid for such an analysis. That the ionic matrix is more complex in urine than serum is further seen in the CITP data presented in Fig. 7. The ITP analysis of a urine blank (Fig. 7A) is shown to produce an ITP stack containing many more components than is obtained with a blank of ultrafiltered serum (Fig. 4A). The patient's urine injected as received provided the data depicted in Fig. 7B, its ITP stack with an expanded time scale being shown in Fig. 7C. This zone structure is about ten times longer than that obtained with the ultrafiltered serum depicted in Fig. 7D. Not surprisingly, identification of salicylate in the complex urine data proved to be more difficult than in serum. However, employing the comparison of normalized absorption spectra of eluting peaks (data not shown) provided the unambiguous presence of this drug in both fluids. It is important to realize that in CITP the detection time interval of a compound is strongly dependent on the sample matrix, this explaining the large difference in salicylate detection times seen in Fig. 7C and D. Hence the presence of salicylate in urine and serum was confirmed in the investigated patient's samples using three different electrokinetic capillary methods, MECC, CZE and CITP.

Fig. 8 represents the (A and B) CZE and (C and D) MECC analyses of antiepileptic drugs. Data for a model mixture consisting of four antiepileptic drugs and uric acid (Fig. 8A and C) and of an ultrafiltered serum sample from a patient under multiple antiepileptic drug pharmacotherapy (Fig. 8B and D) are compared. Using FPIA assays, the patient's serum was found to contain 209 $\mu M$ of ethosuximide and 20 $\mu M$ of primidone. A phenobarbital level of 105 $\mu M$ was determined by an EMIT technique. CZE confirmation with the ultrafiltered serum was possible for ethosuximide and phenobarbital only; primidone in that system co-eluted with matrix compounds. However, all three anticonvulsants could be detected by MECC (Fig. 8D), even by direct injection of the serum (data not shown). The data show differences in the relative detection order of the compounds in the two methods. Primidone elutes in front of ethosuximide in CZE whereas the opposite occurs in MECC, and phenytoin is detected before and after uric acid in the CZE and MECC systems,

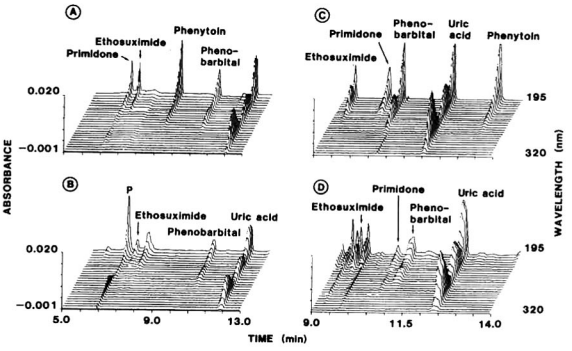


Fig. 8. Three-dimensional (A and B) CZE and (C and D) MECC data representing a model mixture of four antiepileptic drugs and uric acid [25 $\mu$g/ml each (A and C)] and an ultrafiltered serum from a patient under multiple anticonvulsant drug therapy (B and D). The conditions for the CZE and MECC runs are those in Figs. 2 and 1, respectively. P in (B) denotes the peak in which primidone is co-migrating with endogenous compounds.

respectively. Clearly, for anticonvulsants, MECC is preferred to CZE. This sample has not been subjected to CITP.

## CONCLUSIONS

With its distinct advantages, including automation, small sample size, ease of buffer change, direct injection of body fluids and little sample preparation, compared with chromatographic approaches, modern electrokinetic capillary technology appears to be very attractive for the monitoring of intoxications. Three different methods were used in this work, MECC, CZE and CITP. The first two are easily applied whereas CITP requires very careful selection of buffer conditions and typically higher solute concentrations compared with MECC and CZE. Only with the use of the ITP spike technique, in which baseline-resolved UV absorption peaks of solutes are produced by bracketing the solute with discrete, non-absorbing spacers, CITP detection limits become comparable to those observed in MECC and CZE [30]. MECC is the most general approach because it permits the simultaneous determination of acidic, neutral and basic drugs. In cases with high drug concentrations, such as those reported here, body fluids can be injected directly or may have only to be diluted (urine) or ultrafiltered (serum) prior to analysis, providing results within about 30 min. However, in cases with drug concentrations at or below the $\mu M$ ($\mu$g/ml) level, extraction with solute enrichment is required. This has been studied extensively for the MECC confirmation analysis of drugs in human urine [18–22]. Employing this approach, an analytical result is available within about 2 h. Thus, electrokinetic capillary methods can be employed for rapid drug screening, provided that instrumentation with a database for peak identification is available.

With absorption detection towards the capillary end, solute identification can be based on the retention (detection) behaviour and spectral analysis of eluting peaks over a range of wavelengths. In MECC and CZE, detection times are slightly dependent on the sample matrix, which calls for special care when using this parameter for solute identification. In CITP, zone identification by detection times is not possible. Multi-wavelength monitoring is an attractive approach for unambiguous zone assignment. Independent of the method used, the normalized spectrum of a peak is compared with a spectral computer library and segments of a peak can be compared with each other in order to assess peak purity. With all this information, a candidate list could be established followed by peak identification using a multi-parameter technique. If insufficient data or evidence for peak assignment are available, further evaluations and/or tests would have to be performed. Solute detection by other means, including mass spectrometry, could also be anticipated.

## ACKNOWLEDGEMENTS

The authors acknowledge the valuable contributions made by the technicians of the departmental drug assay laboratory and the excellent art work provided by Mrs. M. Kappeler. The generous loan of the UVIS 206 PHD detector by its manufacturer, Linear Instruments (Reno, NV, USA), is gratefully acknowledged. This work was sponsored partly by the Swiss National Science Foundation.

## REFERENCES

1 A.L. Kellermann, S.D. Fihn, J.P. LoGerlo and M.K. Copass, *Ann. Emerg. Med.*, 16 (1987) 1206.
2 P. Martel, D. Lones and R. Rousseau, *Am. Assoc. Clin. Chem.*, 2 (1983) 1.
3 R. DeCresce, A. Mazura, M. Liftshitz and J. Tilson, *Drug Testing in the Workplace*, ASCP Press, Chicago, 1989.
4 S.R. Binder, M. Regalia, M. Biaggi-McEachern and M. Mazhar, *J. Chromatogr.*, 473 (1989) 325.
5 P. Gebauer, V. Dolník, M. Deml and P. Boček, *Adv. Electrophoresis*, 1 (1987) 281, and references cited therein.
6 W. Thormann and M.A. Firestone, in J.C. Janson and L. Rydén (Editors), *Protein Purification*, VCH Weinheim, 1989, pp. 469–492, and references cited therein.
7 J.W. Jorgenson and K.D. Lukacs, *Science*, 222 (1983) 266.
8 B.L. Karger, A.S. Cohen and A. Guttman, *J. Chromatogr.*, 492 (1989) 585.
9 N.A. Guzman, L. Hernandez and B.G. Hoebel, *BioPharm*, 2 (1989) 22.

10 Z. Deyl and R. Struzinsky, *J. Chromatogr.*, 569 (1991) 63.
11 T. Nakagawa, Y. Oda, A. Shibukawa, H. Fukuda and H. Tanaka, *Chem. Pharm. Bull.*, 37 (1989) 707.
12 H. Nishi, T. Fukuyama and M. Matsuo, *J. Chromatogr.*, 515 (1990) 245.
13 D.K. Lloyd, A.M. Cypess and I.W. Wainer, *J. Chromatogr.*, 568 (1991) 117.
14 I.M. Johansson, R. Pavelka and J.D. Henjon, *J. Chromatogr.*, 559 (1991) 515.
15 D.E. Burton, M.J. Sepaniak and M.P. Maskarinec, *J. Chromatogr. Sci.*, 24 (1986) 347.
16 J. Pruñonosa, R. Obach, A. Diez-Cascón and L. Gouesclou, *J. Chromatogr.*, 574 (1992) 127.
17 K. Lee, G.S. Heo, N.J. Kim and D.C. Moon, *J. Chromatogr.*, 608 (1992) 243.
18 W. Thormann, P. Meier, C. Marcolli and F. Binder, *J. Chromatogr.*, 545 (1991) 445.
19 W. Thormann, A. Minger, S. Molteni, J. Caslavska and P. Gebauer, *J. Chromatogr.*, 593 (1992) 275.
20 P. Wernly and W. Thormann, *Anal. Chem.*, 63 (1991) 2878.
21 P. Wernly and W. Thormann, *J. Chromatogr.*, 608 (1992) 251.
22 P. Wernly and W. Thormann, *Anal. Chem.*, 64 (1992) 2155.
23 D.K. Lloyd, K. Fried and I.W. Wainer, *J. Chromatogr.*, 578 (1992) 283.
24 S. Terabe, *Trends Anal. Chem.*, 8 (1989) 129.
25 H. Nishi and S. Terabe, *Electrophoresis*, 11 (1990) 691.
26 P. Trinder, *Biochem. J.*, 57 (1954) 301.
27 P. Gebauer, J. Caslavska and W. Thormann, *J. Biochem. Biophys. Methods*, 23 (1991) 97.
28 W.E. Evans and M. Oellerich (Editors), *Therapeutic Drug Monitoring Clinical Guide*, Abbott Laboratories, Irving, TX, 1984.
29 W. Thormann, *J. Chromatogr.*, 516 (1990) 211.
30 J.C. Reijenga, A. Gaykema and F.E.P. Mikkers, *J. Chromatogr.*, 287 (1984) 365.

*Journal of Chromatography*, 638 (1993) 343–348
Elsevier Science Publishers B.V., Amsterdam

CHROM. 24 871

# Capillary electrophoresis of *o*-phenylenediamine derivatives (quinoxalines) of dicarbonyl sugars

Ivan Mikšík*

*Institute of Physiology, Vídeňská 1083, 142 20 Prague 4 (Czech Republic)*

Jiří Gabriel

*Institute of Microbiology, Vídeňská 1083, 142 20 Prague 4 (Czech Republic)*

Zdeněk Deyl

*Institute of Physiology, Vídeňská 1083, 142 20 Prague 4 (Czech Republic)*

ABSTRACT

Dicarbonyl sugars were separated by capillary electrophoresis as *o*-phenylenediamine derivatives (quinoxalines). Tetrabutylammonium bromide was used as a modifier; D-*arabino*-2-hexosulose (D-glucosone), D-*lyxo*-2-hexosulose (D-galactosone), 7-deoxy-L-*galacto*-2-hexosulose and 5-hydroxy-2,3-dioxohexanal served as standards. The separation procedure was optimized with respect to pH, buffer and solute concentrations. In most instances optimum separations were obtained in 75 m*M* borate buffer (pH 11.0); 0.04 mg/ml was found to be the optimum sample concentration. The detection limit was *ca.* 0.1 pmol. Analyses of a mixture of fermentation products or Maillard reaction products show the applicability of the method.

## INTRODUCTION

The role of dicarbonyl monosaccharides in a number of metabolic pathways seems to be well established; some of these compounds are capable of inhibiting the proliferation of malignant cells and others appear to be involved in diabetes or rat hypoglycaemia. Of particular importance is D-*arabino*-2-hexosulose, the metabolism of which is best known: this sugar is involved in lignin biodegradation and in some fungi it is dehydrated with the formation of an antimicrobial antibiotic, cortalcerone. Other dicarbonyl monosaccharides have been shown to be present in other antibiotics also (for a review, see ref. 1). Dicarbonyl sugars arise also in vertebrate tissues as a result of monosaccharide autoxidation in the presence of the free amino groups. The interest in this respect is stimulated particularly by the fact that dicarbonyl sugars appear to be involved in tissue ageing and in a number of pathological processes. Dioxo compounds (*e.g.*, 3-deoxy-2-hexosulose) were reported to represent the key point in the Maillard (browning) reaction [2,3], which stresses further the need for a reliable separation procedure, preferably complementary to chromatography.

In spite of considerable efforts to separate dicarbonyl sugars in the underivatized form, no completely satisfactory method is available. There are several reasons for this situation: thin-layer chromatography (TLC) is used mostly for screening purposes with limited possibilities of quantification; in high-performance liquid chromatographic (HPLC) procedures (nitrile-bonded

* Corresponding author.

0021-9673/93/$06.00 

phases), dicarbonyl sugars tend to be irreversibly bound to the sorbent; with gas chromatography (GC) the difficulty lies in the instability of the trimethylsilyl derivatives under the analysis conditions. Detection represents another problem. As underivatized sugars are devoid of UV absorbance, their spectrophotometric detection is difficult. It is possible to use short-wavelength UV (typically 185 nm) or IR detection. In the latter instance no satisfactory detection limits serving biomedical purposes can be achieved and in the former the profiles are frequently obscured by the presence of accompanying compounds that absorbing in the same UV region [1].

*o*-Phenylenediamine was introduced some time ago as a suitable derivatization reagent for dicarbonyl sugars. In this derivatization reaction dioxo compounds are converted in the corresponding quinoxalines:

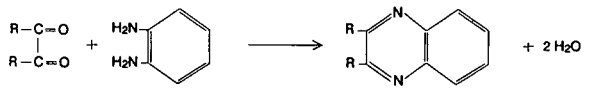


This reaction was successfully applied to the isolation of dicarbonyl sugars from mycelial macerates [4] and for the characterization of various homoglucans [5]. Chromatographic techniques such as ion-exchange chromatography [6], TLC, HPLC [7,8] and GC–MS [5,9,10] have been applied for the separation of *o*-phenylenediamine derivatives of carbohydrates with limited success. All these procedures are fairly insensitive. *o*-Phenylenediamine has also been used as a spray reagent for revealing sugar acids on thin layers [11].

In this paper we report the separation of dicarbonyl sugars by capillary electrophoresis (CE).

## EXPERIMENTAL

### *Chemicals*

*o*-Phenylenediamine was obtained from Sigma (St. Louis, MO, USA). D-*arabino*-2-Hexosulose (D-glucosone), D-*lyxo*-2-hexosulose (D-galactosone) and 7-deoxy-L-*galacto*-2-hexosulose were prepared enzymatically [12] from corresponding aldoses. 5-Hydroxy-2,3-dioxohexanal was prepared enzymatically from 6-deoxy-D-glucose [13]. Tetrabutylammonium bromide and D-(+)-glucose were from obtained Lachema (Brno, Czech Republic) and L-lysine from Serva (Heidelberg, Germany).

### *Quinoxaline formation and preparation of the standards*

Equimolar amounts of *o*-phenylenediamine were added to the solution of a dicarbonyl compound in citrate buffer (pH 4.00). After vigorous stirring for 2 h (40°C) the resulting quinoxalines were extracted with *n*-butanol and recrystallized from ethanol. The structure of the quinoxalines was confirmed with NMR and mass spectral measurements.

### *Capillary electrophoresis*

Separations were carried out with a laboratory-made capillary electrophoresis apparatus [14] with an untreated fused-silica capillary (50 $\mu$m I.D., 70 cm to the detector) at 15 kV; the detection wavelength was set at 220 nm. Calibration was done with an SP 4290 integrator (Spectra-Physics, San Jose, CA, USA).

All measurements were carried out in boric acid of appropriate concentration with 8 mmol/l tetrabutylammonium bromide titrated to the desired pH by 1 mol/l NaOH. This buffer was passed through a 0.5-$\mu$m filter (Waters, Milford, MA, USA) before application. Standards were dissolved in methanol (glucosone, galactosone and 7-deoxy-L-*galacto*-2-hexosulose at 0.5 mg/ml, *o*-phenylenediamine at 2 mg/ml and 5-hydroxy-2,3-dioxohexanal at 3 mg/ml). Aliquots of these stock solutions were evaporated to dryness and the residue was dissolved in separation buffer. The optimum running concentrations of the standards for measurement were 0.04 mg/ml for glucosone, galactosone and 7-deoxy-L-*galacto*-2-hexosulose, 0.08 mg/ml for *o*-phenylenediamine and 0.05 mg/ml for 5-hydroxy-2,3-dioxohexanal.

### *Additional procedures*

The Maillard reaction products were analysed according to the following protocol. A mixture of lysine (2 mmol), glucose (2 mmol) and

*o*-phenylenediamine (1 mmol) was incubated in 10 ml of 0.2 mol/l phosphate buffer (pH 7.4) at 60°C for 20 h. After incubation the sample volume was adjusted to 5 ml. The quinoxalines formed precipitated during the incubation period and were collected by centrifugation (4000 *g*, 15 min). The supernatant was discharged and the pellet was dissolved in methanol (2 mg/ml).

The Maillard reaction products were purified as follows. A mixture of Maillard reaction products was applied to the Silufol UV 254 silica gel thin-layer plates (15 × 15 cm) (Kavalier, Votice, Czech Republic) and developed with chloroform–methanol (22:8, v/v) (20 × 20 × 6 cm chamber, saturated for 0.5 h). The compounds were detected as quenching spots under UV light at 254 nm. The prominent spot occurring at $R_F = 0.33$ was extracted with ethanol and further analysed.

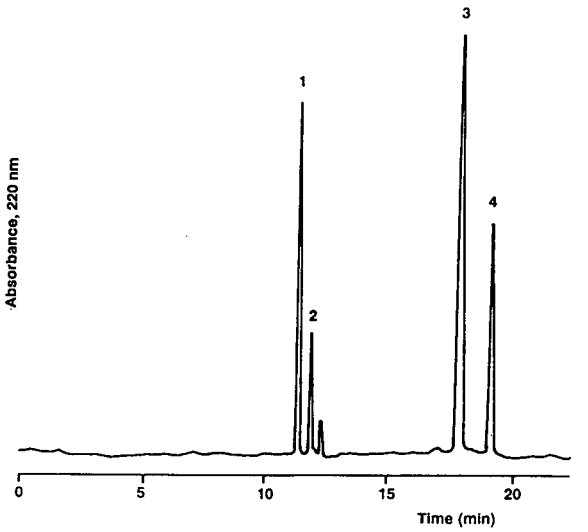


Fig. 1. Electrophoretic profile of standards under optimum condition (75 mmol/l boric acid, pH 11.0). Peaks: 1 = *o*-phenylenediamine; 2 = quinoxaline from 5-hydroxy-2,3-dioxohexanal; 3 = quinoxalines from D-*lyxo*-2-hexosulose (D-galactosone) and 7-deoxy-L-*galacto*-2-hexosulose; 4 = quinoxaline from D-*arabino*-2-hexosulose (D-glucosone).

## RESULTS AND DISCUSSION

Condensation products of D-*arabino*-2-hexosulose (D-glucosone), D-*lyxo*-2-hexosulose (D-galactosone), 7-deoxy-L-*galacto*-2-hexosulose and 5-hydroxy-2,3-dioxohexanal with *o*-phenylenediamine exhibit a strong UV absorbance at 315 nm and, consequently, represent suitable derivatives for the separation of dioxo sugars with UV detection. As the chromatographic techniques used previously for *o*-phenylenediamine dioxo sugar derivatives give relatively high detection limits, capillary electrophoresis appeared to be the method of choice. In preliminary experiments disappointing results were obtained with sodium dodecyl sulphate as micelle-forming reagent; on the other hand, tetrabutylammonium bromide when used as a modifier showed good results. The main separation mechanism seems to be borate complex formation with *cis*-diols. Ion-pair formation of the borate complex with the ammonium salt improves the selectivity. The solute strongly coupled with the borate will migrate slowly to the negative electrode. The separation procedure itself was optimized with respect to pH, buffer and solute concentrations. In most instances optimum separations were obtained with 75 m*M* borate buffer (pH 11.0) and a sample concentration of 0.04 mg/ml. The detection limit is *ca.* 0.1 pmol.

The separation conditions were optimized by using a standard mixture as specified under Experimental. A typical separation of standards is shown in Fig. 1. Here the first peak corresponds to the derivatization reagent (*o*-phenylenediamine) followed by quinoxalines with 5-hydroxy-2,3-dioxohexanal, D-*lyxo*-2-hexosulose (D-galactosone) and 7-deoxy-L-*galacto*-2-hexosulose and D-*arabino*-2-hexosulose (D-glucosone). In preliminary experiments optimum pH conditions and the optimum buffer concentration were established (Figs. 2 and 3). Fig. 2 summarizes the mobility changes relative to the derivatization reagent between pH 9.5 and 11.5. At pH 9.5–10.0 5-hydroxy-2,3-dioxohexanal is not separated from the reagent peak and therefore the higher pH value is advisable for separation. On the other hand, an extremely alkaline pH should be avoided because of solubility problems with tetrabutylammonium bromide. In fact this is not much of a problem because the separation between pH 10.5 and 11.5 is almost equally good. Consequently, pH 11.0 of the

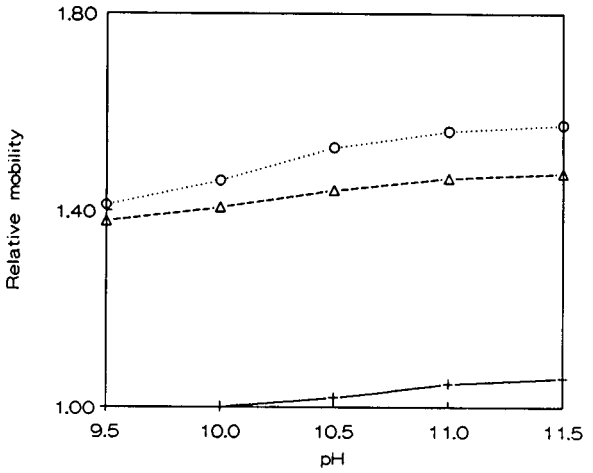


Fig. 2. Influence of pH on the relative mobility (ratio of migration times, *o*-phenylenediamine = 1.00). Measurements were made in 50 mmol/l boric acid. + = 5-Hydroxy-2,3-dioxohexanal; △ = D-galactosone and 7-deoxy-L-*galacto*-2-hexosulose; ○ = D-glucosone.

running buffer appeared to be an acceptable compromise (R.S.D. = 4.8%, $n = 6$).

The optimum boric acid concentration was sought at pH 11.0 in a separate set of experiments. As shown in Fig. 3, with increasing boric acid concentration the relative retention of all components increased and optimum separations were obtained using 75–100 mmol/l boric acid.

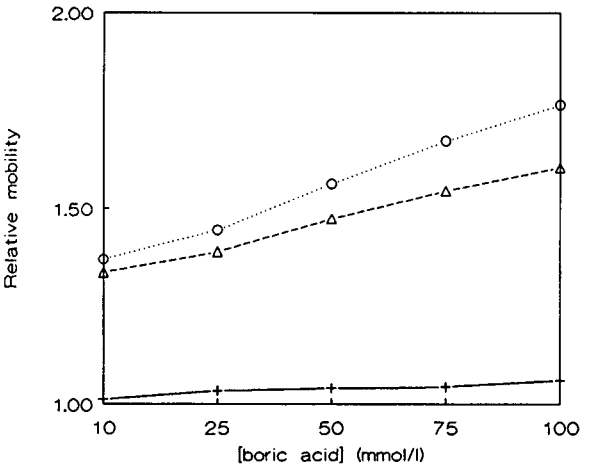


Fig. 3. Influence of boric acid concentration on the relative mobility (ratio of migration times, *o*-phenylenediamine = 1.00). Measurements were made at pH 11.0. + = 5-Hydroxy-2,3-dioxohexanal; △ = D-galactosone and 7-deoxy-L-*galacto*-2-hexosulose; ○ = D-glucosone.

Whereas at a low concentration of boric acid poor separations were obtained, concentrations above 100 mmol/l precluded by excessive heating of the capillary (over 50 μA). Therefore, 75 mmol/l boric acid appeared to be the optimum concentration as it offered baseline separation of the standards and good peak shapes and no cooling of the capillary was necessary. The following calibration graphs were obtained ($y$ = amount in pmol, $x$ = peak area):

for D-glucosone,

$y = 0.595x - 0.026 \quad r = 0.984$

linearity range = 0.5–8 pmol; detection limit = 0.05 pmol;

for D-galactosone,

$y = 0.855x - 0.127 \quad r = 0.990$

linearity range = 0.5–8 pmol; detection limit = 0.05 pmol;

for 7-deoxy-L-*galacto*-2-hexosulose,

$y = 0.653x - 0.215 \quad r = 0.994$

linearity range = 0.5–8 pmol; detection limit = 0.05 pmol;

for 5-hydroxy-2,3-dioxohexanal,

$y = 3.233x - 0.325 \quad r = 0.984$

linearity range = 5–40 pmol; detection limit = 0.15 pmol.

Two practical applications of the method are shown in Fig. 4. In Fig 4A a profile of a crude D-glucosone solution (fermentation broth) is presented. This profile shows the conversion of glucose to glucosone by a mixture of enzymes from the basidiomycete *Phanerochaete chrysosporium* in the presence of *o*-phenylenediamine. The major peak in this profile corresponds to D-glucosone; the smaller peak with a shorter migration time represents an unknown impurity.

Fig. 4B shows the profile of dicarbonyl sugars present in a mixture of Maillard reaction products; the double peak No. 4 (and also other components of the mixture) can be preseparated by TLC and isolates tested for purity by CE. As shown in Fig. 4D, homogenous products can be obtained in this way. By combining TLC with CE it is possible to show the presence of

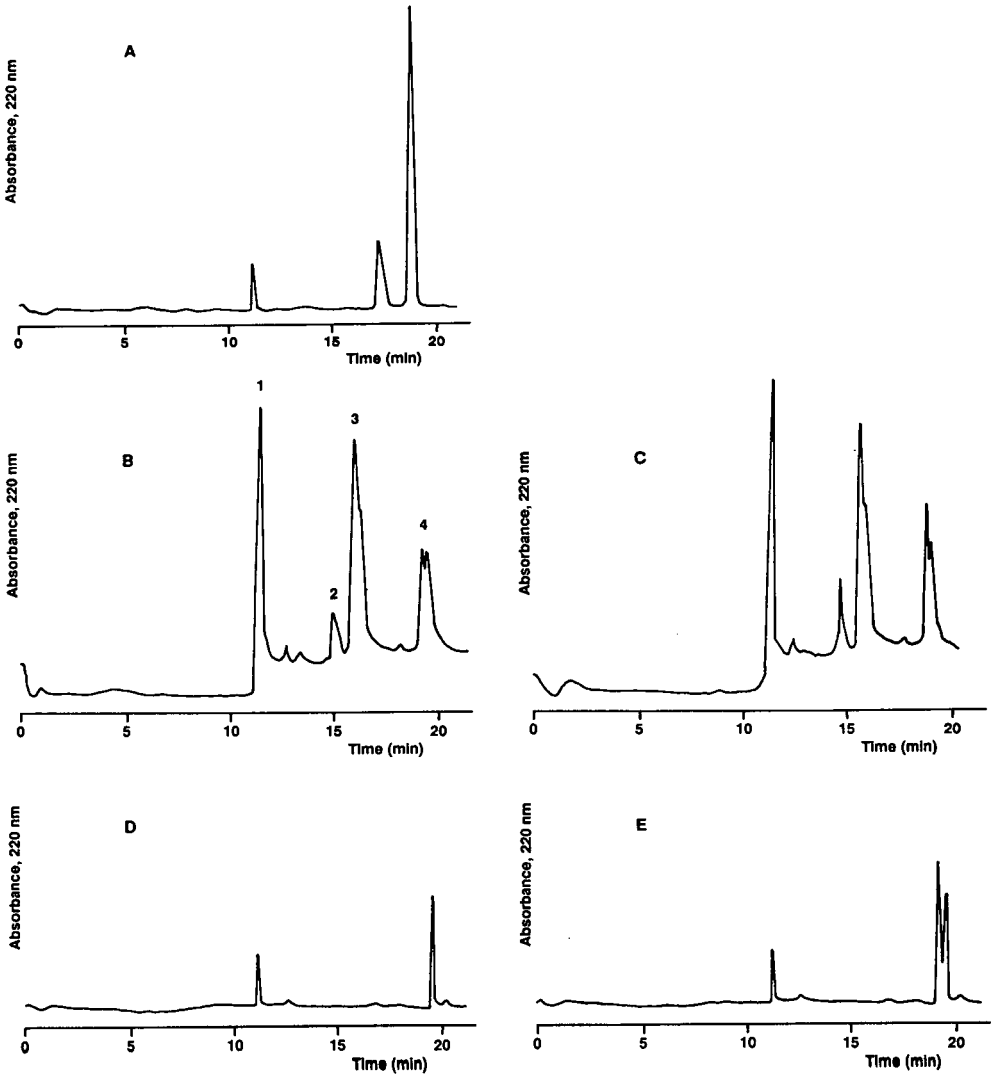


Fig. 4. Application of CE separation of *o*-phenylenediamine derivatives of dicarbonyl sugars. (A) Profile of crude solution of D-glucosone before purification procedures; the smaller peak represents an unidentified impurity; (B) profiles of quinoxalines of Maillard reaction products; (C) same as (B) but spiked with D-glucosone; (D) profile of purified product of Maillard reaction; (E) same as (D) but spiked with D-glucosone. The major peaks in (B) are numbered in the order in which they pass the detection window to facilitate reference in the text (see Results and Discussion).

D-glucosone in this reaction mixture (data not presented) or to isolate, *e.g.*, the accompanying compound in peak No. 4, as shown in Fig. 4E.

ACKNOWLEDGEMENT

This work was supported by the Czechoslovak Academy of Sciences (Grant No. 71129).

REFERENCES

1 J. Gabriel, *Chem. Listy*, 86 (1992) 95.
2 N. Paulsen and K.-W. Pflughaupt, in W. Pigman, D. Horton and J.D. Wander (Editors), *The Carbohydrates*, Vol. 1B, Academic Press, New York, 1985, p. 898.
3 F. Ledl and E. Schleicher, *Angew. Chem. Int. Ed. Engl.*, 29 (1990) 565.
4 M.A. Baute, R. Baute, G. Deffieux and M.J. Filleau, *Phytochemistry*, 16 (1977) 1895.

5 N. Morita, K. Hayashi, M. Takagi and K. Miyano, *Agric. Biol. Chem.*, 47 (1983) 757.
6 M. Takagi, K. Mizutani, I. Matsuda and S. Ono, *Agric. Biol. Chem.*, 35 (1971) 793.
7 W. Slikker, Jr., G.W. Lipe and G.D. Newport, *J. Chromatogr.*, 224 (1981) 205.
8 T. Hayashi, H. Tsuchiya, H. Todoroki and H. Naruse, *Anal. Biochem.*, 122 (1982) 173.
9 N. Morita, K. Nakata and M. Takagi, *Agric. Biol. Chem.*, 53 (1989) 437.
10 N. Morita, Y. Daido, H. Hayashi and M. Takagi, *Agric. Biol. Chem.*, 47 (1983) 765.
11 F. Gosselé, J. Swings and J. De Ley, *Zentralbl. Bakteriol. Parasitenkd. Infektionskr. Hyg. Abt. 1: Orig., Reihe C*, 1 (1980) 178.
12 J. Volc, P. Sedmera and V. Musílek, *Collect. Czech. Chem. Commun.*, 45 (1980) 950.
13 J. Gabriel, *Ph.D. Thesis*, Institute of Microbiology, Prague, 1992.
14 V. Rohlíček and Z. Deyl, *J. Chromatogr.*, 494 (1989) 87.

*Journal of Chromatography*, 638 (1993) 349–356
Elsevier Science Publishers B.V., Amsterdam

CHROM. 24 916

# Determination of explosives residues in soils by micellar electrokinetic capillary chromatography and high-performance liquid chromatography

## A comparative study

Wolfgang Kleiböhmer*, Karl Cammann, Jan Robert and Elmar Mussenbrock

*Institut für Chemo- und Biosensorik, Wilhelm-Klemm-Strasse 8, W-4400 Münster (Germany)*

ABSTRACT

Micellar electrokinetic capillary chromatography (MECC) is investigated for application as a complementary technique to reversed-phase high-performance liquid chromatography (HPLC) in the analysis of explosives residues. Separation efficiency, specificity, sensitivity, reproducibility, analysis time and calibration linearity are examined by comparing the suitability of HPLC and MECC in parallel analyses. Authentic soil samples from a former trinitrotoluene plant are examined, and the results show MECC to be a useful new technique in explosive analysis, yielding good sensitivity, high resolution and short analysis times.

## INTRODUCTION

Concern about the environment has reached new heights in recent years, as evidenced by the 1987 Montreal Protocol and the 1992 Earth Summit in Rio de Janeiro. Many environmental guidelines, regulations and remedies are being initiated which require sound chemical monitoring techniques and analysis methods, in order to ensure that risks are accurately assessed and mandates are properly enacted. Environmental analytical chemistry provides the means to separate, identify and quantitate pollutants found in a variety of matrices including air, land and water [1]. Today, new challenges are being created in this rapidly growing discipline by a changing political climate and increasing environmental concern. One such challenge involves analysis of heavily contaminated soils at military facilities associated with weapons production.

Since the end of the Cold War, various governments have begun to dismantle military installations and munition plants, in accordance with various non-proliferation agreements and disarmament treaties [2]. But as a new world peace and order are being created, major environmental problems are being discovered at many of these locations. Surrounding lands are found to be laden with explosives residues, the most common being 2,4,6-trinitrotoluene (TNT), hexahydro-1,3,5-triazine and associated nitroaromatic and nitramine impurities and degradation products [3]. The highly toxic nature of many of these substances, coupled with their persistence in the environment, requires thorough characterization of contaminated areas.

Some work has been done to analyse these compounds in environmental matrices, including high-performance liquid chromatography (HPLC) [4–6], gas chromatography (GC) [7,8]

* Corresponding author.

0021-9673/93/$06.00 

and supercritical fluid chromatography (SFC) [9]. A forensic analysis has been developed for organic gunshot and explosive constituents using micellar electrokinetic capillary chromatography (MECC) to separate and identify species [10]. MECC has also been used to separate various nitroaromatics [11]. In this study, we investigate the suitability of MECC in routine environmental analysis of soils contaminated by explosives residues. The MECC method is compared with an established HPLC method in terms of separation efficiency, specificity, sensitivity, reproducibility, analysis time and calibration linearity.

## EXPERIMENTAL

### *Micellar electrokinetic capillary chromatography*

MECC analysis was accomplished using a commercially available capillary electrophoresis unit (Dionex, Idstein, Germany) and measurements were made at 20 kV (+polarity) with gravity injection (30 mm, 5 s), and absorbance detection (230 nm). A polyimide-coated fused-silica capillary [57 cm (51 cm to optical window) × 375 μm O.D. × 75 μm I.D.] was utilized in the separation. MECC runs were performed with forced nitrogen cooling of the capillary.

*MECC reagents.* Sodium borate, boric acid, sodium dodecyl sulphate (SDS), Sudan III, HPLC solvents, 2,4-dinitrotoluene and 3-nitrotoluene were purchased from various commercial suppliers. Other explosive components were obtained from Promochem (Wesel, Germany) or by private donation. Buffer was prepared using purified water (SG Reinstwasser system) and contained 2.5 m*M* sodium borate, 12.5 m*M* boric acid and 25 m*M* SDS. Buffer pH was adjusted to 8.5 with phosphoric acid before the solution was vacuum degassed and filtered through a 0.45-μm Duropore membrane filter (Millipore, Eschborn, Germany). Stock solutions of explosives standards were prepared in the range 10–1000 ppm in HPLC-grade methanol (Baker). Serial dilutions were prepared for calibration curves. Prior to MECC analysis, the solutions were further diluted with borate buffer–methanol (95:5).

### *High-performance liquid chromatography*

LC separations were obtained on a modular system composed of a Hewlett Packard 1050 pump, a Rheodyne Model 7010A sample loop injector, a Hewlett Packard 1040M diode-array detector (230 nm) and a Hewlett Packard HPLC Chemstation. The components were separated on a Supelcosil LC-18 column (Supelco, 25 cm × 4.6 mm I.D.) using a linear solvent program at a flow-rate of 1.0 ml/min. The solvent system was water–methanol, with 20-min gradient from 40 to 60% methanol (Baker, HPLC grade). All explosives were dissolved in methanol–water (50:50) to prepare the stock standard. This standard was diluted with methanol–water to the final concentrations of interest.

### *Soil samples*

Authentic contaminated soil samples from Stadtallendorf, Germany, were extracted into organic solvents by Soxhlet extraction as detailed below. All soils were air dried to constant weight and ground with a pestle to pass a 30-mesh sieve [12]. Soils were subjected to exhaustive Soxhlet extraction with 200 ml of diethyl ether for 7 h. The soil extracts were filtered through a 0.45-μm Duropore membrane filter before reducing the solvent to dryness by rotary evaporation. The residue was redissolved under sonication in 10 ml of the buffer solution for MECC analysis or in 50 ml of methanol–water (50:50) for HPLC analysis.

## RESULTS AND DISCUSSION

Two MECC methods for the analysis of nitrocompounds have been published [10,11]. The method of Northrop *et al.* [10] proved to be better suited to this application and was utilized in the work presented. In Table I the various explosive components analysed in the present study are listed.

Fig. 1 shows an MECC and an HPLC separation of explosive constituents in an eleven-component test mixture. Identification of individual components in the electropherogram was made by comparison with the elution order obtained by Northrop *et al.* [10] and by spiking the

TABLE I

COMPOUNDS STUDIED

| Name | Abbreviation |
|---|---|
| 1,3,5-Trinitro-1,3,5-triazacyclohexane | RDX |
| 2,4,6-Trinitrotoluene | TNT |
| 4-Amino-2,6-dinitrotoluene | 4-AMDNT |
| 2,4,6-Trinitrobenzene | TNB |
| 2,4-Dinitrobenzene | DNB |
| 2,6-Dinitrotoluene | 2,6-DNT |
| 2-Nitrotoluene | 2-NT |
| 4-Nitrotoluene | 4-NT |
| 2,4,6,N-Tetranitro-N-methylaniline | Tetryl |
| 1,3,5,7-Tetranitro-1,3,5,7-tetrazacyclooctane | HMX |
| Nitrobenzene | NB |

mixture with single components on subsequent runs.

Surprisingly, the separation order obtained with both methods is nearly the same, although the separation modes are dissimilar. In MECC the elution order of TNT and Tetryl is changed and, more importantly, the aminodinitrotoluene isomers are separated and eluted later than in HPLC. The quality of the MECC separation is readily apparent, as the important degradation products of TNT, the 2 and 4 isomers of amino-dinitrotoluene, are baseline resolved and the complete separation required less than 7 min. The non-aromatic HMX and RDX heterocyclic systems should be solubilized to a lesser degree within the hydrophobic region created by the micellar aggregates than the nitrobenzene and toluene aromatic rings. These theoretical considerations are consistent with the results presented here, which show HMX eluting first, followed by RDX, then the various nitroaromatic substances.

In order to compare the efficiency of HPLC and MECC for the determination of explosives residues, the validation of the method is an

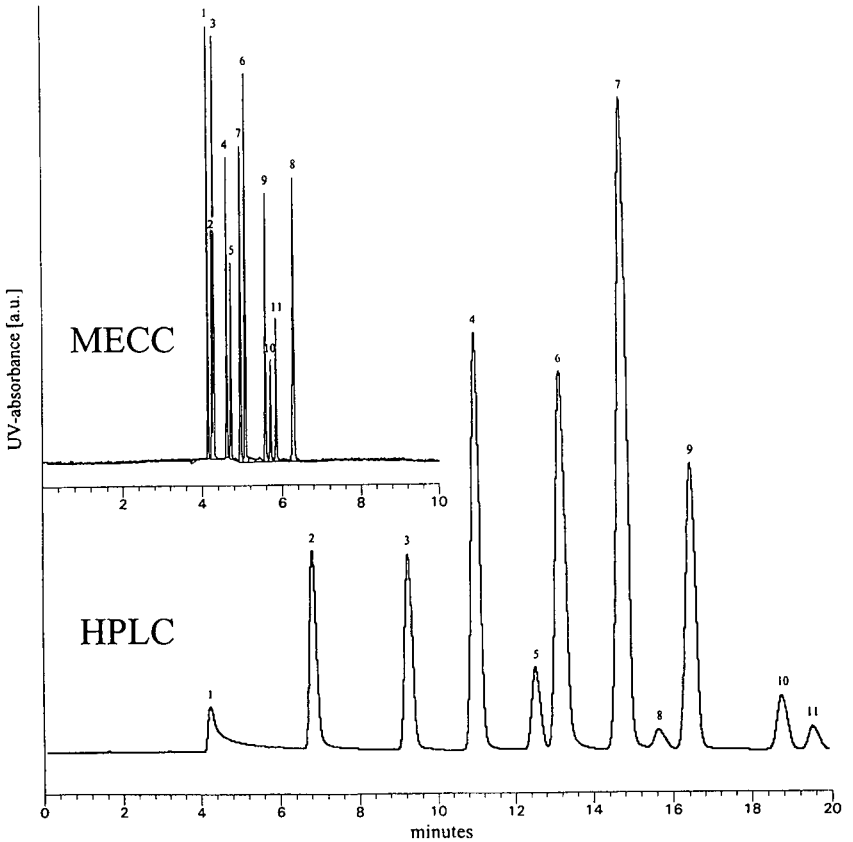


Fig. 1. MECC and HPLC separations of a mixture of explosives. For chromatographic conditions, see text. Peaks: 1 = HMX; 2 = RDX; 3 = TNB; 4 = DNB; 5 = NB; 6 = Tetryl; 7 = TNT; 8 = 4-AMDNT; 9 = 2,6-DNT; 10 = 2-NT; 11 = 4-NT.

TABLE II

AVERAGE VALUES AND RELATIVE STANDARD DEVIATIONS (R.S.D.) OF RETENTION TIMES ($t_R$) AND PEAK AREAS ($A$) FOR STANDARD SOLUTIONS (St) AND SOIL EXTRACTS (E) WITH HPLC

n.q. = Reproducible peak detection but impossible quantification because peak height is below five-fold signal-to-noise ratio.

| Component | Standard solution | | | | Soil extracts | | | |
|---|---|---|---|---|---|---|---|---|
| | $t_{RSt}$ (min) | R.S.D. (%) | $A_{St}$ (AU) | R.S.D. (%) | $t_{RE}$ (min) | R.S.D. (%) | $A_E$ (AU) | R.S.D. (%) |
| RDX | 6.94 | 0.07 | 29.2 | 3.0 | 6.97 | 0.35 | 29.1 | 9.61 |
| TNB | 9.41 | 0.05 | 47.6 | 5.8 | 9.50 | 0.18 | 728.5 | 5.27 |
| DNB | 11.07 | 0.03 | 37.4 | 1.8 | 10.93 | 0.23 | 12.6 | 7.96 |
| TNT | 14.78 | 0.20 | 65.4 | 2.4 | 14.78 | 0.50 | 5274.3 | 4.77 |
| 4-AMDNT | 15.51 | 0.02 | 124.0 | 8.0 | For coelution conditions, see text | | | |
| 2-AMDNT | – | – | – | – | 15.41 | 0.23 | 103.6 | 3.10 |
| 2,6-DNT | 16.25 | 0.40 | 32.5 | 3.6 | 16.22 | 0.22 | 67.4 | 5.59 |
| 2-NT | 18.48 | 0.26 | 20.3 | 4.9 | 18.44 | 0.16 | 9.7 | 11.23 |
| 4-NT | 19.15 | 0.43 | 25.1 | 5.9 | 19.25 | 0.48 | n.q. | n.q. |

important task. The most important requirement for a validation include reproducible retention times and peak areas, minimal interferences, calibration linearity and specificity. In order to determine the within-day precision of the methods, replicate separations were made of standard mixtures of seven components and of soil extracts by HPLC and MECC. In Tables II and III the average values and standard deviations are given for the HPLC retention/MECC migration times and peak areas. For both methods there is, as expected, no difference in elution order for standard solutions or soil extracts. While in HPLC for soil extracts only a slight deterioration in the standard deviations can be observed as compared with the standards, there is a large shift in migration times, and an increase in the standard deviations of migration times and peak areas by the MECC method. So in MECC the peak identification in real probes is impossible

TABLE III

AVERAGE VALUES AND RELATIVE STANDARD DEVIATIONS (R.S.D.) OF MIGRATION TIMES ($t_M$) AND PEAK AREAS ($A$) FOR STANDARD SOLUTIONS (St) AND SOIL EXTRACTS (E) WITH MECC

n.d. = No reproducible peak detection because peak height is below threefold signal-to-noise ratio.

| Component | Standard solution | | | | Soil extracts | | | |
|---|---|---|---|---|---|---|---|---|
| | $t_{MSt}$ (min) | R.S.D. (%) | $A_{St}$ (AU) | R.S.D. (%) | $t_{ME}$ (min) | R.S.D. (%) | $A_E$ (AU) | R.S.D. (%) |
| RDX | 3.39 | 0.34 | 647 141 | 0.6 | 4.12 | 1.84 | For coelution conditions, see text | |
| TNT | 3.39 | 0.34 | – | – | | | | |
| DNB | 3.67 | 0.16 | 772 376 | 0.3 | 4.47 | 2.15 | 7 323 | 42.3 |
| TNT | 3.96 | 0.44 | 1 012 486 | 0.4 | 4.86 | 2.12 | 7 324 807 | 1.9 |
| 4-AMDNT | 4.97 | 0.51 | 271 701 | 0.2 | 6.31 | 2.44 | 20 352 | 42.8 |
| 2-AMDNT | 4.39 | 0.26 | 654 732 | 0.3 | 6.04 | 2.43 | 39 170 | 1.2 |
| 2,6-DNT | 4.44 | 0.60 | 615 941 | 0.3 | 5.52 | 2.28 | 42 479 | 16.5 |
| 2-NT | 4.51 | 0.44 | 31 210 | 7.9 | 5.61 | 3.10 | 8 887 | 14.9 |
| 4-NT | 4.62 | 0.33 | 77 173 | 5.6 | n.d. | n.d. | n.d. | n.d. |

based on migration times of standards. Within a day, differences in migration times were usually less than 1%, and day-to-day or week-to-week variations of up to 4% were observed. This precision has been obtained by capillary temperature control by nitrogen cooling to reduce Joule heating effects.

*Linearity and limit of detection*

For a further comparison of the separation methods, we measured the peak areas for seven explosives from 0.145 to 50 $\mu$g/ml for HPLC and from 0.600 to 50 $\mu$g/ml for MECC samples. UV absorbance was plotted as a function of concentration, and calibration curves were observed to be linear over several orders of magnitude (for regression coefficients, see Table IV). The lower limit of detection of the MECC system was *ca.* 127 ng/ml for the strongly absorbing components, which corresponds to a value of nearly 1 ppm in soil samples. Based upon an injection volume of 2.4 nl for a 75-$\mu$m capillary, a mass detection limit of 1.6 pg was calculated for TNT. To increase sensitivity, larger sample plugs may be introduced onto the capillary by choosing greater values of the sampling height and/or longer sampling times; however, prolonged injection decreases efficiency [10]. In Table IV the lower limit of detection, the regression coefficient and the standardized slope are given for the seven investigated compounds. Slopes were standardized at a single concentration to obtain comparable values. With the exception of the 2 and 4 isomers of nitrotoluene in MECC, all calibration curves were observed to be linear over several orders of magnitude.

*Residue analysis*

Authentic soil samples were obtained from Stadtallendorf, Germany. During World War II, a munitions factory was located in Stadtallendorf situated near Marburg in central Germany, and today local and federal officials are developing guidelines to clean up this environmentally hazardous site. Efforts are under way to analyse the extent of environmental problems at this location and to monitor clean-up procedures [13]. Soil extracts prepared as previously described were analysed by HPLC and MECC, and the results are presented in Fig. 2. One advantage of the MECC technique discovered was that various humic substances that are co-extracted from the soil matrix along with the explosives residues were retained by the micelles. Thus, the micellar separation technique provided a simple and effective means of eliminating potential interferences. On the other hand, in the HPLC analysis of explosives in soils and sediments, these same substances might cause column fouling and require additional clean-up steps [12].

Separation, identification and quantification of several hazardous explosives in Stadtallendorf soil samples were accomplished by the MECC,

TABLE IV

SLOPE, REGRESSION COEFFICIENT AND LIMIT OF DETECTION FOR PEAK AREAS OF SOME SELECTED EXPLOSIVES MEASURED WITH HPLC AND MECC (UV-DETECTION AT 230 nm)

| Component | HPLC | | | | MECC | | | |
|---|---|---|---|---|---|---|---|---|
| | Corrected slope | Regression coefficient | Detection limit (ng absolute)[a] | Detection limit (ng/ml) | Corrected slope | Regression coefficient | Detection limit (pg absolute)[b] | Detection limit (ng/ml) |
| TNB | 206.9 | 0.9999 | 4.8 | 240 | n.d. | n.d. | n.d. | n.d. |
| DNB | 182.7 | 0.9999 | 4.7 | 235 | 81.4 | 0.9997 | 1.6 | 676 |
| TNT | 3.0 | 0.9998 | 10.0 | 500 | 80.8 | 0.9970 | 1.6 | 676 |
| 4-AMDNT | 988.0 | 0.9999 | 2.9 | 145 | 462.1 | 0.9971 | 0.3 | 127 |
| 2,6-DNT | 182.5 | 0.9997 | 5.1 | 255 | 81.3 | 0.9974 | 1.6 | 676 |
| 2-NT | 100.3 | 0.9999 | 4.9 | 245 | 28.3 | 0.7250 | 23.5 | 9940 |
| 4-NT | 177.6 | 0.9999 | 6.3 | 315 | 60.6 | 0.9140 | 13.3 | 5626 |
| TDX | 147.5 | 0.9999 | 5.2 | 260 | 66.2 | 0.9969 | 2.0 | 846 |

[a] Injection volume 20 $\mu$l
[b] Injection volume 2.36 nl.

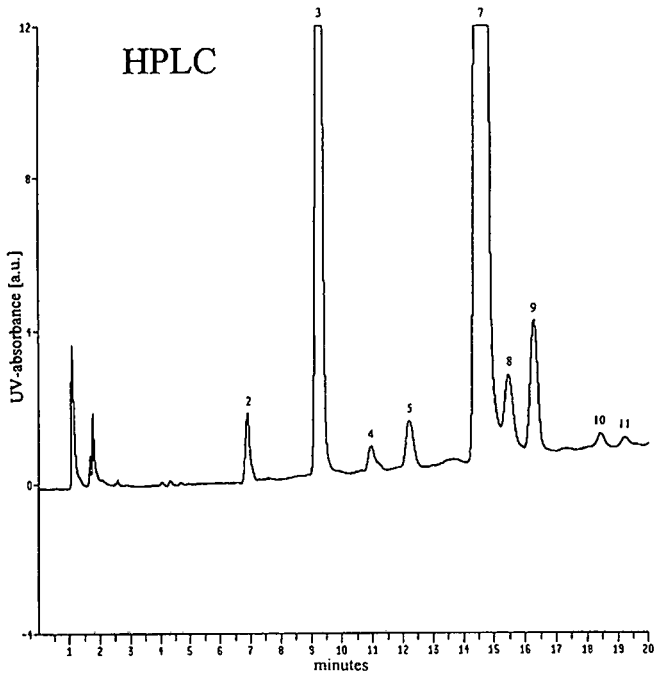


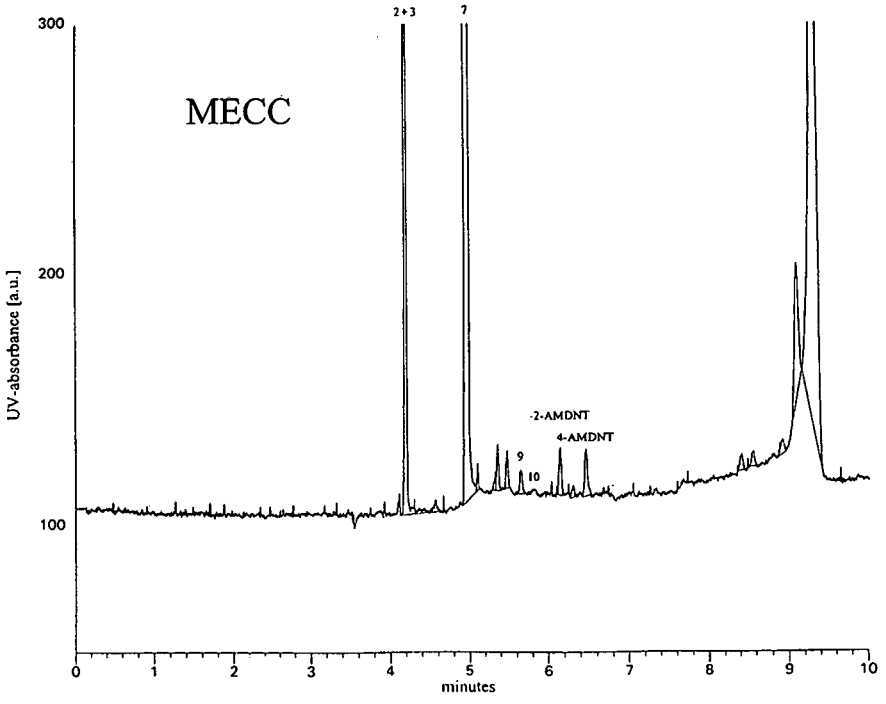


Fig. 2. MECC and HPLC separations of explosives extracted from contaminated soil at site undergoing environmental clean-up. For chromatographic conditions, see text. Peaks as in Fig. 1.

TABLE V

COMPARISON OF CONCENTRATIONS FOUND FOR NITROAROMATIC COMPOUNDS AND DEGRADATION PRODUCTS IN A SOIL FROM STADTALLENDORF (GERMANY), DETERMINED WITH HPLC AND MECC

| Compound | HPLC | | MECC | |
|---|---|---|---|---|
| | Concentration (mg/kg) | R.S.D. (%) | Concentration (mg/kg) | R.S.D. (%) |
| RDX | 22.41 | 9.6 | – | – |
| TNB | 158.27 | 4.6 | – | – |
| DNB | 2.76 | 7.9 | 2.86 | 42.3 |
| TNT | 1409.90 | 4.7 | 1265.85 | 1.9 |
| 2,6-DNT | 24.51 | 5.6 | 6.46 | 42.8 |
| 2-NT | – | – | – | – |
| 2-AMDNT | – | – | 4.59 | 1.2 |
| 4-AMDNT | 14.14[a] | 3.3 | 4.97 | 16.5 |

[a] Sum of 2-AMDNT and 4-AMDNT.

as well as by the HPLC, method. Most of the signals in Fig. 2 were identified, but the presence of unidentified substances believed to be explosive degradation products was also noted in the soil samples using the MECC method, which offers higher efficiency than HPLC. Based upon calibration curves, concentrations of explosives in this case were found to range from 1265 ppm for TNT to 6.4 ppm 2,6-DNT in the original soil. Considering the toxicity of these substances [14], the value of this type of analysis for environmental assessment at military facilities cannot be overstated. In Table V concentrations of several nitroaromatic compounds in the soil determined with MECC and with HPLC are compared. The concentrations found for DNB and TNT are nearly the same for both methods. With MECC, RDX and TNB could not be evaluated, because in the soil probe both compounds had the same migration time. For the aminodinitrotoluene isomers the HPLC method can only give the sum of both amounts. However, considering the relative amounts of each isomer determined by MECC, the resulting sum is close to the HPLC value.

## CONCLUSIONS

The MECC method can be successfully applied to analysis of environmental samples, such as soil extracts, containing explosives residues. The method is fast, economic and generates little organic waste like the comparable HPLC method. Small sample sizes are easily handled, and detection limits are close to those obtained by HPLC. MECC offers high resolution and efficiency, allowing for "fingerprinting" of complex soil extracts. In addition, MECC provides easy removal of interfering humic substances extracted from complex soil matrices. The combined application of HPLC and MECC provides more information about the sample composition. In conclusion, it can be stated that MECC can compete with well-established techniques such as HPLC for the determination of explosives in complex matrices with regard to time of analysis and quantitation. However, better migration time reproducibility for the MECC method is needed. We are currently examining neutral flow markers to calculate MECC capacity factors and improve the precision of MECC results.

## REFERENCES

1 R.E. Clement, M.L. Langhorst and G.A. Eiceman, *Anal. Chem.*, 63 (1991) 270R.
2 M. Reisch, *Chem. Eng. News*, 70 (26) (1992) 7.
3 R.F. Spaulding and J.W. Fulton, *J. Contam. Hydrol.*, 2 (1988) 139.

4 C.F. Bauer, St.M. Koza and T.F. Jenkins, *J. Assoc. Off. Anal. Chem.*, 73 (1990) 541.
5 J.B. Nair and J.W. Huber, *LC·GC*, 6 (1988) 1071.
6 J. Hirata and J. Okamoto, *J. Microcol. Sep.*, 1 (1989) 46.
7 M. Hable, C. Stern, C. Asowata and K. Williams, *J. Chromatogr. Sci.*, 29 (1991) 131.
8 M.H. Mach, A. Pallos and P.F. Jones, *J. Forensic Sci.*, 23 (1978) 446.
9 A. Munder, R.G. Christensen and S.A. Wise, *J. Microcol. Sep.*, 3 (1991) 127.
10 D.M. Northop, D.E. Martire and W. MacCrehan, *Anal. Chem.*, 63 (1991) 1038.
11 Y.F. Yik, H.K. Lee and S.F. Li, *J. High Resolut. Chromatogr.*, 15 (1992) 198.
12 Th.F. Jenkins, M.E. Walsh and P.W. Schumacher, *J. Assoc. Off. Anal. Chem.*, 72 (1989) 890.
13 *Situationsplan, Umweltzentrum der Stadt Stadtallendorf*, Regierungspräsidium Giessen, Landgraf, Giessen, 1989.
14 R. Meyer, *Explosiv Stoffe*, Verlag Chemie, Weinheim, 1973.

*Journal of Chromatography*, 638 (1993) 357–361
Elsevier Science Publishers B.V., Amsterdam

CHROM. 24 930

# High-performance liquid chromatography and micellar electrokinetic chromatography of flavonol glycosides from *Tilia*

Piergiorgio Pietta*
*Università degli Studi di Milano, Via Celoria 2, 20133 Milan (Italy)*

Pierluigi Mauri
*ITBA–CNR, Via Ampere 56, 20131 Milan (Italy)*

Annamaria Bruno and Liliana Zini
*Università degli Studi di Milano, Via Celoria 2, 20133 Milan (Italy)*

ABSTRACT

The determination of nine different flavonol glycosides from *Tilia* using reversed-phase high-performance liquid chromatography (HPLC) and micellar electrokinetic chromatography (MEKC) is described. The analytes were monitored by on-line diode-array UV detection to identify peaks as quercetin or kaempferol derivatives. MEKC is confirmed as a useful complementary technique to HPLC.

## INTRODUCTION

*Tilia cordata* and *Tilia phatyphyllos* have been used as sedatives in folk medicine. They are listed in several pharmacopoeias, and the presence of compounds that behave as ligands for brain benzodiazepine receptors has been described [1]. Most published analyses of *Tilia* flavonol glycosides have involved separations by TLC [2], where the resolution is not sufficient to detect unequivocally components with nearly identical $R_F$ values. Wagner *et al.* [3] proposed a gradient HPLC method, but only quercitrin and tiliroside could be identified.

In this investigation, we applied a previously described HPLC approach [4], based on isocratic elution with 2-propanol and tetrahydrofuran (THF) using $C_8$ columns. The eluate was monitored by diode-array UV detection (DAD) to identify peaks as quercetin or kaempferol derivatives. Flavonol glycosides from *Tilia* were also analysed by micellar electrokinetic chromatography (MEKC) combined with DAD, which has recently been proposed [5] as a complementary technique to HPLC. The structures of the flavonoids analysed are shown in Fig. 1.

* Corresponding author.

0021-9673/93/$06.00 

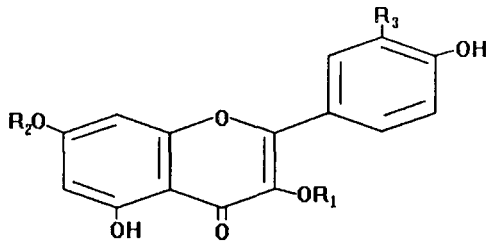


*Quercetin-3-O-glucoside-7-O-rhamnoside (I)*
R =glucose ; R =rhamnose ; R =OH
1 2 3
*Kaempferol-3-O-glucoside-7-O-rhamnoside (II)*
R =glucose ; R =rhamnose ; R =H
1 2 3
*Quercetin-3,7-O-dirhamnoside (III)*
R =R =rhamnose ; R =OH
1 2 3
*Kaempferol-3,7-O-dirhamnoside (IV)*
R =R =rhamnose ; R =H
1 2 3
*Quercetin-3-O-glucoside (isoquercitrin) (V)*
R =glucose ; R =H ; R =OH
1 2 3
*Kaempferol-3-O-glucoside (astragalin) (VI)*
R =glucose ; R =R =H
1 2 3
*Quercetin-3-O-rhamnoside (quercitrin) (VII)*
R =rhamnose ; R =H ; R =OH
1 2 3
*Kaempferol-3-O-rhamnoside (VIII)*
R =rhamnose ; R =R =H
1 2 3
*Kaempferol-3-O-(6-p-coumaroyl)-glucoside (tiliroside) (IX)*
R =6-p-coumaroyl-glucose ; R =R =H
1 2 3

Fig. 1. Structures of *Tilia* flavonol glycosides.

## EXPERIMENTAL

### *High-performance liquid chromatography*

HPLC analyses were performed using a Model 510 pump equipped with a Model U6K universal injector (Waters, Milford, MA, USA) and a model 1040 photodiode-array detector (Hewlett-Packard, Waldbronn, Germany). The column was MOS Hypersil (200 × 4.6 mm I.D.) and the eluent was 2-propanol–THF–water (10:5:85) at a flow-rate of 1.8 ml/min.

### *Micellar electrokinetic chromatography*

MEKC separations were carried out using a Eureka 2000 CE–DAD apparatus (Kontron Instruments, Milan, Italy) equipped with a 72 cm × 75 μm I.D. fused-silica capillary. The running buffer was 30 m*M* sodium borate (pH 8.5)–50 m*M* sodium dodecyl sulphate (SDS). The voltage was 277 V/cm, the injection volume (by gravity) was 10 nl and the temperature was 27°C.

### *Materials*

*Tilia* flowers were obtained from Milanfarma (Milan, Italy), Galke (Gittelde/Harz, Germany) and Birkenweg (Kleinesthein/Main, Germany).

Quercetin-3-O-glucoside (**V**), quercetin-3-O-rhamnoside (**VII**), myricetin-3-O-rhamnoside, kaempferol-3-O-glucoside (**VI**) and kaempferol-3-(*p*-coumaroyl)glucoside (**IX**) were purchased from Extrasynthese (Genay, France). Quercetin-3-O-glucoside-7-O-rhamnoside (**I**), kaempferol-3-O-glucoside-7-O-rhamnoside (**II**), quercetin-3,7-O-dirhamnoside (**III**) and kaempferol-3,7-O-dirhamnoside (**IV**) were obtained in our laboratory from *Tilia* leaves by semi-preparative HPLC.

2-Propanol, THF and water were of HPLC grade (Chromasolv, Riedel-de Haën, Hannover, Germany).

### *Sample preparation*

*Tilia* powdered samples (flowers, leaves and herb) (2 g) were suspended in 50% methanol (20 ml) and left overnight at room temperature. After filtration, the solution was evaporated to dryness *in vacuo* and the residue was dissolved in methanol (2 ml).

*Isolation of* quercetin-3-O-glucoside-7-O-rhamnoside (**I**), kaempferol-3-O-glucoside-7-O-rhamnoside (**II**), quercetin-3,7-O-dirhamnoside (**III**) and kaempferol-3,7-O-dirhamnoside (**IV**). Aliquots of 50 μl of the sample solution were chromatographed on an Aquapore $C_8$ (7 μm) semi-preparative column (250 × 7 mm I.D.) using 2-propanol–THF–water (10:5:85) at a flow-rate of 4 ml/min. Peaks of **I–IV** were collected by means of a Gilson Model 201 fraction collector (Biolabo Instruments, Milan, Italy). Each run yielded 20–30 μg of each compound.

*Hydrolysis*. Aliquots of about 200 μg of **I–IV** were hydrolysed and the resulting aglycones were identified as described previously [6].

*Tilia* (flowers, leaves, herb) sample solutions (0.25 ml) were processed in an analogous manner to obtain the total amount of aglycones.

Glucose and rhamnose were detected by gas chromatography as acetyl derivatives [7].

*Semi-preparative isolation of kaempferol-3-O-(6-p-coumaroyl)glucoside (tiliroside)* (**IX**). A

1-ml volume of the sample solution was diluted to 3 ml with water and applied to a previously activated (5 ml of methanol followed by 5 ml of water) Sep-Pak $C_{18}$ cartridge. After washing with 3 ml of water and 3 ml of 30% methanol, tiliroside was eluted with 3 ml of methanol.

## RESULTS AND DISCUSSION

Previous work [4] on the isolation of flavonoids from officinal plants involved extraction with aqueous methanol or ethanol followed by clean-up through a Sep-Pak $C_{18}$ cartridge. Owing to the absence in *Tilia* of components eluting as a large front, solid-phase extraction was unnecessary, except for the semi-preparative isolation of tiliroside (**IX**).

Using 2-propanol–THF–water (10:5:85) in the isocratic mode, a baseline resolution of all the components was achieved in about 30 min. As shown in Fig. 2A, *Tilia* flowers contain isoquercitrin (**V**), astragalin (**VI**), quercitrin (**VII**), kaempferol-3-O-rhamnoside (**VIII**) and tiliroside (**IX**), the first being the major component. On the other hand, the main flavonols of *Tilia* leaves were the diglycosides **I–IV** and tiliroside, whereas **V–VIII** were present in smaller amounts (Fig. 2B). A chromatogram of *Tilia* herb is shown in Fig. 2C.

Peaks were identified as quercetin (Q), kaempferol (K) or kaempferol-*p*-coumaroyl (T) derivatives on the basis of their on-line UV

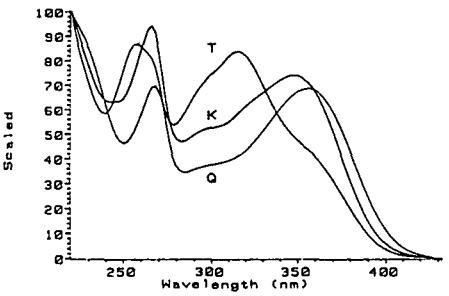


Fig. 3. HPLC–DAD of quercetin (Q), kaempferol (K) and kaempferol-*p*-coumaroyl (T) derivatives.

spectra (Fig. 3). Thus, peaks I, III and II, IV were recognized from the diode-array spectra as quercetin and kaempferol derivatives, respectively. Each peak was isolated and subjected to acid hydrolysis followed by detection of the aglycone by HPLC and sugars by GC. As expected, peaks I and III yielded quercetin, whereas peaks II and IV produced kaempferol. The detected sugars were glucose and rhamnose in the ratio 1:1 for peaks I and II and rhamnose for peaks III and IV.

From these results it can be concluded that peaks I, III and IV are related to the previously reported [8] flavonol glycosides, and peak III may be reasonably assumed to be the analogue quercetin-3,7-dirhamnoside. Peaks V, VI, VII and IX were assigned by co-chromatography with standards, and their identities were confirmed by DAD.

The total amount of quercetin and kaempferol

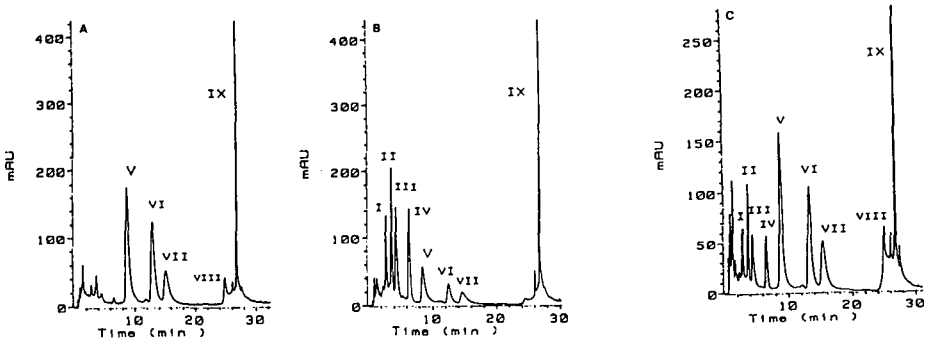


Fig. 2. Typical HPLC traces of (A) *Tilia* flowers, (B) *Tilia* leaves and (C) *Tilia* herb. Column, MOS Hypersil (200 × 4.6 mm I.D.); eluent, 2-propanol–tetrahydrofuran–water (10:5:85); flow-rate, 1.8 ml/min; detection, 270 nm. For peak numbers, see Fig. 1.

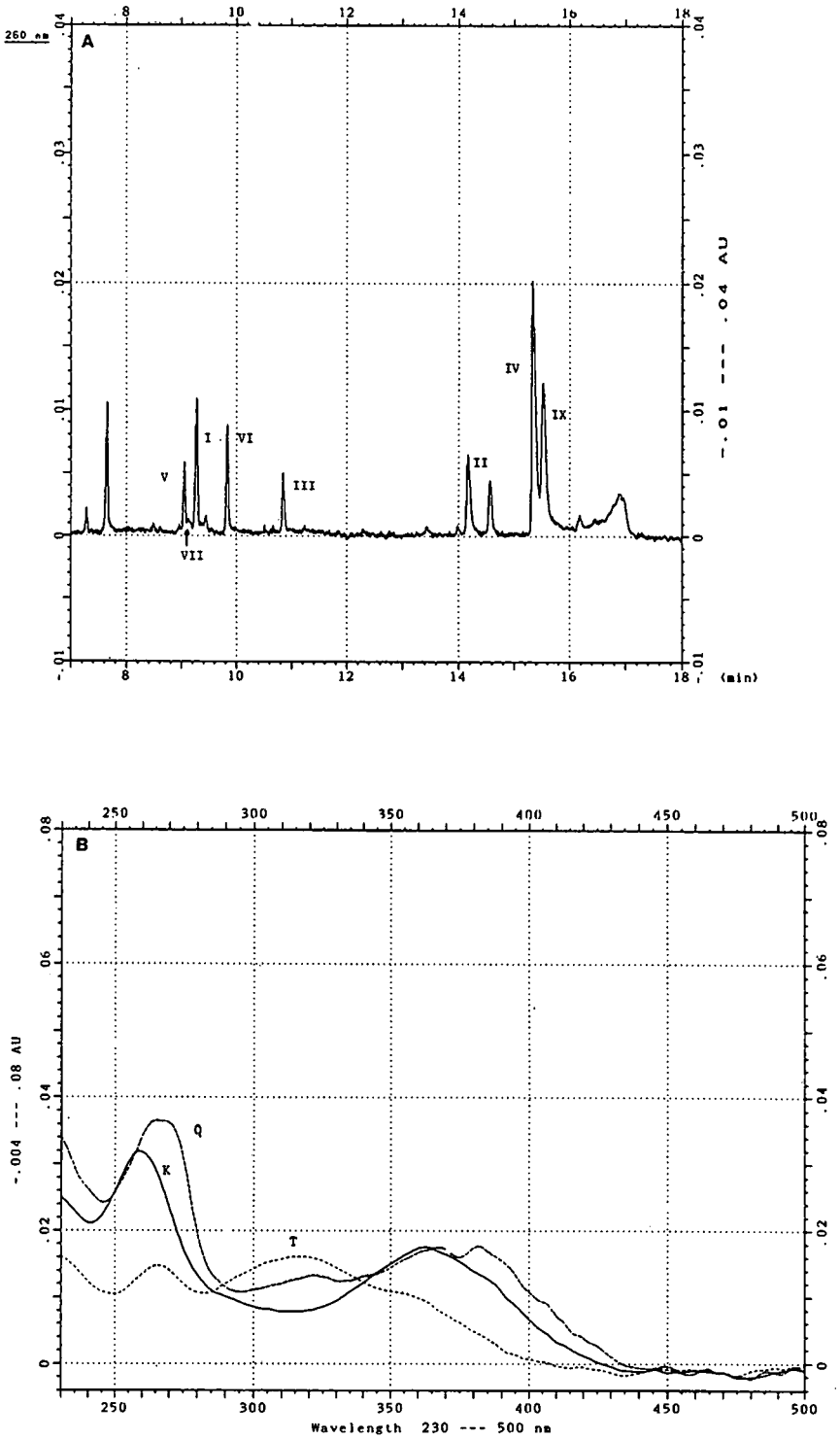


Fig. 4. (A) Typical electropherogram of *Tilia* leaf extract. Conditions: fused-silica capillary (72 cm × 75 μm I.D.); voltage, 277 V/cm; detection, 270 nm; buffer, 30 m*M* borate (pH 8.5)–50 m*M* SDS. (B) MEKC–DAD spectra of quercetin (Q), kaempferol (K) and kaempferol-*p*-coumaroyl (T) derivatives.

TABLE I

TOTAL AMOUNTS OF QUERCETIN AND KAEMPFEROL IN *Tilia* SAMPLES

| *Tilia* | Sample | Quercetin in 250 mg of drug (μg) | Kaempferol in 250 mg of drug (μg) |
|---|---|---|---|
| Flowers | a | 2.21 | 4.54 |
| | b | 2.59 | 3.21 |
| | c | 2.44 | 5.06 |
| Leaves | a | 0.37 | 1.39 |
| | b | 0.44 | 1.47 |
| | c | 0.58 | 1.82 |
| Herb | a | 2.90 | 5.59 |
| | b | 3.49 | 4.41 |
| | c | 3.18 | 5.12 |

derivatives in each sample was obtained by acid hydrolysis and HPLC determination of the resulting aglycones, and the results are given in Table I.

MEKC–DAD of *Tilia* leaf extracts yielded a baseline separation within 16 min (Fig. 4A). Peaks were identified by comparison with authentic specimens and on the basis of their on-line UV spectra (Fig. 4B). The wavelengths of the maximum absorption at around 265 nm of each compound are different from those shown in Fig. 3. This difference is ascribed to the different solvents [borate–SDS (pH 8.5) buffer in MEKC and 2-propanol–THF–water in HPLC] [9].

From these results it can be concluded that MEKC is a valuable alternative to HPLC and recent technological improvements in capillary electrophoresis apparatus for ultraviolet DAD permits on-line spectral information similar to that achieved by HPLC–DAD to be obtained.

ACKNOWLEDGEMENT

The authors are grateful to CNR-PF "Chimica Fine" for providing funds, and to Kontron Instruments for supplying the CE–DAD apparatus.

REFERENCES

1 J.H. Medina, C. Pena, M. Levi de Stein, C. Wolfman and A.C. Paladini, *Biochem. Biophys. Res.*, 165 (1989) 547.
2 V.M. Wichtl, B. Bozek and T. Fingerhut, *Dtsch. Apoth.-Ztg.*, 127 (1987).
3 H. Wagner, G. Tittel and S. Bladt, *Dtsch. Apoth.-Ztg.*, 123 (1983) 515.
4 P.G. Pietta, P.L. Mauri, A. Bruno and A. Rava, *J. Chromatogr.*, 553 (1991) 223.
5 P.G. Pietta, P.L. Mauri, A. Rava and G. Sabbatini, *J. Chromatogr.*, 549 (1991) 367.
6 P.G. Pietta, C. Gardana and P.L. Mauri, *J. High Resolut. Chromatogr.*, 15 (1992) 136.
7 D.J. Nevins, P.D. English and A. Karr, *Carbohydr. Res.*, 5 (1967) 340.
8 L. Horhammer, L. Stich and H. Wagner, *Arch. Pharm. Biol.*, 294 (1961) 685.
9 P.G. Pietta, P.L. Mauri, R. Maffei Facino and M. Carini, *J. Pharm. Biomed. Anal.*, 10 (1992) 1041.

*Journal of Chromatography*, 638 (1993) 363–373
Elsevier Science Publishers B.V., Amsterdam

CHROM. 24 949

# Fraction collection after an optimized micellar electrokinetic capillary chromatographic separation of nucleic acid constituents

Anne-Francesca Lecoq*
*CEC Joint Research Centre, Environment Institute, 21020 Ispra (Italy)*

Sebastiano Di Biase
*Beckman Analytical, Via Cintia 41/F, Naples (Italy)*

Luca Montanarella
*CEC Joint Research Centre, Environment Institute, 21020 Ispra (Italy)*

ABSTRACT

The possible use of capillary electrophoresis (CE) in micellar conditions with fast atom bombardment mass spectrometry (FAB-MS) for the characterization of DNA adducts with the ultimate goal of determining these compounds in biological matrices was explored. A method for fraction collection from an optimized and automated micellar electrokinetic capillary chromatographic (MECC) system is described. Parameters such as the reproducibility of migration times and injection and the maximum mass loadings are addressed. Fractions were collected directly in a small volume (5 $\mu$l) of buffer with sodium dodecyl sulphate (SDS) with recoveries of >75%. The fractions collected were further analysed using MECC and FAB-MS. Preliminary analysis by FAB-MS showed high background signals due to the presence of the SDS, demonstrating the difficulties that will be encountered with fractions deriving from a micellar separation and the need for more detailed investigations of the mass spectrometric conditions in this special case.

## INTRODUCTION

The use of carcinogen–DNA adducts as biological dosimeters of exposure to chemical carcinogens is critically dependent on the development of analytical methods that allow their accurate identification and determination at very low (picomole) levels (*e.g.*, one adduct in $10^8$–$10^{10}$ normal nucleotides). Several techniques have been developed over the past few years to detect and measure DNA adducts. The most widely used is Reddy *et al.*'s $^{32}$P-postlabelling technique [1], in which DNA is digested to 3'-monophosphates of normal and adducted nucleotides which are $^{32}$P-labelled and detected after TLC or HPLC. However, despite its high level of sensitivity, this technique does not reveal any structural information for the identification of unknown adducts that are detected [2]. Identifications are based only on co-chromatography with known standards and, at best, only tentative identifications can be made for unknown adducts.

We therefore developed a capillary electrophoretic (CE) method to evaluate the possibility of its use for the separation, determination and the further identification of normal and modified

* Corresponding author.

0021-9673/93/$06.00 

nucleoside and nucleotide 3′-monophosphates (the form in which nucleotides are phosphorylated in the postlabelling technique). The advantages afforded by CE include multiple separation modes, high resolution, rapid separation times and automation. In a previous paper [3], we reported micellar electrokinetic capillary chromatographic (MECC) separations of normal and some modified nucleic acid bases, including deoxy- and ribonucleosides and deoxynucleotide 5′- and 3′-monophosphates. Together nucleosides and nucleotides are a mixture of neutral and charged species and thus the mechanism of their separation is a combination of both electrophoretic migration and partitioning. An interesting characteristic was that, because of their different behaviours in micellar conditions, deoxyribonucleosides were well separated from the ribonucleosides and from the nucleotides. This cannot be achieved in most chromatographic systems. We and others [4] have shown also that substituted nucleotides generally elute after their unmodified analogues as substitution decreases their polarity and thus increases their partition in sodium dodecyl sulphate (SDS) micelles.

The simultaneous separation of nucleosides and nucleotides was found to be useful because in the nuclease P1 enrichment procedure [5–8] normal nucleotides are preferentially 3′-dephosphorylated to nucleosides whereas bulky aromatic adducted nucleotides are not. In consequence, after enrichment we should find in the nucleotide's elution interval only the adducted compound. For bulky hydrophobic substitutes [*e.g.*, polycyclic aromatic hydrocarbons (PAHs)], the elution behaviour should be confirmed. As adduct standards are not widely available for the development of analytical methodology, we anticipate that fine tuning of the CE conditions will be required for each future system studied. This will require the further availability of synthetic DNA–carcinogen adduct standards that are representative of different chemical classes.

CE has been used for micropreparative applications [9–13] and collected fractions have in some instances been characterized and identified by mass spectrometry. In the future, both CE–MS and micropreparative CE will be utilized in the identification and confirmation of species. Continuous-flow fast atom bombardment (CF-FAB) has proved to be a useful technique for the low-level detection of FAB-amenable analytes, in particular microgram levels of purified nucleosides and carcinogen–nucleoside/nucleotide adducts [14–17], and has been found to lend itself well to interfacing with various separation methods, including in the last few years capillary zone electrophoresis (CZE) [18–21].

In this paper, we explore the use of CE in micellar conditions with FAB-MS for the characterization of DNA adducts. In order to evaluate the possible utilization of purified material obtained after an MECC separation, we collected the micellar separated fractions for preliminary off-line tests. As small-diameter capillaries limit the amount of material that one can inject (*e.g.*, sub-picomoles of material), fractions from multiple runs must be pooled in order to collect sufficient material for subsequent analyses. Automated multiple collection of fractions involves optimization of the separation [*i.e.*, good retention time repeatability and maximum resolution of the components(s) to be purified from the remaining species at the desired loading levels]. Separation conditions (buffer composition, concentration and pH, capillary treatments, temperature and operating conditions) were previously evaluated for their influence on the retention times, resolution and efficiency in the separation of standard deoxynucleoside and deoxynucleotide 3′-monophosphates [22]. The choice of a 50-$\mu$m capillary diameter was based on the resolution required and the high reproducibility of the migration (<1% R.S.D.) that permits collection of repeated separations into the same set of vials with no cross-contamination of adjacent peaks. Under the same conditions (buffer, voltage), a 75 $\mu$m I.D. capillary results in larger mass injection; however, the resolution and repeatability were not inadequate (data not shown). In this work, we evaluated the optimum conditions for the maximum sample loading capacity that maintained a sufficient baseline resolution to allow the collection of the different fractions. After verifying suitable conditions, multiple fraction collection runs were performed into a fraction vial containing 5 $\mu$l of running buffer without SDS. The fractions collected were

directly re-analysed by MECC and then by FAB-MS.

## EXPERIMENTAL

### *Reagents*

All 2′-deoxynucleoside and 2′-deoxynucleotide 3′-monophosphate standards were obtained from Sigma (St. Louis, MO, USA) and were used without further purification. Stock standard solutions were prepared in water purified with a Milli-Q system (Millipore) at a concentration of 5 m*M* and stored at −20°C. The composition of the standard test mixture was 2′-deoxyadenosine (2′dAdo), 2′-deoxycytidine (2′dCyd), 2′-deoxyguanosine (2′dGuo), 2′-deoxythymidine (2′dThd), [2′-deoxyinosine (2′dIno)], 2′-deoxyadenosine 3′-monophosphate (2′dAdo3′mP), 2′-deoxycytidine 3′-monophosphate (2′dCyd3′mP), 2′-deoxythymidine 3′-monophosphate (2′dThd3′mP) and 2′-deoxyguanosine 3′-monophosphate (2′dGuo3′mP) dissolved in water.

All buffer components were obtained from Aldrich, Sigma or Merck and were of HPLC grade. The standard operating buffer 20 m*M* lithium phosphate–5 m*M* borate–100 m*M* SDS–5% acetonitrile prepared fresh each week from stock solutions of 0.2 *M* $Na_2B_4O_7$ and 0.2 *M* $LiOH–H_3PO_4$ (pH 7). The SDS was weighed and dissolved the mixture of buffer, water and acetonitrile and the pH was adjusted to 9.6 at 35°C. The solutions were filtered (0.22 μm), sonicated for 3 min and stored at room temperature.

### *Instrumental*

MECC was performed with a Beckman P/ACE System 2100 controlled with an IBM PS/2 Model 55SX computer with Beckman P/ACE v. 1.1 software. The inlet was held at a positive voltage. The untreated fused-silica capillary (50 μM I.D. × 57 cm total length, 50 cm to the detector) was obtained from Beckman and fitted into a capillary cartridge. Unless mentioned differently, the temperature (strictly controlled by the refrigerating circuit of the P/ACE system) was held at 35°C, the samples were injected by pressure for 10 s and the detection was accomplished by on-column UV absorbance measurement at 254 nm. Data were collected at a rate of 20 points per second and processed with the GOLD software. Relative retention times, when used, were calculated relative to the first peak, 2′dC. FAB mass spectra were generated from the collected fractions by using a VG 70 SEQ high-resolution magnetic sector instrument in an EDqQ configuration. A xenon FAB gun operated at an accelerating voltage of 8 kV was used in all experiments. Spectra were recorded at a resolution of 500. FAB mass spectra were generated by dissolving the fraction in 10 μl of pure glycerol.

## RESULTS AND DISCUSSION

### *Precision: migration time reproducibility*

*Effect of the buffer.* We previously [22] evaluated all the parameters that had an influence on the reproducibility, efficiency and resolution for the separation of our test mixture, *i.e.*, buffer composition (cation type, concentration, organic modifier, surfactant), pH, capillary treatment, applied voltage and operating temperature. The best buffer conditions for our fraction collection purpose was found to be 20 m*M* lithium phosphate–5 m*M* borate containing 100 m*M* SDS and 5% acetonitrile at a pH of 9.6 determined at 35°C. Compared with sodium or potassium phosphate, the lithium phosphate buffer gave a shorter analysis time, better efficiency and good resolution of the peaks. The order of elution is deoxyribonucleosides 3′-monophosphates (C < A < T < G < I) before 2′-deoxyribonucleotide 3′-monophosphates (A < C < T < G < U).

Precise control of the pH of the mobile phase is very important. We previously demonstrated [3] its influence on the resolution of the nucleotide 3′-monophosphates: at pH 7 we were able to separate the nucleotide 5′-monophosphates but not the 3′-monophosphates. To achieve good separation of the 3′-monophosphates we had to increase the pH to >9. At pH 9.6 a good resolution of the peaks was obtained,

but it was observed that the last two eluting peaks of nucleotides, 2′dG3′mP and 2′dU3′mP, which are completely ionized at this pH, tend to have an asymmetric shape and sometimes even show peak splitting (Fig. 1a). This problem could be solved by decreasing the pH (Fig. 1b). As the pH was lowered from 9.6 to 8.8, the time of analysis greatly decreased because of the early elution of the nucleotides mostly as a consequence of the effects of the pH on their degree of ionization. As our purpose was fraction collection and we needed a sufficient resolution to be able to collect the peaks, we decided to continue to work at pH 9.6.

*Effect of the capillary treatment.* For good operation of the capillary and repeatability of the separations, several factors are very important: the initial treatment, the after-run treatment, the storage treatment and the age of the capillary [23]. A systematic study of these treatments was not performed, but the following procedures gave the best reproducibility among those tested. A new capillary was first rinsed for 20 min with water followed by the storage treatment, then equilibrated with the running buffer for 15 min. Rinsing between runs was found to be necessary to return the system to the initial conditions, keeping the current constant from run to run, and consequently reducing the fluctuations in retention times. Rinsing with 0.1 *M* NaOH, followed by the running buffer without SDS at a pH slightly higher than the running buffer, was found to give better reproducibility, re-establishing the working pH gradually. Before a separation the capillary was equilibrated with the running buffer. At the end of a set of separations or for storage, the capillary was treated for 10 min with 0.1 *M* NaOH, 1 min with a first vial of water to remove the residue of NaOH from the outside capillary wall, 20 min with a second vial of water and finally dried with air under pressure from an empty vial. Under these conditions, we were able to perform more than 400 separations with a decrease in resolution. In our case, the loss of resolution occurred for the 2′dA and 2′dT peaks, which were found to be the peaks most sensitive to the operating conditions.

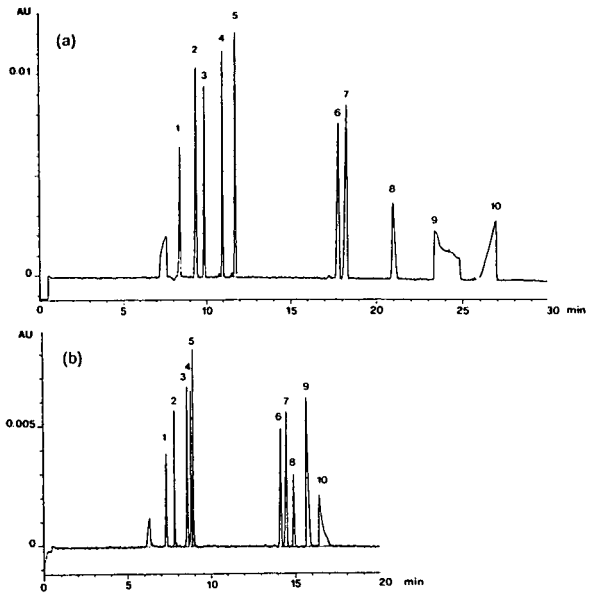


Fig. 1. Electropherograms of the standard mixture. Constant-current mode at 38 μA. (a) pH 9.6; (b) pH 8.8. Peaks: 1 = 2′dCyd; 2 = 2′dAdo; 3 = 2′dThd; 4 = 2′dGuo; 5 = 2′dIno; 6 = 2′dAdo3′mP; 7 = 2′dCyd3′mP; 8 = 2′dThd3′mP; 9 = 2′dGuo3′mP; 10 = 2′dUrd3′mP.

*Effect of instrumental operating conditions.* The best operating temperature was found to be 35°C, giving both good resolution and sufficient efficiency for our purposes [22]. At lower temperatures, the 2′dA and 2′dT peaks were not sufficiently resolved to allow fraction collection. The Ohm's law plot (current *versus* applied voltage) at 35°C exhibited good linearity below an applied voltage of 15 kV, then it began to deviate from linearity owing to less efficient heat dissipation because of the high voltage (Fig. 2). Therefore, for reproducible retention times one should operate below 15 kV. If the voltage is increased, the retention times decreases proportionally for all the solutes but the resolution is unaffected. The efficiency is also similar at all voltages for the nucleosides whereas for the nucleotides the efficiency increased as the voltage increased. This is in agreement with the fact that their separation is mainly due to their electrophoretic mobility and that an increase in the applied voltage leads to a decrease in their longitudinal diffusion [22]. A standard constant voltage of 12 kV or a constant current of 38 μA was generally used throughout this work because

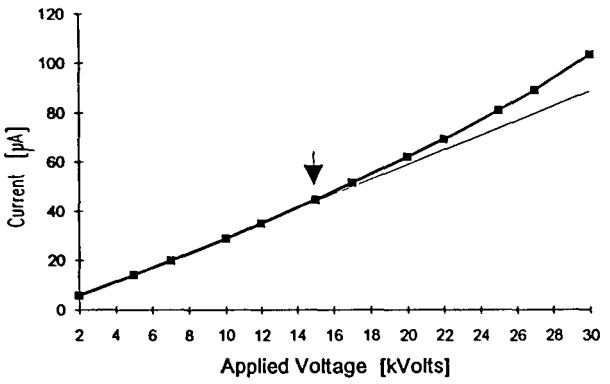


Fig. 2. Plot of current *versus* applied voltage at 35°C. Constant-voltage mode from 2 to 30 kV.

the time of analysis was found to be adequate for our fraction collection purposes.

*Run-to-run repeatability and day-to-day reproducibility*. Run-to-run values of R.S.D. range from 0.2 to 1.5% for the retention time and from 0.1 to 0.8% for the retention time relative to 2'dC. The day-to-day reproducibility of different series of separations, some also with different capillaries and preparations of running buffer, ranges from 0.5 to 4.2% for the retention time relative to 2'dC. It was noted that different preparations of running buffers lead to slight differences in current with consequent slight variations of the retention time. This is probably the most important factor that influences the reproducibility.

*Efficiency and resolution*. For the 57 cm × 50 μm I.D. under our standard operating conditions (electrical field of 21.05 kV/m) and 1 pmol of each standard loaded, the efficiency for the nucleosides is of 350 000 plates/m, greater than that of the nucleotides, 237 000 plates/m. This reflects the greater band broadening that occurs for the later eluting peaks [22]. With regard to the resolution, except for 2'dA3'mP and 2'dC3'mP, it is sufficient to allow the collection of each single peak.

*Minimum detectable concentration*. The minimum detectable concentration (MDC) was calculated using the equation $MDC = 3C(N/S)$ where $C$ = sample concentration, $N$ = detector noise and $S$ = peak signal; the factor 3 represents an arbitrarily chosen minimum signal-to-noise level. The minimum detectable mass (MDM) was calculated as the product of MDC and the injection volume. With on-column UV detection at 254 nm the MDM with a signal-to-noise of 3 was *ca.* 100 fmol. However, given the small injection volumes typically required for good CE performance, the MDC was only from 1–6 μg/ml for a 10-nl injection volume. This is not sufficient to allow the detection of adducts in DNA samples. Moreover, the UV detector does not allow the characterization of the molecules detected unless standards are available.

*Sample injection reproducibility*

Previous comparison of injection methods have generally shown hydrodynamic injections to be more reproducible and linear than electrokinetic injections, primarily because of fluctuating local electric fields at the capillary inlet during electrokinetic injection. It has also been demonstrated that electrokinetic injection induces a sample discrimination that occurs as a consequence of the different mobilities of the sample species [24]. Both procedures depend on the viscosity of the sample solution and therefore care should be exercized with respect to the temperature control of the sample solution for good quantitative reproducibility. Injection volumes can be calculated using the Poiseuille equation: for a capillary with an I.D. of 50 μm and a length to the detector ($L_d$) of 50 cm (6.9 cm less than the total capillary length), the volume of water (viscosity at 30°C = 79.8 P) injected per second is 1.2 nl [25].

To examine the precision of the sample size injected, the peak areas and the peak heights of each solute were calculated under constant injection conditions with five repetitions. The sample injection was performed by pressure for 20 s. The results are shown in Fig. 3a and b. The peak-area and peak-height values were reasonably constant, increasing slightly with successive repetitions because of the evaporation occurring in the sample vial (a 30-μl vial with 10 μl of sample). This can be limited by using a 400-μl vial instead of the 30-μl vial. Other variations can be attributed to errors in the calculation of the area by the Gold software because of the fluctuations of the baseline.

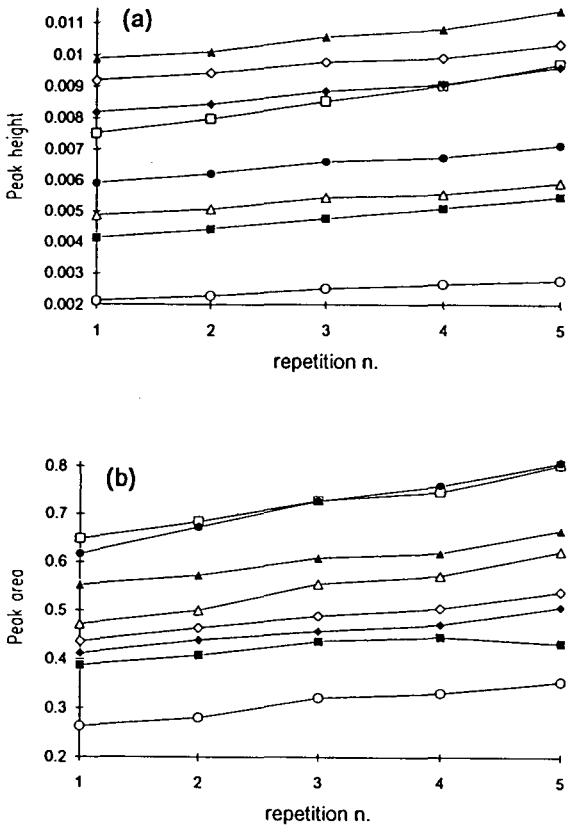


Fig. 3. Plots of (a) peak height and (b) peak area for repeated injections (in arbitrary units as reported by the Beckman Gold peak integrating software). Standard conditions, sample concentration at 0.1 pmol/nl, 20-s pressure injection. ■ = 2′dC; □ = 2′dA; ◆ = 2′dT; ◇ = 2′dG; ▲ = 2′dI; △ = 2′dA3′mP; ● = 2′dC3′mP; ○ = 2′dT3′mP.

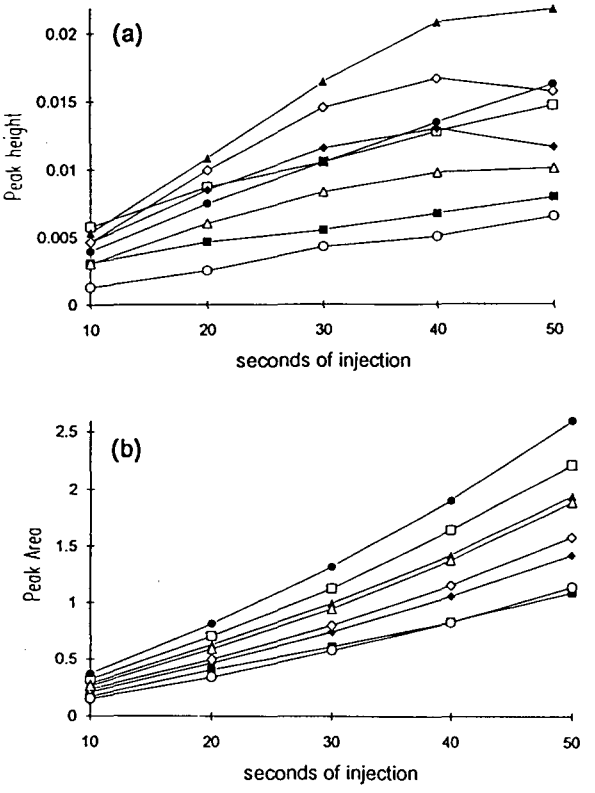


Fig. 4. Plots of (a) peak height and (b) peak area for increasing times of pressure injection (in arbitrary units as reported by the Beckman Gold peak integrating software). Standard conditions, sample concentration at 0.1 pmol/nl. Symbols as in Fig. 3.

*Sample injection linearity*

To determine the sample injection linearity for peak height and peak area we made successive runs with increasing injection times (from 10 to 50 s). Each injection was performed in triplicate. Plots are shown in Fig 4. For a sample concentration of 0.1 pmol/nl the peak-height values reached a plateau at 40 s of injection (4 pmol injected), then no further gain in detectability was obtained for any of the peaks. In contrast, for the peak area, the plateau was not already reached even with a 50-s injection. The slight deviation from the linearity in the plot of peak area *versus* time of injection is due to the evaporation that occurs during the successive runs. To avoid band broadening problems, the injection time must be kept as short as possible (<40 s), otherwise the peak shape and efficiency and consequently the resolution will be compromised. Peak areas were used for quantitative analysis.

*Maximum loadability*

In comparison with HPLC, CE is more limited with respect to the maximum mass load. Consequently, the amounts of material collected from capillaries are relatively small, which constrains further manipulation and analysis. To alleviate this problem, the mass load may be increased by increasing the capillary diameter (in our case ideally >50 $\mu$m). However, eventually the generation of Joule heat caused by the passage of electric current through the capillary will limit the separation efficiency and may impair the

integrity of biological samples. Another approach to solve the mass load problem in micropreparative work is to perform multiple runs with the same collection vial. Thus, the concentration of analyte in the collection vial should increase in proportion to the number of runs.

Peak shape and efficiency deteriorate with increasing injection time and/or sample concentration, owing to the increase in peak width. To establish the limit of overloading with reasonable resolution, we made successive runs with increasing solute concentrations (from 0.125 to 4 pmol/nl) with an injection time of 10 s (*ca.* 10 nl injected). Chromatograms are shown in Fig. 5. At the lowest concentration injected (1.25 pmol injected), the efficiency was at the maximum observed. Apart from 2′dT, which showed peak tailing when overloaded (>10 pmol), the efficiency and the resolution of the other nucleosides remained very good, allowing even higher loadability. The resolution of 2′dA3′mP and 2′dC3′mP began to be degraded above 10 pmol injected, and at 40 pmol we observed the appearance of a third, unidentified, peak eluting before 2′dA3′mP. These two peaks, however, could not be easily collected separately. The efficiency of 2′dT3′mP deteriorated above 20 pmol injected and the peak shape for 2′dG3′mP worsened considerably with overloading. In conclusion, for overloaded runs, concentrated samples should be used, when available, with the time of injection kept as short as possible to main good efficiency.

*Fraction collection*

Fraction collection with CE is technically different from that with HPLC. With electroelution, the end of the capillary must remain in contact with a solution containing buffer and an electrode during the collection of the fraction in order to maintain the electric field that drives the separation. Immediately prior to this step, the field is temporarily interrupted while the outlet buffer vial is replaced with a vial in which the fraction is to be collected. The volume in the latter vial must be kept small (<15 $\mu$l) to minimize analyte dilution. As an alternative to electroelution, pressure-driven mobilization can be used to collect fractions [26].

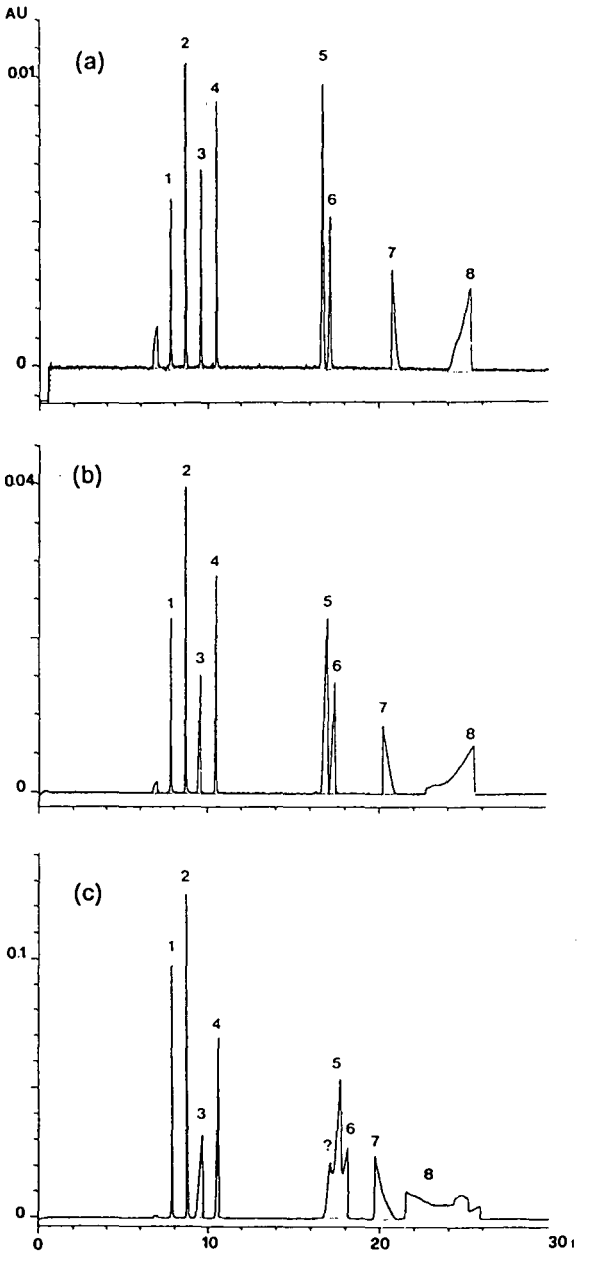


Fig. 5. Electropherograms of increasing concentration o standard mixture with 10-s pressure injection: (a) 0.25; (b) 1 (c) 4 pmol/nl. Peaks: 1 = 2′dCyd; 2 = 2′dAdo; 3 = 2′dThd 4 = 2′dGuo; 5 = 2′dAdo3′mP; 6 = 2′dCyd3′mP; 7 = 2′dThd3′mP; 8 = 2′dGuo3′mP.

We chose to collect two fractions of nu cleosides (2′dT and 2′dG) and one of nu cleotides (2′dA3′mP–2′dC3′mP). Initial run were performed to establish the migration tim

precision under our standard conditions (see Figs. 8a and 9a). After verifying adequate precision, the retention time of the leading edge ($t_{R1}$) of the peak and the peak width was determined. The retention times are those on the appearance of the peak in the detector window. The time that it takes to reach the end of the capillary ($t'_{R1}$) is calculated as follows: $t'_{R1} = (L/l)t_{R1} =$ (56.9 cm/50 cm)$t_{R1}$, where $L$ is the total length of the capillary and $l$ the length from the inlet to the detector window. During the collection period the field strength is reduced to 10 $\mu$A and the autosampler positions the collection vial containing 5 $\mu$l of buffer without SDS at the outlet end of the capillary. The start of the peak collection period is calculated as follows: $t'_{R1} - 0.1 - 0.2 = t_{R1s}$ (0.2 min for safety margin and 0.1 min to compensate for peak migration during the ramp-down period from 38 to 10 $\mu$A). The duration of the collection period at 10 $\mu$A is calculated as (0.2 + peak with + 0.2) · 38 $\mu$A/10 $\mu$A. When two successive peaks were collected the current was maintained at 10 $\mu$A and the corresponding times for collection were calculated in the same way. For multiple fraction collection, several micropreparative separations in an automated sequence were run successively into the same collection vial.

*Recovery*

After the micropreparative sequence was completed, the pooled fractions were re-injected to determine the recovery. For the first fraction collected (2′dT overloaded at a concentration of 4 pmol/nl in a mixture of only 2′dC and 2′dT injected for 40 s in nine successive runs) and re-injected for 60 s, we obtained a peak with a very poor shape (Fig. 6). Using the standard 2′dT in a mixture of 5 $\mu$l of running buffer without SDS plus 1 $\mu$l with SDS (final concentration 0.5 pmol/nl, similar to that of the collected fraction), we tried increasing the time of injection from 10 to 60 s (Fig. 7). Up to a 20-s injection time (*ca.* 10 pmol loaded) the peak had a good shape. For injection times ≥30 s the peak height decreased whereas the peak width increased, leading to a very poor shape of the peak. This is a typical matrix injection-related effect: the high salt concentration and the presence of SDS in the fraction vial lead to zone spreading at the injection end of the capillary when the high voltage is applied. Therefore, we observed peak broadening and slight variations in the retention times of the re-injected fractions (Figs. 8b and 9b). For this reason, the time of re-injection of the fractions collected must be kept as short as possible (<30 s). These effects could be reduced by using a lower salt concentration in the buffer placed in the collection vial.

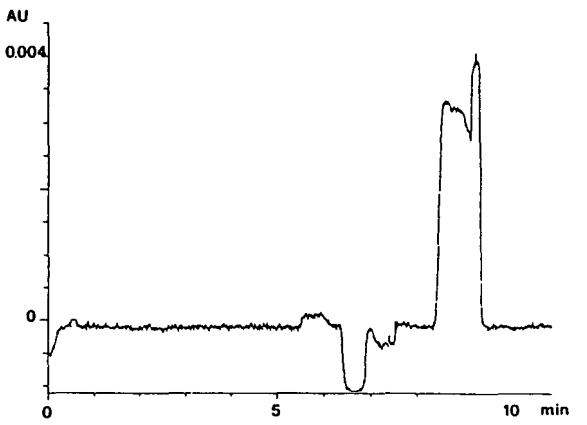


Fig. 6. Electropherogram of the re-injected pooled fraction (nine separations with 40-s pressure injection and a sample concentration of 4 pmol/nl) of 2′dT: 60-s pressure injection, approximate concentration 0.34 pmol/nl.

To determine the mass contained in the collected peak, we first evaluated the amount of solute loaded on the capillary in each run (concentration in pmol/nl × injection volume at 1.2 nl/s). The total amount loaded was deduced by multiplying by the number of successive runs. As this amount was collected in a fraction vial containing 5 $\mu$l of buffer, we estimated the concentration that should be obtained in an hypothetical 100% recovery, and consequently the amount that should be found in the re-injected fraction. The effective amount of the re-injected fraction was calculated either by the external or internal standard method and the recovery was then deduced. The values were always >75% (Figs. 8b and 9b).

*FAB–MS of the collected fractions*

The further analysis of the collected 5-$\mu$l fractions by FAB-MS posed several problems. The extremely high SDS concentration, com-

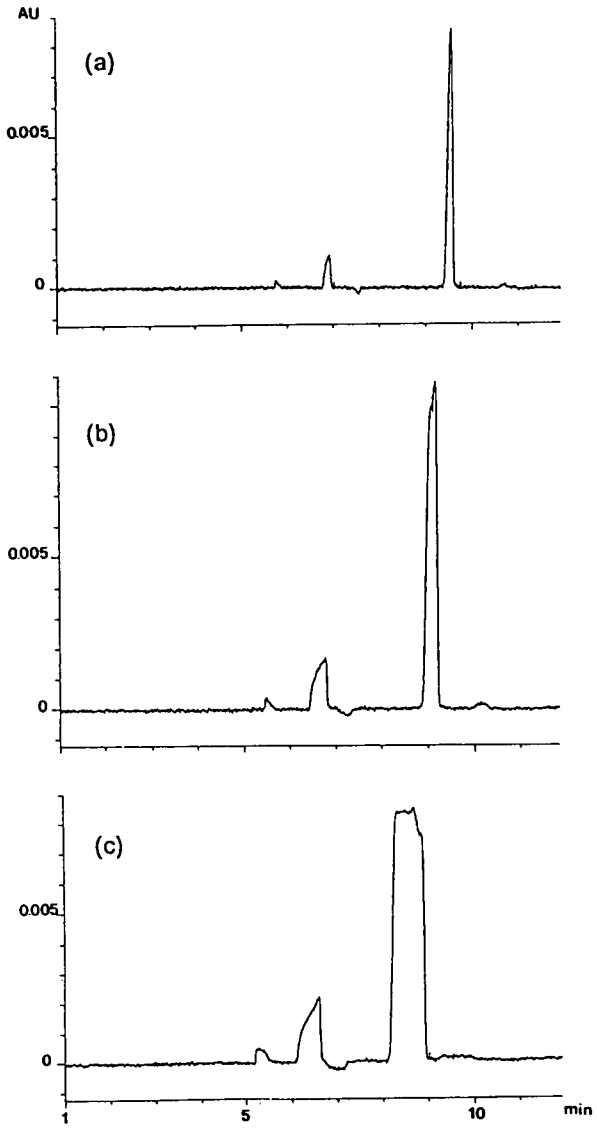


Fig. 7. Electropherograms of standard 2′dT (final concentration 0.5 pmol/nl) in a mixture of 4 $\mu$l of buffer without SDS + 1 $\mu$l of buffer with SDS injected for increasing times of pressure injection: (a) 10 s; (b) 30 s; (c) 60 s.

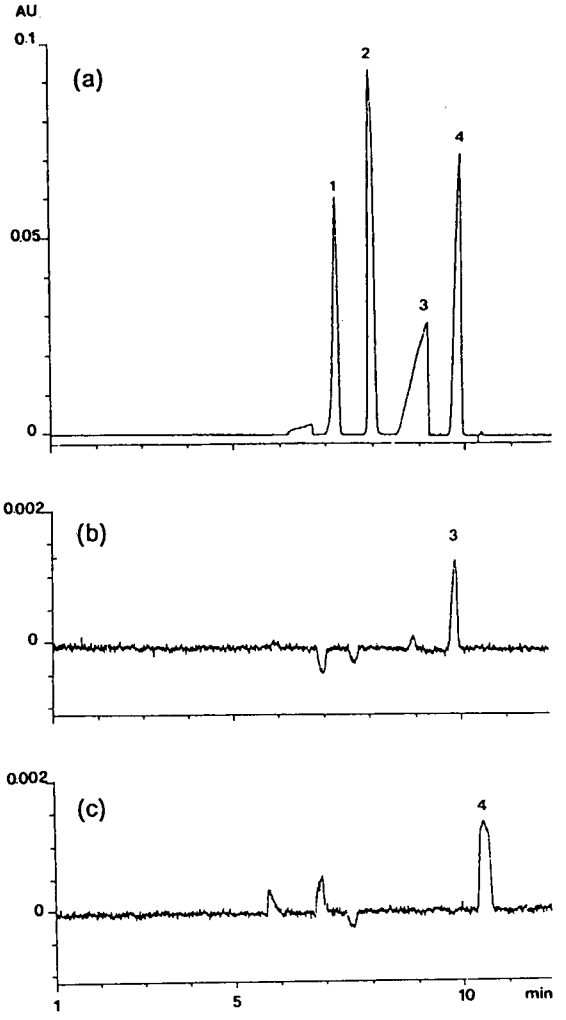


Fig. 8. Nucleoside fraction collection. (a) Electropherogram of the mircopreparative separation: 30-s pressure injection, sample concentration 2 pmol/nl. Peaks: 1 = 2′dCyd; 2 = 2′dAdo; 3 = 2′dThd; 4 = 2′dGuo. (b) Electropherogram of the re-injected pooled fraction (six repetitions) of 2′dT: 20-s pressure injection. Fraction concentration *ca.* 0.05 pmol/nl, recovery 70%. (c) Electropherogram of the re-injected pooled fraction (five repetitions) of 2′dG: 20-s pressure injection. Fraction concentration *ca.* 0.06 pmol/nl, recovery 83%.

pared with the analyte concentration in the fraction, produced a very intense background signal with strong chemical noise at the lower masses. The concentration of the collected nucleosides and nucleotides was too low for an appreciable signal in the presence of this high SDS background. This is probably due to an ion suppression effect of the SDS against the analytes present in the glycerol matrix. The ion suppression effect is a well studied phenomenon [27] in which a compound present in a sample will be recorded at an unusually low intensity or not at all. This has been found to be the result, in large part, of the tendency of the hydrophilic compounds to migrate to the interior of the sample droplet, away from the liquid/vacuum

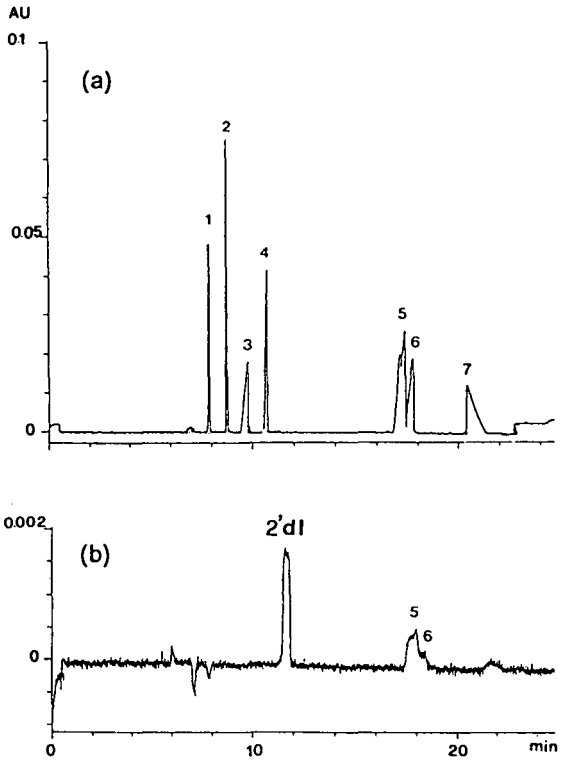


Fig. 9. Nucleotide fraction collection. (a) Electropherogram of the micropreparative separation: 10-s pressure injection, sample concentration 2 pmol/nl. Peaks: 1 = 2'dCyd; 2 = 2'dAdo; 3 = 2'dThd; 4 = 2'dGuo; 5 = 2'dAdo3'mP; 6 = 2'dCyd3'mP; 7 = 2'dTh3'mP. (b) Electropherogram of the re-injected pooled fraction (six repetitions) of 2'dA3'mP–2'dC3'mP: 20-s pressure injection. Internal standard, 2'dI. Fraction concentration *ca.* 0.22 pmol/nl, recovery 93%.

interface. At the same time, hydrophobic compounds tend to migrate to the surface layers of the droplet, suppressing the ionization of other compounds. With SDS we expect it to form a layer on the surface of the glycerol droplet, suppressing completely the ionization of the more hydrophilic nucleosides and nucleotides that migrate to the interior of the droplet (Fig. 10). Indeed, nucleosides in a pure glycerol matrix produced good spectra compared with those from fractions in the presence of SDS, presenting no signal at all for the collected nucleoside or even for the glycerol matrix.

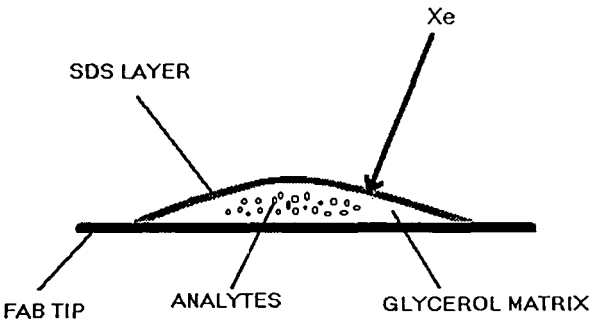


Fig. 10. Schematic representation of the situation at the FAB tip in the presence of SDS.

## CONCLUSIONS

Fraction collection after an optimized MECC separation of nucleic acid constituents has been successfully performed. The recoveries were relatively high (>75%). Nevertheless, the presence of high concentrations of SDS in the collected fractions posed a problem in FAB-MS owing to a strong ion suppression effect. It seems that these types of fractions cannot be directly analysed, at least by FAB-MS, without an intermediate step that could drastically reduce the presence of SDS. This may, however, have the serious disadvantage of leading to sample loss and/or eventual modification in an already very reduced sample volume and concentration. We nevertheless expect an improvement by using a dynamic FAB system, such as CF-FAB, coupled to tandem MS. This will be the subject of future work.

This type of separation with UV detection could still be extremely useful for many purposes, *e.g.*, for the rapid control of the DNA digestion to nucleotides, for the degree of its degradation or digestion in nucleosides, for the determination of RNA contamination and for the detection and determination of normal and some modified deoxy- and ribonucleosides or nucleotides. Moreover, fraction collection after MECC separations could be of interest for other spectroscopic investigations less sensitive to SDS interference.

## REFERENCES

1 M.V. Reddy, R.C. Gupta, E. Randerath and K. Randerath, *Carcinogenesis*, 5 (1984) 231–243.

2 K. Canella, K. Peltonen and A. Dipple, *Carcinogenesis*, 12 (1991) 1109–1114.
3 A.F. Lecoq, C. Leuratti, E. Marafante and S. Di Biase, *J. High Resolut. Chromatogr.*, 14 (1991) 667–671.
4 K.H. Row, W.H. Griest and MP. Maskarinec, *J. Chromatogr.*, 409 (1987) 193–203.
5 M.V. Reddy and K. Randerath, *Carcinogenesis*, 7 (1986) 1543–1551.
6 R.C. Gupta and K. Earley, *Carcinogenesis*, 9 (1988) 1687–1693.
7 J.E. Gallagher, M.A. Jackson, M.H. George, J. Lewtas and I.G.C. Robertson, *Cancer Lett.*, 45 (1989) 7–12.
8 M.V. Reddy, *Carcinogenesis*, 12 (1991) 1745–1748.
9 A.S. Cohen, A. Paulus and B.L. Karger, *Chromatographia*, 24 (1987) 15–24.
10 D.J. Rose and J.W. Jorgensen, *J. Chromatogr.*, 438 (1988) 23–34.
11 X. Huang and R.N. Zare, *J. Chromatogr.*, 516 (1990) 185–189.
12 A. Guttman, A.S. Cohen, D.N. Heiger and B.L. Karger, *Anal. Chem.*, 62 (1990) 137–141.
13 C. Fujimoto, Y. Muramatsu, M. Suzuki and K. Jinno, *J. High Resolut. Chromatogr.*, 14 (1991) 178–180.
14 K.H. Schram, *Trends Anal. Chem.*, 7 (1988) 28–32.
15 H. Moser and G.W. Wood, *Biomed. Environ. Mass Spectrom.*, 15 (1988) 547–551.
16 F.W. Crow, K.B. Tomer, M.L. Gross, J.A. McCloskey and D.E. Bergstrom, *Anal. Biochem.*, 139 (1984) 243–262.
17 R.K. Mitchum, F.E. Evans, J.P. Freeman and D. Roach, *Int. J. Mass Spectrom. Ion Phys.*, 46 (1983) 383–386.
18 K.H. Schram, in A.M. Lawson (Editor), *Clinical Biochemistry: Principles, Methods, Applications, Vol. 1: Mass Spectrometry, Purines and Pyrimidines*, Walter de Gruyter, New York, 1989, p. 507.
19 R.D. Smith, C.J. Barinaga and H.R. Udseth, *Spectra*, 12 (1989) 10–15.
20 R.D. Smith, H.R. Udseth, C.J. Barinaga and C.G. Edmonds, *J. Chromatogr.*, 559 (1991) 197–208.
21 M.A. Moseley, L.J. Deterding, K.B. Tomer and J.W. Jorgenson, *J. Chromatogr.*, 516 (1990) 167–173.
22 A.F. Lecoq, S. Di Biase and L. Montanarella, *J. Microcol. Sep.*, in press.
23 S.C. Smith, J.K. Strasters and M.G. Khaledi, *J. Chromatogr.*, 559 (1991) 57–68.
24 S.E. Moring, J.C. Colburn, P.D. Grossman and H.H. Lauer, *LC · GC*, 8 (1990) 34.
25 G. McLaughlin, R. Biehler, K. Anderson and H.E. Schwartz, *Technical Information Bulletin TIBC-106*, Beckman Instruments, Palo Alto, CA, 1991.
26 R. Biehler and H.E. Schwartz, *Technical Information Bulletin TIBC-105*, Beckman Instruments, Palo Alto, CA, 1991.
27 R.M. Caprioli, W.T. Moore and T. Fan, *Rapid. Commun. Mass Spectrom.*, 1 (1987) 15.

# Author Index

# CHEMOMETRICS TUTORIALS II

edited by **R.G. Brereton**, University of Bristol, Bristol, UK, **D.R. Scott**, U.S. Environmental Protection Agency, Research Triangle Park, NC, USA, **D.L. Massart**, Vrije Universiteit Brussel, Brussels, Belgium, **R.E. Dessy**, Virginia Polytechnic Institute, Blackburg, VA, USA, **P.K. Hopke**, Clarkson University, Potsdam, NY, USA, **C.H. Spiegelman**, Texas A&M University, College Station, TX, USA and **W. Wegscheider**, Universität Graz, Graz, Austria

The journal Chemometrics and Intelligent Laboratory Systems has a specific policy of publishing tutorial papers (i.e. articles aiming to discuss and illustrate the application of chemometric and other techniques) solicited from leading experts in the varied disciplines relating to this subject. This book comprises reprints of tutorials from Volumes 6-11 of this journal, covering the period from mid 1989 to late 1991. The authors of the papers include analytical, organic and environmental chemists, statisticians, pharmacologists, geologists, geochemists, computer scientists and biologists, which reflects the strong interdisciplinary communication. The papers have been reorganized into major themes, covering most of the main areas of chemometrics.

This book is intended both as a personal reference text and as a useful background for courses in chemometrics and laboratory computing.

***Contents:*** Foreword. **Software.** 1. Teaching and Learning Chemometrics with MatLab *(T.C. O'Haver)*. 2. Expert System Development Tools for Chemists *(F.A. Settle, Jr., M.A. Pleva)*. 3. Spectral Databases *(W.A. Warr)*. **Signal Processing.** 4. Specification and Estimation of Noisy Analytical Signals. Part I. Characterization, Time Invariant Filtering and Signal Approximation *(H.C. Smit)*. 5. Specification and Estimation of Noisy Analytical Signals. Part II. Curve Fitting, Optimum Filtering and Uncertainty Determination *(H.C. Smit)*. 6. Fast On-Line Digital Filtering *(S.C. Rutan)*. **Multivariate Methods.** 7. Cluster Analysis *(N. Bratchell)*. 8. Interpretation of Latent-Variable Regression Models *(O.M. Kvalheim, T.V. Karstang)*. 9. Quantitative Structure-Activity Relationships (QSAR) *(W.J. Dunn, III)*. 10. Analysis of Multi-Way (Multi-Mode) Data *(P. Geladi)*. **Factor Analysis.** 11. Target Transformation Factor Analysis *(P.K. Hopke)*. 12. An Introduction to Receptor Modeling *(P.K. Hopke)*. 13. The Spectrum Reconstruction Problem. Use of Alternating Regression for Unexpected Spectral Components in Two-Dimensional Spectroscopies *(E.J. Karjalainen)*. **Statistics.** 14. Analysis of Variance (ANOVA) *(L. Ståhle, S. Wold)*. 15. Multivariate Analysis of Variance (MANOVA) *(L. Ståhle, S. Wold)*. 16. The Validation of Measurement through Inter-laboratory Studies *(J. Mandel)*. 17. Regression and Calibration with Nonconstant Error Variance *(M. Davidian, P.D. Haaland)*. 18. Interpolation and Estimation with Spatially Located Data Sets *(D.E. Myers)*. **Optimization.** 19. Optimization Using the Modified Simplex Method *(E. Morgan, K.W. Burton, G. Nickless)*. 20. Optimization Using the Super-Modified Simplex Method *(E. Morgan, K.W. Burton, G. Nickless)*. **Fractals.** 21. Fractals in Chemistry *(D.B. Hibbert)*. Author Index. Subject Index.

**1992 x + 314 pages**
**Paperback**
**Price: US $ 156.50 / Dfl. 250.00**
**ISBN 0-444-89858-1**

**ORDER INFORMATION**

*For USA and Canada*
**ELSEVIER SCIENCE PUBLISHERS**
Judy Weislogel
P.O. Box 945
Madison Square Station,
New York, NY 10160-0757
Tel: (212) 989 5800
Fax: (212) 633 3880

*In all other countries*
**ELSEVIER SCIENCE PUBLISHERS**
P.O. Box 211
1000 AE Amsterdam
The Netherlands
Tel: (+31-20) 5803 753
Fax: (+31-20) 5803 705

US$ prices are valid only for the USA & Canada and are subject to exchange rate fluctuations; in all other countries the Dutch guilder price (Dfl.) is definitive. Books are sent postfree if prepaid.

ELSEVIER
SCIENCE PUBLISHERS

## PUBLICATION SCHEDULE FOR THE 1993 SUBSCRIPTION

*Journal of Chromatography* and *Journal of Chromatography, Biomedical Applications*

| MONTH | 1992 | J | F | M | A | M | J | |
|---|---|---|---|---|---|---|---|---|
| Journal of Chromatography | 623–627 | 628/1<br>628/2<br>629/1<br>629/2 | 630/1 + 2<br>631/1 + 2<br>632/1 + 2<br>633/1 + 2 | 634/1<br>634/2 | 635/1<br>635/2<br>636/1<br>636/2 | 637/1<br>637/2<br>638/1<br>638/2 | 639/1<br>639/2<br>640/1 + 2 | The publication schedule for further issues will be published later. |
| Cumulative Indexes, Vols. 601–650 | | | | | | | | |
| Bibliography Section | | | | 649/1 | | | 649/2 | |
| Biomedical Applications | | 612/1 | 612/2 | 613/1 | 613/2<br>614/1 | 614/2<br>615/1 | 615/2<br>616/1 | |

## INFORMATION FOR AUTHORS

(Detailed *Instructions to Authors* were published in Vol. 609, pp. 437–443. A free reprint can be obtained by application to the publisher, Elsevier Science Publishers B.V., P.O. Box 330, 1000 AH Amsterdam, Netherlands.)

**Types of Contributions.** The following types of papers are published in the *Journal of Chromatography* and the section on *Biomedical Applications:* Regular research papers (Full-length papers), Review articles, Short Communications and Discussions. Short Communications are usually descriptions of short investigations, or they can report minor technical improvements of previously published procedures; they reflect the same quality of research as Full-length papers, but should preferably not exceed five printed pages. Discussions (one or two pages) should explain, amplify, correct or otherwise comment substantively upon an article recently published in the journal. For Review articles, see inside front cover under Submission of Papers.

**Submission.** Every paper must be accompanied by a letter from the senior author, stating that he/she is submitting the paper for publication in the *Journal of Chromatography.*

**Manuscripts.** Manuscripts should be typed in **double spacing** on consecutively numbered pages of uniform size. The manuscript should be preceded by a sheet of manuscript paper carrying the title of the paper and the name and full postal address of the person to whom the proofs are to be sent. As a rule, papers should be divided into sections, headed by a caption (*e.g.*, Abstract, Introduction, Experimental, Results, Discussion, etc.) All illustrations, photographs, tables, etc., should be on separate sheets.

**Abstract.** All articles should have an abstract of 50–100 words which clearly and briefly indicates what is new, different and significant. No references should be given.

**Introduction.** Every paper must have a concise introduction mentioning what has been done before on the topic described, and stating clearly what is new in the paper now submitted.

**Illustrations.** The figures should be submitted in a form suitable for reproduction, drawn in Indian ink on drawing or tracing paper. Each illustration should have a legend, all the *legends* being typed (with double spacing) together on a *separate sheet.* If structures are given in the text, the original drawings should be supplied. Coloured illustrations are reproduced at the author's expense, the cost being determined by the number of pages and by the number of colours needed. The written permission of the author and publisher must be obtained for the use of any figure already published. Its source must be indicated in the legend.

**References.** References should be numbered in the order in which they are cited in the text, and listed in numerical sequence on a separate sheet at the end of the article. Please check a recent issue for the layout of the reference list. Abbreviations for the titles of journals should follow the system used by *Chemical Abstracts.* Articles not yet published should be given as "in press" (journal should be specified), "submitted for publication" (journal should be specified), "in preparation" or "personal communication".

**Dispatch. Before sending the manuscript to the Editor please check that the envelope contains four copies of the paper complete with references, legends and figures. One of the sets of figures must be the originals suitable for direct reproduction. Please also ensure that permission to publish has been obtained from your institute.**

**Proofs.** One set of proofs will be sent to the author to be carefully checked for printer's errors. Corrections must be restricted to instances in which the proof is at variance with the manuscript. "Extra corrections" will be inserted at the author's expense.

**Reprints.** Fifty reprints will be supplied free of charge. Additional reprints can be ordered by the authors. An order form containing price quotations will be sent to the authors together with the proofs of their article.

# Chromatography of Mycotoxins

## Techniques and Applications

*edited by* **V. Betina**

Journal of Chromatography Library Volume 54

This work comprises two parts, Part A: Techniques and Part B: Applications. In Part A the most important principles of sample preparation, extraction, clean-up, and of established and prospective chromatographic techniques are discussed in relation to mycotoxins. In Part B the most important data, scattered in the literature, on thin-layer, liquid, and gas chromatography of mycotoxins have been compiled. Mycotoxins are mostly arranged according to families, such as aflatoxins, trichothecenes, lactones etc. Chromatography of individual important mycotoxins and multi-mycotoxin chromatographic analyses are also included. Applications are presented in three chapters devoted to thin-layer, liquid, and gas chromatography of mycotoxins.

***Contents:***




**1993 xiv + 440 pages**
**Price: US $ 180.00 / Dfl. 315.00**
**ISBN 0-444-81521-X**





0021-9673(19930528)638:2;1-R